PROVENANCE AND DEPOSITIONAL ENVIRONMENTS OF EARLY CRETACEOUS SEDIMENTS IN THE BREDASDORP SUB-BASIN, OFFSHORE SOUTH AFRICA: AN INTEGRATED APPROACH

By

MOGAMMAD YAASEEN HENDRICKS

Supervisor: Prof. Tapas K. Chatterjee

A thesis submitted in fulfilment of the requirements for the degree of Magister Scientiae in Applied Geology

Department of Earth Sciences
University of the Western Cape, Cape Town
South Africa
October, 2019

DECLARATION

I declare that my research work titled "**Provenance and depositional environments of early Cretaceous sediments in the Bredasdorp sub-basin, Offshore South Africa: An integrated approach**" is my own work, that it has not been submitted before for any degree or examination in any other university, and that all the sources I have used or quoted have been indicated and acknowledged by means of complete references

Mogammad Yaaseen Hendricks October 2019

……..

Signature

ACKNOWLEDGEMENTS

Firstly, all gratitude is due to the Almighty God for granting me the strength and ability to achieve the completion of this research project

I would like to thank Prof. Tapas Kumar Chatterjee, main supervisor on this project, for his guidance, encouragement and patience towards the completion of this research project. His invaluable and extraordinary support has taught me a lot throughout the years, in not only academics but also providing me the beneficial practical skills for my profession.

I am also grateful for the Department of Earth Science at the University of the Western Cape for providing the facilities to complete this research project. I would also like to thank Mrs. Yafah Williams for her constant encouragement and advice towards the completion of the research project. I would also like to thank my colleagues Nehemiah Dominick, Monica Enifome Oghenekome and Kirk Jacobs for their fruitful discussions and help during this research project.

I am also thankful towards the people who have contributed to the completion of this research project such as Dr. Junaid Sadeque and Dr. Ali Jaffri on sedimentological and ichnological analysis, Ms..Mareli Grobbelaar and Ms. Riana Rossouw at the CAF facility (Stellenbosch University) on geochemical analysis, Mrs. Rene Van Der Merwe, Dr. Emese Bordy and Yambi Dinnis on thin section analysis (University of Cape Town) and Ms. Helene G. Hojberg and the EasyCopy team for providing software licenses. I am also indebted to Zain Kamish and Mymoena Stoffels for their help in reconstructing the depositional cartoon models in CorelDraw and help with compiling the references. I am also appreciative to the patience and mentoring of Dr. Eugene Bergh.

I am also beholden for the financial support from the NRF, without their support, this research project would not have been possible. I am also grateful to Mr. Viljoen Storm and Mr. Leon Koopman from the Petroleum Agency South Africa (PASA) for providing me with the data.

Lastly, but not the least, I am grateful to my parents Ebrahim and Gadija Hendricks for their sacrifices and guidance in life as well as my siblings for their encouragement.

ABSTRACT

Southern offshore basins of South Africa are well known as potential provinces of hydrocarbon exploration and production. The complex nature of the Bredasdorp sub-basin's syn-rift architecture (transform fault system) can have adverse effects on reservoir distribution due to periodic local and regional uplift of horsts and grabens. This present investigation focusses on an integrated approach of the 1AT1-V horizon or early Cretaceous sediments in the Bredasdorp sub-basin to identify the depositional environment and provenance of these sediments as well as their role in regionally complex compositional heterogeneities associated with the late stage rifting of Gondwana break-up.

An integrated seismic, sedimentological (including petrography and geochemistry) and ichnologic analysis of the 1AT1-V horizon sediments showed an overall lower regressive element complex assemblage set and an upper transgressive element complex assemblage set that occurred as a >120m thick succession. The analysis identified a mixed-energy deltaic succession followed by an estuarine succession. The 1AT1-V interval (late syn-rift) consisted of nine sedimentary facies associations (and associated petrofacies) on a dipslope setting with variations occurring along the strike and the downdip depositional slope areas.

Two overall sequences were identified as a lower regressive and upper transgressive sequence (Element complex assemblage sets). The regressive sequence consisted of middle to distal delta front lobe fringes, hyperpycnal event beds (sourced from basement highs), offshore migrating tidal bars (and associated inter-bar regions), distal mouth bars, terminal distributary channels (and associated inter-terminal distributary regions). The distal delta plain to proximal delta front consisted of interdistributary bays, distributary channels, crevasse splay sub-deltas, mouth bars, tidal flats and offshore embayments. In the laterally isolated depocenter, these deposits also consisted of basement high slopes with upliftment of the basement highs leading to proximal/central embayment to regressive shoreface/foreshore environments. These sequences consisted generally of low diversity and intensities (impoverished abundances) of trace fossils. The paleoclimate inference from this sequence indicates a humid climate with intermediate degrees of weathering intensities (possibly fluctuating arid-humid conditions). The transgressive sequence consisted of estuarine sedimentation with the occurrence of tidal sand ridges and compound dune fields, embayment facies and tidal bars. These sequences consisted of relatively

higher ichnodiversities and intensities than their relative regressive sequences. The paleoclimate inference during these times consisted of more arid to semi-arid settings with low degrees of weathering in the source terrain. Local tectonic upliftment and subsidence, with exposed basement highs, gave rise to differential process regimes (tidal, wave and fluvial) and hence depositional facies in the diachronous updip/downdip areas (spatial) and within-stratigraphic (temporal) variations. There are several modern analogues that are similar to the 1AT1-V horizon sequence and they are the Mahakam, Ganges-Brahmaputra, Po, Burdekin deltaic and Satpara lake environments.

Compaction and dissolution diagenetic features as well as transportation were responsible for the major compositional heterogeneities concerning the reservoir quality and distribution. Proximal and distal sources were identified with first cycle and polycyclic sediments being deposited in the northern and southern part of the basin during the late stages of rifting in the Bredasdorp sub-basin.

The provenance lithology has been identified as recycled sedimentary rocks (and their meta-equivalents) with an ultimate source terrain that was largely felsic in nature (Cape granite suite). The northern part of the studied section is suggested to have received sediments from the main metasedimentary rocks of the Cape fold belt (including the Table Mountain Group and Bokkeveld Group) whereas the southern sections received more sediments from the basement highs (recycled Malmesbury Group (and Pre-Cape sediments) and Cape granite suite), which is further supported by seismic data. Provenance analysis revealed that the Cape Fold belt (most recent collision) was possibly a provenance terrain but overprinting of several collisions are also acknowledged. The tectonic setting was envisaged to be of a rifted margin during the break-up of Gondwana. This compositional heterogeneity due to facies and provenance-related terrains had major consequences to the reservoir quality and distribution from the northern part to the southern part of the studied section.

Keywords: Bredasdorp sub-basin, early Cretaceous, Depositional environment, Provenance, High-resolution facies analysis, Seismic, Petrography, Geochemistry

CONTENTS

LIST OF FIGURES

List of Tables

List of Tables (Appendix)

Appendix A

Appendix B

Appendix C

CHAPTER 1

BACKGROUND

1.1 Introduction

The Bredasdorp sub-basin has one of the most complex basin-fills in South Africa in terms of its geology. Limited published studies have been performed in the sub-basin based on detailed analysis, but overall research relying on general sequence stratigraphy, biostratigraphy, sedimentology and petroleum geology or petrophysics were performed. These techniques focused mainly on the identification and evaluation of petroleum systems. The complex geological nature of the sub-basin makes it an ideal area to be investigated and even more crucial for an integrated approach to be used to assess the basins depositional history.

In the present work, the depositional environment and provenance of the reservoir sediments will be worked out from a multi-disciplinary approach involving sedimentary facies (lithofacies and ichnofacies), petrographic, geochemical and seismic data analysis for the selected reservoir intervals. Though there are several methods to understand the provenance and depositional environment of sediments, the accuracy of the study depend largely on how these semi-quantitative methods are integrated. To identify the depositional pathways and their possible relationship to hydrocarbon reservoirs, an evaluation of the direction of sediment input into the basin is crucial to understand.

The identification of the depositional environment and the provenance is crucial for the petroleum industry, especially in terms of characterizing the hydrocarbon system for the efficient exploration and exploitation of hydrocarbons. The misinterpretation of the depositional environment and provenance can have catastrophic effects on hydrocarbon extraction (Green & Slatt, 1992). Therefore, the effects of these two factors (encompassing the depositional history) are crucial to the exploration and production phases of hydrocarbon reservoirs.

The interpretation of modern-day processes involved in the sedimentary environment can give rise to reconstructions of ancient depositional environments (Reading, 2009). These ancient sedimentary environments play a major role in characterizing the distribution and the occurrence of petroleum reservoirs. Therefore, for example, the character of petroleum reservoirs can be represented through different methods using seismic facies as well as lithofacies to represent

ancient depositional environments that will be identified in this study, and where the accuracy depends largely on the integration of methods.

The character of sediments is amenable to the various effects of transportation and deposition from the source area to the depositional environment. Thus increasing the need for an integrated approach to predict the depositional environments and identify the provenance. Various researchers use singular methodological approaches to identify the provenance and due to this misinterpretation of the provenance are very common. Some authors do not also consider the depositional pathways when identifying the depositional environment and the provenance. Therefore, to have ascertained a provenance in the past, most studies used a basic approach of combining certain individual and relative combinations of framework minerals like quartz and feldspar, to delineate the source area (Dickinson & Rich, 1972; Dickinson et al., 1983). These studies also aimed at identifying the tectonic setting of the source based on the framework geochemistry or mineralogy that is used and documented in a very broad context (Middleton, 1960; Crook, 1974; Trevena & Nash, 1981; Dickinson et al., 1983; Bhatia & Crook, 1986; McLennan et al., 1993). The problem with a singular approach, for example using mineralogy, can obscure the results and the interpretation of the source area (Macdonald et al., 2006). These petrographic and geochemical methods will be expanded upon and modified in this study with the support of statistical methodologies. The seismic method to provenance is a new but crucial approach in identifying the direction and rate of sediment supply that are important in delineating sediment pathways, as a 'quick' tool for identifying source directions.

The results obtained from these studies can be used in reservoir models for the petroleum industry and for academic research purposes, in terms of evaluating the depositional history of the early Cretaceous sediments. This study will provide insight into the source of sediments and the depositional environment that can be used to characterize a sandstone reservoir model for understanding reservoir quality in unknown parts of a sedimentary basin. The sediment dispersal path is crucial to the development of a reservoir system. An attempt has been made to link modern day source and sink systems (sediment dispersal path) to ancient environments which becomes complicated as there are many factors that influence the distribution of sediments, hence the reservoir distribution (Helland-Hansen et al., 2009). The identification of a source-sink

link can enhance the understanding of modern day or ancient environments as well as global tectonics, paleogeography, climate change and sea-level changes.

There has been no detailed published literature that dealt with the depositional architecture and the provenance of the early Cretaceous sediments of the Bredasdorp sub-basin, therefore this study is crucial for academic research and the petroleum exploration and production stages within the sub-basin.

1.2 Research aim and objectives

1.2.1 Aim

The main aim of the study is to determine and interpret the provenance and depositional environments of the lower Cretaceous sediments. Thus, will provide insight into the detailed sedimentology (including sediment pathways) and paleogeography that characterizes a reservoir system.

1.2.2 Objectives

- To identify facies (including litho and ichnofacies) and seismic facies
- To identify and describe the mineralogy of the rock
- To identify relationships concerning the geochemistry of rocks
- To identify and describe depositional environments
- To identify the provenance using petrographic, geochemical and seismic techniques and compare these findings to the surrounding geology
- Identify how reservoir quality is affected by these changes
- Construct a depositional model with possible modern equivalents

1.3 Location of study area

The study area is located in the offshore Bredasdorp sub-basin, situated along a modern passive continental margin on the southern coast of South Africa and around the Mossel Bay area (Figure 1.3.1). The Bredasdorp sub-basin is a passive marginal sub-basin (with syn-rift half graben) that is structurally complex with an area of around 18000km^2 where thick successions of sedimentary piles occurs offshore. The basin and study area is bounded by crustal scale discontinuities which is located in the west by the Columbine-Agulhas Arc and in the east by the

Infanta Arch (arches which separates the sub-basins). The research focus-area is based on a selected reservoir interval of three wells in the north eastern part of the Bredasdorp sub-basin stretching from the Infanta Arch to a neighbouring basement high (Figure 1.3.1). The studied interval is largely restricted to the 1AT1-V horizons which fall part of the Berriasian and Valanginian stages (early Cretaceous).

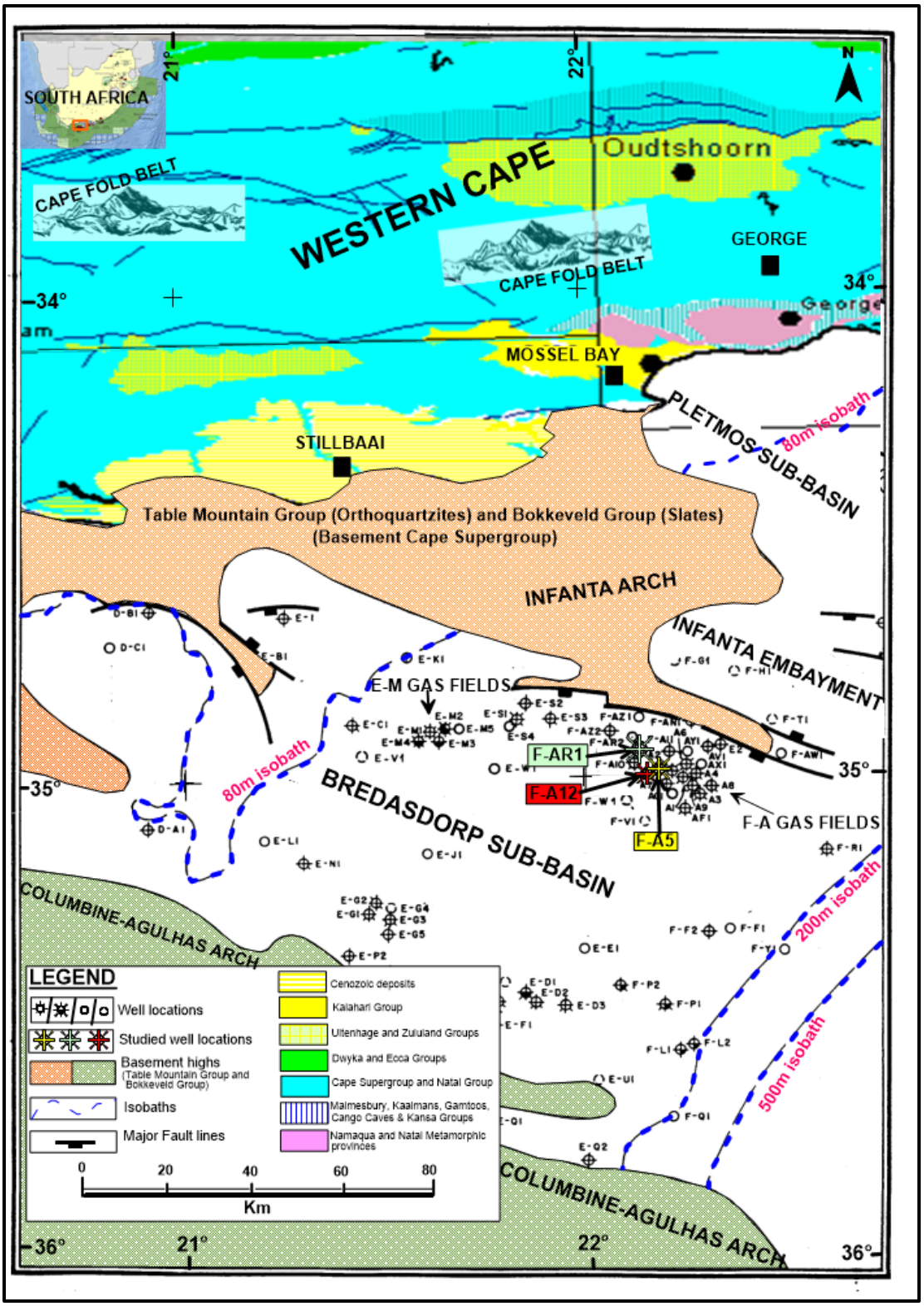

Figure 1.3.1: Study location with simplified geological map of the Bredasdorp sub-basin, offshore South Africa. Study locations and wells situated in the F-A gas fields.

1.4 Literature review

The understanding of petroleum reservoir dynamics depend largely on the depositional realm (including diagenetic setting) and the source area characteristics of the sediments. The source of sediments and the dispersal pattern towards the depositional site (including transport and diagenetic modifications) are important factors to take into account for the construction of petroleum reservoir models.

Sedimentology and stratigraphy involves the study of the processes involved during the formation, timing, transport and deposition of sediments (Nichols, 2009). The depositional environments are areas where sediments are deposited through sedimentary processes governed by certain hydrodynamic or aerodynamic processes.

Depositional environments can be reconstructed in many different ways ranging from seismic facies analysis (including sequence stratigraphy), lithofacies analysis (wireline logs and cores), specialized methods e.g. biostratigraphy, chemostratigraphy, magnetostratigraphy etc. and an integrated or combination of all the methods and interpretations. This contributes to a robust interpretation on depositional environments, usually for the analysis of reservoir zones (reservoir distribution), ore deposits and for academic purposes. Petrographic studies can also yield crucial insights to the conditions under which sediments are deposited in relation to their depositional realm (includes depositional environment and diagenetic environment) which leads to detailed micro-analysis of microfacies and their associated conditions of formation (Esmeray-Senlet et al., 2015).

Most authors identify lithofacies based on grain sizes, where coarse-grained and fine-grained associations can be used to identify certain differences in rocks. This technique is viable to use since it takes into account the hydrodynamic conditions within your depositional setting but it becomes problematic when dealing with multiple depositional systems or paralic depositional environments. Certain authors follow the works and facies characteristics adopted in Miall (1988) and Miall (1996) as a criterion for their facies analysis, incorporating sedimentary structures (with their associated hydrodynamic conditions) and architectural elements. This identification of sedimentary structures (inorganic or organic) forms the basis of determining the depositional processes involved during deposition. The most effective qualitative approach is to

modify Miall (1988)'s descriptions on sedimentary characteristics and comparing the results to modern environments. The problem that occurs with interpreting facies on this generalized approach is that certain details can be overlooked when ascribing facies associations or the basic underlying factors involved in the interpretations of these characteristics such as the fluvial system being an aggradational (distributive) or degradational (tributary) depositional system has been overlooked (Bristow et al., 1999; Nichols & Fisher, 2007; Weissmann et al., 2010). Factors like these, as seen from continental fluvial systems and their modern equivalents, can be grossly exaggerated within the rock record if additional criteria or an integration is not performed.

Another crucial relationship in the identification of depositional environments is the identification of the ecological characteristics of sediments which uses the trace fossils of certain organisms (ichnofacies) to reconstruct the depositional environment. Thus shedding light on crucial information on environmental conditions where facies associations (especially with limited modern equivalents) are unable to denote certain detailed depositional characteristics or profiles (Seilacher, 1967). Therefore, an integrated approach is needed to yield more reliable and accurate results for the identification of the depositional environments, which includes the ichnofabric or bioturbation characteristics (Bromley & Ekdale, 1986; Bromley, 1996; Taylor et al., 2003; Coates & MacEachern, 2009; Ekdale et al., 2012; MacEachern et al., 2012).

Recently, more quantitative methods has been utilized to identify the depositional environments (mostly marginal-marine) based on a set of criteria such as the autogenic (including basinal processes) and allogenic processes involved (Ainsworth et al., 2011; Rossi & Steel, 2016). These methods have resulted in an efficient way to identify subsurface depositional environments with comparison to more modern depositional environments and their processes. Some mineralogical quantitative methods have also been applied to facies analysis where the ratios of certain minerals have been assigned to particular processes involved in the depositional realm. The study of Bordy & Preveck (2008) illustrated this identification by examining semi-quantitatively coarse-grained and fine-grained associations, which were dependent on the percentage ratios between micaceous and feldspathic minerals. These associations can be described in more detail through core analysis (sedimentological observations) or rock outcrop analysis to reconstruct the depositional environments (Bordy & Preveck, 2008). Another form or approach to lithofacies analysis would be to identify all characteristics in thin sections and name these associations as

petrofacies on a more micro-scale as compared to their meso- and macro-equivalents, such as lithofacies and seismic facies (Gonzalez-Acebron et al., 2017)

Seismic facies analysis is a branch in sequence stratigraphy that also plays an essential role during the reconstruction of the depositional environments, especially at observing basin formation at a larger scale and predicting the location of petroleum systems (Veeken, 2013). Vail (1987) provided a detailed description on how sequence stratigraphic analytical techniques, including seismic facies, could be performed with relation to seismic amplitude, reflection geometry (configuration), reflection continuity and the wavelet frequency of seismic profiles. These reflection relationships can be used to evaluate relative sea-level fluctuations and their influence on the depositional environment within depositional systems tracts. Miall (1986) related these relative sea-level changes to the sequence stratigraphic concept where seismic facies distributions relate to global changes in sea level with relation to unconformities and systems tracts. Facies mapping can also be related to particular depositional processes and hence certain paleo-environments to reservoir distribution where drilling is scarce but seismic data are abundant, especially within deep-sea basins (De Ruig & Hubbard, 2006; Johansen, 2013). This method is essential for characterizing the distribution of reservoir intervals. Sequence stratigraphic techniques have become an important segment in petroleum exploration where many authors attempt to characterize the reservoir distribution with its associated depositional environments (Alves et al., 2003; Johansen, 2013). The sequence stratigraphic concept can also be used to define a particular or combination of several possible depositional pathways from the source area (provenance) to the depositional environment (direction of sediment supply). The identification of seismic facies yield important information regarding the source inputs into the basin and upon careful consideration can give clues as to the possible source rock lithology compared to the regional geological setting (Zhu et al., 2014).

The evaluation of wireline logs can also be used to identify the depositional energy based on the shapes of geophysical wireline logs (Rider, 1986). The integration of geophysical well log and core data (including petrography) are calibrated with seismic facies to produce an overall picture of the depositional environments. Thus, characterizing the depositional environment on a micro- and meso-scale with petrographic and core analysis as well as on a macro-scale using seismic sections (Prather et al., 1998).

Analysis of the provenance is usually carried out by sedimentologists to identify the source area and nature of the parent rocks of the sediments. The analysis involves the location, size, lithology, tectonic setting and in some cases the climate or relief of an ancient terrain (Dickinson & Rich, 1972; Crook, 1974). The study of provenance began in the late 1800's, where the provenance of sedimentary rocks dealt mostly on the lithology of source rocks. A provenance study is an important tool for the modern petroleum industry and for academic research interests. The overall composition of the sediments or bulk sediments is largely controlled by their source areas with further compositional variations occurring during transport, deposition and diagenesis (von Eynatten & Gaup, 1999; Kutterolf et al., 2008).

The interpretation of seismic facies and lithofacies are crucial initial techniques due to fundamental information being identified that can lead to the identification of the source directions as possible paleoflows of drainage systems (Lowe et al., 2011; Zhu et al., 2014; Benyon et al., 2016). The determination of the possible direction of the source of sediment is the first step in a provenance study (Boggs, 2009). There are several ways to approach a provenance study and thus includes geochemical, petrographic, magnetic and geochronological approaches.

In terms of the general petrographic method, petrographic discriminant diagrams can be used to define the provenance of a study area. The relative abundance of certain framework minerals (monocrystalline and polycrystalline quartz, feldspars and lithic grains) are used to obtain information on the provenance signature (Dickinson & Suczek, 1979; Ingersoll & Suczek, 1979; Dickinson et al., 1983; Dickinson, 1985; Zuffa, 1985). This method can easily describe the lithology of singular source areas with its provenance signature. This has formed the basis for most petrographic provenance studies throughout the years (Soreghan & Soreghan, 2013). A problem arises with the introduction of two or several source terrains with its own provenance signatures mixing in temporal and spatially dynamic settings within a specific hydrodynamic regime (Velbel, 1985).

Other traditional methods that can also further enhance the provenance signature is to evaluate the characteristics of individual minerals, like the extinction characteristics of quartz to identify the lithology of the source rock (Basu et al., 1975). The abundance or detrital modes of quartz, feldspar and lithic grains are usually counted and plotted on a ternary diagram ('Dickinson ternary plots'). Although this method is not as reliable as more modern methods. von Eynatten et

al. (2003), von Eynatten (2004) and Weltje (2006) introduced a statistical methodology to associate a provenance with detrital grains and to reevaluate the traditional 'Dickinson ternary plots', to yield more reliable results on a more semi-quantitative approach. These modified techniques rely on compositional data analysis (Aitchison, 1982) and are used to explain the provenance more rigorously. The statistical treatment of the data will be done in this study to yield a semi-quantitative approach to provenance. Thus, also keeping in mind the significance of overlapping provenance signatures from sandstone compositions. Therefore, the use of two or more methods can alleviate the significance of overlapping provenance signals (Heller & Frost, 1988; Dallmeyer & Neubauer, 1991; von Eynatten et al., 2003; Kutterolf et al., 2008).

Although these relative mineral abundances are good indicators of provenance, one has to take into account the physical and chemical effects on sediments during weathering, deposition (including transport) and diagenesis (burial). Thus, the use of heavy mineral analysis is considered as one of the most successful and common methods in determining the provenance of sediments and sediment pathways because of their durability (Zack et al., 2004; Ratcliffe et al., 2007; De Barros et al., 2010). Some heavy minerals are easily affected by physical weathering, chemical weathering and diagenesis. The exempted minerals such as garnet, zircon, rutile, chrome spinel (first cycle sedimentation) and apatite are highly resistant to any physical or chemical effects during transport (transport invariance), making it good indicators for provenance studies (Boggs, 2009). The use of these heavy minerals as ratios relative to each other can strongly increase the reliability of these minerals as provenance indicators (Morton & Hallsworth, 1994).

The geochemical approach involves the bulk rock and single grain (heavy mineral or basic mineral) chemistry of rocks. Geochemical analysis has become the basic approach to modern day provenance studies since geochemical analytical techniques improved, like the ICP-MS obtaining trace and REE element concentrations to parts per trillion (ppt) levels. This high-resolution data significantly improves the identification of the geodynamical setting of depositional basins (Crook, 1974; Bhatia, 1983; Roser & Korsch, 1988; McLennan et al., 1993; Belousova et al., 2002; Hoskin & Schaltegger, 2003; Macdonald et al., 2006; Morton & Chenery, 2009; De Barros et al., 2010).

The bulk-rock geochemistry of sediments, especially the stable elements, during diagenesis or metamorphism, is good indicators for provenance studies (McLennan et al., 1993; Ratcliffe et al., 2007). Middleton (1960) was the first to use discriminant diagrams to identify tectonic settings for provenance studies using K_2O/Na_2O ratios. Bhatia (1983) refined the work of Middleton (1960) to include several major elements to refine the provenance in detail. These authors define the tectonic setting of the rocks in a broad context and several problems can be encountered, similar to the petrographic method, such as the complex history for the compositional variation with temporal and spatial changes (Weltje & von Eynatten, 2004). These methods forms the most basic approaches to provenance but more sophisticated or refined methods can yield more detailed or high resolution results, such as the use of trace element chemistry to delineate the tectonic setting (von Eynatten et al., 2003).

Single grain analysis has also become a crucial and modern high-resolution technique for evaluating the provenance of sediments. Heavy minerals are especially used for this method such as rutile geochemistry and zircon geochemistry, which yielded good indicators for provenance (De Barros et al., 2010). Zircon geochronology and heavy mineral analysis, together, are also used to identify the exact location of the source or sources of sediments with associated drainages that can yield accurate results for the identification of sediment pathways (Hallsworth et al., 2000; Thomas, 2011; Benyon et al., 2016). Although zircon geochronology is considered the most appropriate method to use for provenance, drawbacks do occur such as the size of zircons as well as the underlying uncertainty of the analytical instrument (statistical methodology) (Basu, 2017). A further setback in single-grain provenance analysis is that these minerals are restricted to certain source rocks and can only provide part of the picture for that particular mineral grain.

The use of certain methods in obtaining the provenance of sediments has its advantages and disadvantages (Weltje & von Eynatten, 2004). The integration of petrographic and geochemical techniques is crucial to delineating the provenance and depositional environment, because even though they usually complement each other, one can contain important information that the other one may have overlooked (Briggs et al., 2004). This is especially useful when dealing with complex sedimentary basins (Kutterolf et al., 2008). Mader and Neubauer (2004) integrated petrographic and geochemical methods to establish a provenance of sandstones that yielded

results that are more accurate. This integration is important in terms of extracting information that compliments each other or unveiling other underlying factors involved (Etemad-Saeed et al., 2011). The integration of seismic data with these methods can yield further promising results for identifying the provenance and the depositional environment. A recent study by Zhu et al. (2014) revealed an interesting approach to identifying the provenance and depositional environment with the aid of 2D and 3D seismic data of a rift basin.

This study is especially important in environments where complex fault systems occur and integration of methods are crucial. The Bredasdorp sub-basin is such a complex transform rift system where identifying the depositional environment and provenance becomes rather complicated. Thus, an integrated approach is crucial in identifying the tributary and distributary network during an active tectonic regime. There has been a provenance study in the southern part of the Bredasdorp sub-basin (Fadipe, 2012). This study dealt with the geochemical provenance; therefore, to assess the accuracy of that geochemical study an integrated approach was performed and highlight the implications to provenance identification and on reservoir quality and distribution.

CHAPTER 2

REGIONAL GEOLOGICAL BACKGROUND

2.1 Geological setting

2.1.1 Tectono-stratigraphic and structural setting

The Bredasdorp sub-basin is one of five sub-basins that form part of the larger Outeniqua Basin. These sub-basins, which include the Pletmos, Gamtoos, Algoa and southern Outeniqua sub-basins have similar basin evolutionary characteristics. The Bredasdorp sub-basin is bounded by two crustal scale discontinuities that are located and known in the western part of the southern coast as the Columbine-Agulhas Arc and in the east by the Infanta Arch. The latter separates the Pletmos sub-basin from the Bredasdorp sub-basin (Figure 1.3.1).

2.1.2 Tectonic setting

The Bredasdorp sub-basin's tectonic evolution can be divided into the three general tectonic stages viz; pre-rift, syn-rift and post-rift/drift stages (Figure 2.1.1). The breakup of Gondwana during the late Jurassic to early Cretaceous initiated a dextral strike-slip transform boundary (NE-SW trending), which formed in the southern part of the Bredasdorp sub-basin (McMillan et al., 1997). This large-scale fracture system (known as the Agulhas-Falkland Fracture Zone) was initiated due to the more susceptibly weaker nature of the host rocks of the Cape Fold Belt, with the Tristan De Cunha plume and the Bouvet hot spot being the origin (Watkeys, 2006; Hoyer & Watkeys, 2017). Tectonic elements such as horsts and grabens or normal faulting created in this extensional stress regime was formed during the early stages of rifting (syn-rift), with possible reactivation of faults in the compressional Cape Fold Belt (Davies, 1997). The separation of South America from the Falkland Islands and South Africa (Africa), created major en-echelon faults that initiated the formation of the Outeniqua Basin (separated by individual horsts and grabens in the later stage forming the Bredasdorp, Pletmos, Gamtoos and Algoa sub-basins). This regional sequence stratigraphic framework, based on seismic lines and a biostratigraphic study in the Bredasdorp sub-basin, indicates that the regional unconformities does not follow a particular trend to other sub-basins due to the complex tectonic histories of the basin (McMillan, 2003). This complexity or structural complexity has led to the occurrence of the syn-rift I, syn-rift II sequences and post-rift sequences with their associated uplifted and erosional events.

Furthermore, regional sequence stratigraphy during the early-rifted settings would prove to be problematic because of the occurrence of an unstable platform.

2.1.2.1 Pre-rift geology

The Namaqua-Natal metamorphic provinces are the oldest terrains in the southern part of South Africa. These folded terrains consist largely of the Cape Supergroup and Pre-Cape Supergroup sediments. According to McMillan et al., (1997), based on general assumption and proximity to the basement highs, the basin's sediments were derived from the erosion of the Cape Supergroup's orthoquartzites and Karoo Supergroup's sandstone/shales. The Cape Supergroup sediments consist mainly of shallow marine, transitional and deep-sea environment sequences. During the Cape orogeny (Pre-Gondwana landmasses), the Cape Supergroup was largely folded to form the cape fold belt which extended in the offshore and onshore regions of southern Africa (Halbich et al., 1983). The Karoo Supergroup was deposited in a retroarc foreland basin as subduction and erosion commenced (Dingle & Hendry, 1984; Katemaunzanga & Gunter, 2009). The Karoo Supergroup was dominated by glacial, alluvial, marine and deltaic sediments from the late Carboniferous to the early Jurassic periods (Smith, 1990a; Smith, 1990b). It was also believed that the Cape Supergroup has undergone burial metamorphism initially, before the folding event, where thick sequences of the Karoo Supergroup was deposited on top to be eroded at a later stage (De Swardt & Roswell, 1974). After this event, the eastern of Gondwana started showing signs of rifting in the late Jurassic, as the syn-rift's half grabens became evident (McMillan, 2010).

2.1.2.2 Syn-rift stage

The syn-rift stage can be divided into two stages, due to the complex transform fault dynamics, namely the syn-rift I and syn-rift II stages (Jungslager, 1999; Broad et al., 2006). The syn-rift I initial stage (D-1AT1 unconformities) formed possibly in the middle-late Jurassic to early Cretaceous periods. There have been boreholes that intersected rocks of the middle-late Jurassic periods (McMillan et al., 1997). This initial period consisted of claystones, conglomerates and sandstones, which was evident that fluvial environments dominated. This was capped by the occurrence of the first marine intrusion into the basin hosting glauconitic sandstones (Figure 2.1.1). The occurrence of a fluvial environment again became evident followed by another shallow marine glauconitic sandstone due to local tectonics and eustatic sea level changes (Broad et al., 2006). The second syn-rift stage (1AT1-6AT1) consisted of deep-water successions, which

was evident of basin subsidence and the onset of the postrift/drift successions (Broad et al., 2006).

2.1.2.3 Transitional stage

The transitional stage was governed by lowstand (turbidites) and highstand (organic-rich shale) system tracts that were influenced by tectonic instability and eustatic sea-level changes (Broad et al., 2006). These sea level changes can be tracked on a global and local scale due to a number of reasons ranging from first order to fourth order cycles (Brown, 1995).

2.1.2.4 Drift stage (14AT1 and 15AT1 unconformities)

The drift stage started in the middle Albian where it is marked by the clearing of the Falkland plateau from the Columbine-Agulhas arch in the southwest triggering thermal subsidence (Broad et al., 2006). This thermal subsidence led to an overall sea level rise, which was further enhanced by the eustatic sea level rise (1st order). During the Tertiary period (Paleocene age) major uplift occurred and marked the last of the phases of regression (Figure 2.1.1).

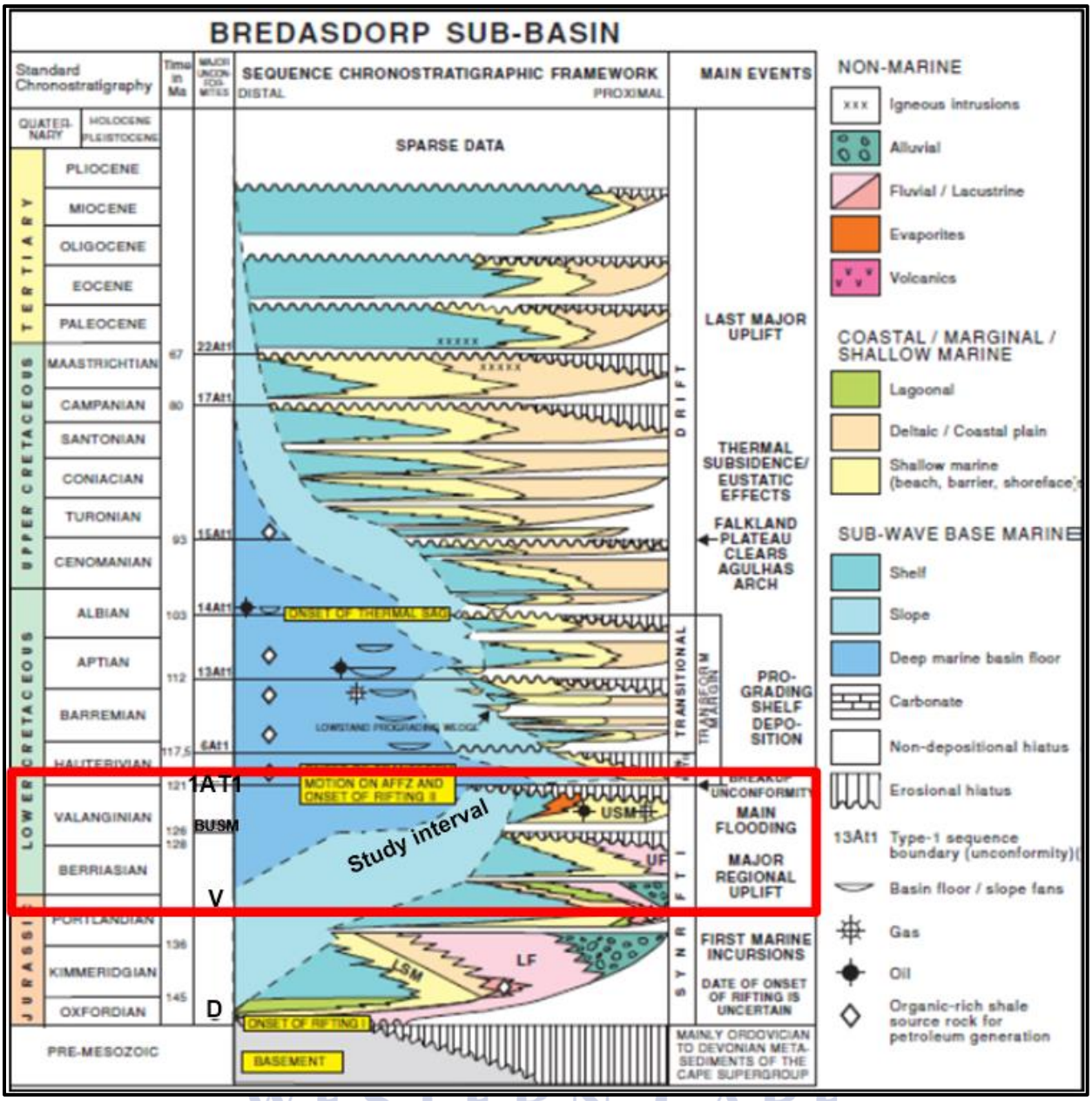

Figure 2.1.1: Sequence stratigraphic framework of the Bredasdorp sub-basin showing major regional unconformities and sedimentary environments. Modified after Broad et al., (2012) with the study interval of this project

2.2 Depositional setting

2.2.1 Middle Jurassic (possibly Oxfordian age) to late Valanginian age

The initial graben fill succession consisted mostly of basal conglomerates, fluvial and alluvial successions (Figure 2.1.1). According to McMillan (1997), the sedimentation rates during this period were largely controlled by differential subsidence (local tectonics). The dominant

environments were of fluvial (possibly braided rivers) and alluvial fan deposits consisting of sandstones interbedded with red/green claystones. McMillan (1997) suggested that an arid climate existed because of evidence of oxidation due to the colours of rocks and caliches observed but this could also have been attributed to sub-basin specific changes. The event was followed by a fossiliferous shelly glauconitic sandstone unit that was identified as beach deposits (McMillan, 2003; Broad et al., 2012). These glauconitic sandstones were interpreted as tidally influenced units of the lower shallow marine deposits (McMillan, 1997). A second fluvial environment was identified as alluvial floodplain and meandering river deposits (McMillan, 1997; Broad et al., 2012). These deposits contained sandstones, red/green claystones and siltstones with no evidence of glauconite (McMillan, 1997). The last or upper shallow marine unit consisted of transgressive sandstones that were possible beach deposits. A cyclical normal regressive phase followed with progradational sets as its dominant stratal arrangement. These successions occurred between the D and 1AT1 unconformities (Figure 2.1.1).

2.2.2 Late Valanginian to early Aptian age

The late Valanginian age showed active erosion or a cease in sedimentation, especially in the northern part of the basin, whereas the southern part showed turbidite systems that were fed by submarine canyons (Brown, 1995). During the early Barremian stage, river-dominated deltaic and prograding shelf deposition occurred possibly due to the combined effects of local tectonics and eustacy (Brown et al., 1995; Broad et al., 2012). Variable changes in sedimentation occurred throughout the basin with turbidity currents dominating during deep marine conditions. These changes are thought to be the result of active fault tectonics through reactivation of fault blocks (McMillan, 1997). There is also evidence of large canyons that provided sediments to deeper parts of the basin. Towards the early Aptian age, turbidite systems dominated the easterly part (towards the Infanta embayment) of the basin as the drifting stage was approached (Brown et al., 1995).

2.2.3 Late Aptian to present

Evidence of submarine canyons persisted during the late Aptian with mass flow deposits and turbidite systems dominating. Ocean floor conditions fluctuated tremendously during these times from oxygen-rich to oxygen-poor conditions (Brown, 1995). During the Turonian to early Coniacian stages (late Cretaceous), progradational sets commenced with local tectonics still

being the driving force for this change. From the Tertiary times, highstand shelf deposition involved mainly clay deposition and minor sandstones during a shallow marine environment (Brown et al., 1995).

CHAPTER 3

METHODOLOGY

Flow chart on the methodology adopted in this study

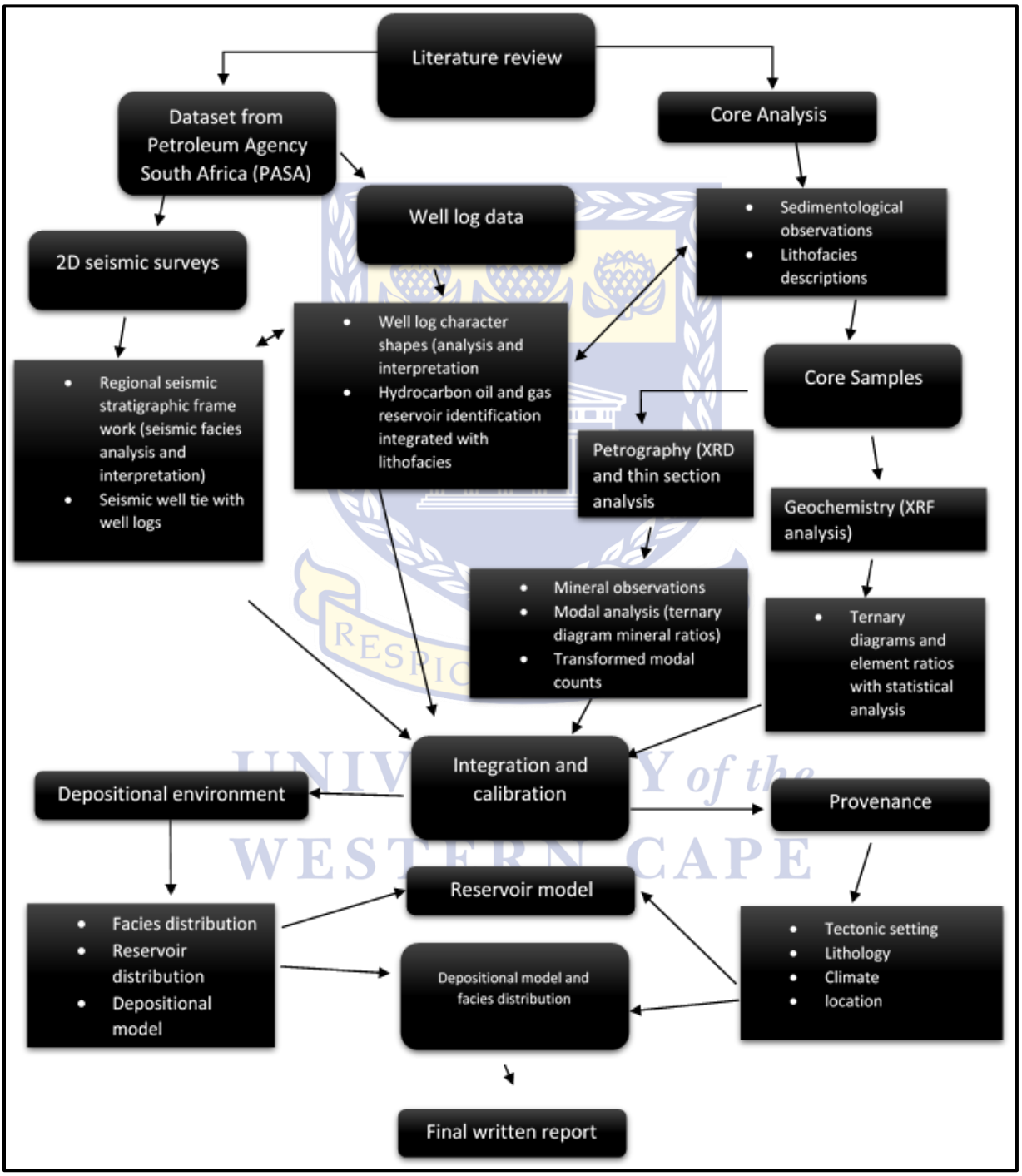

3.1 Seismic facies

3.1.1 Synthetic seismogram and mistie analysis (processing)

The use of 2D data becomes problematic, especially if regional studies are to be undertaken. Initially, the correlation of the 2D seismic lines are to be worked out in order to perform any analysis involving a group of seismic data in the absence of 3D seismic data. The 2D seismic data has been taken during different times or individually and with different equipment (different companies), therefore an offset exists with overlapping 2D seismic lines. A mistie analysis is performed to correct for this offset by applying a correlation that involves all the seismic lines and referenced fixed lines (usually the lines intersecting the wells) and are adjusted accordingly.

A synthetic seismogram can then be generated to represent accurately a correlation between the seismic data and the well data. The synthetic seismogram is created through the convolution process. During the interpretation stage, correlation with the logs and a well-to-seismic tie is attempted using a synthetic seismogram (Onajite, 2013). The sonic log is used to acquire the acoustic impedances and the density formation log is used to acquire the density of the formation. During the convolution process, the earth's reflection series (reflection coefficient) is convolved with a seismic wavelet (minimum-phase and zero phase wavelets) to produce a synthetic seismic trace (Onajite, 2013). This process can occur either theoretically (computed software) or practically by using the seismic trace from the wellbore data in correlation with reservoir zones to produce seismic wavelets. A general precursor wavelet should be used as a baseline and consists of various forms such as the Ricker wavelet, Ormsby wavelet, Stevison-Levison and the Klauder wavelet. A zero phase Ricker wavelet usually represents a frequency of 30 Hz, which is considered as the general frequency for seismic interpretations to be performed (Dey & Lines, 1998). This Ricker wavelet is being used in the present study as it represents the general criteria for offshore basins along the southern offshore coast (extracted from several unpublished well completion reports). Dey & Lines (1998) found that the Ricker wavelet and the Klauder wavelet is almost identical with minor offsets with response to Ziolkowski et al. (1998)'s interpretation on deconvolution.

3.1.2 Seismic characteristics

In the present work, seismic facies was interpreted using the Petrel™ software package based upon seismic reflection characteristics. Reflection terminations were identified first, followed by

the general criteria of identification of seismic facies. The general criteria consist of identifying the reflection configuration, reflection continuity, reflection amplitude and wavelet frequency. The external form and direction of sediment input from source to basin was considered based on 2D dip- and strike-orientated seismic lines. The occurrence of large incised valleys or clinoforms (deltaic clinoform scale) can be used to assess the direction of sediment supply on a regional scale for possible sediment pathways (methodology outlined in Zhu et al., 2014). The seismic lines were specifically chosen for their intersection of the wells and the regional seismic lines (inline and crosslines) were chosen to cover most of the sub-basin especially the landward edge of the sub-basin and local depocenters (Figure 3.1.1).

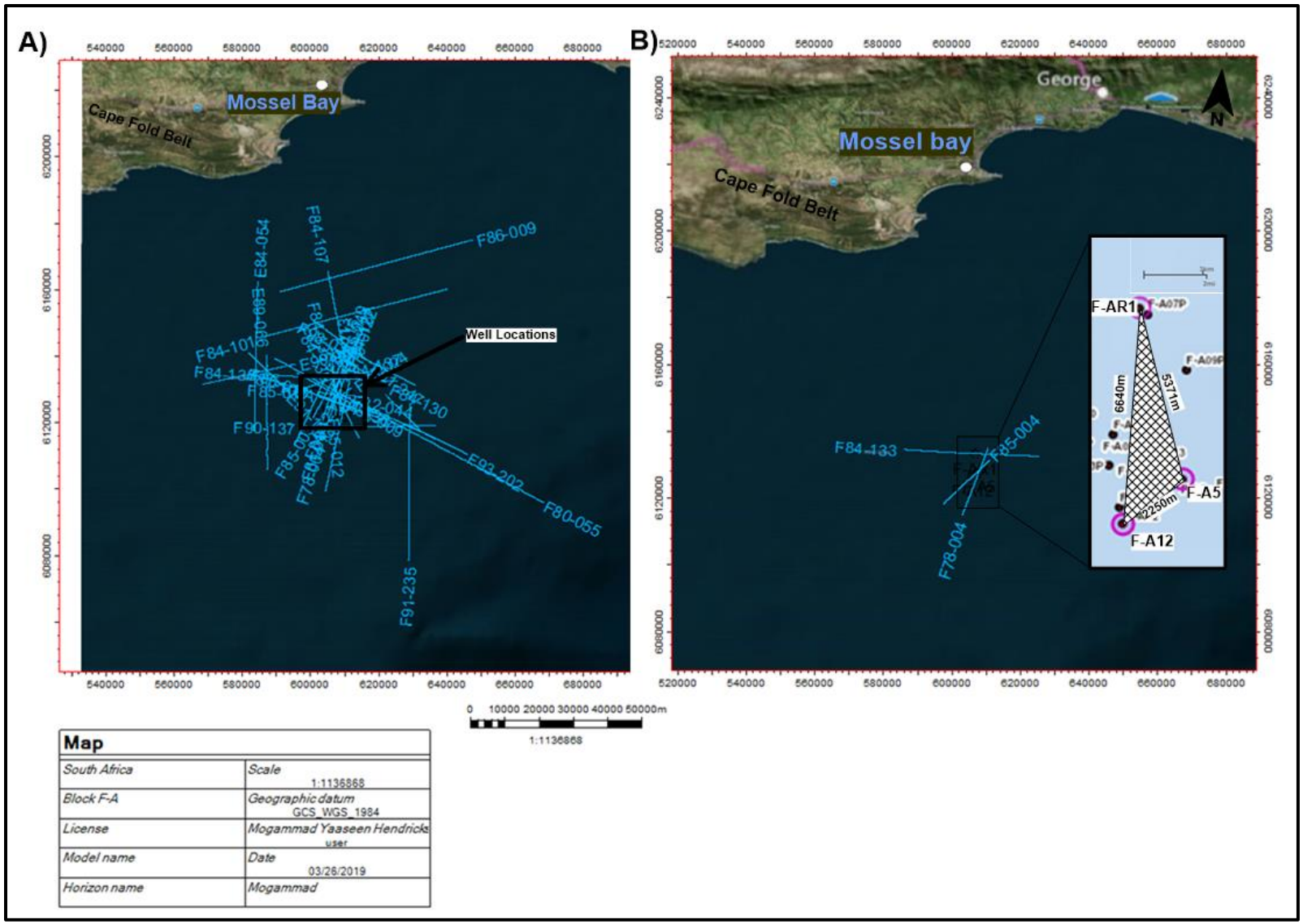

Figure 3.1.1: 2D seismic lines and well locations used in this study (A). Also shown are the represented 2D lines with well intersections and relative distances.

3.2 Depositional environment and reservoir potential from geophysical logs

3.2.1 Gamma Ray log

The Gamma-ray log measures the total natural radioactivity in rocks where an array of receivers designed to measure radioactivity is attached to a wireline or steel cable and records the different radiation wavelengths (Gluyas & Swarbrick, 2013). The main radioactive elements that accounts for the variation in these rocks are Potassium (K), Uranium (U) and Thorium (Th).

A response on the gamma ray log, to either the right or left (deflections) is encountered when a change in depositional energy occurs (from a base line). A deflection to the left indicates a permeable lithology, with an increase in depositional energy (sandstone or limestone), and a deflection to the right indicates a less permeable lithology, with a decrease in depositional energy (shale) which can be related to the depositional environments and hence sequence stratigraphic surfaces (Selley, 2014; Rider, 1986).

A cylindrical shape with a sharp top and base represents mostly aggradational environments such as braided fluvial, aeolian, channel-fills etc. (Figure 3.2.1) (Rider, 1986). A funnel shape or coarsening upwards pattern represents prograding environments such as crevasse splays, river mouth bars and delta fronts etc. (Figure 3.2.1) (Rider, 1986). A bell shape or fining-upward pattern represents channel deposits such as tidal flats, fluvial and tidal point bars and deep tidal channel-fill (Figure 3.2.1) (Rider, 1986). A symmetrical shape represents prograding and retrograding environments such as regressive to shoreface deltas being overlain by estuarine systems (Figure 3.2.1). A serrated shape represents aggrading environments such as flood plains, deep marine slopes and storm-dominated shelves.

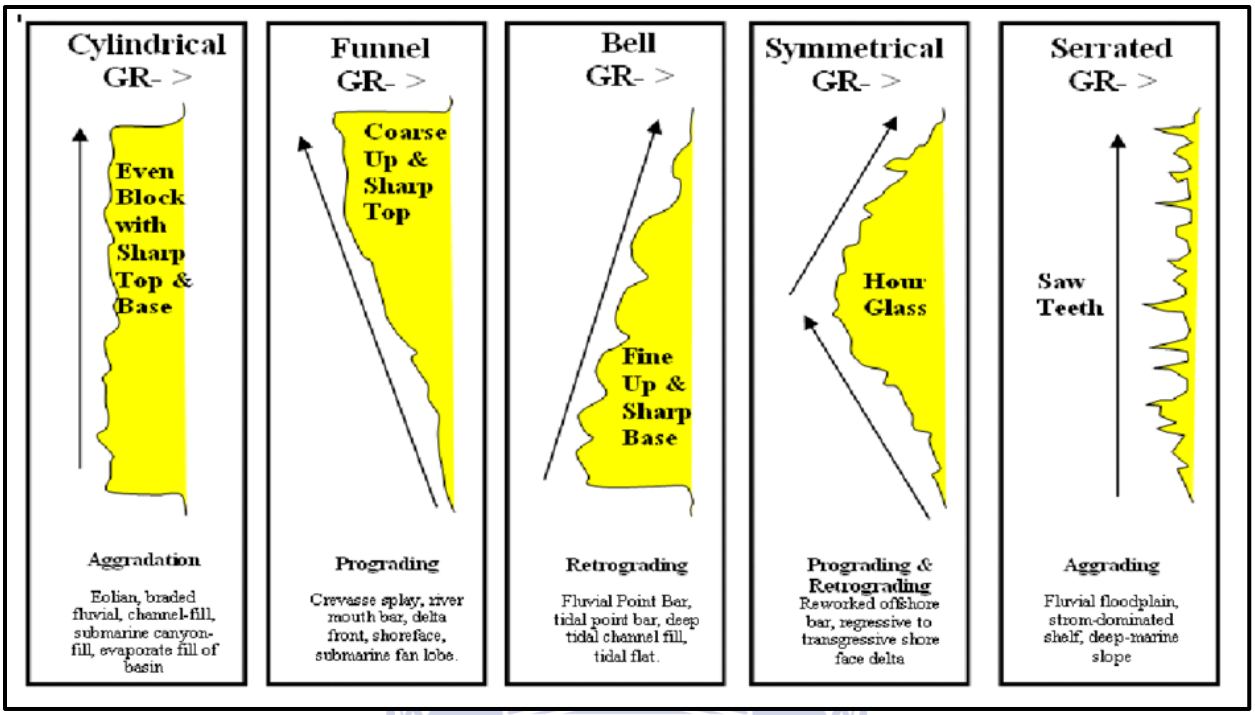

Figure 3.2.1: Sedimentary environments defined by gamma ray log shapes, after Futalan et al. (2012)

3.2.2 Neutron-density log

The neutron-density logs are known for measuring the porosity of rock formations. The neutron log tool measures gamma rays but induces or bombards a rock formation with neutrons causing the rock to emit gamma rays in proportion to their hydrogen content (Selley, 2014). The hydrogen atom concentration is recorded which relates to hydrogen occurring in the fluid phases. The formation density tool measures the electron density of a formation where gamma rays are emitted into the formation and interacts with the electrons. These gamma rays are scattered in the formations and the bulk density can be determined. A crossover between the two logs represents possible hydrocarbons or water saturated zones in pores (Rider, 1986).

3.2.3 Sonic log

The sonic tool measures the time taken for a sound pulse to travel from a source to the receiver through the formation. The transit time in low porosity layers is short and in porous layers the transit time is longer (Rider, 1986). The sonic log is also used for the calibration with seismic data to create well-to-seismic ties where acoustic impedances can be calculated and produce a synthetic seismic trace.

3.2.4 Resistivity logs

The resistivity logs measures the resistivity or conductivity of formations. There are three types of resistivity logs, namely: those that measure the deep, medium and shallow resistance with relative penetration of the formations (horizontal readings). The medium resistivity measures possible intrusions of drilling fluid in the middle section of a logged borehole. The shallow and deep resistivity logs measures the electric resistivity for the formation at shallow and deep intervals of the formation. The resistivity logs are used to differentiate between hydrocarbons and water saturated areas. Hydrocarbons usually show high resistivity values as compared to water zones that show a low resistivity, therefore increasing conductivity (Rider, 1986).

3.2.5 Correlation

The well log correlation was performed based upon the well tops or regional unconformities of South African basins. These well tops were received from the Petroleum Agency South Africa (PASA) for each well. The main regional second-order sequence is bounded by 1AT1 and D unconformities, which range through the lower Cretaceous period. This regional correlation was used to constrain the main features of the wells. In addition, whenever the wells are being compared, it is attributed to the lateral and updip variations that occur. The wells used in the correlation are displayed in measured depth and are not inclined (vertical wells).

3.3 Facies analysis

Core descriptions

In order to obtain a correlation, the core depths had to be shifted with the GR depths. F-A12 and F-A5 needed to be shifted in order for the core depth to be correlated with the gamma ray log. The correlation was done according the main fining upward units within the wells, as well as the shale or finer grained sediments of the core to match the increased gamma ray response of the log. This process can easily be performed on the EasyCore software for matching. Regional correlations for the major unconformities were based on unpublished reports of micropalaeontological and seismic data for the 1AT1-V horizon in which the core of F-A12 consisted of 120m, F-AR1 around 50m and F-A5 around 55m of continuous cores. The well F-A12 and F-A5 cores were extensive and mostly covered the entire 1AT1-V horizon with F-AR1 only covering the upper parts of the sequence.

Facies descriptive analysis were based on the occurrence of sedimentary structures, grain size, bioturbation index (abundance according to Taylor & Goldring (1993)), rock colour, trace fossil identification and characteristics (diversity of species) and bed thickness (including upper and lower bed contacts). F-AR1 facies characteristics had to be based upon the visible sedimentary structures and evidence of trace fossils. The core has been logged at a 1:10 scale to provide a robust study with limited wells.

Reservoir characteristics obtained from the core was solely based on petrographic thin sections and geophysical log signatures with descriptions based on poor or good reservoir quality of the sandstones, siltstone and claystones (or mudstones). Micro-facies was partly recognized (Appendix B) within samples taken, but due to the vast number of cores and facies, certain samples were better chosen according to reservoir quality from the obtained geophysical logs.

3.4 Petrography

3.4.1 Mineralogy (general mineral descriptions)

Forty-three selected core samples were studied in detail for petrographic analysis. All the samples were collected along three vertical borehole sections (Appendix A, Sedimentary logs). These samples were siliciclastic lithologies and consisted of sandstones, mudstones, siltstones and claystones. The mean grain size (Wentworth, 1922; Folk, 1980), roundness (Powers, 1953) and sorting (Pettijohn et al., 1972) was estimated (visual estimation) using the standard grain size chart. All minerals identified through the microscope were based on the optical properties of the minerals and no staining was performed.

There were no XRD analysis performed on the F-A12 and F-A5 wells, but the analysis was performed on the F-AR1 well, therefore the clay mineral analysis and identification is restricted to visual estimation for the two wells F-A12 and F-A5 only. Clay diagenesis therefore was a minor part of this study but was summarized briefly.

The framework components will be identified and consist of monocrystalline quartz, polycrystalline quartz, K-feldspar, plagioclase feldspar, lithic rock fragments, possible heavy minerals, micas (focusing on biotite and muscovite) and any clays found within the petrographic view. Authigenic components will also be identified such as kaolinite, anatase, and dolomite.

The occurrence of specific grains and their characteristics are also a criterion used to evaluate the provenance. The textural properties of quartz, feldspars, lithic fragments and heavy minerals with their petrographic characteristics can be used to delineate the provenance area. The role of quartz, with its distinctive features can indicate possible source rock lithologies. The relative abundances of the feldspars are also largely indicative of the source area, with inference of the climatic conditions as well. Lithic fragments are also crucial to the understanding of the source area since this becomes direct evidence for their source rock equivalents.

The occurrence of sedimentary lithic fragments such as siltstones, claystones and even the unstable sandstone clasts can indicate a sedimentary source (not including intrabasinal clasts). Igneous rock fragments such as volcanic rock fragments (with olivine, feldspars, pyroxenes etc.) indicate an igneous source.

The occurrence of slate, phyllite, schist and quartzite fragments can all indicate a metamorphic provenance. This is largely dependent on the arrangement or alignment of grains such as muscovite, chlorite and altered feldspars that generally is indicative of a low-rank metamorphic provenance (Rank 1 to rank 3) (Garzanti et al., 2003). The occurrence of schist rock fragments, gneissic rock fragments, muscovite, biotite, chlorite and sheared metaquartzites assemblages are all indicative of middle- to high-rank metamorphic provenances.

3.4.2 Modal analysis

Modal analysis was carried out for twenty-one samples with the coarser grained fraction greater than 63µm grain sizes (sandstones and minor silty sandstones). For every thin section analyzed in the modal analysis work, 300 points were counted using the traditional method of Dickinson and Suczek (1979), Dickinson et al. (1983) and Ingersoll et al., (1984). Sample criteria that have been excluded for this analysis were mostly based on grain sizes less than 63µm and for severely altered samples based on carbonate cements.

The minerals that will be crucial for the study will consist of quartz, feldspars and rock fragments. Quartz will be divided into monocrystalline quartz (separated according to a 5° maximum and minimum angle) and polycrystalline quartz (separated by the amount of crystal units present). The feldspars will be divided into K-feldspar (potassium feldspar) and plagioclase feldspar (with possible albite). Rock fragments will be divided into chert, volcanic rock

fragments/plutonic, claystone/siltstone (and its metapelitic equivalents) fragments and sandstone fragments.

The analyzed samples were plotted on traditional QtFL, QmFLt, QpLvmLsm, QpQmuQmn ternary plots (Basu et al., 1975; Dickinson and Suczek, 1979; Dickinson et al., 1983; Ingersoll et al., 1984; Arribas et al., 1985) as well as their counterparts that are modified in compositional space (Weltje, 2006). Detrital grains counted were according to Dickinson et al. (1983) and Ingersoll et al. (1984)'s recalculated assemblages of the Gazzi-Dickinson method, and excluded cements and matrix (including glauconite, opaque, chlorite, heavy minerals and carbonate grains or fragments). The excluded minerals were not plotted as part of the 300 points but counts were made when these minerals intersected the grid point.

Dickinson & Suczek (1979), developed ternary diagrams that is well established among many authors where tectonic setting of the provenance area can be identified. With any method, there is always a level of uncertainty and the qualitative descriptions should be transformed into more quantitative means. It is also well understood that the effects of selective transport, mixing in the source area and enrichment or depletion of grains are factors that changes the compositional variability from the source area to the sink (Weltje, 2006). In addition, the modal analysis was evaluated using an alr (additive log ratio) transformation of QFL ternary plots (Weltje 2002; Weltje, 2006). Therefore, the use of log-transformations in statistical analysis has proven itself very useful where compositional data has been quantified (Weltje, 1994; von Eynatten et al., 2003; Weltje, 2006).

3.5 Geochemistry

Thirty samples were selected for geochemical analysis with major elements determined by X-Ray Fluorescence Spectrometry (XRF) analysis and the trace elements determined by the Inductively Coupled Plasma Mass Spectrometer (ICP-MS). Among the thirty samples, twenty-three samples consisted of a coarse-grained fraction (sandstones and brecciated burrowed unit and the remaining seven samples consisted of a fine-grained fraction (siltstones, mudstones and claystones). All samples were collected from three petroleum exploration wells namely F-AR1, F-A12 and F-A5 of the Bredasdorp sub-basin (Figure 3.1.1).

The geochemical bulk-rock analysis was carried out at Stellenbosch University, South Africa using the Central Analytical Facilities (CAF). Major element chemistry was determined using the Panalytical Axios WDXRF spectrometer machine (detection limits of 0.05ppm) with polished mounts of XRF fusions. Loss on Ignition (LOI) were calculated by heating a sample at a 1000° Celsius, allowing volatiles to escape until the mass ceases to change and the difference (in weight) is calculated afterwards. The trace elements were determined using the Resolution M-50-LR Excimer laser ablation system with the Argilent 7700 ICP-MS.

The average chemical components were compared to Post-Archean Average Shale (PAAS), North American Shale Composite (NASC) and Upper Continental Crust normalization values (UCC) (Appendix C). The comparison was to evaluate whether the source rock had basic rock features or not (Hu et al., 2014). This deviation of values will help to identify vital information regarding the enrichment and depletion of certain elements.

In order to identify the provenance, certain aspects had to be addressed that affects the geochemistry of the source. Pe-Piper et al. (2008) used a systematic approach, modified from various studies and the approach of McLennan et al. (1993), to evaluate the effect of weathering and diagenesis, the effects on grain size and sorting on element variation, which correlated with petrographic techniques performed. The maturity can also be assessed using the SiO_2/Al_2O_3 ratio with a value greater than 5 indicating that a rock is chemically mature (Roser et al., 1996)

Plots of Al_2O_3 vs SiO_2, P_2O_5/Al_2O_3 vs CaO/Al_2O_3 and FeO_T/Al_2O_3 vs CaO/Al_2O_3 evaluates the major element variation and diagenetic cements to identify the samples that has undergone severe diagenesis. Samples that were severely affected by diagenesis were added (for comparison) and were accounted for when using major elemental chemistry.

The role of the depositional environment is also crucial to minimizing the error involved in evaluating provenance changes. Therefore, the separation of the coarse-grained fraction from the finer-grained fraction is crucial and the analysis should be carried out separately for each group of grain sizes to minimize the effects of the hydrodynamic changes (Roser & Korsch, 1985; Garcia et al., 1994)

The chemical index of alteration (CIA) and A-CN-K ternary diagram (Al_2O_3 (mol.) - Na_2O+CaO* (mol)-K_2O). With CaO* representing the CaO content in silicate minerals only,

corrected for the Calcium content in relation to carbonates and phosphates)-K_2O (mol.)) of Nesbitt & Young (1982), is used for evaluating the relationship of weathering and diagenesis and the possible character of the source. The CIA uses the molar proportions of oxides to obtain the losses and gains of mobile silicate bearing elements (CIA=100(Al_2O3/Al_2O_3+CaO*+Na_2O+K_2O) molar proportions). The CIA index evaluates the degree of chemical weathering, with a higher value producing more aluminous clays such as kaolinite-dominated mudstones within a tropical environmental setting (Nesbitt & Young, 1982). Although these diagrams are based majorly on the alteration or destruction of feldspars, certain care has to be taken in terms of evaluating the effects of CaO and Na2O within rock samples. For example, the Index of compositional variation (ICV) is used to mitigate the effects of residual diagenesis and takes into account the CaO content from all sources (Cox et al., 1995; Potter et al., 2005). The ICV (ICV= [($CaO+Na_2O+K_2O+Fe_2O_3+MgO+MnO+TiO_2$)/$Al_2O_3$)] uses the major oxide percentages to evaluate compositional changes with respect to these major oxides.

In addition, the CIA_{molar} has proved valuable in determining the paleoclimate for certain basins (Goldberg & Humayun, 2010). The CIA_{molar} can be calculated as calculating the proportion, in molar, between alkalis plus calcium and alumina (CIA_{molar}= $Al_2O_{3(molar)}$/$CaO^*_{(molar)}$ + $Na_2O_{(molar)}$ + $K_2O_{(molar)}$). Thus evaluating the degree of loss of these elements will correspond to humid or arid conditions. PIA, and CIW values has also been calculated which involves the alteration of plagioclase with silicate chemical alteration in general along weathering trends and can also be linked to weathering intensity. The PIA (PIA= [(Al_2O_3.K_2O)$_{molar}$/(Al_2O_3+ CaO*+Na_2O.K_2O)$_{molar}$).100]) monitors plagioclase weathering and provide additional support to the other indexes (Fedo et al., 1995; Fedo et al., 1996)). The CIW ((Al_2O_3/Al_2O_3+CaO+Na_2O).100) (Harnois, 1988) evaluates the degree of silicate weathering in general and correlates well with the other indices (Selvaraj & Chen, 2006). The use of ratios, such as he K/Rb or Rb/Sr ratios, can also give an indication of the degree of weathering that occurred.

Studies carried out by several researchers have shown that using major and trace element geochemistry of sandstones and mudstones reflects a provenance signature related to tectonic setting (eg. Bhatia &Crook 1986; Roser & Korsch, 1985; Cingolani et al., 2003; Briggs et al., 2004; Pe-Piper et al., 2008; Hofer et al., 2013; Verma & Armstrong-Altrin, 2013; Puy-Alquiza et

al., 2014; Castillo et al., 2015; Tawfik et al., 2017). Immobile trace elements have become useful for the inference of provenance and the determination of tectonic setting as well (McLennan et al., 1993). This immobility is particular useful due to the masking nature of sedimentary processes on provenance signatures.

There are also serious doubts as to whether the tectonic setting can be distinguished based on certain bulk-rock chemical elements because of the autocyclic and allocyclic factors involved in the formation of sedimentary rocks (Ryan & Williams, 2007; Pe-Piper et al., 2008; von Eynatten et al., 2003, von Eynatten & Dunkl, 2012). These factors include source-rock composition, lithology (depositional environment), tectonic setting, climate and relief. Therefore, single grain chemistry or statistical rigorous techniques should be applied to evaluate single grain provenance or provenance in general, in addition to the modifications involved within the depositional realm. Traditional diagrams (based on Bhatia, 1983; Bhatia & Crook, 1986; Roser & Korsch, 1985) have become common and should be treated with extreme caution. The problem with these traditional data is the fact that compositional data analysis has not been applied and certain characteristics of certain elements can almost certainly be affected by autocyclic and allocyclic controls (Weltje, 2006; Armstrong-Altrin, 2009; Caracciolo et al., 2012).

As a solution to this problem, Verma & Armstrong-Altrin (2013) has proposed new discriminant diagrams, based on compositional data analysis (ilr (isometric log ratio) and alr (additive log ratio) transformations), to evaluate tectonic settings using major element oxides. The new tectonic regimes are classified as ARC (active volcanism), RIFT (extension regime) and Col (collisional compression). The effects of lithology, climate or relief are minimized by dividing the sediments into high-silica (>63%) and low-silica siliciclastic sediments (<63%). This statistical discriminant technique has shown to be extremely reliable with success rates of >90% for tested samples. As noted by Verma & Armstrong-Altrin (2013), the effects of weathering, recycling (local), diagenesis and even analytical error can be minimized based on this new statistically rigorous technique.

3.6 Statistical analysis

Statistical analysis involved descriptive statistics, Principle Component Analysis (PCA), regression analysis, canonical discriminant function analysis and F-tests, which were performed to look at the relationship between elements, the relationship between samples (inter-sample

variability) and the relationship between samples and elements (intra-sample variability). The results of the F-tests (parametric test) has not been added but was just used as an initial test to evaluate the statistical significance of the variation within the normal data. The statistical significance was evaluated and deemed significant at a 95% confidence interval with p-values and f-values. In addition, PCA was performed on normal and transformed data, to evaluate the differences within the two datasets. Following the PCA, a discriminant function analysis was run to confirm the occurrence of special groups within the dataset and their relation to the provenance and facies classification that can be used in unknown parts of the sub-basin. These statistical techniques were performed on fine-grained and coarse-grained geochemical samples separately. The modal count data has also been transformed using the clr (centered log ratio) transformation and plotted on ternary compositional plots of Weltje (2006).

The general statistics are usually performed based on the assumption that the data is normally distributed (parametric) and assumes that variables are independent. This brings about the problem of the constant sum constraint (1 or 100) and non-negativity in terms of compositional geochemical data (100% for majors and ppm for trace elements). Aitchison (1982) introduced the concept of compositional data analysis or methods on approaching compositional data whereby the data is transformed from a D-part simplex (Sd) to real space. This D-part simplex, as defined by Aitchison (1982), only represents a part of the sample, not taking into account the constant sum problem. Trend analysis becomes spurious when using compositional data that is not normally distributed and constrained (Sd), since most parametric tests assumes normal distributions of the dataset. This transformation was usually based on centered log-ratio (clr) transformation (Aitchison, 1982), although there is other transformations (additive log ratio (alr) and isometric log ratios (ilr)), this transformation was common and was used with great success (von Eynatten, 2003; Hofer et al., 2013; Pe-Piper et al., 2008; Caracciolo et al., 2012). The clr transformation was done according to Aitchison (1982)'s method and was computed by:

$$y = ln(\frac{x}{g(x)})$$

Where x represents the elemental composition, g(x) the geometric mean of the element samples. This transforms the data from the simplex to the real space, escaping the constant-sum constraint.

The geochemical data is portrayed in this study as normal data (those 'closed' by 100) and transformed data (open).

The log-ratio transformations can be performed on petrographic modal data and geochemical data. For example, the quantitative re-evaluation of the Dickinson (1979) traditional diagrams made use of the concept of compositional data analysis and the calculation of rigorous statistical confidence regions has been applied to define the provenance and tectonic settings. These new confidence regions based on compositional trends has proven to show more accurate and reliable results (Weltje, 2006). The transformations can also be used to evaluate the degree of weathering within the source area (Weltje, 1994) as well as the modal petrographic classification.

Once the data has been transformed, it can be analyzed using multivariate statistical techniques. Principle Component Analysis (PCA) is the most recognized method in evaluating source to sink chemistry. This method employs a search criterion such as identifying orthogonal linear combinations as vectors to represent the variability or correlation among variables (Caracciolo et al., 2012). PCA can be performed on normal and transformed geochemical data. PCA is a statistical data reduction technique which can also be used as a visualization technique and display certain relationships between elements and samples. This visualization can be assessed using biplots that plots the variation or correlation of the principle components (based on Eigen-value decomposition or singular value decomposition). Principle components calculated through singular value decomposition has been used more effectively to represent the results of transformed data (Aitchison, 1982). Subcompositional trends can then be outlined for further analysis, with the elements showing the largest variability representing a subcomposition. Principle components are new variables with vector quantities (magnitude and direction) created on an axis that is rotated to represent the sample space. The number of components are based on the amount of variables with the first component containing most of the variability within the dataset compared to the others (variability decreases as component numbers increase). The biplots that are created are based on the first two components since most of the variability can be explained by the first and second principle components.

Aitchison (1997) also showed that PCA could easily be interpreted based on clr transformed data. The relationship between variables and the principle components can be interpreted based on the links between two rays or vectors (von Eynatten et al. 2003; Tolosana-Delgado et al.

2005). These magnitudes are based on the covariance matrix, but the relationships are still the same once a correlation matrix is used. A short link between rays suggests that the components are proportional in some way. Collinear links between variables shows that a single process was involved in forming them. In addition, the smaller the angle between the links the more correlated they are in terms of formation processes. The links that are perpendicular to one another (orthogonal) suggest that there was no correlation based on the processes involved in the formation of those variables. At an angle of 120°, the links have no correlation between variables and different processes of formation should be considered for the variables or groups of variables. Also, the compositional trends within the data can also be outlined using a variation array of clr-transformed data. The detailed description of the methods corresponding to subcompositional trend analysis can be found in Martin-Fernandez et al. (2005).

Discriminant function analysis will also be performed on the transformed variables. This method involves the classification of patterns that occurs between variables (inter- and intra-sample variables) to define groups within the dataset. The dataset will be assessed on whether the identified variables related to depositional environments and provenance- or unconformity-related (sequence stratigraphic) elements can be identified specifically within this basin for future regional or local correlational studies.

CHAPTER 4

RESULTS

4.1 Facies analysis

Three wells were selected for this study namely well F-A12, F-AR1 and F-A5. F-A12 was used as a reference well and was 2250m away from F-A5 and 6640m away from F-AR1 (displacements, Figure 3.1.1)). Well F-A5 and F-AR1 were 5371m away (Figure 3.1.1).

4.1.1 Well: F-A12

4.1.1.1 Seismic facies

Seismic facies 1.1 is characterized by wavy-divergent to progradational basinward-dipping reflection patterns with variable to moderate amplitudes and moderate to high frequencies (Figure 4.1.1). The progradational reflectors (possibly shelf edge) are largely tangential/oblique. The external form is characterized by an erosive complex or chaotic fill (overall not channel scale). The lateral change in facies is contorted by the occurrence of faults. Further down dip there is the occurrence of migrating wave mounds that are indicative of high-energy sub-marine fans (Figure 4.1.1). The sediment transport direction shows that most of the sediments were derived from the NNE direction (Proximal basement high).

Interpretation: The seismic facies 1.1 described here is similar to the SF-2 facies described by Lin et al. (2018) as shelf edge or delta front deposits. The onlap fill towards the top is characterized by base level rises to fill the depocenters created by the faults and the onset of the drift phase. A divergent reflection pattern indicates syn-depositional differential tectonic movement (indicated by local depocenters) (Veeken, 2013).

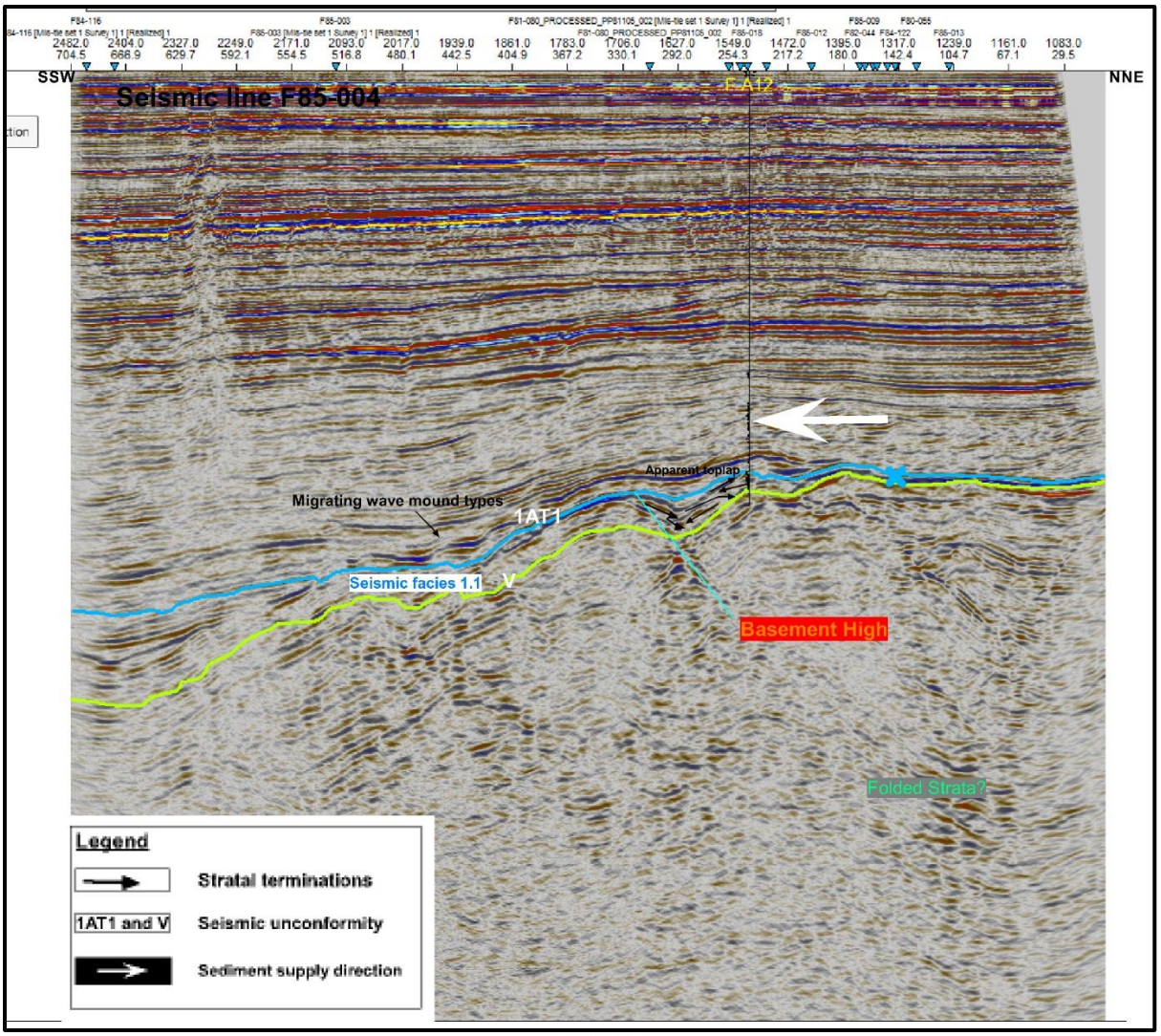

Figure 4.1.1: Study interval with interpreted seismic horizons (1AT1-V horizon) showing seismic facies 1.1 and stratal terminations. In addition, the basement high with possibly folded strata? The sediment supply direction (white arrow) is also displayed.

4.1.1.2 Reservoir zones

This well was divided into five compartmentalized reservoir zones (stacked plays) separated by minor potential fluid barriers or flooding surfaces (Figure 4.1.2). These zones were confined by two major unconformities, the 1AT1 occurring at a depth of 2659m and the horizon V unconformity situated at a depth of 2798m. The gamma ray log shapes that occur in F-A12 are cylindrical, bell-shaped (serrated and smooth), saw-teeth serrated and funnel shaped. These shapes occur throughout the succession and represent various depositional associations.

As seen from Figure 4.1.2, reservoir zone 5 contains minor to rare porous intervals and therefore are of poor reservoir quality. The gamma ray readings shows a range of high to low values with neutron density cross-overs indicating no visible occurrence of hydrocarbons. Reservoir zone 4 is similar in nature to reservoir zone 5 and shares the same reservoir characteristics or electrolog character. Reservoir zone 5 was the only zone that was not cored but showed a similar nature to reservoir zone 4. Reservoir zone 3, 2 and 1 shows hydrocarbon-bearing zones with fluid barriers or flooding surfaces developing a compartmentalized reservoir zone. The gamma ray readings for these reservoir zones are low due to its diminishing argillaceous material (or K, Th and U values). The neutron-density logs show that there is an occurrence of hydrocarbons. The resistivity logs indicate the occurrence of oil with some or rare water-bearing beds towards the top of each compartmentalized reservoir. The detailed observations of petrophysical characteristics were well beyond the scope of this study. This observation was confirmed using well core analysis reports and the geophysical well log shapes.

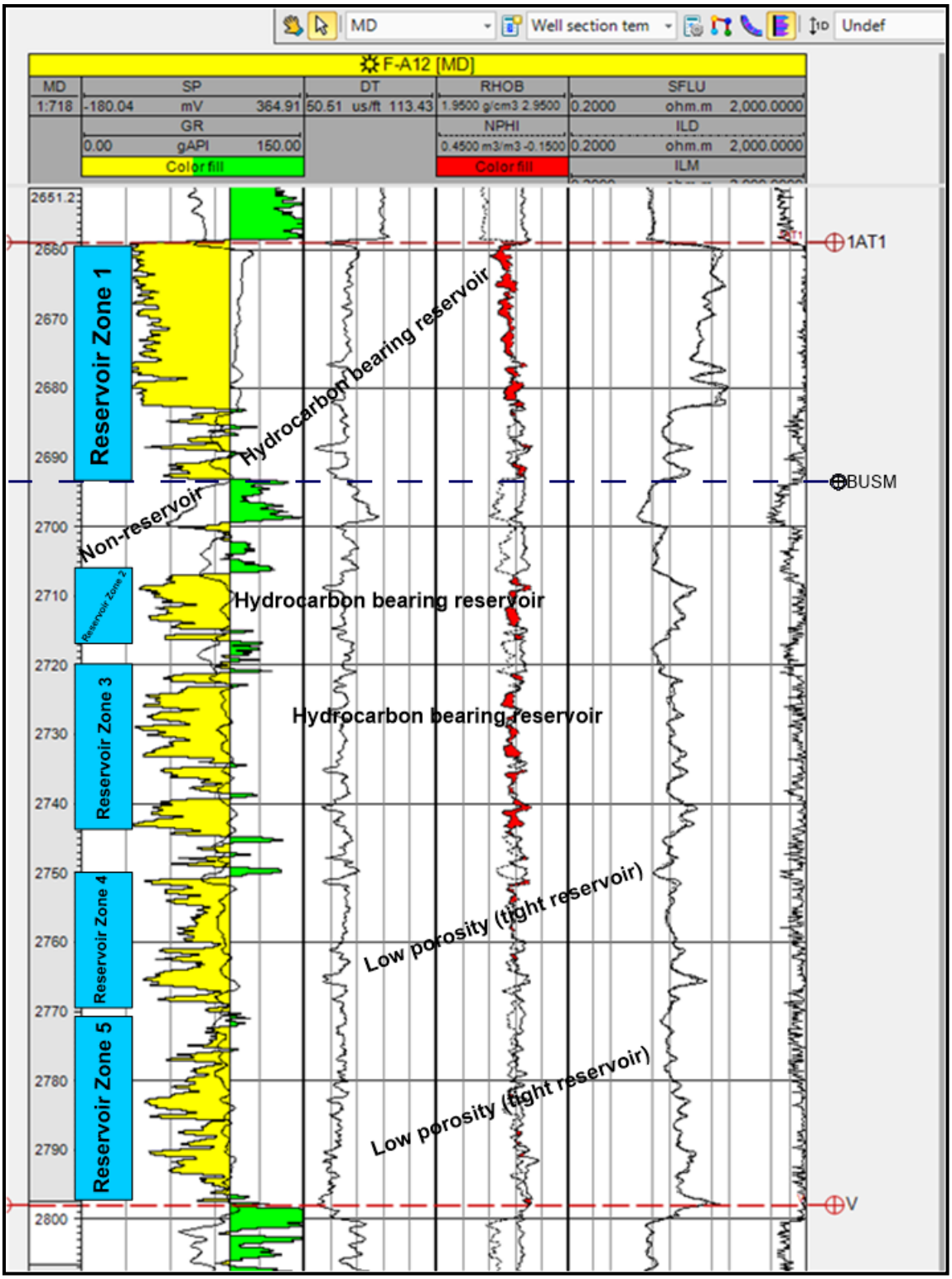

Figure 4.1.2: Reservoir zones and corresponding geophysical logs with interpreted hydrocarbon potential of F-A12. GR- Gamma Ray log, DT-Sonic log, RHOB-Density log, NPHI-Neutron log, SFLU-shallow resistivity, ILD- Deep resistivity logs and ILM-Medium Resistivity logs

4.1.1.3 Lithofacies

Facies associations of the regressional element complex assemblage set (Table 1)

Facies association 1 (Distal-middle Delta front platform/mud rich delta front sheet and lobe facies) (Figure 4.1.3A)

Facies 1.1 (Figure 4.1.3B)

Heterolythic parallel (lenticular) to undulating low-angle wavy bedded, vfL-fU medium grey massive-ripple laminated sandstone interbedded with very fine to medium grey/brown mudstone drapes (>1m thick). Sedimentary structures consist of Sm, Sw, Shl, and Sr (including SM1 and SM2). There are abundant soft-sediment deformational structures related to density contrasts such as fluid escape structures, load and flame structures (rapid deposition). The thickness of these bodies varies but ranges from 10cm to >1.1m. These facies also occur interbedded with facies 1.2. This is further supported by the massive bedding nature of interbedded sandstones. Interbeds of massive to faintly laminated, coarsening upward, light/medium grey sandstone (ranging from 1cm-17cm in thickness) are moderately well sorted with subrounded grains.

Mud drape thickness decreasing towards the top of the unit. Disseminated claystone rip-up clasts, with carbonaceous fragments are also evident. The mudstone drapes contain silt grains that are fine to coarse in part and shows evidence of carbonaceous material (generally less than 1cm thick) (Sedimentary structure, C). Evidence of carbonaceous material is common with the mud drapes based on the colouration (oxidation haloes). There is also the occurrence of festoon-shaped ripple laminations within the interbedded sandstone of the wavy beds but are largely structureless. This is the result of combined flow with predominant oscillatory flow and minor unidirectional flows.

Bioturbation is absent to rare. Trace fossils encountered are *Bergaueria*-like sedimentary structures and *Planolites*. Imbricated clasts are found at 2769.74m and 2768.76m. Shell fragments are also abundant towards the top of the unit (2768.74m). A coarsening upward and thickening upward trend exist within composite bedsets ranging from lenticular bedding (vfL sandstone) at 2769.74m to wavy bedding with fU sandstone towards the top (2769.06m). Lenticular bedding shows evidence of starved ripples. Thin section analysis reveals that the clay drapes are in fact silty claystone that are well sorted with quartz grains being the dominant

mineral. Muscovite flakes are common throughout. At 2769.01m the wavy beds conforms to the bedding angle with increase in dip (low angle wavy bedding). An imbrication lag is also found at 2769.74m, which contains carbonaceous ripped-up clasts (3cm elongated clasts). Well log signatures consisted of low and moderate gamma ray values and area largely serrated. There are also low neutron values and low-density values, but carbonaceous rip-up clasts are present.

Interpretation: These heterolythic type (wavy and lenticular bedding) deposits usually occur in tidally influenced environments (Reineck & Wunderlich, 1968). The occurrence of double mud layers is largely indicative of tidal influences but there is no detailed cyclicity as are usually found in confined settings. These facies are characterized to be part of the middle-distal delta front region (subaqueous subtidal platform) where wave processes dominate (above FWB). The occurrence of the interbedded mudstone drapes does not contain much carbonaceous matter with respect to the low neutron log values and thin section analysis as would be found in supratidal heterolythic mud flats. Also, thin section analysis (F-A12#15) reveals that the interbedded mudstone contains abundant quartz grains (silt-sized) usually indicative of high energy events than the predicted slack-water stages in tidal settings (Density flow mud of Talling et al., 2007; Talling et al., 2012).

The coarsening upward nature of this unit and thickening of the sandbodies and increase in grain size towards the top can be interpreted as distal mouth bar heterolythic deposits (Nordahl et al., 2006). These facies represents the unconfined channel fill on the subtidal-subaqueous platform with their relative association with FA 1.2 (Eide et al., 2016). Rapid aggradation occurred possibly from the formation of large subaqueous crevasse sub-deltas further updip (Rossi & Steel, 2016). The massive to laminated sandstone suggest that there was a flow under upper flow regime conditions (low ichnodiversity and abundance) followed by a flow decrease with a high sediment supply (no ripple drift because the turbulence was too high). This is also interpreted to be very close to the subaqueous unconfined-confined channel bars as flooding continued, together with penecontemporaneous deformation. The absence or low diversity of ichnofabrics reflects stressed environmental conditions caused by small colonization windows due to rapid aggradation after suspension settling (MacEachern et al., 2008; Van Capelle et al., 2016). This is further supported by the high-energy *Bergaueria*-like traces (Knaust, 2017). The salinity could also have been too low for burrowing organisms due to fluctuating river floods (Shanmugam et

al., 2000). This is supported by the overlying Facies 2.1, which has been interpreted because of strong river floods due to hyperpycnal flows either from basement highs or from the main distributary, which is evidence that the distal parts of subaqueous terminal distributary channels were approached. These fluctuations were possibly driven by periodic influxes of river floods (Martinius et al., 2001). Ripped-up and imbricated clasts (rounded) also serves as evidence for fluid-mud beds (supercritical flows) further upstream or updip, possibly from terminal distributary channels (Eide et al., 2016).

Mud drapes usually represents tidal-dominant fluctuations of slackwater stages between high or low tides, but the absence of any cyclicity points towards another interpretation. The inter-channel areas on the delta front lobe can produce similar facies. The ripple bedforms (festoon cross-lamination) in between are indicative of combined flows, small-scale anisotropic hummocky cross stratification that are non-amalgamated (Van Straaten & Kuenen, 1957; Martel & Gibling, 1994; Legler et al., 2013). Also, the fact that the sandstone units are pinching, together with the low-angle of the undulating beds, the festoon-shaped low angle ripple cross-laminations corresponds strongly to the interpretation put forward by Arnott and Southard (1990), Cheel & Leckie (1993), Molgat and Arnott (2001) and Nordahl et al. (2006) for wave to current ripple cross-laminations of undulating cross-laminated to graded rhythmites in the delta front environment. These combined flows shows that fluvial and wave processes were dominant (Ainsworth et al., 2016), and this is further supported by swaley cross stratification and hyperpycnites higher up in the sequence.

It should also be noted that dynamically deposited mudstones occur throughout the succession. These fluid-mud layers similar to the SM1 and UM2 layers described by Mackay & Dalrymple (2011) are usually attributed to tidal deposition in turbidity maximum zones within tidal channels. There has been no flume study that points toward fluid-mud layers produced under higher energy wave deposition in a mud-rich setting. Therefore, it could be possible for combined flows to produce similar sedimentary features. The abundance of SM1 layers that have mud-dominated ripple lee slopes can be attributed to unidirectional flows and turbulence suppression in the ripple troughs (Baas & Best, 2008) but can also be attributed to anisotropic combined flows with a dominant unidirectional flow (Nordahl et al., 2006). The interbedding of

facies 1.2 (tidal bars) are possibly indicative of tidal energy increasing towards the top of these successions with wave energy increasing towards the bottom.

Carbonaceous clasts or shale fragments suggest that nearby vegetation were eroded and transported through subaqueous terminal distributary channels (Oomkens, 1974; Staub & Gastaldo, 2003; Olariu & Bhattacharya, 2006; Van Capelle et al., 2016). The imbricated intra clasts are ripped-up bedding due to the nature of subaqueous crevasse channels and flooding on a solidified and partly water-saturated underlying unit. These facies are also equivalent to the subtidal-mudflats as proposed by Shanmugam et al. (2000), the heterolythic delta front facies of Martinius et al. (2001) and the abandoned subaqueous distributary channels of Van Capelle et al. (2016).

Facies 1.2 (Delta front tidal bar) (Figure 4.1.3C)

Facies 1.2A1 and 1.2A2

These facies are characterized by fining-upward and coarsening-upward sequences (element complex), which is divided into two sub-facies and represented by facies 1.2A1 and 1.2A2 (0.51 to 0.66m thick sequences).

Facies 1.2A1 is a basal unit that is defined by light-medium grey mL-fU cross-bedded sandstone (Spb) unit (simple bedsets that range from 0.08m to 1.3m thick), with dark grey carbonaceous laminae (mud drapes). These facies are planar erosively underlain by facies 1.1. Facies 1.2A1 (basal unit) consist of a bioclastic sandstone (inferred bar bottom). The basal boundary unit is missing but unpublished reports confirm that it is an 'inferred' channel bottom. Since there is no evidence for a channel bottom, this unit has been taken as a tidal bar that is largely confined in most places. These facies shows sub-rounded grains and are very well sorted. Facies 1.2A1 shows a planar erosive base with a gradational or non-erosive sharp contact towards the top. Shell fragments are abundant and disseminated throughout the facies, which makes the bed highly calcareous. Carbonaceous debris occurs mixed with silt. Composite bedsets are common and a change in hydrodynamic conditions occurs as fining-upward sequences occurs with siltstone and claystone heterolyths (Facies 1.1). The bioturbation index ranges from 1-4 with an ichnofabric dominated by *Macaronichnus* (under fairweather conditions). There are also possible casts of bivalves (Bi) which occurs synonymously with shell debris. Sedimentary structures

consist of Sp with foresets that are tabular and largely sigmoidal to tangential. The cross-bedded sandstone also shows carbonaceous mud drapes. These mud drapes are not erosional but their boundaries exist as sharp contacts. The quantity of broken shell fragments tend to decrease towards the top with woody fragments and carbonaceous-rich drapes increasing.

Facies 1.2A2 consist of ripple laminated (Sr) vfU sandstone that is non-calcareous (0.04m to 0.53m thick). The grain shapes are sub-rounded and are very well sorted. The sedimentary structures consist of Sr with bidirectional ripples or small scale herringbone-like structures also present. Facies 1.2A2 grades to Facies 1.2A1 and is largely gradational. Facies 1.1 is also found interbedded within this facies association but is well sorted and grains are sub-angular in shape. These carbonaceous drapes become browner towards the top. These facies have boundaries or contacts that are sharp. Occasional pebble stringers or clasts are possibly due to a nearby major tidal inlet of flooding of nearby subaqueous channels. Facies 1.1 also occurs interbedded with facies 1.2 as evidence of a decrease in fluvial effectiveness. Therefore, Facies 1.2A1 tends to transition to Facies 1.2A2 (fining-upward sequence) and Facies 1.1 transitions to Facies 1.2A1 (coarsening-upward sequence). Trace fossil index and occurrences are the same as in facies 1.2A1.

Interpretation: This sequence represents tidal confined bars forming subaqueous ripple and dune bedforms (medium scale and large scale cross bedding) on a distal to middle delta front (subtidal to intertidal shoals) platform. The occurrence of thin layers (lamina-scale) being bidirectional is indicative of reversal of flow due to tidal processes (Reineck & Singh, 1980). The grading of facies 1.2A1 to facies 1.2A2 is the result of periodic subaqueous flows from nearby subaqueous channels/terminal channels. This is further supported by the four stages of delta lobe development as seen in the Atchafalaya deltaic system whereby distal tidal bars are rather interlinked with prodeltaic or distal delta front deposits (Olariu & Bhattacharya, 2006). Trace fossils are dominated by a dense ichnofabric of *Macaronichnus* that can be attributed to a delta front environment under fairweather conditions (Seike, 2008; Knaust, 2017). There is a decrease in the thickness of the beds towards the top of the bed with decreased thickness within the mud drapes. This interpretation of tidal bars rather than tidal compound dunes is preferred since there are coarsening-upward and fining-upward sequences of beds. The coarsening upward nature is

because currents and wave energy are greatest at the crest of the ridge in subaqueous or offshore settings (Olariu et al., 2012a).

The subordinate current was less dominant therefore the mud drapes are not eroded in many cases. The overall coarsening upward nature of these sandstones (made up of fining-upward sequences) is representative of subaqueous distal tidal bar deposits, which occurs synonymously with facies 1.1. Facies 1.2 is interpreted to be part of migrating (progradational) tidal sand bars within the subaqueous platform of the delta front, fed by subaqueous channels. Facies 1.2A1 are interpreted as a storm surge lag deposits since the shells are fragmented, have planar erosive bases and gradational tops as described by Brenner & Davies (1973) and Reading (1982). These deposits are concentrated usually in the troughs of the tidal sandbars, which can be synonymous to unconfined and confined tidal bars (Eide et al., 2016). Facies 1.2A is interpreted as the tidal bar with minor depressions or troughs to allow some sort of confined flow on the bar (evidence of small bidirectional ripples). Thus, could have been the result of storm surges waning or the occurrence of a subordinate current reacting to a bar that migrated obliquely (laterally). Evidence for this is the fining upward nature of facies 1.2 into the inter-bar region of Facies 1.1. The initial coarsening upward trend from Facies 1.1 is the result of tidal bar migration (Facies 1.2A1) with a strong input of current speeds and wave energy on an open setting or delta front setting (Olariu et al., 2012b). These units can also be described as interdistributary islands (extensions forming subaqueous shoals) interfingering on delta front deposits (Kuehl et al., 2005). In addition, these units with the overlying hyperpycnites can be described as turbidites or /distal delta front hyperpycnites formed due to hyperpycnal flows.

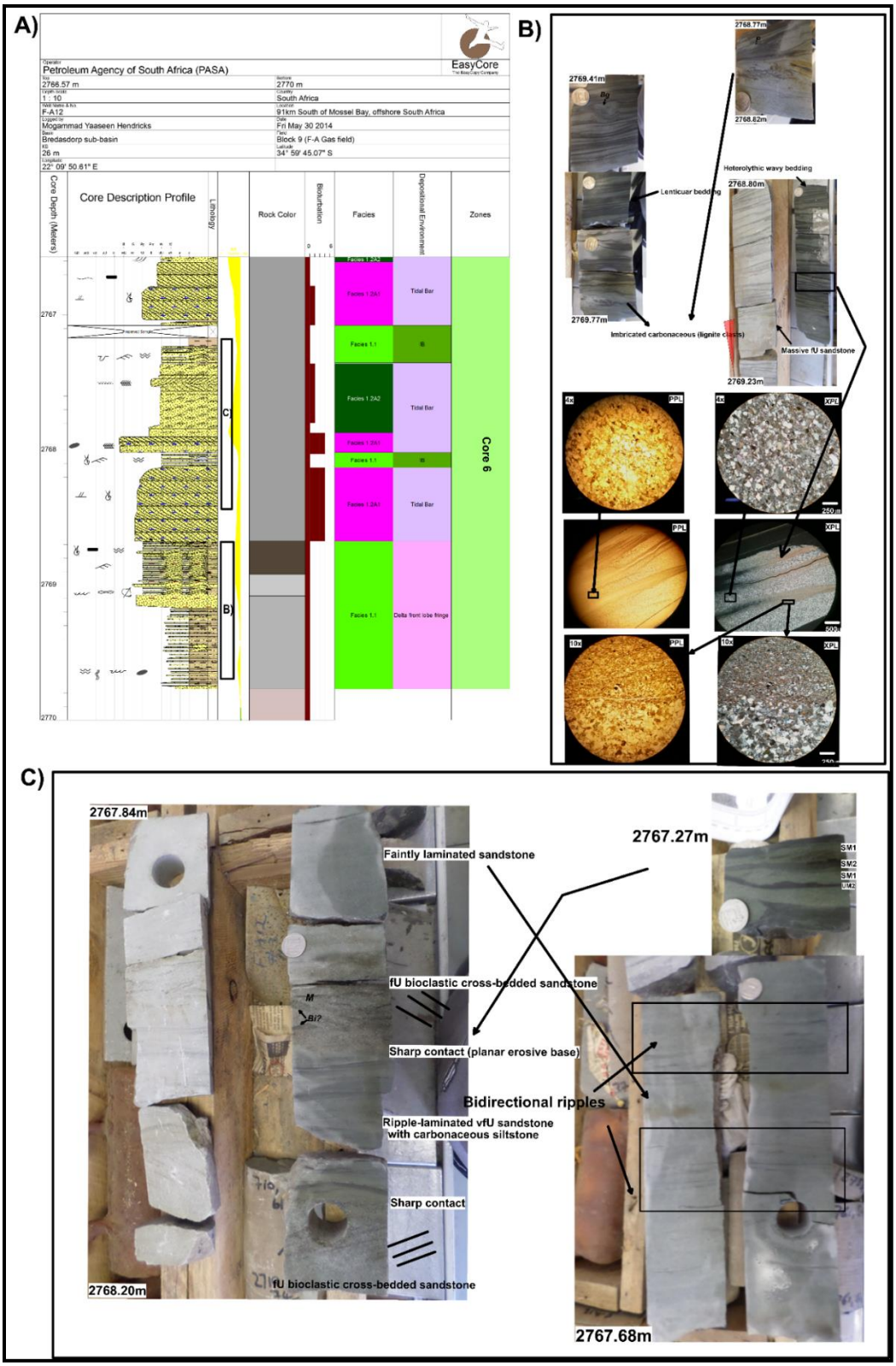

Figure 4.1.3: Examples of facies association 1 showing proximal to distal delta front lobes with offshore migrating tidal bars. A) Sedimentological log with gamma ray log, bioturbation index,

facies and depositional environments. B) Facies 1.1 showing coarsening-up upward composite beds and lenticular bedding with thin section analysis of these units. C) Facies 1.2 showing bioclastic sandstone interbedded with facies 1.1. Bidirectional ripples are also present indicative of tidal processes. Trace fossils consist of Bergaueria (Be) (Facies 1.1) and Macaronichnus (M) and Bivalve (Bi) trace-producer casts (Facies 1.2)

Facies Association 2 (Proximal delta front)

Channelized delta front lobe facies/Terminal distributary channels (with turbidites/hyperpycnal event flows (debrites)) (Figure 4.1.4)

Facies 2.1

These facies consist of fU-fL low-angle heterolythic cross-bedded units that are synonymous with Facies 1.2A, but the partially carbonaceous to fully sediritic claystone drapes are light brown and this unit contains more pebble grade para-conglomerate stringers that are oligomictic in origin (Figure 4.1.4B, C). In certain parts, it shows siltstone units that are ripple laminated. This unit ranges in thickness from 0.34m to 1.62m thick. Granule to pebble clasts is found disseminated throughout the succession that are usually well rounded and oblate. There is a gradation within the foresets that tends to coarsen upward (hyperpycnites). The low angle heterolythic cross-bedding (Splx and Shl) grades to high angle cross bedding (Sp) towards the top. The sediritic and mud clasts are aligned parallel to the bedding plane or parallel to the bedding foresets. The low angle bedding grades into horizontal bedding (Sh) in certain parts. The grains are very well sorted with subrounded grain shapes. Sedimentary structures also consist of unidirectional ripples (Sr) (festooned shape) and planar cross-laminated units (Spl) that are tabular in nature. There is a gradational change from planar cross lamination (facies 1.2) towards the base of the unit to planar cross bedding towards the top. Small-scale cross-bedding and large-scale cross-bedding is evident. Claystone (carbonaceous) drapes are light brown with oxidation haloes. Starved backflow ripples also occur with mud drapes. Double mud layers are also present. An oligomictic paraconglomerate stringer consists of clay (sideritic) clasts. These clasts are also found scattered throughout the unit. The dune foresets tend to show an inverse grading texture (2cm-4cm) until a gradational contact with the siltstone ripples and eventually the brown claystone drapes that lead to abandonment. The Bioturbation index is 0 as there are no visible traces. Wood fragments are also present.

Facies 2.2

These facies consist of inversely graded units that are made up of a basal massive claystone (Fm) unit (greenish brown) that grades to a vfL sandstone (medium grey) and to a top unit that consist of mL-mU sandstone (grey) (Sin). This unit is around 0.74m thick. Faint cross laminations are seen in the coarser vfL and mL-mU sandstone but are largely inversely graded. This coarser unit is also made up of comminuted shell debris. Wood debris are common with sideritic and claystone clasts. Grains are sub-angular and are well sorted. The bioturbation index is 0 and no traces are found in this unit. The unit is around 25 cm thick. There is a sharp contact between these facies and facies 2.1.

Facies 2.3

mL-fU medium grey planar horizontal (Sh) to low angle-massive sandstone (Splx to Sm) and interbedded ripple laminated (Sr) dark brown fL to vfL-siltstone (swaley cross-stratification (Sw)/wave influenced turbidites) (Figure 4.1.4C). The overall unit is 1.41m thick. Double mud layers also occur. The grains are subrounded to subangular and are very well sorted. Shell debris is common making the unit calcareous. The floating clasts (oblate) are usually stretched and are 2cm in diameter (long axis). This low angle cross-bedded unit is around 39cm thick and the laminasets tend to coarsen upward. Bioturbation index is 0-1 and consist mostly of *Thalassinoides* and *Ophiomorpha* burrows. This unit also tends to grade to a finer climbing ripple to ripple laminated (Sr) unit towards the top of the overall facies 2 with evidence of escaped burrows and sand injectites or fluid escape pipes.

Facies 2.4

These facies consist of an intra-formational oligomictic para-breccia (Gmd) (Figure 4.1.4B). This unit is largely matrix-supported, poorly sorted, oligomictic, grey breccia dominated by angular and subangular, prolate to oblate mud chips. The unit is around 0.2m thick. Some rounded intra-formational granules also occur towards the base of the unit with some traction flow indicated by some sort of imbrication initially. The lower contact consists of a planar undulating erosive to gradational base. Clast sizes show two main sizes: 4 mm for the smallest clasts and 20mm for the largest clast sizes (granule to pebble-size). The matrix comprises mostly of mL to mU sandstone that are massive and grey in colour. Convoluted (Shc) laminae sections (overturned laminae) are

also evident within this unit. Towards the top of the sequence, these units tend to increase in clast size (up to 4cm in size) and slumped sequences become evident. There are no evidence of trace fossils (BI=0)

Interpretation: The colour of the mud drapes tend to change therefore it is likely that this unit was deposited in a subaqueous setting or close to the terrestrial side with the influx of more oxygenated fluids and absence of mud cracks. There is no evidence of emergence but the colour of the mud drapes changes to light brown possibly because of the influence of more oxygenated fluids. There is a strong tidal influence due to the occurrence of mud drapes or quiescent periods (Allen, 1982). This can also be attributed to wave-influenced turbidity currents during the waning stage of the turbidite deposition (Lamb et al., 2008). Double mud layers are usually representative of tidal fluctuations with time-velocity changes in a subtidal setting (Visser, 1980). These layers could also be the result of changes in hydrodynamic conditions with episodic pulses from a fluvial input, thus contributing to the occurrence of internal waves as possible drivers for deposition in this zone. This is further supported by the intercalated siltstone that is ripple laminated with organic material that forms part of a waning sustained turbulent flow, which resulted in an increased fallout from suspension (turbidites). The low bioturbation index is the result of rapid aggradation (comminuted shell debris- high-energy event) over a prolonged hyperpycnal flow with the fluctuation or changing salinity (Zavala et al., 2011). This is supported by the occurrence of inverse grading of Facies 2.2 with hyperpycnal waxing and waning flows.

The horizontal stratification has been interpreted by Shanmugam et al. (2000) as tidal sand bars and is the result of diurnal tidal inequality and mud drapes as pause planes. The position of these tidal bars could have been largely on the shelf because the occurrences of massive sandstone with ripple laminations (Facies 2.3) are more indicative of a proximal-middle delta front setting (Olariu & Bhattacharya, 2006). The occurrence of floating mud chips and pebbles could be the result of an approaching channel or proximal mouth bar/terminal distributary channel further updip or laterally. In addition, these high energy or high velocity events are supported by the horizontal stratification that is indicative of a possible fluvial origin (Ainsworth et al., 2016). The occurrence of dunes and ripples (Facies 2.1) is the result of hydrodynamic changes, with the fluctuating supply of sand to mud and change in flow velocities and vortices during a

hyperpycnal flow producing turbidites (Zavala et al., 2011). The episodic grading points largely towards turbidite deposition of terminal distributary channels. The occurrence of starved ripples can be attributed to possible backflow ripples migrating on larger dune foresets (macroforms). These facies also show a normal grading trend within each foreset (simple) and coarsening upward laminasets indicating large asymptotic foresets of macroforms (Reineck & Singh, 1980). This type of cross bedding could also be the result of heterolythic inclined cross stratification with the migration of the tidal bars but the occurrence of back flow ripples and abundant mud chips is largely indicative of hyperpycnites. There is also a grading that takes place from horizontally laminated sandstone to climbing ripples towards the top, which is indicative of hyperpycnite gradation of suspended material to bedload material (Zavala et al., 2011) or storm-influenced swaley cross stratification (low angle erosional surfaces) within the shoreface zone. The occurrence of shell debris in this unit points largely to a storm dominated interval for the inverse graded unit. This ripple-laminated unit also shows signs of escaped burrows and sand injectites, which is the result of an increase in sediment supply and fluctuating current speeds. These deposits are equivalent to the sub-tidal creeks as described by Hovikoski et al. (2008), proximal high-energy tidal bars (Tanavsuu-Milkeviciene & Plink-Bjorklund, 2009) possibly as a result of the hyperpycnal flows, syn-rifted flood-tidal deltas (Jackson et al., 2005), proximal river dominated delta front (Coates & MacEachern, 2009). These facies has also been described as subtidal channel deposits that are usually connected to their distributary equivalents in the lower delta plain (Kuehl et al., 2005; Rossi & Steel, 2016). Klausen et al. (2018) described these facies as tidal distributary channels, but the lack of an erosional base and the floating clasts of facies 2.4 are largely still indicative of hyperpycnal flows. However, the occurrence of these hyperpycnal flows are known to occur in fluvial or tidal inter-channel areas, but the lack of finer material and erosional bases with its associated sedimentary features is largely indicative of a subtidal setting (Zavala & Pan, 2018). The influences of riverine currents are clear with the occurrence of rip-up clasts, wood fragments and coaly fragments. The gradation of hyperpycnal flows with increased clast sizes towards the top is a result of the proximal basement high event flows interbedded with terminal distributary channels (Pattison et al., 2007) which is further supported by the debrites and overturned laminated sequences (convoluted) possibly from nearby basement high failures. The top unit can be described as possible delta front mouth bars as well.

A marine influence is evident with the occurrence of marine trace fossils such as *Thalassinoides* and *Ophiomorpha* burrows.

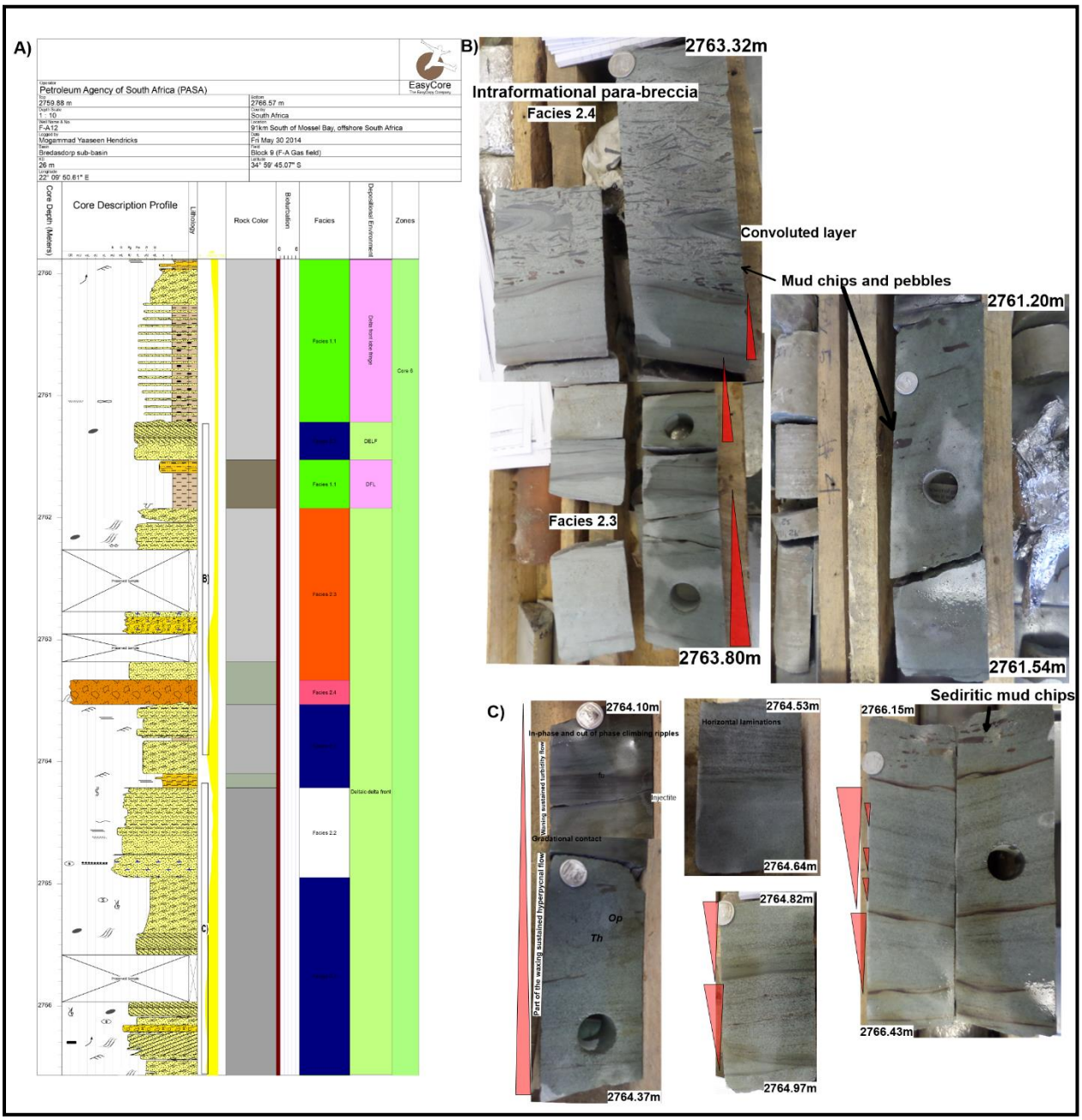

Figure 4.1.4: Examples of facies association 2 showing channelized delta front lobe facies or terminal distributary channels with hyperpycnal to turbidity event deposits. A) Sedimentological log showing coarsening-upward and fining-upward sequences. B) The occurrence of a non-cohesive debris flow (debrite bed), associated convoluted soft-sediment deformation of facies 2.4 and cross-bedded sandstone. The flow tends to grade into a cross bedded unit with aligned clasts. C) Normally and inversely graded units also occur with organic rich mudstone drapes (facies 2.3 and 2.2) and heterolythic units (facies 2.1). Bioturbation is common and restricted to

certain intervals with trace fossil ichnospecies consisting of Ophiomorpha rudis (Op) and Thalassinoides (Th)

Facies association 3 (Lower delta plain to proximal delta front mouth bars with associated terminal distributary channels, interdistributary bays (sand flats) and associated crevasse splay sub-deltas or lobes)

Facies 3.1 (Inter-terminal subaqueous distributary regions)

Dark grey massive claystone/siltstone (Fm) with vfL sandstone/siltstone interbeds (Fl). The boundary contacts are sharp (with Facies 3.4) and ranges from undulating to planar horizontally laminated and consist of gradational contacts (with facies 3.2) with ripped up clasts. The thickness of these beds varies from 0.09m to 1.56m thick. Microscale gradational contacts are evident with overall coarsening upward cycles occurring as well. Some intervals also occur as wavy bedding. These facies are not calcareous and are largely massive in nature but occurs as fluid mud layers (SM2) in certain parts. This unit sometimes exist as massive siltstone bedding (Fm) on its own. Bioturbation is rare but towards the top mantle and swirl structures and *Paleophycus* occur (BI=1). The upper part of this unit becomes siltier and contains more carbonaceous partings as Facies 3.2 is reached. These distal interdistributary bay islands are usually associated with mouth bars. These facies also tend to grade to wave rippled laminae with bioturbation of marine trace fossils becoming evident.

Facies 3.2 (Terminal distributary channels/Crevasse splay sub deltas or lobe deposits)

Coarsening upward and fining-upward units that consist of massive (Sm) to faintly horizontally laminated fL sandstone (Sl) grading to cross-stratified fL sandstone (Spb) with rare to no occurrence of mud drapes (mostly trough cross-bedding, planar tabular cross-bedding and ripple cross-lamination). In some parts (the top part of the unit), the cross-stratified sandstone is cL-mU in grain size with trough cross-stratification or planar tabular cross-bedding dominating. The unit varies in thicknesses from 0.2m to 5m thick throughout. The faintly laminated unit contains discontinuous mud drapes (crinkled in some cases) and in certain cases, grades to vfU ripple laminated sandstone or massive bioturbated siltstone (this part has been interpreted as facies 3.1 because it represents an abandonment phase). These facies can be divided into two parts; the terminal distributary lobes (crevasse splay sub-deltas) and the channelized facies (with a basal monomictic orthobreccia). The lobes have sharp bases whereas the channels have erosional

bases. These units are moderately to poorly sorted and consist of subangular to subrounded grains.

Towards the top, the unit tends to grade from claystone to planar horizontally laminated and massive sandstones that are very well sorted. Wood fragments, shell debris (associated with calcareous intervals) and quartz pebble floating clasts tend to increase towards the top of the facies or usually associated with bedding planes of cross-stratified units. The horizontally laminated fU/vfU sandstone shows normal grading textures. A bioturbation index of 0-2 (low diversity) with *Fugichnia*-like traces (possibly *Conichnus*), *Paleophycus* and *Macaronichnus* occurring towards the top of units or restricted to certain intervals. Slumped bedding or convoluted bedding also occurs as soft-sediment deformation. These facies shows a sharp to slightly erosive contact with Facies 3.1 at the base and top of the unit. These deposits are always bounded by Inter-terminal distributary channels. The proximal part of this unit shows more claystone clasts and fining-upward sequences more indicative of channelized proximal crevasse splay subdeltas and terminal distributary channels associated with slumped deposits and proximal tidal bars with wavy mud drapes (Gugliotta et al., 2015). The tidal energy started to increase since the lower delta plain and confined settings has been reached. Where these caliches are present bioturbation also tend to increase. Higher up in the sequence these facies tend to similar in characteristics to crevasse splay deltas but are more associated with high velocity channel fills.

Facies 3.3 (Tidal sand flat)

These facies consist of Interbedded medium to light grey cU sandstone and dark grey mudstone (Shl with Sm and Fm). The unit is 0.6m thick. The grains are well sorted and consist of subangular to subrounded grains. Sedimentary structures consist of massive sandstone and massive mudstones with soft sediment deformation by loading occurring as rhythmic layers. Flaser bedding occurs towards the base of the facies and grades to wavy bedding towards the top. Bioturbation is restricted to *Ophiomorpha* and *Paleophycus* trace fossils. Double mud drapes also occur.

Facies 3.4 (Tidal- to wave-dominated and river-influenced mouth bars)

Horizontal to low-angle laminated mL-fU sandstone (Sl to Splx) that grade to wave ripple laminated fL-vfU sandstone beds (Sw) with light brown single and double claystone drapes. The facies has a thickness that ranges from 0.44m to 4.88m. The overall sequence tends to coarsen upwards but fining upward micro-sequences of horizontal planar laminated fU sandstones to wave rippled fL-vfU sandstone/siltstone that contains double and single light brownish claystone drapes occurs. There is a sharp to gradational contact between these three units. The sandstone is well to very well sorted with subangular to subrounded grains. Certain intervals tend to be calcareous. The ripple laminated (Sr) units consist largely of wave ripples and climbing ripple laminations. The climbing ripples to normal ripple laminated units, usually showing a unidirectional component, are rarely found with the drapes. Soft sediment deformation by loading (Shc) is common where the massive to horizontal lamination is deposited on the ripple-laminated unit. Flasers are common throughout the unit, which is lined with the brown claystone usually associated with the troughs (shale partings) of the wave ripples. The clay drapes are massive in nature. The claystone rip-up intra-clasts are light brown. There is also the occurrence of large pebble clast that is greater than 4mm. Ripples shows herringbone-like structures but these are the results of combined flows on wave ripples with climbing ripples (type 1 and type 2) as well. Undulating wave ripple bedforms are common which is aligned with the bedding plane of the larger asymmetrical wave ripples and largely associated with the drapes. The ripple-laminated units are usually very silty and are referred to as siltstone in parts. Wood clasts, wood fragments and lignite flakes are common. The carbonaceous material tends to increase towards the top from being restricted to laminae to occurring randomly (alignment). Bioturbation is low (low abundance and diversity) with a few *fugichnia-like* traces and biogenic structures are only restricted to carbonaceous wood fragments and plant material. Floating clasts are rare but does occur (mostly light brown claystone intraclasts). The transition of the interdistributary bay and open marine conditions occurs with the presence of marine trace fossils and wave ripples. This is possibly because of a fourth-order relative sea level rise within the outer embayment part of the distributary channel.

Interpretation: These facies has been described as mouth bars and terminal distributary channels intercalated with either intervals of channel delta abandonment (further updip) or inter-terminal or mouth bar deposits (facies 3.1) found in between. A distal crevasse splay sub-delta intercalation would also produce a similar succession on the distal intertidal delta platform or

transgressive coaly mudstones (Mellere et al., 2016). These transgressions could be the result of delta lobe switching (autocyclic controls) on the platform on an asymmetric delta. This is supported by the sharp contact to the heterolythic unit, which is a result of full abandonment to interdistributary bays as the tidal mouth bars migrated across the lower delta plain, or upper delta front. This could also be the result of storm action above the fairweather wave base. There is also evidence for hyperpycnal lofting (hypopycnal?) deposits occurring as planar laminated fluid-mud siltstone/mud layers. Where micro-scale coarsening-upward units occur, it is possibly due to the distal nature of the restricted embayment. In addition, the non-bioturbated nature of the sandstones and fluid mud layers could be the result of distal terminal distributary channel lobes from a waning hypopycnal flow along the shoreline. The calcareous units or shell-bearing units is related to interdistributary bay deposits/lagoons/restricted bay deposits in a coastal plain setting (Rossi & Steel, 2016) with bars migrating across and shell debris from nearby beach bars through wave action. The occurrence of Facies 3.2 is the result of sporadic crevasse splay sub-deltas due to the occurrence of massive-planar laminated to cross-stratified and sparse granules (Gugliotta et al., 2015). These units are also described by Ainsworth et al. (2016) to be part of the proximal tidal mouth bars. Also the occurrence of double mud drapes are representative of tidal action becoming more dominant (Shanmugam et al., 2000). These facies are the upper part of the interdistributary bay where tidal sand flats dominate. The well sorted nature of this unit is probably due to wave action together with the parallel lamination as post-vortex structures. These facies has been combined with interdistributary bays and collectively known as the coastal plain facies. The tidal sand flat facies are not very thick and occurs as a thin-bedded unit. The tidal mouth bars are usually cut by channels or shows a sharp contact with interdistributary bay deposits. Facies 3.2 units are also similar to the terminal distributary channels and mouth bars described by Olariu & Bhattacharya (2006) and Mellere et al. (2016).

Facies association 3.3 does not occur often in the vertical succession but has been interpreted as tidal sand flats as their nature are similar to the tidal sand flats proposed by Shanmugam et al. (2000).

Facies 3.4 shows planar horizontal lamination (Sl) (upper flow regime) and massive sandstone (Sm) that is attributed to a rapid aggradation and high flow velocities (Einsele, 2000). The fining-upward sequences could be the result of waxing and waning hyperpycnal flows. This

sequence has been attributed to proximal mouth bar deposits (upper delta plain), close to the transition between the interdistributary bay/terminal distributary channel and mouth bar complexes. This unit could also be described as mouth bar-interdistributary bay complexes that are influenced by wave activity (Elliott, 1974). The distinct alternation between the darker brown claystone drapes towards the bottom grading to light brown claystone drapes towards the top is attributed to the heterogeneous nature of a mouth bar complex (Ainsworth, 2016).

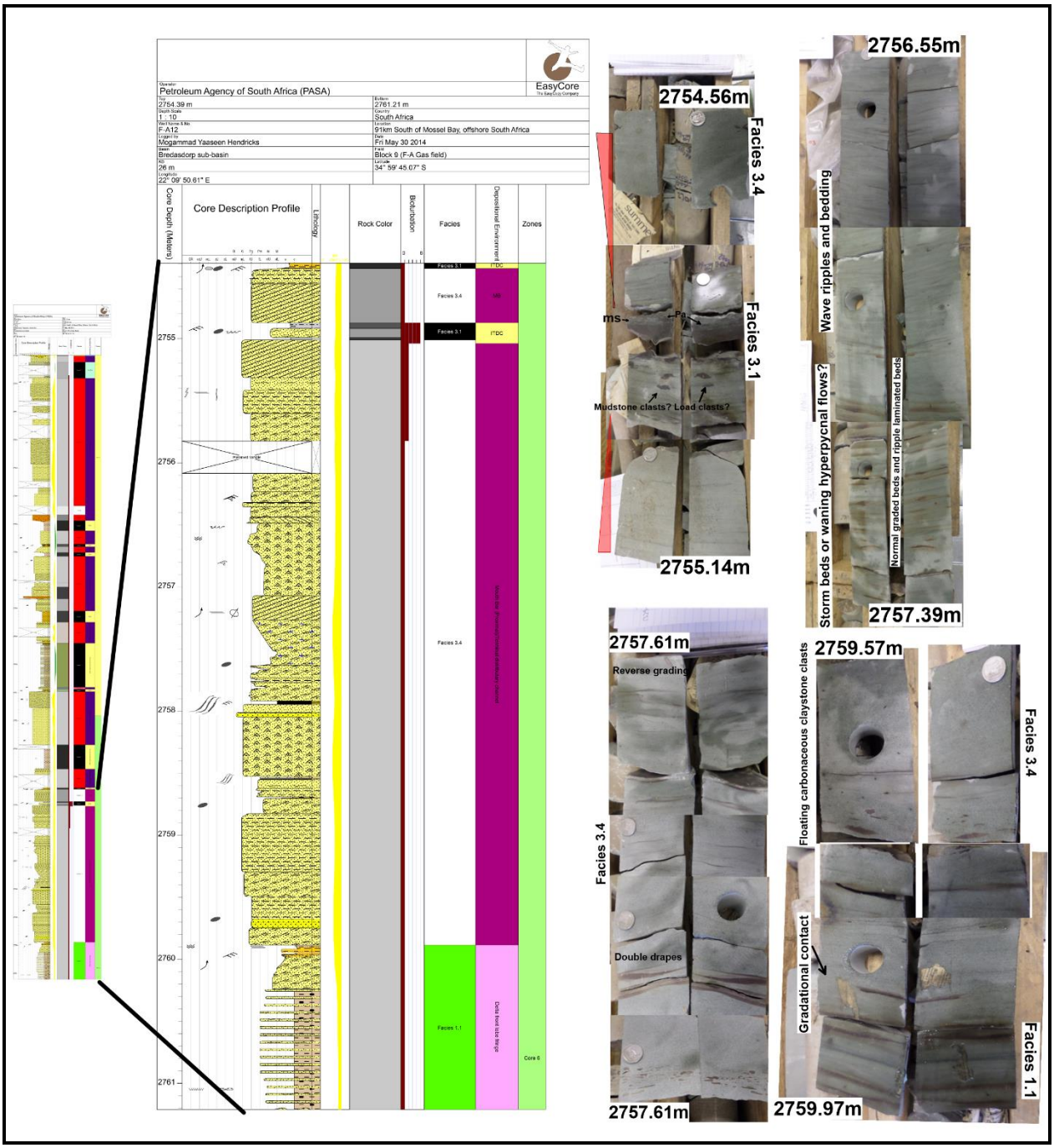

Figure 4.1.5: Examples of facies association 3 (Lower delta plain to proximal delta front) showing mouth bars. Trace fossils consist of Paleophycus (Pa) and mantle/swirl structures (ms). Double mud drapes are common with reverse grading

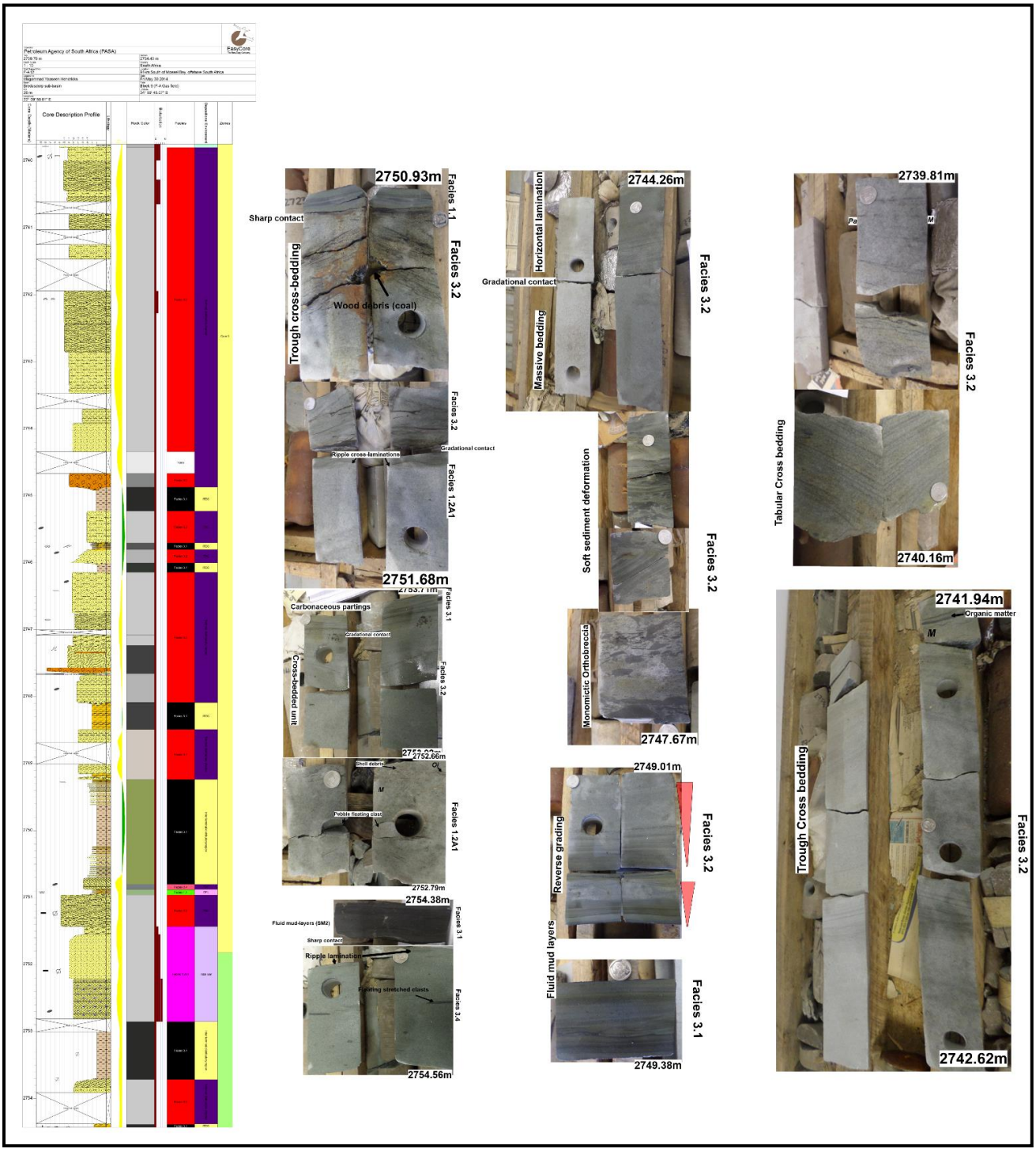

Figure 4.1.6: Examples of facies association 3 showing terminal distributary channels, interdistributary bays and associated crevasse splay subdeltas. Trace fossils consist of Macaronichnus (M), Ophiomorpha irregulaire (Oi) and Paleophycus (Pa). Shell debris, floating clasts and coal (wood) fragments are common

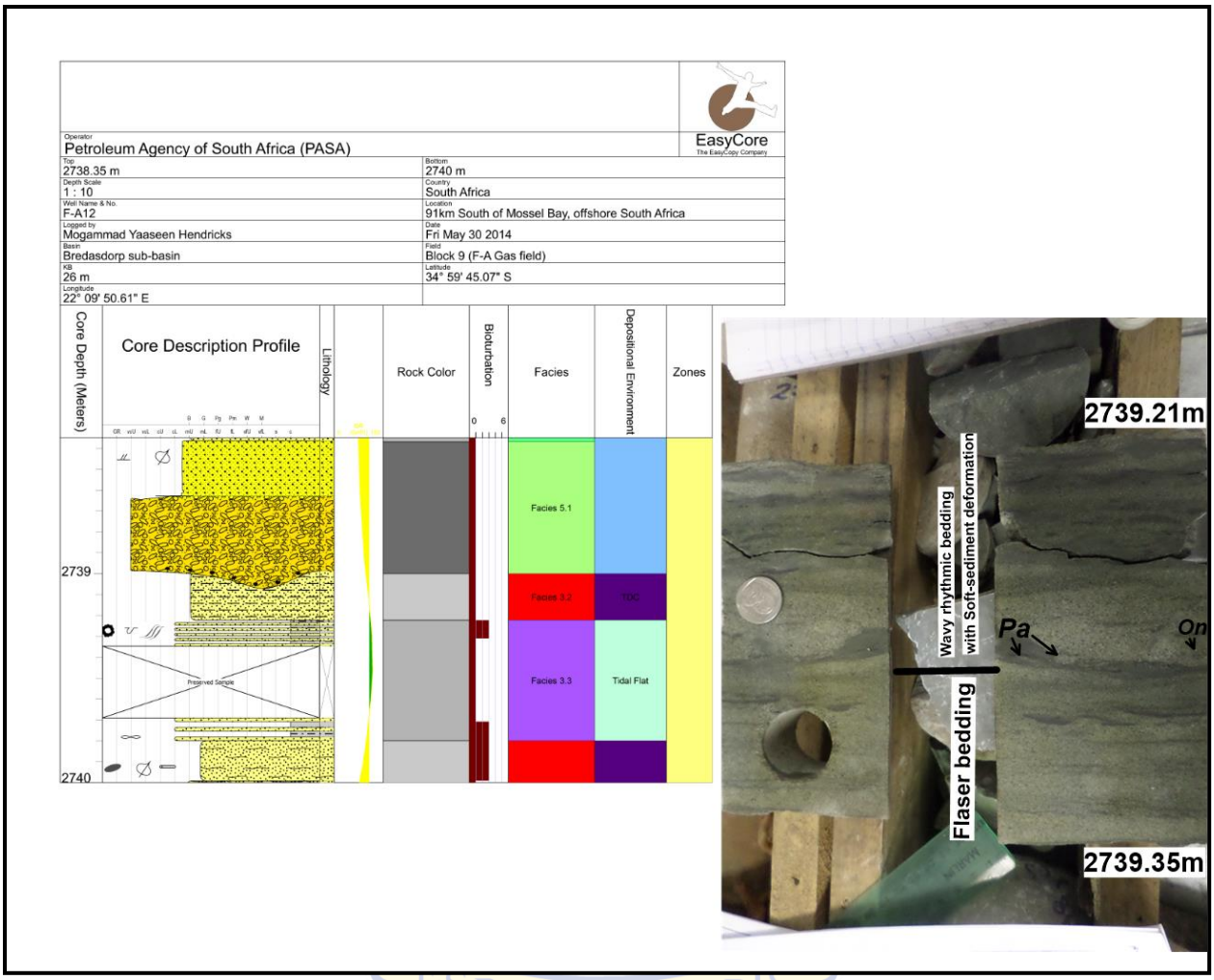

Figure 4.1.7: Example of Facies association 3 showing isolated tidal sand flats on the interdistributary bay. Trace fossils consisted of Paleophycus (Pa) and Ophiomorpha nodosa (On).

Facies association 4 (Coastal plain)

Distributary channels

Fining upward units that consist of a basal conglomerate and fines upwards towards a finer grained deposit that are usually claystone and vfL sandstone-siltstone interbeds.

Facies 4.1 (Figure 4.1.8)

Oligomictic ortho-conglomerate (Gp). Clast-supported unit that is poorly sorted and consist of grey sandstone matrix and dark grey/greenish claystone and siltstone intraclasts. Minor sandstone clasts with sediritic pebbles (calcareous) also occur but the unit is largely oligomictic.

Sedimentary structures consist largely of cross-stratification (Spl and Spb) with the alignment of granules and cobbles to the bedding planes. Rounded clasts are more common with bladed to prolate shapes. The unit ranges in thickness between 0.16m and 0.62m. The clast size ranges from cobbles to granules (4cm in the upper sequences and >4cm in the lower sequence). The matrix consists of mL-fU sandstone that is medium grey in colour. Carbonaceous fragments also occur aligned parallel to the bedding plains. This unit tend to grade to a granule or vcU sandstone that shows an alignment to the cross-beds. Lignite or carbonaceous material is common. The basal boundary is an angular erosional contact and usually cuts into Facies 3.1 or 3.2 (synonymous to 4.1). The upper boundary surfaces are usually gradational. Bioturbation is absent (BI=0).

Facies 4.2 (Figure 4.1.8)

Cross-stratified medium to light grey mL sandstone (Spl and SpB). In parts, the grains are coarse, especially towards the top of the unit. Sedimentary structures consist of planar tabular (SpB), low angle cross-bedding (Splx), ripple cross laminations (Sr) and slumping (Shc). The unit ranges in thickness between 0.13 and 2.3m. The grains are moderately to moderately well sorted with subangular to subrounded shapes. Claystone clasts are more common in this unit than facies 5.3. Towards the top of these units, the angle of dip increases which points towards trough cross-bedding. The foresets also tends to have a normal grading texture with carbonaceous laminae and spaced or stepped laminae. The foresets tend to grade to thick bedded units towards the top. Furthermore, this unit also occurs as inclined cross-stratified and ripples laminated heterolythic alternations of fU to vfU sandstone and mudstone. Finer grained material such as the heterolythic (more lenticular bedding) is associated with ripple laminations. This unit usually shows no bioturbation but towards the top with associated backfilled estuarine deposits *Macaronichnus* and *Paleophycus* burrows occur (BI=3). The unit occurs as interchannel bars associated with distributary channels or as crevasse splays (more finely grained with ripple laminations) associated with interdistributary bays.

Facies 4.3 (Figure 4.1.8)

Massive (Sm) to planar horizontal laminated (Sh) fU to mU sandstones. The unit is usually moderately well sorted but poorly sorted units also occur throughout the succession. The unit ranges in thickness between 0.15 and 3.3m. The horizontal laminations (Sh) are also normally

graded in some intervals (spaced lamination). In some parts also consist of parallel bedded cL sandstone with interlaminated fluidized carbonaceous mud, which is associated with fine-grained channels. The grains are subangular to subrounded in shape. The upper and lower contacts are usually gradational. Carbonaceous material and pyritic nodules are common and bioturbation is rare (BI=0-1) with the occurrence of *Fugichnia* burrows. These facies shows normal grading textures within horizontal sets as well. The contact boundaries are gradational to erosional gradational between the massive and planar horizontal bedding. These facies also tend to grade into Facies 5.2 possibly because of trough cross bedding.

Facies 4.4 (lower delta plain Interdistributary bay and crevasse splay subdeltas) (Figure 4.1.9)

Olive to dark grey claystone with vfU-vfL sandstone/siltstone interbeds (Heterolythic). The boundary contacts are sharp, ranges from undulating to planar horizontally laminated (Fl), and gradational contacts with ripped up clasts (mantle and swirl structures). This unit is similar in composition to the inter distributary terminal channel regions but they are largely associated with distributary channels (some overlap does occur). The unit ranges in thicknesses between 0.45m and 2.35. The unit especially becomes thicker with associated crevasse splays (2.35m). Microscale gradational contacts are evident with overall coarsening upward cycles occurring as well. Massive claystone (Fm) usually grades to interbedded and interlaminated vfL sandstone and claystone/siltstone and eventually towards a massive to faintly laminated vfL sandstone at the top of the sequence. These facies are not calcareous and are largely massive in nature. These units sometimes exist as massive siltstone bedding on its own. The olive grey-green siltstone shows planar horizontal to undulating lamination (Close to wave-rippled bedding) with plant or coal fragments as carbonaceous laminae in between. Carbonaceous material consists of wood fragments. Ripple laminations (Sr) are also common with shale partings especially towards the transitional zone between interdistributary bays and backfilled estuarine embayments. Bioturbation is rare with associated crevasse splay but can become locally highly bioturbated (BI 3-4) with some horizontal burrows occurring (*Paleophycus*) (BI=1). These floodplain/interdistributary bays associated with channels contains highly bioturbated tops with calichified tunnel burrows of *Camborygma* or *Loloichnus* traces as well as mantle and swirl structures. In general, the ichnodiversity and ichnofacies abundances are low. The upper part of this unit becomes siltier as Facies 3.2 is reached. These facies also occurs interbedded with cL

sandstone that shows double mud drapes (Facies 4.1). The unit that occurs with Facies 4 (Channels) is more calcareous with caliches (and finer grained siltstone/claystone) towards the top of the unit. These facies also tend to grade to wave rippled laminae with bioturbation of marine trace fossils towards the top as Facies 5.1 is reached.

Interpretation: These deposits are classified as part of the lower delta plain facies. Erosive to sharp based lower boundaries with fining upward sequences are related to channelized bodies (Rossi & Steel, 2016). These channels tend to incise into interdistributary bays/floodplain deposits and mouth bars towards the bottom of the sequence. The carbonaceous material is the result of anoxic swampy conditions with interbeds of sandstone as the result of bank-full flooding of nearby channels into interchannel areas (Miall, 1996). Towards the top, the unit tends to grade to estuarine or lagoonal bay mudstone (thin bedded) or erosionally-based sequences. The distributary channels consist predominantly of planar bedding and lamination and a lack of cross-bedding, which could be a result of major flooding within the major channel (Tunbridge, 1981) and on the floodplain or due to shallow-water depth channels that promotes upper flow regime conditions (Reineck & Singh, 1980). Kastner et al. (2017) found that distributary channels associated with large mouth bar and terminal distributary channels are shallow and wide due to deposition occurring at the mouth of the river. This coincides with this unit occurring stratigraphically above older terminal distributary/mouth bar deposits. Also, the occurrence of low-angle to planar horizontal lamination and good sorting can be attributed to wave influence on these bar forms (Rossi & Steel, 2016), but the erosionally-based bottom and the occurrence of floating claystone clasts has been interpreted as wave/tide influenced distributary channels (Hovikoski et al., 2008). The absence of beach-ridge facies or classifying these units as foreshore-backshore facies or even tempestites is due to the lack of concrete facies evidence indicative of these zones (such as high angle cross-bedding, plant debris and representative ichnofacies assemblages) (Davies et al., 1971; Dickinson et al., 1972).

Erosionally based finer-grained channels (mud-dominated channel fills of Legler et al., 2013) also occur. These channels are dominated by planar horizontal laminated claystone and siltstone, which is possibly because of transitional turbulent, or plug flow forming ‘fluidized mud’ (Mackay and Dalrymple, 2011). This is further supported by the occurrence of low angle heterolythic alternations of ‘fluidized mud’ (with ripple laminations (SM1 facies of Mackay and

Dalrymple, 2011)) and sandstones that is indicative of higher energy settings. These facies also tend to occur in channel-fill sequences that are possibly because of the turbidity maximum zone (Van den Berg et al., 2007; Mackay and Dalrymple, 2011).

The low bioturbation indexes with rare occurrences of bioturbated intervals can be attributed to a stressed environment where the occurrence of highly bioturbated intervals being restricted to channel abandonment with low ichnodiversities but higher ichnodensities (Rossi & Steel, 2016). The occurrence of calichified burrows is largely restricted to emergence of the channel and subsequent abandonment.

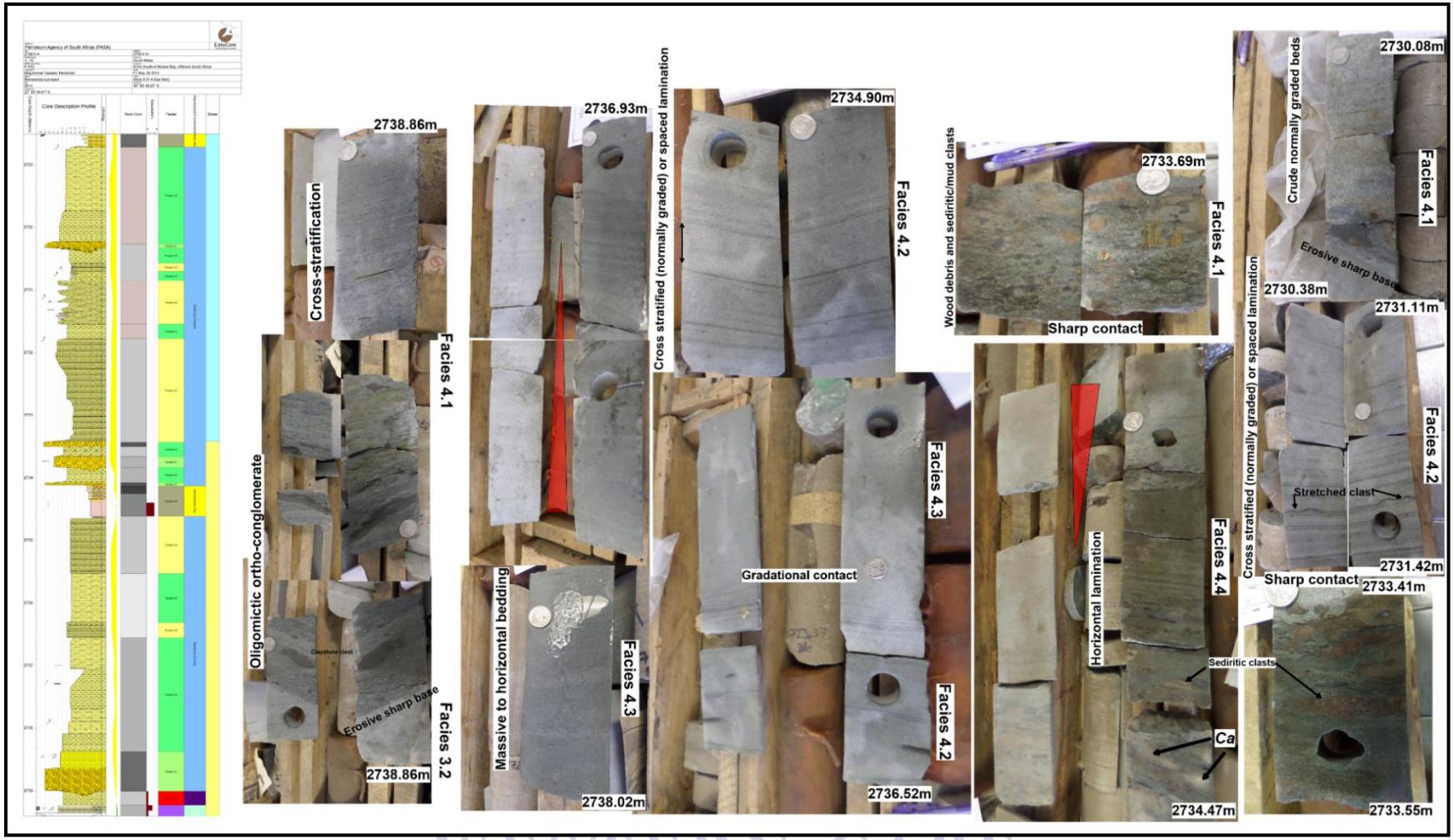

Figure 4.1.8: Examples of facies association 4 showing distributary channels with their finer grained counterparts or interdistributary bay deposits. Trace fossils consisted of fugichnia-like traces, Camborygma (Ca), Paleophycus (Pa) and Macaronichnus (M). Sediritic clasts and inversely graded units are also common.

Figure 4.1.9: Examples of facies association 4 showing interdistributary bays and crevasse splay deposits. Trace fossils consisted of Paleophycus (Pa), mantle/swirl structures (ms) and Camborygma (Ca). Pyrite nodules are also a common diagenetic mineral. Thick bottomsets also occur that are irregularly structured indicative of transitional type tidally influenced environments.

Table 1: Summarized facies associations of the regressive element complex assemblage set section F-A12 with associated facies elements and complexes. Refer to Appendix A (Table A1) for facies element code descriptions

Facies elements	Facies complex	Facies association
Sm, Sw, Shl, and Sr (including SM1 and SM2)	Facies 1.1 (Middle to distal delta front area and delta fringe facies)	FA1.1 (Distal-middle Delta front platform/mud rich delta front sheet and lobe facies)
Spb, Sp, Sr	Facies 1.2 (1.2A1 and 1.2A2)	FA1.2 (Tidal bar) Middle to distal delta front subtidal sand bars), offshore tidal bar.
Splx and Shl, Sp, Sh, Sr, Spl Fm, Sin Sh, Sw, Sr, Splx to Sm Gmd, Shc	Facies 2.1 Facies 2.2 Facies 2.3 Facies 2.4	FA2 (Proximal delta front/intertidal shoal with channelized delta front lobe facies or terminal distributary channels) or (Proximally confined tidal bars on the upper delta front with turbidites/hyperpycnal event flows (debrites))
Fm, Fl, SM2 Sm, Sl, Spb Shl with Sm and Fm Sl to Splx, Sw, Sr, Shc	Facies 3.1 Facies 3.2 Facies 3.3 Facies 3.4	FA3 (Lower delta plain to proximal delta front (distal intertidal delta platform) mouth bars with associated terminal distributary channels and interdistributary bays with crevasse splay subdeltas (inter-terminal distributary regions)
Gp, Spl and Spb Spl and SpB, Splx, Sr, Shc Sm, Sh Fl, Fm, Sr	Facies 4.1 Facies 4.2 Facies 4.3 Facies 4.4	FA4 (Coastal plain) Distributary channels with Interdistribtary bays and crevasse splay sub-deltas

Facies associations of the transgressional phase or transgressive element complex assemblage set (Table 2)

Facies association 5 (Outer embayment or offshore transgressive mudstones with proximal tidal bars)

Facies 5.1 (Figure 4.1.10)

Interbedded light greenish grey massive (Fm) (olive green and light to medium grey) to faintly laminated siltstone and mudstone (Fl). Intercalated massive (Sm) vfL to fU sandstone beds occur, especially towards the top with an erosional base. Carbonaceous fragments occur as lignite flakes in part but not abundant, more argillaceous. Floating quartz, siltstone and claystone clasts occur, usually associated with transgressive lags. Siderite and calcareous concretions and staining occur throughout the facies (diagenetic halos). This unit shows a thickness that ranges between 0.17m and 14m. Sedimentary structures consist mostly of massive bedding (Mb) but where parallel lamination occurs is mostly disrupted by bioturbation. Ripple laminations and climbing ripple laminations also occur frequently, especially towards the top of the whole unit. A BI index of 2-4 occurs. Trace fossils consist of *Planolites (P), Paleophycus (Pa)* (abundant), *Chondrites (Ch), Skolithos (Sk), Taenidium (Ta)* and *Epichnia*-type burrows and *Thalassinoides (Th).* Claystone clasts occur as disrupted saturated clasts.

Facies 5.2 (Proximal tidal bars) (Figure 4.1.11)

A cross-bedded (Spb) fL sandstone that grades to a horizontally laminated heterolythic (Fl) argillaceous siltstone and massive claystone (facies 5.1). The facies is 4.3m in thickness. This unit shows fining-upward sequences with planar erosive or erosional external basal contacts and gradational internal bedding contacts. Calcareous in nature with sparatic calcite grains which could be representative of shell fragments. Bioturbation is restricted to certain intervals but consist largely of *Macaronichnus (M)* burrows (low diversity but high abundance ichnofabric) and rarer *Paleophycus (Pa).*

Interpretation: The occurrence of abundant bioturbation, finer grain sizes, are indicative of a low-energy setting (Visher, 1969; Chen et al., 2014). This type of setting can be interpreted as a central embayment environment (Jackson et al., 2005) or lagoon environment. This unit is also equivalent to the mud flats in an estuarine setting that is capped by an erosively based vfL sandstone that is indicative of tidal creeks or small scale channels (equivalent to the crevasse splay deposit in a deltaic setting) (Lin et al., 2018). The abundant trace fossils (low ichnodiversity) are indicative of conditions that allowed certain organisms to strive (opportunistic organisms). The massive bedding, due to fluidized mud deposition (as evidence from saturated claystone clasts) and bioturbation, is evident that periodic influxes of sediment occurred, thus indicating zones of intense bioturbation as fluctuations in fluvial power. Facies 5.1

resembles the open bay and offshore lacustrine facies of Ta et al. (2002) and Melchor (2004). The only difference is the occurrence of intercalated vfL sandstone that is a result of high-frequency flooding (Rossi & Steel, 2016) proximal to a major fluvial output. The association of these facies with major distributary channels are representative of minor half cycle transgressions (allocyclic possibly) where channels are backfilled as estuarine deposits (Salahuddin & Lambiase, 2013; Lambiase et al., 2017).

The siderite staining makes the burrows more visible which is referred to as ‘preferred tube cementation’ that enhances the variability of diagenetic changes (Knaust and Bromley, 2012). This unit is similar to the subaqueous delta platform as described by Mellere et al. (2016) but the finer grained facies with similar sedimentary structures are rather suggested as outer embayment facies with migrating tidal bars.

Figure 4.1.10: Examples of facies association 5 showing offshore transgressive or embayment mudstones. Trace fossils consisted of chondrites (Ch), Skolithos (Sk), Paleophycus (Pa), Thalassinoides (Th), Taenidium (Ta) and cryptically bioturbated structures (fine matrix). Pyrite and siderite nodules and staining are common.

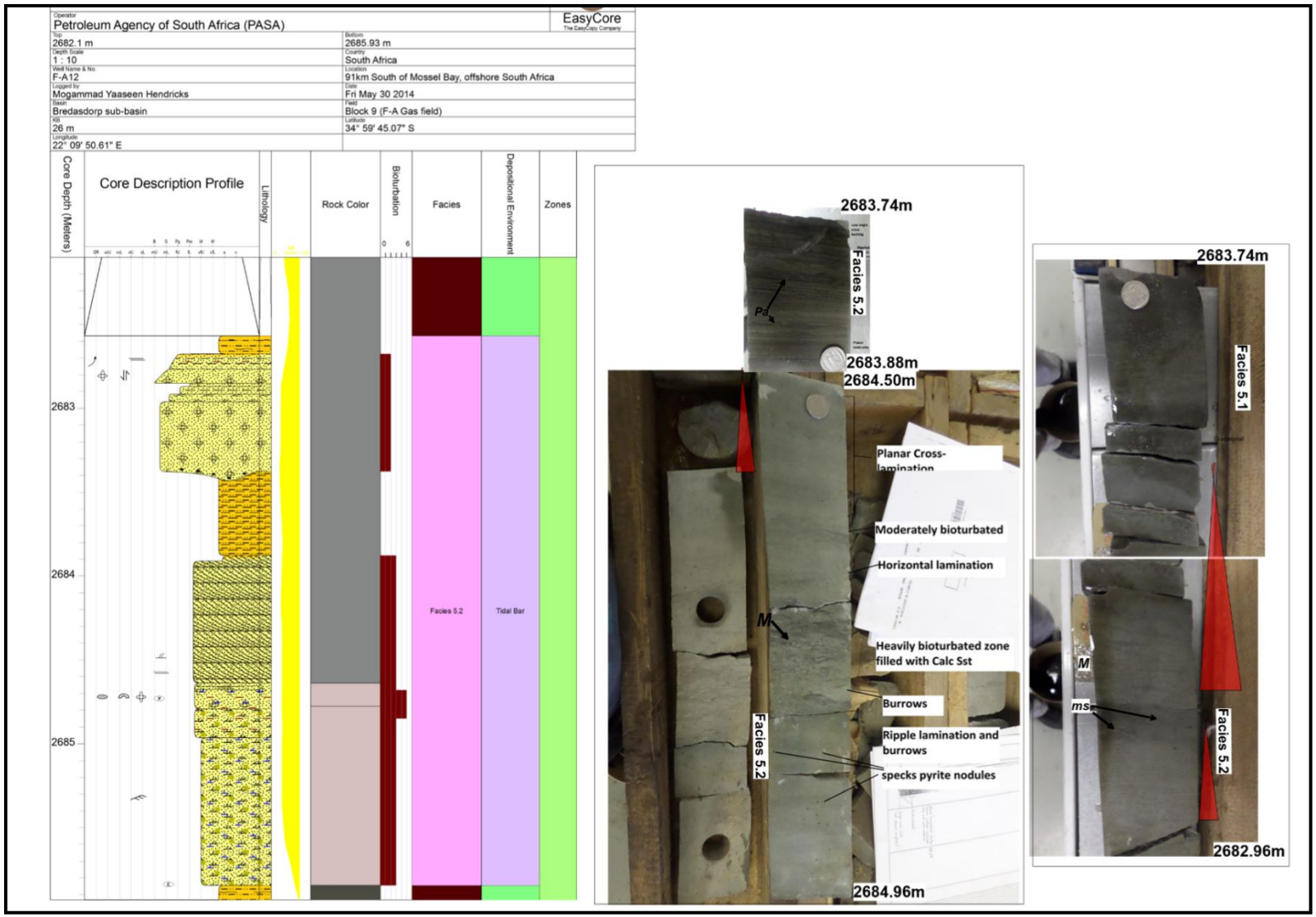

Figure 4.1.11: Examples of facies association 5 showing tidal bars. Trace fossils included dense populations of Macaronichnus (M) with minor occurrences of mantle/swirl (ms) structures and Paleophycus (Pa). Paleophycus burrows are more restricted to the finer grained material. Fining-upward sequences also occur regularly.

Facies association 6 (Figure 4.1.12) Subaqueous subtidal sand ridges and compound dune fields

Facies 6.1

Facies 6.1 consists of a massive (Sm) light-medium green-grey, mL-fU (make this into two) moderately to highly bioturbated (Sb) glauconitic sandstone. Abundant *Crinoid* shell fragments (coarse) with medium-grey pyritic mud drapes are very common. Grains are moderately well to well sorted and are subrounded to rounded in shape. Subangular grains also occur but are restricted to particular beds. Abundant quartz and feldspars with minor argillaceous mica grains (restricted to the mud drapes). Minor silty-sand (vfU to fL) texture with floating claystone and quartz clasts (1-4mm) also occur, which usually forms part of fining-upward sequences. The unit ranges in thickness between 4.62m to 14.6m. Evidence of mL sandstone associated with highly bioturbated areas is common.

Sedimentary structures are rare, but low-angle to horizontal lamination (Splx to Sh) with weakly defined disturbed mud drapes does occur. Evidence of cross-stratification (planar tabular cross-bedding and trough cross-bedding (Spl/Spb)) and ripple lamination (Sr) occurs but very faintly. Cross-bedded foresets are usually tangential or asymptotic and consist of mud drapes. Where planar lamination (Sh) occurs undisturbed, the laminae are usually argillaceous (micaceous bands) and carbonaceous in composition. The boundary between low-angle/horizontal bedding and cross bedding is usually master surfaces on which the foresets terminate. Disturbed bedding is also common due to bioturbation, but syn-depositional structures such as slumping and micro-faults are common.

The bioturbation index is in the range of 3-6 (6 in intensely bioturbated zones). Weakly defined to Cryptic heterogeneities of bioturbation (mud drapes altered) is common with *Macaronichnus (M)*, *Ophiomorpha rudis (Or)*, *Paleophycus (Pa)*, *Siphonichnus ophthalmoides (Si)*, *Beaconites*/*Scolicia (Be/Sc)*, *Thalassinoides* and possible *Planolites* (*P*). Macaronichnus occurs throughout the interval as cryptic small-diameter burrows but the other trace fossils dominate certain intervals. The grain sizes within these burrows are coarser (homogeneous active fills) and contain mU sandstone grains, as noted earlier with areas of high bioturbation. Thin section analysis reveals the occurrence of echinoderms that commonly forms the trace fossil Scolicia or *Beaconites*. Bivalve casts also occurs which are completely diagenetically altered with burrow-

fills that are calcareous in nature where the surrounding or host-rock is not calcareous. Occasional floating claystone clasts occur throughout the facies. Diagenetic minerals are also found throughout the facies, which consist largely of calcareous concretions (casts), pyritic nodules and pyritized zones. Glauconite also tends to decrease from top to bottom of the unit.

Facies 6.2

These facies consist of an interlaminated black shale (claystone) and medium-dark grey siltstone (Fl). Sedimentary structures consist of planar laminations (Fl) between shale and medium-grained siltstone. The facies is 0.06m thick and forms the possible fining-upward boundary of the proximal tidal bars with gradational overlying compound dune fields and tidal sand ridges. Unpublished paleontological reports suggest it contains diverse radiolarian assemblages and benthonic foraminifera. There are no visible trace fossils that occur throughout these facies.

Facies 6.3

These facies consist of granule to pebble stringers of clasts that are largely matrix-supported and polymictic (Gmd). The granule-pebble conglomerate is light grey, indurated, poorly sorted, contains green to grey claystone and siltstone, quartz and green sandstone clasts (ranging from 2mm to 10mm). Shows predominantly low sphericity, rounded, oblate to prolate siltstone and claystone clasts. The quartz grains are bladed and subrounded with a high sphericity. Coarse shell debris is commonly found aggregated in the conglomerate. The unit has a thickness of 0.03m. Bioturbation is rare (BI=0). The matrix is composed of the surrounding fine-grained sandstone (possibly intraformational). Occurs at the base of fining upward sequences.

Interpretation: The glauconite in these facies has been interpreted as allochthonous glauconite as revealed by thin section analysis of glauconite minerals and the surrounding mineral grains (Amorosi et al., 2012). According to Odin (1985), the occurrence of glauconite are usually indicative of continental shelves and slopes (water depths of 50 to 500m), therefore Shanmugam et al. (2000) interpreted these units as shelf deposits or an open shallow marine setting. The fluctuating bioturbation intensities, cross-stratification with master surfaces (2D and 3D dunes) and interlaminated claystone/siltstone all points towards tidal sandridges with its accompanied inter-trough regions with the migration of initial tidal bars and evolving to sand ridges or sand sheets on an open shelf setting (Desjardins et al., 2012; Olariu et al., 2012a).

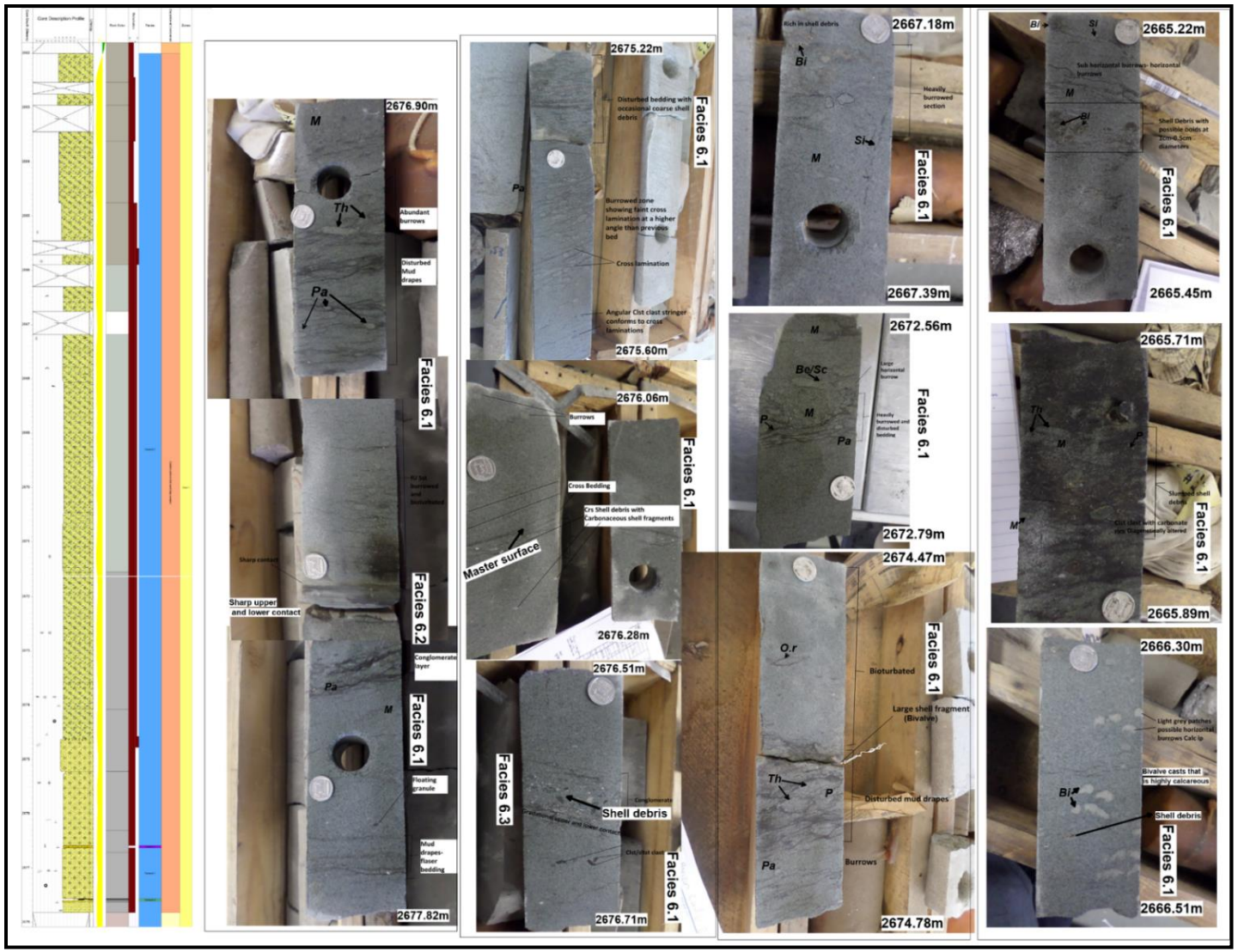

Figure 4.1.12: Examples of facies association 6 showing tidal sand ridges and compound dune fields. Trace fossils are abundant and consisted of Macaronichnus (M), Paleophycus (Pa), Thalassinoides (Th), Planolites (P), Ophiomorpha rudis (O.r), Beaconites/ Scolicia (Be/Sc), Siphonichnus ophthalmoides (Si) and bivalve casts (Bi).

Table 2: Summarized facies associations of the transgressive element complex assemblage set section F-A12 with associated facies elements and complexes. Refer to Appendix A (Table A1) for facies element code descriptions

Facies elements	Facies complex	Facies association
Fm, Fl, Sm, Mb Fl, Spb	Facies 5.1 Facies 5.2	FA5 ((Outer embayment or offshore transgressive mudstones and proximal tidal bars)
Sm, Sb, Splx to Sh, Spl/Spb, Sr, Sh Fl Gmd	Facies 6.1 Facies 6.2 Facies 6.3	FA6 (Subaqueous subtidal sand ridges and compound dune)

4.1.2 Well: F-AR1

The blocky nature (Aeolian (sand dunes, tidal sands)) and slight coarsening upward nature of the gamma ray log shapes shows a uniform or monotonous grain size throughout the cored interval indicating a reworked uniform energetic environment with an aggradational signature and minor 5^{th} to 6^{th} order fluctuations of paleo-shoreline activity. The evidence of glauconite (accessory 15-20% rock volume) throughout the cored section indicates that it is part of a siliciclastic shallow reworked marine environment (Amorosi et al., 2012).

4.1.2.1 Seismic Facies

Seismic Facies 2 consist of sub-parallel (2A) and shingling reflection (2B) configurations (Figure 4.1.13). Further down-dip there is a change from sub-parallel to sigmoid progradation and shingled configurations (associated with bottomsets) (ABC method shows two seismic facies). There is a moderate to high amplitude and the reflections are semi-continuous. Low to high frequencies occurs throughout the seismic facies. Sediment supply (or sediment transport direction) came from the SW.

Interpretation: The resolution of the seismic section was poor and no detailed seismic facies within one unit could be performed. The topsets are marked by continuous to semi-continuous reflections and this is usually indicative of sedimentation conditions were rather uniform. Towards the bottom of the sections the conditions changes to rather semi-continuous to

discontinuous reflectors which indicates rapid changes in depositional energy levels, indicative of fluvial to marine transitional facies.

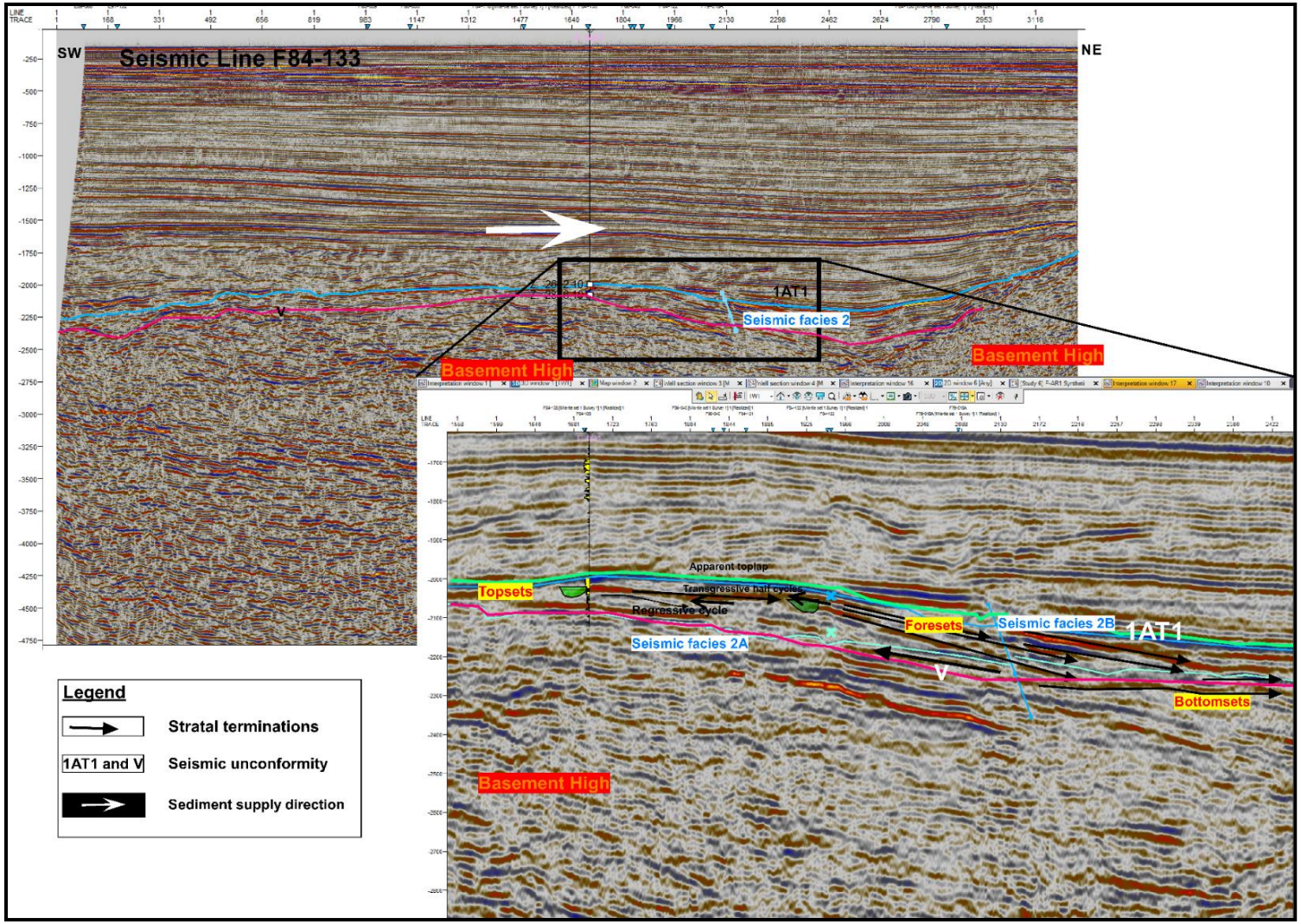

Figure 4.1.13: Study interval with interpreted seismic horizons (1AT1-V horizon) showing seismic facies 2 (2A and 2B) and stratal terminations. Topsets, foresets and bottom sets are seen within the studied interval. The sediment supply direction (white arrow) is shown.

4.1.2.2 Reservoir zones

There were four reservoir zones identified in this well (Figure 4.1.14), but only the top interval of this unit was cored (reservoir zone 1) and formed the focus of this study. This reservoir zone formed a 65m interval that is capped by an extensive regional unconformity or subsequent transgressive, offshore shales (extremely low gamma ray values). The large difference in the density and neutron logs (lower neutron and hydrogen interactions in gas) largely indicates a gas zone that is very porous (high resistivity readings) (Figure 4.1.14). The porosity readings are supported by conventional unpublished reports and are expanded upon in Table B3, Appendix B. Thus showing that this unit is indicative of an excellent porosity but poor permeability. Reservoir zone 2, 3 and 4 shows a very high sand-shale ratio indicating that connectivity between the reservoirs are quite high with minor fluid barriers (as compared to the other 2 wells). Reservoir zone 3 and 4 shows rare to no indication of porous or hydrocarbon-bearing units. Reservoir zone 2 indicates an oil-bearing reservoir with low gamma ray values, high resistivity values and neutron/ density cross-overs. Reservoir zone 2 shows that the flooding surfaces acts as fluid barriers and therefore can be identified as a compartmentalized reservoir interval.

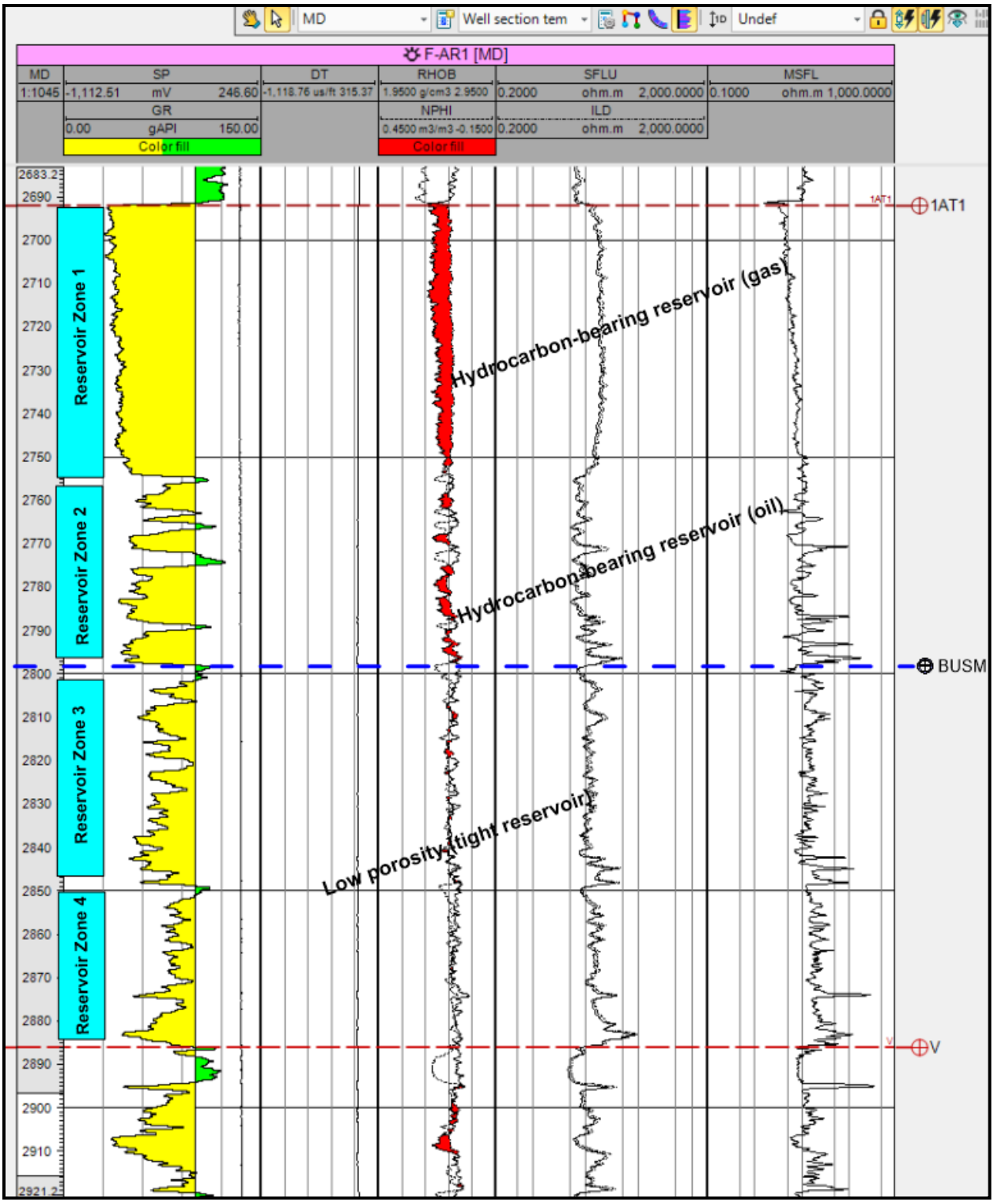

Figure 4.1.14: Reservoir zones and corresponding geophysical logs with interpreted hydrocarbon potential of F-AR1. GR- Gamma Ray log, DT-Sonic log, RHOB-Density log, NPHI-Neutron log, SFLU-Shallow resistivity, ILD- Deep resistivity logs and MSFL-Medium Resistivity logs.

4.1.2.3 Lithofacies

Facies Association 6 (Figure 4.1.15A and Table 3) Tidal sand ridges and compound dune fields

This facies association correlates with facies association 6 from well F-A12. Facies 6.1 has been divided into two parts in this well because of their features being more distinct than the facies 6.1 in well F-A12. This variation has been recorded here as separate due to the lateral facies variations, especially in trace fossil diversities and intensities).

Facies 6.1a (Figure 4.1.15B)

Massive (Sm) to faintly or wavy laminated (Slf), light grey to off-white (some places clean white), hard, compacted, fU-mL sandstone (ranges from 0.15m to 7.5m thick amalgamated bedsets) with calcareous nodules and thin drapes of carbonaceous mudstone. Sedimentary structures are Sm, Sh mud draped cross bedding (Spb). Grains are subrounded and well sorted. At several places throughout the unit it shows a bimodal distribution of vfU sandstone well to moderately well sorted can be seen. Cryptic to weakly defined bioturbation is evident as well as horizontal burrows. *Ophiomorpha Irregulaire (Oi)* burrows are common and starts at 2740.75m (visible). The occurrence of *Macaronichnus segregatis (M), Planolites (P), Skolithos (Sk), Paleophycus (Pa), Beaconites (Be), Siphonichnus ophthalmoides (Si)* with casts of producing bivalves (Bi) and horizontal burrows of *Thalassinoides* which occurs throughout(Figure 4.1.16A, B, C, D, E). Mud drapes are organic rich (around <8mm thick) and are distributed in a random manner (no evidence of cyclicity) as seen in figure as well. These drapes occur disseminated and as single or double mud layers (crinkled and straight) and where thick layers are found to be partly laminated. These continuous and disseminated drapes are largely carbonaceous but some occurs as mudstone drapes (Figure 4.1.15). Drapes occurs, in part, as weakly defined low-angle cross-stratified and horizontal bedded drapes (2°-9°) and are found at places where bioturbation intensity has decreased. Calcareous nodules range in diameter from 1-2cm and occur as poikilotopic cemented patches or nodules (equant) (Figure 4.1.15). Quartz grain boundaries are sutured with plagioclase alteration common. Pyrite nodules occur disseminated and as pyritized zones (2701.63m), but large nodules found at 2735.74m and 2698.9m. At 2735.74m, ‘weakly defined’ bioturbation with the disappearance of the calcareous nodules is evident. Asymptotic cross beds are also found but believed to be part of larger bedform migration at 2728.81m. The

interconnected trace fossils accounts possibly for most of the massive nature of the sediment. Occasional shell fragments occur at around 2713.2m.

Facies 6.1b (Figure 4.1.15C)

Low to high angle cross-stratified (Splx and Spb) (some places bidirectional Shb)), light grey to off-white, hard, compacted, fL-fU sandstone (ranges from 0.08m to 1.5m thick bedsets). Occasional vfU sandstone intercalated. The grains are moderately well sorted with rounded to subrounded grains. This unit can be described as trough cross-bedding based on the gradational change of bedding angle and reactivation surfaces. Sedimentary structures are Sp and Sr. This unit is largely synonymous and gradational to facies 6.1a. The unit is largely disturbed and shows cryptically bioturbated sandstone in some places, but evidence of an increase and decrease in the dip angles (low angle maximum dip of 8°) occur throughout as well as evidence of large scale cross bedding (trough or planar but large scale subaqueous dunes (Spb)). The trace fossils that occur are the same as facies 6.1a with the occurrence of *Fugichnia-like* traces (Figure 4.1.16F). Calcareous nodules also occur within this unit. Herringbone cross stratification is also recorded (Figure 4.4). Occasional granules occur locally. Mud drapes consist largely of siltstone. Steeply dipping drapes occur at 2704.75m.

Facies 6.3 (Figure 4.1.15D)

Low-angle cross-bedded to planar bedded (Splx to Sh), medium grey, hard, compacted, fL pebbly sandstone (Gmd) (0.38m thick bedset). Sedimentary structures are Sh and Splx. Matrix is well sorted and contains rounded to subrounded grains. Pyrite nodules are also common throughout. Pebble-granule clasts are less than 0.5cm. Bioturbation is moderate to rare. Rare to absent trace fossils. Pebbles are disseminated and not particularly aligned with bedding planes.

Interpretation: These facies are similar to the association in F-A12 but their variations, especially in sedimentary structure-visibility or trace fossil occurrences are more distinct. The massive and faint laminations could be interpreted as due to bioturbation and rapid aggradation. This is considered a high-energy environment from gamma ray logs (fine grain size under a marine hydraulic regime), so the places where bioturbation is evident, it can be considered the sole reason for the massive nature of the sandstone. The faint lamination or pseudo laminations can be interpreted as wave ripple bedding according to Gietelink (1973), but not all drapes are curved

and this interpretation should be avoided if there is not sufficient evidence. The comminuted and disseminated shell fragments can be considered as the result of reworking from barrier bar complexes through tidal, wave or oceanic currents. Compacted glauconite and sutured boundaries provides evidence towards the compaction of this unit.

An increase in drape intensity (tidal settings) is a result of the decrease in bioturbation and reworking (Gingras & MacEachern, 2012; Gingras et al., 2012b). The nature of these sediments being highly bioturbated, fully and partially, makes it difficult to interpret in terms of interpreting the depositional environment using sedimentary structures. Trace fossil assemblages and glauconite occurrence can contribute immensely to the identification of the depositional environment.

The evidence of single or double mud layers and the massive nature of this unit cannot be attributed to tidal action as the only driving force and careful consideration of other factors, like an abnormally high suspended sediment concentration, low current velocities and low wave intensity over a long period could be evidence for their occurrence (McCave 1970; Allen, 1982). Since facies 6.2 is absent in this well, a high suspended sediment concentration can be ruled out in the proximal part of this association and the occurrence of facies 6.2 in well F-A12 would be attributed to a high suspended sediment concentration in the distal part of the association. The high-suspended sediment concentration can be due to the proximal basement highs.

There are evidence of ‘weakly defined’ and ‘cryptic’ bioturbation which suggest deposition within an upper (close to foreshore)-middle subtidal environment (Gingras et al., 2012a). This bioturbation is common among trace fossils of *Ophiomorpha irregulaire (Oi)* and *Thalassinoides* ichnofacies. The sudden increase in the visibility of burrows (in general) can be attributed to a ‘colonization window’ (Gingras et al., 2012a). The sub-environment of deposition for this unit has been interpreted to be part of a migrating compound dune field that grades to a sandsheet (sandwave or tidal sand ridges). This is also further supported by the occurrence of a clean white sandstone and large-scale trough cross-bedding of Facies 6.2 (with *Thalassinoides* burrows) that are indicative of close-to-shoreline settings. The evidence of ‘true’ mud drapes that are indicative of subaqueous controlled (channelized) flows also further supports this shoreline proximal setting. The lower part of this unit is rarely visibly bioturbated and this nature can be attributed the compound dune fields with thick mud drapes. This unit is characterized by its moderate-high

sedimentation rates, high to moderate energy environment with abundant reactivation surfaces (crinkled mud drapes) and mud deposition occurring on low angle to planar horizontal beds of bottomsets. The large-scale planar bedding, low-angle and high angle cross-bedded sandstone is the result of subaqueous dune migration within the subtidal zone. This unit can be interpreted to have a small 'colonization window' due to rapid aggradation (Desjardins et al., 2012). The upper unit (where bioturbation intensity increases) is interpreted to be part of the sandsheet core-margin within the subtidal environment. This environment can be characterized based on its increased evidence of bioturbation and the low dipping angles of depositional dune fields (Desjardins et al., 2012).

In addition, glauconite is unlikely to form in a transitional environment and are restricted in their formation to shoreface (upper, middle and lower) or offshore zones, but reworking and winnowing can occur during marine regressions and transgressions (personal communication, Compton; Wigley and Compton, 2007; Amorosi et al., 2012). The occurrence of glauconite (Figure 4.1.15B) is evident that there was a marine influence (oxygenated to slightly reducing conditions) in an upper shoreface or subtidal zone. There is evidence that the glauconite was reworked (under 3rdto 4th order transgressions) due to the unit being thicker than 10m, the well sorted nature of the glauconite with surrounding grains, the common occurrence of glauconite within finer grained sediments (fU) and the percentage range of glauconite within the host rock all contributes to an allochthonous origin (Amorosi et al., 2012). In addition, the mud drapes, discussed earlier, is evident of tidal currents, which is a major contributor and enhancer to the remobilization of glauconite grains.

The pebbles from Facies 6.3 are interpreted to have been reworked pebbles from the updip inlet (Jackson et al., 2005). The fact that these facies does not occur with erosional surfaces cannot be assumed that they formed under an erosional transgression (transgressive lag or wave ravinement surfaces). This is also further supported by the carbonaceous laminations that can be attributed to a major distributary or inlet channel further updip where woody material was common and the sedimentation rate was high within the depositional realm.

.

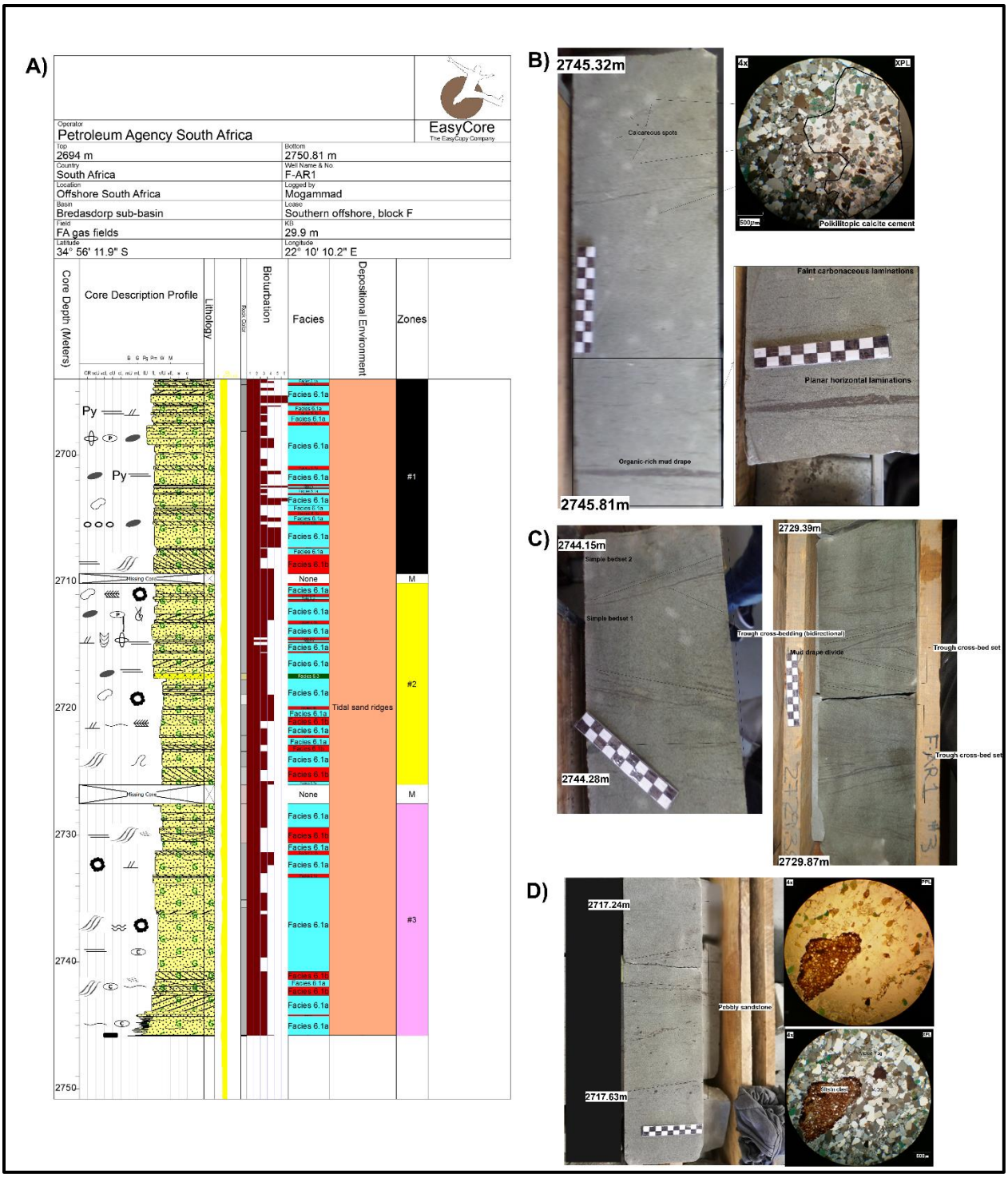

Figure 4.1.15: Examples of facies association 6 of F-AR1 showing tidal sand ridges and compound dune fields. A) Sedimentological log showing variable amounts of bioturbation. B) The occurrence of facies 6.1 showing cryptic bioturbation and massive bedding with occasional disrupted mud drapes. C) Large scale trough cross bedding and simple bedset boundaries (Facies 6.1b). D) Thin section analysis with siltstone clasts and pyrite nodules scattered in an isolated interval (Facies 6.3).

Figure 4.1.16: Trace fossils are diverse but abundant Macaronichnus (M) is common throughout the interval (forming cryptic bioturbation). Trace fossils species (ichnospecies) consisted of A) Thalassinoides (Th), Planolites (P) and Macaronichnus (M). B) Dominant Macaronichnus (M). C) Paleophycus, Macaronichnus (M), Ophiomorpha irregulaire (Oi). D) Thalassinoides (Th), Macaronichnus (M), Paleophycus (Pa), Skolithos (Sk) and Beaconites (Be). E) Bivalve casts (Bi) with associated Siphonichnus ophthalmoides (Si), Macaronichnus (M) and Paleophycus (Pa). F) Trace fossil occurrence is restricted to forsets of cross bedding as well with Planolites (P), Macaronichnus (M) and Fugichnia-like traces (fu). The fugichnia-like traces is due to rapid overloading of the cross bedded units sandwiched between bottomsets in migrating compound dune fields.

Table 3: Summarized facies associations of the transgressive element complex assemblage sets section of F-AR1 with associated facies elements and complexes. Refer to Appendix A (Table A1) for facies element code descriptions

Facies elements	Facies complex	Facies association
Sm, Slf, Sh, Spb	Facies 6.1a	FA 6 (Subaqueous subtidal sand ridges and compound dune)
Sr, Sp, Splx and Spb, minor Shb	Facies 6.1b	
Sh and Splx, Splx to Sh	Facies 6.3	

4.1.3 Well: F-A5

4.1.3.1 Seismic facies

Seismic facies 1.2 consist of chaotic to discontinuous and imbricated progradational seismic reflections, moderate to high amplitudes, medium to high frequencies (Figure 4.1.17). The red reflectors are abundant towards the bottom that is largely indicative of shale and shows external convex-upward geometries. The foresets present is largely intact and no indication of slumped external forms is seen. The sediment transport direction shows that most of the sediments were derived from the SSW direction (Proximal basement high).

Interpretation: These deposits have been interpreted as lacustrine basin-margin deposits. The seismic facies indicate a restricted basement with abundant and thick red reflectors. An imbricated progradational package is representative of progradation with early transgressions (Lin et al., 2018).

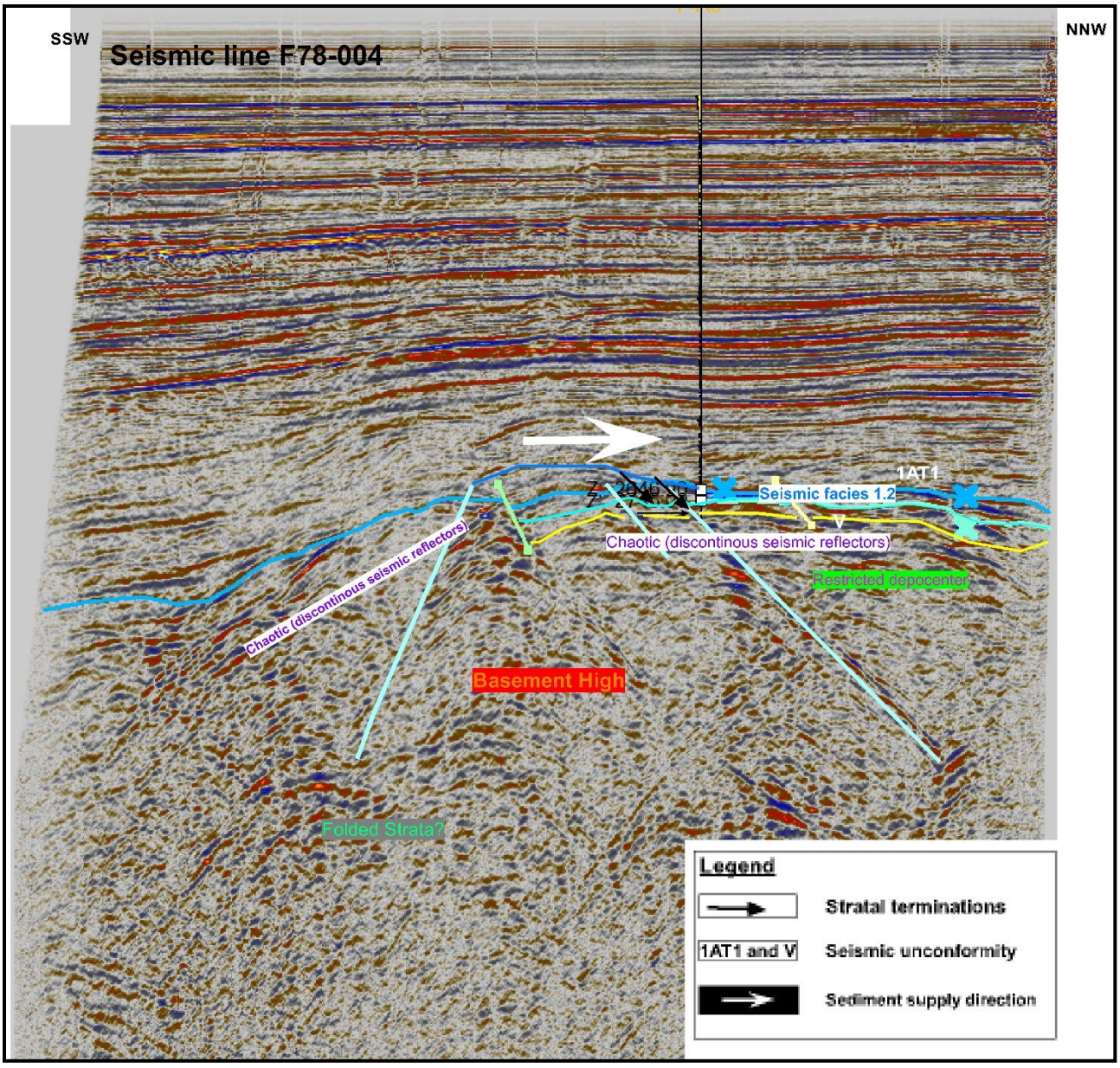

Figure 4.1.17: Study interval with interpreted seismic horizons (1AT1-V horizon) showing seismic facies 1.2 and stratal terminations. In addition, the basement high with possibly folded strata? The sediment supply direction (white arrow) is also displayed. This area is highly faulted with basement uplifts occurring.

4.1.3.2 Reservoir zones

Four reservoir zones have been identified in this wells cored section. Reservoir zone 4 occurs above the V-horizon and is underlain and overlain by shale (high gamma ray values). The zone shows some indication of hydrocarbon-bearing intervals but is not of good reservoir quality (high water content-low resistivity in places) and is identified as a tight reservoir with low

porosity. Reservoir zone 3 and 1 shows neutron-density cross-overs indicative of hydrocarbon-bearing fluids but the fluctuating resistivity values indicate that there are water-bearing units as well. These zones are also compartmentalized as they are separated largely by fluid barriers or non-reservoir units. Reservoir zone 2 shows a good indication of hydrocarbon bearing units with low gamma ray values, a neutron-density cross over and high resistivity values. The non-reservoir units or seals show good fluid barriers to the compartmentalized reservoir zones.

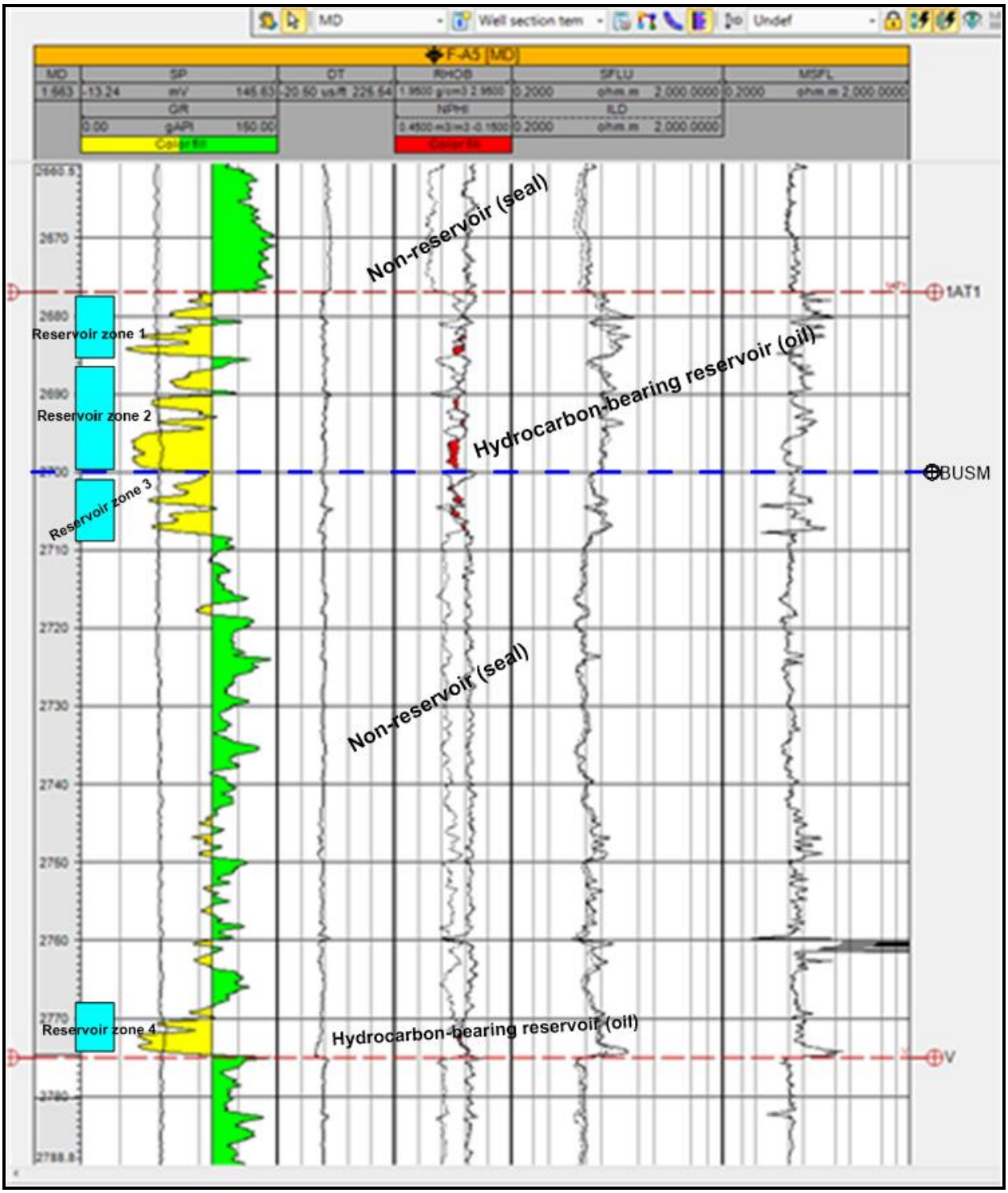

Figure 4.1.18: Reservoir zones and corresponding geophysical logs with interpreted hydrocarbon potential of F-A5. GR- Gamma Ray log, DT-Sonic log, RHOB-Density log, NPHI-Neutron log, SFLU-shallow resistivity, ILD- Deep resistivity logs and ILM-Medium Resistivity logs

4.1.3.3 Lithofacies

Regressional phase of F-A5 (Summarized in Table 4)

Facies Association 5 (Figure 4.1.19) Outer embayment or offshore transgressive mudstones

The occurrence of facies association 5 occurs in well F-A5 and F-A12. There is a clear distinction between the two wells (lateral variations) in terms of their trace fossil diversities and therefore it is envisaged that F-A5's occurrence is largely due to the restriction and anoxic conditions in a more distal setting than F-A12 association. Furthermore, facies association 5 in F-A12 occurs vertically with proximal tidal bars and therefore their paleo geographic position would be more proximal than F-A5.

Facies 5.1a

Massive claystone (Fm), dark greyish that occurs in part as dark green/grey claystone (thin section analysis), hard, comprising sub-angular to angular silt-sized grains (mostly quartz). The thickness of this unit ranges between 0.7m to 7.2m. This unit shows a gradational change from claystone to silty claystone and then mudstone (Facies 5.1b). This is typical of reverse grading. In addition, the boundary is a result of maximum alteration between the two lithologies and is indicative of the low permeability of facies 5.1a. Bioturbation is absent. No visual evidence of carbonaceous material. No evidence of marine/terrestrial trace fossils seen except for *Zoophycos?* and *Chondrites*? (BI=0).

Facies 5.1b

Massive mudstone (Fm) with siltstone in part, medium dark olive green, hard, comprising silt-sized fraction that are poorly sorted (bimodal grain size) and has subangular-angular quartz grains. The upper and basal contact of this unit is largely gradational. The unit thickness ranges from 1.44m to 3.6m. The clay matrix consists mainly of clay minerals such as smectite-illite. Thin section analysis revealed an iron-rich calcite. Sideritic and pyrite staining and nodules occurs (common from 2724.17m) and associated within fractures or synsedimentary micro-faults. Pyrite staining and nodules occur (occurring mostly from 2710.24m). Bioturbation is rare or indistinct (BI=0).

Interpretation: The dark claystone could be the result of carbonaceous material. The dark olive green and dark grey claystone is the result of anoxic conditions in a restricted estuarine embayment or offshore area (below storm wave base). The rare occurrence of opportunistic trace fossils usually indicates fluctuating anoxic-oxic conditions; this is also further supported by the occurrence of *Zoophycos ichnospecies* that during the Cretaceous were adapted to these conditions (Zhang et al., 2015). The claystone shows an inverse grading towards the mudstone indicating an increase in energy. Multiple pulses of higher energy increases, resulted in coarsening upward trends within the interbedded mudstone and claystone. These could be interpreted as multiple events of waxing and waning with suspension settling as the dominant depositional process during hyperpycnal flows (Li et al., 2015). The scarce bioturbation also proves this with waxing and waning flows, with the relative occurrence of opportunistic organisms, in a distal stressed environmental setting (prodelta/shelf environment) in addition to the mottled appearance and their relative stratigraphic position with facies association 7 (Gietelink, 1973; Li et al., 2015). Mellere et al. (2016) interpreted these deposits as suspension fall-out deposits (spillover) from nearby major channels on the distal intertidal delta platform or quiet environmental setting of the offshore shelf. Oanh Ta et al. (2002) interpreted these facies as outer embayment deposits with carbonate nodules occurring throughout the interval. Carr et al. (2003), Jackson et al. (2005) and Van Capelle et al. (2016) also interpreted this unit as an offshore environment below fairweather wave base. Yang et al. (2010) interpreted these deposits as a low-energy oxygenated shallow embayment. The shallow embayment interpretation can easily be accepted since the level of diagenetic alteration of sediments is abundant with a high level of pore-fluid percolation in a reduced subsurface setting.

This unit is diagenetically altered (green) and evidence of interstratal percolation of reducing water circulation can be seen (formation of illite). The colour can be attributed to the colour of illite and chlorite minerals. This intensity can only be observed if this unit was saturated with fluids (subaqueous reducing water setting) under increased water depths and coinciding pressures or a fluctuating water table column. The overall thickness of this unit and their relative stratigraphic location on seismic data suggest that this facies association was part of a mud-dominated marine depocenter (Young et al., 2000; Jackson et al., 2005)

The bioturbation intensity is rather complex since no visible burrows can be seen except for diagenetically altered nodules which could be attributed to *Chondrites* ichnogenus. These facies are the same as the offshore lacustrine facies association of Melchor (2004). The absence of visible ichnofossils does not necessarily mean that there were no bioturbation present and the massive nature of the unit could be due to intense bioturbation and supports the interpretation put forward by Mellere et al. (2016). However, as noted by Taylor et al. (1995), these ferroan carbonate nodules can also be attributed to near seafloor cementation during reduced sedimentation rates.

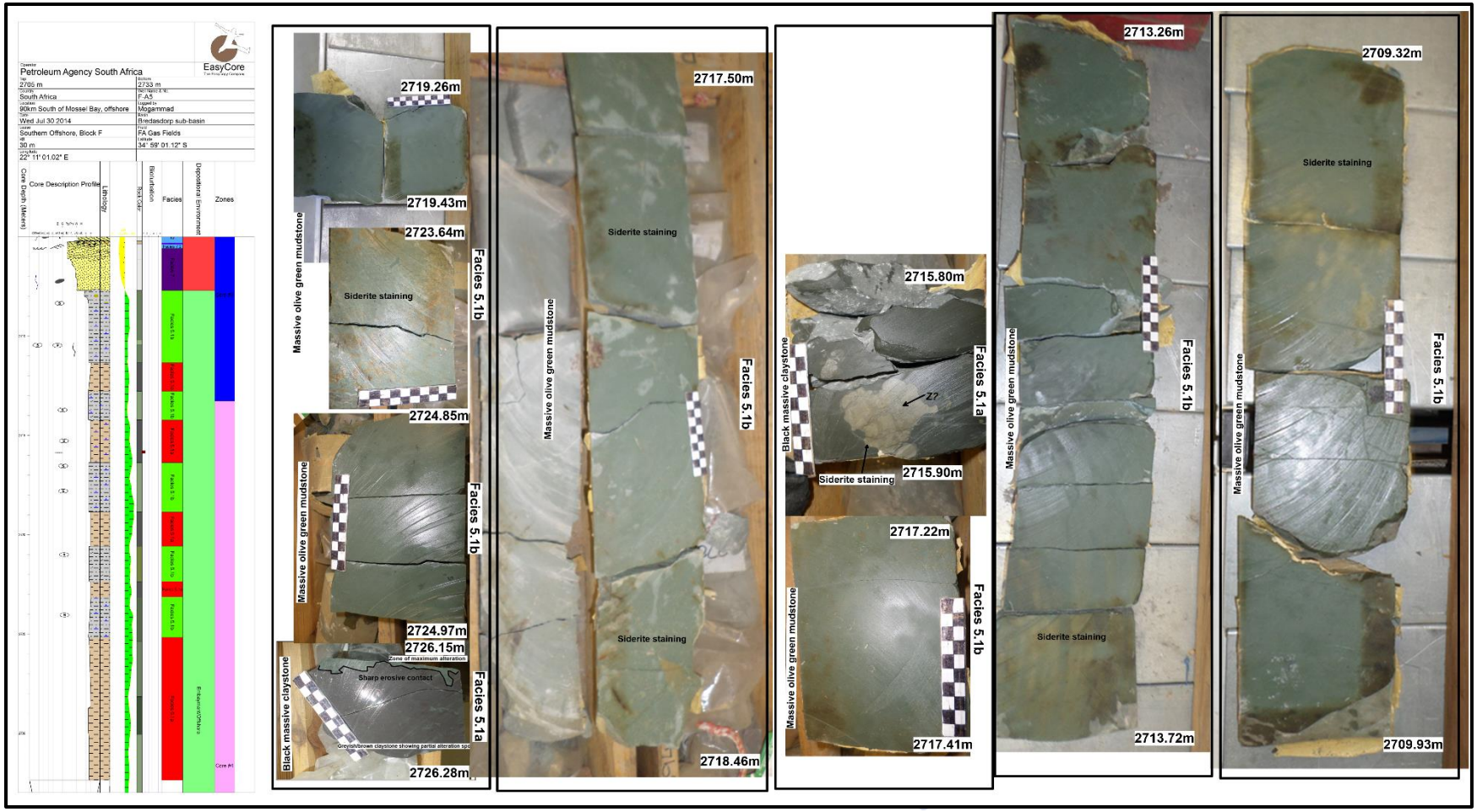

Figure 4.1.19: Examples of facies association 5 (F-A5) consisting facies 5.1a and 5.1b showing offshore transgressive mudstones and outer embayment depositional environments. Thick bedded green and black mudstone (purely claystone and siltstone also occur) with siderite staining occurring frequently throughout these intervals. There are rare to no occurrences of trace fossils (isolated Zoophycos isp? (Z)) but siderite concretions are evident which could be the result of remnant burrowing.

Facies Association 7 (Basement high slopes with hyperpycnite deposits and slope failures or breaching)

Facies 7.1 (Figure 4.1.20, coarsening upward units)

Massive to faintly cross-stratified (Sm to Slf and Spb), vfL- fU sandstone (2m thick), light grey to white, comprising of subrounded-subangular grains that are tightly packed and moderately well sorted (porosity low). Fractured units are common with syn-sedimentary faults and mud injectites. Disseminated clasts are present. The contact between the underlying mudstone and this sandstone unit is a sharp undulatory contact with injected mud or ripped up clasts. The sandstone shows a coarsening upward trend of vfL sandstone at the base to a fU sandstone towards the top of the unit. There is no evidence of any trace fossils and remains massive due to rapid aggradation (BI=0). Faint cross-laminations occur towards the top at the facies contact between Facies 7.2 and 7.1. These laminations are in alignment with the bedding angle of facies 7.2.

Facies 7.2 (Figure 4.1.20)

Interbedded high angle cross-bedded (Spb), vfU-fU sandstone and medium to coarse climbing ripple laminated siltstone/mudstone (Sr). This unit conforms to the high-angle cross-bedded depositional dip and shows a general coarsening upward trend. The fU sandstone is massive (Sm) in part but grades to cross-laminations (Spl), light grey in colour, comprising angular-subangular grains that are moderately well sorted (bimodal). The whole facies ranges in thickness from 0.07m to 2.11m thick.

Thin section analysis (refer to Appendix B for details) revealed that grains are compacted with sutured and concave-convex boundaries. Mono-crystalline quartz (showing strain shadows and undulatory extinction) and microcline (k-feldspar) is evident. The fU sandstone occurs at the top and at the base of this unit. The vfU sandstone occurs at the upper part of the unit and shows evidence of syn-sedimentary faulting (throw of 1cm) and fractures and flame structures. The medium to coarse, light grey to medium grey siltstone interbed contains counter-ripple or backflow ripples (antidune structure under upper flow regime conditions) and in-phase climbing ripples. This unit has angular to sub-rounded grains that are moderately well sorted. The upper and lower boundary of this unit shows undulatory or wavy contacts. The mudstone is greenish grey that contain a fine silt-sized fraction and forms flame structures with the fU sandstone. This

unit also occurs as mud flasers (stretched clasts) indicating possible rapid aggradation and burial of erosive lag with clasts being semi-plastic in nature. Bioturbation is rare but interval-specific burrows occur as *Macaronichnus* trace fossils with cryptic bioturbation.

Facies 7.3 (Figure 4.1.20)

Granule-pebble grade stringers (3-5 cm thick), massive-matrix supported, indurated, oligomictic light-grey parabreccia (Gmd). It is dominated by sub-angular to subrounded, oblate to bladed greenish/grey claystone clasts. Clast-size ranges from 0.2-1cm. These facies range from 0.03m to 0.05m thick. Occurs at the base of facies 7.2. The matrix consists mostly of fU sandstone. This unit comprises an erosional surface with intraformational clasts present. Clasts are poorly aligned or show weak imbrication conforming to bedding planes. (Possible base of minor inter-bar or bar top channel fill). Bioturbation is absent.

Facies 7.4 (Figure 4.1.20)

Horizontal planar laminated (Sh), light grey mL sandstone. The grains are rounded to subangular grains that are moderately well sorted. The facies occur as an isolated unit that is 0.89m thick. Plagioclase alteration is common, as well as strained quartz and polycrystalline quartz (figure). Microcline and zircon crystals are evident but rare. The upper boundary of this unit shows a sharp contact and lower boundary shows a gradational change. Bioturbation is rare to absent.

Interpretation: Facies 7.1 directly overlies facies association 5 and the lower boundary contact is erosional in part suggesting that rapid aggradation took place where a higher density sand was deposited on a still water-saturated mudstone below. The high-angle depositional dips of these units suggest that these layers were deposited rapidly on a slope environment. The occurrences of green claystone clasts (from Facies 7.3) oriented and aligned at a high angle suggest that a high energy or turbulent event took place that ripped up the beds of Facies association 5. In addition, the whitish sandstone revealed that it was in a high-energy environment possibly reworking from a shoreline parallel shoreface.

These massive/structureless, erosive pebble lags and cross-laminated sandstone is indicative of breaching turbidites with the occurrence of high-angle depositional dips are attributed to a slope environment. There is no evidence of slumping, which could be have been attributed to the stability of the slope. The occurrence of counter current ripples and climbing ripples are

indicative of an increased suspension fallout or increase in sediment concentration. However, the occurrence of horizontal lamination and climbing ripples are largely possible hyperpycnites in the lateral distal part of channels. The hyperpycnites could be the result of breaching within the channel walls or levees, thus forming an erosive event overlying cross-laminations (parallel laminated hydraulic regime on a high angle depositional dip) on the outer parts of the main channels (Van den Berg et al., 2017). This interpretation, with the thickness of the unit, coincides with crevasse splay deposits, middle and proximal crevasse splays forming adjacent to major channels or distributary (Gugliotta et al., 2015). Therefore, these splays as described here is rather splays formed by the breaching of slopes as proposed by Van den Berg et al. (2017). Three sequences occur amalgamated which suggests a trend that is controlled and are not sporadic. This coincides with major flooding from the main distributary channels or intrabasinal turbidites (Zavala & Arcuri, 2016).

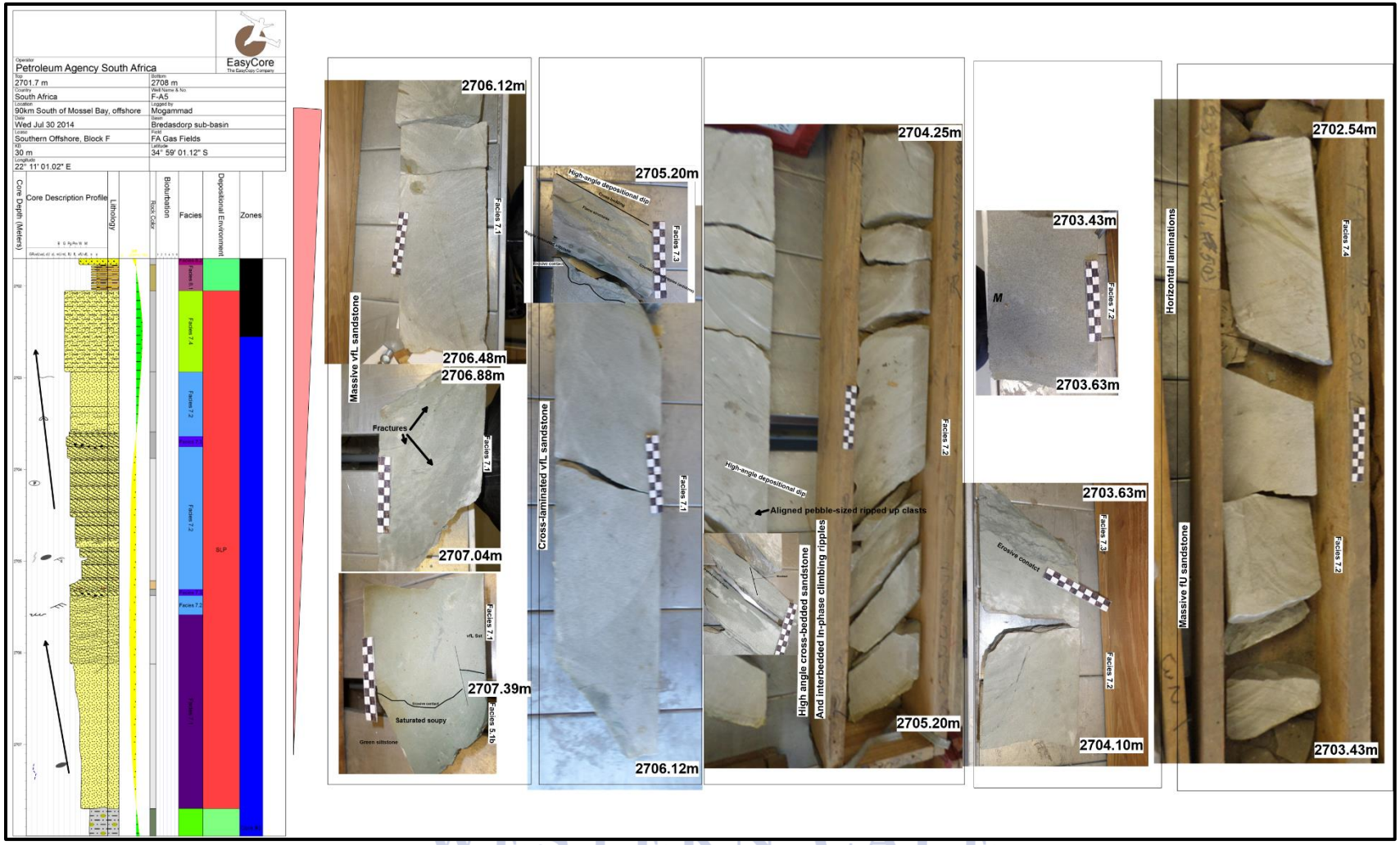

Figure 4.1.20: Examples of facies association 7 with facies 7.1, 7.2, 7.3 and 7.4 showing basement high slopes with hyperpycnite (breaching) deposits. The erosive contacts with liquefied mud are evidence of breaching. The core broke along the bedding planes with pebbles aligned parallel to the bedding planes as well.

Facies Association 8 (Figure 4.1.21) Proximal/central embayment to shoreface/foreshore environment

Facies 8.1

Interlaminated claystone and coarse siltstone (Sh) (30cm thick). The dark olive green claystone is massive (Fm) and fissile in part with faint laminations (Fl). The light to medium grey siltstone shows parallel laminations and is largely gradational with the claystone. Bioturbation is rare with *Planolites* and *Chondrites* (BI=1). The boundary bedding contacts are sharp.

Facies 8.2

Cross-stratified pebbly vfU light grey to off-white vfU sandstone (Gp), indurated sandstone that grade to an ortho-conglomerate towards the top (inversely graded). The planar cross-bedded unit tends to grade to low angle cross bedding usually indicative of hummocky cross-stratification (Sw). The clasts show an alignment (in thin section as well) with the bedding planes which shows some form of stratification, not randomly arranged. There is also evidence of soft sediment deformation towards the top. The pebbly vfU sandstone (0.24cm thick) consist of <0.8cm pebble clasts that is prolate in shape. This unit also shows a sharp contact with Facies 8.1. The quartz grains are moderately well sorted and shows rounded grains, with altered feldspars. The distribution in some parts is bimodal. Thin section analysis revealed an argillaceous matrix but is largely affected by compaction with sutured quartz grain boundaries, as well as elongated plagioclase grains are evident. Porosity is fair to poor. Pyrite occurs as disseminated patches. Laminations are draped rarely with organic matter and are non-calcareous. These beds are gradational with Facies 8.3.

Facies 8.3

Clast-supported, indurated, poorly sorted, polymictic, greenish/brown pebble conglomerate (Gmd) (31cm thick). The unit is dominated by bladed and oblate clasts of claystone, siltstone and quartz pebble clasts. Clasts are generally rounded to subrounded, poorly sorted and up to 5cm in size. Matrix consists of vfU sandstone of Facies 8.2. This unit tends to grade to a matrix-supported conglomerate towards the top and eventually grades to Facies 8.4 (gradational contact). Bioturbation is rare to absent (BI=0).

Facies 8.4

Wave-rippled bedded (Sw), medium to dark grey vfU sandstone with occasional mL sandstone within the interbeds (trough and crest) and siltstone drapes. The grains are well to moderately well-sorted, and consist of sub-angular to sub-rounded grains. The wave ripples are in part truncated which suggest a possible high-energy event with the mL sandstone-filled troughs and crests at the bottom. These grades to normal wave ripple laminations towards the top (2700.50m). The normal wave ripples tend to grade further into critically climbing ripples (type 1=Type A) and finally to parallel horizontal laminations of facies 8.2. The grading of this structure could be indicative of in phase standing waves of the upper flow regime. These facies also marks the initial appearance of pyrite nodules. There is also soft sediment deformation in the form of syn-sedimentary faults. Bioturbation is rare but marine trace fossils occur as *Thalassinoides* burrows. The upper and lower boundary contacts are gradational and the unit is 23-50cm thick.

Facies 8.5

Planar laminated, medium to dark grey, indurated, vfU sandstone with medium grey coarse siltstone inter-laminations (Sl and Fl). The grains are moderately well sorted and consist of angular to sub-rounded grains of quartz. The distribution is partly bimodal with siltstone in part. Large amount of opaque minerals are present which can be identified as pyrite. Siderite is also evident as diagenetically altered staining as *Paleophycus* burrows (BI=1). This unit also shows a gradational upper and lower contact with Facies 8.4 but shows a sharp contact with facies 8.6. This unit ranges in thicknesses from 27 to 34cm thick.

Facies 8.6

Faintly laminated (Slf), dark brownish to grey, indurated, vfU-fL bioclastic/fossiliferous sandstone (83cm thick). The grains are well sorted and subrounded to rounded in shape. This unit shows post-depositional alteration of siderite and diagenetic pyrite (could be the mixing of pyrite with fossil debris to create a siderite or ferroan-carbonate staining). The intensity of the alteration increases towards the top with increased shell debris (2698.79m). There is evidence of randomly aligned shell debris or broken up shells throughout this unit but the alteration intensity and shell debris quantity increase towards the top. Pebbles occur disseminated throughout

(equant) and are <1cm in size. This unit shows clear burrows towards the top of the unit but cryptic bioturbation towards the center. Burrows are restricted to visible actively filled *Paleophycus, Macaronichnus (passive fill), Thalassinoides* and small-diameter actively filled burrows (BI=2). The basal boundary and upper boundary is sharp with facies 8.5 and 6.1a)

Interpretation: These deposits have been interpreted as proximal embayment to shoreface and foreshore environments. Facies 8.1 occurs similar to facies association 5 but are coarser grained therefore these facies have been placed as a different facies. The rapid change in environments is due to the rapid rate of erosion in F-A5 due to the basement highs. The occurrence of marine trace fossils is largely indicative of a shallow marine environment (Knaust, 2017). Facies 8.1 also contains more visible burrows such as *Planolites* and *Chondrites* than Facies association 5. These facies (Facies 8.1) has been interpreted as outer embayment facies with its relative stratigraphic position above slope/offshore deposits with its associated characteristics (Jackson et al., 2005). It is suggested that the pebbles or the occurrence of aligned clasts is the result of nearby inlets. The interbedded small-scale amalgamated anisotropic swaley cross-stratification is also largely indicative of a lower shoreface or upper shoreface wave influenced shallow marine environment (Dott & Bourgeois, 1982; Swift et al., 1983; Duke et al., 1991, Van Capelle et al., 2016). The finer grain size of facies 8.4is suggested to have been deposited in an energetic wave climate within a turbidity maximum zone since the occurrence of wave ripples and climbing ripples are both evident. The interpretation is strongly related to hummocky cross stratification during waxing and waning isolated storm events but not strong enough to form tempestites. The bioturbation intensity and diversity increase towards the top, which is largely indicative of a lower shoreface environment for the upper section of this unit (Facies 8.5/8.6) (Taylor & Gawthorpe, 1993). The lower section is more indicative of a higher energy event (Facies 8.1, 8.2 and 8.3). Yang et al., (2010) interpreted this facies association as high-energy littoral and front deposits. The occurrence of shell debris and fine-grained character is a common attribute to high-energy swash events in the foreshore to upper shoreface zones in a wave influenced/ dominated setting (Gietelink, 1973). These can also be attributed to the wave ravinement surface but a sequence stratigraphic study is beyond the scope of this study. However, Rossi & Steel (2016) interpreted these deposits as mixed energy interdistributary bay deposits especially where the shell debris is randomly orientated (suggesting in-situ formation) and a high degree of bioturbation (Facies 8.6). The bioturbation tends to increase upward following the storm event,

which supports the interpretation of a waning storm event in the upper shoreface to foreshore environment.

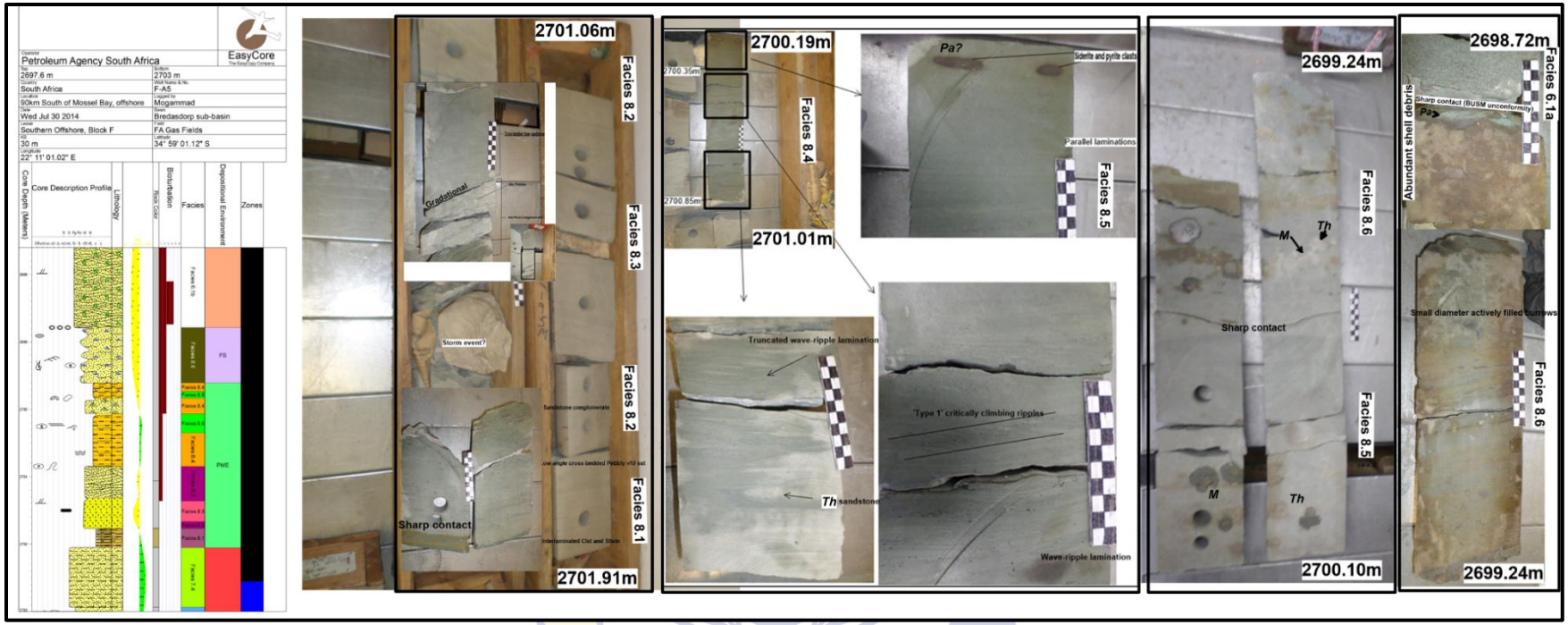

Figure 4.1.21: Examples from facies association 8 with facies 8.1, 8.2, 8.3, 8.4, 8.5 and 8.6 showing proximal/central embayment to shoreface/foreshore environment. Shell debris is common in the carbonate stained units. Trace fossils consisted of Macaronichnus (M), Thalassinoides (Th) and Paleophycus? (Pa). Type B (Type 2) critically climbing and wave ripples (truncated forms as small-scale hummocky cross stratification) occurs in these unit.

Table 4: Summarized facies associations of the regressive element complex assemblage set section of F-A5 with associated facies elements and complexes. Refer to Appendix A (Table A1) for facies element code descriptions

Facies elements	Facies complex	Facies association
Fm Fm	Facies 5.1 Facies 5.2	FA 5 (offshore prodelta/shelf deposits or outer embayment)
Sm to Slf and Spb Spb, Sr, Spl, Sm Gmd Sh	Facies 7.1 Facies 7.2 Facies 7.3 Facies 7.4	FA 7 (Basement high slopes with hyperpycnites and slope failures or breaching)
Sh, Fm, Fl Gp, Sw Gmd Sw Sl and Fl Slf	Facies 8.1 Facies 8.2 Facies 8.3 Facies 8.4 Facies 8.5 Facies 8.6	FA 8 (Proximal/central embayment to shoreface/foreshore environment)

Transgressional phase of well F-A5 (Summarized in Table 5)

Facies association 6 (Figure 4.1.22) (Tidal sand ridges and compound dune fields)

Facies 6.1b

Cross-bedded (Spb), light to medium greenish grey/off white, indurated, fU glauconitic sandstone (137cm). The change in dip angle from a low- angle (Facies 6.1a) to high angle (Facies 6.1b) is largely indicative of trough cross-stratified bedding. The internal and external facies contact is sharp between simple bedsets and composite bedset boundaries. Porosity is poor due to compaction. Quartz grains are well sorted and are subrounded to rounded in shape. Glauconite occurs throughout this unit and appears largely compacted in some places. Rock fragments are common. Plagioclase is common with their alteration products (sericite). The unit has a thickness of 1.37m. Cross-laminations (Spl) are draped with siltstone and are largely disturbed due to bioturbation (BI=2-4). Horizontal burrows are common at the base of this unit

(indicative of *Cruziana* ichnofacies). The small diameter burrows of *Macaronichnus* (*M*) are indicative of *Skolithos* ichnofacies Burrows are restricted to ichnospecies of *Thalassinoides* (*Th*), *Macaronichnus* (*M*), *Planolites* (*P*) and *Paleophycus* (*Pa*). *Macaronichnus* burrows are the most dominant trace fossils and forms cryptic bioturbation.

Facies 6.3/6.1a

Low-angle cross-bedded (Splx) to massive sandstone (Sm), light to medium grey, indurated, mU glauconitic pebble sandstone (2.8m or 280cm). In some parts, planar horizontal laminations are evident. Quartz grains are well rounded and well sorted. Glauconite occurs throughout the unit and is well sorted with the host detrital grains. Most grains are altered and highly fractured. The pebbles are of different types (polymictic) consisting of claystone, quartz and siltstone pebbles. These clasts ranges in size from 2mm to <1mm (granules). These clasts are equant to bladed. The bedding contacts are largely gradational between these two facies (6.1b and 6.3/6.1a). The siltstone drapes contain coal or organic matter towards the top of the unit and increases towards the top. The unit has a thickness of 3.32m. The dip direction changes in this unit as oppose to facies 6.1b. The bioturbation intensity increases in these facies but are still dominated by the same ichnospecies as Facies 6.1b (BI=4).

Interpretation: The occurrence of trough-cross stratified units is largely indicative of 3D dune migration as tidal compound dune fields. These facies can also be as tidal sand ridges with comparison to the other wells showing less bioturbation. This could be due to temporal or spatial changes with dune migration. The occurrence of mud drapes is indicative of dominating tidal processes. In addition, the abundance of trace fossils is largely indicative of a large tidal prism that occurs coeval with proximal depositional settings (Gingras et al., 2012b). The occurrences of glauconitic grains are indicative of shallow marine environments and the well-sorted nature is largely indicative of reworked grains on tidal sand ridges (Shanmugam et al., 2000; Amorosi et al., 2012). This is further supported by the occurrence of *Cruziana* and *Skolithos* ichnofacies that is largely indicative of lower shoreface and upper offshore transitional zones. In addition, relatively to the other wells, these facies are the distal equivalents of F-AR1 and F-A12 (FA6) and the trace fossil density has decreased.

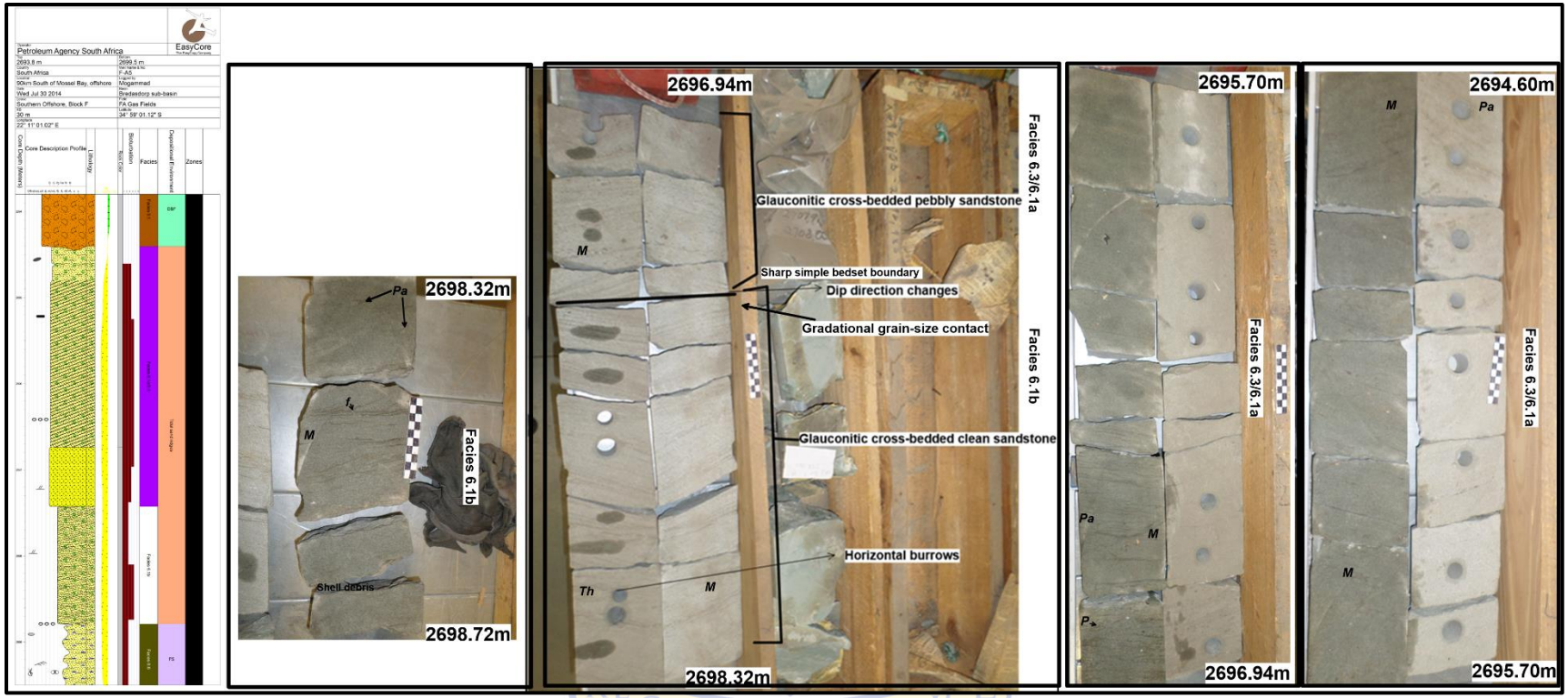

Figure 4.1.22: Examples of facies association 6 showing compound dune fields with glauconitic sandstones. Trace fossils consisted of Macaronichnus (M), Paleophycus (Pa), Planolites (P) and Thalassinoides (Th).

Facies Association 9 (Figure 4.1.23) Deep lacustrine channels and lobes

Facies 9.1 (Channel breaching)

Matrix supported, poorly indurated, poorly size-sorted, polymictic, grey breccia (Gmb) dominated by angular mud clasts and minor equant quartz pebbles. Clast shape shows two ranges with intraformational angular claystone clasts and intraformational well-rounded quartz clasts. Angular claystone clast size ranges from 2cm to 5cm and the quartz pebble size ranges from <0.5cm to 1cm. The matrix consists of dark grey vfU sandstone with pebbles. This conglomerate can be classified as a polymictic parabreccia but towards the top, the unit tends to become more monomictic, which are associated with larger clasts greater than 10cm. The thickness of this unit ranges from 0.45 to 0.5m. Forms the base of a non-cohesive debris flow and shows an erosive contact with Facies association 6 but internal facies are gradational (with facies 9.2). The clasts are randomly arranged but towards the top, the unit usually shows some sort of alignment. The clasts show an internal fabric that is massive and laminated. Bioturbation is absent with a BI=0.

Facies 9.2 (Breaching turbidites and deep lacustrine channels)

Planar stratified, stepped planar laminae (Sh to Sm), massive to cross-laminated (Sm to Spl), medium/dark grey vfL-vfU sandstone and siltstone. The unit has a thickness that ranges from 1.3 to 2.6m. Grains are moderately well to moderately poorly sorted. Siltstone bands are common with planar cross-laminations occurring towards the base of the unit. These further grades to a coarsening-upward massive and planar-bedded vfL-vfU sandstone or an increase in organic rich drape intensity. The unit is rich in organic material. Low angle truncations also occur and are possibly hummocky cross-stratification but no evidence of tempestites sequences are presents and are rather restricted to an isolated bed. Thin section analysis revealed a compacted sandstone with abundant sutured grain boundary contacts. Plagioclase is altered in places. Muscovite also evident. Monocrystalline quartz is abundant. Syn-sedimentary faults are evident as well. Bioturbation is rare but consist of *fugichnia* traces and *Nereites (N)* with an index of 0-2 (Figure 4.1.23).

Deep lacustrine lobes

Facies 9.3

Heterolythic alternations (Shl) of vfL dark grey sandstone to coarse siltstone and organic-rich mudstone/coaly shales. The unit has a thickness of 4.74m. Sedimentary structures consist of planar horizontal laminations, faint ripple cross-laminations, low-angle laminations and wavy bedding are present. Soft sediment deformation is also common with flame and load structures. Fluid mud layers are also common throughout (SM1 and SM2). Abundant to moderate organic matter (carbonaceous laminations). Grains are moderately well sorted with subrounded-rounded grains. Thin section analysis reveals a tightly packed unit with argillaceous matrix in some areas. Feldspars are altered in part. Carbonaceous claystone clasts occur throughout the unit as well. Bioturbation is highly variable restricted to certain intervals (BI=0-5).

Interpretation: Facies association 9 has been described as non-cohesive debris flows with turbidites in the breaching or slope failure of basement highs to form submarine channels and lobes (intraformational turbidites). There is a close resemblance of these facies to deep-water inrtrabasinal turbidites (Zavala & Arcuri, 2016). These channels and lobes consisted of turbidite architectures or sequences (Dodd et al., 2019). The relative stratigraphic position of these facies (with their underlying reworked glauconitic unit) does not exclude an interpretation as estuarine channels and mudflats as proposed by Van den Berg et al. (2017) in the Tilje formation. Therefore, the high abundance of organic matter and organic rich clasts in channels could be the result of the erosion of nearby vegetation (Rossi & Steel 2016).

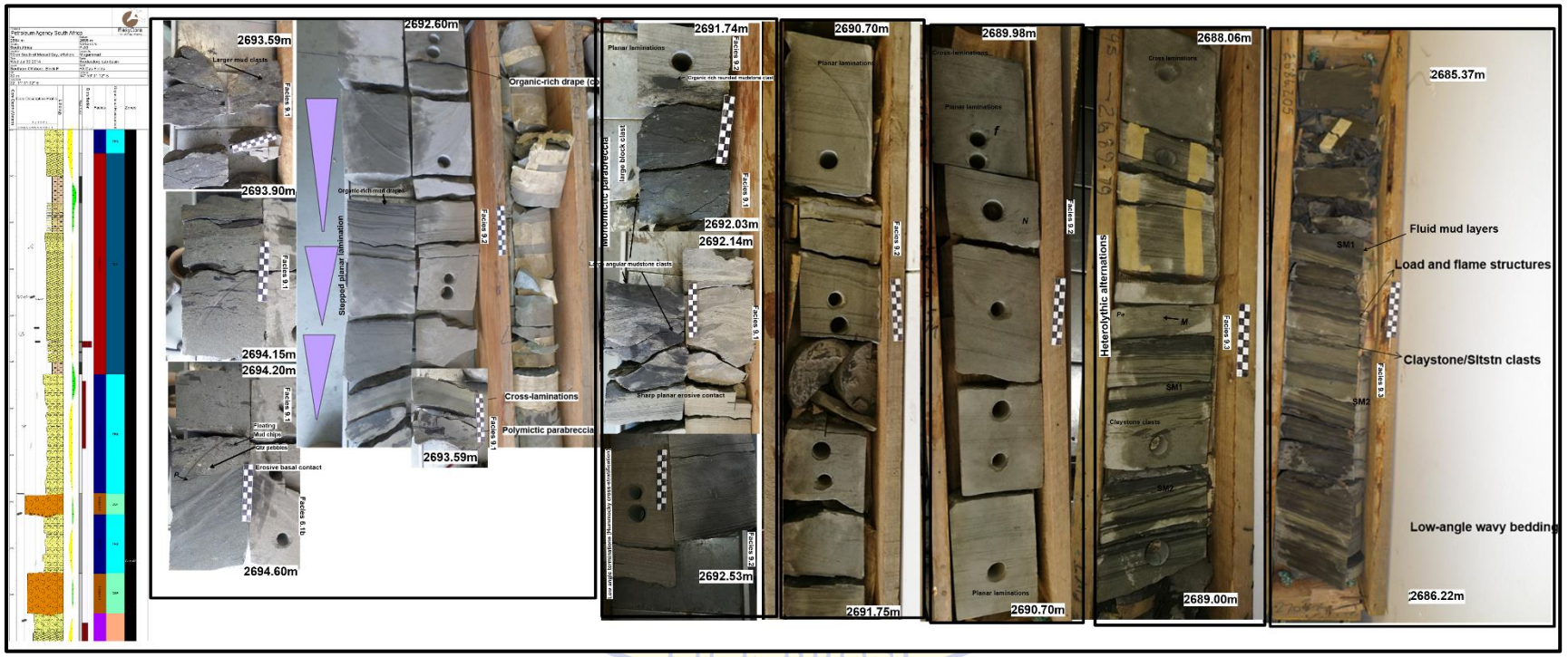

Figure 4.1.23: Examples of facies association 8 and 9 with deep lacustrine channels and lobes. Coarsening upward sequences are common with trace fossils consisting of Planolites (P), Macaronichnus (M), Nereites (N) and Paleophycus (Pa). Fluid mud layers are common with disseminated claystone clasts. Organic matter is also abundant with mud drapes usually rich in organic matter.

Table 5: Summarized facies associations of the transgressive element complex assemblage set section of F-A5 with associated facies elements and complexes. Refer to Appendix A (Table A1) for facies element code descriptions

Spl, Spb Splx, Sm	Facies 6.1b Facies 6.1a/6.3	FA 6 (Compound dune fields)
Gmb Sm to Spl, Sh to Sm Shl, SM1 and SM2	Facies 9.1 Facies 9.2 Facies 9.3	FA 9 (Breaching channels (including turbidites) and lobes

4.1.4 Facies correlation, lateral variations, and stacking patterns

A regional correlation was constructed based on unpublished reports of seismic marker horizon depths (1AT1, V or D horizons) and has been integrated into this study (Figure 4.1.24). The seismic data indicated that F-A5 sediments were deposited in a separate depocenter to F-A12 and F-AR1, making a correlation of facies difficult. However, a correlation based on element complex assemblages (regional zones such as shoreface, foreshore, delta plain, prodelta etc.) can be performed (Figure 4.1.25). It should also be noted that a regional correlation is problematic since each depocenter went through local subsidence and uplift therefore different characteristic stacking patterns cannot be correlated.

The stacking patterns can become rather complex within rift-systems with the interplay between accommodation space and sediment supply caused by a tectonically active region. Therefore, the seismically defined unconformities acts as high order, low frequency sequences within a rift sequence stratigraphic framework (Martins-Neto & Catuneanu, 2009). The low order, high frequency sequences are governed by flooding surfaces that can be seen in figure 4.1.24. F-A12's lower section (above the V horizon) consisted of a series of fining upward and coarsening-upward high frequency sequences that are common with syn-rifted sequences (Martin-Neto & Catuneanu, 2009). The facies stacking pattern of this lower section reveals a net regressive sequence or regressive element complex assemblage set (high order sequence) with deeper zoned facies (delta front) overlain by proximal facies (delta plain). The upper section is rather complex

with retrogradational packages (below BUSM), within a net transgressive stacking pattern (element complex assemblage set), which shows transgressive mudstones overlain by a subtidal platform (above BUSM). F-A5's lower sections are dominated by massive green mudstones with minor intercalations of siltstone that shows a restriction of these facies within a diachronous framework with F-A12 (Figure 4.1.24 and Figure 4.1.25). F-AR1, however shows a well-developed sequence and conforms to the sequences of F-A12 with minor deviations possibly due to autocyclic processes (Figure 4.1.24).

The relative proportion of major minerals in the facies does not change much in the different kinds of facies associations. Therefore, minor and lithic fragments compositional variations are due to provenance changes or possibly sequence stratigraphic changes. It is emphasized that no specific assemblage of framework minerals can be attributed to facies changes and therefore microfacies analysis are restricted to changes in abundances due to hydrodynamic conditions and grain sizes (detailed descriptions of microfacies and facies associations in Appendix B).

The relative trace fossil variations among facies associations are restricted to diversity changes from proximal to distal equivalents. Most of the ichnofossil assemblages are restricted to *Cruziana* and *Skolithos* ichnofacies assemblages but the continental or *Scoyenia* (mostly delta plain) also occurs. Facies association 5 are absent in the proximal part or northern part of the sub-basin (F-AR1) of the depositional system and possibly has a variably defined trace fossil diversity because of certain environmental factors (closer to the alluvial plain). The trace fossil diversities in the distal part of this facies association are also variable with an increased diversity occurring on F-A12's part of the depositional system compared to F-A5's isolated depocenter. The occurrence of ichnospecies in well F-A12 and F-AR1 are more diverse (showing fluctuating oxygen conditions) with the occurrence of *Planolites*, *Paleophycus*, *Chondrites*, *Skolithos*, *Taenidium*, *Epichnia*-types burrows and *Thalassinoides.* As compared to F-A5's isolated depocenter, the ichnospecies are closely related to low-oxygen traces such as *Zoophycos* and *Chondrites.* Facies Association 6 among all the wells (lateral and updip variation) is similar with the occurrence of certain species being better developed in certain areas than others are. The trace fossil assemblage in this association is rather diverse with respect to the relative proportions of traces but the overall basin-wide occurrences are considered as relatively low (Buatois et al., 1999). Trace fossils consist of *Macaronichnus, Ophiomorpha ispp, Paleophycus, Siphonichnus*

ophthalmoides, *Beaconites/Scolicia*, *Thalassinoides*, *Planolites* and *fugichnia*-like traces. The ichnodensity of certain burrows (especially *Macaronichnus* and *Paleophycus*) are extremely high especially in one depocenter (F-A12 ad F-AR1) compared to the other depocenter (F-A5). Facies association 4 consists of a low diversity and low density with *Macaronichnus*, *Paleophycus*, *Fugichnia*-like traces and *Loloichnus/ Camborygma*. The distal equivalents to this association are related to facies association 8 (diachronous facies assemblages) with the occurrences of *Planolites*, *Chondrites*, *Thalassinoides* and *Paleophycus* ichnospecies. Facies association 1, 2, 3, 7 and 8 associated with delta front environments contains low occurrences of trace fossils in general but random low abundance traces (restricted to certain beds) occurs with ichnospecies made up of *Bergaueria*, *Planolites*, *Thalassinoides*, *Conichnus*, *Chondrites*, *Macaronichnus*, *Paleophycus*, *Ophiomorpha* trace fossils as well as mantle and swirl structures. Facies association 8 is mostly made up of facies-crossing traces and facies association 9 is made up of *Nereites* and *fugichnia*-like traces indicative of offshore environments.

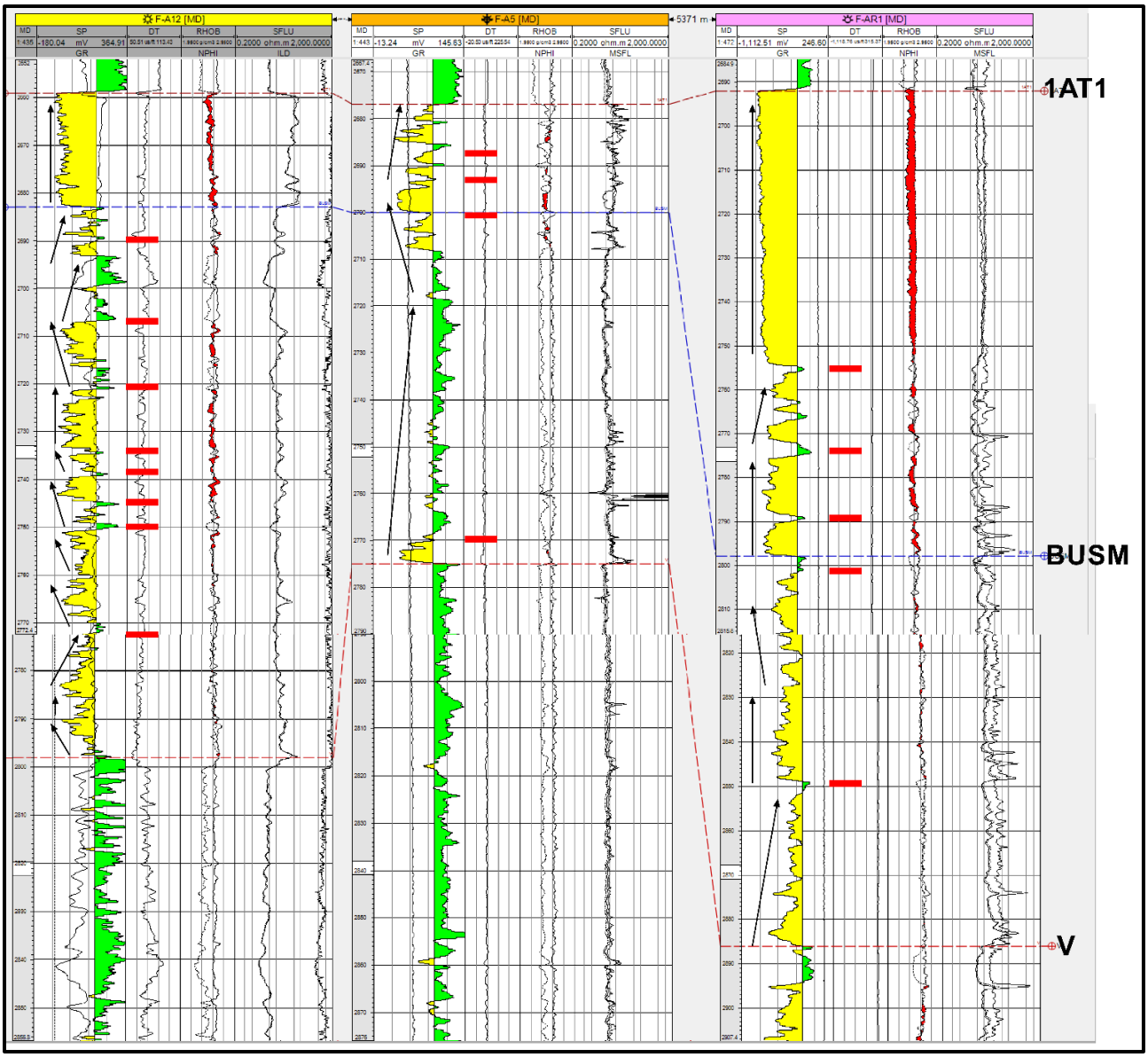

Figure 4.1.24: Well correlation based on regional seismic horizons as based on seismic sequence stratigraphic techniques. The regional high order, low frequency unconformities (horizons) has been obtained from unpublished reports from PASA and is 1AT1, BUSM (Bottom Upper Shallow Marine) and V horizon. The solid thick red lines are flooding surfaces with black arrows indicative of low order, high frequency sequences of progradation, retrogradation and aggradation.

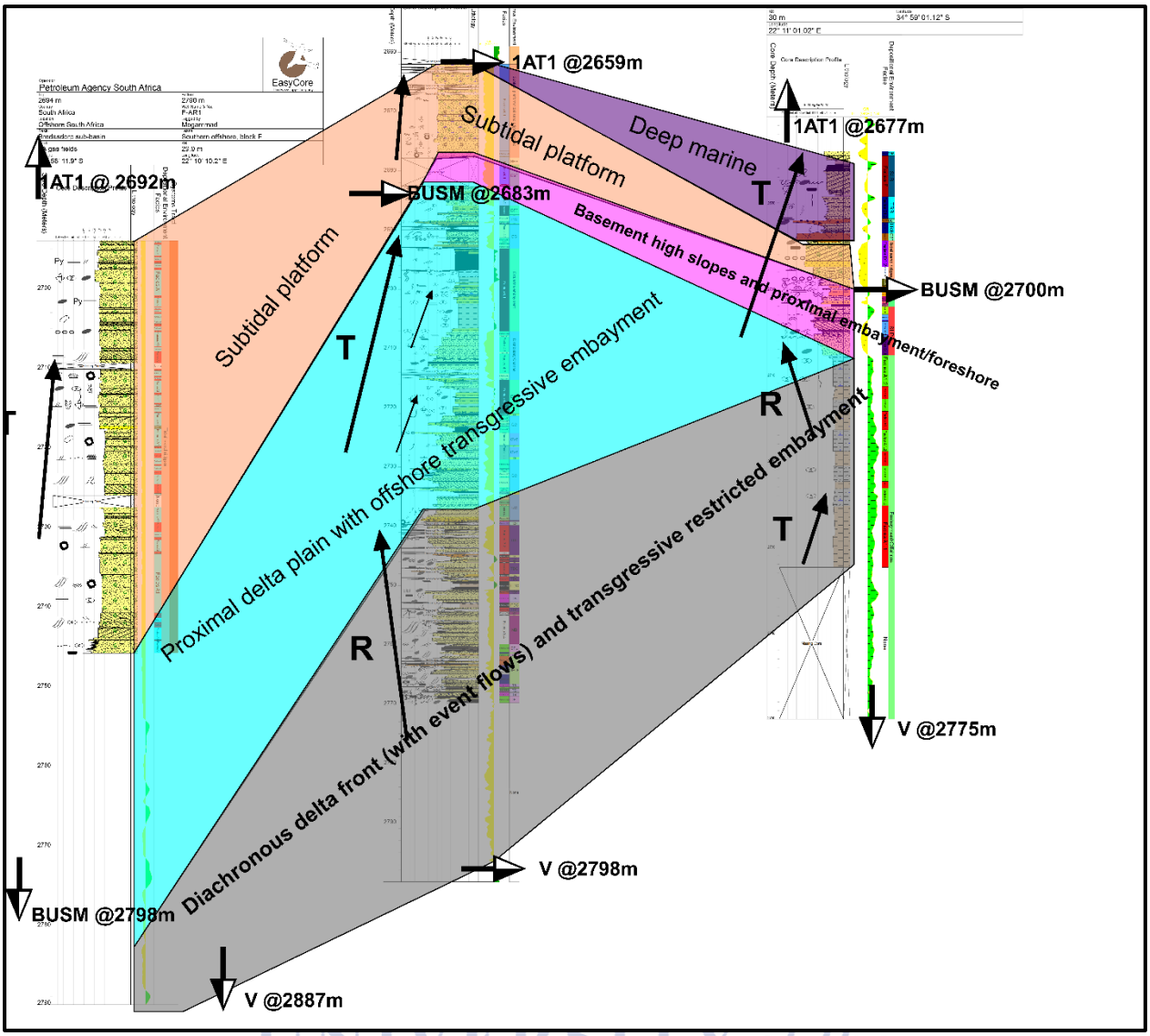

*Figure 4.1.25: Regional element complex assemblage correlation for the 1AT1-V horizon. The arrows represent the location of the seismic unconformity horizons. An arrow pointing down means that the unconformity is based further down at a specific depth. The Regressive phase or element complex assemblage set (**R**) and transgressive phase or element complex assemblage set (**T**) is also shown*

Table 6: Diachronous facies correlation with updip/downdip and lateral variations

Facies correlation (element complex)	Depositional elements	Interpretation and depositional processes
F-AR1= Facies association 6 F-A12= Facies association 6 F-A5= Facies Association 6	Tidal sand ridges and compound dune fields	Tidal dominated
F-AR1= N/A F-A12= Facies Association 5 F-A5= Facies association 5	Estuarine offshore embayment	Wave-dominated to fluvially-influenced and tide-affected
F-A12= Facies association 4 F-AR1= lower section purely fluvial F-A5= Facies association 8	Delta plain (distributary channels) Proximal embayment to shoreface/foreshore environments	Fluvial and wave dominated
F-A12= Facies association 3, 2 and 1 F-AR1= lower section F-A5= Facies association 7 and 8	Delta front environments	Fluvial dominated and tidal to wave modulated
F-A5= Facies association 7 F-A5= Facies association 9	Basement high slopes Deep sea lacustrine channels and lobes	Breaching related turbidity currents Turbidity currents due to slope stability

4.2 Petrography

Petrographic analyses of sedimentary rocks are important for the identification of sedimentary processes for detrital sediments during depositional and post-depositional/diagenetic changes. The identification of the characteristics of certain mineral grains can yield important information about the provenance (Basu et al., 1975; Dickinson and Suczek, 1979; Dickinson et al., 1983;

Ingersoll et al., 1984; Arribas et al., 1985). This can also further be enhanced by bulk-rock geochemical analysis. Detailed petrographic descriptions of the 1AT1-V horizon can be found in Appendix B, Table B3. Due to a large number of sandstone samples studied for petrographic descriptions, a summary of the analysis is presented here.

Textural data of the analyzed samples suggest that the matrix content was <15% for majority of the samples (detailed descriptions can be found in Appendix B, Table B3). Petrographic visual estimation of the samples indicates mostly poorly to well sorted and with mL to vfL grain sizes with subangular-subrounded grains. The average framework grain composition is $Q_{72}F_{21}L_{7.}$ The framework minerals that were evaluated for compositional variation and modal point counting were >5° undulose monocrystalline quartz, <5° undulose monocrystalline quartz, non-undulose (normal) quartz, polycrystalline quartz, K-feldspar, plagioclase feldspar, biotite, muscovite, opaques, heavy minerals and lithic fragments (sedimentary, metamorphic and plutonic/volcanic fragments). There were not much lithic fragments present in the samples but wherever present are interpreted to be of sedimentary in origin with minor metamorphic and igneous lithic fragments. The amount of feldspars could largely be underestimated/overestimated because of their alteration products (fully altered) being similar to micaceous lithic fragments (Rotzien et al., 2018).

Framework grains constituted around 85% of the samples whereas the rest of the sample or the average consisted of matrix, cement and pore spaces. Majority of the samples consisted of abundant extrabasinal (non-carbonate) monocrystalline quartz (undulose (38.3%) and non-undulose (61.7%) extinct quartz) and the values ranged from 47.6%-75.3% (Figure 4.2.1). The monocrystalline content had an average of 62.3% ±1.6%. The grain contact boundaries consisted mostly of sutured, concavo-convex and long contacts (Figure 4.2.1C, D; 4.2.3A, B). There are rare quartz inclusions to be seen in some of the samples, consisting of zircon and muscovite grains. Most of the quartz in the samples is rounded to subrounded with minority masked by overgrowths (Figure 4.2.1). Some quartz grains also have vacuoles with cloudy appearances. Polycrystalline quartz ranged from 2.6%- 19% with an average of 8.74% ± 0.98% (Pure polycrystalline quartz (Figure 4.2.1E, F)). Polycrystalline quartz is not restricted to grain sizes (Tawfik et al., 2017) and is abundant in most of the samples throughout the succession. Sub

crystals within the polycrystalline quartz consist of straight, sutured and crenulated intercrystalline boundaries (Figure 4.2.1A, B and 4.2.1E, F).

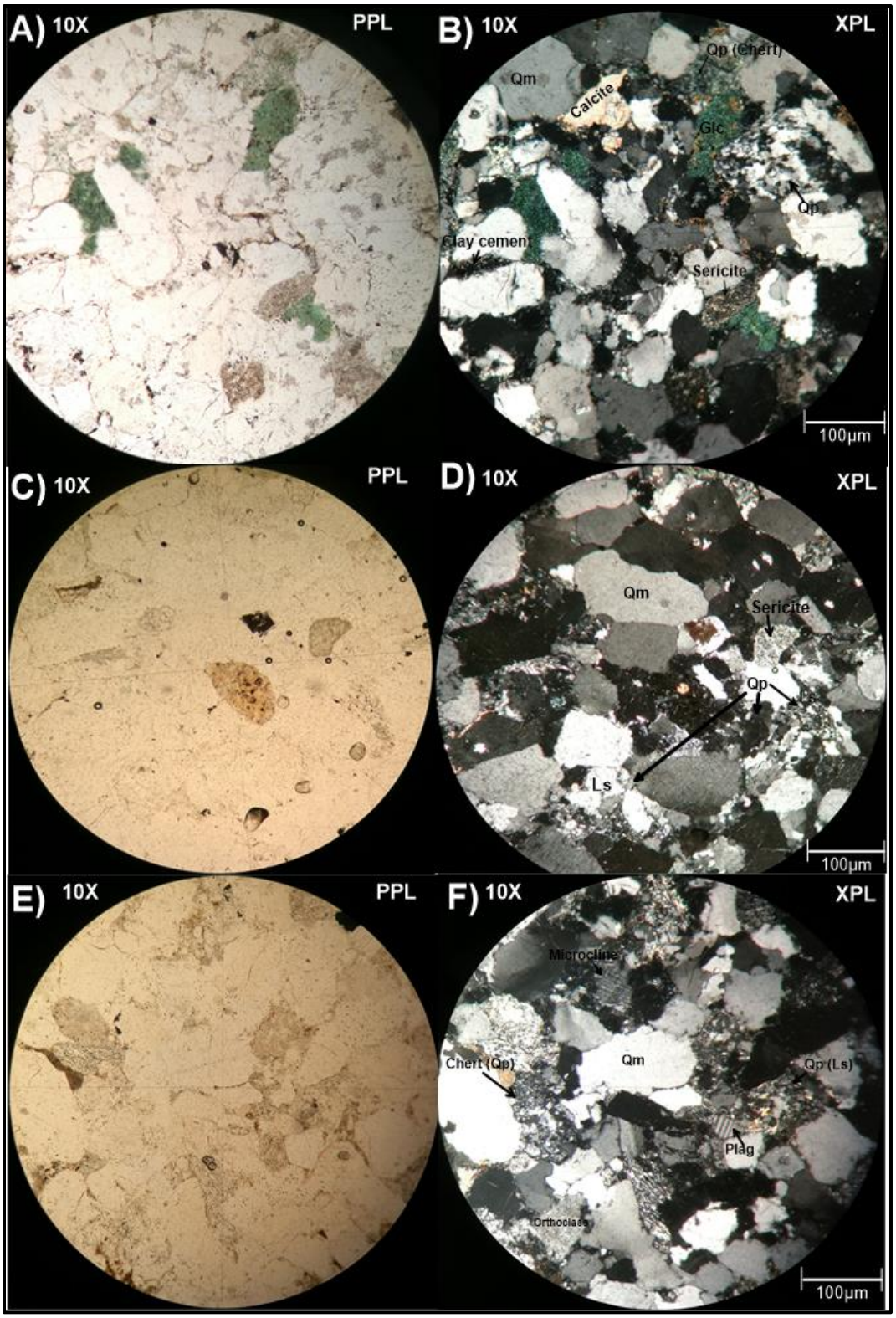

Figure 4.2.1: A) Plain polar and B) Cross polars (Sample F-A5 #4, at a depth of 2697.18m), polycrystalline fragment (Qp) (metamorphic in origin, sheared metaquartzite) consisting of

micro and mega elongated, crenulated quartz crystals that is welded together. Detrital chert is also present towards the top of this section. Clay cement with abundant sulphide mineral inclusions that is indicative of organic matter (Left). Alteration products such as sericite and glauconite (Glc) are also evident. C) Plain polar and D) Crossed polar (Sample F-A12 #1, at a depth of 2662.27m), showing a polycrystalline (megaquartz only) that occurs as pure quartz and metasedimentary lithic fragments, rank 1 (Ls). E) Plain polar and F) Cross polar (Sample F-A5 #8, at a depth of 2702.84m), showing a detrital chert fragment with microquartz and megaquartz welded together. There is also polycrystalline quartz that is considered to be a sedimentary lithic fragment. Plagioclase (Plag), microcline and orthoclase feldspars also occur in this section.

In terms of abundance, the feldspars are second after quartz and ranges between 7% and 37% with an average of 20.8% ± 2.1%. Plagioclase feldspars were the most dominant as compared to the alkali-varieties. Some of the feldspars are partially to fully altered to their alteration products such as sericite (Figure 4.2.2C). The brittle nature of plagioclase feldspar is also evident, especially those grains with well-developed cleavages (Figure 4.2.2A). Compaction, together with quartz grains, causes the twin planes to deform in the direction of maximum stress. Presence of certain plagioclase feldspar grains that shows complex twinning were also noticed (amalgamation of albite and Carlsbad twinning) (Figure 4.2.2E). The alkali varieties consisted of microcline (Figure 4.2.2B) and orthoclase (Figure 4.2.2C, D), with the latter being identified only based on optical properties. Orthoclase grains are in appearance (Figure 4.2.2C) with a few exhibiting Carlsbad twinning (Figure 4.2.2D). There are also evidence of plagioclase feldspar overgrowths (Figure 4.2.8D, E), orthoclase overgrowths and calcite replacement textures that are largely due to the result of diagenetic and burial processes.

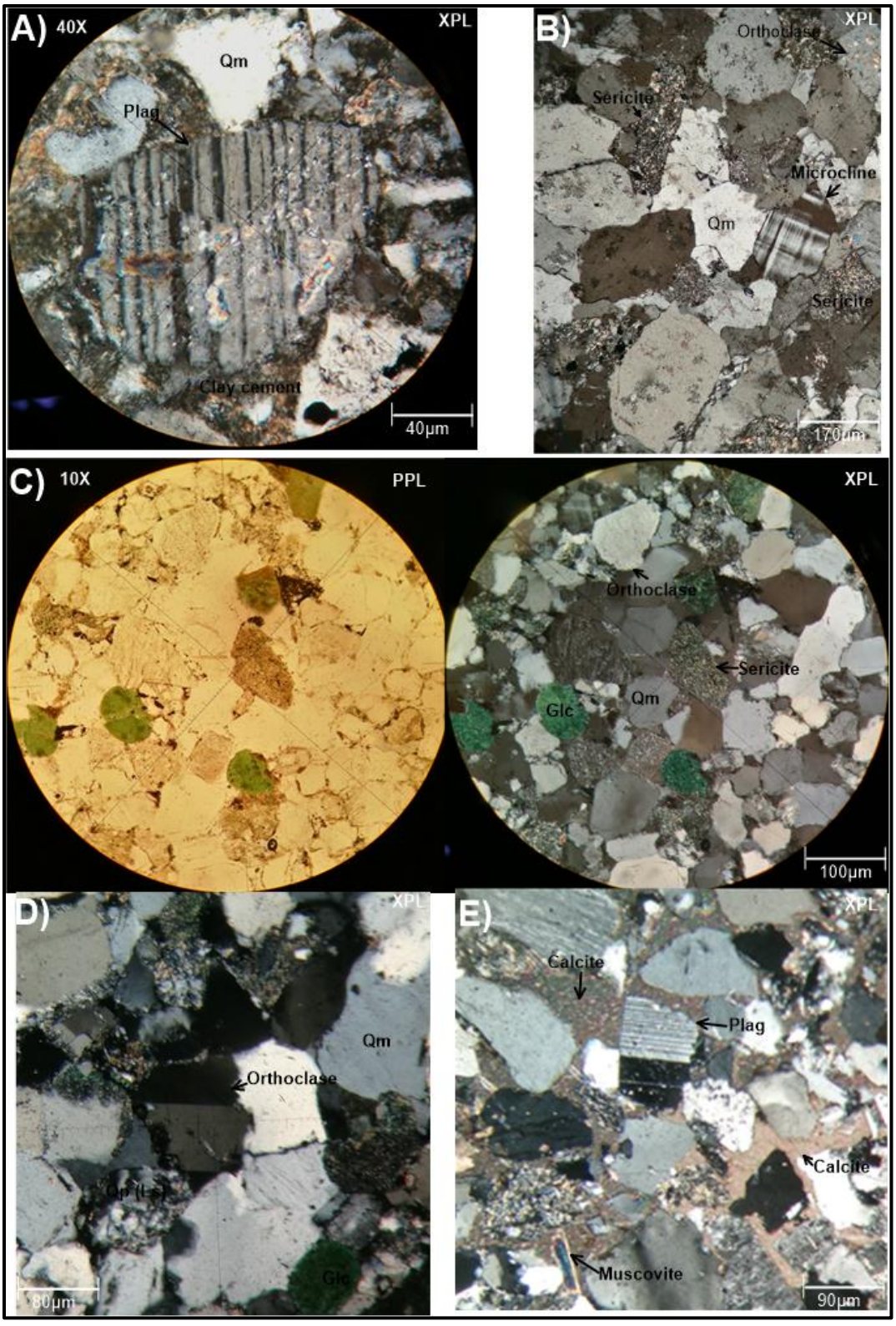

Figure 4.2.2: Under cross polars, plagioclase feldspar showing well defined lamellae with monocrystalline quartz (Qm) surrounding the grain (Sample F-A5 #9, at a depth of 2705.20m).

The brittle nature of plagioclase can be seen with quartz squashing the plagioclase feldspar to deform the lamellae twins. There is also sericitic alteration with minute flakes developing. B) Microcline showing its well-defined tartan texture with orthoclase, sericite and monocrystalline grains in the sample (Sample F-A5 #10, at a depth of 2706.12m). Orthoclase alteration occurs with no Carlsbad twinning. C) Under plain polar (left) and cross polar (right), showing orthoclase with well developed speckled alteration (partly altered), sericite, glauconite (Glc), unit extinct quartz and undulose extinct quartz (Sample F-AR1 #6, at a depth of 2729.63m). D) An orthoclase grain showing well-defined rare carlsbad twinning (Sample F-A12 #2, at a depth of 2674.78m). E) Plagioclase feldspar grain showing complex twinning with both carlsbad and albite twinning. Poikilotopic calcite cement is also evident with quartz (abundant) and muscovite flakes 'floating' around (Sample F-A12 #13, at a depth of 2747.70m)

Clay minerals present comprises mainly of illite, smectite and kaolinite. Clay minerals consisted of smectite and illite within the claystone samples, F-AR1 samples were mostly restricted to glauconite and kaolinite (restricted to the upper parts of the other two wells), with cements being quartz, as confirmed by XRD results. Vermicular kaolinite, as a secondary replacement mineral, also occurs within calcite grains (Figure 4.2.3E). The calcite precipitated in the pore space and kaolinite replaced the calcite afterwards (2^{nd} cycle replacement). The clays also occur as cement with abundant opaque minerals and carbonaceous material (Figures 4.2.3A, B and F). There is also the occurrence of clay coatings surrounding the edge of the grains (Figure 4.2.1A, B).

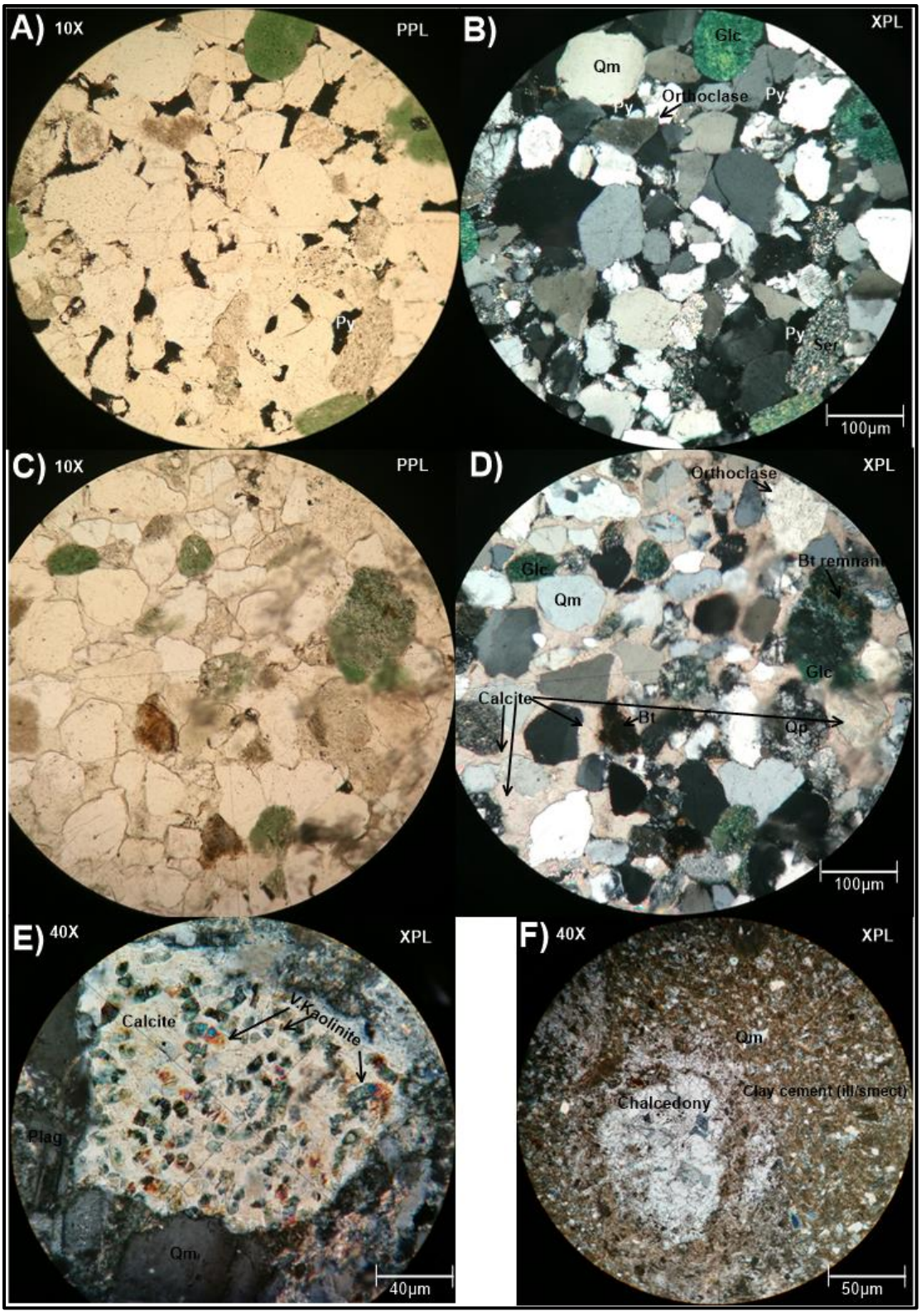

Figure 4.2.3: A) Plain polar and B) Cross polar, showing pyrite-filled (pyrite-Pyr) pore spaces that acted partly as cement and followed the replacement of a precursor carbonaceous material

(organic matter). Other minerals that also occur are 'plain' orthoclase (no special twinning), glauconite (Glc), sericite (feldspar alteration) and monocrystalline quartz with unit extinction (Sample F-AR1 #2, at a depth of 2713.91m). C) Under plain polar and D) under cross polar, showing poikilotopic calcite cement forming as a 'displacive' texture. Other minerals include non-undulose and >5° undulose monocrystalline quartz, polycrystalline quartz, glauconite, orthoclase and biotite (Bt). The biotite in the center has been partially-fully altered to glauconite Sample F-AR1 #11, at a depth of 2744.81m). E) Vermicular kaolinite replacing a pore-filled calcite grain (secondary replacement of orthoclase). Presence of 'worm-like' structure of the vermicular kaolinite with very high birefringence colours possibly taking on the optical properties of calcite (Sample F-A5 #9, at a depth of 2705.20m). F) Blobs of chalcedonic quartz possibly forming as a replacement texture. Other minerals include monocrystalline quartz with a clay rich matrix and cement (illite/smectite) (Sample F-A5 #13, at a depth of 2711.05m)

Rock fragments are the least abundant component with an average of 1.7% ± 0.7%. The sedimentary lithic fragments (average 78.5% of total lithic grains) were more dominant over igneous (average 11.7%) and metamorphic rock fragments (average 10.3%). Coarse igneous rock fragments are common with plagioclase laths and some with porphyritic-like textures (Figure 4.2.4A, B). Metamorphic rock fragments consist mostly of sheared (crenulated) polycrystalline quartz (quartzite) fragments (Figure 4.2.6A, B and Figure 4.2.1A, B), with some rare varieties of metapelite grains of 'rank 1' (Figure 4.2.1D). Sedimentary rock fragments consisted of chert (Non-pure polycrystalline quartz) (Figure 4.2.4D), siltstone and minor claystone fragments that are mostly subrounded in shape (Figure 4.2.4E, F). The low abundance of metamorphic rock fragments in the modal count is mostly due to the grains being counted as a polycrystalline quartz. There is a large amount of 'rank 1' metapelites with lesser amounts of metafelsitic and metabasitic lithic fragments. If the sheared polycrystalline quartz were counted as metamorphic rock fragments, it would be relatively sub-equal to the sedimentary lithic fragments.

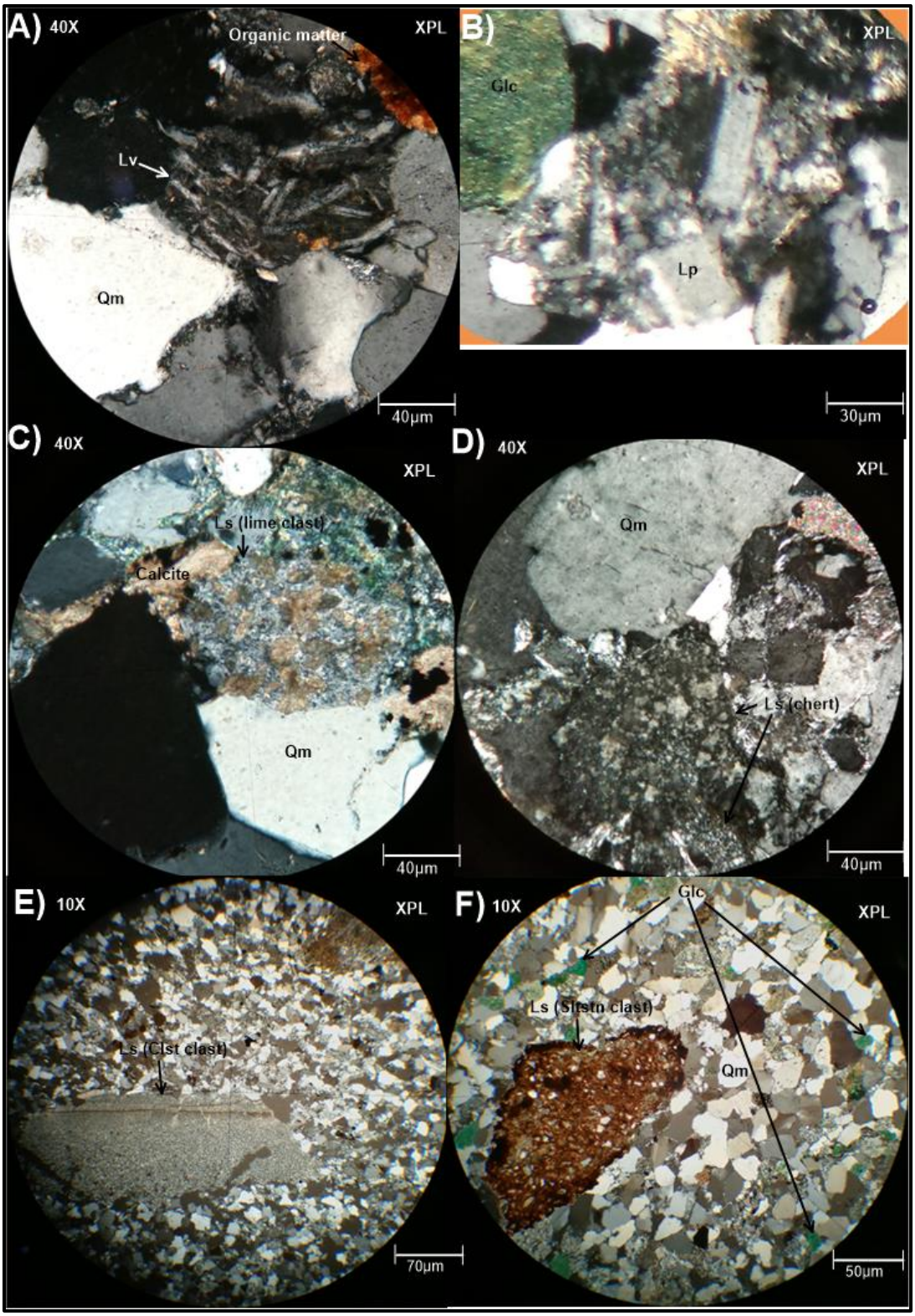

Figure 4.2.4: A) Volcanic lithic fragment (basaltic), with plagioclase feldspar laths in a finer grained matrix, cross polar (Sample F-A5 #8, at a depth of 2702.84m).B) Plutonic rock fragment

with large (relative) orthoclase grains showing Carlsbad twinning (F-A12 #1, at a depth of 2662.27m). C) Sedimentary pelagic carbonate fragment (Rank 1) with dolomitic crystal grains encased in a micritic calcite matrix (Sample F-A12 #3, at a depth of 2677.82m). D) Sedimentary lithic fragment (that is classified as a polycrystalline quartz fragment) showing mega- and micro-quartz fragments (sutured contacts) (Sample F-A12 #9, at a depth of 2713.30m. E) Sedimentary lithic fragment showing a claystone (Clst) clast with relict horizontal laminations (Sample F-A5 #7, at a depth of 2701.54m). F) Sedimentary lithic fragment that is portrayed as a siltstone clast with monocrystalline quartz encased in a finer clay matrix (Sample F-AR1 #3, at a depth of 2717.41m)

The accessory minerals are only abundant (5% < x <10%) in certain samples. Muscovite (Figure 4.2.2E) and biotite (Figure 4.2.3C, D) is the least common with biotite being rare. The occurrence of glauconite can be roughly attributed to the presence of biotite since biotite could be one of the point sources for glauconite formation (Figure 4.2.3C, D), whether from secondary smectite or primary biotite. Detrital muscovite occurs as minute flakes and occurs disseminated throughout the interval (Figure 4.2.2E). These muscovite flakes are sometimes aligned to the bedding panes and are bent due to compaction. There is also the occurrence of chalcedonic quartz balls within a silty claystone sample, which could have had a fossilized precursor or could just largely be a replacement mineral for another mineral (Figure 4.2.3F). Heavy minerals constitute zircon and rutile. Zircons (and heavy minerals) were only found in some samples (Figure 4.2.5C, D). These zircon grains were mostly rounded in shape with some showing abraded terminals (Figure 4.2.5E, F).

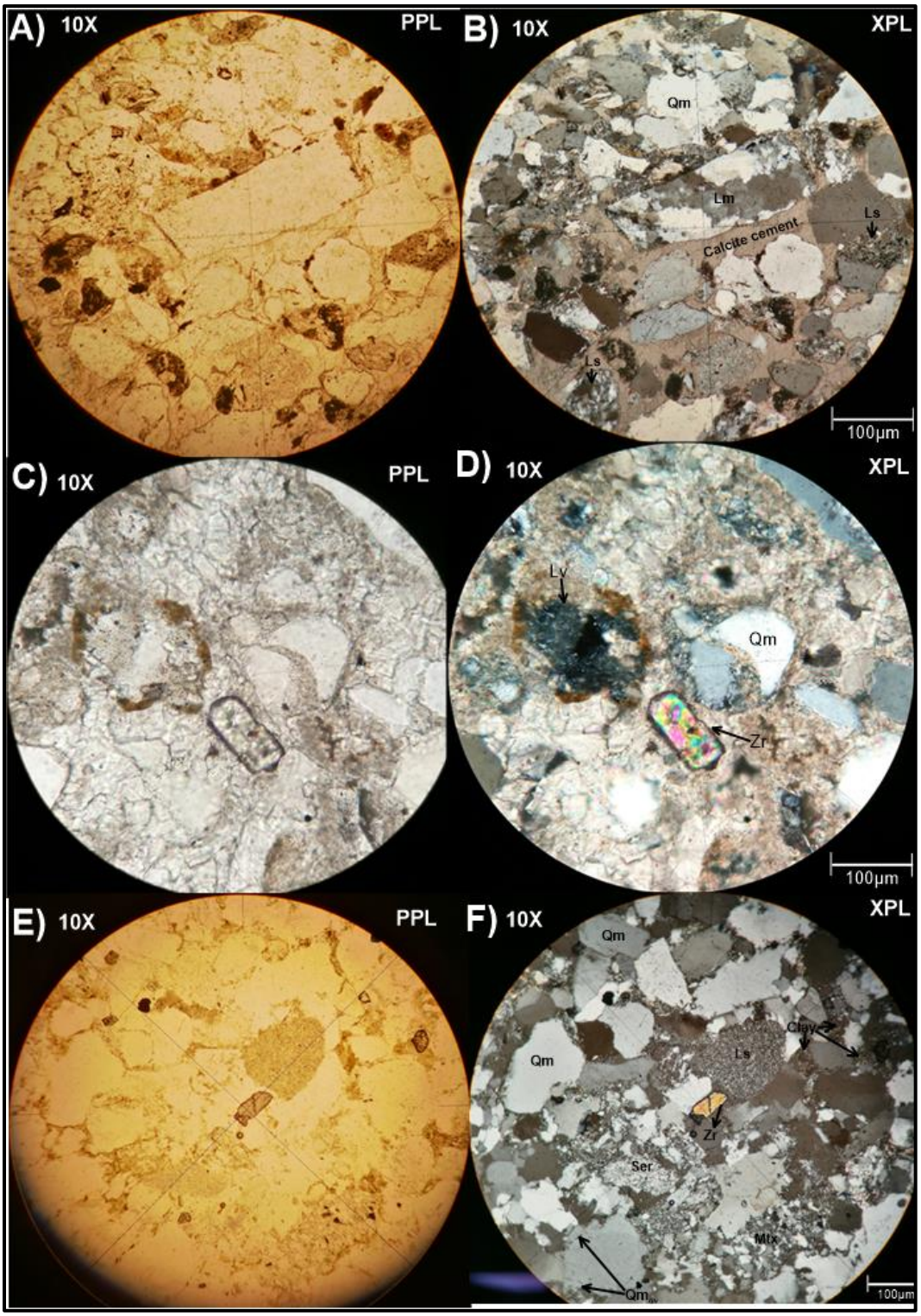

Figure 4.2.5: A) Under plain polar, B) under crossed polar showing a metamorphic polycrystalline quartzite lithic fragment that is possibly indicative of metamorphic origin (Sample F-A12 #13, at a depth of 2747.79m). The intercrystalline subcrystals of the

polycrystalline quartz have sutured quartz grain boundaries within the fragments, which is also encased in the poikilotopic calcite cement. C) Plain Polar, D) Crossed polar showing a zircon grain with a volcanic lithic fragment (F-A12 #13, at a depth of 2747.79m). There is also the occurrence of a large phenocryst in a glassy-fine groundmass. E) Plain Polar, F) Crossed polar showing a zircon grain with a volcanic lithic fragment (fine-grained groundmass) and monocrystalline quartz (Qm) (F-A5 #8, at a depth of 2702.84m). The occurrence of the abraded zircon grains is indicative of polycyclic reworking.

There are many different types of diagenetic features that could be seen in most of the samples, including pore fluid circulation (alteration), compaction, cementation (precipitated minerals in fractures and around grains), dissolution textures and mineral grain replacement features. These processes are destructive in many ways, such as decreasing permeability and porosity as well as causing difficulties in identification of some of the mineral grains for provenance analysis. It does however; provide useful information regarding the diagenetic modifications of the sediments.

Mechanical compaction was largely evident in most of the samples. This process could be seen from the compactional deformation of 'soft' glauconite (Figure 4.2.6A, B), bending and fracturing of muscovite and the interpenetration of quartz and feldspar grains (Figure 4.2.6C, D) (decreasing porosity further without additional cementation). Chemical compaction and dissolution is also evident with the occurrence of sutured boundaries and concave-convex grain boundaries (Figure 4.2.6C, D). This, rarely, also occur together with point contacts that is indicative of the differential stresses (compaction) involved within one sandstone unit with the selective mechanical durability of minerals. This is further amplified by the occurrence of quartz overgrowths that are at the early to intermediate stages and is indicative of first cycle diagenetic textures. The occurrence of polycyclic quartz grains exhibiting overgrowths is also evident in some samples (Figure 4.2.6E, F).

The alteration of the feldspars was also very common. The occurrence of alteration products such as sericite occurs in most of the samples (Figure 4.2.6D). Vacuolization is not as common as sericitization but does occur in some of the samples (even quartz grains). Replacement/Displacive textures of feldspars can also be seen, especially when a poikilotopic calcite cement is present (Figure 4.2.7A, B and C). Feldspar overgrowths rarely occurs but it is evident in some of the samples (indicative of weathering in the source area when alteration is visible) (Figure 4.2.7D, E).

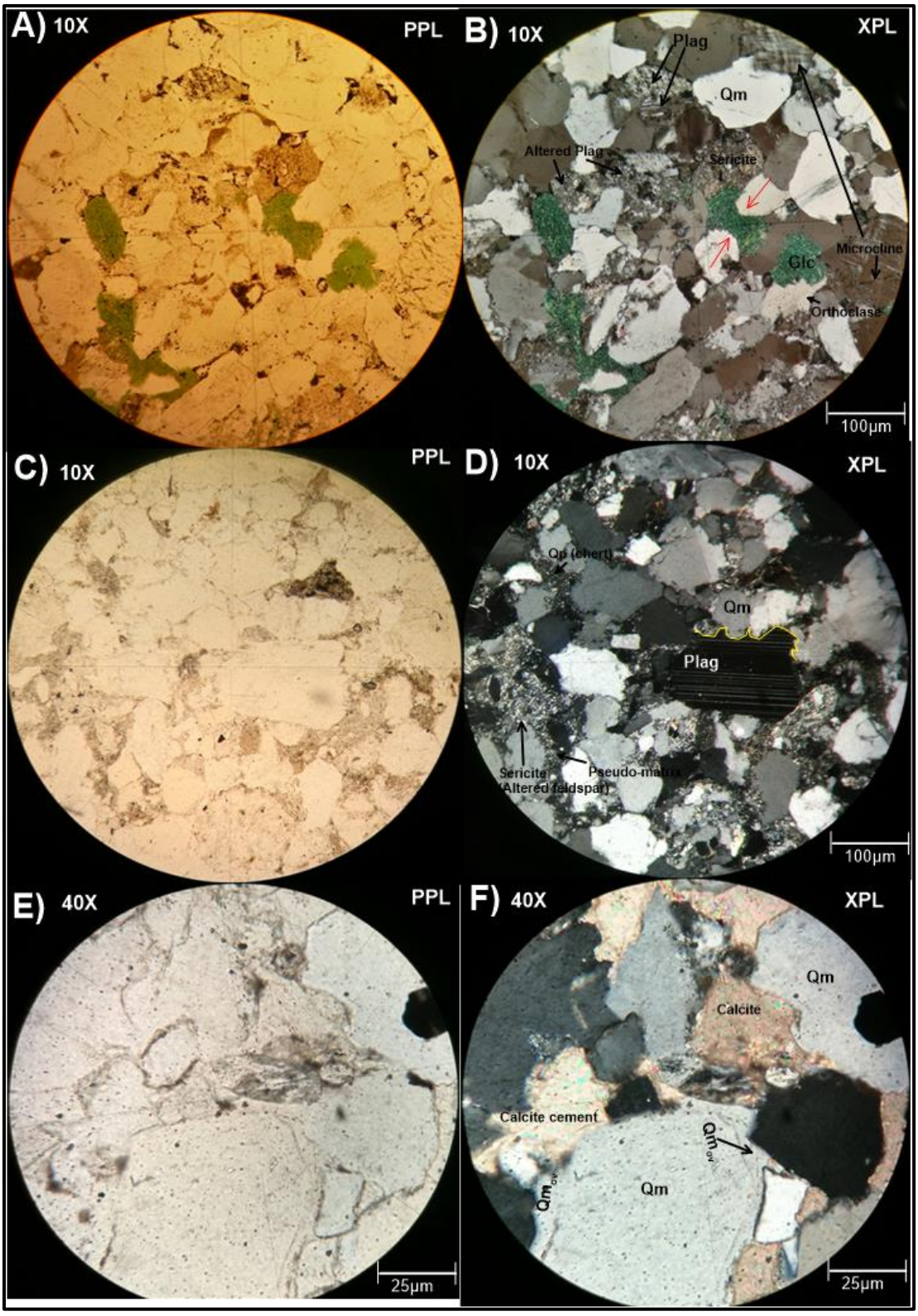

Figure 4.2.6: Mechanical and chemical compaction within the 1AT1-V succession. A) Plain polar (PPL), B) Crossed polars (XPL), Compaction of glauconite (Glc) in between two

monocrystalline quartz (M.Qtz), as indicated by red arrows, evident of the 'soft' nature of glauconite that is extremely vulnerable to compaction (Sample F-AR1#11, at a depth of 2744.81m) . The interpenetration of quartz into plagioclase feldspar (Plag) (yellow outline) with the surrounding quartz grains exhibiting sutured, concavo-convex and long contacts as illustrated in C) Plain polar and D) Cross polar (Sample F-A5#8, at a depth of 2702.84m). This is evidence of differential compaction (stresses within one sample). Dissolution by compaction of quartz to form early-intermediate stage of quartz overgrowths (idiomorphic), which can be seen and identified by its inclusion-free euhedral rim as illustrated in E) under plain polar and F) under crossed polar (Sample F-A12#13, at a depth of 2747.79m). There are also the occurrence of caries texture of quartz and calcite (upper right).

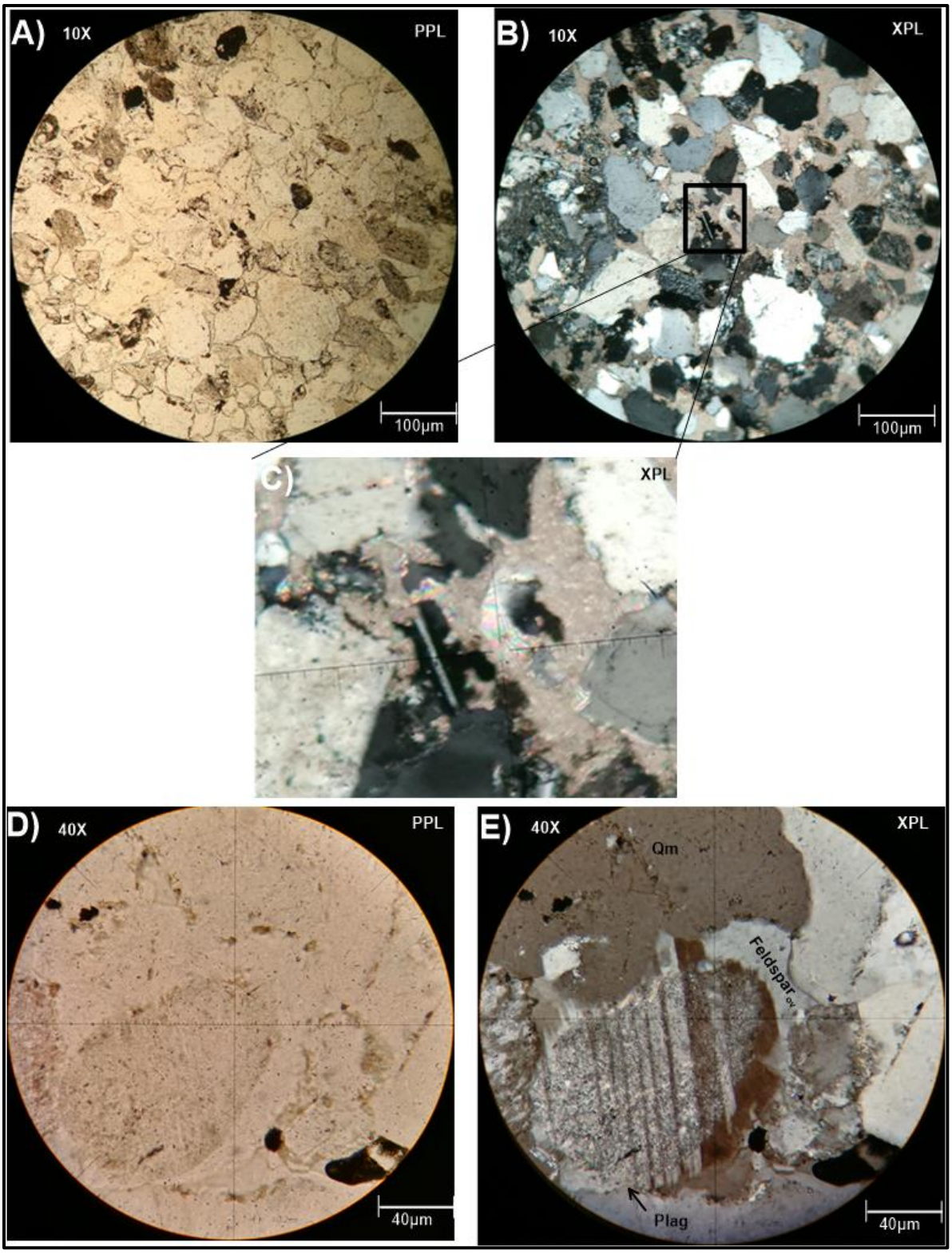

Figure 4.2.7: Replacement textures (A, B and C). Plagioclase being replaced by calcite that is common through diagenetic alterations (Sample F-A12 #13, at a depth of 2747.79m). D) Plain

polar, E) Crossed Polar, showing plagioclase overgrowths (Sample F-A5#5, at a depth of 2698.49m), which can be identified by the inclusion-free rim with a partially-fully altered core which is also in optical continuity with the host grain.

Clay minerals also form diagenetic cements but its occurrence is restricted to certain samples or, more specifically, depositional facies. Smectite and illite was both found in the claystone samples but its analysis falls well beyond the scope of this study. Some claystone clasts were also stretched and compacted to create a pseudo-matrix (Figure 4.2.6D).

Opaque minerals are also common with pyrite nodules being the dominant grains. Opaque minerals (mostly pyrite) are also restricted, to some extent, with the occurrence of clay minerals (as well as organic matter) in the sandstone samples (Figure 4.2.3B) which is further related to the depositional environment.

Calcite cements are also one of the abundant features within the samples usually occurring as a poikilotopic calcite cement (Figure 4.2.7B) (around 1% of all samples and 30% in extreme cases) thus having a major effect on the permeability and porosity of these samples (filling of pores). Calcite is also found as a replacement texture for plagioclase feldspars (Figure 4.2.7C). Quartz cement is restricted to the quartz overgrowths that interlock with the surrounding grains.

Unstable minerals such as K-feldspar, biotite (related to glauconite formation) and carbonate cements all contribute to the dissolution and precipitation more 'readily' than their stable counterparts do. Partial and full alteration or replacement of certain minerals is common. The alteration of K-feldspar and plagioclase feldspar is evident where sericite or illite becomes the end- product (Figure 4.2.2, 4.2.7E). This also occurs synonymously with partial and full dissolution and replacement of feldspars by calcite (calcium carbonate phase). K-feldspar is also observed to be replaced by vermicular kaolinite (Figure 4.2.3E).

4.2.1 Classification

The classification of sandstones can be attributed to the mineralogical composition, texture, porosity and permeability, including the matrix and cement, or a combination of these factors. On average, the modal composition of sandstones in the 1AT1-V horizon are $Q_{72}F_{21}L_{7}$, which falls mostly under the arkose and subarkose fields, with remnants occurring in the sublitharenite and lithic arkose fields (McBride, 1963) (Figure 4.2.8A). Thus acknowledging the fact that this

composition could have been slightly different at the time of deposition due to diagenetic effects (McBride, 1977; Tawfik et al., 2017). So overall, the samples in the 1AT1-V horizon exhibit a quartzofeldspathic composition, with very low lithic grains and low feldspar grains (based on visual estimation). The log-ratio six-fold compositional space diagrams of Weltje (2006) further confirm this (Figure 4.2.8B).

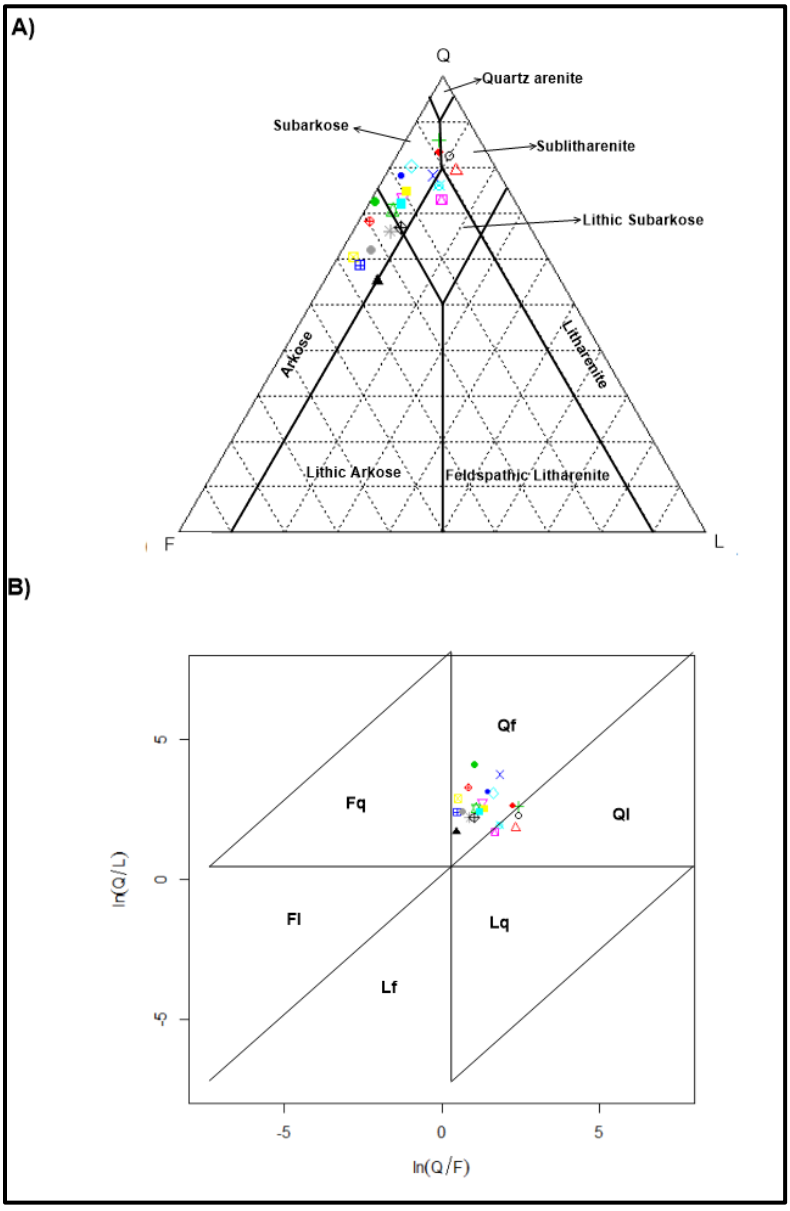

Figure 4.2.8: A) Sandstone classification QFL diagram with the modal compositions of the sandstones of the 1AT1-V horizon succession, after McBride (1963). B) Six-fold subdivision of compositional log-ratio space, after Weltje (2006). Qf-Quartzofeldspathic, Ql-Quartzolithic, Fq-Feldspathoquartzose, Fl-Feldspatholithic, Lf-Lithofeldspathic, Lq-Lithoquartzose.

4.2.2 Provenance and tectonic setting

The general petrographic descriptions of geological samples can provide reliable evidence for the source characteristics or provenance of the deposited sediments (grain shape, types of quartz, alteration products etc.). One can obtain clues for the compositional changes that the sediments have gone through from the source to the sink.

Most of the samples in the 1AT1-V horizon are indicative of a sedimentary (and meta-equivalents) provenance with subordinate low to middle rank metamorphic rock fragments indicative of metamorphic parent material (largely metasedimentary). This is largely based on the occurrence of undulose monocrystalline quartz, polycrystalline quartz, altered and fresh feldspars, siltstone and claystone clasts, metaquartzite grains, chert and some muscovite grains. The occurrence of igneous rock fragments is also indicative of another subordinate or ultimate provenance. Thus, enhancing the interpretation of mixing of different provenances as a crucial factor in the compositional variation of the sediments.

The results of the counted grains can be found in Appendix B. Provenance categories were based on the traditional QtFL (Dickinson, 1985), QmFLt, QpLvmLsm (Dickinson, 1985), undulose-based ternary plots (Basu et al., 1975). The main category fields for provenance/tectonic setting are Continental block provenance (stable craton and basement uplift), magmatic arcs and recycled orogens.

Abundant sedimentary and low to high-grade metamorphic clasts are largely indicative of a quartzose-recycled orogen. This is further confirmed by triangular plots that show that the 1AT1-V horizon samples plot in the quartzose-recycled field, transitional continental field and mixed provenance fields (Figure 4.2.10). With respect to the tectonic setting the sediments plots in the transitional continental field and recycled quartzose field on the QtFL (Figure 4.2.9). Thus is further supported by the collisional suture zone field on the QpLvmLsm diagram (Figure 4.2.12). The quantitative analogues to these ternary plots of Dickinson (1979) indicates largely continental block provenance settings and recycled orogenic sediments (Figure 4.2.13A, B) with its correlative provenance terrain fields (Figure 4.2.13C). These diagrams has been modified after Dickinson's (1979) provenance fields and represents a more quantitative illustration of the confidence regions of the provenance fields.

Furthermore, the parent rock type are supported by the ternary plot of Basu et al. (1975) and is part of the low-middle rank metamorphic field as well as the plutonic (possibly high-rank metamorphic) fields (Figure 4.2.11). This type of inference from traditional diagrams for provenance characteristics shows that the provenance of the basin has a complex history from different sources.

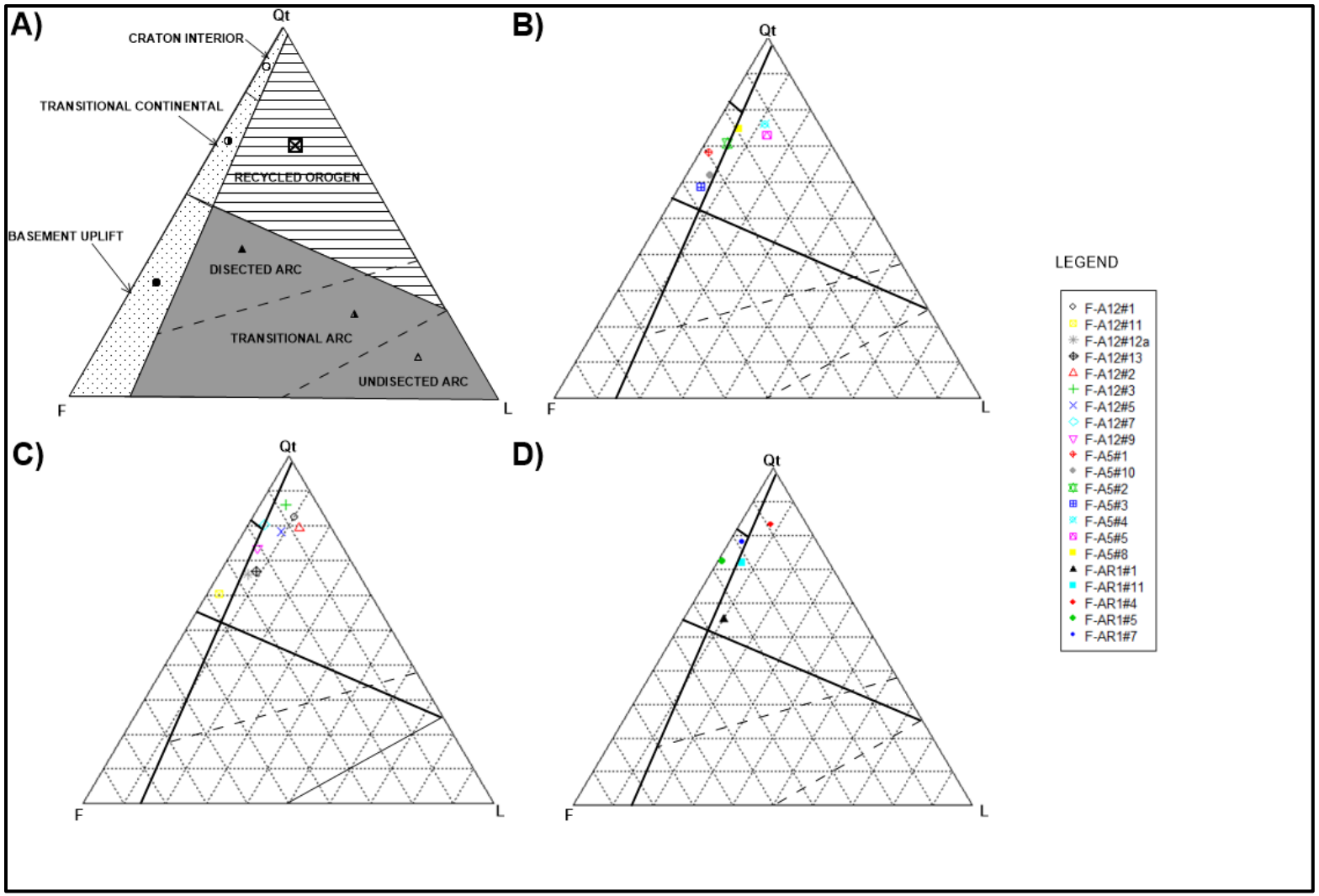

Figure 4.2.9: A) QtFL diagram with provenance fields (after Dickinson, 1975). Individual boreholes plotted as indicated by B) F-A5, C) F-A12 and D) F-AR1

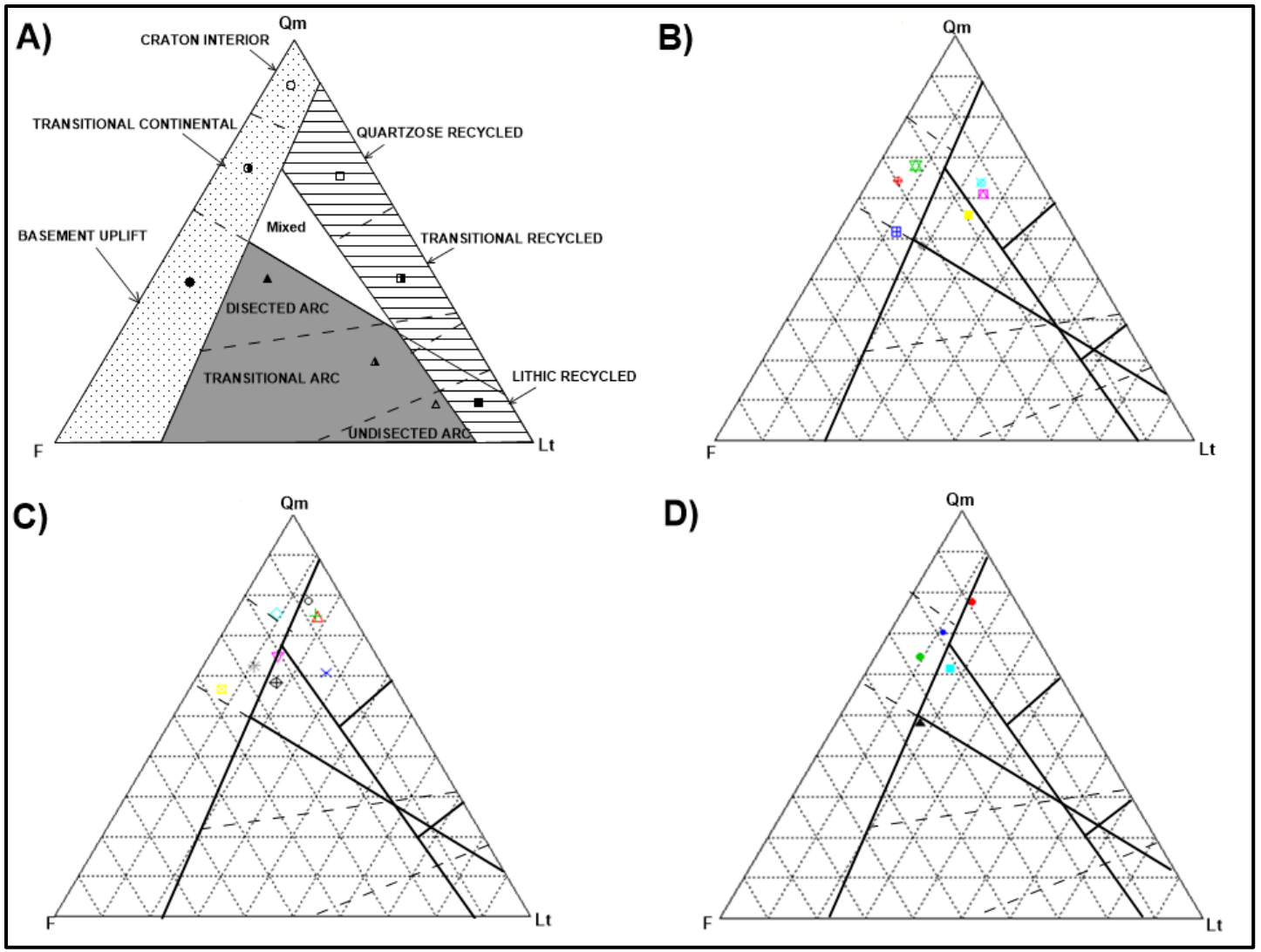

Figure 4.2.10: A) QmFLt diagram with provenance fields (after Dickinson, 1975). Individual boreholes plotted as indicated by B) F-A5, C) F-A12 and D) F-AR1

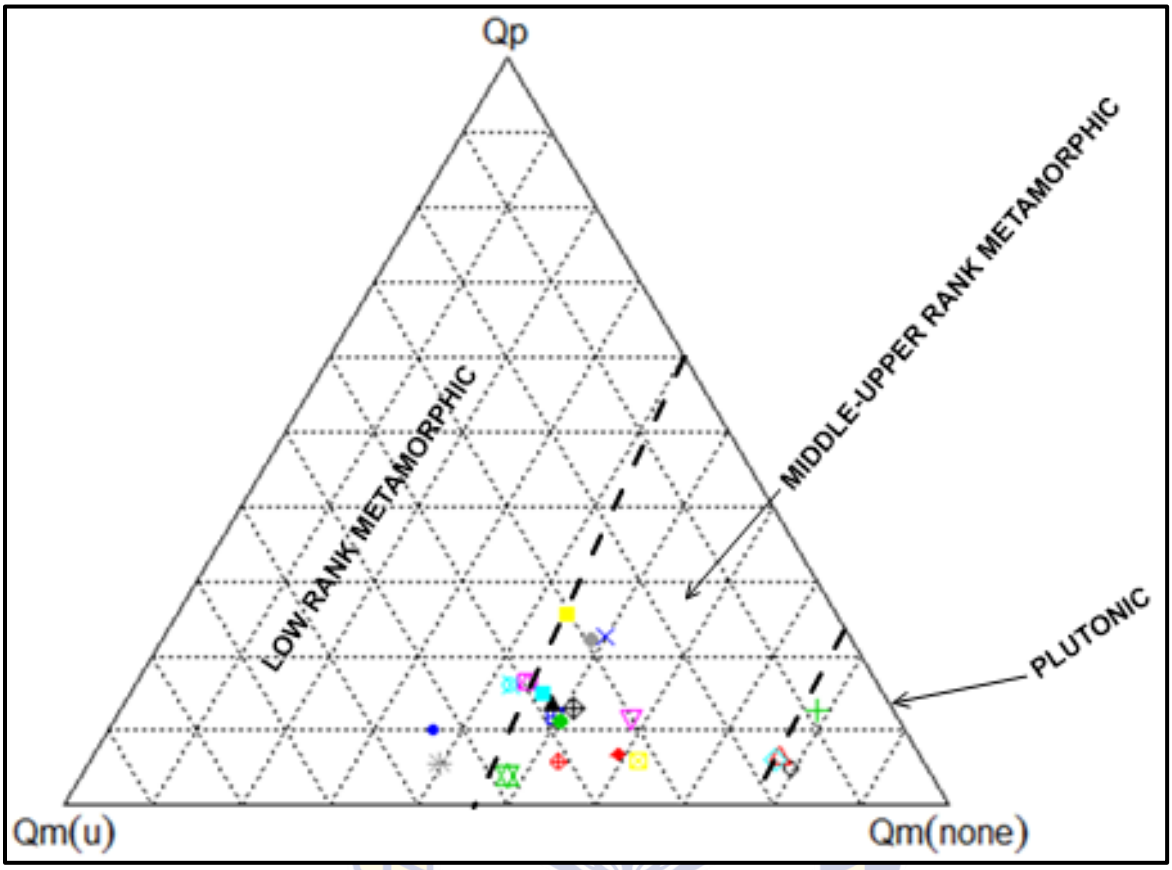

Figure 4.2.11: Significance of quartz grain provenance plotted on a QpQ(u)Q(non) diagram, after Basu et al., 1975. Qp=Polycrystalline quartz, Q(u) =undulose extinct quartz and Q(none)=none undulose extinct quartz

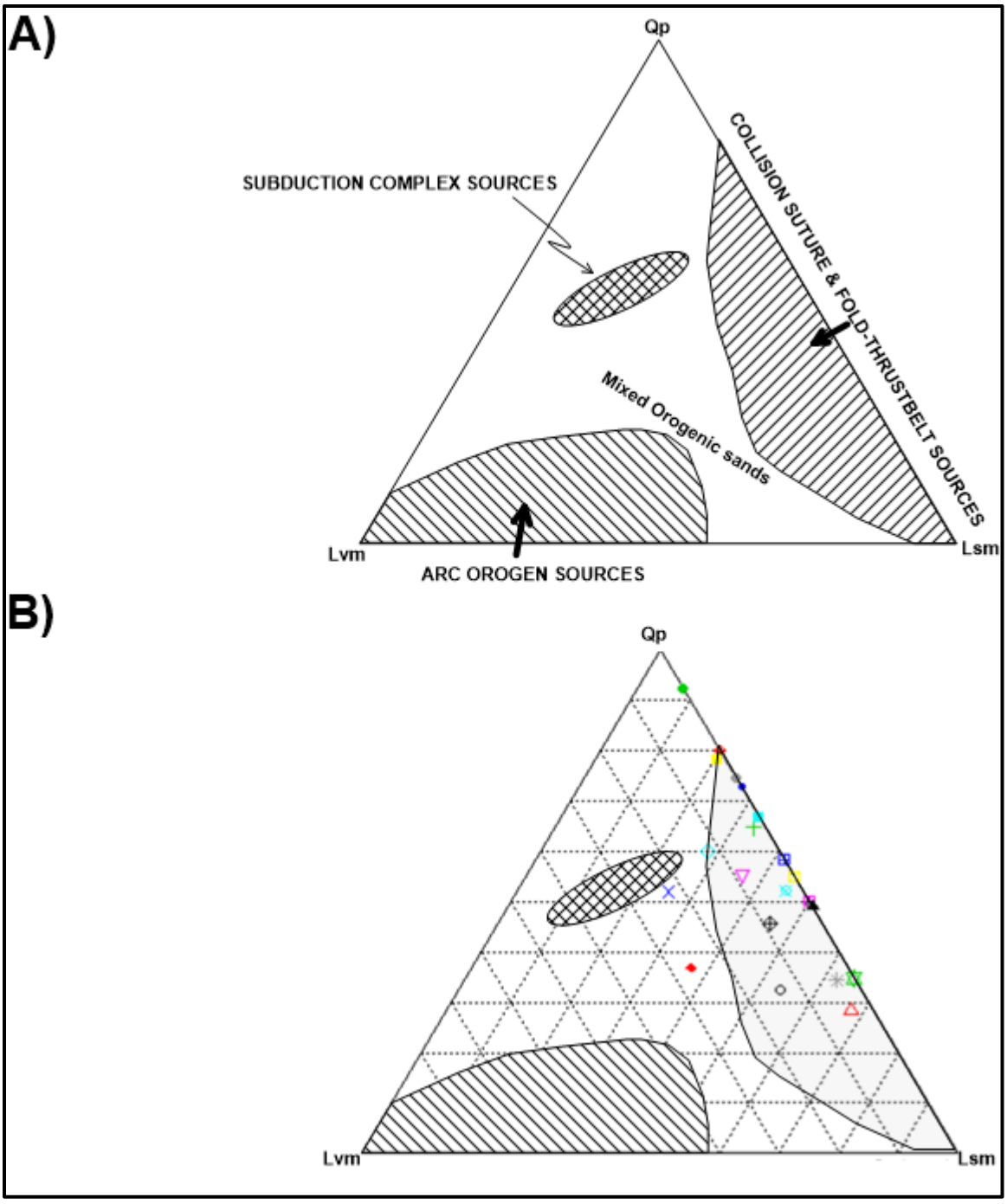

Figure 4.2.12: Ternary plots showing the tectonic setting of the samples plotted, A) General provenance fields after Dickinson (1975) and Dickinson et al. (1983) and B) Samples of the 1AT1-V horizon plotting in the collision-suture zone field.

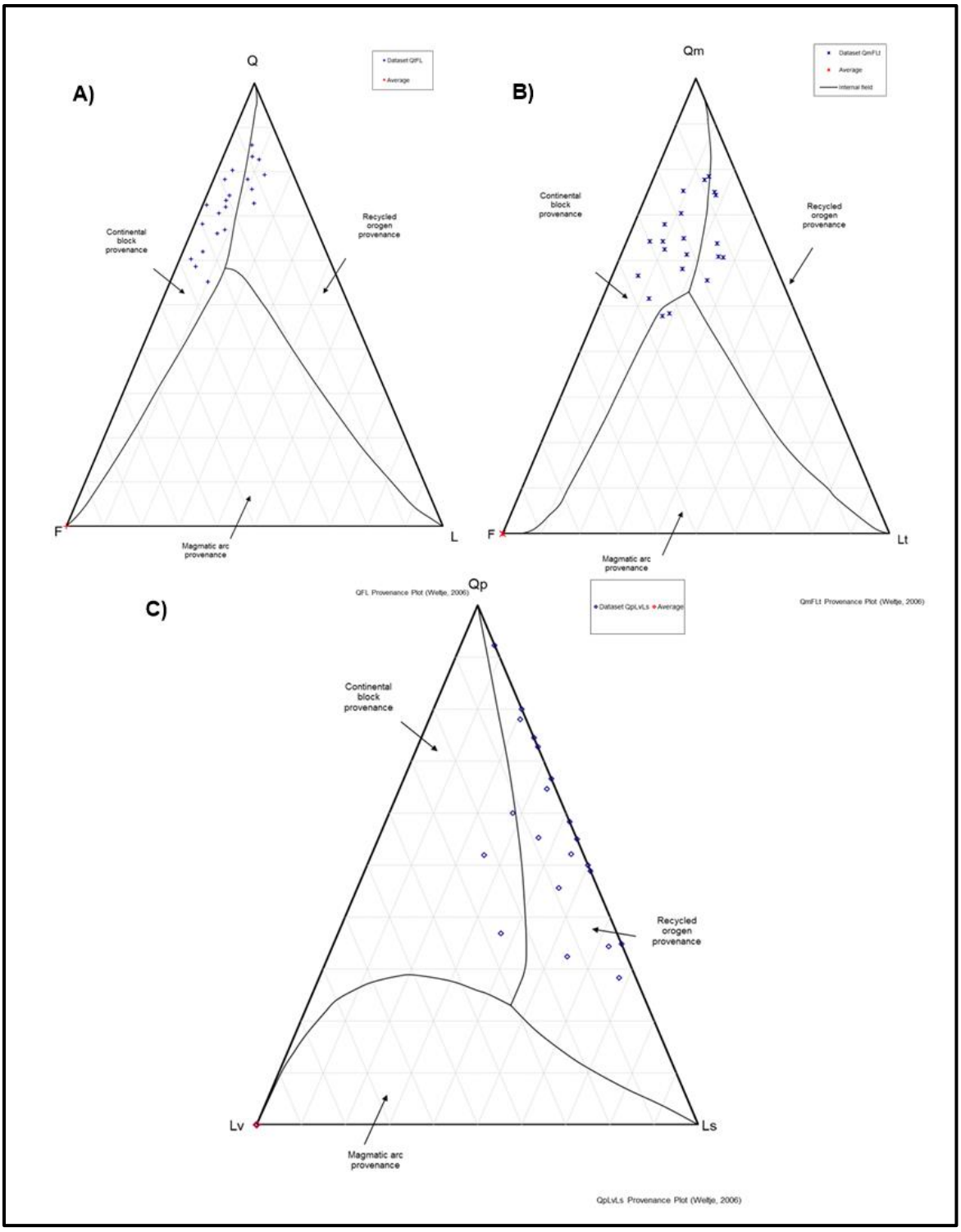

Figure 4.2.13: Quantitative ternary plots for provenance identification (after Weltje, 2006). A) QtFL ternary plot, B) QmFLt and C) QpLvLs ternary plots showing all samples plotted in compositional space.

4.3 Geochemistry

Thirty XRF/ICP-MS geochemical analysis from the three wells (F-A12, F-AR1 and F-A5) have been selected within the boundary of the 1AT1 to V unconformities and contain sandstones (coarser grained fraction) with a few finer grained components (mudstones and siltstones). F-A12 and F-A5 samples run throughout the interval whereas F-AR1 is limited to the upper reaches of the interval (close to the 1AT1 unconformity), which was solely accessible based on the cores available.

The whole-rock chemical composition of the sandstones and fine sediments (mudstone, claystone and siltstone) shows a wide range of values (Appendix C). The bulk rock geochemistry of the samples is taken as the average composition of the elements in the sample and care should be taken on the possible sources and external or internal factors (transport, weathering etc.) that might affect this.

Furthermore, the average of the chemical component concentrations was calculated and when compared indicates that the SiO_2 was higher (with lower MgO, CaO and $Fe_2O_3^T$) than the reference values (Appendix C, Table C1). Thus, indicating that source rocks does not have basic rock features according to Hu et al. (2014), which means that there was mixing of sources or diagenetically altered samples occurring in the vertical sequences of the chosen wells. The K_2O and Al_2O_3 average concentrations are low indicating that the content of clay is low within the samples. The SiO_2/Al_2O_3 ratio is greater than 5 and indicates that there could have been mature sedimentary or meta-sedimentary rocks within the source area. Petrographic studies reveal that the framework grains are mainly monocrystalline quartz (Qm), polycrystalline quartz (Qp), plagioclase feldspars and microcline, minor muscovite and minor rock fragments with abundant types of clay minerals. The K-feldspars are rather not ubiquitous but present in variable amounts and the geochemical results confirms this (mean value of K_2O=2.029 wt%, with 8 samples above 4 wt%).

4.3.1 Classification

Sandstones and siltstones have SiO_2 content >80% whereas mudrocks or shales have a SiO_2 content <70%, therefore the distinction between the two can be recognized geochemically on a geochemical plot (Pettijohn, 1963; Herron, 1988; Pettijohn et al., 1972). The geochemical

classification diagram of Herron (1988) indicates that majority of the samples plots in litharenite, sublitharenite and wackes with minor (one or two samples) plotting in arkose, shale and Fe-sand fields. F-A12 and F-A5 is spread equally throughout the fields but F-AR1 only plots in the sublitharenite field. The geochemical classification of Pettijohn et al. (1972) shows that majority of the samples plots in the sublitharenite, subarkose and litharenite fields with some samples plotting n the arkose field. All the samples belonging to the subtidal platform tidal sand ridges all plots in the sublitharenite fields that suggest that there was hydrodynamic recycling and sorting occurring as well as quartz dilution. The mudstones or shales plots in the shale, wackes and arkose fields because of the high content of Al-Fe bearing clay minerals. However, the sorting diagram of Garcia et al. (1994) (Figure 4.3.13A) better shows a classification with samples ranging from immature to mature sediments and are largely quartzofeldspathic in nature, which coincides with the petrographic classification.

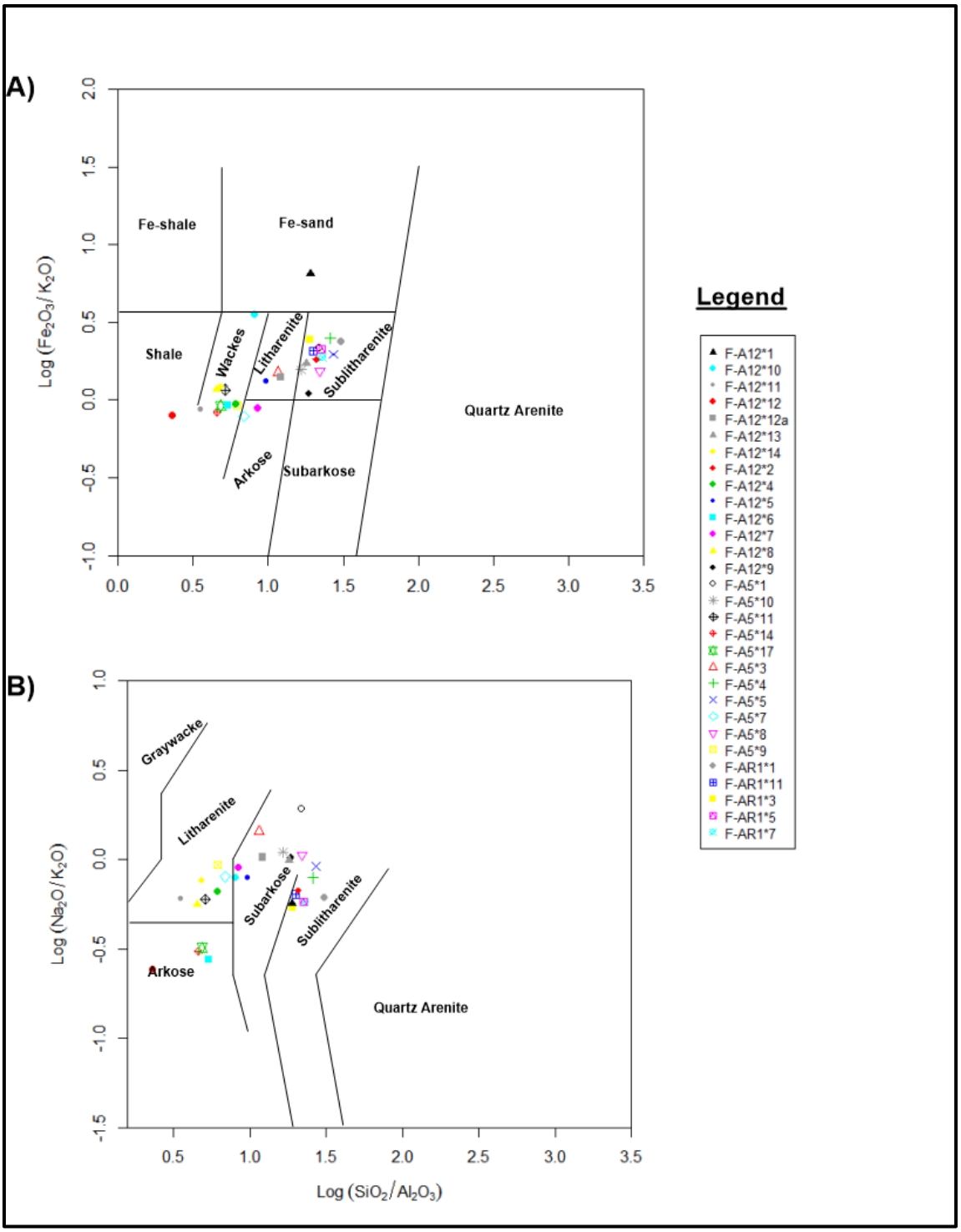

Figure 4.3.1: The log of A) (SiO_2/Al_2O_3) vs log (Fe_2O_3/K_2O) plot for the classification of sandstones after Herron (1988) and B) after Pettijohn et al. (1972).

4.3.2 *Major element variation* (Appendix C, Table C1 and C2)

The samples of the 1AT1-V horizons, in general, have high SiO_2 content (av. 79.93 wt%) with negative correlations to TiO_2 (av. 0.34wt%), Al_2O_3 (av. 6.39wt%), K_2O (av. 1.47wt%), Fe_2O_3 (av. 2.41wt%) and MgO (av. 0.79wt%) (Figure 4.3.4).

The variability in element distribution unrelated to provenance has to be identified in order to eliminate incorrect observations of the geochemical source characteristics. Diagenetic reactions can obscure the characteristics of the source, so careful treatment of the geochemical data has to be observed for this compositional variation.

Four samples have been identified geochemically with severe diagenesis (carbonate cements) from the general dataset which falls off the general trend on plots of Al_2O_3 vs SiO_2, P_2O_5/Al_2O_3 vs CaO/Al_2O_3 and FeO_T/Al_2O_3 vs CaO/Al_2O_3 (Figure 4.3.2). These four samples are F-A12#13 (lower), F-A12#1 (upper), F-A12#5 (middle) and F-A12#10 (lower). These diagrams assume that clay minerals are largely a result of feldspar alteration, and general trends of average published rock compositions from standards can be compared with Post-Archean Australian Shale (PAAS; Taylor and McLennan, 1985), Proterozoic craton sandstones and North American Shale Composite values (Gromet et al. 1984; Condie, 1993) to geochemical datasets to establish differences within a general trend (Pe-Piper et al., 2008). These diagrams are in agreement with each other and identify the samples that have undergone severe diagenesis, which is supported by petrographic data with poikilotopic calcite cements. The samples has not been omitted but has been added to the dataset to evaluate the significance of these samples with their corresponding provenance diagrams that does not use the diagenetically-related (post depositional) elemental compositions. These samples were excluded from the clr transformations with PCA analysis.

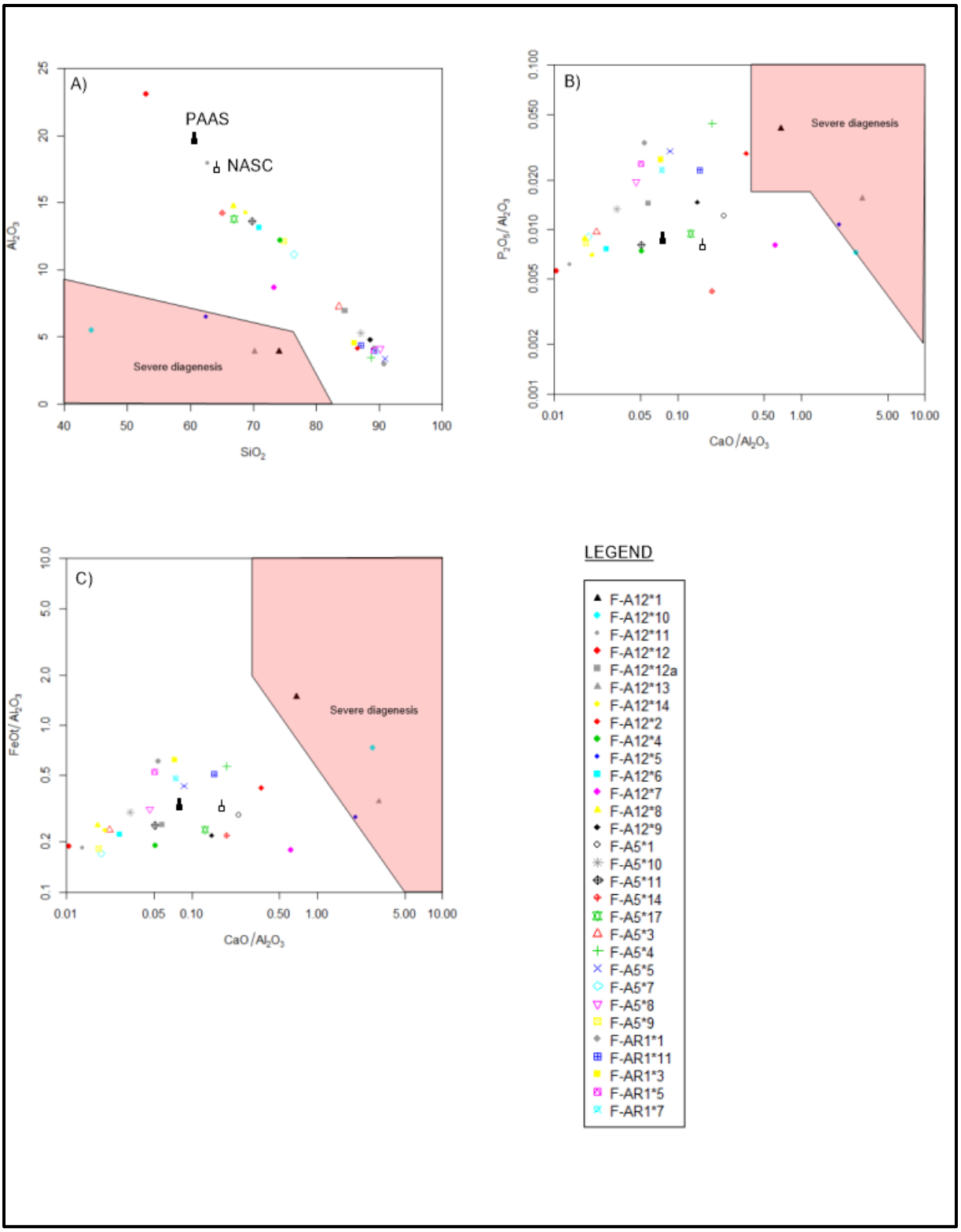

Figure 4.3.2: Plots of A) Al_2O_3 vs SiO_2; B) P_2O_5/Al_2O_3 vs CaO/Al_2O_3 and C) $FeOt/Al_2O_3$ vs CaO/Al_2O_3 showing the effects of diagenesis on the chemical composition from abundant

carbonate cement, modified after Pe-Piper et al. (2008). These altered samples fall off the clustering trend and has been confirmed from thin sections and basic statistics (box plots, histograms), the degree of diagenesis from carbonate cements.

In general (all samples), there is a negative correlation between SiO_2 (no covariants) and Al_2O_3 (co-vary with TiO_2, Na_2O, K_2O and Fe_2O_3) with $f > f_{critical}$ during an F-test (unequal variances) (Figure 4.3.4). On average, the samples show that the coarser fraction are more enriched in SiO_2 and MnO, and depleted in other elements (TiO_2, Fe_2O_3, Al_2O_3, Na_2O, K_2O) as compared to the UCC geochemical values (Figure 4.3.3). In contrast, the finer fraction shows mostly depleted values for elements compared to PAAS except for SiO_2, K_2O and Na_2O (Figure 4.3.3), with K_2O and Na_2O being the weathering sensitive cations (K^+ and Na^+). In addition, the finer fraction compared to UCC shows that K_2O is enriched in the fine fraction whereas the other elements are either constant or depleted. This is mostly due to the presence of illite with some anomalously high ratios of K_2O:Na_2O in the finer fraction. This ratio is usually used as an indicator of the relative abundance of K-feldspar and plagioclase with constant ratios generally falling close to one or below indicating subequal amounts of plagioclase to K-feldspars.

In the finer grained fraction, PCA was applied to major element oxides (SiO_2, Al_2O_3, TiO_2, Fe_2O_3, CaO, Na_2O and K_2O) (Figure 4.3.5). The first principle component explains 96.6% of variance and shows positive loadings for Al_2O_3 and K_2O (strong and weak loadings respectively) with strong negative loadings for SiO_2. The second principle component explains 2.5% of variance and shows positive loadings for SiO_2, Al_2O_3 and Na_2O with strong negative loadings for CaO. The proportion of total variability is retained by the first and second principle components and is equal to 99.1%. Thus clearly shows that CaO, SiO_2 and Al_2O_3 show the largest variability. The rest of the elements are linked to Al_2O_3, which suggest that they occur as a singular process (although in three dimensions they would plot on different planes but overlapping one another, spurious correlations).

In the finer grained fraction, there is a strong negative Pearson correlation between SiO_2 (co-vary with CaO) and Al_2O_3 (which co-vary with TiO_2, Na_2O, K_2O and Fe_2O_3) with r=-0.94 (Figure 4.3.5) and $f < f_{critical}$ (equal variances). CaO and MnO show a weak and strong positive Pearson correlation with SiO_2 respectively. A low negative correlation between Al_2O_3 and CaO (r=-0.27) suggest that not all Ca is of marine origin but possibly because of detrital Ca-bearing minerals at

the source (Plagioclase feldspar, eg. anorthite). Therefore, the use of Na_2O as a substitute for CaO* is not applicable but has been accounted for by determining the ratio (CaO/Na_2O) and using the values of reference criteria (eg. PAAS and UCC) to calculate the CaO within the silicate fraction only (CaO*). Also, a positive weak correlation between CaO and L.O.I ($r=0.33$, $f > f_{critical}$) confirms that Ca is not largely derived from the carbonates but also from a silicate bearing phase (von Eynatten, 2003; Hofer et al., 2013).

In the coarser grained fraction, PCA was applied to eight major element oxides (SiO_2, Al_2O_3, Fe_2O_3, MgO, CaO, K_2O, Na_2O and TiO_2) (Figure 4.3.5). The first principle component (PC1) explained 97% of the variance and shows positive loadings for SiO_2 (strong positive correlation and negative loadings on Al_2O_3 (strong negative correlation), Fe_2O_3, MgO, K_2O, Na_2O and TiO_2. PC2 explains 2% of variance and shows positive loadings for CaO (strong positive correlation) with negative loadings for all other elemental oxides (based on covariance matrix). Sample scores show some variation within the sandstones, especially the glauconitic shallow marine environment for F-AR1, F-A12 and F-A5 (well correlation).

In the coarser grained fraction, there is also a strong negative Pearson correlation between SiO_2 and Al_2O_3 (co-vary with MgO, TiO_2, Na_2O, K_2O and Fe_2O_3) with $r=-0.85$ (Figure 4.3.4). This relationship is weaker than the finer fraction because of the aluminous clay content.

The coarser grained fraction (sandstones) has higher SiO_2 values than the finer grained fraction (variance being equal ($f < f_{critical}$)). Thus making the use of SiO_2 as a defining factor between these two groups not statistically significant, in terms of variations. This would increase the probability that the samples were derived from a common process, mainly hydrodynamic sorting process, but sample size could be a factor for type 1 and type 2 errors. The CaO content is also enriched in the coarser fraction (av. 2.44wt%) relative to the fines (av. 0.95wt%) with the variance being unequal ($f > f_{crit}$). Thus, showing that CaO can be used as a discriminant factor among the fine- and coarse-grained rocks (relating to diagenetic calcite cement). This means that the CaO derived from the fine and coarser sediments was derived from two different processes. In addition, the Fe_2O_3, MgO, Na_2O and P_2O_5 concentrations are higher within the finer fraction than the coarse fraction.

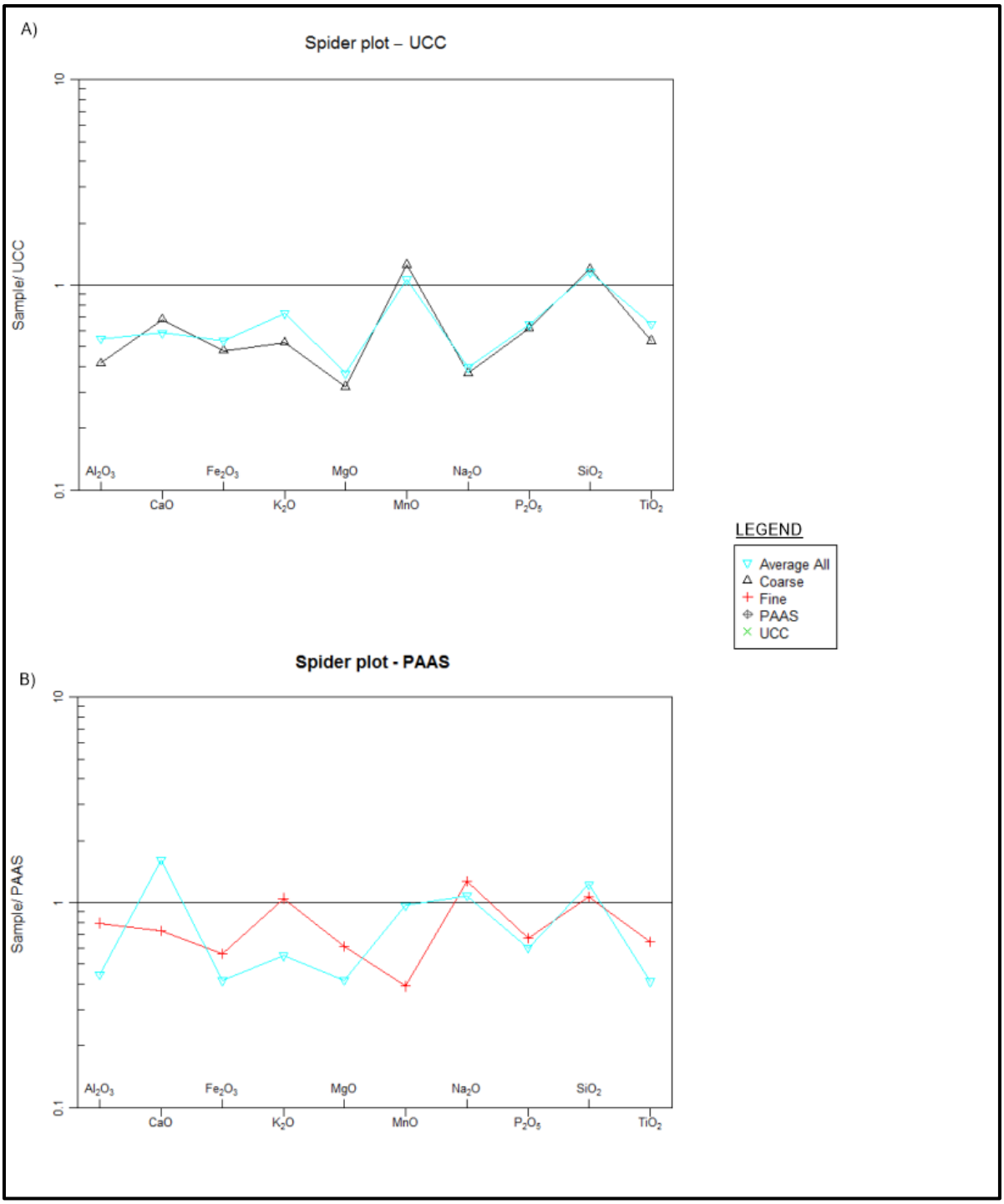

Figure 4.3.3: Major element chemistry of 1AT1-V horizon showing a) Average of samples compared to Upper Continental Crust (UCC after Rudnick & Gao, 2003) and B) compared to Post Archean Australian Shale (PAAS) after Taylor & McLennan, 1985)

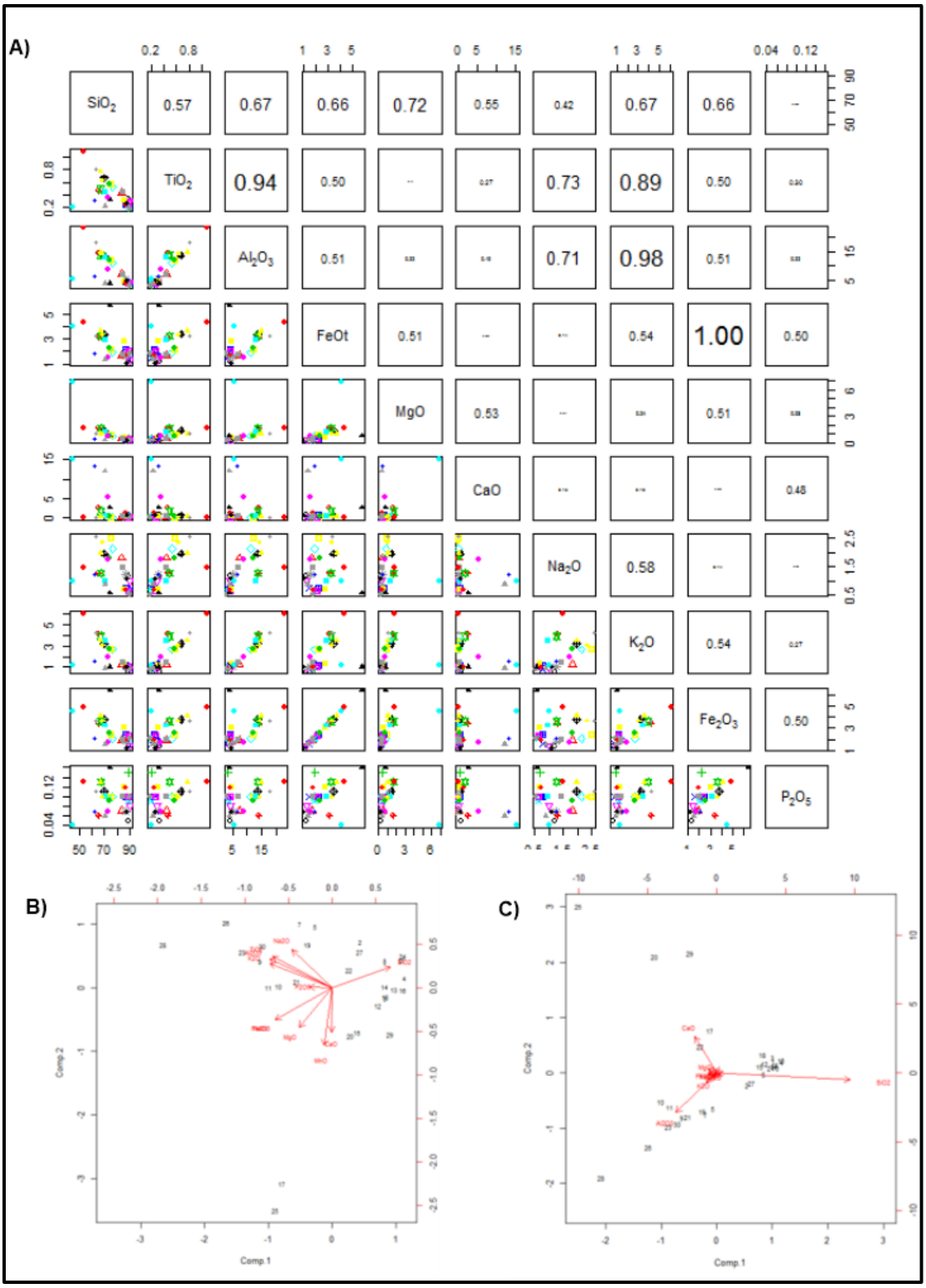

Figure 4.3.4: A) Correlation matrix of all samples (Sandstones and finer fraction (mudstone, siltstone, claystone) with component vectors based on B) Correlation matrix and C) Covariance

(Refer to Table C6 (Appendix C) for lithology, detailed correlation matrix (Appendix C) and Legend in Figure 4.3.2)

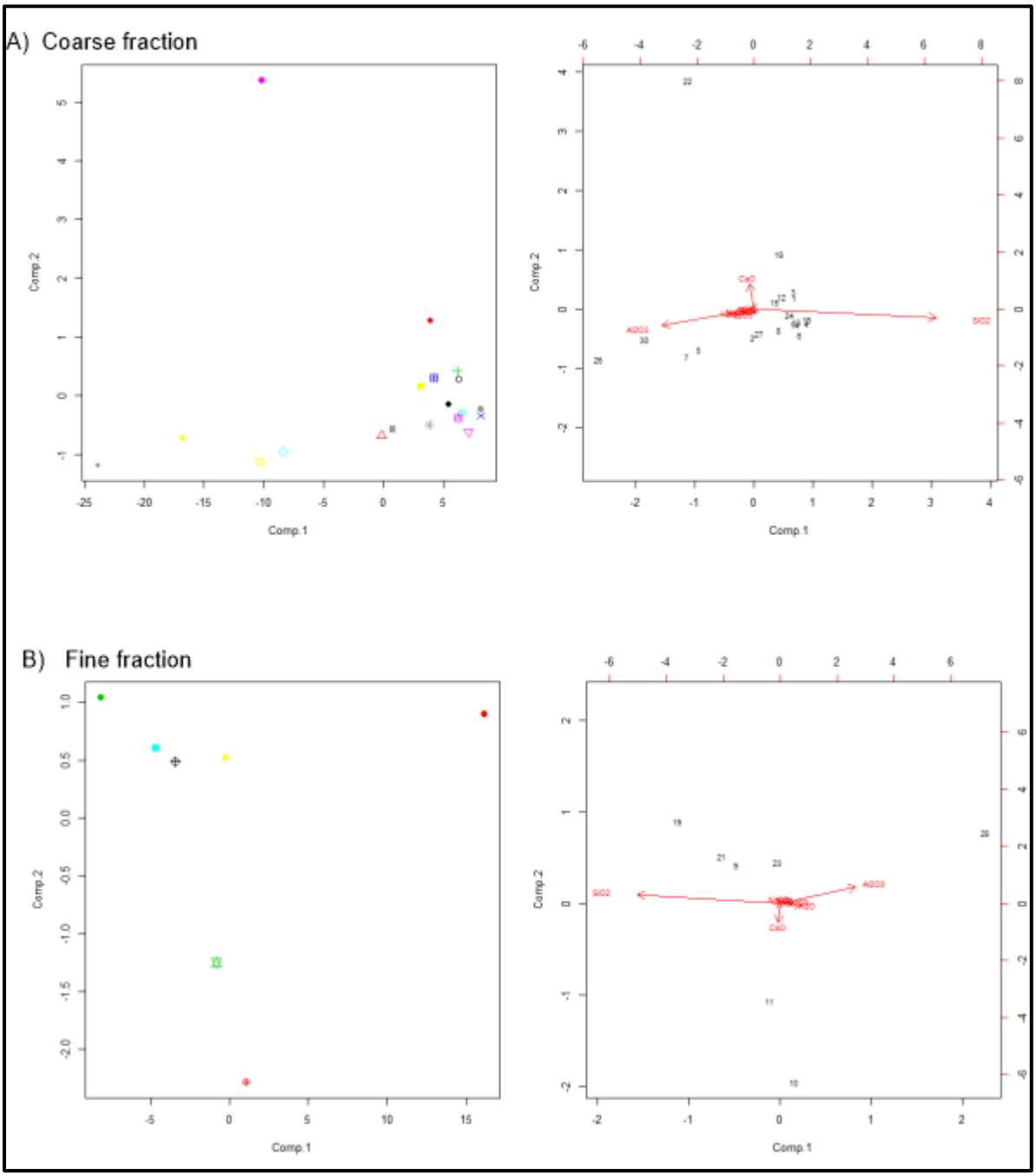

Figure 4.3.5: Principle component analysis of A) coarse grained and B) finer grained fraction showing major oxides based on the covariance matrix for the normal (untransformed) data.

The concentrations, vertically (stratigraphic), also shows slight compositional fluctuations (Major element oxides conc.) but this is mostly as a result of the positive correlation between

SiO_2 and Al_2O_3 with a decrease in grain size and depositional environment, therefore a need to group these variables was not necessary.

Si/Al elemental ratios (proxy for quartz) are low and constant in general (average= 4.15±0.37) with K/Al (proxy for illite content (Hofmann et al., 2001)) and Na/Al (proxy for smectite content (Hofmann et al., 2001)) remaining constant with an average of 0.404±0.014 and 0.15±0.017, respectively, within the finer grained fraction. The Th/K is quite high which is the proxy for kaolinite (Parkinson, 1996; Deconinck et al., 2003; Zhang et al., 2014). The Plot of K/Al vs Na/Al (with K_2O vs Na_2O) shows that these elements does not vary much between the two wells but rather a strong correlation exist with one another. There is also a weak negative correlation between Si/Al and K/Al. F-A12#6 and F-A12#12 shows a high illite and low smectite content, F-A5#17 and #14 shows a very high illite and low-medium smectite content and F-A12#8, F-A12#4 as well as F-A5#11 shows low illite with high relative smectite contents (Figure 4.3.6). The K_2O/Al_2O_3 ratios are very low as indicators for the relative quantity of illite and kaolinite.

Also, the influence of heavy minerals are usually accounted for by using TiO_2 in binary diagrams, which can occur in clay minerals and heavy minerals or is largely retained with Al_2O_3 (change in hydrodynamic conditions) in the finer fractions (Garcia et al., 1994). A strong positive correlation between Al_2O_3 and TiO_2 (r=0.943) and Nb and Al_2O_3 (r=0.974) suggest that clay minerals could be a possible source for adsorbed titanium. There is a weak negative correlation between Si/Al and K/Al suggesting that most of the illite content were diagenetic in origin. The weak negative correlation between TiO_2 and K/Al also suggest that $TiO_2$was not derived (adsorbed) from illite but possibly from other clay mineral, authigenic anatase or heavy mineral (ilmenite and rutile). The TiO_2 content, whether adsorbed by clay minerals or a source of ilmenite should be acknowledged. This statement should be observed within the depositional environment. There is also a high value for K/Rb (av.200).

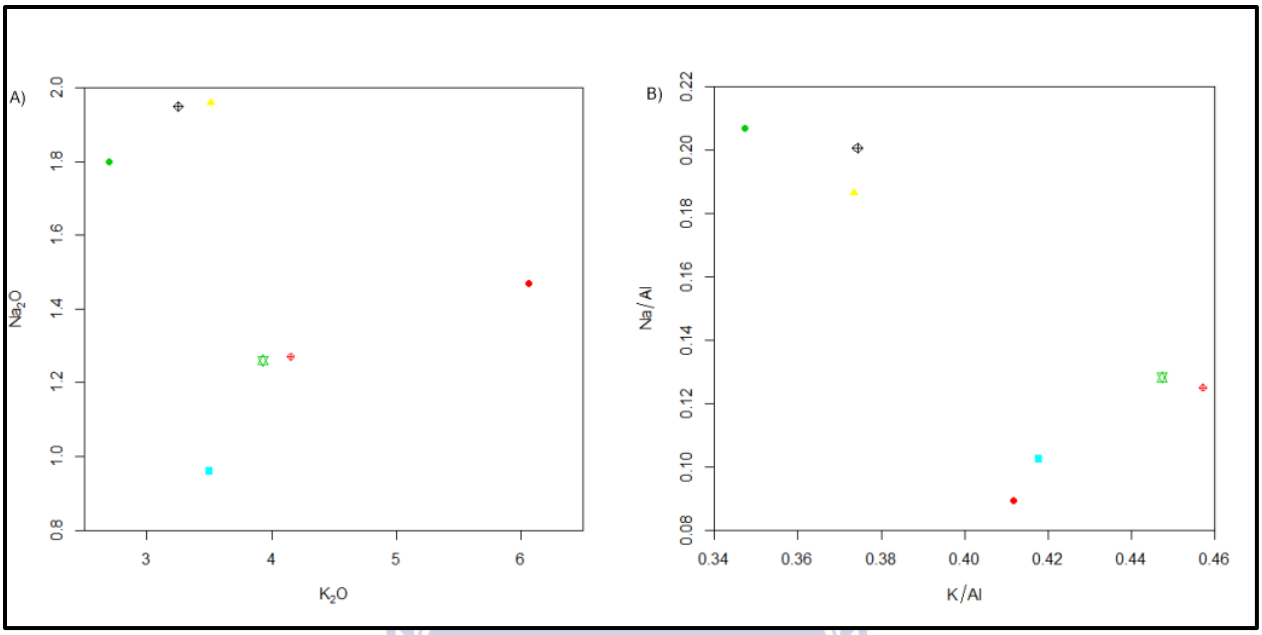

Figure 4.3.6: Illite vs Smectite relative occurrence based on geochemical percentages of K2O and Na2O (left) with Na/Al and K/Al as well (Right)

The relationship between major elements is crucial to delineate possible geochemical 'families' (high correlation factor). The enrichment of silica in sandstones relative to mudstones and siltstones with negative correlation of Al_2O_3, TiO_2, Al_2O_3, Fe_2O_3, MgO and K_2O means that most of the silica present within samples are present in quartz grains (Figure 4.3.4) (Tawfik et al., 2017). The major differences between the sandstones and mudstones would be the dilution factor of quartz (Cullers, 2000). This dilution factor and K-Feldspar dissolution (during illite formation) plays a role in the reasoning behind some of the claystone samples that are geochemically not portrayed as shales. Another factor could also be the dirty nature of the sandstone or claystone (some sandstone with siltstone bands) and high amount of Al-bearing clay minerals. The low values of K_2O/Na_2O ratios accounts for the occurrence of plagioclases over K-feldspar, which only increases as the illite-trend composition is reached (Table C4 (Appendix C), Figure 4.3.11).

4.3.3 Trace and rare earth element variation (Appendix C, Table C2 and within stratigraphic variation)

Trace and rare earth elemental analysis were carried out for 30 samples (23 coarse and 7 fines). On average, most of the samples show concentration below 100ppm except for V (42-145ppm, one sample showing high value of 145ppm), Cr (47.55-467.75ppm), Zn (16.65-176.35ppm, one

sample above 100ppm), Rb (26.54-271.25ppm), Sr (38.2-903.5ppm), Zr (95.05-576.5ppm), Ba (190.15-3680ppm) and Ce (31.73-130.95ppm). On Average, compared to UCC, all the samples shows that it is more enriched in Zr, Hf, Sm, Eu, Tb, Yb and Lu and depleted in the other trace elements (Figure 4.3.7). Within the stratigraphic section, HFSE (High field strength elements are higher in F-A12 and F-A5 (shallow and deeper depths) with F-AR1 (shallow depth) showing more depleted values as compared to UCC (Figure 4.3.7, Appendix C). Trace element concentrations are more depleted in the coarser fraction than the finer fraction. In fact, trace elements are more enriched within the finer fraction than the average in all trace elements except for Sr. On average, compared to PAAS, samples show that it is more depleted in trace elements except for Zr and Hf (Figure 4.3.7). As compared to PAAS, trace elements are more enriched within the finer fraction than the coarse fraction.

The Strontium (Sr) content for three samples (F-A12#10, F-A12#5 and F-A12#13) are also highly enriched (Figure 4.3.7). The Chromium (Cr) content is also well beyond the average of the UCC value (92ppm) with samples ranging from 47.55-467.75ppm (Av. 234.13ppm). Cr/V values range from 0.64-7.76ppm with Y/Ni ranging from 0.4-3.82ppm, which is higher than the PAAS and UCC values. The relative abundances of Cr, Ni, Co, Sc (depleted as compared to the UCC) indicates a possible mixing or provenance from a mafic source, but no literature evidence indicates that there is a presence of first-cycle mafic sources for the Bredasdorp sub-basin, therefore another explanation should be considered (Cingolani et al., 2003). In general, there exists a strong positive correlation between elements of Ti, Zr and V (V being relatively low compared to UCC).

Heavy Rare Earth Elements (HREE) shows a flat trend, whereas the Light Rare Earth Elements (LREE) normalized to chondrites (after Boynton, 1984) shows an enriched trend but decreases as Gadolinium (Gd) is approached. One sample, F-A12#12 being particularly enriched in HREE compared to other samples.

The average ratios of La/Sc, Sc/Th, Cr/Th and Co/Th in the coarse-grained samples are 3.21, 1.10, 38.73 and 0.77, respectively. In the finer fraction, the ratios of La/Sc, Sc/Th, Cr/Th and Co/Th are 3.26, 0.82, 5.84 and 0.44, respectively (Table C4, Appendix C). There are also lower values of La/Sc and Cr/Th ratios in UCC and PAAS, with higher values for Sc/Th and Co/Th in

UCC and PAAS compared to the average of the coarser and finer fraction. The relatively high ratios of Th/Sc (av. 0.95) and high values of Zr/Sc (max. 73,53) suggest that there was extensive recycling and sorting due to zircon enrichments (some minor samples that shows little recycling). In addition, there is a negative correlation between Th and Th/U. The Rb/Al_2O_3 ratios are also quite high as compared to UCC. There is also a good positive correlation between TiO_2 and Zr (r=0.64)

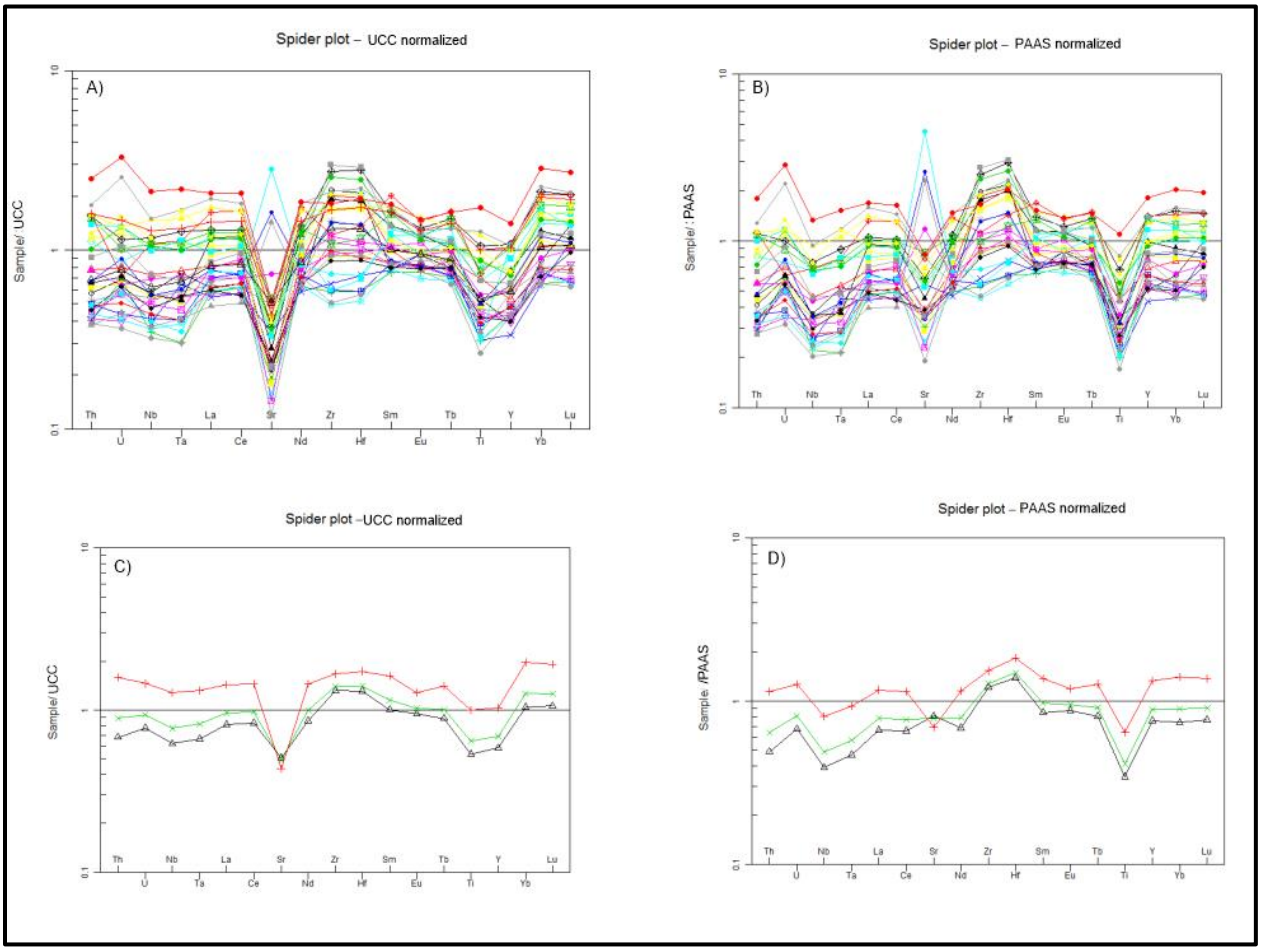

Figure 4.3.7: Trace element variation A) compared to UCC, B) PAAS with the average elemental compositions, the coarser grained fraction and finer grained samples compared to C) UCC and D) to PAAS

4.3.4 Major element and Trace element transformed (clr) variation

4.3.4.1 Classification and variations

The clr-transformed data was evaluated and can be found in the Appendix C (Compositional data summary statistics (Table C8 and C9)). Correlation and covariance matrices can also be found in the appendix. As seen above three subcompositions were outlined in the PCA (normal) but the other elements were shadowed and over exaggeration of the data occurred (very high correlation effects). This makes data interpretation problematic especially when observing subcompositional trends within the dataset (Martin-Fernandez et al., 2005).

PCA was applied to eight major oxides using clr-transformed data (Figure 4.3.8, Table C8). The elements are SiO_2, Al_2O_3, Fe_2O_3, MgO, CaO, K_2O, Na_2O and TiO_2, which were used to evaluate provenance characteristics and weathering effects. Samples affected by severe diagenesis have been removed.

In the coarse-grained fraction (Figure 4.3.8A), the first component explains 68.7% of variance with positive loadings for all elements except for SiO_2 and CaO. The second component explains 20% of the variance with negative loadings for Al_2O_3, K_2O, CaO, Na_2O and TiO_2 and positive loadings for SiO_2 and Fe_2O_3. The total proportion of the variance by the first two components can be explained by 88.7%. This making the results significant in terms of their variation (Thió-Henestrosa & Martín-Fernández, 2005). In the finer fraction (Figure 4.3.8B), the first component explains 79% of the variance with positive loadings for all elements except for CaO (high negative loading) and MgO. The second component explains 15% of the variance with positive loadings for CaO, Na_2O, SiO_2, TiO_2 and negative loadings for Al_2O_3, Fe_2O_3, K_2O and MgO. The total proportion of variance can be explained by 94%.

PCA analysis for transformed major elements in the coarser grained fraction shows that Al_2O_3, Fe_2O_3-SiO_2 and CaO are orthogonal (Figure 4.3.8A). These links can be described as these elements forming separately or under different processes (Tolosana-Delgado et al., 2005). Also, the normal data (untransformed) shows subcompositional linear trends (SiO_2, CaO and Al_2O_3) that are largely exaggerated because of the constant-sum problem. The variations are quite small between the transformed data and untransformed data, but the use of the untransformed data might give misleading results as to the variations made by individual proportions of

subcompositions, if the method outlined, by Martin-Fernandez et al. (2005), Aitchison & Greenacre (2002) and Aitchison & Pawlowsky-Glahn (1997) were to be followed on PCA characteristics.

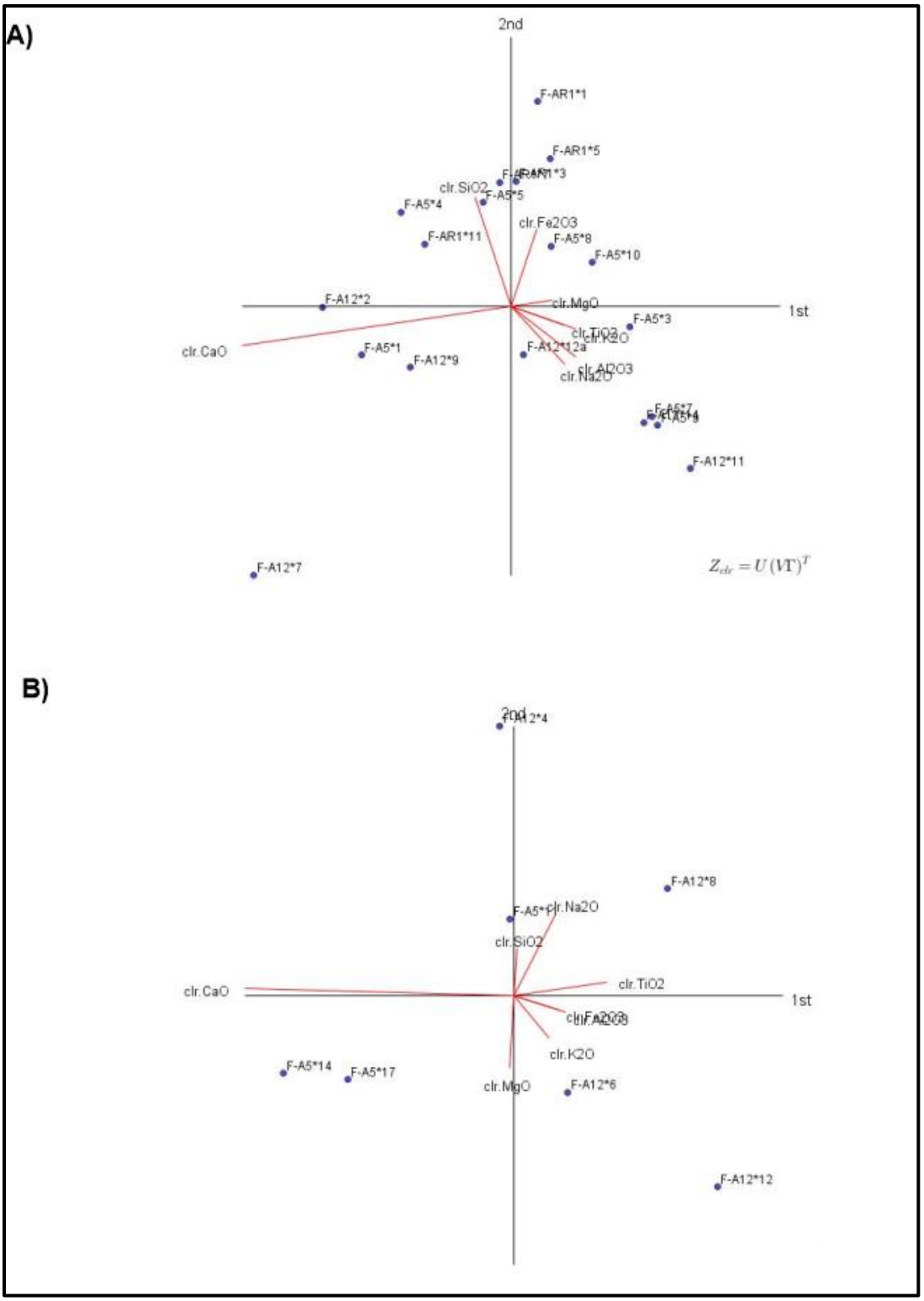

Figure 4.3.8: Principle component analysis (PCA) based on transformed data. PCA was performed on eight major oxides within the A) coarser grained samples and B) finer grained samples. Principle components are based on the covariance matrix.

PCA was applied to trace elements (Table C9) with a detrital signature or that is more indicative of source rock composition (Pe-Piper et al., 2008). PC1 in the coarse fraction explains 42% of the total variability with low positive loadings for Sr, Rb, Nb, Ta, Th and U as well as high positive loadings for Zr-Hf subcompositions (Figure 4.3.9A). This shows that PC1 variation is mostly caused by the trace elements associated with heavy minerals. PC1 shows negative loadings for V-Co-Ni subcompositions with the other elements showing weaker correlations with the principle component. PC2 explains 24% of the total variability with strong positive loadings for Rb and Sr and strong negative loadings for Zr, Hf and Co. The strong positive loadings of Rb and Sr is most probably as a result of feldspars and mica minerals, which is confirmed by the modal counts for the samples that plots close to these vectors (Pe-Piper et al., 2008). The total proportion of variability can be explained by 66% within the first two principle components. A vague discrimination can be seen with F-AR1 (Northern borehole) that has a higher correlation with Ni, Co, La, Gd, Y and Sc. These are elements closely associated with mafic sources. There is also a third subcomposition forming with Nb-Ta-U-Yb group of elements with strong relation to the Sr-Rb subcomposition. These elements were used solely because they best represent the ultimate source of the sediments (Bhatia & Crook, 1986; McLennan 1993; Totten et al., 2000; McLennan, 2001; Ryan & Williams, 2007).

In the finer fraction (Figure 4.3.9B), PCA was performed on the same trace elements as the coarser fraction. PC1 explains 59% of the total variability with strong negative loadings for Zr and Hf. PC1 has weak positive loadings for all other trace elements (with Th, Co, Sc and Rb showing the highest). PC2 explains 28% of the total variability with strong positive loading for U (with weak positive loadings for mafic associated elements V and Co (Ni and Sc shows negative loadings). Strong negative loadings on PC2 are found with Gd and Sr. The proportion of total variability can be explained by 87% within the first two principle components.

The method of Caracciolo et al. (2012) proved to be successful in determining the provenance and tectonic setting of three sub-basins of different environments. The K_2O, SiO_2, Al_2O_3, CaO, Na_2O, TiO_2, MgO, Fe_2O_3, Ni, Sc, La, Rb, Zr, Th, Sr and Hf clr transformations were used to perform PCA on the coarse-grained fraction (Figure 4.3.10). PC1 explained 55% of the total variability with strong positive loadings for CaO. PC2 explained 29.6% of the total variability with strong negative loadings for Zr, Hf, Na_2O and CaO. The proportion of total variability can

be explained by 87.5% within the first two principle components. Thus making the results for non-correlation between samples and elements very strong. The V, Ni, Fe_2O_3 groups together and these elements shows a possible indication of an intermediate felsic-mafic input. This is further confirmed on provenance-related elements in discriminant function analysis (Appendix C)

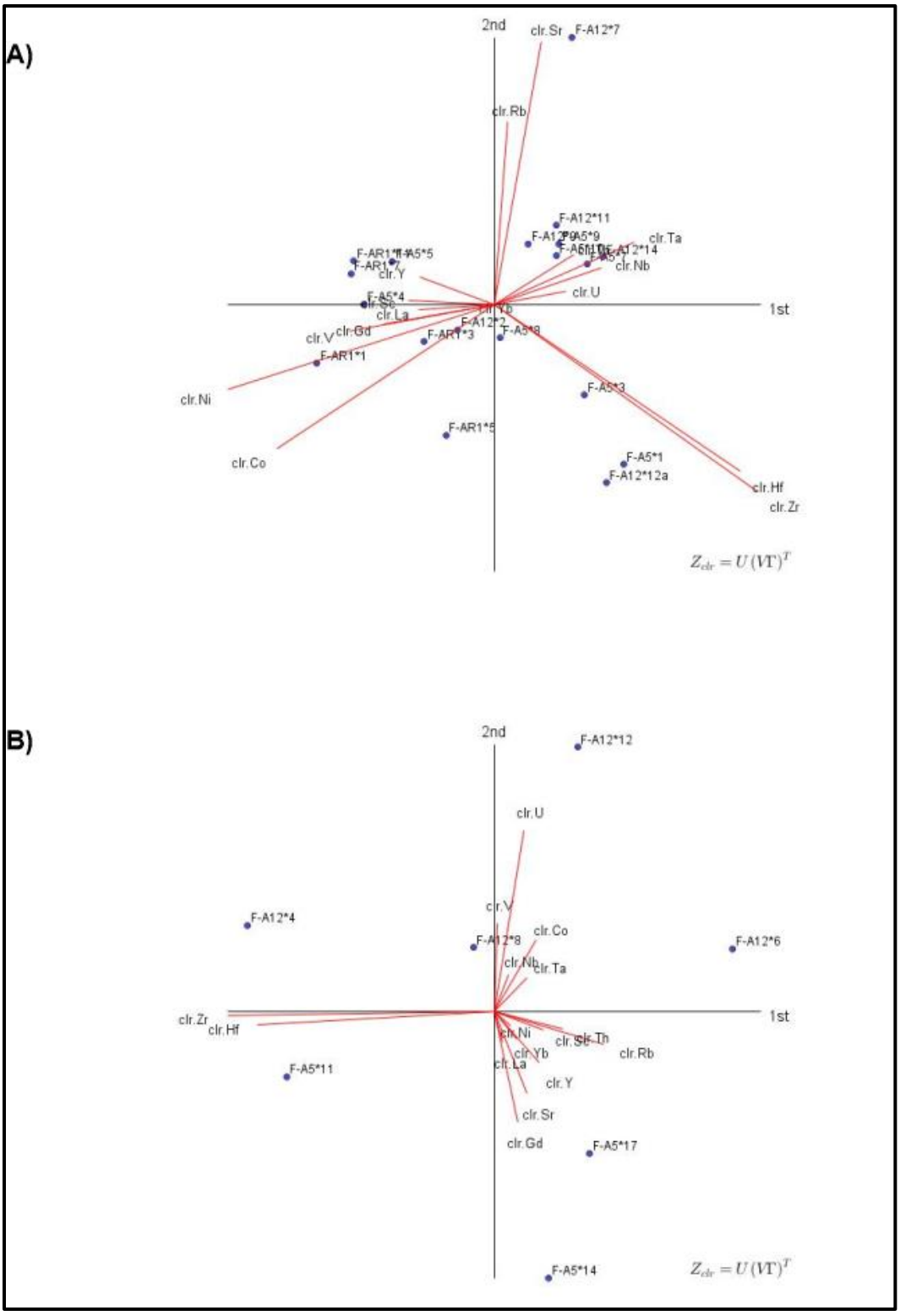

Figure 4.3.9: PCA performed on the trace elements within the A) coarser grained fraction and B) finer grained fraction. Principle components are based on the covariance matrix.

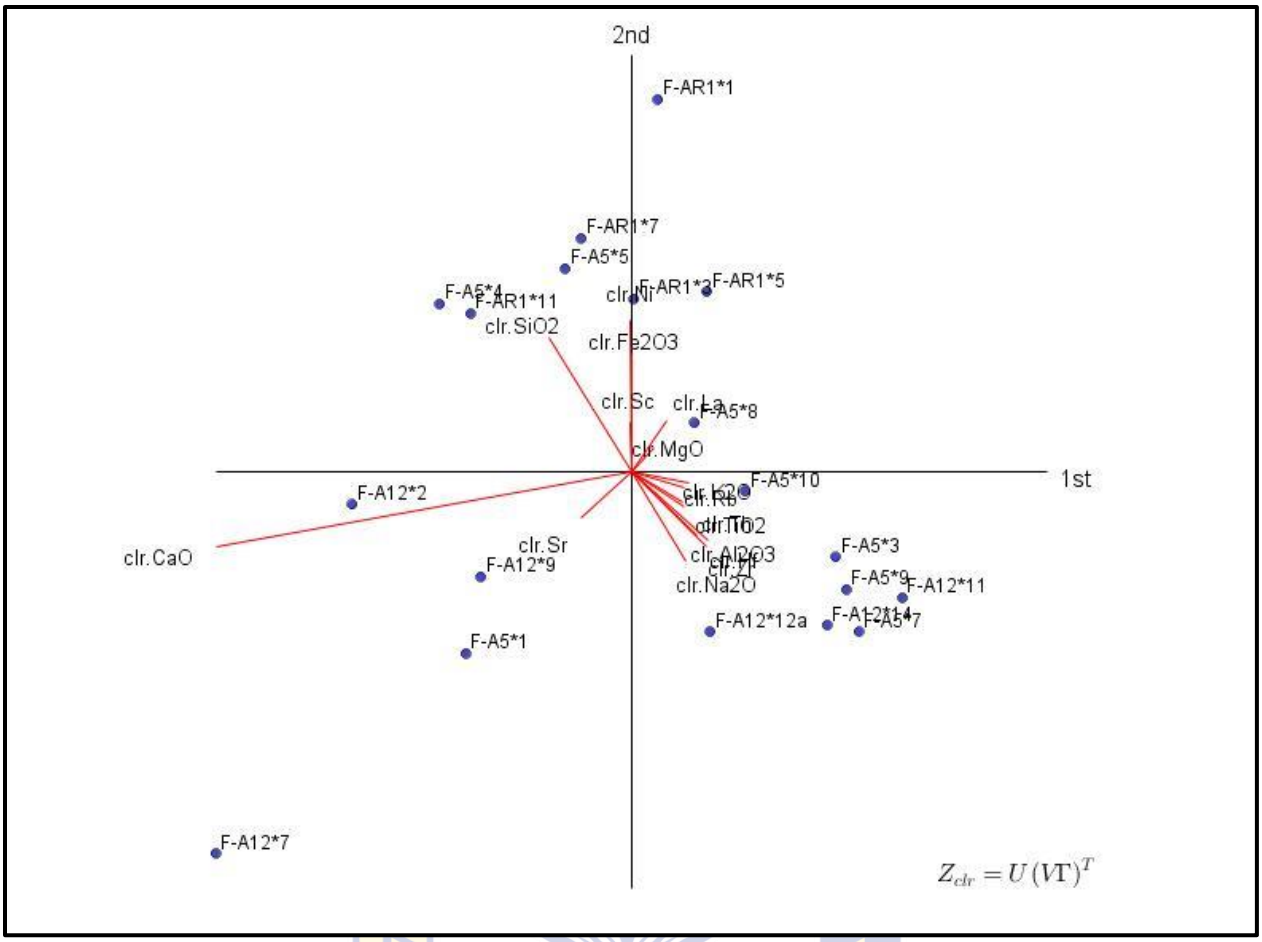

Figure 4.3.10: PCA performed by the method of Caracciolo et al. (2012) whereby trace elements are compared to certain major elements. There are different units of measurements so the principle components were based on the correlation matrix. Only the coarser grained samples were chosen for this analysis.

The role of the use of discriminant function analysis in this study was to assess the viability of groups identified in the provenance and facies correlation identification within a rifted setting using geochemical variations.

The major element chemistry showed a variation as discussed above with the occurrence of transgressive sequences and regressive diachronous sequences (element complex assemblage sets) using discriminant analysis with a 96.7% correct classification based on P_2O_5, MnO and Fe_2O_3 (Appendix C) in the Bredasdorp sub-basin. The trace element chemistry showed much more and accurate variations with facies correlative variations indicating a 100% correct classification. Trace elements that can be used to discriminate element complex assemblage sets

in the Bredasdorp sub-basin are Sc, Co, Sr, Cs, Mo, La, Nd, Rb, Y and Pr. A relationship between facies association 8 and facies association 5 (negative function 1) can be seen from discriminant function analysis. This is rather a unique relationship since they occur in separate depocenters and are relatively different facies. Facies association 9 and facies association 6 can also be distinguished because they occur in transgressive element complex assemblage sets (Appendix C).

4.3.5 Weathering indices

The values for CIA, CIW, PIA, CIA_{molar}, WIP and ICV are presented in Appendix C, Table C3. CIA values range from 48.56 (F-A5#1)-71.04 (F-A12#12) with an average of 59.41. The CIA values for all samples tend to fall above the line for unaltered feldspars (CIA=50) except for sample F-A5#1. CIA_{molar} values range from 2.36 (F-A5#1)-53.00 (F-A12#12). The finer fraction has higher CIA (65.69) and CIA_{molar} (20.72) values than the coarser fraction that has values of 57.59 and 11.69, respectively.

ICV values range between 0.67 (highly weathered) to 5.33 (least weathered) with an average of 1.41. The coarse-grained fraction (1.59) has higher average ICV values than the finer grained samples (0.81). Most of the sample trends towards a basic granitic source composition (parallel to granite trend), but a second trend line also occurs that trends closer to the basalt line (indicative of more than one source or mixing of two provenances, not really basaltic in composition with samples F-A5#4, F-A5#5, F-A5#8, F-A5#10, F-AR1#1, F-AR1#3, F-AR1#5, F-AR1#7, F-AR1#11, F-A12#2 and F-A12#7) (Figure 4.3.12).

The CIW values ranges from 53-89 (av.70.5) which coincides with moderate to low losses of Ca, Na and Sr (minus the diagenetically altered samples) from the source area or a low content of these elements in the source area (Figure 4.3.3). The mineralogy shows quartz, feldspars, minor illite/smectite and calcite that confirm this interpretation of incipient to moderate chemical weathering for most of the samples. The WIP values ranges from 10-59 (av.27.8).

In general, the samples trends towards the illite-muscovite line from a possible granitic-granodiorite source on the A-CN-K diagram (intersects Feldspar join) (Figure 4.3.11A). However, one has to also consider that the trend line does not follow (not parallel to the A-CN join) the general trend line of Nesbitt & Young (1982), therefore possible mixing (sources and

multiple weathering trends due to recycling) or a second source should be considered (McLennan et al., 1993).

Within-trend facies variation (Appendix C, within stratigraphic variation), indicates that the lower part of the stratigraphic section was dominated by tropical-subtropical conditions whereas the upper part of the stratigraphic section was possibly dominated by more arid to semi-arid conditions.

The K/Rb index has also been used as a proxy and values range from 196-296. This indicates a weathering intensity of incipient to intermediate weathering (Selvaraj& Chen, 2006). The PIA values shows a range of 55-77.6 which indicates that the source (Plagioclase weathering, since the source contained more plagioclase than K-feldspar (Figure 4.3.11A) experienced intermediate weathering of plagioclase feldspars within the source (also enhanced due to the low resistivity of Plagioclase rather than K-feldspar to weathering). Although K-metasomatism occurred, the source of the Na could have come largely from a felsic input, which correlates with the PIA values of containing albite and anorthite (with more abundant albite) (Fedo et al., 1996). As seen from figure 4.3.11B, there is not much biotite encountered within the samples. The occurrence of muscovite is also low due to the low Rb/K_2O ratios, with the exception of some sample (F-A12#12). The petrography also confirms that there is abundant plagioclase than microcline or orthoclase.

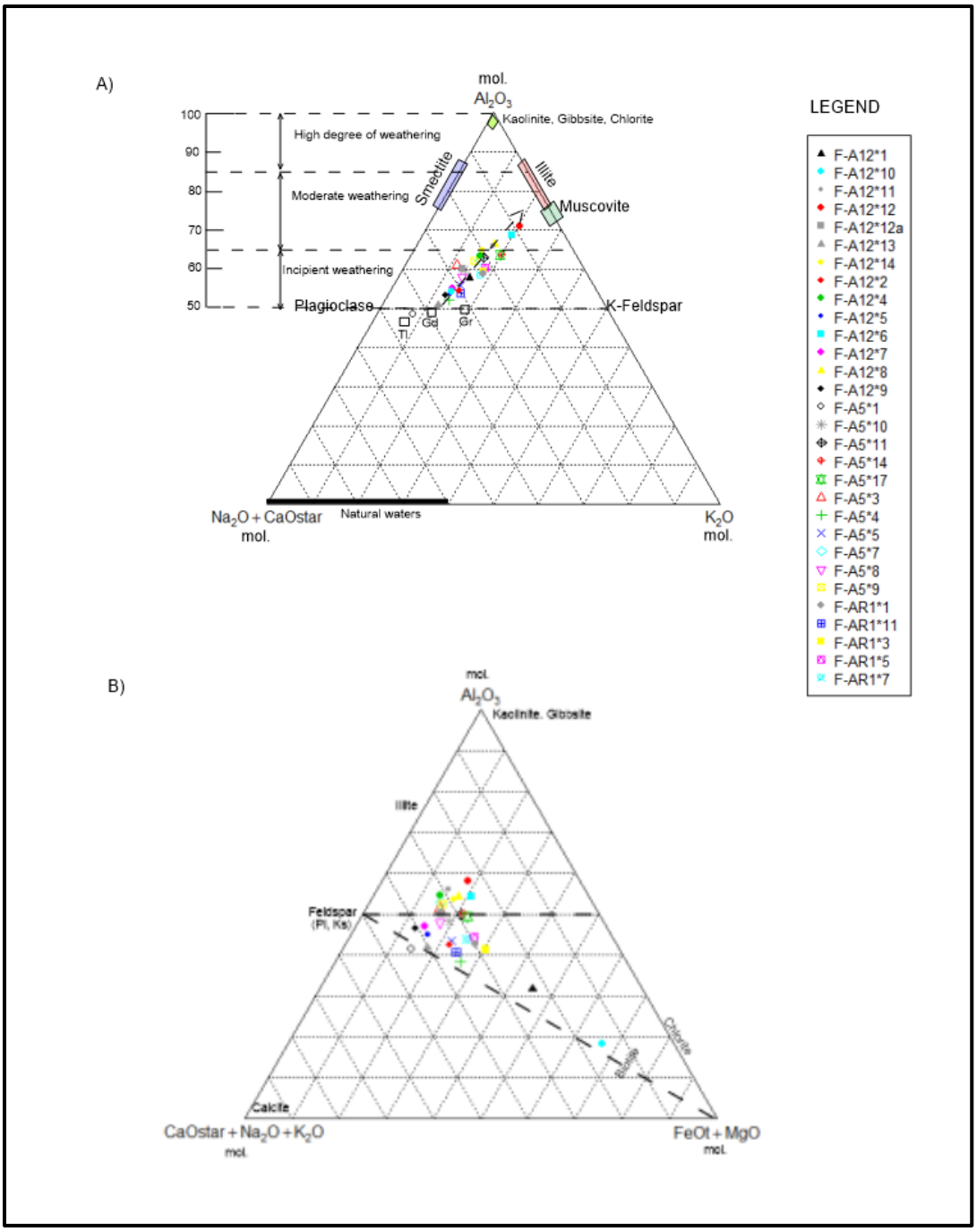

Figure 4.3.11: Weathering trends evaluated graphically showing A) A-CN-K diagram, after Nesbitt & Young (1982), and B) Mineralogical ternary plot showing feldspar weathering trends after McLennan et al., (1993)

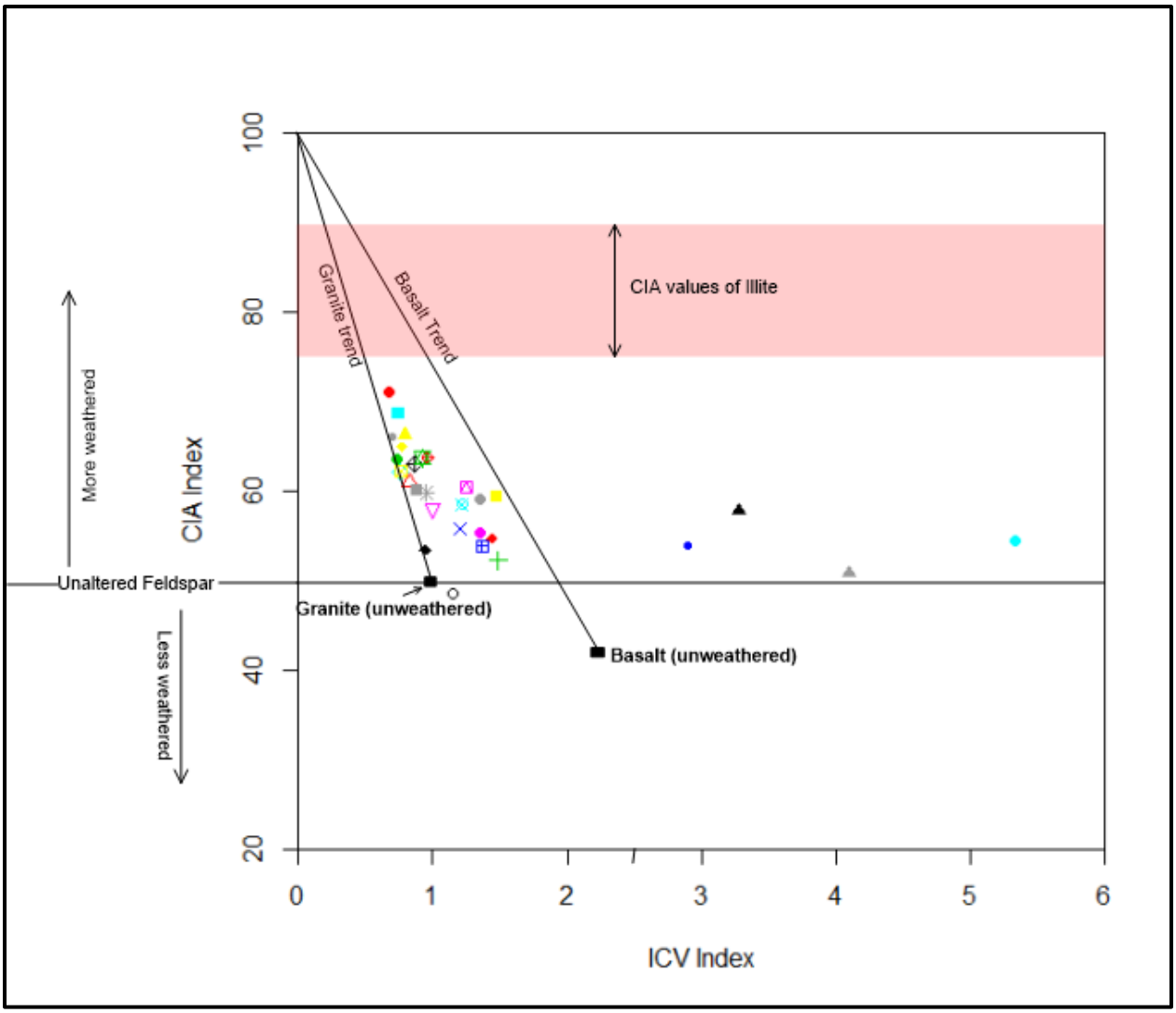

Figure 4.3.12: Showing CIA index vs ICV index, the possible weathering trends as well as the intensity of the weathering within the source region. Granitic and basaltic compositions are also added, after Lee (2002).

4.3.6 Sorting and recycling

The finer fraction does not show much increased sorting due to polycyclic recycling or hydraulic sorting except for samples F-A5#11 (Figure 4.3.13A). F-AR1 shows samples that are more likely affected by hydraulic sorting than polycyclic recycling, except for sample F-AR1#5. F-A12 shows two samples (F-A12#1 and F-A12#12a) that are more affected by polycyclic recycling, three samples (F-A12#12, F-A12#7, F-A12#8) that are not affected by both processes and the rest of the samples are more affected by hydraulic sorting and polycyclic recycling. F-A5 shows two samples less affected by hydraulic sorting and polycyclic recycling (F-A5#14 and F-A5#17),

with the rest of the samples, indicating polycyclic recycling and hydraulic sorting (Figure 4.3.13A). These assumptions are based largely on first cycle sedimentation of a singular area when compared to Horton group sandstones (Pe-Piper et al., 2008). The polycyclic nature of sediments is also enhanced in the plot of Th/Sc vs Zr/Sc (Figure 4.3.14). The other components used for sorting is V and Ti where a strong positive correlation between these two elements are evident that ilmenite occurs in this formation. The ilmenite content is not as resistant as zircon. Therefore, as V or Ti remains constant, with increased concentration of Zr the samples will show polycyclic or recycling. The Zr and Th can also be used to evaluate the effect of the concentration of heavy minerals due to polycyclic provenances (McLennan et al., 1993).

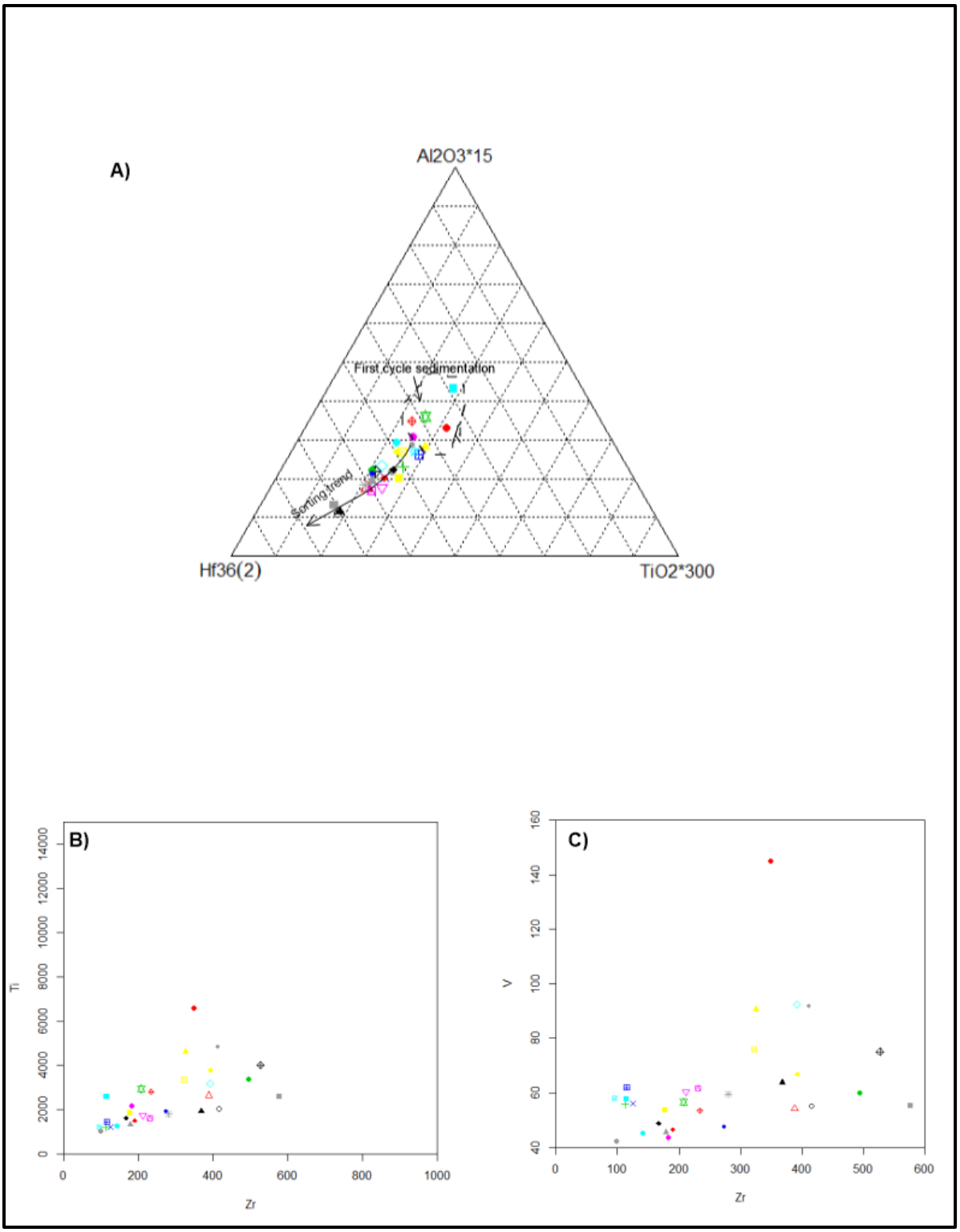

Figure 4.3.13: Sorting and first cycle sedimentation compared to polycyclic sedimentation. A) Sorting trend for evaluating first cycle sedimentation and polycyclic sedimentation (Garcia et

al., 1994). Evaluation of a possible granitic source showing fist cycle sedimentation with ilmenite as the dominant mineral (B and C), after Pe-Piper et al. (2008)

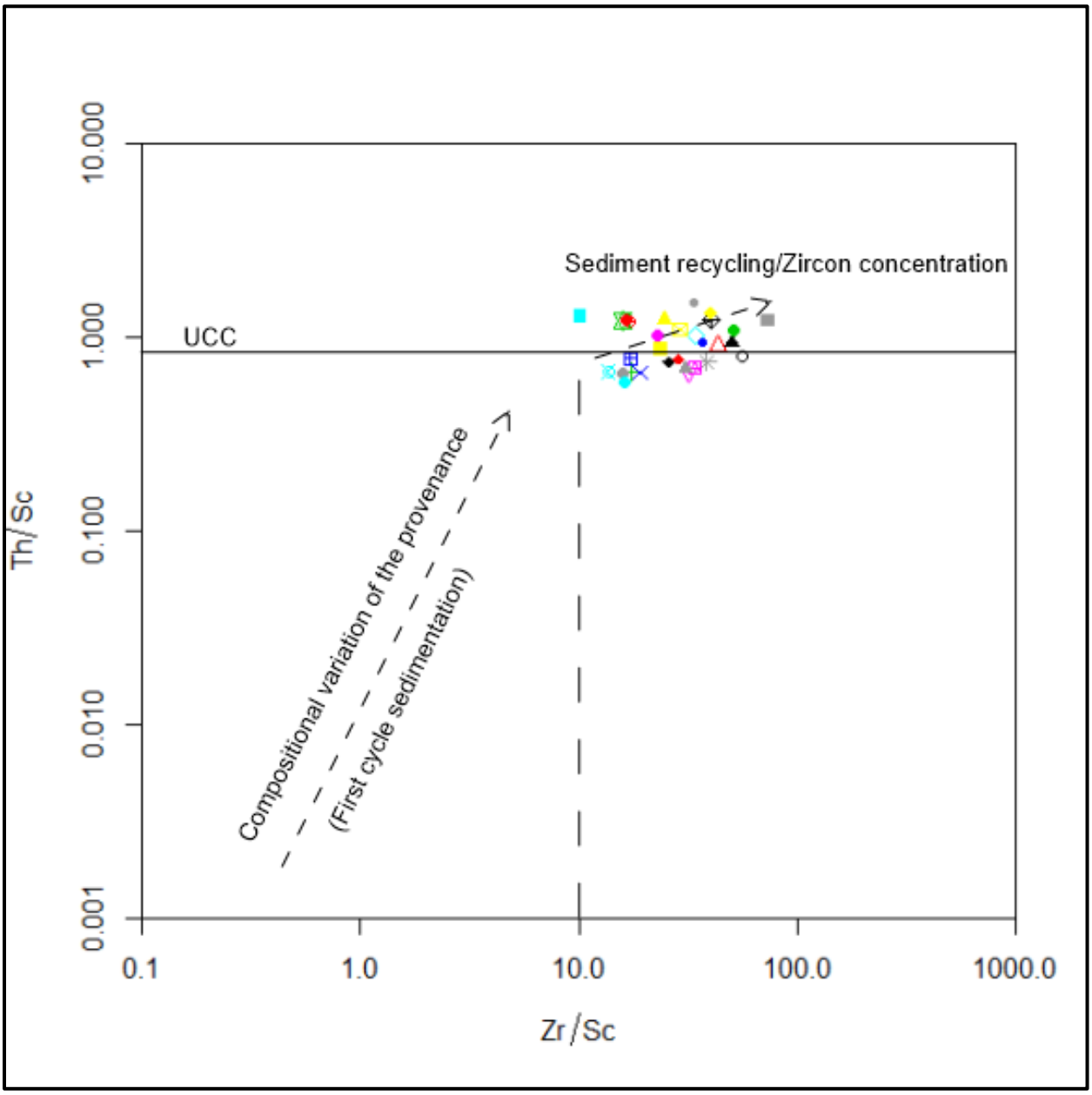

Figure 4.3.14: Plot of Th/Sc vs Zr/Sc used to assess chemical variation due to first cycle sedimentation or polycyclic sedimentation or sediment recycling (heavy mineral enrichment), after McLennan et al. (1993)

4.3.7 Provenance and tectonic setting

Most of the samples of the 1AT1-V horizon interval plot in the quartzose recycled field with a minor influence or samples plotting in the felsic region (Figure 4.3.18A and B). This indicates

that the source rock lithology is of recycled sedimentary/metasedimentary material as well as signs of an igneous input.

The high average ratio of La/Sc (3.18) suggest that it falls part of the active continental margin (ACM) and passive continental margins (PCM) regimes which is possible since the ACM usually evolves into a PCM (Bhatia & Crook, 1986). This is visualized with major element chemical diagrams of SiO_2 vs log (K_2O/Na_2O) plot (Figure 4.3.15). The plot of Ti/Zr vs La/Sc and the ternary plot of La-Th-Sc (Figure 4.3.16) show a transitional phase between active continental island arc and passive/active continental margins.

According to Verma & Armstrong-Altrin (2013)'s discriminant diagrams, all the samples (not diagenetically altered) falls within the Rift field (Figure 4.3.17). These diagrams have been assessed through rigorous quantification of tectonic plate boundaries that focused on the depositional basin.

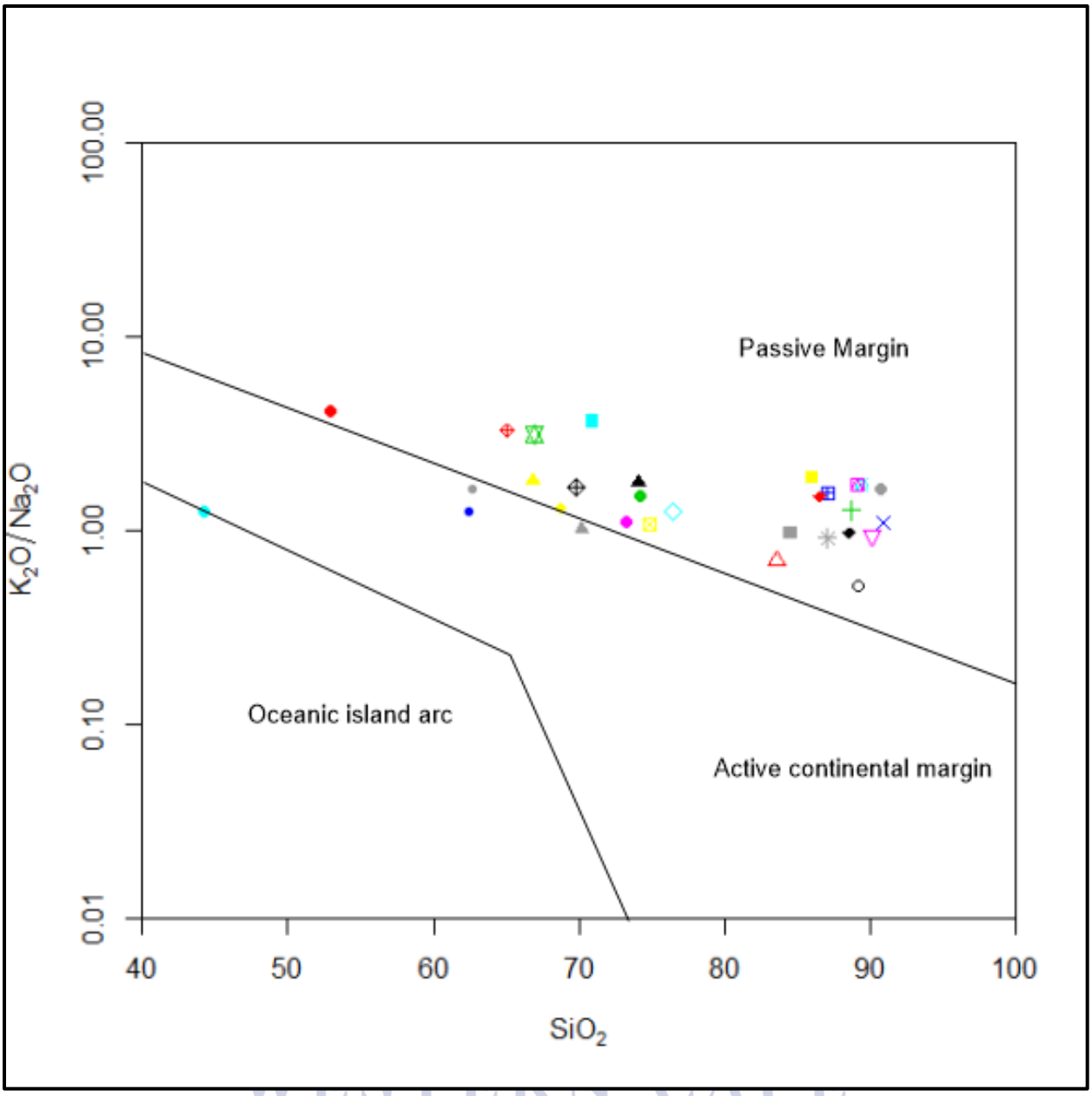

Figure 4.3.15: SiO2 vs K2O/Na2O diagram for the illustration of tectonic settings using geochemical data (after Bhatia & Crook, 1986)

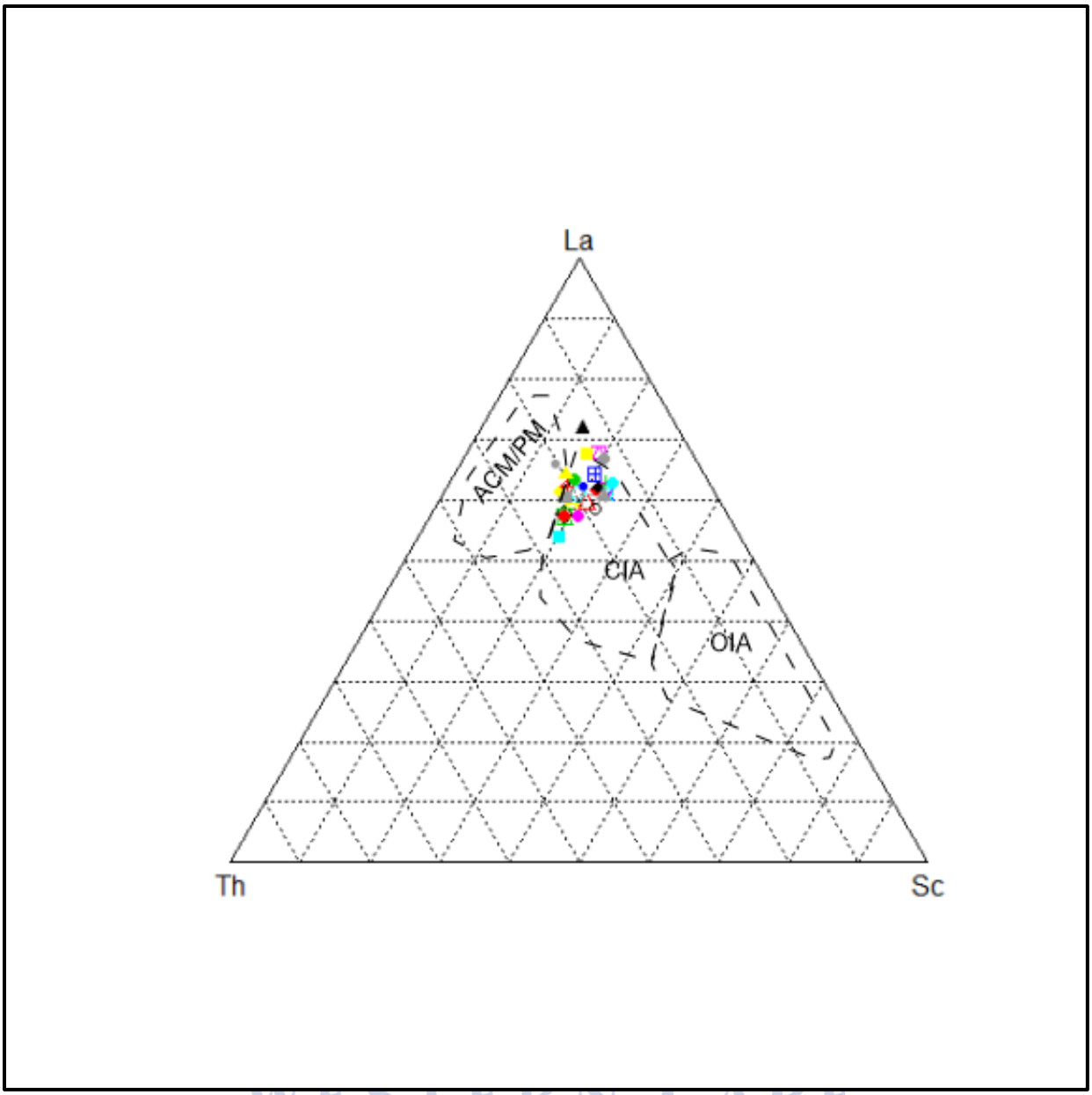

Figure 4.3.16: La-Th-Sc plot showing tectonic settings using geochemical data, after Bhatia & Crook (1986). Tectonic fields are ACM-active continental margin, PM- Passive margin, CIA-continental island arc and OIA-oceanic island arc.

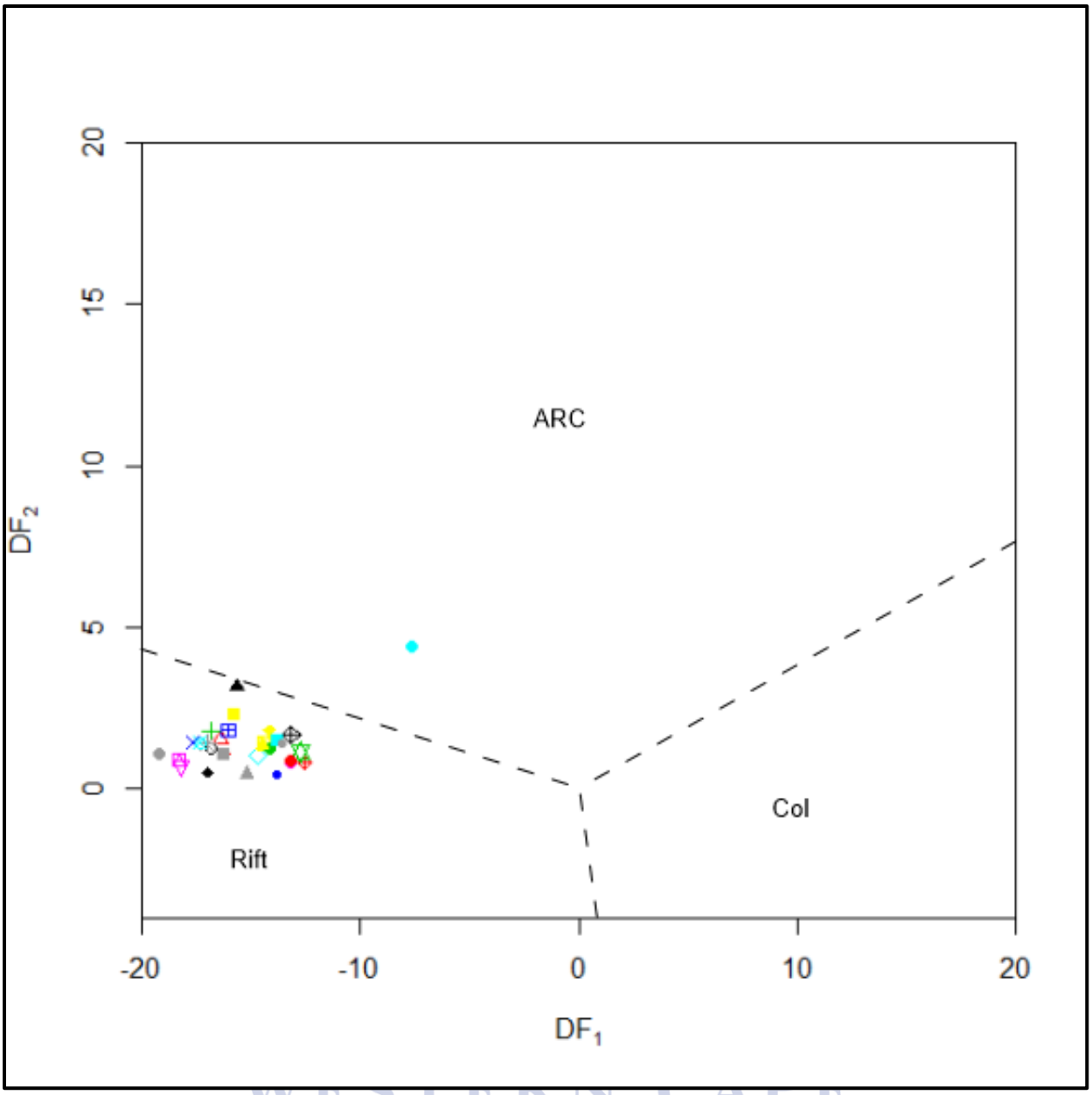

Figure 4.3.17: Discriminant diagrams distinguishing between tectonic boundaries using transformed variables in compositional data analysis, after Verma & Armstrong-Altrin (2013). ARC-active volcanism, Rift-extensional tectonics and Col-collisional tectonic regime. [Where DF_1 *= [-0.263*(ln*TiO_2*)] + [0.604*(ln*Al_2O_3*)] + [-1.725*(ln*Fe_2O_3*)] + [0.660*(lnMnO)] + [2.191*(lnMgO)] + [0.144*(ln*CaO*)] + [1.304*(ln*Na_2O*)] + [0.054*(ln*K_2O*)] + [-0.330*(ln*P_2O_5*)] - [1.588] and* DF_2 *= [-1.196*(ln*TiO_2*)] + [1.064*(ln*Al_2O_3*)] + [0.303*(*Fe_2O_3*)] + [0.436*(lnMnO)] + [0.838*(lnMgO)] + [-0.407*(ln*CaO*)] + [1.021*(ln*Na_2O*)] + [-1.706*(ln*K_2O*)] + [-0.126*(ln*P_2O_5*)] – [1.068)].*

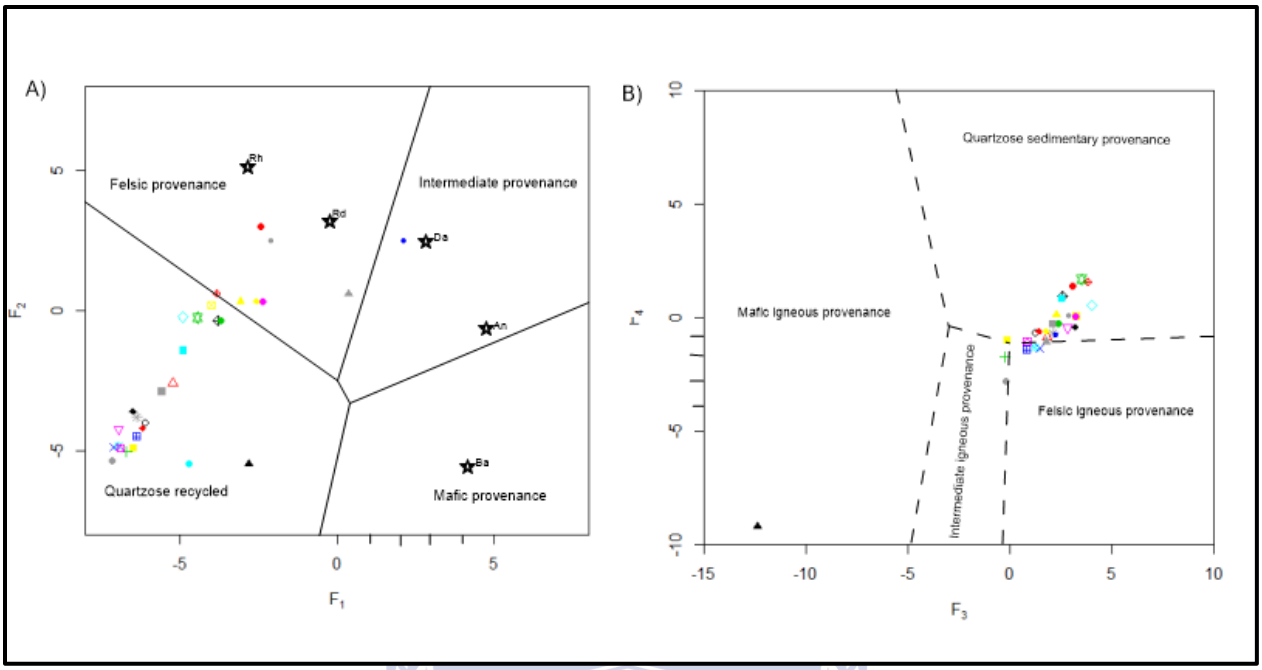

Figure 4.3.18: Source rock lithology identification and classification from geochemical data a) F1 Vs F2 and B) F3 vs F4, after Roser & Korsch (1985).

There was no clear discrimination between the F-AR1 borehole (North) and F-A12/F-A5 boreholes (South) using the normal data for provenance identification. A linear discriminant function analysis on the clr-transformed data revealed a clear discrimination between a borehole in the north (F-AR1) and the boreholes in the South (F-A12 and F-A5). The misclassification percentage was around 6.7% (Appendix C, Discriminant function analysis). Discriminant function 1 was represented mostly by Ni and V that also showed a close relationship with well F-AR1. Discriminant function 2 was represented by Hf, Zr, Sc, U, Th and Rb that was closely associated with well F-A12 and F-A5. This is also further supported by the subcompositions formed from trace elements in the PCA but adding more discriminative power to the differentiation based on provenance-specific elements.

CHAPTER 5

DISCUSSION

5.1 Depositional model and paleogeography

Seismic data and well log correlations identified inclined stratigraphic units with F-AR1 being located on the delta plain and F-A12 to F-A5 being situated in the delta front (proximal prodelta) to delta plain platforms. F-A12 and F-A5 shows bidirectional downlapping (shelf-edge deltas) indicating a proximal sediment supply from basement highs (uplifted block) to hanging wall depocenters similar to the study of Lin et al. (2018) in a strike-oriented seismic line. This is described as a dual sediment-supply system or part of a hanging-wall dipslope setting in a rift basin (Muravchik et al., 2018). These can be described as 'walking out' lateral facies transitions in two fault-bounded depocenters (Carr et al., 2003). Two depositional systems are envisaged for the studied interval with F-A5 having its own depositional system compared to F-A12 and F-AR1 (diachronous). The diachronous deposition of F-A5 sediments are restricted to above the V horizon (Figure 4.1.24 and Figure 4.1.25) as compared to the other two wells. A regional correlation confirms a lower section within the F-A12/F-AR1 depocenter undergoing rapid upliftment of the fault block producing a high sediment supply that outpaces subsidence. The second depocenter (F-A5) possibly undergone rapid subsidence that outpaced the rate of sediment supply during these times (Figure 5.1.1). These changes brought about provenance-related and facies-related geochemical variations.

In the 1AT1-V horizon tidal, wave and fluvial processes dominated throughout the succession, making the lower succession a mixed-energy (fluvial dominated/wave influenced and tide affected) deltaic system and an upper section dominated by a tide-dominated to wave-influenced estuarine system. Mixed energy deltaic or marginal-marine settings are common in modern environments and therefore should be abundant in ancient settings (Yoshida et al., 2007).

Regional facies distribution revealed that there were nine facies associations within the 1AT1 and V horizons. The lower section (not cored for F-AR1) were dominated by a net-regressive or regressive element complex assemblage set (Figure 5.1.1) and autocyclic fining-upward sequences with the outbuilding of the middle to distal delta front comprising of delta front lobe fringes, hyperpycnal event beds, offshore migrating tidal bars (and associated inter-bar regions),

mouth bars and terminal distributary channels (and associated inter-terminal distributary regions). This net regressive phase is confirmed by Broad et al. (2012) to have occurred during a major upliftment event within the Bredasdorp sub-basin. Interestingly, there is a regional facies correlation with a relationship with trace element geochemistry showing a high correlation with facies from the opposite side of the basement high. These facies can be seen from Figure 5.1.1 showing the basement high slope deposits correlating with deposits from the distal delta front of the opposing depocenter (Discriminant function analysis on trace element data). The proximal/middle embayment and regressive shoreface/foreshore environments are also envisaged to occur laterally in an isolated depocenter during the regressive phase, possibly due to the uplift history of the basement high.

The lower delta plain to proximal delta front consisted of interdistributary bays, distributary channels, crevasse splay subdeltas, mouth bars, tidal flats and offshore embayments. The coarsening-upward base of the cored section is indicative of a regression unit on a wave and fluvial dominated prodeltaic/distal delta front succession followed by the migration of offshore/distal tidal bars indicative of minor tidal influences offshore (mud drapes) (Olariu et al., 2012b). The middle to distal delta front is made up of mouth bars (shoals) with event beds of hyperpycnites from the nearby basement high because of steepening coastlines along a secondary depositional system (shelf-edge type delta system). The proximal delta front is made up of terminal distributary channels that overlie the mouth bars and are rather difficult to distinguish from each other with terminal distributary channels showing more parallel to trough-cross stratified sandstones (Olariu & Bhattacharya, 2006). Further updip along the depositional plain, the result of delta lobe switching became common, which resulted in the stacking of several shallow channelized units, with a strong input from the secondary depositional system or basement highs. It is believed that the shallow channels were the result of a prograding delta plain on an extensive but gentle slope of mouth bars and terminal distributary channels on the delta front. The occurrence of several crevasses splays along each main distributary channel became evident with coarsening-upward and fining upward sequences that resulted from minor transgression and regressions or lobe switching due to a rapidly uplifted environment (tectonically active).

The occurrence of interdistributary bays and crevasse splay subdeltas with interbedded mouth bars are possibly the result of reworked mouth bars by longshore currents as wave processes start to dominate towards the top of the section (Elliot, 1974). The interfingering of interdistributary bay islands (interdistributary bay extensions) and mouth bars are a common attribute in the Ganges-Brahmaputra deltaic system. The occurrence of distributary channels can be attributed to a fluvial influx as a driver of sediments from the NNW regions (Cape fold belt) (Lin et al., 2018). The dominant processes in the lower section were wave and river influenced environments. The tidal influences are rare in the lower sections and only become dominant towards the top with the incoming transgressions and increased basin width (Yoshida et al., 2007). The occurrence of wave-dominated structures is evident in both the net regressive and net transgressive phases of the formation (presence of small-scale and large scale hummocky cross stratification (truncated wave ripples or symmetrical wave ripples). The occurrence of these deposits is similar to the Bryne-Sandnes formations in the Sogne Basin of Mellere et al. (2016) where the occurrence of wave-influenced characteristics is subordinate to the dominant fluvial and tidal regimes.

The paleogeographic constraints during the net-regressive sections (regressive element complex assemblage set) is crucial in the interpretation of the depositional environments since major depocenters evolved during these times and became tectonically active with respect to their syn-rifted tectonics and associated punctuated transgressions. The occurrence of the lower stratigraphic sequences of F-AR1 (high sand to shale ratios) would be restricted to the subaerial setting with the position of F-A12 occurring in the outer parts of a prograding deltaic platform. Even though F-A12 and F-A5 has a low gradient depositional platform from the main depositional system, a secondary depositional system providing sediments from the basement highs produced a high gradient platform. With respect to the main depositional system, F-A12 and F-A5 environments were mainly focussed on a subtidal to intertidal platform.

The modern equivalents to these environments are restricted to the Mahakam, Ganges-Brahmaputra (Figure 5.1.4D), Po (Figure 5.1.4A, B and C) and Burdekin (Figure 5.1.3) deltaic environments but with the occurrence of active tectonics, a rather late stage of the Satpara lake (Figure 5.1.4E) depositional system is also envisaged. The thickness of the mouth bar deposits of the delta front region is similar to thicknesses occurring on the Mahakam Delta (Salahuddin and

Lambiase, 2013; Lambiase et al., 2016). The distributary channels are filled with backfilled finer (marine-influenced) sediments equivalent to major transgressions on a deltaic platform (seen on the Mahakam and Po deltas (Figure 5.1.4C). The Po deltaic plain (Figure 5.1.4A) shows a vast area for the interdistributary bay zone (including sand spits (Figure 5.1.4B) and tidal bars) and therefore becomes a common feature in this setting similar to the vast nature of the interdistributary bay deposits of this study. The distributary channels in the Po deltaic system are dominated by suspended sediment (Correggiari et al., 2005), thus making them likely to contain abundant fluid mud layers and the presence of upper plane bed laminations with a high fluvial discharge. The occurrence of mouth bars interbedded with interdistributary bays is also common in the Burdekin delta (Figure 5.1.3A). This occurs coeval laterally with abandoned mouth bars showing vegetated tops similar to the inter-terminal distributary regions in this study (Figure 5.1.3C and D). These can also be confused with tidal bars which also shows a fining-upward nature (Olariu et al., 2012) which should be reevaluated, but the occurrence of less bioturbated tops (or ichnospecies-specific changes) can be used to evaluate these differences.

Crustal scale discontinuities or uplifted fault blocks can cause the deposition of separate depocenters with its own characteristics, such as each depocenter containing their own salinity and hence their own facies (including biofacies) changes (Ganges-Brahmaputra delta (Figure 5.1.4D), (Kuehl et al., 2005)). This setting is also seen in the Satpara Lake or modern day lacustrine environment and the Burdekin delta's promontory (Figure 5.1.3B and 5.1.4E).

The upper part of the 1AT1-V horizon were mostly dominated by transgressive estuarine sedimentation with the deltaic platform converting to an estuarine system with the occurrence of tidal sand ridges and compound dune fields, embayment sedimentation and tidal bars (Figure 5.1.2) (Mellere et al., 2016). Broad et al. (2012) confirm this sedimentation pattern of the net transgressive phase with the occurrence of a major flooding event possibly related to an increase in overall basin subsidence with the incoming drift stage. At this stage, tidal processes became the dominant process with fluvial processes declining because of the increasing width of the basin with maximum accommodation space being created (Yoshida et al., 2007). The estuarine system was tide dominated because of abundant tidal-indicators such as herringbone cross bedding and mud drapes indicative of tidal processes on a subtidal platform. The increase in tidal power towards the top can be attributed to the paleotopography gaining a gentle gradient as the

basin is being filled (with the end of the syn-rift) (Lin et al., 2018). A speculative transition zone between the prograding and small scale retrograding packages are noted because of the subsequent occurrence of back-filled distributary channels, such as the occurrence of the green transgressive back-filled mudstones (Lambiase et al., 2016). These deposits are usually associated with offshore embayments with extensive thicknesses. The seismic facies character in F-A5 showing a restricted embayment due to active fault tectonics with high angle foresets and thick bottomsets of claystone close to the basement high. In the eastern part of the study area F-A5 showed thick bedded offshore/embayment facies that was largely restricted, but no attributed stacking pattern could be assigned due to the deposits occurring within the lower stratigraphic intervals associated with a net-regressive package equivalent to facies in F-A12. Active fault propagation was the major reason for the restricted embayment and stratigraphic variability between F-A5 and F-A12. These restricted and open embayments are similar to the embayment facies within the Burdekin delta with restrictions occurring due to bedrock promontories (Figure 5.1.3A) (Fielding et al., 2005). A similar setting is seen in the Satpara lake deposit and Ganges-Brahmaputra deltas with promontories occurring creating a secondary depositional system perpendicular to the main distributary system.

This mixed-energy marginal-marine setting is also further enhanced by the occurrence of the *Skolithos* and *Cruziana* ichnofacies with minor continental-zoned *Scoyenia* ichnofacies as well as facies-crossing trace fossils. Certain parts of the succession are dominated by high ichnodiversities (based on the relative selected wells) and abundances but overall they are impoverished throughout. High-density monospecific traces, a combined *Skolithos* and *Cruziana* ichnofacies, an abundance of certain taxa, with overall low-diversity assemblages points towards stressed environmental conditions possibly opposed upon it by brackish water zones or salinity differential stresses (Wightman et al., 1987; Pemberton & Wightman, 1992; Buatois et al., 2005), differential oxygenation and erratic sedimentation (high turbidity) conditions in the environment (Moslow & Pemberton, 1988; Hubbard et al., 2004). In addition, the trace fossil diversity also starts to increase during the net transgressive phases as opposed to the net regressive phases of deposition.

All these ancient depositional elements occurred in a still-active tectonic setting making the interpretation of the depositional environment rather complex and largely representative of an overall paralic system.

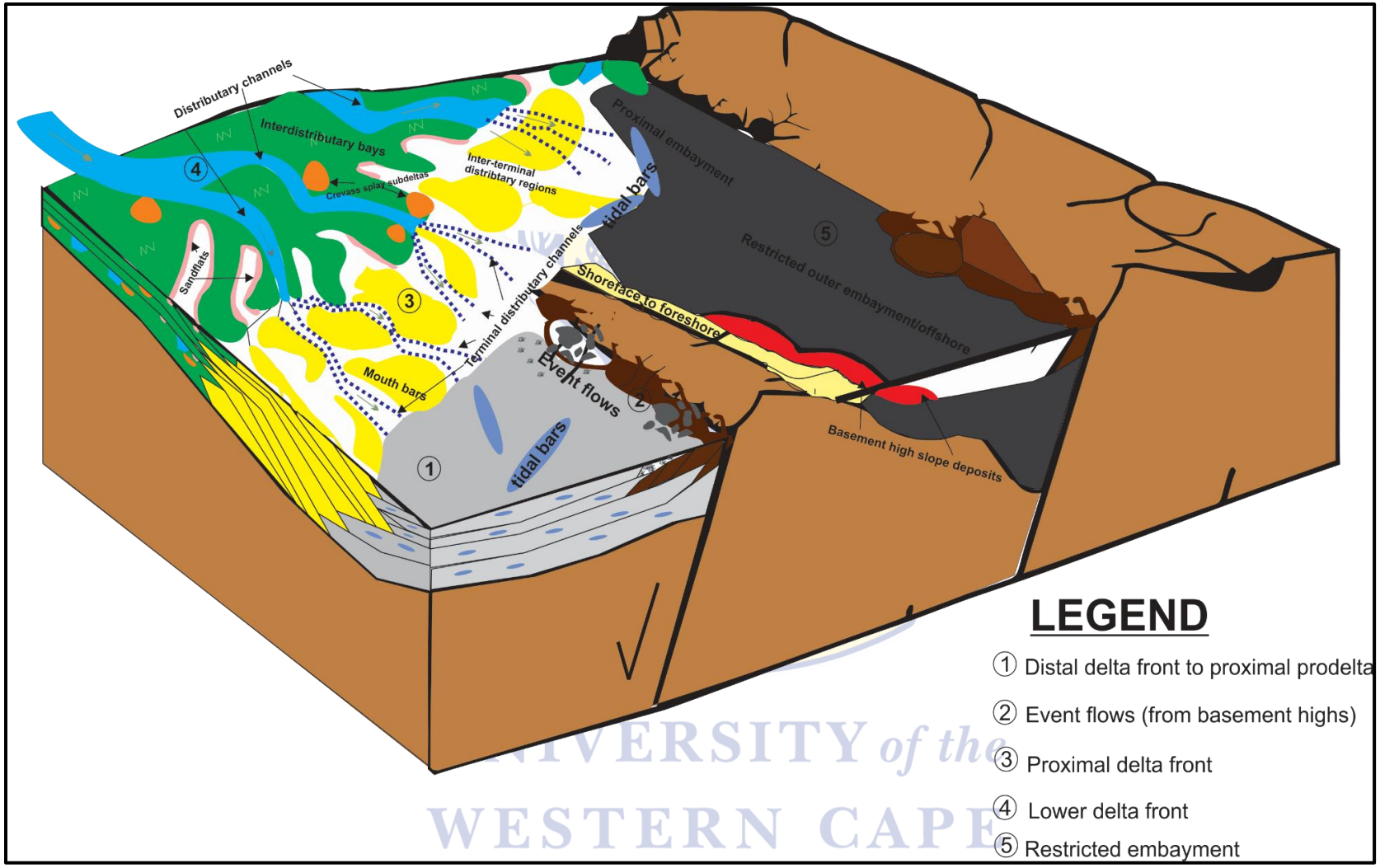

Figure 5.1.1: Depositional model of the lower net-regressive element complex assemblage set section of the 1-AT1-V horizon with active fault tectonics forming two depocenters. Not to scale

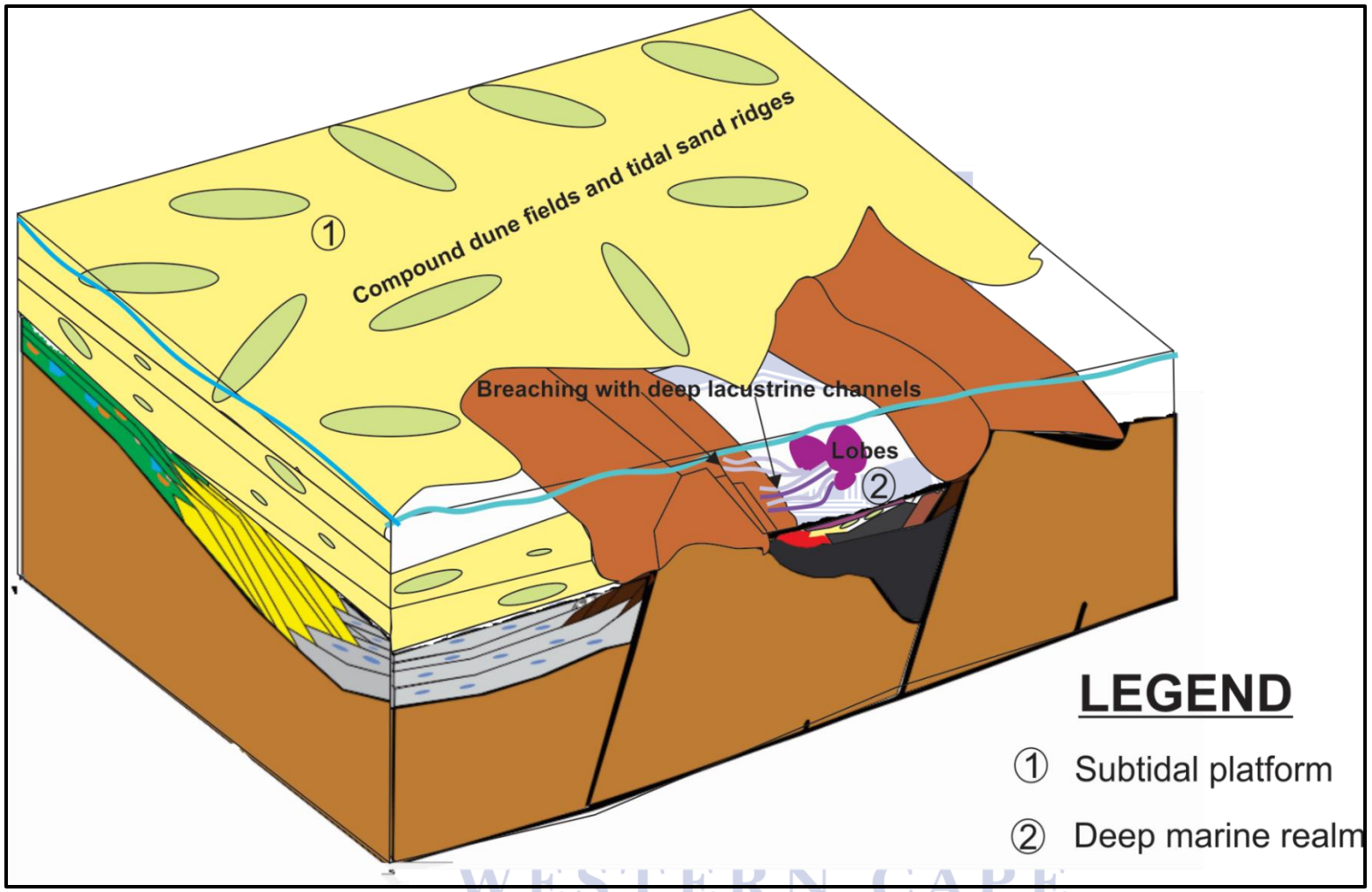

Figure 5.1.2: Depositional model for the net transgressive sequence or element complex assemblage set (high order) of the 1-At1 to V horizon. The deep lacustrine channels are a result of breaching of a basement high. The composition of the basement high is that of the Cape fold belt with its characteristic formations. Not to scale.

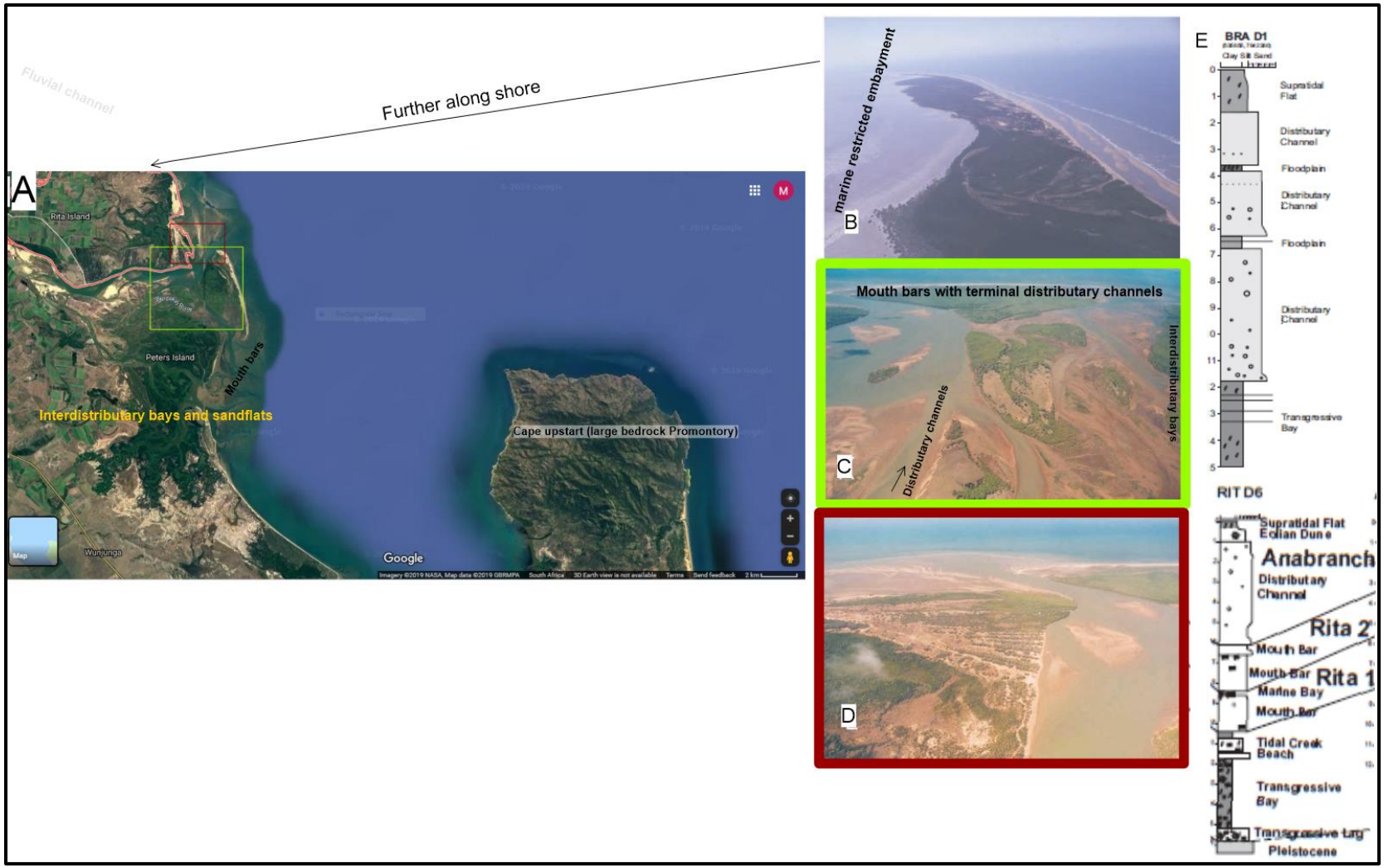

Figure 5.1.3: A) Aerial view of the Burdekin delta showing the interdistributary bays/sandflats intercalated with mouth bars and distributary channels. The Cape upstart is also present which is a bedrock promontory and acts as a barrier (Google earth image). B)

A marine embayment that occurs further along shore from the Burdekin delta. Notice the different colours and detachment from the open sea with the embayment (this is a spit not a basement uplift but can cause the same effect). C) And D) Mouth bars intercalated with terminal distributary channels and distributary channels. The abandonment of the mouth bars can form a vegetated surface with organic material similar to this study with terminal distributary channels containing carbonaceous material. E) Sedimentary log of the Burdekin delta showing transgressive bay deposits, mouth bars, distributary channels, floodplain and interdistributary bay deposits. B, C, D and E images are taken and modified after Fielding et al., (2005)

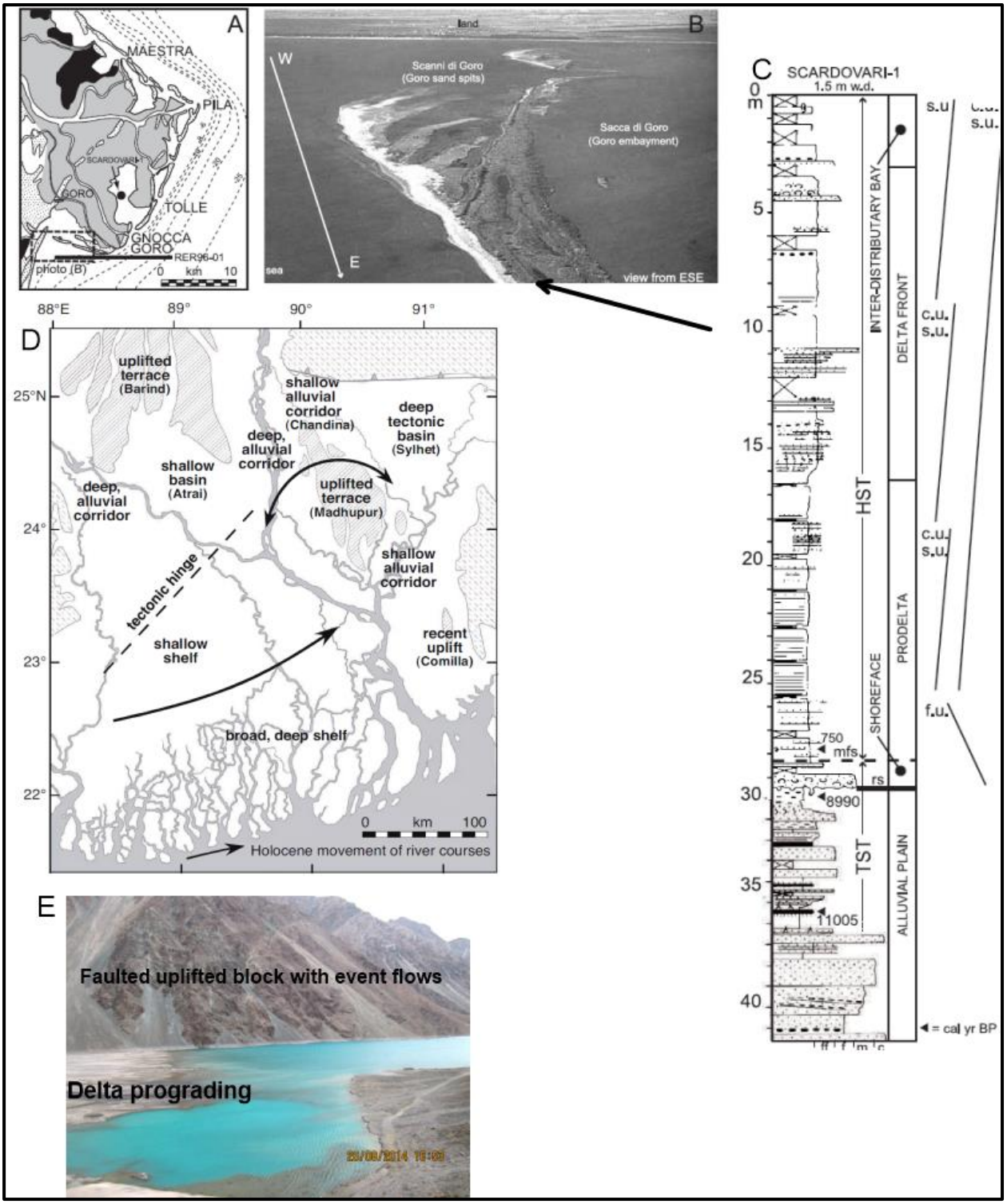

Figure 5.1.4: A) Aerial view of the Po deltaic system showing a relatively narrow prodeltaic platform with extensive mouthbars and distributary channels. B) A spit growth similar to the Burdekin extensive spit that forms an open embayment. C) Sedimentary log section of the Po delta (after Correggiari et al., 2005). Delta front mouth bars being overlain by interdistributary bay deposits with high frequency stacking patterns caused by autocyclic controls. D) The Ganges-Brahmaputra delta aerial view showing the effect of uplifted regions or modern tectonics on the sedimentation pattern. Each depocenter created has its

own facies characteristics with the prograding delta (Kuehl et al., 2005). E) Satpara lake (Pakistan) showing event flows (with episodic turbidites) from fault-uplifted blocks and a prograding delta front region (Google image).

5.2 Statistical methodology

The difference between the normal data and the transformed data can clearly be seen, as the over-simplified and extreme correlation between variables exists in the normal (untransformed) data. The use of statistical analysis on the normal raw data yielded rare to no variability in the data therefore principle component variation was restricted largely to the first components in the finer and coarser grained fractions. An important difference is also seen in the finer fractions for normal and transformed data on the PCA plots whereby SiO_2shows a higher variability in the normal data whereas in the transformed data SiO_2has a smaller variability, which is possibly due to the relatively high proportion of SiO_2 in the samples, which overshadows the other elements (silica dilution). Thus, if a recycled source is found, the SiO_2 content can be misleading if used for geochemical classification or provenance diagrams especially if a confidence region is attached. Therefore, the variability of the transformed SiO_2 content can be more easily attributed to the proportion of quartz in the modal count data.

There is a slight difference in the modified ternary plots of Weltje (2006), with samples plotting mostly in the continental block provenance fields. The inferred continental block provenances, concerning the tectonic provenance, yields more accurate results in compositional space with the occurrence of basement block uplifts (Columbine-Agulhas arc and Infanta arcs) during the break-up of Gondwana. Thus confirming the syn-rift nature of the sub-basin. This is also confirmed by the geochemical compositional variation of the 'rifted' tectonic setting of Verma & Armstrong-Altrin (2013). Since the relative proportion of quartz is exaggerated, the tectonic setting regime posted as passive margin is also over exaggerated and is more related to active continental margins than passive continental margins (Figure 4.3.15). There is also a level of uncertainty when inferring these provenance tectonic settings with the occurrence of recycled provenances, with temporal and spatial changes in the provenance terrains or depositional basins as upliftment occurs with the emergence of different geological formations (Garzanti et al., 2003).

The discriminant function analysis in the normal data shows a violation (possibly due to spurious correlations) and could not be computed whereas the transformed data could be

evaluated because there were no restrictions on the data. Discriminant function analysis on transformed data was 'easier to interpret' compared to the normal (untransformed) data and therefore yielded more accurate and correlative results to the other methods of the study.

5.3 Classification

Triangular plots of the studied wells suggest that sandstone samples plots within the arkose and subarkose fields, with remnants occurring in the sublitharenite and lithic arkose fields. This is further supplemented by the alr log-ratio transformed space plot of Weltje (2006). The quartzofeldspathic field in log-ratio space holds true as compared to the average and general composition (visual estimation) of most of the sandstone samples (Table B3, Appendix B). Geochemically, the results yielded a greater variation within the data but most of the samples plotted in the sublitharenite fields because of the sorting and immaturity of majority of the samples. The sorting plot of Garcia et al. (1994) (Figure 4.3.13A) using Zr, Hf and TiO_2 revealed a classification ranging from immature to mature sediments and are largely attributed to quartzofeldspathic samples. This classification yielded similar results to the petrographic modal count data. Discriminant function analysis also revealed a 0% misclassification for the two types of environments represented by marine to transitional environments. This is largely a result of glauconitic sandstone units that is partially represented by the P_2O_5 and Fe_2O_3 content. This large variation in the Fe content could be the cause of the classification of litharenitic compositions rather than subarkosic or arkosic in the untransformed geochemical classification (this is also further supported by the large variation of Fe in the clr-transformed data). So using the Fe content in geochemical classification diagrams should be carefully examined, even if there are minor or minute diagenetic changes.

5.4 Diagenesis

Diagenetic processes can affect the original composition on its own, if one had to ignore the other factors involved in the compositional variation from the source to sink. These processes include largely compaction and cementation (including dissolution). An attempt to minimize the effects of diagenesis was performed to exclude the samples that have been affected by severe diagenesis (those with abundant carbonate cements or phosphate minerals). This is especially important in minimizing the diagenetic effects on principle component analysis. The high variation of Ca (in calcite)is still evident which can be related to minute amounts of diagenetic carbonate cements, which was still evident in thin sections (Zhang et al., 2014).

Except for two finer grained samples (F-A5 #14 and #17), the Ca content was rather low in all the finer grained samples and can be attributed to pore fluid circulation.

Mechanical compaction has been seen throughout the succession such as the bending of ductile glauconite and the fractured feldspar grains. Severe compaction is seen, especially based on the occurrence of long and sutured contacts in most of the samples (Akinlotan, 2017). This is evidence of compositional variation within the depositional realm and has major effects in identifying the provenance as well as having a devastating effect on the porosity/permeability of the formation. Pressure solution (chemical compaction) through sutured boundaries and interpenetration textures has a major effect on the porosity and permeability of these rocks (highly compacted). So even though these rocks might show a good-poor porosity (in this case) it has an even lower permeability because of these factors (Wilson & McBride, 1988). Thus also keeping in mind that this is solely based on visual estimation of the thin sections and an in-depth diagenetic study is well beyond the scope of this study.

Thus, the lowering of porosity and permeability is further amplified by the occurrence of cementation. The quartz cement (overgrowths) and a poikilotopic calcite cement are largely indicative of a very low porosity as a factor of burial depth (Stone & Siever, 1996). The depositional environment is a crucial contributor to this factor, since shallow marine waters can supply Ca and Fe and bicarbonate ions. Geochemical studies revealed that four samples are diagenetically altered and this was further confirmed by petrographic studies as the increase in carbonates usually indicated severe diagenesis (poikilotopic calcite cements). This is also further supported by the high amount of Sr within the altered samples. The Sr content are usually associated with diagenetic carbonate cements (within the source-sink system, Sr is mobile and therefore concentrates where significant pore fluid circulation (drivers as organic or inorganic) occur in the depositional setting) (Nelson et al., 1986). This is further confirmed in the PCA analysis where Ca and Sr are strongly correlated with respect to a single process involved in their compositional variation (Figure 4.3.10, Figure 4.3.7A and 4.3.7B). The weak negative correlation in the finer fraction between CaO and Al_2O_3 (r=-0.26) as well as the weak positive correlation between CaO and LOI (r=0.32) suggest that the CaO is of marine origin and that most of the CaO was derived from carbonates (von Eynatten, 2003; Hofer et al., 2013). Petrographic studies revealed a Fe-rich calcite in some of the finer grained rocks therefore, the expelling of carbonates could have been problematic in the finer

fraction. The PCA data (transformed) for the coarser grained fraction confirms that most of the calcium derived was from diagenetic origins (subcomposition) with a strong correlation between the CaO and LOI (r=0.55) (Pe-Piper et al., 2008). Even though samples was excluded that portrayed severe diagenesis, due to the increased carbonate contents (possibly Fe-rich calcite), the effects of the diagenetic environment was still evident (Pe-Piper et al., 2008; Zhang et al., 2014). These carbonates possibly formed through sea-floor diagenesis (Okwese et al., 2012). Nevertheless, high loadings for CaO content in both the coarser fraction and the finer fraction suggest that there were Ca-bearing carbonates involved (Zhang et al., 2014).

The fossil content (disseminated shell debris in some facies) is also a large contributor to the calcite cement with silica cementation being enhanced by the volume of pore water circulation and silica-rich source regions (Willey, 1974; Berner, 1980). The silica derived from skeletons or siliceous organisms has been established by the strong negative correlation between SiO_2 and Al_2O_3 within the finer fraction, which suggests that there were siliceous skeletons involved in the contributor of silica into the distributary network (Hofer et al., 2013). The coarser fraction has mostly been affected by mechanical compaction and silica was mostly derived in situ. This silica dilution is one of the possible reasons for the SiO_2 being relatively so high in the samples.

The partial and full alteration or dissolution of feldspars was a major factor in masking the provenance characteristics. The fact that these samples were buried deep is a crucial problem because the dissolution of feldspars during diagenesis can affect the modal count of the K-feldspars and K_2O concentrations (Montanez, 1997; Wilkinson et al., 2001; Zhang et al., 2014). Replacement textures are also evident within most of the samples, especially the replacement of feldspars by poikilotopic calcite and sericite as well as the replacement of quartz by calcite (Figure 4.7F). This becomes a problem in identifying grains during modal counting (Gonzalez-Acebron et al., 2010). Thus, the overall feldspar content could be underestimated in this case, but most fully altered sericite has been added to the overall feldspar content. Thus weakens source-rock interpretation in this provenance study and becomes a primary source of uncertainty. Furthermore, the effects on permeability are also destructive leading to a porosity-poor or largely heterogeneously permeable formation (low K-feldspar dissolution). In terms of abundance, the petrographic modal counts indicated more feldspars than the untransformed geochemical data predicted. The transformed data, however,

played a crucial role in accurately determining that most of the K_2O (forming a constituent in a relevant subcomposition) was an important factor in the overall compositional variation of sediments, as indicated by the petrographic modal counts. This compositional variation was different in the finer fraction and that of the coarser fraction, with the occurrence of clay minerals.

Clay mineral diagenesis was also a large factor in the samples of 1AT1-V horizon. The presence of vermicular kaolinite, glauconite and illite-smectite are crucial to the understanding of the petroleum reservoir and the nature of the diagenetic environment. Thus identifying that most of the authigenic clay minerals (Figure 4.3.8B), with K_2O, Na_2O and CaO being orthogonal, were probably formed in the eogenetic-mesogenetic stages (Bjorlykke, 1983). A crucial part to the sudden enrichment of K_2O which is related to the formation of illite from kaolinite or smectite with deeper buried samples (F-A5#17 and #14) but their abundance is rather restricted to the finer fraction with variability of K_2O in the PCA being relatively low (Maynard, 1992). The Fe_2O_3 and P_2O_5 content do not show much variation in the dataset, but their distinguishing characteristics for sedimentary facies of the marine realm and transitional realm is well established. The identification of vermicular kaolinite and kaolinite (XRD results from F-AR1) is probably a result of telogenesis but a further detailed study into diagenetic reactions related to clay minerals should be performed.

Therefore, with the loss of provenance information, the effects seen on porosity and permeability are destructive. This is solely based on primary porosity and further studies have to be done in order to evaluate how these factors influenced the secondary porosity as indicated by Schmidt & McDonald (1979).

In summary, diagenetic processes plays a crucial role in the altering of the bulk-rock geochemistry. Therefore, this has devastating effects on the provenance- or weathering-related diagrams that makes use of major element oxides. The major elements are more prone to source and weathering (including diagenesis) conditions (Zhang et al., 2014). The accessory elements, however, are less prone to be affected by weathering and are more representative of the source and the hydrodynamic sorting during transport. These factors accounts for the compositional variability within the sediments (Weltje et al., 1998).

5.5 Transport

Mechanical weathering is evident based on the textural maturity of sediments and transportation occurring over long distances as well as short distances. This is largely based on grain shapes being well-rounded to subangular grains in some places as well as the geochemical behavior with respect to maturity. The geological samples had a high variability that is attributed to the depositional environments or the distributary network. In order to evaluate the source and paleoclimate conditions, the effects of sorting and recycling has to be assessed.

The trace element concentrations are the least affected by weathering and are prone to give valuable information on the source area. Density-specific grain changes are largely controlled by the hydrodynamic conditions (sorting), where the elemental concentrations of Ti and Zr can be assessed irrespective of a particular grain size (Sawyer, 1986, Garcia et al., 1994; Zhang et al., 2014).

McLennan et al. (1993) suggested that Zr/Sc and Th/Sc could be used to assess the role of sedimentary sorting as well as recycling (Figure 4.3.14). Most of the samples are indicative of a recycling nature, which is represented by the zircon or heavy-mineral enrichment (Sawyer, 1986; Garcia et al., 1994). There is a clustering of elements with a strong relation to heavy minerals (Zr, Hf) in the PCA analysis that suggests that polycyclic recycling occurred (Figure 4.3.9). In addition, the low correlation between Zr and TiO_2/Ce are indicative of a low influence of hydraulic sorting in the finer grained fraction (Mondal et al., 2012; Wang et al., 2012; Zhang et al., 2014).

The provenance interpretation of quartz can be assessed for a polycyclic recycling nature. Although the interpretation of the polycyclic quartz can also become distorted due to intrastratal solution, the occurrences of the poikilotopic calcite cement suggest that the pH was not in the range for dissolution of quartz during diagenesis. Therefore, quartz overgrowths with abraded rims should be considered polycyclic (Dutton & Diggs, 1990). There are also other factors involved besides pH such as pore water chemistry (including the total CO_2 in the system), temperature and organic matter. The presence of organic matter is largely indicative of an externally derived buffer system. In the sample that contain polycyclic quartz overgrowths, the facies below this unit usually consist of a carbonaceous claystone, therefore clay-mineral dewatering can promote CO_2 content in the system, thus

irrespective of pH (presumably at a range of 4-8) can promote carbonate precipitation with no silica dissolution (Kharaka et al., 1979). Therefore, the abraded quartz overgrowths can be considered as polycyclic, especially if the timing of these minerals can be depth related.

The strong positive correlation between TiO_2 and Al_2O_3 suggest that the compositional variation of these elements is probably the result of the source area (Garcia et al., 1994; Zhang et al., 2014). There is also local sorting and recycling due to the depositional environment (hydraulic sorting). This can be seen on figure 4.3.13, where F-AR1 samples plots closer to the increased Ti and lower Zr content (scattered section, Figure 13B and 13C), as evidence of first cycle Ti-bearing phases (Piper et al., 2007; Zhang et al., 2014). This is further enhanced by the low WIP values of F-AR1 which has been recently considered as an index of provenance, rather than an index of weathering, and indicates first cycle sedimentation (ICV values of >1) but from a recycled source terrain such as a sedimentary or metamorphic provenance (Garzanti & Resentini, 2016). This is also seen on the biplot (Figure 4.3.9, Figure 4.3.10) with the clustering of F-AR1 samples. Thus indicating that samples of F-AR1 is indicative of first cycle sedimentation but is also well sorted due to local hydraulic sorting in the coarser fraction (Figure 4.3.13A, close to first cycle sedimentation trend). The visual estimation of the plagioclase feldspars is much more in the F-AR1 well than the other two wells, therefore a provenance change has been attributed as the 1AT1 horizon is reached, thus probably exposing different source terrains with rapid upliftment during active tectonic activity.

The effect of hydraulic sorting can be distinguished from the effects of the concentration of heavy minerals from polycyclic provenances (geochemically). The coarser fraction samples from the 1AT1-V horizon, in general, shows a trend towards the Hf apex on the diagram of Garcia et al. (1994) (Figure 4.3.13). Thus indicating enrichment of heavy minerals in most of the samples. In addition, the weak positive correlation between Th/Sc and Zr/Sc is indicative of sedimentary recycling during multiple cycles of sedimentation (McLennan et al., 1993; Asiedu et al., 2004). The Zr and TiO_2 content covary, so the variability of these trace elements is controlled largely by zircon, which is supported by the petrographic data (Zhang et al., 2014).

The effect of sedimentary processes that have affected mineral abundances can also be shown geochemically (McLennan et al., 1993). The plots of Zr/Sc vs Th/Sc are used to evaluate zircon enrichment relative to the Th content (McLennan et al., 1993) (Figure 4.3.14).

Recycled/mature sources have Th/Sc ratios >0.8 with relatively high Zr/Sc (not much influenced by grain sizes). Sedimentary recycling within the source area is confirmed with relatively high ratios of Th/Sc and Zr/Sc, with the exception of a few samples with relatively low values of Th/Sc and Zr/Sc within all three wells. Major element ratios can also be used to evaluate sediment maturation within the depositional environment (in transport and recycling). SiO_2/Al_2O_3 ratios for F-AR1 is higher than for the other two wells indicating a higher maturity due to transport and hydraulic recycling within the depositional environment (reworking), rather than polycyclic recycling (Figure 4.3.13).

5.6 Paleo-climatic inferences

The proximity to the basement high and horizon mapping revealed that there was a topographic steepening towards the North East or Eastern direction (F-A12 and F-A5). The relief in the source area is rather complex because of the basin being bounded by a basement high on the eastern and western parts of the basin. These basement highs were crucial in controlling the major depositional architectures and hence the proximal provenance.

The relative quantity of illite over kaolinite is a good indicator for paleoclimate reconstruction. The occurrence of kaolinite (detrital) as a phase in XRD is largely indicative of humid conditions (Singer, 1980; 1984). Usually the occurrence of feldspar preservation is indicative of an arid environment (Tucker, 2001). However, there is a relatively stable occurrence of sub-equal amounts of feldspar and its alteration products. This is usually indicative of rapid erosion in an area of high relief under humid conditions. This is further confirmed by the high accumulation rates in the early Cretaceous times within the sub-basin (Tinker et al., 2008)

According to Tucker (2001), samples that plots in the upper section of the QFL diagram (Figure 4.2.9 and 4.2.10) are a result of humid weathering conditions compared to samples that plot in the lower section indicating arid conditions in the source area, whether it is from a metamorphic or plutonic source. The 1AT1-V horizon samples plots in the center region of plutonic and metamorphic source terrains indicating humid-arid climatic source conditions. This can also be supported by the degree of weathering and climatic conditions as noted by Weltje (1994) on transformed modal counts. The trend in compositional space shows an intermediate plutonic-metamorphic source terrain (mixed), with incipient to moderate degrees of weathering (Figure 5.1.5). The comparison of data of Mann & Cavaroc (1973) with its

transformations modified after Weltje et al. (1998), shows that the 1AT1-V horizon samples are largely indicative of moderate to high slopes under subhumid climatic conditions with sedimentary recycling. Even though the sediments have undergone recycling, a sub-humid to arid climate are further supported by the relative abundance of monocrystalline-polycrystalline quartz to unstable grains and the amount of feldspars over volcanic rock fragments which are usually indicative of humid and arid climatic conditions (Young et al., 1975; Mack & Jerzykiewicz, 1989).

The geochemical variation as a function of climatic conditions should be assessed since there are various other factors involved in controlling climatic conditions (Guo et al., 2018). The relative constraints on major element data (constant-sum problem), as well as autocyclic and allocyclic controls (excluding climate) should be assessed before evaluating the climatic conditions of the source area.

The SiO_2/Al_2O_3 ratio can be used to assess recycling and weathering of the provenance terrain, since quartz is more stable than the other minerals in the depositional realm (Roser & Korsch, 1985; Dingle & Lavelle, 1998). The level of sandstone maturity is then governed by the percentage of SiO_2 within a sample (Dingle & Lavelle, 1998). This maturity, together with CIA values can indicate possible climatic conditions. The SiO_2/Al_2O_3 ratios are relatively high with majority occurring above 5 for progressively matured sediments (Roser et al. 1996; Dingle & Lavelle, 1998). The strong negative correlation between the SiO_2/Al_2O_3 and the CIA ratios suggests that as the chemical index of alteration increased, the degree of maturity decreased (Dingle & Lavelle, 1998). High SiO_2/Al_2O_3 ratios will indicate low degrees of weathering when the CIA value is used. Therefore, to assess the nature of chemical weathering in the source area, a positive correlation between SiO_2/Al_2O_3 ratios and the CIA values should exist to make the CIA value more robust.

All the three wells shows a relatively high SiO_2 abundance (F-A5: 80.2wt%, F-AR1: 88.44wt%, F-A12: 70.02 wt%) as compared to the values of PAAS and UCC (Figure 4.3.3). The problem with these high contents of SiO_2 is the quartz dilution phenomenon (McLennan, 1989; Aitchison & Pawlowsky-Glahn, 1997). Therefore, certain measures need to be taken for the treatment of the geochemical data to eliminate spurious correlations. The low-medium values and a relatively constant Si/Al ratio indicates that there were some dilution of detrital quartz within the finer fraction (although one sample indicates a very low amount of detrital quartz) (Hofer et al., 2013). F-AR1 samples are more mature (shallow marine wave

reworking) with F-A5 being less mature and F-A12 the least mature based on averages (hydrodynamically). The F-AR1 samples does not have finer grained samples (sampling is limited) as in the case for the other wells, in general, this well will be dominated by quartz-rich assemblages.

The effects of grain size is also a factor that controls the weathering index, therefore the 'coarser fraction' are mostly in the range of fine to medium sandstones thus attaching a sense of 'transport invariance' to the use of weathering indices. Although this level of invariance has been taken into account, the issue of grain sizes on indices of weathering is still evident (Nesbitt & Young, 1982)

The depletion of mobile weathering cations (Figure 4.3.3) are also largely indicative of their relative quantity in the source area being depleted (Garzanti & Resentini, 2016). This is largely evident in the coarser fraction, whereas in the finer fraction there are differences in weathering cations therefore careful analysis using the CIA values has to be considered. Borges et al. (2008) and Garzanti & Resentini (2016) concluded that collisional belt provenances can become complicated concerning weathering indices, especially where the relief is high, obscuring weathering indices to reflect provenance terrains rather than specific climatic conditions.

There is a positive linear co-variance of Al_2O_3 with several major oxides (Fe_2O_3, TiO_2, MgO, Na_2O and K_2O) indicating that these elements (also confirmed by PCA), in general (except for F-A12), are derived from or associated with silicates (clay minerals or alluminosillicates) (Jin et al., 2006; Sciscio & Bordy, 2016). Thus contributing to moderate-incipient chemical weathering affecting the 1AT1-V horizon samples (Sciscio & Bordy, 2016). PCA confirms that CaO, Na_2O and K_2O behave independently in the finer fraction (Figure 4.3.8). This means that the correction for CaO from marine origins should be accounted for, since the loss of Ca and Na from feldspars did not occur together. The Mg and Fe content is constant and is not affected by significant marine influence. This is probably due to the mobility and solubility of Mg^{2+} and Fe^{2+} in the marine realm Siderite and pyrite is evident within the stratigraphic section but not much variation within the Fe content was observed (except for depleted amounts) (Figure 4.3.3). These depleted amounts, especially Mg^{2+}, can be directly related to the depleted amounts in the source region.

The finer grained fractions will also show lower SiO_2 with higher Al_2O_3 (and co-variants) contents compared to the coarser grained fraction solely due to grain sizes and mineralogy (CIA will also be higher) (Guo et al., 2018). There is a positive correlation between CIA and the SiO_2/Al_2O_3 ratios, which makes the finer fraction more prone to indicate weathering conditions in the source area rather than local hydraulic conditions.

Although the CIA index is a fairly good approximation of weathering, the ICV (Index of compositional variability) and CIA_{molar} (highly sensitive to humid conditions) is more reliable when it comes to evaluating the weathering conditions under different climatic conditions within a formation. ICV takes into account all possible geochemical parameters with minimal effects of diagenesis, unlike the CIA values that are largely affected by diagenetic alterations (Potter et al., 2005; Sciscio & Bordy, 2016). Usually to ascertain climatic conditions, Suttner and Dutta (1986)'s SiO_2 vs $Al_2O_3+K_2O+Na_2O$ diagram is used to determine the climate of ancient sediments, but due to the recycled nature of the plotted samples (Figure 4.3.14) this diagram's accuracy is based largely on the nature of first cycle sedimentation and erosion. The drawback with the CIA index and most other indices is based on the assumption that the source had a high content of feldspar that eventually breaks down to clay minerals. Therefore, the CIA value does not account for diagenetic alterations, provenance, physical weathering and sorting (Goldberg & Humayun, 2010; Sciscio & Bordy, 2016). However, the degree of silicate weathering can be assessed using the CIA index of an overall formation within the finer fraction (Selvaraj & Chen, 2006). The effects of provenance and contributions of different source rocks are evaluated using the A-CN-K plots and ICV values.

Most of the CIA values indicate that the source was undergoing incipient to moderate degrees of chemical weathering. The petrographic data reveals that mechanical weathering was a major constituent with in the tributary network. During weathering, Al, K, Mg, Cs and Rb are kept within the system whereby Na, Ca and Sr are lost due to dissolution and contribute majorly to the diagenetic realm of sediments. Figure 4.3.11A shows that most of the sediment was deposited during the early to middle stages of chemical weathering/diagenesis. In addition, the loss of independent CaO and Na_2O during weathering of plagioclase did not occur together (Pe-Piper et al., 2008). However, the A-CN-K diagram illustrates that Na_2O and CaO were lost within the system (CaO*, Figure 4.3.11A). PCA confirms that the finer grained fraction indicated an oppositely trended, Ca and Na, which suggest that Ca was possibly derived from a Ca-rich mineral (anorthite-plagioclase), whereas the coarser grained

fraction shows that some of the Ca^{2+} was derived from seawater (CaO being orthogonal to Na_2O). Thus indicating that the CaO* within the finer fraction is used correctly for further source-weathering conditions. The loss of Na^{2+} and Ca^{2+} projects a trend towards the illite composition ultimately. In addition, the trendline is not parallel to the A-CN join that could be the result of smectite interference as shown in some samples and compositional variation due to mixing in the source terrain (Figure 4.3.11A). In addition, the illite is not detrital but diagenetic based on the low correlation between Si/Al and K/Al contents.

The finer fraction should yield better results for evaluating the source-climatic conditions. The finer fraction has values that range from 63.055-71.04. These values are relatively low-medium when compared to the average CIA values of fine grained rocks at 70-75. These values plot above the feldspar line, which indicates incipient-moderate weathering conditions (supported by PIA, CIW, Rb/Sr and K/Rb ratios). This is supported by petrographic data as well plotted on Weltje (1994)'s weathering diagram. The finer fraction is also plotted on the diagram of Goldberg & Humayun (2010) which suggest that these sediments were deposited in subtropical climatic conditions. The high ICV and CIA_{molar} values suggest that chemical weathering, with equal physical weathering, was a major constituent in the changing geochemistry of samples. Thus showing more humid conditions within the source region (as confirmed by the CIA_{molar} values in the finer fraction after Goldberg & Humayun, 2010). The K_2O/Al_2O_3 ratios are also very low and point towards sub-tropical conditions with occasionally average values that periodically changes (Gallet et al., 1998). This is also confirmed by the paleolatitude of the offshore southern Africa to be at 50°S (Smith & Briden, 1977; McMillan et al., 1997; Torsvik & Cocks, 2016) which indicated a temperate, cool and wet to dry climate.

Additionally, petrographic analysis on these samples suggests that illitization was only common in one sample (mixed-layer illite and smectite) but the occurrence of illite is quite low. In addition, K-feldspar content was quite low (in abundance) in the petrographic analysis so the effect of metasomatism is minimized. It is also assumed that there was no significant K^+ addition to the system to cause erratic results. The fact that the finer fraction shows subtropical conditions and the coarser fraction indicating arid conditions with low CIA values can be explained with relation to the provenance area and grain size (Price & Velbel, 2003; Garzanti & Resentini, 2016). A felsic source weathers easily within a system, therefore the CIA values will be quite high, whereas a quartzose recycled source will not weather

easily. Therefore, the CIA value (silicate weathering) indicates low degrees of weathering within the source region because of the chemical stability of the source area. The finer fraction which yields better results for weathering and the CIA_{molar} value (ultra-sensitive to humid conditions) shows more humid conditions within this region but the coarser fraction indicates more arid conditions which is also supported by the modal count data.

These indices compliment SiO_2/Al_2O_3 ratios, which indicate mature sediments at relatively incipient-moderate degrees of chemical weathering. Therefore facies associations (based on grain sizes) plays a key role in the variability of these units (Sciscio & Bordy, 2016). It is crucial that knowledge of other factors involved in the variation of CIA values should also be taken into account. So fluctuations of the CIA values can be related to fluctuations in temperature (Dingle & Lavelle, 1998).

Within-stratigraphic (temporal distribution) sections or as the drift unconformity is approached, the environment becomes more arid/dry (low CIA_{molar} values) as confirmed by McMillan (1997) but initially (samples occurring well below in the stratigraphic column) more subtropical-tropical humid conditions prevailed. In conclusion, the finer fraction and the coarser fraction were derived from rocks that were undergoing both incipient and moderate degrees of chemical weathering due to the stability of the provenance terrain. In addition, the use of multiple proxies for weathering is advised because of the vulnerabilities of using single proxies as weathering indicators in the source area (Garzanti & Resentini, 2016). The PIA values were synonymous with CIA values and their trends were sufficient to represent low feldspars in the source regions. This study serves as a baseline quantitative study for further palaeo-climatic studies, and thus further studies based on more samples and methods need to be incorporated through quantitative and qualitative means.

The use of weathering indices should be evaluated carefully, since the petrographic and bulk-rock geochemical data can indicate completely different climatic conditions. In this instance, the weathering intensity is supported by both the geochemical data and petrographic data for the coarser fraction. The original authors of the CIA (Nesbitt & Young 1982; McLennan et al., 1993) only used finer grained sediments and this was crucial, since the finer grained material is more susceptible to weathering conditions. There are still modern authors that use these CIA values on coarser grained sediments and careful observations should be made that accounts for other factors as well (besides chemical weathering in the source region). Sedimentological (carbonaceous coal drapes), petrographic and geochemical analysis (finer-

grained material) all point towards warm humid-subtropical with arid climatic conditions occurring at certain time intervals in the early Cretaceous. This is further supported by fluctuating climatic imbalances shown with isotopic data (Föllmi, 2012) and paleogeography maps of Gondwana during the early Cretaceous, which represented a variety of climates, as there was fluctuations from humid-arid conditions (Torsvik & Cocks, 2016). This is also supported by Hay & Floegel (2012)'s paleogeographic reconstructions of the early Cretaceous climate with fluctuations between arid and warm humid belts (mid latitude).

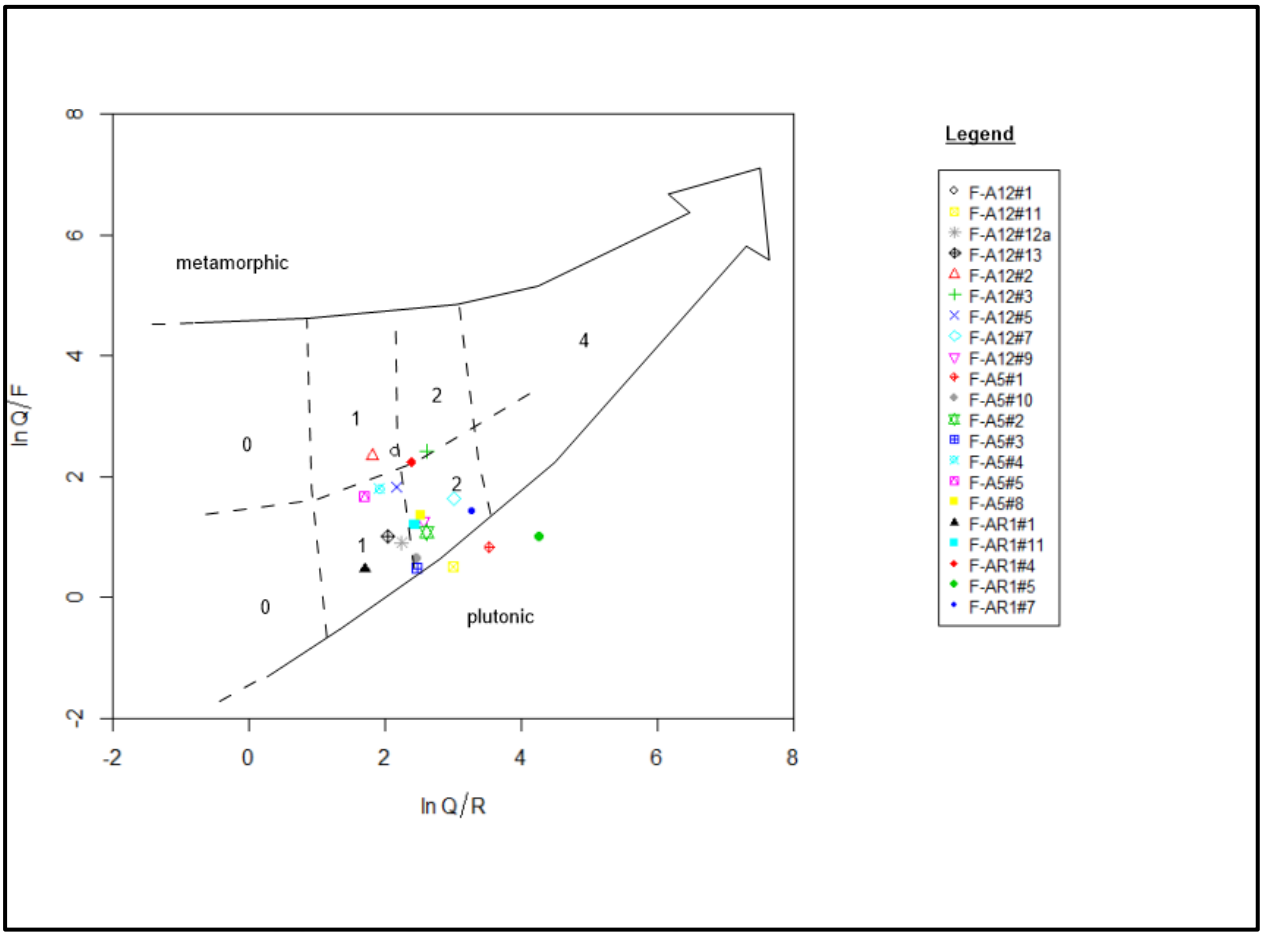

Figure 5.6.1: Bivariate log-ratio plot of 1AT1-V horizon samples showing the weathering intensity of modal counts (after Weltje, 1994).The symbol numbers indicate weathering intensity where 0-unweathered, 1-slightly weathered, 2-moderately weathered and 4-intensely weathered.

5.7 Provenance and Tectonic setting

5.7.1 Provenance lithology

Till date, there has not been a single robust provenance study performed in the Bredasdorp sub-basin, therefore no comparison can be made as to evaluate the classification scheme and provenance characteristics. This study acts as an inference towards a more detailed

provenance study. Studies that are more detailed can be performed using different techniques within the constraints of data and equipment availability.

The occurrence of quartz and its associated characteristics has long been used as a grain for the identification of the provenance of sediments. Quartz inclusions were restricted to the minor occurrence of muscovite and zircon grains with some grains also being clear with no inclusions. These clear grains are usually an indication that the ultimate source of these quartz grains is volcanic in origin (Boggs, 2009). This is further confirmed by major element data indicating a subordinate or ultimate source input that is of felsic composition (with an average composition ranging from granodiorite-granite (Figure 4.3.11)). The subordinate source input is also confirmed by the high values of Rb, K, Ba, major elemental oxides, an enrichment of the LREE with small negative Eu anomalies, constant or flat HREE and considerably high Hf and Zr content, although the latter can be due to recycling representative of an ultimate source terrain (av. K/Rb of 200, Eu/Eu* of 0.51-0.89) (Floyd et al., 1989). Incompatible to compatible element ratios (La/Sc, Th/Sc and Th/Co) indicates that the samples are of ultimate felsic and recycled source compositions (Floyd & Leveridge, 1987). This is further confirmed by the occurrence of felsitic igneous lithic fragments (Figure 4.2.4B). Ratios of K_2O and Rb are quite high which implies a possible 'acidic' source but with compositions that are more feldspar-rich (indicated by petrography) such as an albitic-rich granite (Floyd & Leveridge, 1987). XRD and petrographic analysis confirms the occurrence of plagioclase in the form of albite, which supports an ultimate/recycled albitic rich granitic source.

The occurrence of plagioclase feldspars over the alkali feldspars could be due to the chemical/mechanical durability and abundance of these minerals in the source area. According to Pittman (1970), the occurrence of orthoclase, microcline and abundant plagioclase should point towards parent material that consists of igneous and metamorphic rocks. Abundant biotite usually points to an igneous source terrain, but the occurrence of detrital biotite is restricted to some of the samples. This 'rare' abundance can be explained by the occurrence of glauconitic grains from which biotite are usually a precursor for glauconite formation (Figure 4.2.3). Thus also noting that a K-poor/Fe-rich smectite and illite can also be a precursor for glauconite formation (Bjorlykke, 1983; Amorosi et al. 2012).

The Th/Sc ratio, which is highly sensitive to average provenance compositions, indicates a higher silicic provenance (Taylor and McLennan, 1985; Lee, 2009; Hofer et al., 2013). The

Cr content was extremely high which was due mainly to contamination (milling machine uses a Cr ring). According to the regional geology, an ultramafic source is unlikely which is supported by the low Y/Ni and high La/Y ratios (ratios based on Bhatia & Crook, 1986). Even though these values were also relatively low (as compared to UCC and PAAS) a mafic recycled origin is envisaged. Thin sections reveal that plagioclase was more abundant than K-feldspars (K-feldspar mostly in the form of microcline and orthoclase). The A-CN-K diagram also illustrates this phenomenon with the trend line intersecting the K-feldspar/plagioclase line at a more enriched plagioclase source composition.

The major element content, shown in Figure 4.3.18A and 4.3.18B, indicates a principal input from a primary recycled source (sedimentary/metasedimentary) and a secondary input from an igneous source (Roser and Korsch, 1988). With the increasing sediment maturity and multiphase quartz, samples would plot in the quartzose recycling field, which is further confirmed by the recycled nature of the sediments based on the petrographic data (Figure 3.3.14). Thus implying that the samples of the 1-AT1-V horizon samples are mostly the products of polycyclic provenances with respect to the trace element composition as well. Furthermore, the depleted values of weathering cations (Figure 4.3.3) are indicative that the source area was already depleted in these cations, also largely indicative of a recycled source terrain.

The feldspars were not that scarce in the sandstone and siltstone samples as noted by the geochemical analysis. The samples that do show abundant feldspars are less likely to be recycled sediments. Since most of the samples are recycled, the occurrence of moderately abundant feldspars is most likely due to the presence of an igneous source terrain (Islam, 2010). Therefore, there would be a fine line between sediments that has been recycled and first cycle sedimentation (the occurrence of well-rounded zircon grains and euhedral zircons). This is supported by the heavy mineral proxy data of hydraulic sorting and polycyclic recycling as discussed earlier (Figure 4.3.13 and 4.3.14). This points out to a reworked provenance terrain from older meta-sedimentary (low-grade) and a possible first cycle/recycled igneous bearing source terrains (Boggs, 2009).

The polycrystalline and undulatory extinct quartz grains can also be used to infer a provenance (Basu et al., 1975). Most of the samples indicate a low-medium grade metamorphic origin with minor evidence of plutonic source terrains (Figure 4.2.13). This is further supported by the nature of the polycrystalline quartzitic clasts that are stretched,

which is usually indicative of a metamorphic provenance (Scholle, 1979). These sediments are not considered compositionally mature (Pettijohn, 1975), and therefore meets the requirements for the study of undulatory extinct and polycrystalline quartz grains of Basu et al. (1975). The recycled nature of these sediments are still a crucial factor for masking the actual provenance of the sediments, since Basu et al. (1975) dealt with first cycle sediments. This is confirmed by the geochemical data as well with a primary quartzose/recycled origin and minor influences of igneous terrains (Figure 4.3.18).

The presence of different types of lithic fragments is crucial to the understanding of the provenance since lithic fragments are a direct link to the possible source rock lithology. Therefore, the occurrence of metaquartzite and chert in most of the samples are usually indicative of metasedimentary and metafelsitic source rocks (Garzanti & Vezzoli, 2003). Whether this was part of a first cycle sedimentary process (proximal source area) or multiple recycled proxies are still unknown, due to the overlapping nature of these fields based on lithic fragments. Multiple recycled proxies are supported by the spatial and temporal evolution of the tectonic settings (Figure 4.2.13) (Garzanti et al., 2003; Caracciolo et al., 2012). The metafelsitic origin is supported by the geochemical data (Figure 4.3.18A), but there is a low correlation between the modal counts and the same samples evaluated under geochemical analysis. This has been accounted for by using compositional data analysis.

The relative occurrence of these lithic rock fragments does not indicate a specific time where all of these source rocks were present within the source terrain. The processes of selective enrichment and depletion of these grains within the sediment dispersal system should be taken into account for further quantitative provenance studies. Therefore, the provenance did not change much vertically and was largely sedimentary/metasedimentary (grade 1) and acidic igneous source (metafelsitic) terrains as confirmed by petrography and geochemistry (the latter based on lithic grains but could have been largely recycled). The temporal change that does occur is mostly the result of a spatial and temporal distribution of different formations (Garzanti et al., 2003; Weltje, 2012). The compositional changes that do occur laterally could be attributed to the depositional changes within the system.

Interestingly, the CaO (Na_2O) and K_2O content is relatively low compared to the UCC and may reflect a source rock being dominated by an albitic-rich plagioclase and/ or a source with low K-feldspar metasedimentary rocks (Pe-Piper et al., 2008). However, PCA and correlation analysis confirms that some of the CaO content was diagenetically derived, but it does not

necessarily mean that it reflects a source terrain that is dominated by K-feldspar but rather, a source terrain dominated by an albitic plagioclase composition with possibly sub-equal, but lesser proportions of K-feldspar as well (confirmed by petrographic modal counts). The diagenetic origin is also clearly seen from f-tests for the finer grained and coarser grained fractions. The weathering stability of these minerals is also a major contributor for the selective compositional variation of these minerals within the samples.

The CaO-Ni-Hf/Zr is orthogonal and suggests that they possibly came from three sources or formed by three different processes (Caracciolo et al., 2012). PCA also confirms the upper part of F-A5 is enriched by K_2O (result of K-feldspars or rather illite formation) and the lower part (deeper depths) more dominated by plagioclase feldspars which is more enriched in the felsic input (Figure 4.3.10).

The Ni and Ti contents of sediments can be used to indicate a mafic source. The high variation within the Ni content in this context does not make it an appropriate discriminator for first cycle provenance (standard deviation of 5.8); this could be due to various other reasons such as chemical properties of mobility and solubility, as well as the source region (recycled origin). The relatively high TiO_2 content is due to derivation from ilmenites (high correlation between V and Ti) and pelitic meta-sediments (Pe-Piper et al., 2008; Zhang et al., 2014). This is confirmed by the low angle between links for Zr-Hf-TiO_2 (Figure 4.3.10). The high correlation between Zr with V and TiO_2 (Ti) suggest that most of the Ti was derived from the ilmenite in the source region. This is further confirmed in the finer fraction and coarser fraction as well with TiO_2, Zr and Hf sharing the same variations in PCA. The negative low correlation between illite proxy (K/Al) and Ti suggest that it was not adsorbed during weathering or soil formation. The high correlation between TiO_2 and Al_2O_3 suggest an authigenic response or adsorption onto other clay minerals (excluding smectite and illite) or possibly other Ti-bearing alluminosillicates. These TiO_2 bearing minerals could well be linked to a peralkaline granite (Birkett et al., 1996).

5.7.1.1 Provenance lithology compared to the surrounding terrains

It is proposed that majority of the sediments were possibly derived from the sedimentary rocks of the basement highs (Table Mountain quartzites and possibly the Malmesbury Group (pre-Cape), minor onshore provenances (Malmesbury Group) and a second ultimate source of felsic composition could have been from the Cape granite suite (tectonic pre-Cape inlier). The Cape granite suite is the only known source of felsic derived igneous provenance in the

area and are usually associated with the Malmesbury Group sediments along the southern coast (Figure 1.3.1, Frimmel et al., 2013). These granites are also confirmed to have very high amounts of albite, as compared to anorthite, especially the Blanco Albitite from the George pluton (Browning & Macey 2015). These S-type granites (Cape granite suite) also contain more plagioclase feldspar than alkali feldspar minerals, low biotite and abundant zircon and ilmenite minerals (Farina et al., 2012). This confirms the geochemical results of an ultimate igneous source that contained more plagioclase with lesser K-feldspar grains as an ultimate source terrain. The extent of the Cape granite suite offshore is yet unknown but majority of the upliftment occurred within the western part (Cape Town) where exposures of the granites are seen. This is further supported by fission track analysis of Tinker et al. (2008), which suggest high rates of sediment coming into the basin during the early Cretaceous times from the Northern part of the sub-basin.

An ultimate igneous source can be due to the weathering of the Cape granite suite. Another speculation would be if the biotite can be considered as an equivalent to the formation of glauconite, then with its other associated characteristics, an igneous ultimate source terrain can certainly be inferred (recycled/first cycle, proximal/distal) (Islam, 2010). Bordy & America (2016) also performed a provenance analysis of the late Mesozoic Pletmos sub-basin (alluvial proximal terrains) and confirmed that a proximal provenance occurred from the Maalgaten Granite where they are usually associated with the Blanco Albitite that is envisaged to have undergone recycling further offshore.

The occurrence of subangular to subrounded grain shapes does confirm provenances from proximal and distal source areas (bimodal distribution in samples). Therefore, an inference can be made that most of the sediments came from the NW and NE, which agrees with the sediment source directions of Brown (1995). Also, the assumption that the Karoo Supergroup (Ecca or Dwyka groups) could have contributed to the overall 1AT1-V sedimentary succession as suggested by Tinker et al. (2008) should be reevaluated since the provenance of the Ecca group points to a source that is more enriched in K-feldspar than plagioclase (Baiyegunhi et al., 2017). The source for the 1AT1-V sequence points to an ultimate source that is more enriched in plagioclase than the amount of K-feldspars (Table Mountain Group and Bokkeveld Group).

It is also suggested that F-AR1 (in the North) was sourced more from sediments of the Table Mountain Group and Bokkeveld Group with a higher recycled mafic content, especially from

the south western part of South Africa (Fourie et al., 2011), whereas F-A12 and F-A5, was sourced more from the felsic metasedimentary or recycled uplifted meta-sedimentary felsic source from the older Pre-Cape sediments (Buggisch et al., 2010) and the Cape Granite suite (based on the biplot vectors of Zr and Hf content together with TiO_2, Na_2O content). PCA confirms that Fe_2O_3, Ni and V group together, this could largely be due to the effects of recycling (provenance signature preserved in the sedimentary provenance) and points towards samples of F-AR1. This could also reflect the occurrence of a sedimentary quartzose recycled source that is more enriched in these elements in the North (F-AR1) or received more detritus from the Table Mountain Group (which is rich in a mafic/felsic component). This is further confirmed by the low WIP values and discriminant function analysis of F-AR1, which indicates an enriched content of recycled quartz (Garzanti & Resentini, 2016).

5.7.2 Tectonic setting

The tectonic setting using the modal counts points largely to the occurrence of a provenance terrain that exists as a collision-foreland orogenic terrain, with possible overprinting of precursor transitional-continental terrains (Dickinson& Suczek, 1979; Dickinson, 1983; Suczek & Ingersoll, 1985). This is further confirmed by source rocks that consist of sedimentary/metasedimentary (metapelite) cover, with plutonic basement rocks (Dickinson, 1985). These tectonic settings can be further supported by the rigorous statistical revaluation of the Dickinson model by Weltje (2006) (Figure 4.2.13A, B and C). Most of the samples plots in the continental block provenance and recycled (collisional)-orogen fields. This can be attributed to the evolution of the recycled tectonic terrains, such that the temporal compositional changes from quartzofeldspathic and quartzolithic samples could have been due to the erosion from older source terrains (uplifted regions) to younger source terrains with their own tectonic setting (Gonzalez Acebron et al., 2010; Caracciolo et al., 2012). The plot of Ti/Zr vs La/Sc and the ternary plot of La-Th-Sc (Figure 4.3.16) gives two paleo-tectonic settings probably because of the mixed and recycled provenance (immobile nature of these elements). This can, however be attributed to the evolution of different tectonic settings, as confirmed by petrographic data (4.2.13). As the transform-rift margin progressed, active sedimentary/meta-sedimentary source directions became available during the break-up of Gondwana (Hofer et al., 2013). This recycled nature of the sedimentary source, with older provenance signatures, can disrupt the trend (Pe-Piper et al., 2008). In addition, bulk rock geochemistry for trace element discriminant analysis has come under scrutiny due to the recycled nature of sources, especially of mafic derived Sc content (Bock et al., 2000;

Kutterolf et al., 2008; Hofer et al., 2013). The immobility, in this case, for trace elements has actually become a problem since the bulk rock geochemistry records overall provenance signatures of recycled sediments, and not precise source-rock end-members.

This is especially true for the fact that PCA (transformed data) shows a clear relationship between V, Ni and Sc (angle <45°) which indicates that it has been derived from a source that was possibly derived from older mafic provenances with its associated tectonic settings (Table Mountain Group) (Figure 4.3.9A). So overall, abundant sedimentary and metamorphic rock fragments points towards source rock lithology of quartzose recycled orogenic terrains, part of a collisional suture or fold thrust zone provenance terrain. In addition, the occurrence of the samples in the transitional-continental field (continental block provenances) means that the provenance could have evolved from this terrain towards a more quartzose-recycled terrain (Okuzawa & Hisada, 2008).

The high quartz content, low plagioclase and K-feldspars, low polycrystalline/monocrystalline quartz ratios and low lithic fragments all point towards plate boundaries (depositional basins) of a rifted margin with associated collisional to foreland-uplifted provenance terrains (Dickinson & Valloni, 1980). This is further supported by Verma & Armstrong-Altrin (2013)'s geochemical discriminant diagrams, where all the samples (excluding diagenetically altered) falls within the Rift field (Figure 4.3.17). The plate boundary (tectonic setting) coincides with the tectonic setting proposed by the break-up of Gondwana (Brown, 1995; Jungslager, 1996; Broad et al., 2012).

This is further supported by the confidence regions of the dataset that indicates a temporal change possibly from an ultimate source (possibly PAN-African orogeny or Kaapvaal craton interior) to multiple recycled source terrains (including the Cape fold belt) and finally evolving into the basement uplifted area (rifted setting) during the early Cretaceous age (Figure 4.2.13). The tectonic setting (plate boundaries) is much more complicated, because of the transform-rifted nature of the tectonic setting (Gondwana break-up), showing reactivation of faults and enhanced compressional phases overprinting the Cape Fold Belt. Therefore, two tectonic provenance settings are inferred. It is proposed that the Falkland Plateau was still moving, within this sub-basin, towards the south that formed part of the larger nature of the transform-transpressional boundary.

5.7.2.1 Tectonic setting in response to the surrounding terrains

The initial provenance inference (Brown, 1995) that the source rocks were the sedimentary successions of the Table Mountain group orthoquartzites and Bokkeveld group (Cape Supergroup) holds true. These successions with pre-Cape successions were also largely metamorphosed during the Cape Fold event.

The occurrence of the metaquartzites or metapelites is largely indicative of this metamorphic event. The presence of low-medium metamorphic grade (Basu et al., 1975) is largely due to a decrease in deformation intensity from the Southern to the Northern part of the Cape fold belt (Halbich et al. 1993; Blewett & Phillips, 2016). This is further supported by the occurrence of metapelitic 'rank 1' lithic fragments within some of the samples (Garzanti & Vezzoli, 2003). The Cape fold belt contains rocks from Paleozoic sedimentary and pre-Cape basement rocks that have largely gone through low-grade metamorphism (Frimmel et al., 2001). Interestingly, the diagram of Basu et al. (1975) shows that there was a secondary provenance of medium grade with high-grade metamorphic material (including igneous terrains). Thus could largely be the result of the pre-Cape successions. This also confirms that a possible pre-Cape (Pan-African orogeny (medium grade) and syn-Cape (Cape fold event (low-grade)) metamorphic overprint occurred with lower-middle greenschist facies (overprint) being reached (Frimmel et al., 2001). Also, this could have largely been the result of the complex transform-rifted nature of the basin, but the absence of a proper regional study concerning the transpressional or transtensional stresses on the deformed provenance terrains involved during the syn-rift or Gondwana break-up, no inference can be made that involves the deformational history of these events. Halbich et al. (1993) confirmed that the deformation intensity (grades) increased towards the south; therefore, an offshore accumulation possibly has higher rank metamorphic material than its onshore equivalents. These high-grade to igneous subordinate terrains can also be attributed to the Natal group (Pre-Cape sediments), which was entirely removed during syn-rift stage of Gondwana break-up (Marshall & von Brunn, 1999).

The change in grain shapes indicate that the Cape fold belt was extensive, from provenance terrains that are proximal (basement highs) and distal (Great escarpment). Tinker et al. (2008) confirm the distal provenance, as well as the uncertainty in the study related to the input of the Basement highs during the early Cretaceous. Blewett & Phillips (2016) also confirm the extensive nature of the Cape Fold Belt. Nonetheless, these grains or the overall provenance is

definitely an indication of recycled provenance terrains. The recycled nature is also confirmed by the occurrence of polycyclic quartz overgrowths, rounded zircon grains, the abundance of meta-quartzite and chert rock fragments (ultra-stable). Thus falls part of the provenance terrains with its associated plate boundaries.

5.8 Reservoir potential

In well F-A12, five reservoir zones were identified where reservoir zone 1, 2 and 3 were hydrocarbon bearing and reservoir zone 4 and 5 were tight reservoirs. In F-AR1 Reservoir zone 1 and 2 were hydrocarbon bearing whereas 3 and 4 were tight reservoirs. Well F-A5 had hydrocarbon bearing units in reservoir zone 1, 2 and 4 whereas reservoir zone 3 was identified as a tight reservoir.

Relatively, the porosity and permeability fluctuations are mostly due to the facies changes that occur but the role of the provenance on reservoir distribution and reservoir quality was crucial. The effect of diagenesis destroyed permeability due to compaction and cementation. The porosity in most cases was preserved as secondary porosity and was a function of the abundance of feldspars and their alteration products. It is well known that plagioclase and orthoclase as well as their alteration products are crucial to the porosity distribution of hydrocarbon reservoirs (reservoir quality). It is clearly seen that F-AR1 with its specific provenance characteristics and first cycle sedimentation yields an excellent porosity but poor permeability. The permeability was mostly a function of depth whereby the shallow samples displayed good permeability readings which was mostly a function of diagenesis. Transport also played a crucial role in the ‘packing’ structure of grains but was largely modified, therefore only certain samples (shallower depths) are attributed to the enhanced porosity and permeability due to transportation for some compartmentalized reservoir zones. The heterogeneous composition and distribution of feldspars within samples are controlled by their recycled counterparts and is therefore a contributor to the porosity of the reservoir. F-A12 and F-A5 were sourced from the basement highs predominantly therefore will yield different porosities and hence permeability as well.

CHAPTER 6

CONCLUSION AND RECOMMENDATIONS

6.1 Conclusion

Detailed sedimentological analysis has identified nine facies associations in the studied interval of 1AT1-V horizon. Two overall sequences were identified as lower regressive and upper transgressive sequences (Element complex assemblage sets). The regressive sequence consisted of middle to distal delta front lobe fringes, hyperpycnal event beds, offshore migrating tidal bars (and associated inter-bar regions), mouth bars, terminal distributary channels (and associated inter-terminal distributary regions). The distal delta plain to proximal delta front consisted of interdistributary bays, distributary channels, crevasse splay subdeltas, mouth bars, tidal flats and offshore embayments. Laterally, these deposits also consisted of basement high slopes with upliftment of the basement highs and proximal/central embayment to regressive shoreface/foreshore environments. These sequences consisted generally of low diversity and intensities (impoverished abundances) of trace fossils. The paleoclimatic inference from this sequence indicates a humid climate with intermediate degrees of weathering intensities (possibly arid conditions).

The transgressive sequence consisted of estuarine sedimentation with the occurrence of tidal sand ridges and compound dune fields, embayment facies and tidal bars. These sequences consisted of relatively higher ichnodiversities and intensities than their relative regression sequences. The paleoclimatic inference during these times consisted of more arid to semi-arid settings with low degrees of weathering in the source terrain. The dominant processes involved in the lower section were fluvial dominated, wave-influenced and tide-affected type of deposits with the strength of tidal processes increasing towards the top and dominating the transgressive sequence. A major tectonic shift gave rise to different processes and hence depositional facies. It is proposed that there are several modern analogues that are similar in most cases and they are the Mahakam, Ganges-Brahmaputra, Po, Burdekin deltaic and Satpara lake environments.

Diagenetic processes played a crucial role in the compositional heterogeneity with compaction and dissolution dominating the process regime. These had major effects on the reservoir quality and distribution with the change in provenance as well. Transport distances

were also a major contributor since a proximal and distal source were identified with first cycle and polycyclic sedimentation characteristics.

The provenance lithology has been identified as recycled sedimentary rocks (and their meta-equivalents) with an ultimate source terrain that was largely felsic in nature (Cape granite suite). The northern part of the studied section is suggested to have received sediments from the main metasedimentary rocks of the Cape fold belt (including the Table Mountain Group and Bokkeveld Group) whereas the southern sections received more sediments from the basement highs (recycled sections of the Malmesbury Groups and Cape granite suite). This compositional heterogeneity due to facies and provenance-related terrains had major consequences to the reservoir distribution from the northern part to the southern part of the studied section.

6.2 Recommendations

It is recommended that additional wells should be added to constrain this interpretation. Furthermore, zircon geochronology using ID-TIMS should be performed as well as single grain feldspar chemistry to evaluate the recycled nature of the provenance for ultimate provenance lithologies. End-member modelling can be performed on samples from the basement highs to evaluate proximal provenance terrains.

More detailed biostratigraphic analysis can also be performed to evaluate time intervals of these deposits and be correlated with onshore-extensions for stratigraphic nomenclature. This study can also be evaluated further based on high frequency sequence stratigraphic analysis that will require more well data to evaluate ravinement, regressive and surfaces of erosion. This has especially become complicated because of the overprinting of high-resolution sequence stratigraphic surfaces and bedding surfaces but more well data can constrain this. Isotopic analysis on onshore invertebrate fossils can also be performed to identify the paleoclimate variability during these times. The structural regime should also be evaluated which went beyond the study aims and objectives. The timing of faults (apatite fission track analysis) should be recorded to constrain this interpretation as well.

(43944 words)

REFERENCES

Ainsworth, R. B., Vakarelov, B. K., MacEachern, J. A., Nanson, R. A., Lane, T. I., Rarity, F., & Dashtgard, S. E. (2016). Process-driven architectural variability in mouth-bar deposits: A case study from a mixed-process mouth-bar complex, Drumheller, Alberta, Canada. *Journal of Sedimentary Research*, *86*(5), 512–541. https://doi.org/10.2110/jsr.2016.23

Ainsworth, R. B., Vakarelov, B. K., & Nanson, R. A. (2011). Dynamic spatial and temporal prediction of changes in depositional processes on clastic shorelines: Toward improved subsurface uncertainty reduction and management. *AAPG Bulletin*, *95*(2), 267–297. https://doi.org/10.1306/06301010036

Aitchison, J. (1982). The statistical analysis of compositional data. *Journal of the Royal Statistical Society: Series B (Methodological)*, *44*(2), 139–160.

Aitchison, J., & Pawlowsky-Glahn, V. (1997). The one-hour course in compositional data analysis or compositional data analysis is simple. *Proceedings of IAMG*, *97*, 3–35.

Aitchison, J., & Greenacre, M. (2002). Biplots of compositional data. *Journal of the Royal Statistical Society: Series C (Applied Statistics)*, *51*(4), 375–392.

Akinlotan, O. (2017). Mineralogy and palaeoenvironments: the Weald Basin (early Cretaceous), Southeast England. *The Depositional Record*, *3*(2), 187–200.

Allen, J. R. L. (n.d.). 1982, Sedimentary Structures: Their Character and Physical Basis, Volume II. *Developments in Sedimentology*, *30*, 71004–71009.

Alves, T. M., Gawthorpe, R. L., Hunt, D. W., & Monteiro, J. H. (2003). Cenozoic tectono-sedimentary evolution of the western Iberian margin. *Marine Geology*, *195*(1–4), 75–108.

Amorosi, A., Guidi, R., Mas, R., & Falanga, E. (2012). Glaucony from the Cretaceous of the Sierra de Guadarrama (Central Spain) and its application in a sequence-stratigraphic context. *International Journal of Earth Sciences*, *101*(2), 415–427. https://doi.org/10.1007/s00531-011-0675-x

Armstrong-Altrin, J. S. (2009). Provenance of sands from Cazones, Acapulco, and Bahía Kino beaches, Mexico. *Revista Mexicana de Ciencias Geológicas*, *26*(3), 764–782.

Arnott, R. W., & Southard, J. B. (1990). Exploratory flow-duct experiments on combined-flow bed configurations, and some implications for interpreting storm-event stratification. *Journal of Sedimentary Research*, *60*(2), 211–219.

Arribas, J., Marfil, R., & de la Pena, J. A. (1985). Provenance of Triassic feldspathic sandstones in the Iberian Range (Spain); significance of quartz types. *Journal of Sedimentary Research*, *55*(6), 864–868.

Baas, J. H., & Best, J. L. (2008). The dynamics of turbulent, transitional and laminar clay-laden flow over a fixed current ripple. *Sedimentology*, *55*(3), 635–666. https://doi.org/10.1111/j.1365-3091.2007.00916.x

Baiyegunhi, C., Liu, K., & Gwavava, O. (2017). Diagenesis and reservoir properties of the Permian Ecca Group sandstones and mudrocks in the Eastern Cape Province, South Africa. *Minerals*, *7*(6), 88.

Basu, A. (2017). Evolution of siliciclastic provenance inquiries: A critical appraisal. In *Sediment provenance* (pp. 5–23). Elsevier.

Basu, A., Young, S. W., Suttner, L. J., James, W. C., & Mack, G. H. (1975). Re-evaluation of the use of undulatory extinction and polycrystallinity in detrital quartz for provenance interpretation. *Journal of Sedimentary Research*, *45*(4), 873–882.

Belousova, E., Griffin, W. L., O'Reilly, S. Y., & Fisher, N. L. (2002). Igneous zircon: trace element composition as an indicator of source rock type. *Contributions to Mineralogy and Petrology*, *143*(5), 602–622.

Benyon, C., Leier, A. L., Leckie, D. A., Hubbard, S. M., & Gehrels, G. E. (2016). Sandstone provenance and insights into the paleogeography of the McMurray Formation from detrital zircon geochronology, Athabasca Oil Sands, Canada. *AAPG Bulletin*, *100*(2), 269–287. https://doi.org/10.1306/10191515029

Berner, R. A. (1980). *Early diagenesis: a theoretical approach*. Princeton University Press.

Bhatia, M. R. (1983). Plate tectonics and geochemical composition of sandstones. *The Journal of Geology*, *91*(6), 611–627.

Bhatia, M. R., & Crook, K. A. W. (1986). Trace element characteristics of graywackes and tectonic setting discrimination of sedimentary basins. *Contributions to Mineralogy and Petrology*, *92*(2), 181–193.

Birkett, T. C., Trzcienski, W. E., & Stirling, J. A. R. (1996). Occurrence and compositions of some Ti-bearing minerals in the Strange Lake intrusive complex, Quebec-Labrador boundary. *The Canadian Mineralogist*, *34*(4), 779–801.

Bjørlykke, K. (1983). Diagenetic reactions in sandstones. In *Sediment diagenesis* (pp. 169–213). Springer.

Blewett, S. C. J., & Phillips, D. (2016). An overview of Cape Fold Belt Geochronology: Implications for sediment provenance and the timing of Orogenesis. In *Origin and Evolution of the Cape Mountains and Karoo Basin* (pp. 45–55). Springer.

Bock, B., Bahlburg, H., Wörner, G., & Zimmermann, U. (2000). Tracing crustal evolution in the southern central Andes from late Precambrian to Permian with geochemical and Nd and Pb isotope data. *The Journal of Geology*, *108*(5), 515–535.

Boggs Jr, S. (2009). *Petrology of Sedimentary Rocks*. Cambridge University Press.

Bordy, E. M., & America, T. (2016). Sedimentology of granite boulder conglomerates and associated clastics in the onshore section of the late Mesozoic Pletmos Basin (Western Cape, South Africa). *Journal of African Earth Sciences*, *119*, 67–77.

Bordy, E. M., & Prevec, R. (2008). Sedimentology, palaeontology and palaeo-environments of the Middle (?) to Upper Permian Emakwezini Formation (Karoo Supergroup, South Africa). *South African Journal of Geology*, *111*(4), 429–458.

Borges, J. B., Huh, Y., Moon, S., & Noh, H. (2008). Provenance and weathering control on river bed sediments of the eastern Tibetan Plateau and the Russian Far East. *Chemical Geology*, *254*(1–2), 52–72.

Boynton, W. V. (1984). Cosmochemistry of the rare earth elements: meteorite studies. In *Developments in geochemistry* (Vol. 2, pp. 63–114). Elsevier.

Brenner, R. L., & Davies, D. K. (1973). Storm-generated coquinoid sandstone: Genesis of high-energy marine sediments from the upper Jurassic of Wyoming and Montana. *Bulletin of the Geological Society of America*, *84*(5), 1685–1698. https://doi.org/10.1130/0016-7606(1973)84<1685:SCSGOH>2.0.CO;2

Briggs, R. M., Middleton, M. P., & Nelson, C. S. (2004). Provenance history of a late Triassic-Jurassic Gondwana margin forearc basin, murihiku terrane, North Island, New Zealand: Petrographic and geochemical constraints. *New Zealand Journal of Geology and Geophysics*, *47*(4), 589–602. https://doi.org/10.1080/00288306.2004.9515078

Bristow, C., Skelly, R. L., & Ethridge, F. G. (1999). Crevasse splays from the rapidly aggrading sand bed, braided Niobrara River, Nebraska: effect of base level rise. *Sedimentology*, *46*(6), 1029–1047.

Broad, D. S., Jungslager, E. H. A., McLachlan, I. R., Roux, J., & Van der Spuy, D. (2012). South Africa's offshore Mesozoic basins. In *Regional Geology and Tectonics* (pp. 534–564). https://doi.org/10.1016/B978-0-444-56357-6.00014-7

Broad, D. S., Jungslager, E. H. ., McLachlan, I. R., & Roux, J. (2006). Offshore Mesozoic Basins. In *The Geology of South Africa* (pp. 553–572). Geological Society of South Africa.

Bromley, R. G. (1996). *Trace Fossils: Biology, Taphonomy and Applications*. Psychology Press.

Bromley, R. G., & Ekdale, A. A. (1986). Composite ichnofabrics and tiering of burrows. *Geological Magazine*, *123*(1), 59–65.

Brown, L. F. (1995). Sequence Stratigraphy in Offshore South African Divergent Basins: An Atlas on Exploration for Cretaceous Lowstand Traps by Soekor (Pty) Ltd, AAPG Studies in Geology 41. AAPG.

Browning, C., & Macey, P. H. (2015). Lithostratigraphy of the George pluton units (Cape granite suite), South Africa. *South African Journal of Geology*, *118*(3), 323–330.

Buatois, L. A., Mangano, G., & Carr, T. (1999). *Sedimentology and ichnology of Paleozoic estuarine and shoreface reservoirs, Morrow Sandstone, Lower Pennsylvanian of southwest Kansas, USA*.

Buatois, L. A., Gingras, M. K., MacEachern, J., Mángano, M. G., Zonneveld, J. P., Pemberton, S. G., Martin, A. (2005). Colonization of brackish-water systems through time: evidence from the trace-fossil record. *Palaios*, *20*(4), 321–347.

Buggisch, W., Kleinschmidt, G., & Krumm, S. (2010). Sedimentology, geochemistry and tectonic setting of the Neoproterozoic Malmesbury Group (Tygerberg Terrane) and its relation to neighbouring terranes, Saldania Fold Belt, South Africa. *Neues Jahrbuch Für Geologie Und Paläontologie-Abhandlungen*, *257*(1), 85–114.

Caracciolo, L., von Eynatten, H., Tolosana-Delgado, R., Critelli, S., Manetti, P., & Marchev, P. (2012). Petrological, geochemical, and statistical analysis of Eocene–Oligocene sandstones of the Western Thrace Basin, Greece and Bulgaria. *Journal of Sedimentary Research*, *82*(7), 482–498. https://doi.org/10.2110/jsr.2012.31

Carr, I. D., Gawthorpe, R. L., Jackson, C. A. L., Sharp, I. R., & Sadek, A. (2003). Sedimentology and sequence stratigraphy of early syn-rift tidal sediments: the Nukhul Formation, Suez Rift, Egypt. *Journal of Sedimentary Research*, *73*(3), 407–420.

Castillo, P., Lacassie, J. P., Augustsson, C., & Hervé, F. (2015). Petrography and geochemistry of the Carboniferous-Triassic Trinity Peninsula Group, West Antarctica: Implications for provenance and tectonic setting. *Geological Magazine*, *152*(4), 575–588. https://doi.org/10.1017/S0016756814000454

Cheel, R. J., & Leckie, D. A. (1993). Hummocky cross-stratification. In *Sedimentology review 1* (Vol. 1, pp. 103–122). Blackwell Scientific Publications Oxford.

Chen, S., Steel, R. J., Dixon, J. F., & Osman, A. (2014). Facies and architecture of a tide-dominated segment of the Late Pliocene Orinoco Delta (Morne L'Enfer Formation) SW Trinidad. *Marine and Petroleum Geology*, *57*, 208–232. https://doi.org/https://doi.org/10.1016/j.marpetgeo.2014.05.014

Cingolani, C. A., Manassero, M., & Abre, P. (2003). Composition, provenance, and tectonic setting of Ordovician siliciclasticrocks in the San Rafael block: Southern extension of the Precordillera crustal fragment, Argentina. *Journal of South American Earth Sciences*, *16*(1), 91–106. https://doi.org/10.1016/S0895-9811(03)00021-X

Coates, L., & MacEachern, J. A. (2009). The ichnological signatures of river-and wave-dominated delta complexes: differentiating deltaic and non-deltaic shallow marine successions, Lower Cretaceous Viking Formation and Upper Cretaceous Dunvegan Formation, west-central Alberta.

Condie, K. C. (1993). Chemical composition and evolution of the upper continental crust: contrasting results from surface samples and shales. *Chemical Geology*, *104*(1–4), 1–37.

Correggiari, A., Cattaneo, A., & Trincardi, F. (2005). The modern Po Delta system: lobe switching and asymmetric prodelta growth. *Marine Geology*, *222*, 49–74.

Cox, R., Lowe, D. R., & Cullers, R. L. (1995). The influence of sediment recycling and basement composition on evolution of mudrock chemistry in the southwestern United States. *Geochimica et Cosmochimica Acta*, *59*(14), 2919–2940. https://doi.org/10.1016/0016-7037(95)00185-9

Crook, K. A. W. (1974). Lithogenesis and geotectonics: The significance of compositional variation in flysch arenites (graywackes).

Cullers, R. L. (2000). The geochemistry of shales, siltstones and sandstones of Pennsylvanian–Permian age, Colorado, USA: implications for provenance and metamorphic studies. *Lithos*, *51*(3), 181–203.

Dallmeyer, R. D., & Neubauer, F. (1991). 40Ar/39Ar age of detrital muscovite, Carnic Alps: evidence for Cadomian basement in the Eastern Alps. *Terra Nostra Abstracts*, *3*, 12–13.

Davies, C. P. N. (1997). Unusual biomarker maturation ratio changes through the oil window, a consequence of varied thermal history. *Organic Geochemistry*, *27*(7–8), 537–560.

Davies, D. K., Ethridge, F. G., & Berg, R. R. (1971). Recognition of barrier environments. *AAPG Bulletin*, *55*(4), 550–565.

De Barros, C. E., Nardi, L. V. S., Dillenburg, S. R., Ayup, R., Jarvis, K., & Baitelli, R. (2010). Detrital minerals of modern beach sediments in southern Brazil: a provenance study based on the chemistry of zircon. *Journal of Coastal Research*, 80–93.

De Ruig, M. J., & Hubbard, S. M. (2006). Seismic facies and reservoir characteristics of a deep-marine channel belt in the Molasse foreland basin, Puchkirchen Formation, Austria. *AAPG Bulletin*, *90*(5), 735–752.

De Swart, A. M. J., & Rowsell, D. M. (1974). Note on the relationship between diagenesis and deformation in the Cape Fold-belt. *South African Journal of Geology*, *77*(3), 239–245.

Deconinck, J. F., Hesselbo, S. P., Debuisser, N., Averbuch, O., Baudin, F., & Bessa, J. (2003). Environmental controls on clay mineralogy of an Early Jurassic mudrock (Blue Lias Formation, southern England). *International Journal of Earth Sciences*, *92*(2), 255–266. https://doi.org/10.1007/s00531-003-0318-y

Desjardins, P. R., Buatois, L. A., & Mángano, M. G. (2012). Chapter 18 - Tidal Flats and Subtidal Sand Bodies. In *Developments in Sedimentology*: *Vol.Volume 64* (pp. 529–561). https://doi.org/http://dx.doi.org/10.1016/B978-0-444-53813-0.00018-6

Dey, A. K., & Lines, L. R. (1998). Seismic source wavelet estimation and the random reflectivity assumption. In *SEG Technical Program Expanded Abstracts 1998* (pp. 1088–1091). Society of Exploration Geophysicists.

Dickinson, K. A., Berryhill Jr., H. L., & Holmes, C. W. (1972, January 1). Criteria for Recognizing Ancient Barrier Coastllnes* (J. K. Rigby & W. K. Hamblin, Eds.). *Recognition of Ancient Sedimentary Environments*, Vol. 16, p. 0. https://doi.org/10.2110/pec.72.02.0192

Dickinson, W. R. (1983). Provenance of North American Phanerozoic sandstones in relation to tectonic settings. *Geological Society of America Bulletin*, *94*(2), 222–235. https://doi.org/10.1130/0016-7606(1983)94<222:PONAPS>2.0.CO;2

Dickinson, W. R. (1985). Interpreting Provenance Relations from Detrital Modes of Sandstones. In *Provenance of Arenites* (pp. 333–361). https://doi.org/10.1007/978-94-017-2809-6_15

Dickinson, W. R., & Suczek, C. A. (1979). Plate tectonics and sandstone compositions. *AAPG Bulletin*, *63*(12), 2164–2182.

Dickinson, W. R., & Valloni, R. (1980). Plate settings and provenance of sands in modern ocean basins. *Geology*, *8*(2), 82–86.

Dingle, R. V, & Hendry, Q. B. (1984). Late Mesozoic and Tertiary sediment supply to the Eastern Cape Basin (SE Atlantic) and palaeo-drainage systems in southwestern Africa. *Marine Geology*, *56*(1–4), 13–26.

Dingle, R. V, & Lavelle, M. (1998). Late Cretaceous–Cenozoic climatic variations of the northern Antarctic Peninsula: new geochemical evidence and review. *Palaeogeography, Palaeoclimatology, Palaeoecology*, *141*(3–4), 215–232.

Dodd, T. J. H., McCarthy, D. J., & Richards, P. C. (2019). A depositional model for deep-lacustrine, partially confined, turbidite fans: Early Cretaceous, North Falkland Basin. *Sedimentology*, *66*(1), 53–80.

Dott Jr, R. H., & Bourgeois, J. (1982). Hummocky stratification: significance of its variable bedding sequences. *Geological Society of America Bulletin*, *93*(8), 663–680.

Duke, W. L., Arnott, R. W. C., & Cheel, R. J. (1991). Shelf sandstones and hummocky cross-stratification: new insights on a stormy debate. *Geology*, *19*(6), 625–628.

Dutton, S. P., & Diggs, T. N. (1990). History of quartz cementation in the Lower Cretaceous Travis Peak Formation, East Texas. *Journal of Sedimentary Research*, *60*(2), 191–202.

Eide, C. H., Howell, J. A., Buckley, S. J., Martinius, A. W., Oftedal, B. T., & Henstra, G. A. (2016). Facies model for a coarse-grained, tide-influenced delta: Gule Horn Formation (Early Jurassic), Jameson Land, Greenland. *Sedimentology*, *63*(6), 1474–1506. https://doi.org/10.1111/sed.12270

Einsele, G. (2000). *Sedimentary Basin, Evolution, Facies and Sediment Budget*. https://doi.org/10.1007/978-3-662-04029-4

Ekdale, A. A., Bromley, R. G., & Knaust, D. (2012). The ichnofabric concept. In *Developments in Sedimentology* (Vol. 64, pp. 139–155). Elsevier.

Elliott, T. (1974). Interdistributary bay sequences and their genesis. In *Sedimentology* (Vol. 21).

Esmeray-Senlet, S., Özkan-Altiner, S., Altiner, D., & Miller, K. G. (2015). Planktonic foraminiferal biostratigraphy, microfacies analysis, sequence stratigraphy, and sea-level changes across the Cretaceous–Paleogene boundary In the Haymana Basin, Central Anatolia, Turkey. *Journal of Sedimentary Research*, *85*(5), 489–508.

Etemad-Saeed, N. A., Hosseini-Barzi, M. A., & Armstrong-Altrin, J. S. (2011). Petrography and geochemistry of clastic sedimentary rocks as evidences for provenance of the Lower Cambrian Lalun Formation, Posht-e-badam block, Central Iran. *Journal of African Earth Sciences*, *61*(2), 142–159.

Fadipe, O. A. (2012). *Reservoir quality, structural architecture, fluid evolution and their controls on reservoir performance in block 9, F-O gas field, Bredasdorp Basin, offshore South Africa*. The University of the Western Cape. Unpublished thesis

Farina, F., Stevens, G., & Villaros, A. (2012). Multi-batch, incremental assembly of a dynamic magma chamber: the case of the Peninsula pluton granite (Cape Granite Suite, South Africa). *Mineralogy and Petrology*, *106*(3–4), 193–216.

Fedo, C. M., Eriksson, K. A., & Krogstad, E. J. (1996). Geochemistry of shales from the Archean (~ 3.0 Ga) Buhwa Greenstone Belt, Zimbabwe: implications for provenance and source-area weathering. *Geochimica et Cosmochimica Acta*, *60*(10), 1751–1763.

Fedo, C. M., Wayne Nesbitt, H., & Young, G. M. (1995). Unraveling the effects of potassium metasomatism in sedimentary rocks and paleosols, with implications for paleoweathering conditions and provenance. *Geology*, *23*(10), 921–924.

Floyd, P. A., & Leveridge, B. E. (1987). Tectonic environment of the Devonian Gramscatho basin, south Cornwall: framework mode and geochemical evidence from turbiditic sandstones. *Journal of the Geological Society*, *144*(4), 531–542.

Floyd, P. A., Winchester, J. A., & Park, R. G. (1989). Geochemistry and tectonic setting of Lewisian clastic metasediments from the Early Proterozoic Loch Maree Group of Gairloch, NW Scotland. *Precambrian Research*, *45*(1–3), 203–214.

Folk, R. L. (1980). *Petrology of sedimentary rocks*. Hemphill Publishing Company.

Fourie, P. H., Zimmermann, U., Beukes, N. J., Naidoo, T., Kobayashi, K., Kosler, J., Theron, J. N. (2011). Provenance and reconnaissance study of detrital zircons of the Palaeozoic Cape Supergroup in South Africa: revealing the interaction of the Kalahari and Río de la Plata cratons. *International Journal of Earth Sciences*, *100*(2–3), 527–541.

Föllmi, K. B. (2012). Early Cretaceous life, climate and anoxia. *Cretaceous Research*, *35*, 230–257.

Frimmel, H. E., Basei, M. A. S., Correa, V. X., & Mbangula, N. (2013). A new lithostratigraphic subdivision and geodynamic model for the Pan-African western Saldania Belt, South Africa. *Precambrian Research*, *231*, 218–235.

Frimmel, H. E., Fölling, P. G., & Diamond, R. (2001). Metamorphism of the Permo-Triassic Cape Fold Belt and its basement, South Africa. *Mineralogy and Petrology*, *73*(4), 325–346.

Futalan, K., Mitchell, A., Amos, K., & Backe, G. (2012). Seismic facies analysis and structural interpretation of the Sandakan sub-basin, Sulu Sea, Philippines. *AAPG International Conference and Exhibition (Singapore), Www. Searchanddiscovery. Com/Pdfz/Documents/2012/302 54futalan/Ndx_futalan. Pdf. Html*.

Gallet, S., Jahn, B., Lanoë, B. V. V., Dia, A., & Rossello, E. (1998). Loess geochemistry and its implications for particle origin and composition of the upper continental crust. *Earth and Planetary Science Letters*, *156*(3–4), 157–172.

Garcia, D., Fonteilles, M., & Moutte, J. (1994). Sedimentary fractionations between Al, Ti, and Zr and the genesis of strongly peraluminous granites. *The Journal of Geology*, *102*(4), 411–422.

Garzanti, E., Andò, S., Vezzoli, G., & Dell'era, D. (2003). From rifted margins to foreland basins: investigating provenance and sediment dispersal across desert Arabia (Oman, UAE). *Journal of Sedimentary Research*, *73*(4), 572–588.

Garzanti, E., & Resentini, A. (2016). Provenance control on chemical indices of weathering (Taiwan river sands). *Sedimentary Geology*, *336*, 81–95.

Gietelink, G. (1973). Sedimentology of a linear prograding coastline followed by three high-destructive delta-complexes (Cambro-Ordovician, Cantabrian Mountains, NW Spain). *Leidse Geologische Mededelingen*, *49*(1), 125–144.

Gingras, M. K., & MacEachern, J. A. (2012a). Tidal ichnology of shallow-water clastic settings. In *Principles of Tidal Sedimentology* (pp. 57–77). Springer.

Gingras, M. K., MacEachern, J. A., & Dashtgard, S. E. (2012b). The potential of trace fossils as tidal indicators in bays and estuaries. *Sedimentary Geology*, *279*, 97–106.

Gluyas, J., & Swarbrick, R. (2013). *Petroleum geoscience*. John Wiley & Sons.

Goldberg, K., & Humayun, M. (2010). The applicability of the Chemical Index of Alteration as a paleoclimatic indicator: An example from the Permian of the Paraná Basin, Brazil. *Palaeogeography, Palaeoclimatology, Palaeoecology*, *293*(1–2), 175–183.

González-Acebrón, L., Arribas, J., & Mas, J. R. (2010). *Sand provenance and implications for paleodrainage in a rifted basin: the Tera Group (N. Spain)*.

González-Acebrón, L., Pérez-Garrido, C., Mas, R., Arribas, J., & Götze, J. (2017). Provenance signatures recorded in transgressive sandstones of the Upper Cretaceous Iberian seaway. *Journal of Sedimentary Research*, *87*(2), 152–166.

Gromet, L. P., Haskin, L. A., Korotev, R. L., & Dymek, R. F. (1984). The "North American shale composite": Its compilation, major and trace element characteristics. *Geochimica et Cosmochimica Acta*, *48*(12), 2469–2482.

Gugliotta, M., Flint, S. S., Hodgson, D. M., & Veiga, G. D. (2015). Stratigraphic record of river-dominated crevasse subdeltas with tidal influence (Lajas Formation, Argentina).*Journal of Sedimentary Research*, *85*(3), 265–284. https://doi.org/10.2110/jsr.2015.19

Guo, Y., Yang, S., Su, N., Li, C., Yin, P., & Wang, Z. (2018). Revisiting the effects of hydrodynamic sorting and sedimentary recycling on chemical weathering indices. *Geochimica et Cosmochimica Acta*, *227*, 48–63.

Hälbich, I. W., Fitch, F. J., & Miller, J. A. (1983). Dating the Cape orogeny. In *Geodynamics of the Cape Fold Belt*.

Hallsworth, C. R., Morton, A. C., Claoué-Long, J., & Fanning, C. M. (2000). Carboniferous sand provenance in the Pennine Basin, UK: constraints from heavy mineral and detrital zircon age data. *Sedimentary Geology*, *137*(3–4), 147–185.

Harnois, L. (1988). The CIW index: a new chemical index of weathering. *Sedimentary Geology*, *55*, 319–322.

Hay, W. W., & Floegel, S. (2012). New thoughts about the Cretaceous climate and oceans. *Earth-Science Reviews*, *115*(4), 262–272.

Helland-Hansen, W., Martinsen, O. J., & Thurmond, J. B. (2009). Relationships between morphological and sedimentological parameters in source-to-sink systems: a basis for predicting semi-quantitative characteristics in subsurface systems. *Basin Research*, *21*(4), 361–387.

Heller, P. L., & Frost, C. D. (1988). Isotopic provenance of clastic deposits: application of geochemistry to sedimentary provenance studies. In *New perspectives in basin analysis* (pp. 27–42). Springer.

Herron, M. M. (1988). Geochemical classification of terrigenous sands and shales from core or log data. *Journal of Sedimentary Research*, *58*(5), 820–829.

Hofer, G., Wagreich, M., & Neuhuber, S. (2013). Geochemistry of fine-grained sediments of the upper Cretaceous to Paleogene Gosau Group (Austria, Slovakia): Implications for paleoenvironmental and provenance studies. *Geoscience Frontiers*, *4*(4), 449–468.

Hofmann, P., Ricken, W., Schwark, L., & Leythaeuser, D. (2001). Geochemical signature and related climatic-oceanographic processes for early Albian black shales: Site 417D, North Atlantic Ocean. *Cretaceous Research*, *22*(2), 243–257.

Hoskin, P. W. O., & Schaltegger, U. (2003). The composition of zircon and igneous and metamorphic petrogenesis. *Reviews in Mineralogy and Geochemistry*, *53*(1), 27–62.

Hovikoski, J., Lemiski, R., Gingras, M., Pemberton, G., & MacEachern, J. A. (2008). Ichnology and Sedimentology of a Mud-Dominated Deltaic Coast: Upper Cretaceous Alderson Member (Lea Park Fm), Western Canada. *Journal of Sedimentary Research*, *78*(12), 803–824. https://doi.org/10.2110/jsr.2008.089

Hoyer, L., & Watkeys, M. K. (2017). Using magma flow indicators to infer flow dynamics in sills. *Journal of Structural Geology*, *96*, 161–175.

Hu, J., Li, Q., Fang, N., Yang, J., & Ge, D. (2015). Geochemistry characteristics of the Low Permian sedimentary rocks from central uplift zone, Qiangtang Basin, Tibet: insights into source-area weathering, provenance, recycling, and tectonic setting. *Arabian Journal of Geosciences*, *8*(8), 5373–5388.

Hu, J., Li, Q., Fang, N., Yang, J., & Ge, D. (2014). Geochemistry characteristics of the Low Permian sedimentary rocks from central uplift zone, Qiangtang Basin, Tibet: insights into source-area weathering, provenance, recycling, and tectonic setting. *Arabian Journal of Geosciences*, *8*(8), 5373–5388.

Hubbard, S. M., Gingras, M. K., & Pemberton, S. G. (2004). Palaeoenvironmental implications of trace fossils in estuarine deposits of the Cretaceous Bluesky Formation, Cadotte region, Alberta, Canada. *Fossils and Strata*, *51*, 1–20.

Husein, S., & J. Lambiase, J. (2013). Sediment dynamics and depositional systems of the Mahakam Delta, Indonesia: Ongoing delta abandonment on a tide-dominated Coast. In *Journal of Sedimentary Research* (Vol. 83). https://doi.org/10.2110/jsr.2013.42

Ingersoll, R. V, Bullard, T. F., Ford, R. L., Grimm, J. P., Pickle, J. D., & Sares, S. W. (1984). The effect of grain size on detrital modes: a test of the Gazzi-Dickinson point-counting method. *Journal of Sedimentary Research*, *54*(1), 103–116.

Ingersoll, R. V, & Suczek, C. A. (1979). Petrology and provenance of Neogene sand from Nicobar and Bengal fans, DSDP sites 211 and 218. *Journal of Sedimentary Research*, *49*(4), 1217–1228.

Islam, M. A. (2010). Petrography and provenance of subsurface Neogene sandstones of Bengal Basin, Bangladesh. *Journal of the Geological Society of India*, *76*(5), 493.

Jackson, C. A. L., Gawthorpe, R. L., Carr, I. D., & Sharp, I. R. (2005). Normal faulting as a control on the stratigraphic development of shallow marine syn-rift sequences: the Nukhul and Lower Rudeis Formations, Hammam Faraun fault block, Suez Rift, Egypt. *Sedimentology*, *52*(2), 313–338.

Johansen, S. E. (2013). Composition of seismic facies: A case study. *AAPG Bulletin*, *97*(10), 1645–1656.

Jungslager, E. H. A. (1996). Geological evaluation of the remaining prospectivity for oil and gas of the pre-1At1 "synrift" succession in Block 9, Republic of South Africa. *Unpubl. SOEKOR Rep*.

Jungslager, E. H. A. (1999). Petroleum habitats of the Atlantic margin of South Africa. *Geological Society, London, Special Publications*, *153*(1), 153–168.

Kästner, K., Hoitink, A. J. F., Vermeulen, B., Geertsema, T. J., & Ningsih, N. S. (2017). Distributary channels in the fluvial to tidal transition zone. *Journal of Geophysical Research: Earth Surface*, *122*(3), 696–710. https://doi.org/10.1002/2016JF004075

Katemaunzanga, D., & Gunter, C. J. (2009). Lithostratigraphy, sedimentology, and provenance of the Balfour Formation (Beaufort Group) in the Fort Beaufort–Alice area, Eastern Cape Province, South Africa. *Acta Geologica Sinica-English Edition*, *83*(5), 902–916.

Kharaka, Y. K., Lico, M. S., Wright, V. A., & Carothers, W. W. (1979). Geochemistry of formation waters from Pleasant Bayou No. 2 well and adjacent areas in coastal Texas. *Proc 4th Geopressured-Geothermal Energy Conf*, 168–193.

Klausen, T. G., Torland, J. A., Eide, C. H., Alaei, B., Olaussen, S., & Chiarella, D. (2018). Clinoform development and topset evolution in a mud-rich delta–the Middle Triassic Kobbe Formation, Norwegian Barents Sea. *Sedimentology*, *65*(4), 1132–1169.

Knaust, D. (2017). *Atlas of trace fossils in well core: Appearance, taxonomy and interpretation*. Springer.

Knaust, D., & Bromley, R. G. (2012). Trace Fossils as Indicators of Sedimentary Environments, *Developments in Sedimentology*, *64*.

Kuehl, S. A., Allison, M. A., Goodbred, S. L., Kudrass, H., Giosan, L., & Bhattacharya, J. P. (2005). The Ganges-Brahmaputra Delta. *Special Publication-SEPM*, *83*, 413.

Kutterolf, S., Diener, R., Schacht, U., & Krawinkel, H. (2008). Provenance of the Carboniferous Hochwipfel formation (Karawanken Mountains, Austria/Slovenia)-Geochemistry versus petrography. *Sedimentary Geology*, *203*(3–4), 246–266.

Lamb, M. P., Myrow, P. M., Lukens, C., Houck, K., & Strauss, J. (2008). Deposits from wave-influenced turbidity currents: Pennsylvanian Minturn Formation, Colorado, USA. *Journal of Sedimentary Research*, *78*(7), 480–498.

Lambiase, J. J., Riadi, R. S., Nirsal, N., & Husein, S. (2017). Transgressive successions of the Mahakam Delta Province, Indonesia. *Geological Society, London, Special Publications*, *444*(1), 335 LP – 348. https://doi.org/10.1144/SP444.2

Lee, Y. Il. (2002). Provenance derived from the geochemistry of late Paleozoic–early Mesozoic mudrocks of the Pyeongan Supergroup, Korea. *Sedimentary Geology*, *149*(4), 219–235.

Lee, Y. Il. (2009). Geochemistry of shales of the Upper Cretaceous Hayang Group, SE Korea: Implications for provenance and source weathering at an active continental margin. *Sedimentary Geology*, *215*(1–4), 1–12.

Legler, B., Johnson, H. D., Hampson, G. J., Massart, B. Y. G., Jackson, C. A., Jackson, M. D., … Ravnas, R. (2013). Facies model of a fine-grained, tide-dominated delta: lower Dir Abu Lifa Member (Eocene), Western Desert, Egypt. *Sedimentology*, *60*(5), 1313–1356.

Li, Z., Bhattacharya, J., & Schieber, J. (2015). Evaluating along-strike variation using thin-bedded facies analysis, Upper Cretaceous Ferron Notom Delta, Utah. *Sedimentology*, *62*(7), 2060–2089.

Lowe, D. G., Sylvester, P. J., & Enachescu, M. E. (2011). Provenance and paleodrainage patterns of Upper Jurassic and Lower Cretaceous synrift sandstones in the Flemish Pass Basin, offshore Newfoundland, east coast of Canada. *AAPG Bulletin*, *95*(8), 1295–1320.

MacEachern, J. A., Bann, K. L., Hampson, G. J., Steel, R. J., Burgess, P. M., & Dalrymple, R. W. (2008). The role of ichnology in refining shallow marine facies models. In *Recent advances in models of siliciclastic shallow-marine stratigraphy* (Vol. 90, pp. 73–116). Society for Sedimentary Geology (SEPM) Tulsa, USA.

MacEachern, J. A., Bann, K. L., Gingras, M. K., Zonneveld, J.-P., Dashtgard, S. E., & Pemberton, S. G. (2012). The ichnofacies paradigm. In *Developments in sedimentology* (Vol. 64, pp. 103–138). Elsevier.

Mack, G. H., & Jerzykiewicz, T. (1989). Provenance of post-Wapiabi sandstones and its implications for Campanian to Paleocene tectonic history of the southern Canadian Cordillera. *Canadian Journal of Earth Sciences*, *26*(4), 665–676.

Mackay, D. A., & Dalrymple, R. W. (2011). Dynamic mud deposition in a tidal environment: the record of fluid-mud deposition in the Cretaceous Bluesky Formation, Alberta, Canada. *Journal of Sedimentary Research*, *81*(12), 901–920.

Mader, D., & Neubauer, F. (2004). Provenance of Palaeozoic sandstones from the Carnic Alps (Austria): petrographic and geochemical indicators. *International Journal of Earth Sciences*, *93*(2), 262–281.

Mann, W. R., & Cavaroc, V. V. (1973). Composition of sand released from three source areas under humid, low relief weathering in the North Carolina Piedmont. *Journal of Sedimentary Research*, *43*(3).

Marshall, C. G. A., & von Brunn, V. (1999). The stratigraphy and origin of the Natal Group. *South African Journal of Geology*, *102*(1), 15–25.

Martel, A. T., & Gibling, M. R. (1994). Combined-flow generation of sole structures, including recurved groove casts, associated with Lower Carboniferous lacustrine storm deposits in Nova Scotia, Canada. *Journal of Sedimentary Research*, *64*(3a), 508–517.

Martins-Neto, M. A., & Catuneanu, O. (2009). Rift sequence stratigraphy. *Marine and Petroleum Geology*, *30*, 1–7.

Martinius, A. W., Kaas, I., Helgesen, G., Kj, J. M., & Leith, D. A. (2001). Sedimentology of the heterolithic and tide-dominated Tilje Formation (Early Jurassic, Halten Terrace, offshore mid-Norway). In *Norwegian Petroleum Society Special Publications* (Vol. 10, pp. 103–144). Elsevier.

Maynard, J. B. (1992). Chemistry of modern soils as a guide to interpreting Precambrian paleosols. *The Journal of Geology*, *100*(3), 279–289.

McBride, E. F. (1963). A classification of common sandstones. *Journal of Sedimentary Research*, *33*(3), 664–669.

McBride, E. F. (1977). Secondary porosity-importance in sandstone reservoirs in Texas. *Gulf Coast Association of Geological Societies Transactions*, *27*, 121–122.

McCave, I. N. (1970). Deposition of fine-grained suspended sediment from tidal currents. *Journal of Geophysical Research*, *75*(21), 4151–4159.

McLennan, S. M. (1989). Rare earth elements in sedimentary rocks: influence of provenance and sedimentary processes. *Geochemistry and Mineralogy of Rare Earth Elements, Reviews in Mineralogy 21*, 169–200.

McLennan, S. M., Hemming, S., Mcdaniel, D. K., & Hanson, G. N. (1993). Geochemical approaches to sedimentation, provenance, and tectonics.

McLennan, S. M. (2001). Relationships between the trace element composition of sedimentary rocks and upper continental crust. *Geochemistry, Geophysics, Geosystems*, *2*(4).

McMillan, I. K. (2003). Foraminiferally defined biostratigraphic episodes and sedimentation pattern of the Cretaceous drift succession (Early Barremian to Late Maastrichtian) in seven basins on the South African and southern Namibian continental margin. *South African Journal of Science*, *99*(11–12), 537–576.

McMillan, I. K. (2010). The foraminifera of the Portlandian (late Jurassic) Bethelsdorp Formation of the onshore Algoa Basin, Eastern Cape province: Their stratigraphic position

compared with other early graben infill successions of the South African continental margin. *Les Rosalines*.

McMillan, I. K., Brink, G. I., Broad, D. S., & Maier, J. J. (1997). Late Mesozoic sedimentary basins off the south coast of South Africa. In *Sedimentary Basins of the World* (Vol. 3, pp. 319–376). Elsevier.

Melchor, R. N. (2004). Trace fossil distribution in lacustrine deltas: examples from the Triassic rift lakes of the Ischigualasto-Villa Unión basin, Argentina. *Geological Society, London, Special Publications*, *228*(1), 335–354.

Miall, A. D. (1986). Eustatic sea level changes interpreted from seismic stratigraphy: a critique of the methodology with particular reference to the North Sea Jurassic record. *AAPG Bulletin*, *70*(2), 131–137.

Miall, A. D. (1988). Reservoir heterogeneities in fluvial sandstones: lessons from outcrop studies. *AAPG Bulletin*, *72*(6), 682–697.

Miall, A. D. (1996). The geology of fluvial deposits: sedimentary facies, basin analysis, and petroleum geology.

Middleton, G. V. (1960). Chemical composition of sandstones. *Geological Society of America Bulletin*, *71*(7), 1011–1026.

Molgat, M., & Arnott, R. W. C. (2001). Combined tide and wave influence on sedimentation patterns in the Upper Jurassic Swift Formation, south-eastern Alberta. *Sedimentology*, *48*(6), 1353–1369. https://doi.org/10.1046/j.1365-3091.2001.00424.x

Mondal, M. E. A., Wani, H., & Mondal, B. (2012). Geochemical signature of provenance, tectonics and chemical weathering in the Quaternary flood plain sediments of the Hindon River, Gangetic plain, India. *Tectonophysics*, *566*, 87–94.

Montañez, I. P. (1997). Secondary porosity and late diagenetic cements of the Upper Knox Group, Central Tennessee region: a temporal and spatial history of fluid flow conduit development within the Knox regional aquifer.

Morton, A. C., & Hallsworth, C. (1994). Identifying provenance-specific features of detrital heavy mineral assemblages in sandstones. *Sedimentary Geology*, *90*(3–4), 241–256.

Morton, A., & Chenery, S. (2009). Detrital rutile geochemistry and thermometry as guides to provenance of Jurassic–Paleocene sandstones of the Norwegian Sea. *Journal of Sedimentary Research*, *79*(7), 540–553.

Moslow, T. F., & Pemberton, S. G. (1988). An integrated approach to the sedimentological analysis of some Lower Cretaceous shoreface and delta front sandstone sequences.

Muravchik, M., Gawthorpe, R. L., Sharp, I. R., Rarity, F., & Hodgetts, D. (2018). Sedimentary environment evolution in a marine hangingwall dipslope setting. El Qaa Fault Block, Suez Rift, Egypt. *Basin Research*, *30*, 452–478.

Nelson, B. K., DeNiro, M. J., Schoeninger, M. J., De Paolo, D. J., & Hare, P. E. (1986). Effects of diagenesis on strontium, carbon, nitrogen and oxygen concentration and isotopic composition of bone. *Geochimica et Cosmochimica Acta*, *50*(9), 1941–1949.

Nesbitt, H. W., & Young, G. M. (1982). Early Proterozoic climates and plate motions inferred from major element chemistry of lutites. *Nature*, *299*(5885), 715.

Nichols, G. J., & Fisher, J. A. (2007). Processes, facies and architecture of fluvial distributary system deposits. *Sedimentary Geology*, *195*(1–2), 75–90.

Nichols, G. (2009). *Sedimentology and stratigraphy*. John Wiley & Sons.

Okwese, A. C., Pe-Piper, G., & Piper, D. J. W. (2012). Controls on regional variability in marine pore-water diagenesis below the seafloor in Upper Jurassic–Lower Cretaceous prodeltaic sandstone and shales, Scotian Basin, Eastern Canada. *Marine and Petroleum Geology*, *29*(1), 175–191.

Olariu, C., & Bhattacharya, J. P. (2006). Terminal distributary channels and delta front architecture of river-dominated delta systems. *Journal of Sedimentary Research*, *76*(2), 212–233.

Olariu, C., Steel, R. J., Dalrymple, R. W., & Gingras, M. K. (2012a). Tidal dunes versus tidal bars: The sedimentological and architectural characteristics of compound dunes in a tidal seaway, the lower Baronia Sandstone (Lower Eocene), Ager Basin, Spain. *Sedimentary Geology*, *279*, 134–155.

Olariu, M. I., Olariu, C., Steel, R. J., Dalrymple, R. W., & Martinius, A. W. (2012b). Anatomy of a laterally migrating tidal bar in front of a delta system: Esdolomada Member, Roda Formation, Tremp-Graus Basin, Spain. *Sedimentology*, *59*(2), 356–378.

Onajite, E. (2013). Seismic data analysis techniques in hydrocarbon exploration. Elsevier.

Oomkens, E. (1974). Lithofacies relations in the Late Quaternary Niger delta complex. *Sedimentology*, *21*(2), 195–222.

Parkinson, D. N. (1996). Gamma-ray spectrometry as a tool for stratigraphical interpretation: examples from the western European Lower Jurassic. *Geological Society, London, Special Publications*, *103*(1), 231–255.

Pemberton, S. G., & Wightman, D. M. (1992). Ichnological characteristics of brackish water deposits.

Pe-Piper, G., Triantafyllidis, S., & Piper, D. J. W. (2008). Geochemical identification of clastic sediment provenance from known sources of similar geology: the Cretaceous Scotian Basin, Canada. *Journal of Sedimentary Research*, *78*(9), 595–607.

Pettijohn, F. J. (1963). Chemical composition of sandstones, excluding carbonate and volcanic sands: Representative analyses. US Government Printing Office.

Pettijohn, F. J. (1975). *Sedimentary rocks* (Vol. 3). Harper & Row New York.

Pettijohn, F. J., Potter, P. E., & Siever, R. (1972). *Sands and sandstone*. Springer-Verlag.

Piper, D. J. W., Pe-Piper, G., Hundert, T., & Venugopal, D. V. (2007). The lower Cretaceous Chaswood formation in southern New Brunswick: provenance and tectonics. *Canadian Journal of Earth Sciences*, *44*(5), 665–677.

Potter, P. E., Maynard, J. B., & Depetris, P. J. (2005). Mud and mudstones: Introduction and overview. Springer Science & Business Media.

Powers, M. C. (1953). A new roundness scale for sedimentary particles. *Journal of Sedimentary Research*, *23*(2), 117–119.

Prather, B. E., Booth, J. R., Steffens, G. S., & Craig, P. A. (1998). Classification, lithologic calibration, and stratigraphic succession of seismic facies of intraslope basins, deep-water Gulf of Mexico. *AAPG Bulletin*, *82*(5), 701–728.

Price, J. R., & Velbel, M. A. (2003). Chemical weathering indices applied to weathering profiles developed on heterogeneous felsic metamorphic parent rocks. *Chemical Geology*, *202*(3–4), 397–416.

Puy-Alquiza, M. J., Miranda-Aviles, R., Cruz-Cruz, M., Pérez-Arbizu, O., Vega-González, M., & Ana-Zanor, G. (2014). Geochemistry and depositional environment of the Losero Formation in the Mesa Central, México. *Boletín de La Sociedad Geológica Mexicana*, *66*(3).

Ratcliffe, K. T., Morton, A. C., Ritcey, D. H., & Evenchick, C. A. (2007). Whole-rock geochemistry and heavy mineral analysis as petroleum exploration tools in the Bowser and Sustut basins, British Columbia, Canada. *Bulletin of Canadian Petroleum Geology*, *55*(4), 320–336.

Reading, H. G. (1982). Sedimentary basins and global tectonics. *Proceedings of the Geologists' Association*, *93*(4), 321–350.

Reading, H. G. (2009). Sedimentary environments: Processes, facies and stratigraphy. John Wiley & Sons.

Reineck, H.-E., & Singh, I. B. (1980). *Depositional sedimentary environments*: with reference to terrigenous clastics.

Rider, M. H. (1986). *The geological interpretation of well logs*.

Roser, B. P., Cooper, R. A., Nathan, S., & Tulloch, A. J. (1996). Reconnaissance sandstone geochemistry, provenance, and tectonic setting of the lower Paleozoic terranes of the West Coast and Nelson, New Zealand. *New Zealand Journal of Geology and Geophysics*, *39*(1), 1–16.

Roser, B. P., & Korsch, R. J. (1985). Plate tectonics and geochemical composition of sandstones: a discussion. *The Journal of Geology*, *93*(1), 81–84.

Roser, B. P., & Korsch, R. J. (1988). Provenance signatures of sandstone-mudstone suites determined using discriminant function analysis of major-element data. *Chemical Geology*, *67*(1–2), 119–139.

Rossi, V. M., & Steel, R. J. (2016). The role of tidal, wave and river currents in the evolution of mixed-energy deltas: Example from the Lajas Formation (Argentina). *Sedimentology*, *63*(4), 824–864.

Rotzien, J. R., Browne, G. H., & King, P. R. (2018). Geochemical, petrographic, and uranium–lead geochronological evidence for multisourced polycyclic provenance of deep-water strata in a hybrid tectonic setting: The upper Miocene upper Mount Messenger Formation, Taranaki Basin, New Zealand. *AAPG Bulletin*, *102*(9), 1763–1802.

Rudnick, R. L., &Gao, S. (2003). Composition of the continental crust. *Treatise on Geochemistry*, *3*, 659.

Ryan, K. M., & Williams, D. M. (2007). Testing the reliability of discrimination diagrams for determining the tectonic depositional environment of ancient sedimentary basins. *Chemical Geology*, *242*(1–2), 103–125.

Sawyer, E. W. (1986). The influence of source rock type, chemical weathering and sorting on the geochemistry of clastic sediments from the Quetico metasedimentary belt, Superior Province, Canada. *Chemical Geology*, *55*(1–2), 77–95.

Schmidt, V., & McDonald, D. A. (1979). The role of secondary porosity in the course of sandstone diagenesis.

Scholle, P. A., & Foundation, A. A. of P. G. (1979). *A color illustrated guide to constituents, textures, cements, and porosities of sandstones and associated rocks* (Vol. 28). American Association of Petroleum Geologists. Tulsa.

Sciscio, L., & Bordy, E. M. (2016). Palaeoclimatic conditions in the Late Triassic-Early Jurassic of southern Africa: a geochemical assessment of the Elliot Formation. *Journal of African Earth Sciences*, *119*, 102–119.

Seike, K. (2008). Burrowing behaviour inferred from feeding traces of the opheliid polychaete Euzonus sp. as response to beach morphodynamics. *Marine Biology*, *153*(6), 1199–1206.

Selley, R. C., & Sonnenberg, S. A. (2014). *Elements of petroleum geology*. Academic Press.

Selvaraj, K., & Chen, C.-T. A. (2006). Moderate chemical weathering of subtropical Taiwan: constraints from solid-phase geochemistry of sediments and sedimentary rocks. *The Journal of Geology*, *114*(1), 101–116.

Shanmugam, G., Poffenberger, M., & Toro Alava, J. (2000). Tide-dominated estuarine facies in the Hollin and Napo (“T” and" U") formations (Cretaceous), Sacha field, Oriente basin, Ecuador. *AAPG Bulletin*, *84*(5), 652–682.

Singer, A. (1980). The paleoclimatic interpretation of clay minerals in soils and weathering profiles. *Earth-Science Reviews*, *15*(4), 303–326.

Singer, A. (1984). The paleoclimatic interpretation of clay minerals in sediments—a review. *Earth-Science Reviews*, *21*(4), 251–293.

Smith, A. G., Smith, W., & Briden, J. C. (1977). *Mesozoic and Cenozoic paleocontinental maps*. Cambridge University Press.

Smith, R. M. H. (1990). Alluvial paleosols and pedofacies sequences in the Permian Lower Beaufort of the southwestern Karoo Basin, South Africa. *Journal of Sedimentary Research*, *60*(2), 258–276.

Smith, R. M. H. (1990). A review of stratigraphy and sedimentary environments of the Karoo Basin of South Africa. *Journal of African Earth Sciences (and the Middle East)*, *10*(1–2), 117–137.

Soreghan, G. S., & Soreghan, M. J. (2013). Tracing Clastic Delivery to the Permian Delaware Basin, USA: Implications for Paleogeography and Circulation In Westernmost Equatorial Pangea. *Journal of Sedimentary Research*, *83*(9), 786–802.

Staub, J. R., & Gastaldo, R. A. (2003). Late Quaternary sedimentation and peat development in the Rajang River delta, Sarawak, east Malaysia.

Stone, W. N., & Siever, R. (1996). Siliciclastic diagenesis and fluid flow: Concepts and applications. SEPM (Society for Sedimentary Geology) Special Publication 55.

Suczek, C. A., & Ingersoll, R. V. (1985). Petrology and provenance of Cenozoic sand from the Indus Cone and the Arabian Basin, DSDP sites 221, 222, and 224. *Journal of Sedimentary Research*, *55*(3), 340–346.

Suttner, L. J., & Dutta, P. K. (1986). Alluvial sandstone composition and paleoclimate; I, Framework mineralogy. *Journal of Sedimentary Research*, *56*(3), 329–345.

Swift, D. J. P., Figueiredo, A. G., Freeland, G. L., & Oertel, G. F. (1983). Hummocky cross-stratification and megaripples; a geological double standard? *Journal of Sedimentary Research*, *53*(4), 1295–1317.

Ta, T. K. O., Nguyen, V. L., Tateishi, M., Kobayashi, I., Saito, Y., & Nakamura, T. (2002). Sediment facies and Late Holocene progradation of the Mekong River Delta in Bentre Province, southern Vietnam: an example of evolution from a tide-dominated to a tide- and wave-dominated delta. *Sedimentary Geology*, *152*(3), 313–325. https://doi.org/https://doi.org/10.1016/S0037-0738(02)00098-2

Tanavsuu-Milkeviciene, K., & Plink-Bjorklund, P. (2009). Recognizing tide-dominated versus tide-influenced deltas: Middle Devonian strata of the Baltic Basin. *Journal of Sedimentary Research*, *79*(12), 887–905.

Tawfik, H. A., Ghandour, I. M., Maejima, W., Armstrong-Altrin, J. S., & Abdel-Hameed, A.-M. T. (2017). Petrography and geochemistry of the siliciclastic Araba Formation (Cambrian), east Sinai, Egypt: implications for provenance, tectonic setting and source weathering. *Geological Magazine*, *154*(1), 1–23.

Taylor, A. M., & Gawthorpe, R. L. (1993). Application of sequence stratigraphy and trace fossil analysis to reservoir description: examples from the Jurassic of the North Sea. *Geological Society, London, Petroleum Geology Conference Series*, *4*(1), 317–335. Geological Society of London.

Taylor, A. M., & Goldring, R. (1993). Description and analysis of bioturbation and ichnofabric. *Journal of the Geological Society*, *150*(1), 141–148.

Taylor, A., Goldring, R., & Gowland, S. (2003). Analysis and application of ichnofabrics. *Earth-Science Reviews*, *60*(3–4), 227–259.

Taylor, S. R., &McLennan, S. M. (1985). *The continental crust: its composition and evolution*.

Thió-Henestrosa, S., & Martín-Fernández, J. A. (2005). Dealing with compositional data: the freeware CoDaPack. *Mathematical Geology*, *37*(7), 773–793.

Thomas, W. A. (2011). Detrital-zircon geochronology and sedimentary provenance. *Lithosphere*, *3*(4), 304–308.

Tinker, J., de Wit, M., & Brown, R. (2008). Mesozoic exhumation of the southern Cape, South Africa, quantified using apatite fission track thermochronology. *Tectonophysics*, *455*(1–4), 77–93.

Tolosana-Delgado, R., Otero, N., & Pawlowsky-Glahn, V. (2005). Some basic concepts of compositional geometry. *Mathematical Geology*, *37*(7), 673–680.

Torsvik, T. H., & Cocks, L. R. M. (2016). *Earth history and palaeogeography*. Cambridge University Press.

Totten, M. W., Hanan, M. A., & Weaver, B. L. (2000). Beyond whole-rock geochemistry of shales: the importance of assessing mineralogic controls for revealing tectonic discriminants of multiple sediment sources for the Ouachita Mountain flysch deposits. *Geological Society of America Bulletin*, *112*(7), 1012–1022.

Trevena, A. S., & Nash, W. P. (1981). An electron microprobe study of detrital feldspar. *Journal of Sedimentary Research*, *51*(1), 137–150.

Tucker, M. E. (2001). *Sedimentary Petrology: An Introduction to the Origin of Sedimentary Rocks*. Blackwell. *Scientific Publication, London*.

Tunbridge, I. P. (1981). Sandy high-energy flood sedimentation—some criteria for recognition, with an example from the Devonian of SW England. *Sedimentary Geology*, *28*(2), 79–95.

Vail, P. R. (1987). Seismic stratigraphy interpretation using sequence stratigraphy: Part 1: Seismic stratigraphy interpretation procedure.

Van Cappelle, M., Stukins, S., Hampson, G. J., & Johnson, H. D. (2016). Fluvial to tidal transition in proximal, mixed tide-influenced and wave-influenced deltaic deposits: Cretaceous lower Sego Sandstone, Utah, USA. *Sedimentology*, *63*(6), 1333–1361.

Van den Berg, J. H., Boersma, J. R., & van Gelder, A. (2007). Diagnostic sedimentary structures of the fluvial-tidal transition zone – Evidence from deposits of the Rhine and Meuse. *Netherlands Journal of Geosciences*, *86*(3), 287–306. https://doi.org/DOI: 10.1017/S0016774600077866

Van den Berg, J. H., Martinius, A. W., & Houthuys, R. (2017). Breaching-related turbidites in fluvial and estuarine channels: Examples from outcrop and core and implications to reservoir models. *Marine and Petroleum Geology*, *82*, 178–205.

Van Straaten, L., & Kuenen, P. H. (1957). *Accumulation of fine grained sediments in the Dutch Waddensea*.

Veeken, P. C. H. (2013). *Seismic stratigraphy and depositional facies models*. Academic Press.

Velbel, M. A. (1985). Geochemical mass balances and weathering rates in forested watersheds of the southern Blue Ridge. *American Journal of Science*, *285*(10), 904–930.

Verma, S. P., & Armstrong-Altrin, J. S. (2013). New multi-dimensional diagrams for tectonic discrimination of siliciclastic sediments and their application to Precambrian basins. *Chemical Geology*, *355*, 117–133.

Visher, G. S. (1969). Grain size distributions and depositional processes. *Journal of Sedimentary Research*, *39*(3), 1074–1106. https://doi.org/10.1306/74D71D9D-2B21-11D7-8648000102C1865D

Visser, M. J. (1980). Neap-spring cycles reflected in Holocene subtidal large-scale bedform deposits: a preliminary note. *Geology*, *8*(11), 543–546.

von Eynatten, H. (2003). Petrography and chemistry of sandstones from the Swiss Molasse Basin: an archive of the Oligocene to Miocene evolution of the Central Alps. *Sedimentology*, *50*(4), 703–724.

von Eynatten, H. (2004). Statistical modelling of compositional trends in sediments. *Sedimentary Geology*, *171*(1–4), 79–89.

von Eynatten, H., Barceló-Vidal, C., & Pawlowsky-Glahn, V. (2003). Composition and discrimination of sandstones: a statistical evaluation of different analytical methods. *Journal of Sedimentary Research*, *73*(1), 47–57.

von Eynatten, H., & Dunkl, I. (2012). Assessing the sediment factory: the role of single grain analysis. *Earth-Science Reviews*, *115*(1–2), 97–120.

von Eynatten, H., & Gaupp, R. (1999). Provenance of Cretaceous synorogenic sandstones in the Eastern Alps: constraints from framework petrography, heavy mineral analysis and mineral chemistry. *Sedimentary Geology*, *124*(1–4), 81–111.

Wang, W., Zhou, M.-F., Yan, D.-P., & Li, J.-W. (2012). Depositional age, provenance, and tectonic setting of the Neoproterozoic Sibao Group, southeastern Yangtze Block, South China. *Precambrian Research*, *192*, 107–124.

Watkeys, M. K. (2006). Gondwana break-up: a South African perspective. *The Geology of South Africa.* Johannesburg & Pretoria*: Geological Society of South Africa &the Council for Geoscience*, 531–539.

Weissmann, G. S., Hartley, A. J., Nichols, G. J., Scuderi, L. A., Olson, M., Buehler, H., & Banteah, R. (2010). Fluvial form in modern continental sedimentary basins: distributive fluvial systems. *Geology*, *38*(1), 39–42.

Weltje, G. J., Meijer, X. D., & De Boer, P. L. (1998). Stratigraphic inversion of siliciclastic basin fills: a note on the distinction between supply signals resulting from tectonic and climatic forcing. *Basin Research*, *10*(1), 129–153.

Weltje, G. J. (1994). Provenance and dispersal of sand-sized sediments: reconstruction of dispersal patterns and sources of sand-sized sediments by means of inverse modelling techniques (Vol. 121). Utrecht University.

Weltje, G. J. (2002). Quantitative analysis of detrital modes: statistically rigorous confidence regions in ternary diagrams and their use in sedimentary petrology. *Earth-Science Reviews*, *57*(3–4), 211–253.

Weltje, G. J. (2006). Ternary sandstone composition and provenance: an evaluation of the 'Dickinson model.' *Geological Society, London, Special Publications*, *264*(1), 79–99.

Weltje, G. J. (2012). Quantitative models of sediment generation and provenance: state of the art and future developments. *Sedimentary Geology*, *280*, 4–20.

Weltje, G. J., & von Eynatten, H. (2004). Quantitative provenance analysis of sediments: review and outlook. *Sedimentary Geology*, *171*(1–4), 1–11.

Wentworth, C. K. (1922). A scale of grade and class terms for clastic sediments. *The Journal of Geology*, *30*(5), 377–392.

Wightman, D. M., Pemberton, S. G., & Singh, C. (1987). Depositional modelling of the Upper Mannville lower Cretaceous East Central Alberta: Implications for the Recognition of Brackish Water Deposits.

Wigley, R., & Compton, J. S. (2007). Oligocene to Holocene glauconite–phosphorite grains from the Head of the Cape Canyon on the western margin of South Africa. *Deep Sea Research Part II: Topical Studies in Oceanography*, *54*(11–13), 1375–1395.

Wilkinson, M., Milliken, K. L., & Haszeldine, R. S. (2001). Systematic destruction of K-feldspar in deeply buried rift and passive margin sandstones. *Journal of the Geological Society*, *158*(4), 675–683.

Willey, J. D. (1974). The effect of pressure on the solubility of amorphous silica in seawater at 0°C. *Marine Chemistry*, *2*(4), 239–250.

Wilson, J. C., & McBride, E. F. (1988). Compaction and porosity evolution of Pliocene sandstones, Ventura Basin, California. *AAPG Bulletin*, *72*(6), 664–681.

Yang, W., Feng, Q., Liu, Y., Tabor, N., Miggins, D., Crowley, J. L., Thomas, S. (2010). Depositional environments and cyclo-and chronostratigraphy of uppermost Carboniferous–Lower Triassic fluvial–lacustrine deposits, southern Bogda Mountains, NW China: A terrestrial paleoclimatic record of mid-latitude NE Pangea. *Global and Planetary Change*, *73*(1–2), 15–113.

Yoshida, S., Steel, R. J., & Dalrymple, R. W. (2007). Changes in depositional processes—an ingredient in a new generation of sequence-stratigraphic models. *Journal of Sedimentary Research*, *77*(6), 447–460.

Young, M. J., Gawthorpe, R. L., & Sharp, I. R. (2000). Sedimentology and sequence stratigraphy of a transfer zone coarse-grained delta, Miocene Suez Rift, Egypt. *Sedimentology*, *47*(6), 1081–1104.

Young, S. W., Basu, A., Mack, G. H., Darnell, N., & Suttner, L. J. (1975). Use of size composition trends in Holocene soil and fluvial sand for paleoclimate interpretation. *Proceedings of the 9th International Sedimentological Congress, Theme*, *1*, 201–209.

Zack, T. v, Von Eynatten, H., & Kronz, A. (2004). Rutile geochemistry and its potential use in quantitative provenance studies. *Sedimentary Geology*, *171*(1–4), 37–58.

Zavala, C., & Arcuri, M. (2016). Intrabasinal and extrabasinal turbidites: Origin and distinctive characteristics. *Sedimentary Geology*, *337*, 36–54.

Zavala, C., Arcuri, M., Meglio, M. Di, Diaz, H. G., & Contreras, C. (2012). A genetic facies tract for the analysis of sustained hyperpycnal flow deposits (R. M. Slatt & C. Zavala, Eds.). *Sediment Transfer from Shelf to Deep Water—Revisiting the Delivery System*, Vol. 61, p. 0. https://doi.org/10.1306/13271349St613438

Zavala, C., & Pan, S. X. (2018). Hyperpycnal flows and hyperpycnites: Origin and distinctive characteristics. *Lithologic Reservoirs*, *30*(1), 1–27.

Zhang, L. J., Fan, R.-Y., & Gong, Y. M. (2015). Zoophycos macroevolution since 541 Ma. *Scientific Reports*, *5*, 14954.

Zhang, Y., Pe-Piper, G., & Piper, D. J. W. (2014). Sediment geochemistry as a provenance indicator: Unravelling the cryptic signatures of polycyclic sources, climate change, tectonism and volcanism. *Sedimentology*, *61*(2), 383–410.

Zhu, H., Yang, X., Liu, K., & Zhou, X. (2014). Seismic-based sediment provenance analysis in continental lacustrine rift basins: An example from the Bohai Bay Basin, China. *AAPG Bulletin*, *98*(10), 1995–2018.

Ziolkowski, A., Underhill, J. R., & Johnston, R. G. K. (1998). Wavelets, well ties, and the search for subtle stratigraphic traps. *Geophysics*, *63*(1), 297–313.

Zuffa, G. G. (1985). Optical analyses of arenites: influence of methodology on compositional results. In *Provenance of arenites* (pp. 165–189). Springer.

APPENDICES

Appendix A: Sedimentological data

Facies codes

Table A1: Facies analysis codes used in this study

Facies codes	Sedimentary structures	Description	Interpretation	Depositional environment occurrence
Gmd	Disorganized fabric (or weak imbrication)	Floating clasts that are matrix supported and are largely monomictic (especially breccias) but polymictic characteristics does occur as extrabasinal clasts in conglomerates.	Freezing of non-cohesive debris flows due to hyperconcentrated flow (channel lags) or turbulent flows (Hyperpycnites)	Proximal delta front (base of terminal distributary channels), Subaqueous subtidal sand ridges and compound dune fields, Basement high slopes, Proximal/central embayment to shoreface/foreshore environment.
Gp	Planar tabular or trough cross-stratified	Oligomictic orthoconglomerate	Transverse or linguoid bars as the migration of 2D and 3D dunes on channel floors	Distributary channels, Proximal/central embayment to shoreface/foreshore environment.
Spl or Spb	Planar to trough cross- stratified (laminated and bedded) vfL to cL sandstone.	Moderately to Well sorted. Mud drapes occurs occasionally (organic or silt draped). Occasionally pebbly.	Migration of 2D and 3D dunes (lower flow regime) small and megaripple bedding (change in hydrodynamic conditions)	Subtidal-sand sheet progradation (subtidal sand ridges and compound dune fields), migrating offshore tidal bars, Channelized proximal delta-front lobes (part of terminal distributary channel sequence),

				Distributary channels, Basement high slopes with hyperpycnites and slope failures or breaching, Deep lacustrine channels. (Lower delta plain to proximal delta front (distal intertidal delta platform) mouth bars with associated terminal distributary channels
Sm	Massive vfL to cL sandstone	Moderately to well sorted, occasional pebbles	Rapid deposition or aggradation, intense Bioturbation	Subtidal-sand sheet progradation (subtidal sand ridges and compound dune fields), Middle to distal delta front area and delta fringe facies. Channelized proximal delta-front lobes (part of terminal distributary channel sequence), Lower delta plain to proximal delta front mouth bars with associated terminal distributary channels, Distributary channels, Outer embayment or offshore transgressive

				mudstones, Subaqueous subtidal sand ridges and compound dune fields, Basement high slopes with Hyperpycnites and slope failures or breaching, Deep lacustrine channel.
Shb	Herringbone cross-stratified fL-mU sandstone (medium scale and small scale)	Moderately well sorted, occasional pebbles	Suspension settling to lower flow regime (dune or ripple migration)	Subtidal-sand sheet progradation (subtidal sand ridges and compound dune fields).
Sh	Horizontally stratified vfL to cL sandstone	Moderately to well sorted. Occasional disseminated granules	Upper plane bed, upper flow regime (lower flow regime plane bed cL-cU sandstone)	Subaqueous subtidal sand ridges or compound dune fields (bottomset), Proximal delta front/intertidal shoal, Distributary channels Basement high slopes with Hyperpycnites and slope failures or breaching. Proximal/central embayment to shoreface/foreshore environment, deep lacustrine channels.
Slf	Faintly laminated sandstone	Moderately to well sorted	Lower flow regime bedforms with suspension and benthic feeders (primary and secondary	Subaqueous subtidal sand ridges or compound dune fields, Interdistributary

			structures)	bay (lower delta plain). Basement high slopes with Hyperpycnites and slope failures or breaching. Proximal/central embayment to shoreface/foreshore environment.
Splx	Low angle cross-stratified vfL to mU sandstone	Organic rich drapes, in some places non-organic	Washed-out dunes under upper flow regime; toesets of larger bedforms,	Subtidal-sandsheet progradation (forsets of subtidal sand ridges and compound dune fields), proximal delta front, Proximal delta front/intertidal shoal, Tidal to wave dominated and river influenced mouth bars, Distributary channels, Subaqueous subtidal sand ridges and compound dune fields
Shl	Heterolythic alternations of vfL sandstone and mudstones/claystones	The coarser grained units are usually poorly to moderately sorted with subangular grains.	Suspension settling to rapid aggradation (associated with (Shc)) or hyperconcentrated flow under upper flow regime conditions.	Delta front (distal mouth bar) or delta front sheet and lobe (fringe), proximal delta front Middle to distal delta front area and delta fringe facies. Proximal delta front/intertidal

				shoal, Tidal sand flat, Deep lacustrine lobes.
Sr	Ripple laminated sandstone, largely unidirectional but occurs as bidirectional ripples as well, climbing ripples are also present in some places	Very well sorted	Migration of 2D or 3D ripples under lower flow regime, with suspension settling or increased suspended sediment concentration with forward migration	Delta front with prograding tidal bars, Middle to distal delta front area and delta fringe facies, Proximal delta front/intertidal shoal, Tidal to wave dominated and river influenced mouth bars, Distributary channels Subaqueous subtidal sand ridges and compound dune fields, Basement high slopes with hyperpycnites and slope failures or breaching.
Sw	Wave rippled (combined flow (anisotropic) or isolated isotropic wave ripples) vfL to fL sandstone consisting of hummocky or swaley cross stratification	Truncated ripple-forms are common with thick lamina of climbing ripples indicative of wave ripples	Combined flows with wave action and fluvial-derived unidirectional flows	Delta front sheets, Middle to distal delta front area and delta fringe facies, Proximal delta front/intertidal shoal, Tidal to wave dominated and river influenced mouth bars, Proximal/central embayment to shoreface/foreshore environment.

Sb	Bioturbated sandstone	The unit is usually poorly to moderately sorted.	Organism disruption of sediments through burrowing associated with quiescent periods and active deposition	Subaqueous subtidal sand ridges and compound dune fields
Mb	Bioturbated mudstone or siltstone	Usually associated with massive bedding	Organism disruption of sediments through burrowing associated with quiescent periods	Outer embayment or offshore transgressive mudstones
Fm	Massive mudstone to siltstone	Non-bioturbated	Suspension settling with turbulent currents.	Channelized delta front lobe facies/Terminal distributary channels, Lower delta plain to proximal delta front mouth bars with associated terminal distributary channels and interdistributary bays, Distributary channels, Outer embayment or transgressive mudstones, Proximal/central embayment to shoreface/foreshore environment.
SM1 and SM2	Stratified fluidized mud layers	Occurs as two forms. Horizontally stratified (SM2) or ripple cross laminated (SM1).	Increased suspended sediment concentration with unidirectional or bidirectional	Middle to distal delta front area and delta fringe facies, Distributary channels, Deep lacustrine lobes, Lower delta plain to proximal delta

			flows	front mouth bars with associated terminal distributary channels and interdistributary bays
Fl	Laminated to faintly laminated mudstone	Contains mica flakes and are rare	Suspension settling during quiescent periods	Lower delta plain to proximal delta front mouth bars with associated terminal distributary channels and interdistributary bays, Distributary channels, Outer embayment or offshore transgressive mudstones, Proximal tidal bars, Subaqueous subtidal sand ridges and compound dune fields, Proximal/central embayment to shoreface/foreshore environment.
Sin	Inversely graded or normally graded mudstone and sandstone	Occurs as thin bedded distal turbidites	Suspension settling following or preceding high energy events	Channelized delta front lobe facies (Terminal distributary channel sequences)
Shc	Convoluted bedded, overturned cross stratification and slumped bedding	These units are associated with coarser grained units (fL sandstone and above)	Soft sediment deformation by loading and high current velocity flows over semi-consolidated sediments (High	Channelized delta front lobe facies (Terminal distributary channel sequence), (Lower delta plain to proximal delta front mouth bars

			energy events).	with associated terminal distributary channels and interdistributary bays, Distributary channel sequence

Detailed sedimentary log sections (logged at 1=10cm)

Operator: Petroleum Agency of South Africa (PASA)	EasyCore
Top: 2661 m	Bottom: 2770 m
Depth Scale: 1: 10cm	Country: South Africa
Well Name & No.: F-A12	Location: 91km South of Mossel Bay, offshore South Africa
Logged by: Mogammad Yaaseen Hendricks	
Basin: Bredasdorp sub-basin	Field: Block 9 (F-A Gas field)
KB: 26 m	Latitude: 34° 59' 45.07" S
Longitude: 22° 09' 50.61" E	

Lithologies

- Breccia
- Claystone
- Conglomerate
- Mudstone
- Paleosol
- Pebbly Sandstone
- Sandstone
- Siltstone

Admixture

- Argillaceous
- Calcareous
- Glauconitic
- Organic
- Pyritic
- Sandy
- Siliceous

Grain Type

- Intra-formational Clasts

Structure

- Bioturbated
- Cross Laminated
- Current Ripple Laminated
- Faintly Laminated
- Herringbone
- Low-angle Planar Laminated
- Planar Cross-bedded
- Planar Laminated
- Relict-bedded
- Ripple Laminated
- Slumped
- Trough Cross-bedded
- Wave Ripple Laminated

Support

- Clast Supported
- Matrix Supported

Contacts

- Bioturbated
- Erosional Lag
- Gradational
- Scoured
- Straight
- Undulating

Accessories

- Calcite Nodules
- Coal
- Pebbles
- Pull-apart Structure
- Pyrite Nodules
- Py Pyrite
- Shale Clasts
- Siderite Nodules
- Synsedimentary Microfaults

Fossils

- Fossils Broken
- Plant Fragments
- Wood Silicified

Sedimentary Structures

- Convolute Lamination
- Faint Lamination
- Fining Upward
- Flame Structure
- Fluid Escape Pipe
- Herringbone Cross-bedding
- Inverse grading
- Lenticular Bedding
- Load Structure
- Mottled Bedding
- Parallel Wavy Bedding
- Planar Cross Lamination
- Planar Lamination
- Ripple Lamination
- Sand Lamina
- Slickensides
- Slumped Bedding
- Wispy Lamination
- mud drapes with sand

Trace Fossils

- Bioturbation (undifferentiated)
- Escape Structure
- Horizontal Spreiten
- Macaronichnus
- Ophiomorpha
- Paleophycus
- Planolites
- Scolicia

Skolithos

Thalassinoides

Facies

Cross-bedded sandstone that grades to horizontally lami siltstone

Cross-stratified sandstone

Heterolythic hyperpycnites

Horizontal-massive to ripple laminated sandstone

Horizontally to massive bedded sandstone

Interbedded claystone and siltstone

Interbedded massive bioturbated siltstone and mudstone

Interbedded medium to light grey cU sandstone and dark mudstone

Interlaminated claystone and siltstone

Intraformational oligomictic para-breccia

Inversely graded unit

Massive to faintly laminated grading to cross straification

Matrix-supported paraconglomerate

None

Oligomictic cross-stratified orthoconglomerate (cross bedded)

Olive/dark grey claystone with vfL sandstone and siltston

Planar laminated-massive-ripple laminated sandstone

Ripple laminated sandstone with bidirectional ripples

Wavy interbedded Sst with claystone

cL-mL bioclastic cross-bedded sandstone bidirectional ip

mL-fU glauconitic cross-stratified sandstone

Depositional Environment

CVS Crevasse Splay

DFL Delta front lobe fringe

DC Distributary Channel

EST Estuarine embayment

ITDC Inter terminal distributary region

IB Interbar/trough region

IDB Interdistributary Bay

DELF Middle to distal delta front

MB Mouth Bar (Proximal)/Terminal distributary channel

No None

OS Offshore Shelf

SHF Shelf

SP Subtidal platform tidal sand ridge complex

TDC Terminal distributary channel

TB Tidal Bar

TDF Tidal Flat

Zones

Core 1

Core 2

Core 3

Core 4

Core 5

Core 6

None no core

Core Depth (Meters)

Core Photographs

Core Description Profile

Lithology

Petrography sample depths

Geochemical sample depths

Rock Color

Facies

Depositional Environment

Notes

Bedding Dip Angle

Zones

2662

2663

2664

Missing Core

Preserved Sample

Preserved Sample

fU to mI light grey to greenish grey glauconitic sandstone with medium greyish to brown mud drapes. The grains are subrounded to rounded and are moderately to moderately well sorted. Sedimentary structures consist of cross stratification and horizontal planar stratification (complexity gives rise to changes in bedding character or angle which are possibly indicative of master surfaces of large scale dune migration or compound dune migration). The unit tends to become argillaceous in some parts. Bioturbation (ranges from 3 to 6) is common with the occurrence of coarse shell fragments. Bioturbation often leads to disturbed bedding (waning flows). The burrows consist largely of calcareous fills with some burrows intensely diagenetically altered (selective carbonate cementation). Trace fossils that occur are *Paleophycus, Ophiomorpha (rudis and nodosa), Scolicia, Macaronichnus,Thalassinoides* and *Planolites* (found within *Thalassinoides* burrows). The burrows are randomly distributed but does occur within intervals with high concentration of trace fossils. Floating greenish grey clasts (largely angular to rounded (oblate)) are also common with coarse shell debris which provides evidence for high energy and low energy colonization windows. The clasts are also aligned parallel to foresets but could also be the result of bioturbation reworking on the bedding planes. Carbonaceous fragments also occur which are more prone to occur in association with mud drapes. Pyrite nodules and pyritized mud drapes aslo occur. Interbedded intraformational conglomerates also occur with greenish grey claystone and siltstone clasts (range from 0.1mm to 0.5mm in long diameter axis (oblate)) and quartz pebbles with sandstone clasts as well.

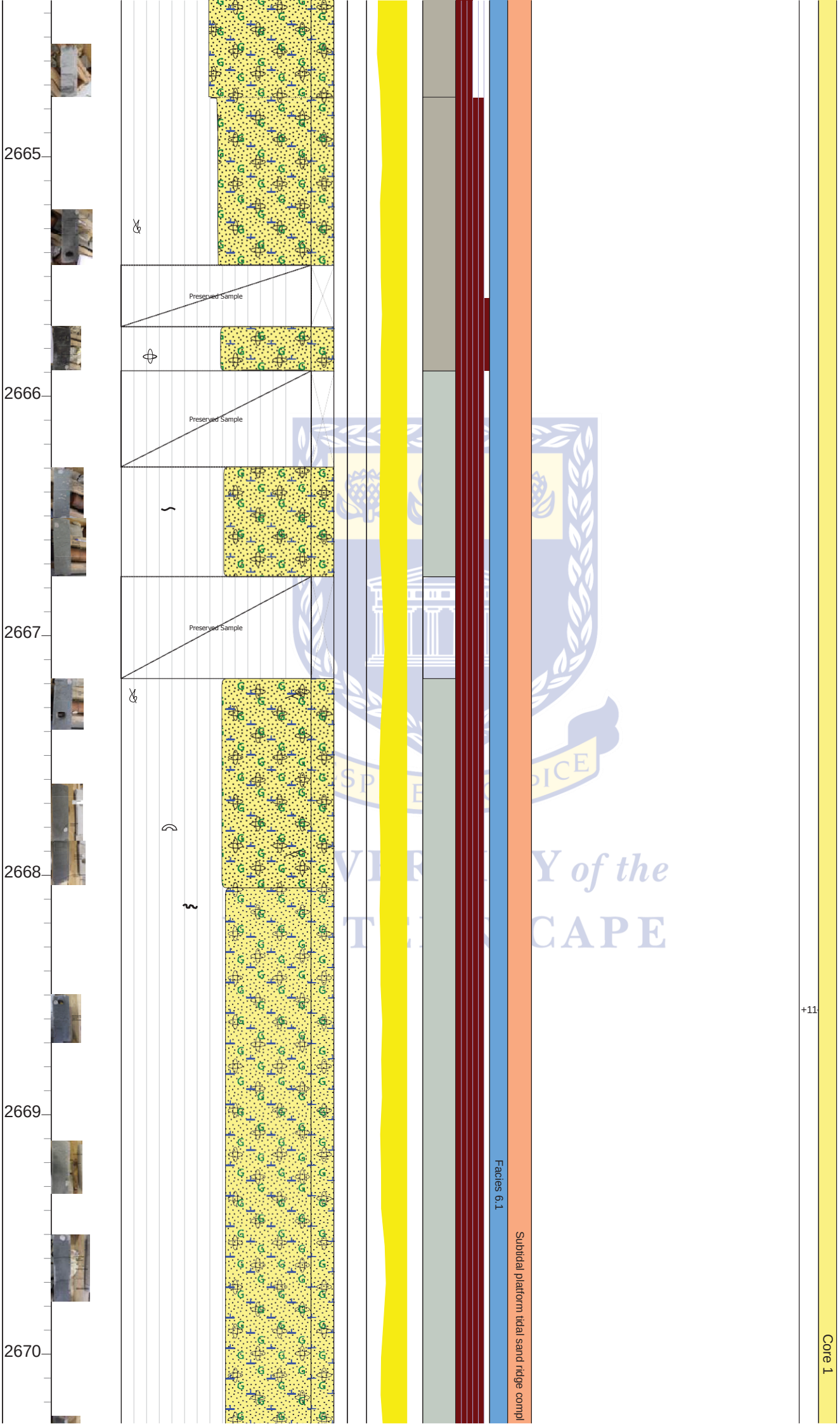

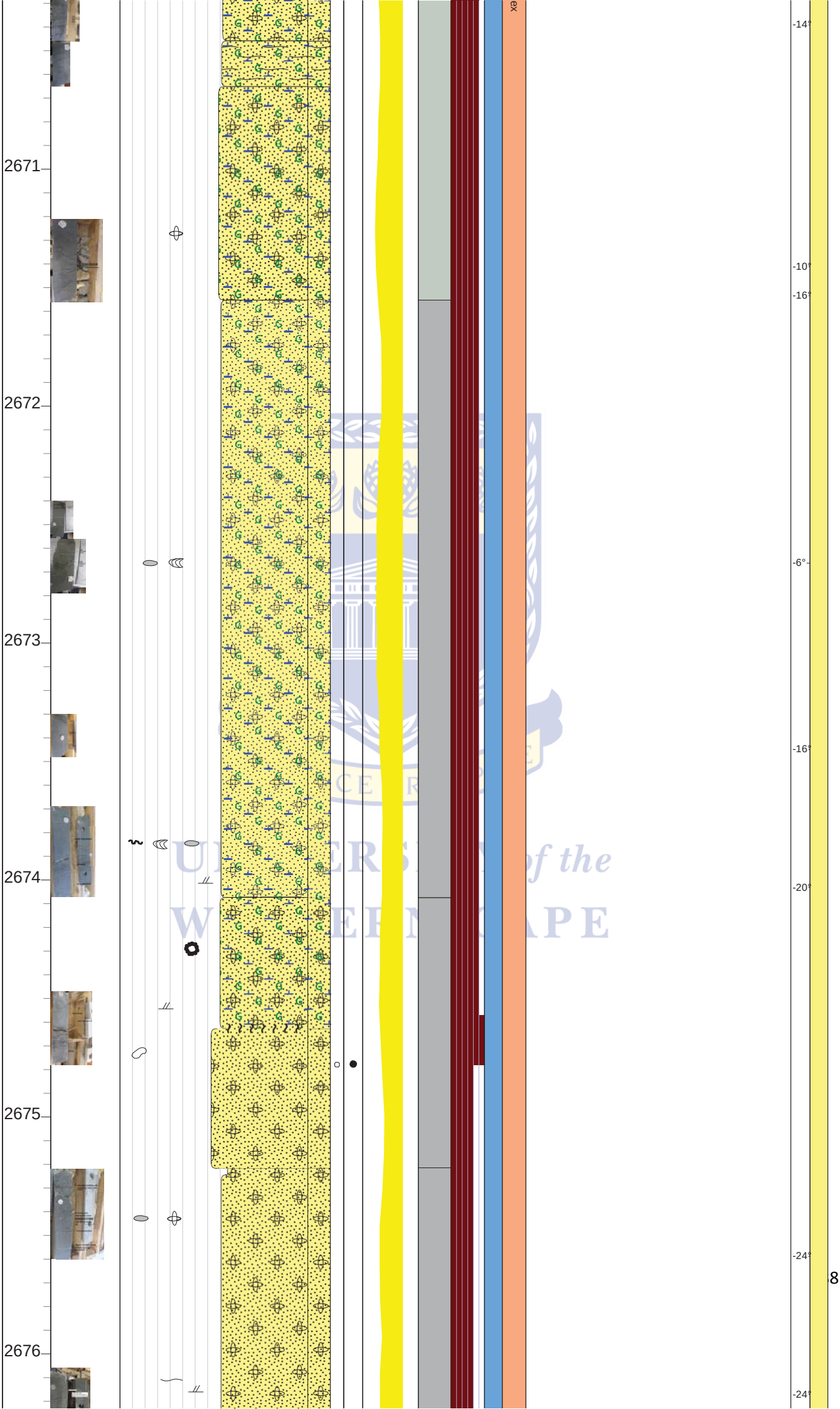

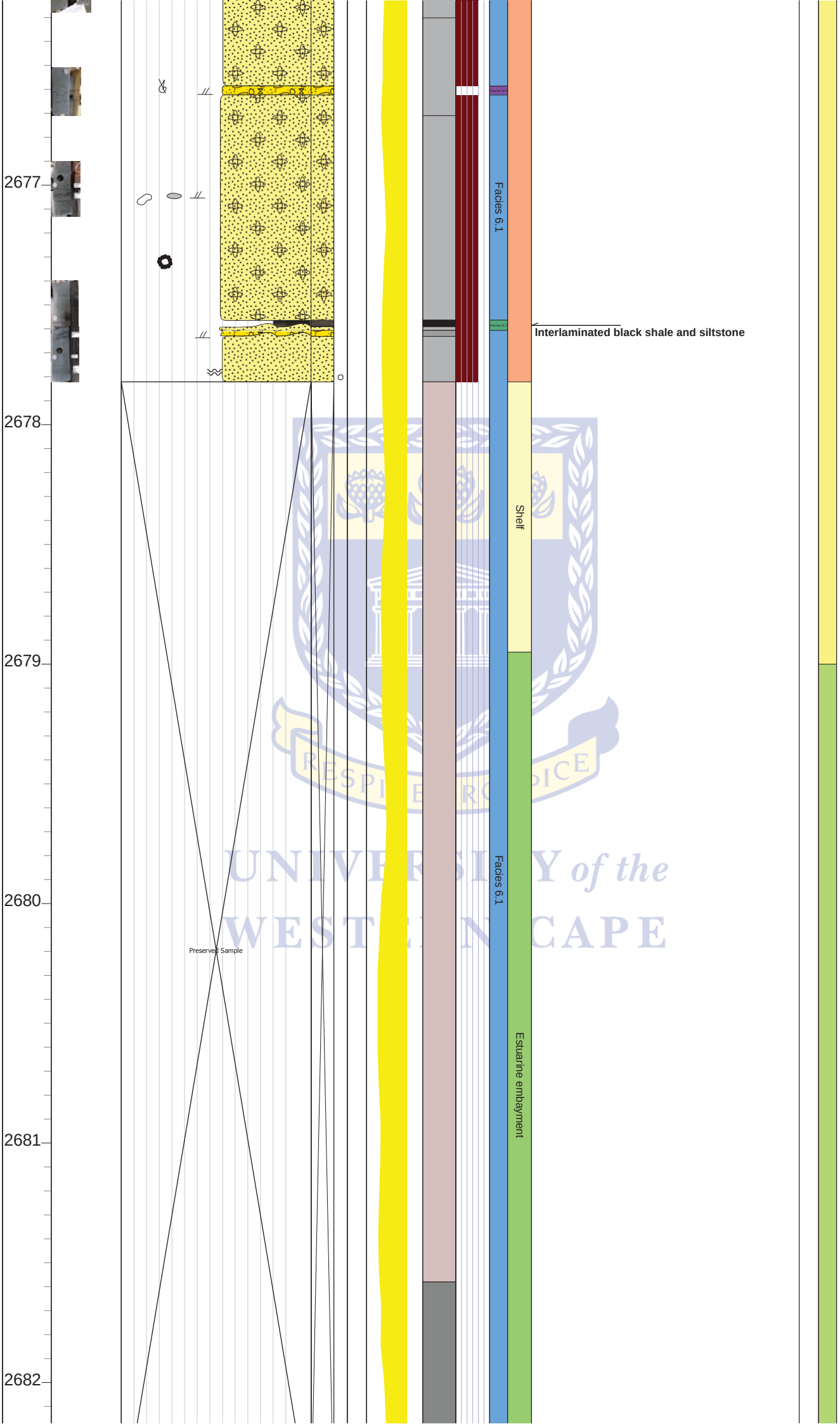

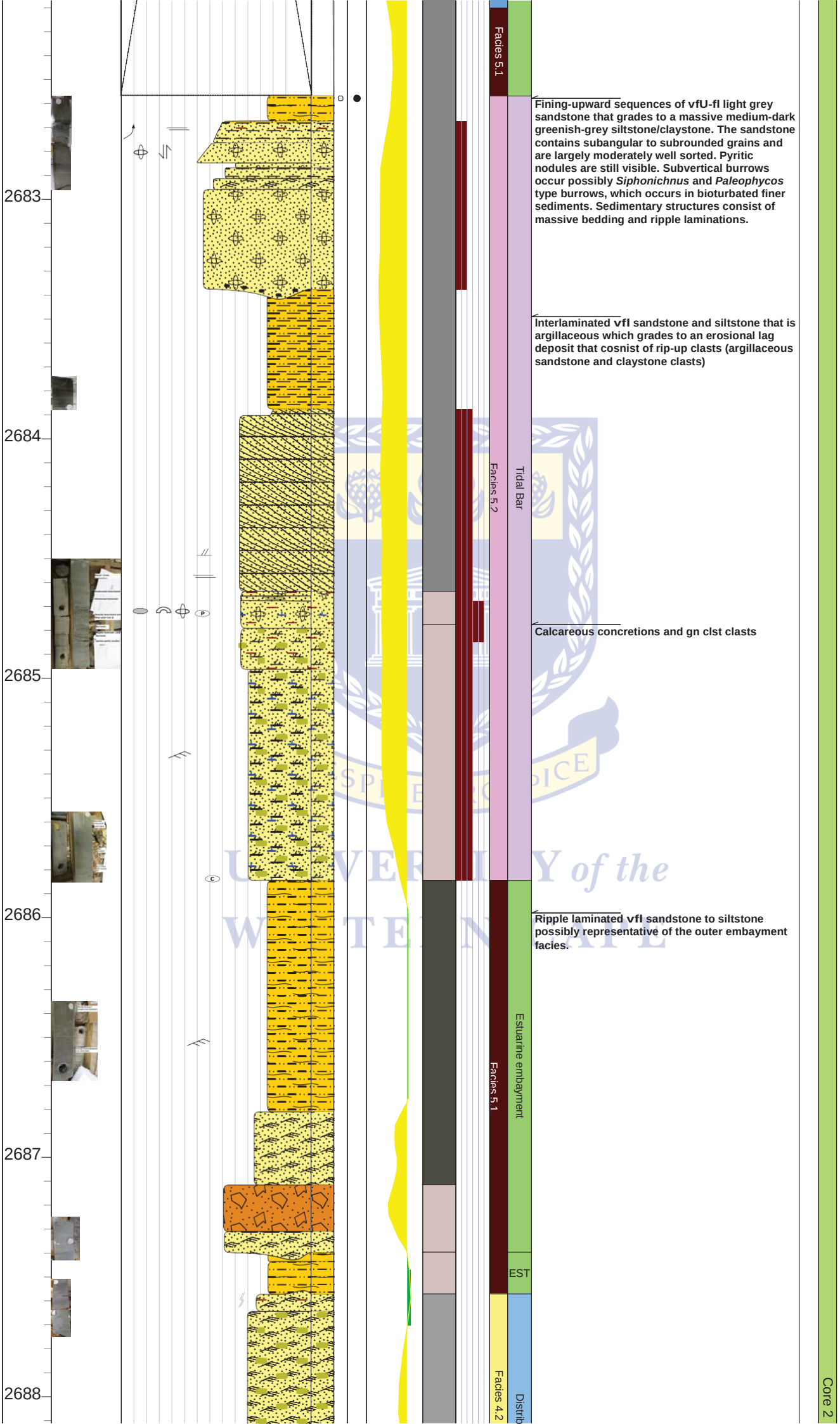

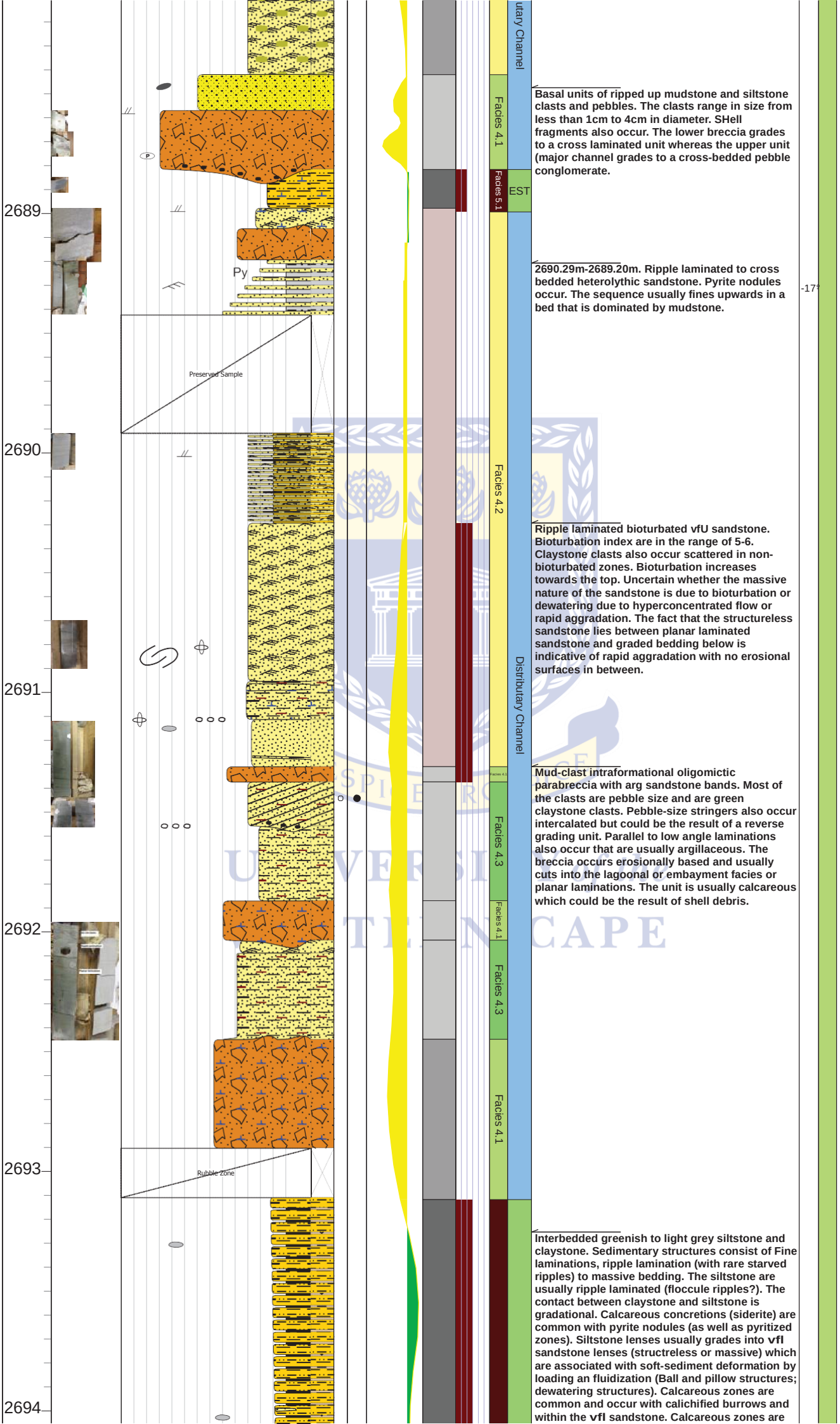

Basal units of ripped up mudstone and siltstone clasts and pebbles. The clasts range in size from less than 1cm to 4cm in diameter. SHell fragments also occur. The lower breccia grades to a cross laminated unit whereas the upper unit (major channel grades to a cross-bedded pebble conglomerate.

2690.29m-2689.20m. Ripple laminated to cross bedded heterolythic sandstone. Pyrite nodules occur. The sequence usually fines upwards in a bed that is dominated by mudstone.

Ripple laminated bioturbated vfU sandstone. Bioturbation index are in the range of 5-6. Claystone clasts also occur scattered in non-bioturbated zones. Bioturbation increases towards the top. Uncertain whether the massive nature of the sandstone is due to bioturbation or dewatering due to hyperconcentrated flow or rapid aggradation. The fact that the structureless sandstone lies between planar laminated sandstone and graded bedding below is indicative of rapid aggradation with no erosional surfaces in between.

Mud-clast intraformational oligomictic parabreccia with arg sandstone bands. Most of the clasts are pebble size and are green claystone clasts. Pebble-size stringers also occur intercalated but could be the result of a reverse grading unit. Parallel to low angle laminations also occur that are usually argillaceous. The breccia occurs erosionally based and usually cuts into the lagoonal or embayment facies or planar laminations. The unit is usually calcareous which could be the result of shell debris.

Interbedded greenish to light grey siltstone and claystone. Sedimentary structures consist of Fine laminations, ripple lamination (with rare starved ripples) to massive bedding. The siltstone are usually ripple laminated (floccule ripples?). The contact between claystone and siltstone is gradational. Calcareous concretions (siderite) are common with pyrite nodules (as well as pyritized zones). Siltstone lenses usually grades into vfl sandstone lenses (structreless or massive) which are associated with soft-sediment deformation by loading an fluidization (Ball and pillow structures; dewatering structures). Calcareous zones are common and occur with calichified burrows and within the vfl sandstone. Calcareous zones are

restricted to certain parts. Bioturbation index are in th range of 3-4 but can extend to zones with bioturbation indeices of 5-6. Vertical burrows are common (oppurtunistic organisms such as *Skolithos).*

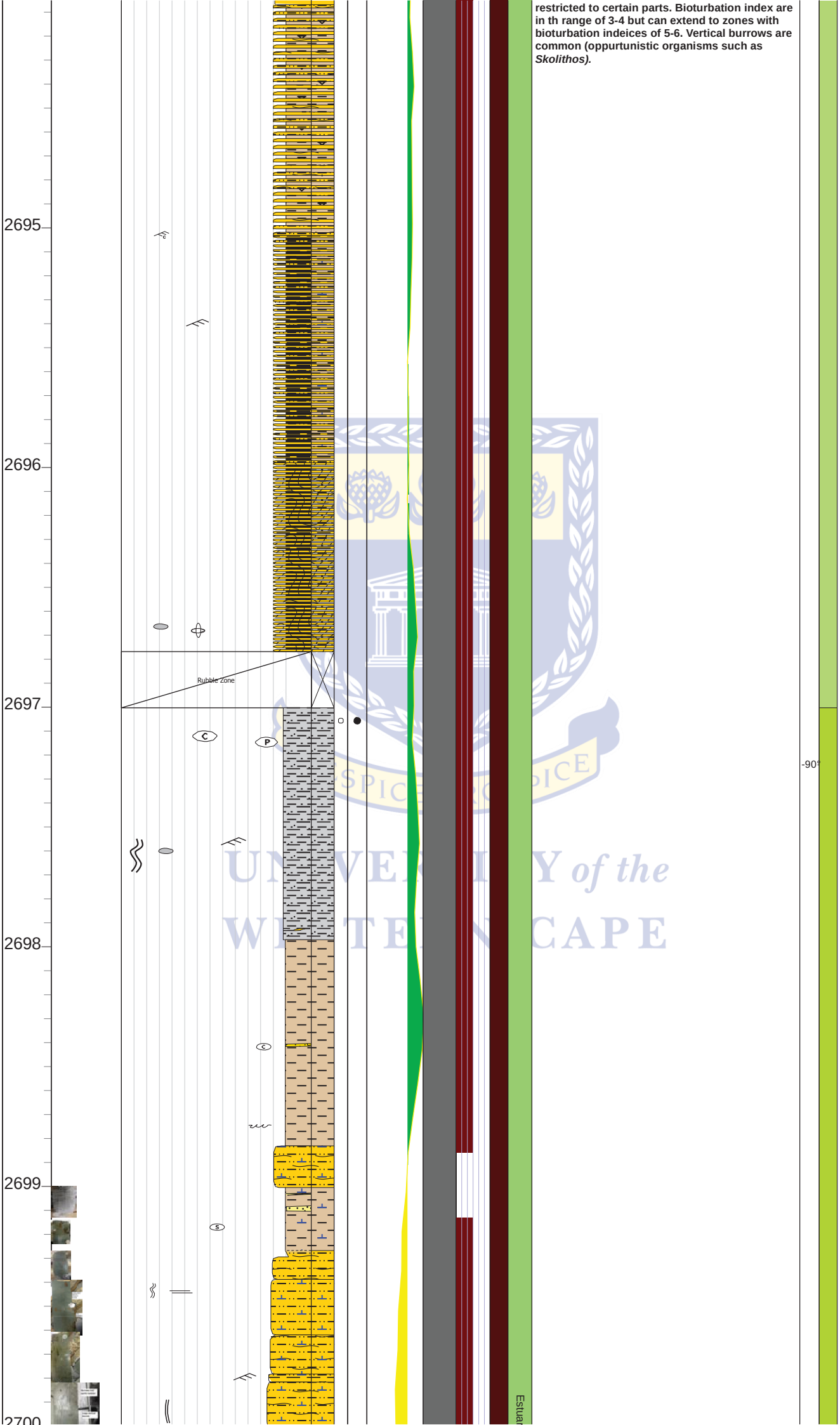

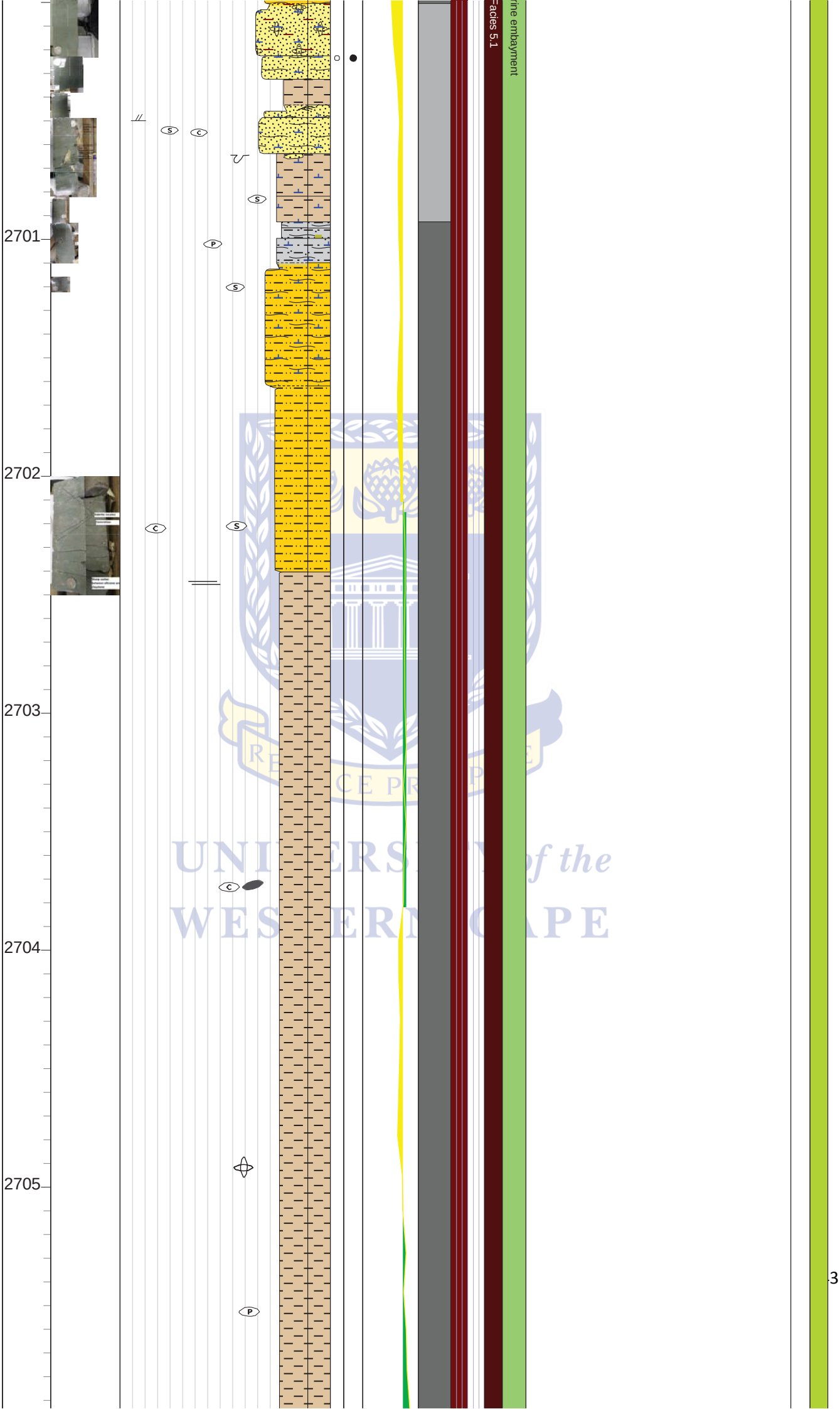

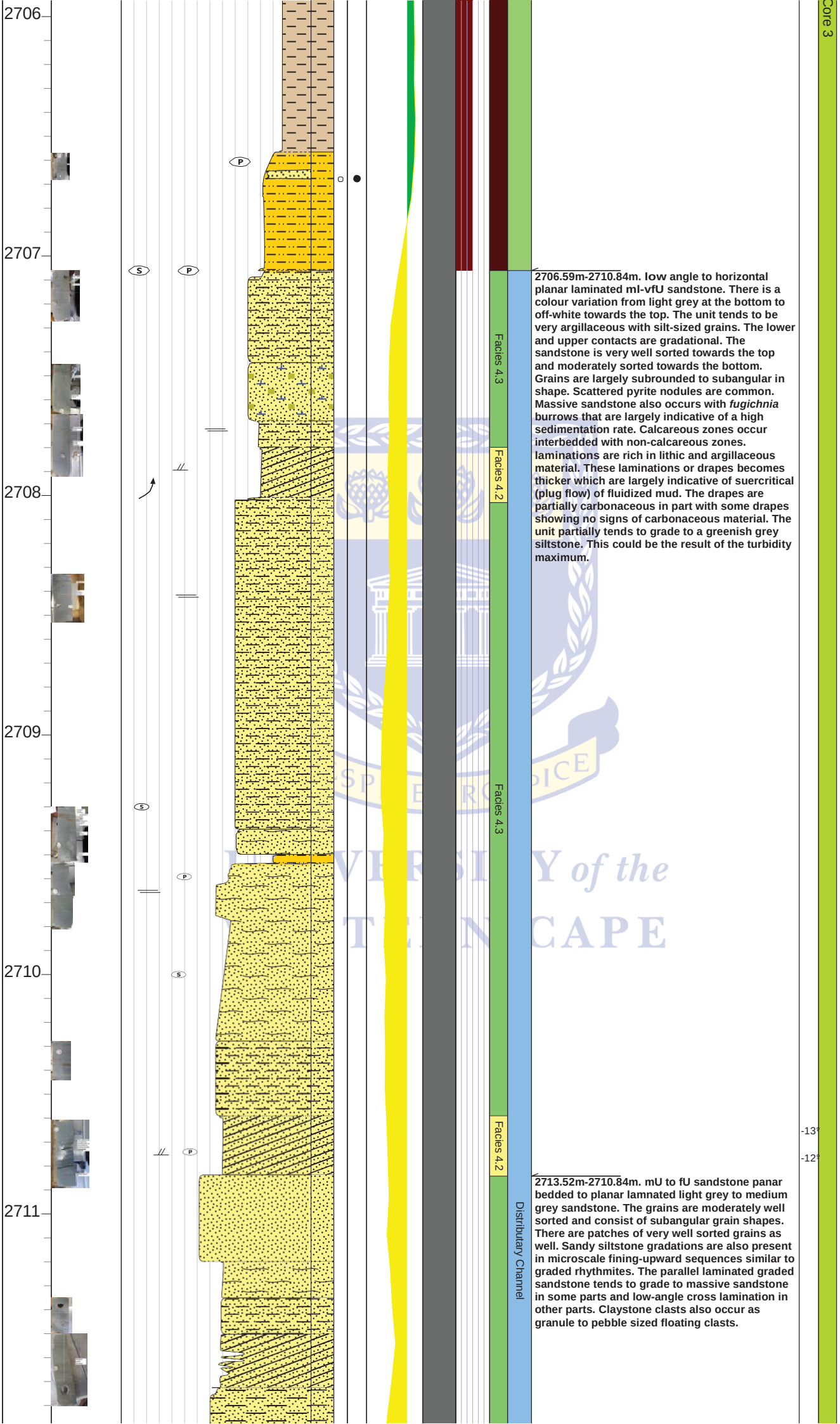

2706.59m-2710.84m. low angle to horizontal planar laminated ml-vfU sandstone. There is a colour variation from light grey at the bottom to off-white towards the top. The unit tends to be very argillaceous with silt-sized grains. The lower and upper contacts are gradational. The sandstone is very well sorted towards the top and moderately sorted towards the bottom. Grains are largely subrounded to subangular in shape. Scattered pyrite nodules are common. Massive sandstone also occurs with *fugichnia* burrows that are largely indicative of a high sedimentation rate. Calcareous zones occur interbedded with non-calcareous zones. laminations are rich in lithic and argillaceous material. These laminations or drapes becomes thicker which are largely indicative of suercritical (plug flow) of fluidized mud. The drapes are partially carbonaceous in part with some drapes showing no signs of carbonaceous material. The unit partially tends to grade to a greenish grey siltstone. This could be the result of the turbidity maximum.

2713.52m-2710.84m. mU to fU sandstone panar bedded to planar lamnated light grey to medium grey sandstone. The grains are moderately well sorted and consist of subangular grain shapes. There are patches of very well sorted grains as well. Sandy siltstone gradations are also present in microscale fining-upward sequences similar to graded rhythmites. The parallel laminated graded sandstone tends to grade to massive sandstone in some parts and low-angle cross lamination in other parts. Claystone clasts also occur as granule to pebble sized floating clasts.

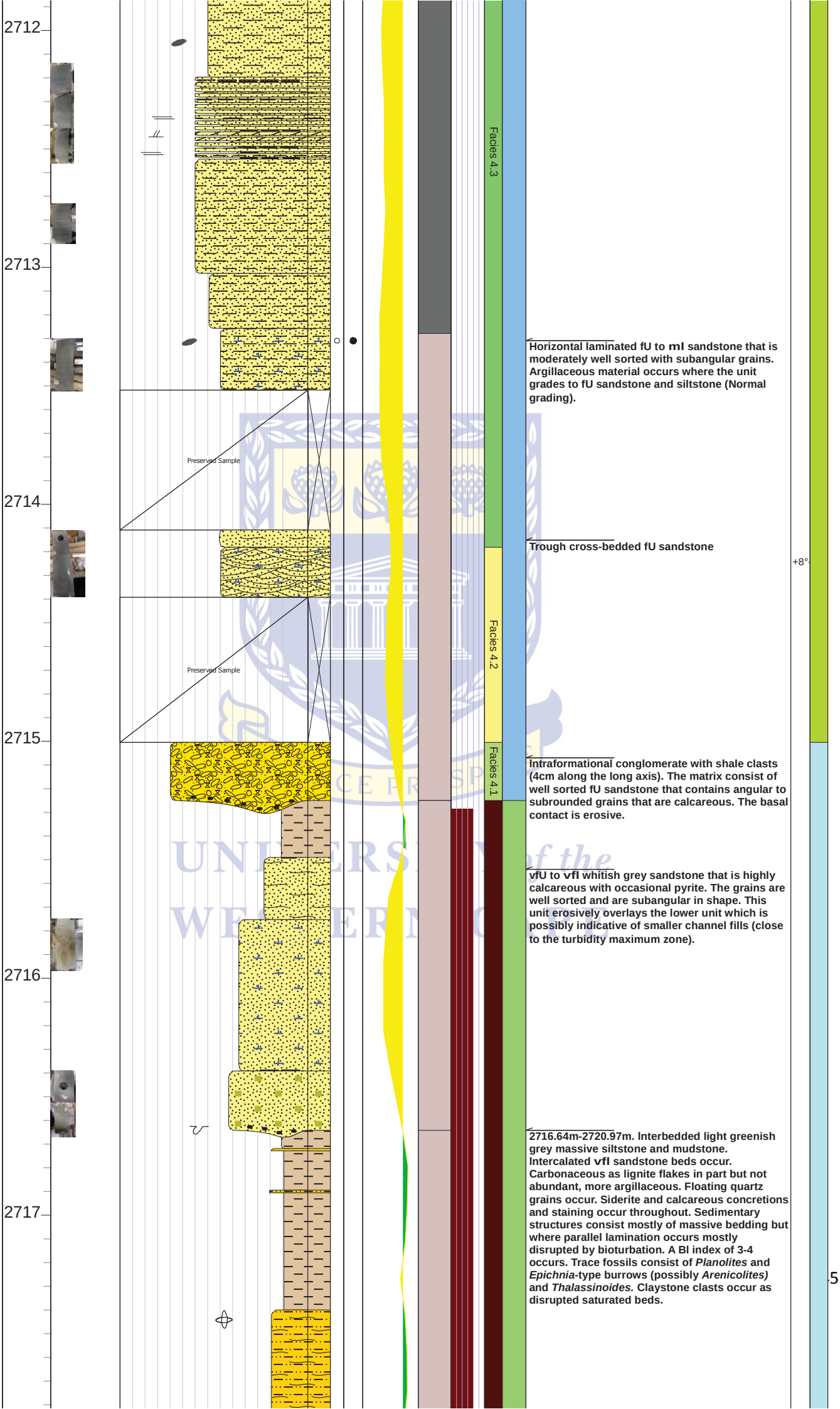

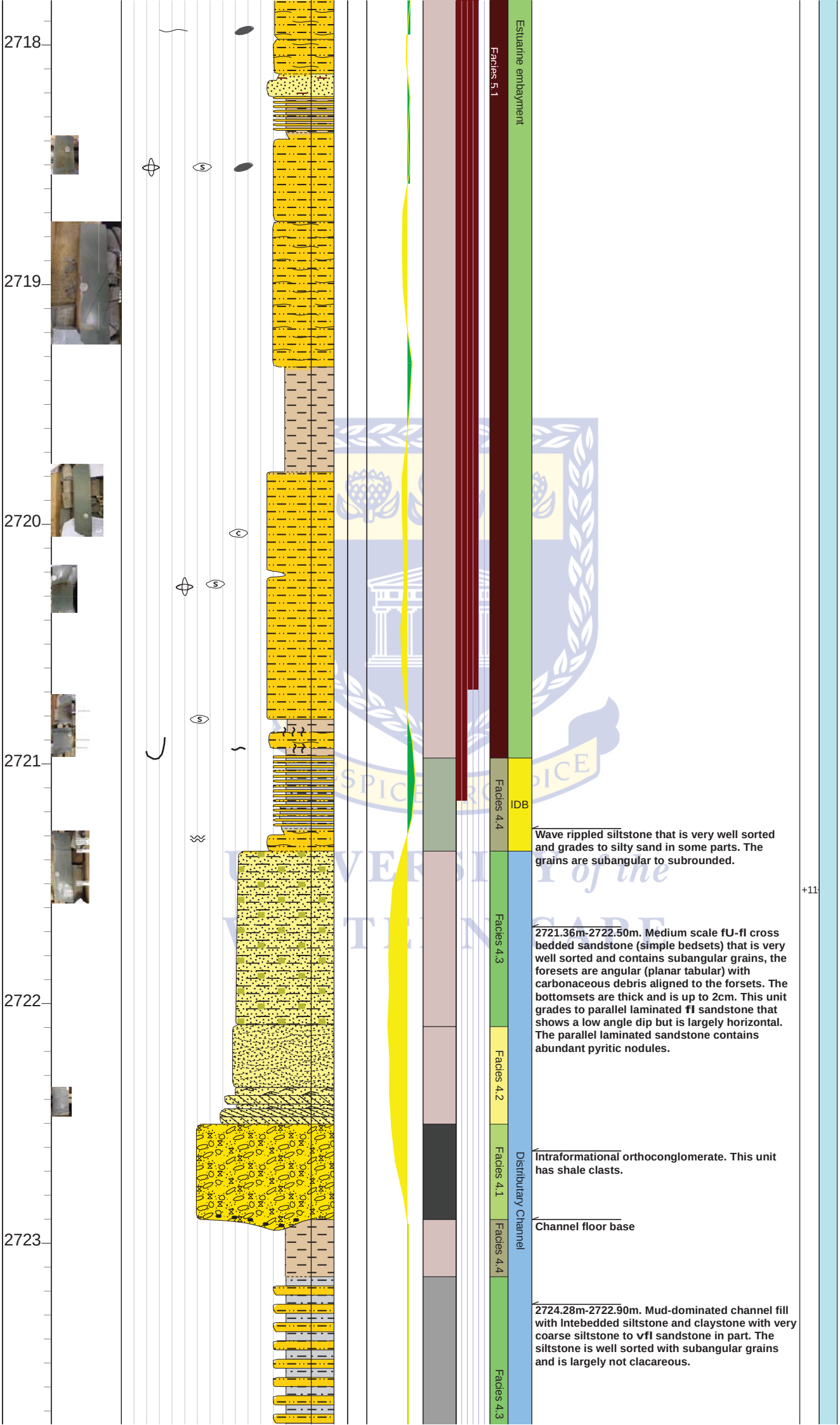
2718
2719
2720
2721
2722
2723
Estuarine embayment
Facies 5.1
Facies 4.4
IDB
Facies 4.3
Facies 4.2
Facies 4.1
Facies 4.4
Facies 4.3
Distributary Channel
+11
Wave rippled siltstone that is very well sorted and grades to silty sand in some parts. The grains are subangular to subrounded.
2721.36m-2722.50m. Medium scale fU-fl cross bedded sandstone (simple bedsets) that is very well sorted and contains subangular grains, the foresets are angular (planar tabular) with carbonaceous debris aligned to the forsets. The bottomsets are thick and is up to 2cm. This unit grades to parallel laminated fl sandstone that shows a low angle dip but is largely horizontal. The parallel laminated sandstone contains abundant pyritic nodules.
Intraformational orthoconglomerate. This unit has shale clasts.
Channel floor base
2724.28m-2722.90m. Mud-dominated channel fill with Intebedded siltstone and claystone with very coarse siltstone to vfl sandstone in part. The siltstone is well sorted with subangular grains and is largely not clacareous.

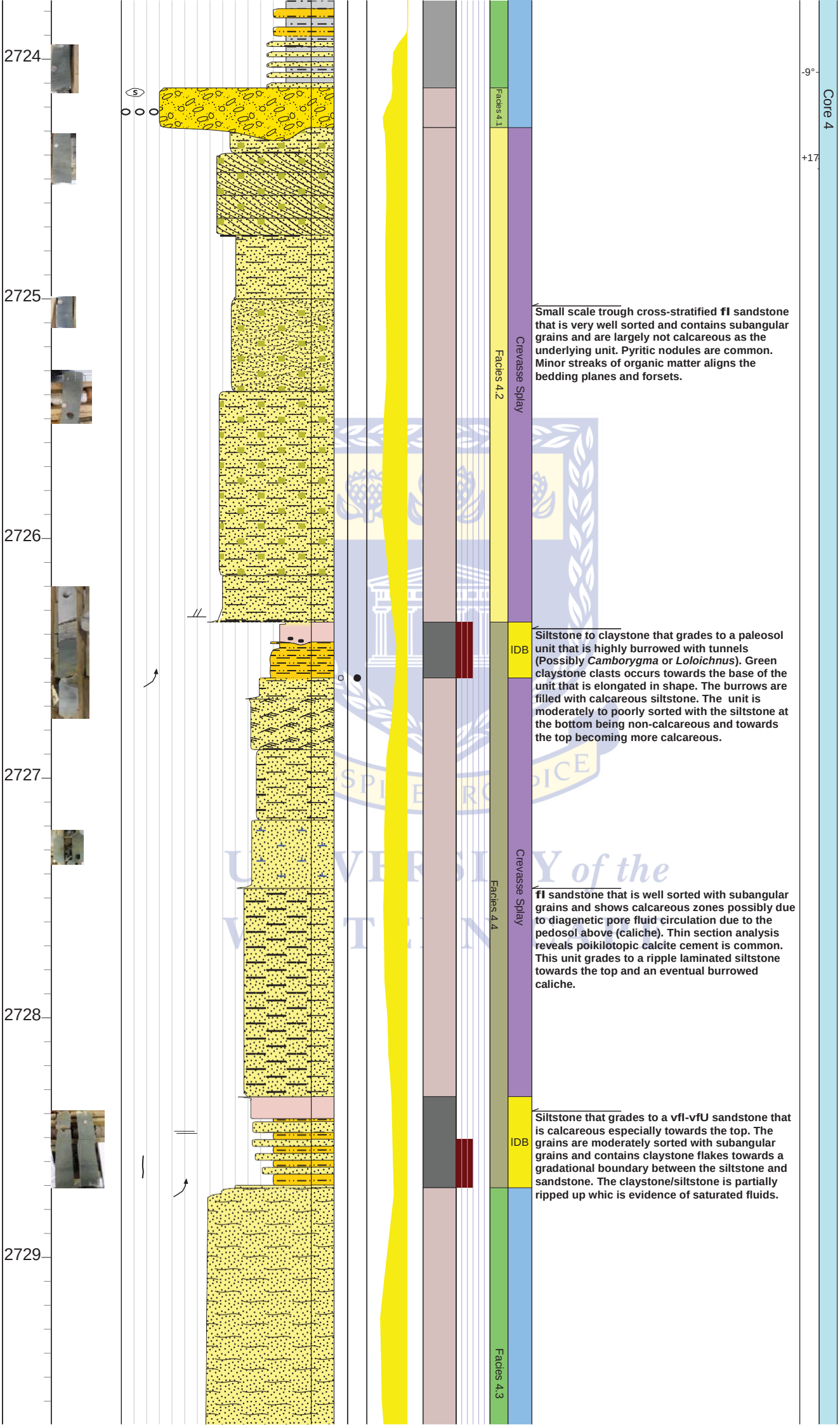
2724
2725
2726
2727
2728
2729
Facies 4.1
Facies 4.2
Facies 4.4
Facies 4.3
Crevasse Splay
Crevasse Splay
IDB
IDB
-9°
+17
Core 4
Small scale trough cross-stratified fl sandstone that is very well sorted and contains subangular grains and are largely not calcareous as the underlying unit. Pyritic nodules are common. Minor streaks of organic matter aligns the bedding planes and forsets.
Siltstone to claystone that grades to a paleosol unit that is highly burrowed with tunnels (Possibly Camborygma or Loloichnus). Green claystone clasts occurs towards the base of the unit that is elongated in shape. The burrows are filled with calcareous siltstone. The unit is moderately to poorly sorted with the siltstone at the bottom being non-calcareous and towards the top becoming more calcareous.
fl sandstone that is well sorted with subangular grains and shows calcareous zones possibly due to diagenetic pore fluid circulation due to the pedosol above (caliche). Thin section analysis reveals poikilotopic calcite cement is common. This unit grades to a ripple laminated siltstone towards the top and an eventual burrowed caliche.
Siltstone that grades to a vfl-vfU sandstone that is calcareous especially towards the top. The grains are moderately sorted with subangular grains and contains claystone flakes towards a gradational boundary between the siltstone and sandstone. The claystone/siltstone is partially ripped up whic is evidence of saturated fluids.

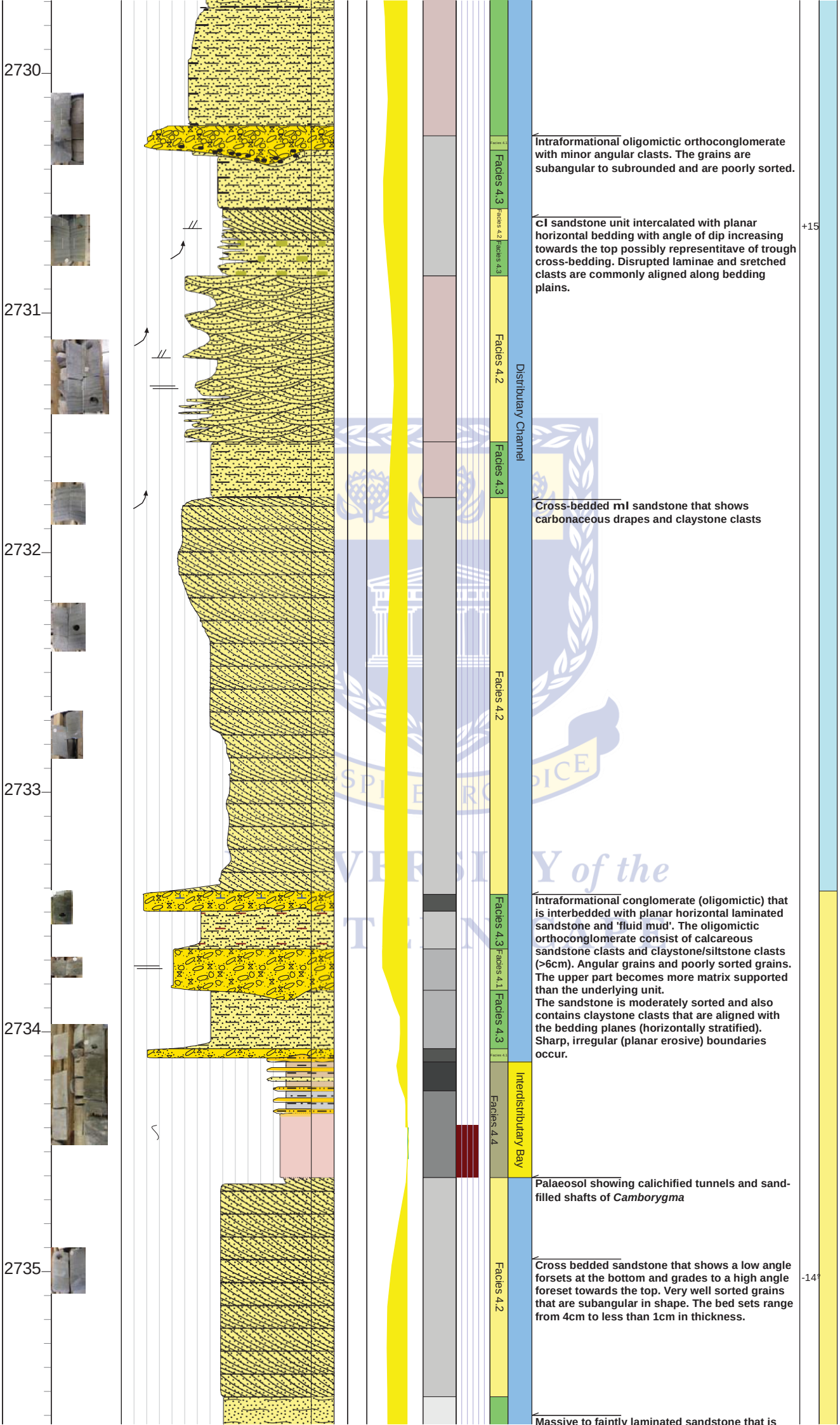
2730
2731
2732
2733
2734
2735
Facies 4.3
Facies 4.2
Facies 4.3
Facies 4.2
Facies 4.3
Facies 4.2
Facies 4.3
Facies 4.1
Facies 4.3
Facies 4.4
Facies 4.2
Distributary Channel
Interdistributary Bay
+15
-14
Intraformational oligomictic orthoconglomerate with minor angular clasts. The grains are subangular to subrounded and are poorly sorted.
cl sandstone unit intercalated with planar horizontal bedding with angle of dip increasing towards the top possibly representitave of trough cross-bedding. Disrupted laminae and sretched clasts are commonly aligned along bedding plains.
Cross-bedded ml sandstone that shows carbonaceous drapes and claystone clasts
Intraformational conglomerate (oligomictic) that is interbedded with planar horizontal laminated sandstone and 'fluid mud'. The oligomictic orthoconglomerate consist of calcareous sandstone clasts and claystone/siltstone clasts (>6cm). Angular grains and poorly sorted grains. The upper part becomes more matrix supported than the underlying unit.
The sandstone is moderately sorted and also contains claystone clasts that are aligned with the bedding planes (horizontally stratified). Sharp, irregular (planar erosive) boundaries occur.
Palaeosol showing calichified tunnels and sand-filled shafts of *Camborygma*
Cross bedded sandstone that shows a low angle forsets at the bottom and grades to a high angle foreset towards the top. Very well sorted grains that are subangular in shape. The bed sets range from 4cm to less than 1cm in thickness.
Massive to faintly laminated sandstone that is

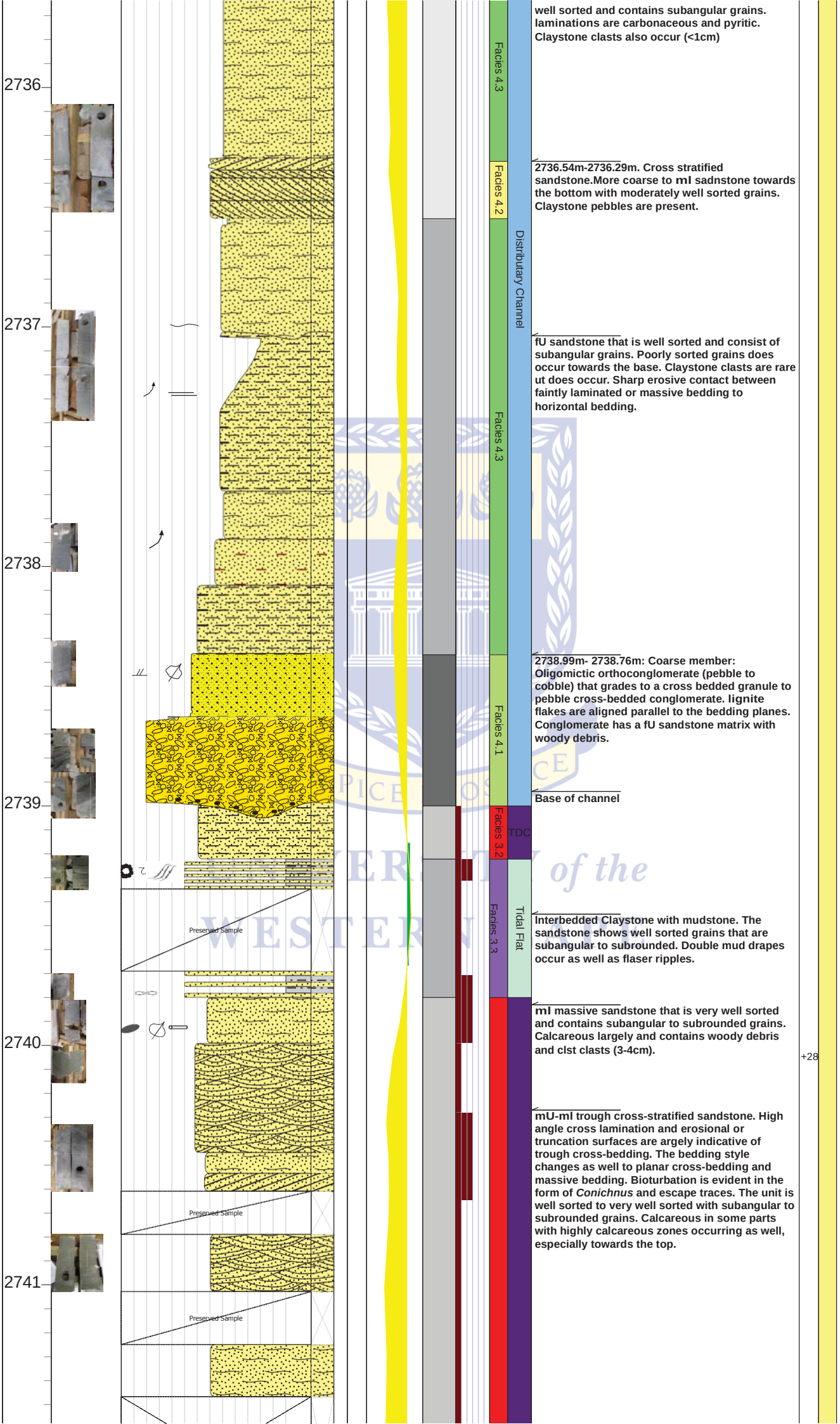

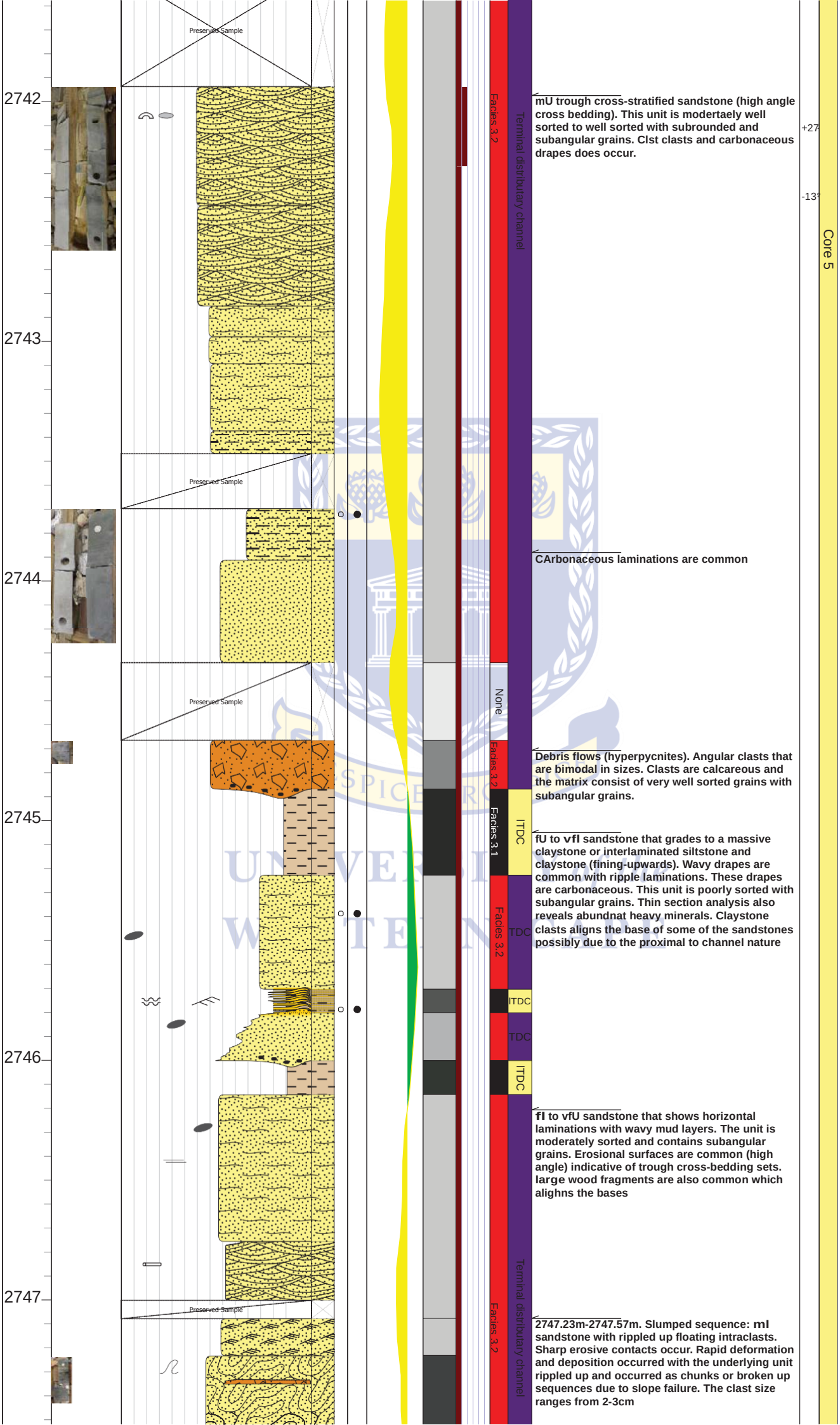

mU trough cross-stratified sandstone (high angle cross bedding). This unit is modertaely well sorted to well sorted with subrounded and subangular grains. Clst clasts and carbonaceous drapes does occur.

CArbonaceous laminations are common

Debris flows (hyperpycnites). Angular clasts that are bimodal in sizes. Clasts are calcareous and the matrix consist of very well sorted grains with subangular grains.

fU to vfl sandstone that grades to a massive claystone or interlaminated siltstone and claystone (fining-upwards). Wavy drapes are common with ripple laminations. These drapes are carbonaceous. This unit is poorly sorted with subangular grains. Thin section analysis also reveals abundnat heavy minerals. Claystone clasts aligns the base of some of the sandstones possibly due to the proximal to channel nature

fl to vfU sandstone that shows horizontal laminations with wavy mud layers. The unit is moderately sorted and contains subangular grains. Erosional surfaces are common (high angle) indicative of trough cross-bedding sets. large wood fragments are also common which alighns the bases

2747.23m-2747.57m. Slumped sequence: ml sandstone with rippled up floating intraclasts. Sharp erosive contacts occur. Rapid deformation and deposition occurred with the underlying unit rippled up and occurred as chunks or broken up sequences due to slope failure. The clast size ranges from 2-3cm

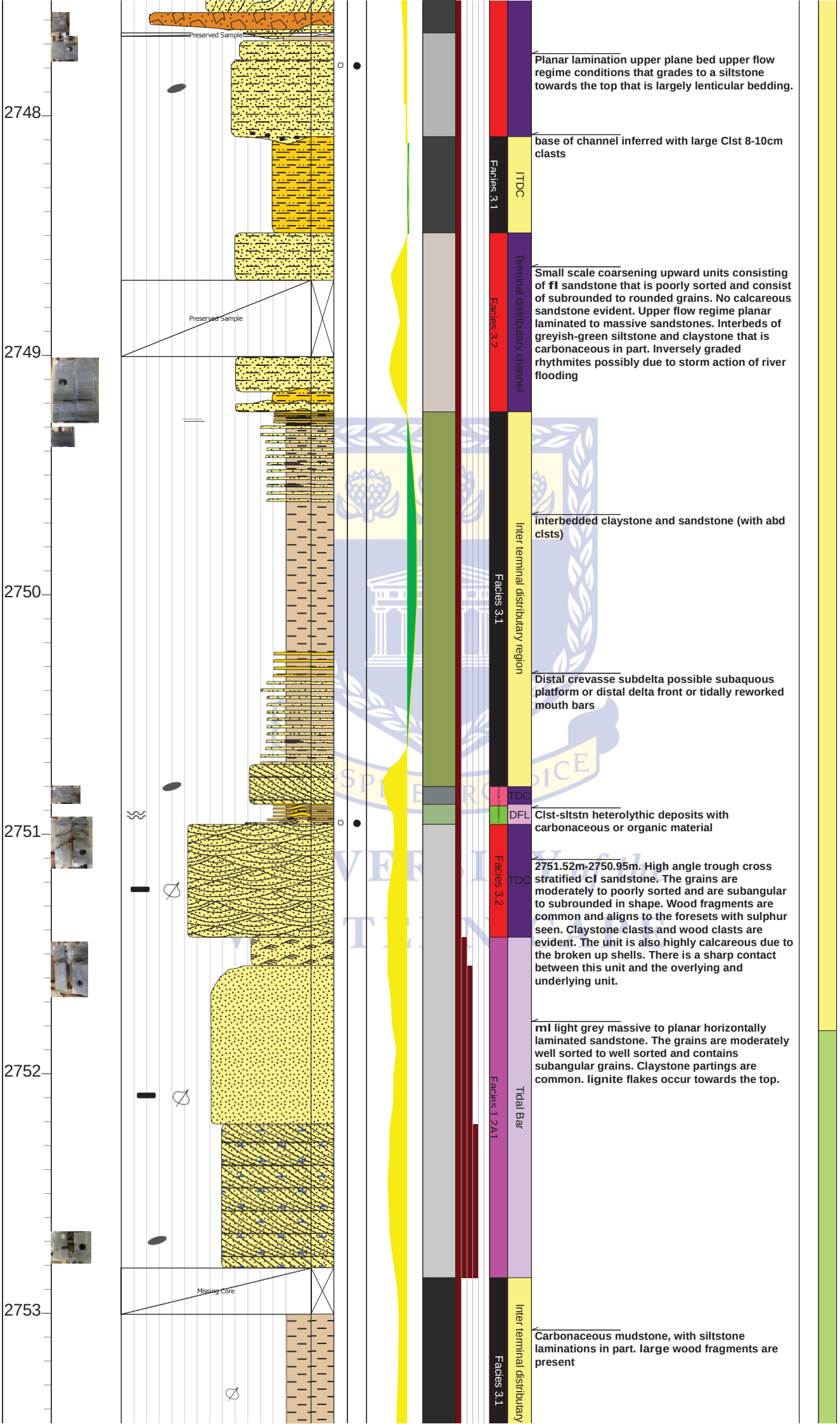
2748
2749
2750
2751
2752
2753
Preserved Sample
Preserved Sample
Missing Core
Facies 3.1
ITDC
Facies 3.2
Terminal distributary channel
Facies 3.1
Inter terminal distributary region
TDC
DFL
Facies 3.2
TDC
Facies 1 2A1
Tidal Bar
Facies 3.1
Inter terminal distributary
Planar lamination upper plane bed upper flow regime conditions that grades to a siltstone towards the top that is largely lenticular bedding.
base of channel inferred with large Clst 8-10cm clasts
Small scale coarsening upward units consisting of fl sandstone that is poorly sorted and consist of subrounded to rounded grains. No calcareous sandstone evident. Upper flow regime planar laminated to massive sandstones. Interbeds of greyish-green siltstone and claystone that is carbonaceous in part. Inversely graded rhythmites possibly due to storm action of river flooding
interbedded claystone and sandstone (with abd clsts)
Distal crevasse subdelta possible subaquous platform or distal delta front or tidally reworked mouth bars
Clst-sltstn heterolythic deposits with carbonaceous or organic material
2751.52m-2750.95m. High angle trough cross stratified cl sandstone. The grains are moderately to poorly sorted and are subangular to subrounded in shape. Wood fragments are common and aligns to the foresets with sulphur seen. Claystone clasts and wood clasts are evident. The unit is also highly calcareous due to the broken up shells. There is a sharp contact between this unit and the overlying and underlying unit.
ml light grey massive to planar horizontally laminated sandstone. The grains are moderately well sorted to well sorted and contains subangular grains. Claystone partings are common. lignite flakes occur towards the top.
Carbonaceous mudstone, with siltstone laminations in part. large wood fragments are present

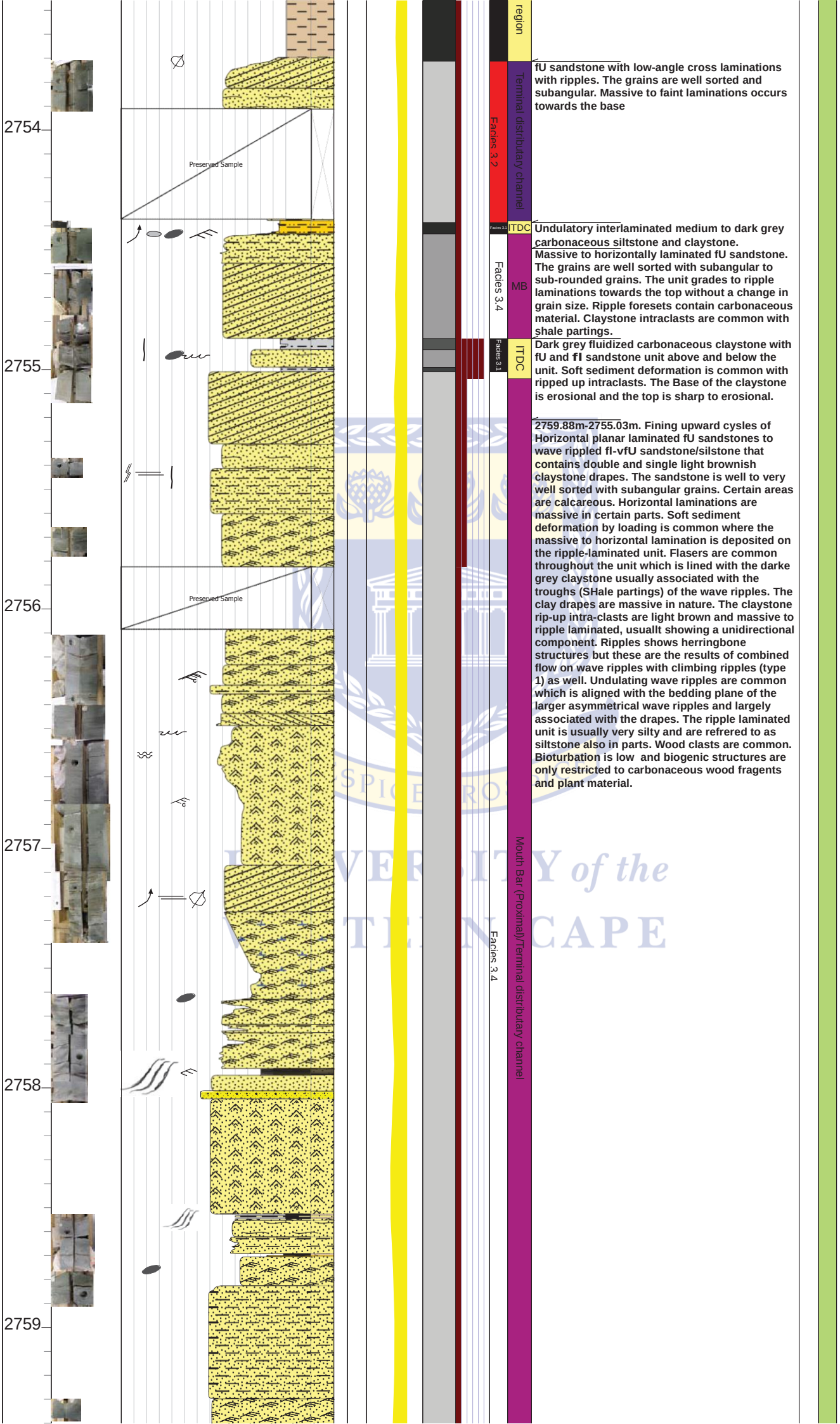

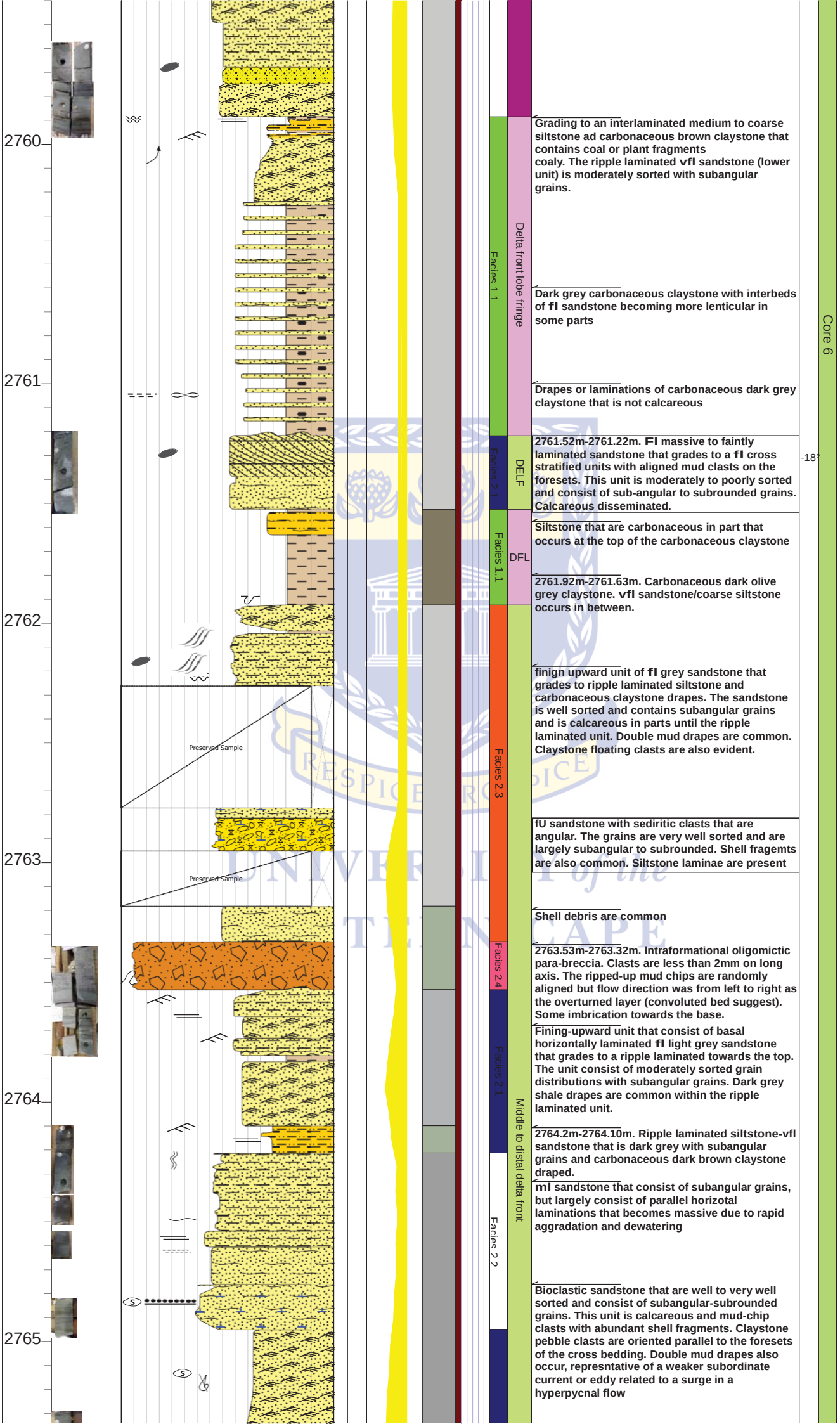

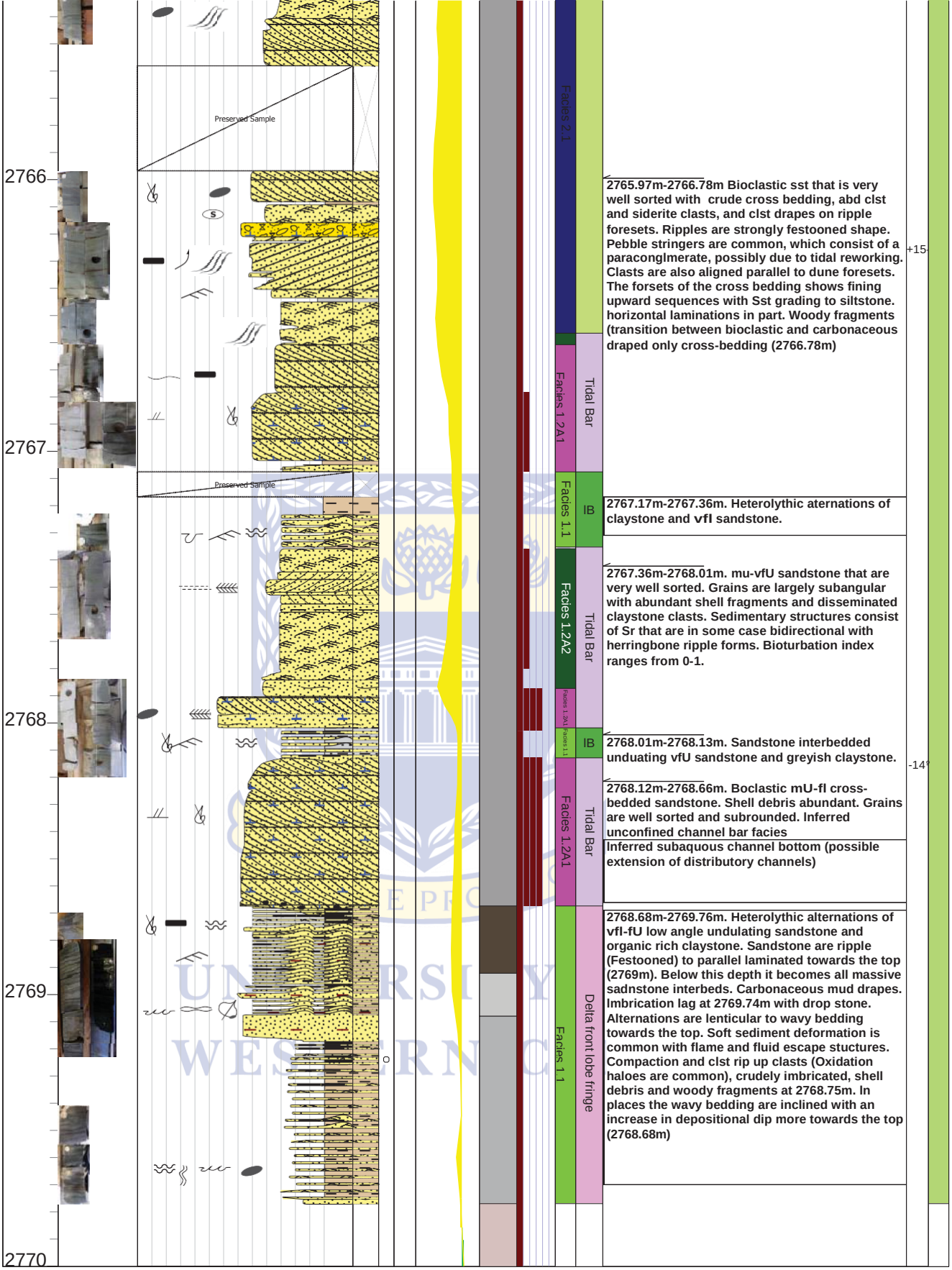
2766
2767
2768
2769
2770
Preserved Sample
Preserved Sample
Facies 2.1
Facies 1.2A1
Tidal Bar
Facies 1.1
IB
Facies 1.2A2
Tidal Bar
IB
Facies 1.2A1
Tidal Bar
Facies 1.1
Delta front lobe fringe
2765.97m-2766.78m Bioclastic sst that is very well sorted with crude cross bedding, abd clst and siderite clasts, and clst drapes on ripple foresets. Ripples are strongly festooned shape. Pebble stringers are common, which consist of a paraconglmerate, possibly due to tidal reworking. Clasts are also aligned parallel to dune foresets. The forsets of the cross bedding shows fining upward sequences with Sst grading to siltstone. horizontal laminations in part. Woody fragments (transition between bioclastic and carbonaceous draped only cross-bedding (2766.78m)
+15
2767.17m-2767.36m. Heterolythic aternations of claystone and vfl sandstone.
2767.36m-2768.01m. mu-vfU sandstone that are very well sorted. Grains are largely subangular with abundant shell fragments and disseminated claystone clasts. Sedimentary structures consist of Sr that are in some case bidirectional with herringbone ripple forms. Bioturbation index ranges from 0-1.
2768.01m-2768.13m. Sandstone interbedded unduating vfU sandstone and greyish claystone.
-14
2768.12m-2768.66m. Boclastic mU-fl cross-bedded sandstone. Shell debris abundant. Grains are well sorted and subrounded. Inferred unconfined channel bar facies
Inferred subaquous channel bottom (possible extension of distributory channels)
2768.68m-2769.76m. Heterolythic alternations of vfl-fU low angle undulating sandstone and organic rich claystone. Sandstone are ripple (Festooned) to parallel laminated towards the top (2769m). Below this depth it becomes all massive sadnstone interbeds. Carbonaceous mud drapes. Imbrication lag at 2769.74m with drop stone. Alternations are lenticular to wavy bedding towards the top. Soft sediment deformation is common with flame and fluid escape stuctures. Compaction and clst rip up clasts (Oxidation haloes are common), crudely imbricated, shell debris and woody fragments at 2768.75m. In places the wavy bedding are inclined with an increase in depositional dip more towards the top (2768.68m)

Operator	EasyCore
Petroleum Agency South Africa	

Top 2684 m	Bottom: 2732.6 m
Depth scale: 1 : 10cm	Country: South Africa
Well Name & No.: F-A5	Location: 90km South of Mossel Bay, offshore
Logged by: Mogammad	Lease: Southern Offshore, Block F
Basin: Bredasdorp sub-basin	
Field: FA Gas Fields	KB: 30 m
Latitude: 34° 59' 01.12" S	Longitude: 22° 11' 01.02" E

Lithologies

Breccia
Claystone
Mudstone
Pebbly Sandstone
Sandstone
Siltstone

Admixture

Anhydritic
Argillaceous
Calcareous
Glauconitic
Organic
Pyritic
Sandy

Structure

Cross Laminated
Faintly Laminated
Hummocky
Low-angle Planar Laminated
Planar Cross-bedded
Planar Laminated
Ripple Laminated
Slumped
Trough Cross-bedded
Wave Ripple Laminated

Support

Matrix Supported

Contacts

Erosional Lag
Gradational
Scoured
Straight
Undulating

Accessories

Cemented Fractures
Coal
Open Fractures
Pebbles
Pyrite Nodules
Shale Clasts
Siderite Nodules
Synsedimentary Microfaults

Fossils

Plant Fragments

Sedimentary Structures

- Climbing Ripples
- Flame Structure
- Load Structure
- Parallel Wavy Bedding
- Planar Cross Lamination
- Planar Lamination
- Ripple Lamination
- Slumped Bedding
- Wispy Lamination

Trace Fossils

- Escape Structure
- Macaronichnus
- Nereites
- Paleophycus
- Thalassinoides
- Zoophycos

Facies

- Bioclastic sandstone
- Cross-bedded glauconitic san d
- Grey black claystone
- Heterolythic alternations of vf siltstone and organic-rich mu d
- High angle Ripple-laminated f beds
- Horizontal laminated/bedded sst
- Interbedded Claystone/siltsto n
- Low angle cross-bedded pebbly sandstone
- Massive to planar laminated sandstone
- Mudstone green with calcareou nodules
- None
- Planar laminated vfU sst-siltst t
- Rip-up clast conglomerate
- Sandstone orthoconglomerate
- Wave-rippled bedding
- vfU sst occasional ripped up clasts

Depositional Environment

- DBF Debris Flow
- FS Foreshore
- Outer embayment/ Offshore
- PME Proximal to middle embayme
- SLP Slope
- Suaqueous subtidal platform tidal sand ridges
- SLB Submarine lobe facies
- TRB Turbidite

Zones

- #2 Core #2
- #3 Core #3
- #4 Core #4

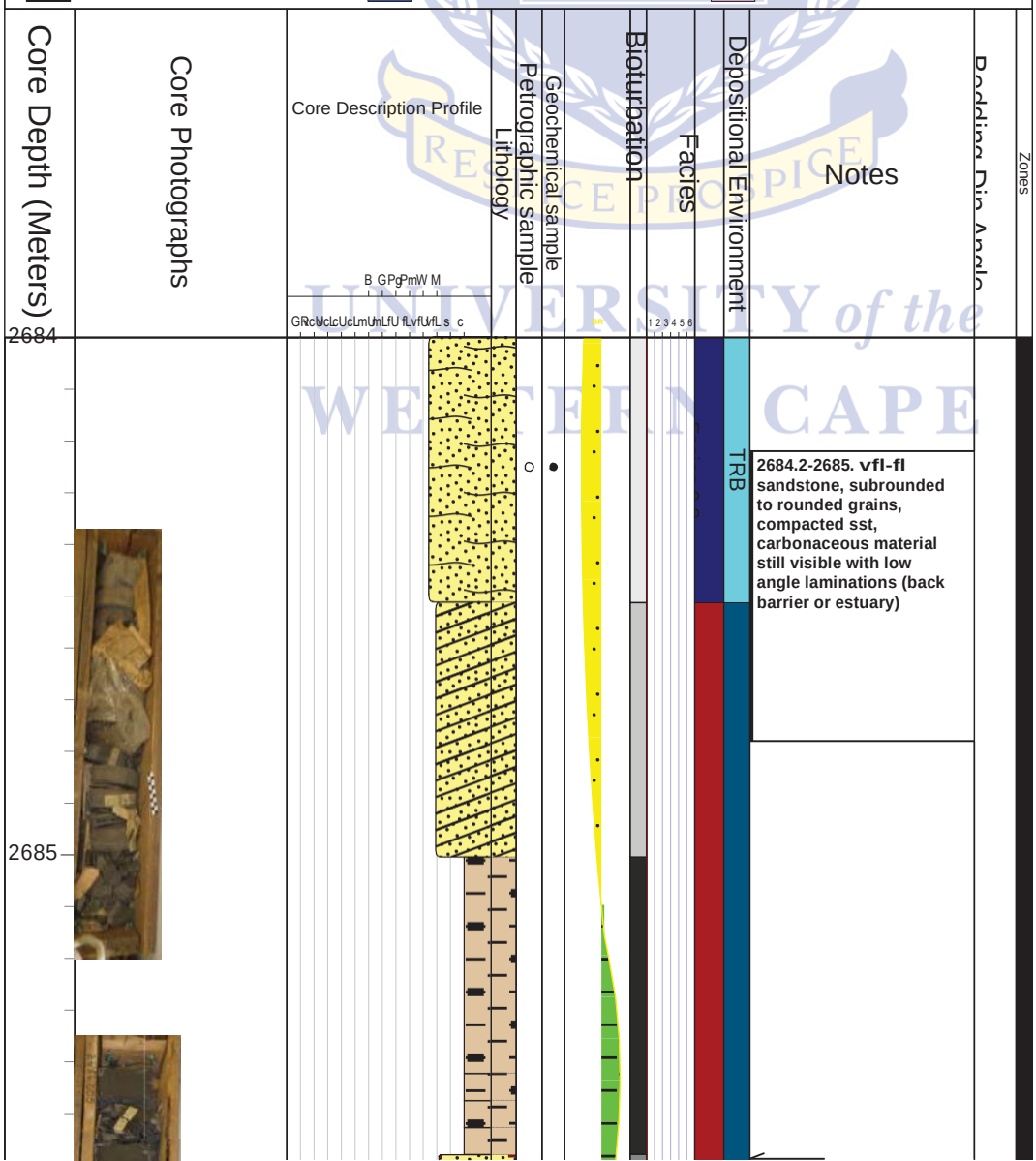

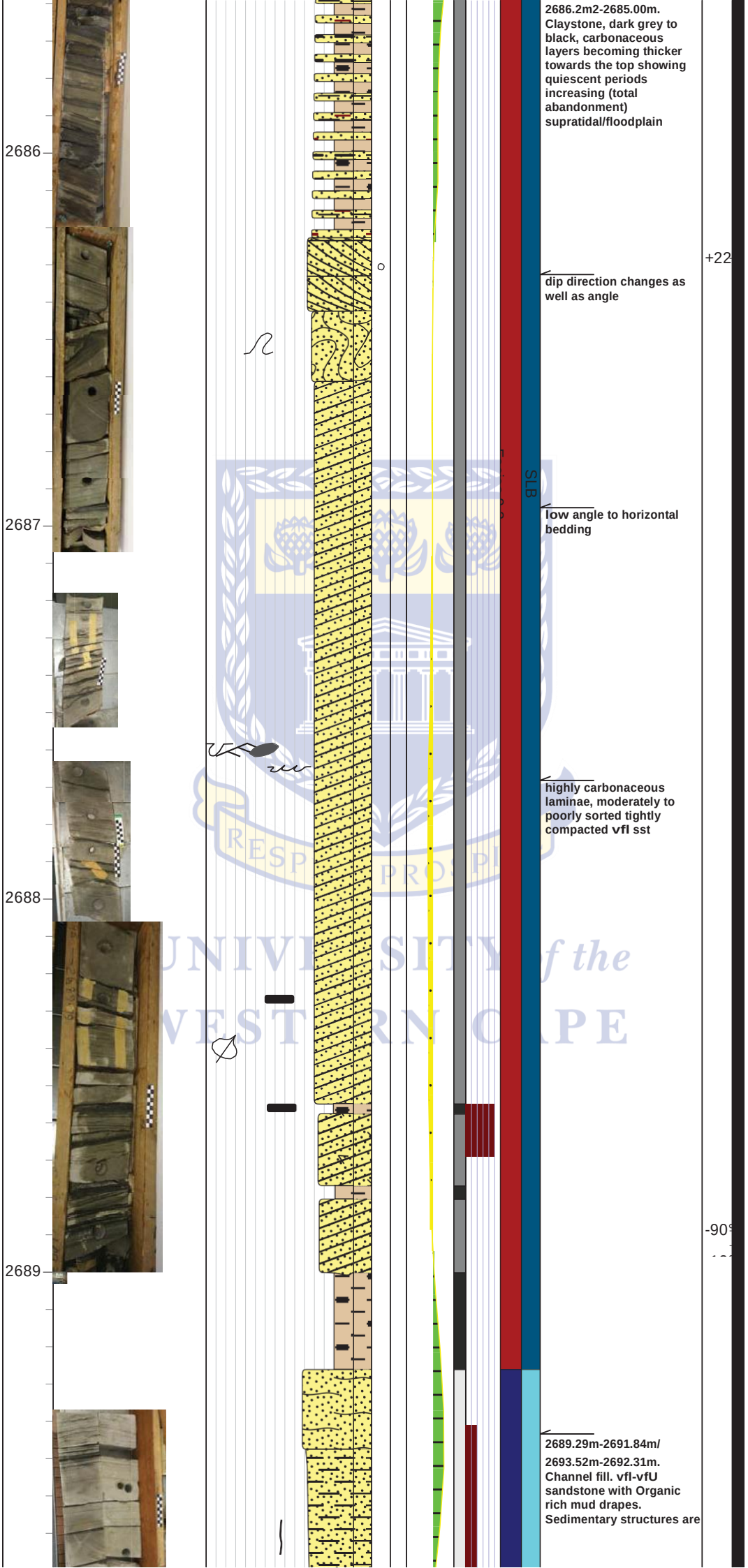

planar laminations and low angle laminations. laminae are idsrupted in some cases, with cross laminations and massive sandstone towards the bottom.

2690

2691

2692

2693

TRB

DBF

2692.3m-2691.85m/ 2693.52m-2694.12m. Channel bottom. Matrix supported, poorly indurated, poorly size-sorted, polymictic, grey breccia dominated by angular clasts and minor equant quartz pebbles (46-62cm thick). Clast shape shows two ranges with intraformational angular claystone clasts and intraformational well-rounded quartz clasts. Angular claystone clast size ranges from 2cm to 5cm and the quartz pebble size ranges from <0.5cm to 1cm. The matrix consist of dark grey vfU sandstone with pebbles. This conglomerate can be classified as a polymictic parabreccia. Forms the base of the channel. Some of the clasts shows relict bedding from ripped-up nature.

TRB

DB

Facies

Core #2

+15

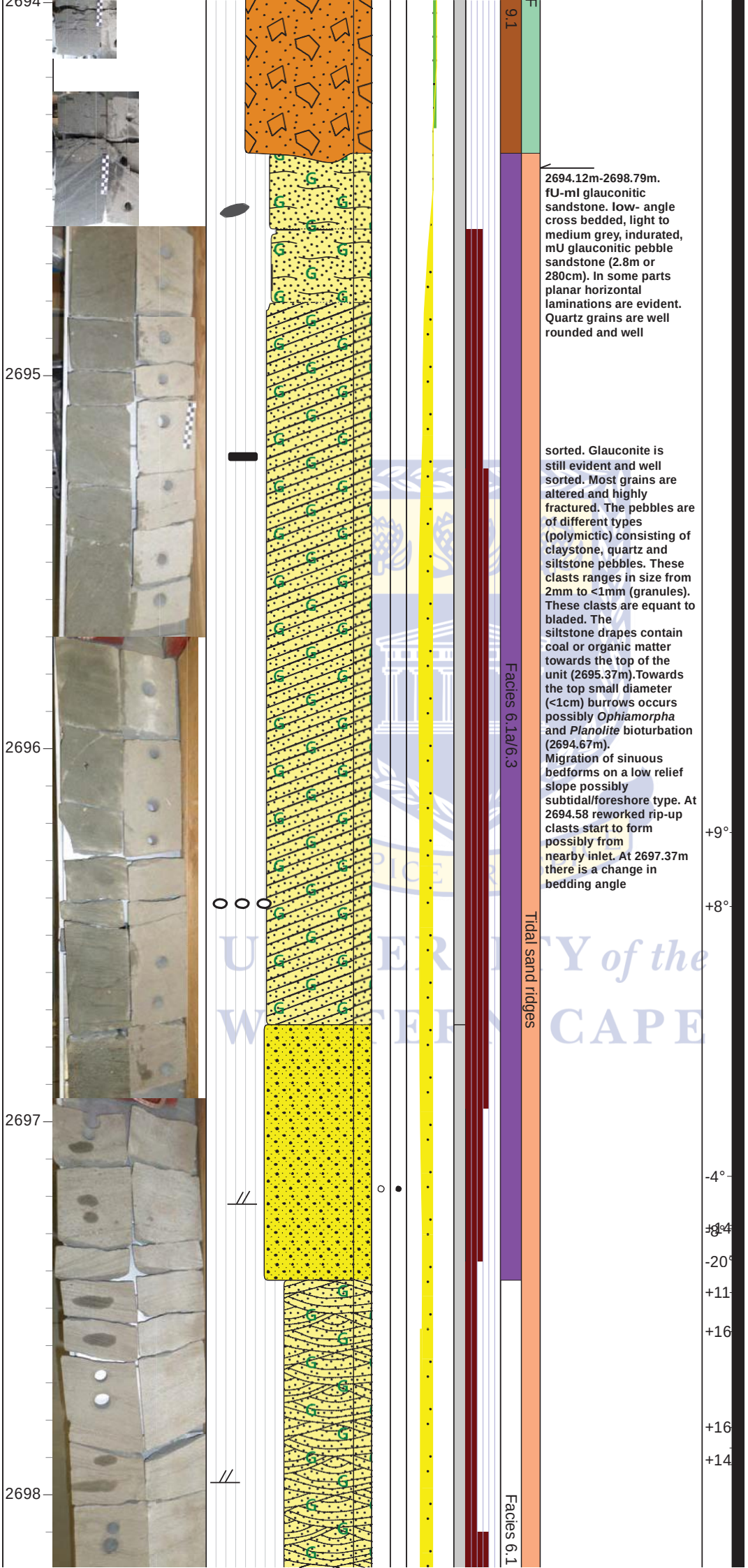

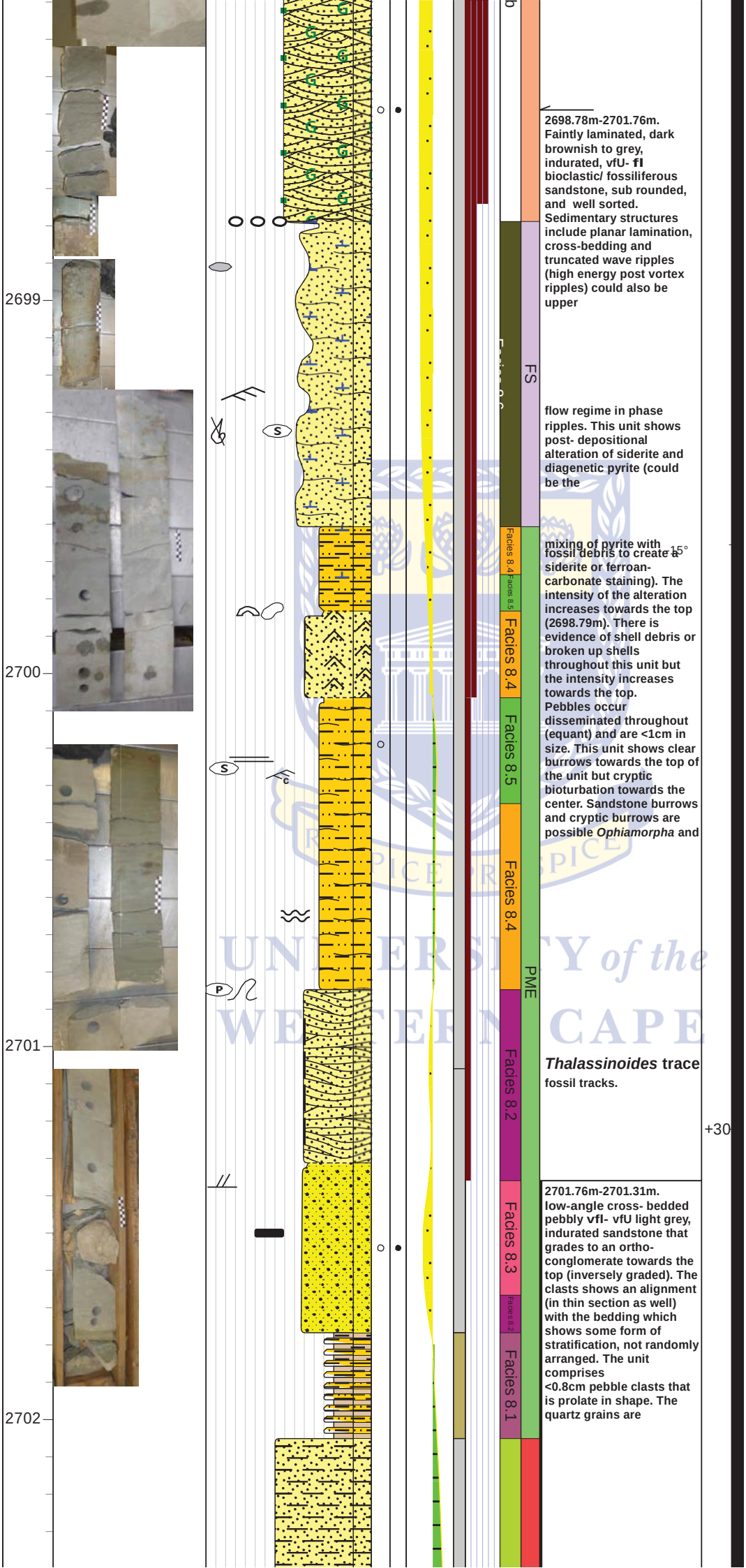

2698.78m-2701.76m. Faintly laminated, dark brownish to grey, indurated, vfU- **fl** bioclastic/ fossiliferous sandstone, sub rounded, and well sorted. Sedimentary structures include planar lamination, cross-bedding and truncated wave ripples (high energy post vortex ripples) could also be upper

flow regime in phase ripples. This unit shows post- depositional alteration of siderite and diagenetic pyrite (could be the

mixing of pyrite with fossil debris to create a siderite or ferroan-carbonate staining). The intensity of the alteration increases towards the top (2698.79m). There is evidence of shell debris or broken up shells throughout this unit but the intensity increases towards the top. Pebbles occur disseminated throughout (equant) and are <1cm in size. This unit shows clear burrows towards the top of the unit but cryptic bioturbation towards the center. Sandstone burrows and cryptic burrows are possible *Ophiamorpha* and

***Thalassinoides* trace** fossil tracks.

2701.76m-2701.31m. **low-angle cross- bedded pebbly vfl- vfU light grey, indurated sandstone that grades to an ortho-conglomerate towards the top (inversely graded). The clasts shows an alignment (in thin section as well) with the bedding which shows some form of stratification, not randomly arranged. The unit comprises <0.8cm pebble clasts that is prolate in shape. The quartz grains are**

2703

2704

2705

2706

Facies 7.4

moderately well sorted and shows rounded grains, with altered feldspars. The distribution in some parts are bimodal. Porosity is fair to poor. Pyrite occurs as disseminated patches.

Facies 7.2

2702.04m-2701.76m. Interbedded Claystone and coarse siltstone. The dark olive green claystone is massive and fissile ip with faint laminations. The light to medium grey siltstone shows parallel laminations and are largely gradational with the claystone.

Facies 7.3

2703.78m-2702.06m. mI-fU, light grey-medium grey sandstone that shows pebbles or ripped up clasts towards the bottom at 2703.78m. These clasts are green in colour. This unit is largely erosive at the base

Facies 7.2

2703.78m-2705.39m. vfU-fU cross bedded sandstone unit that shows an erosive base with deformation structures (flame structures)

Mud flasers or clasts stretched (2704.83m) and in- phase climbing ripples on high angle cross-bedding (2705m)

Ripple interlaminated cross-beds with erosional lag towards the bottom

Facies 7.2

2705.37m-2707.68m. Massive vfI-fU sandstone unit. Faint cross laminations are evident. light grey to white in colour, comprised of subrounded- subangular grains that are tightly packed and moderately well sorted (porosity low). Fractured units are common with syn-sedimentary faults. Disseminated clasts are present.

The contact between the underlying mudstone and this sandstone unit is a

SLP

-90°

+27

+30

+32

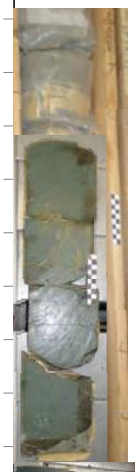

2707

2708

2709

2710

sharp undulatory contact with injected mud or ripped up clasts. The sandstone shows a coarsening upward trend of **vfl** sandstone at the base to a fU sandstone towards the top of the unit.

There is no evidence of any trace fossils. Claystone injected fractures occurring within this unit. . The clasytone injections is olive green in colour.

2707.69m-2732.36m. Interbedded

Siltstone- Claystone. Claystone, dark greyish to reddish- brown but occurs in part as dark green/ grey claystone (thin section analysis), hard, comprising sub-angular to angular silt-sized grains (mostly quartz). Bioturbation is absent. No visual evidence of carbonaceous material. No evidence of marine or terrestrial fossils or trace fossils
seen. Mudstone with medium dark olive green, hard, comprising silt- sized fraction that are poorly sorted (bimodal grain size) and has subangular-angular quartz grains. No evidence of trace fossils marine or terrestrial. The clay matrix consist mainly of clay minerals such as smectite-illite.
Thin section analysis revealed an iron-rich calcite.
Sideritic staining, as well as nodules are common from 2724.17m and occurs in fractures as well. Pyrite staining and

nodules occurring at

Facies 7.1

Facies 5.1b

Core #3

S

P

S

P

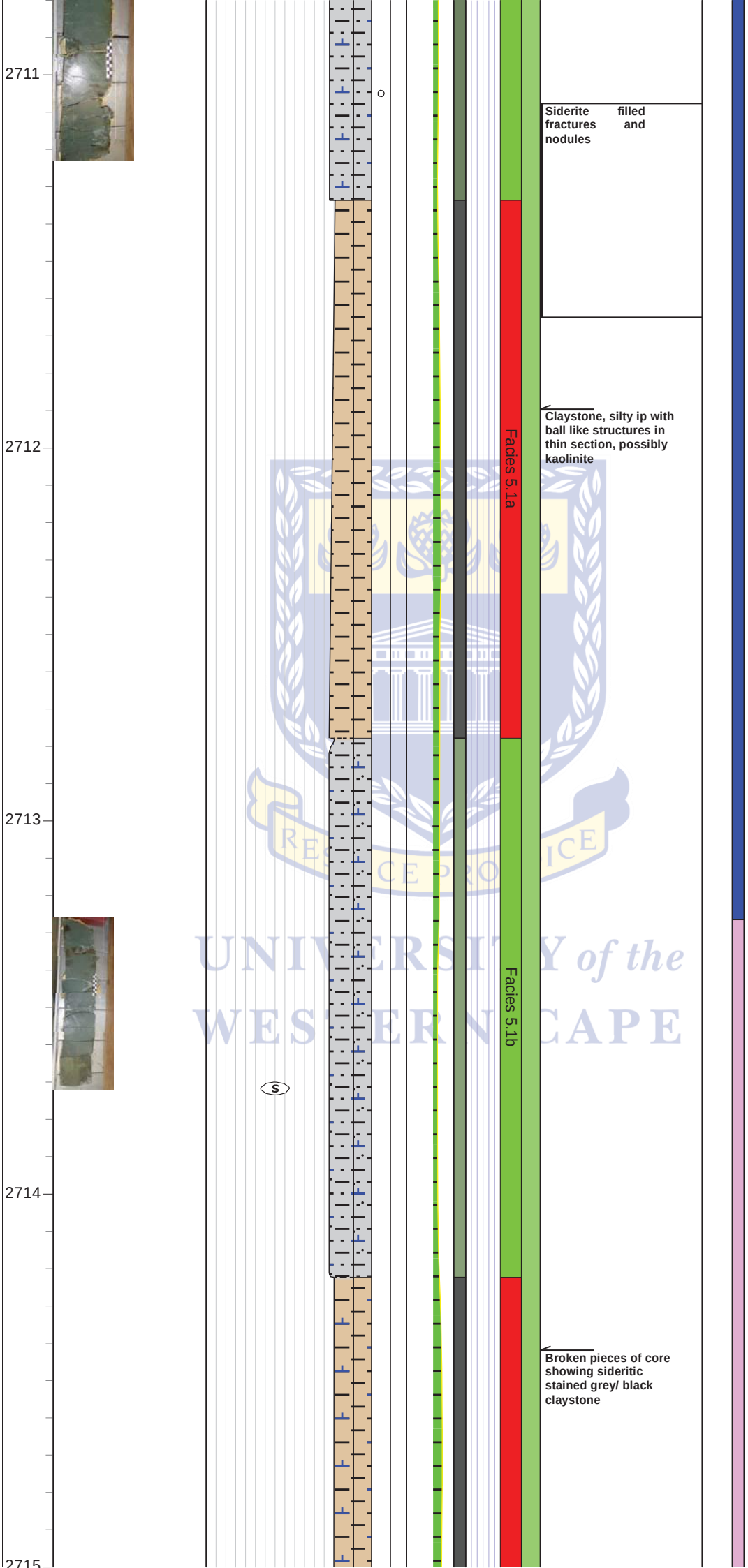

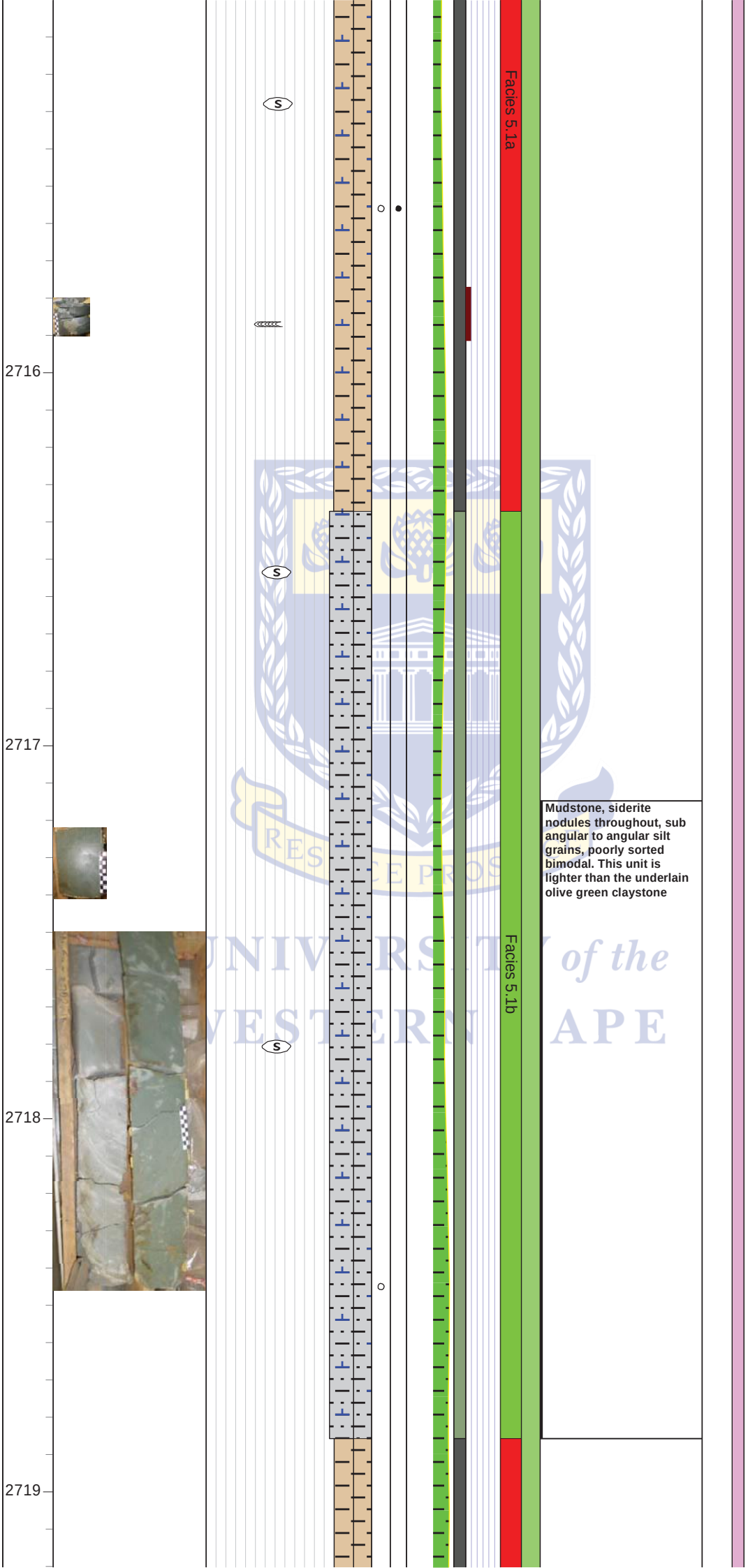

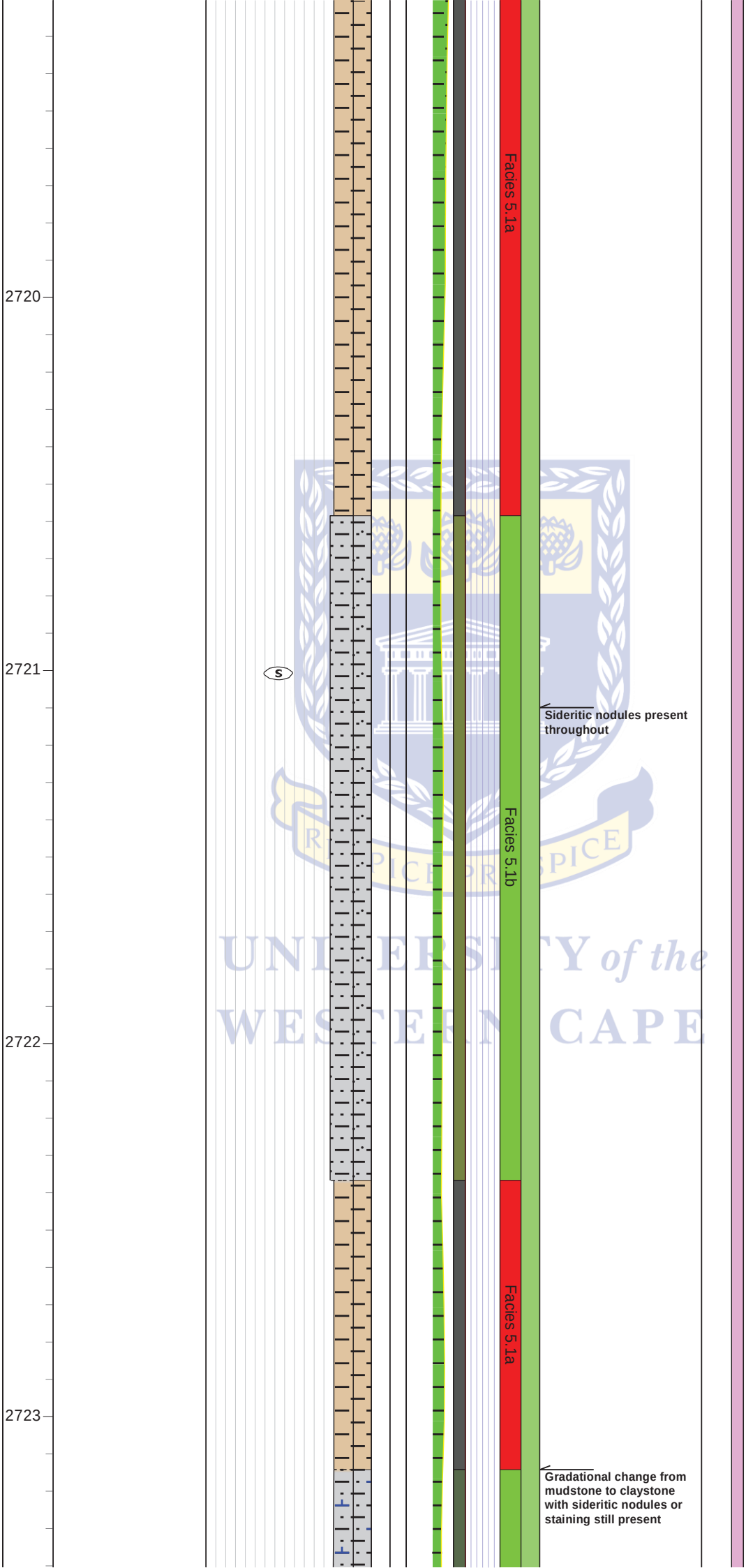

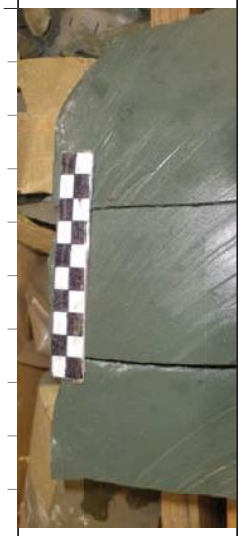

2724

2725

2726

2727

S

Facies 5.1b

Dark olive green mudstone with sideritic nodules starting at 2724.17m

Diagentically altered claystone (dark green-grey), possibly chlorite-smectite-illite clay, that grades to silty claystone towards the top. Silt-sized subangular to subrounded quartz grains showing evidence of a gradational change (microfacies change) from claystone (100% argillaceous) to pure mudstone (50% argillaceous matrix) towards the top

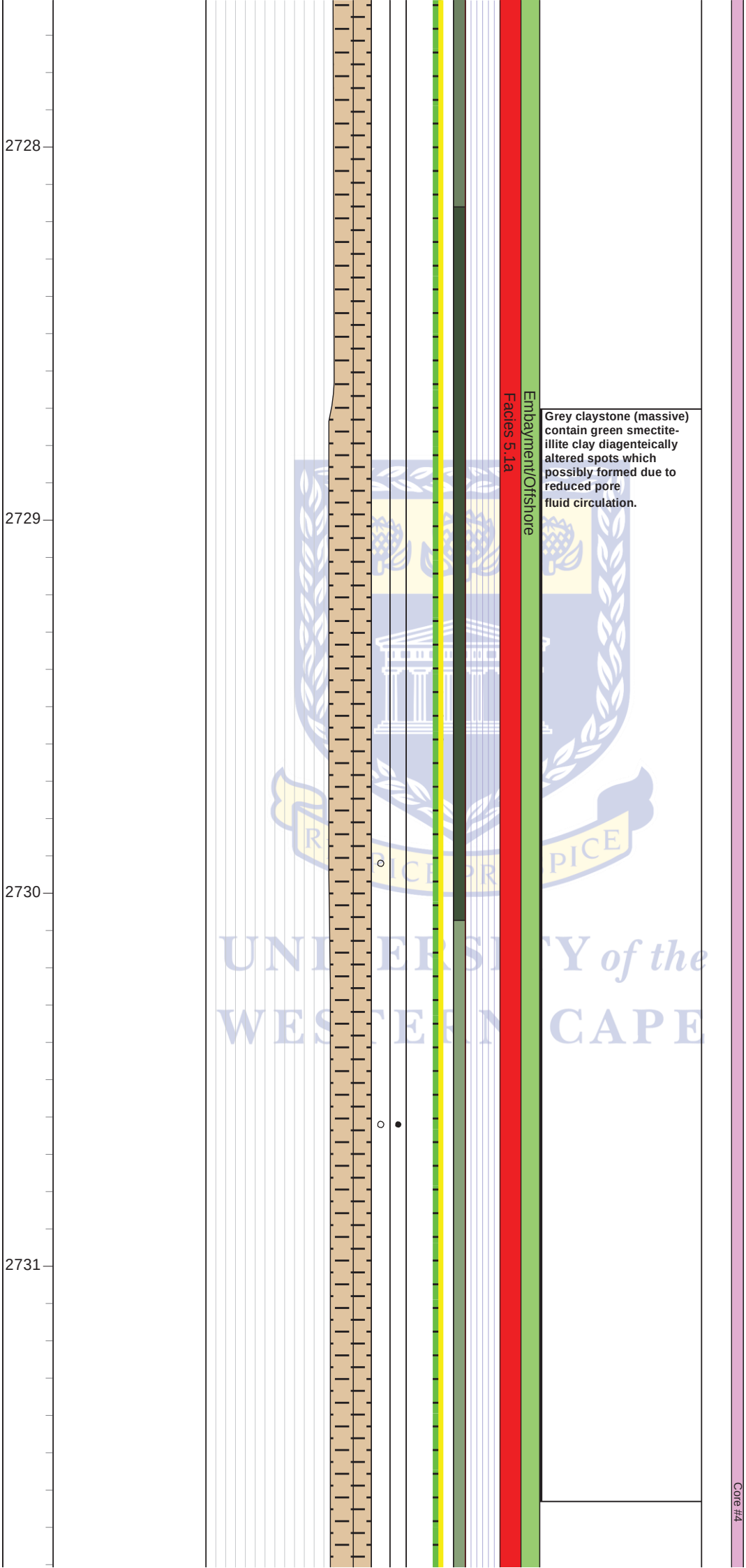

Operator

Petroleum Agency South Africa

EasyCore
The EasyCopy Company

Top: 2694 m	Bottom: 2747 m
Depth Scale: 1 : 10cm	Country: South Africa
Well Name & No.: F-AR1	Location: Offshore South Africa
Logged by: Mogammad	Basin: Bredasdorp sub-basin
Lease: Southern offshore, block F	Field: FA gas fields
KB: 29.9 m	Latitude: 34° 56' 11.9" S
Longitude: 22° 10' 10.2" E	

Lithologies

Mudstone

Pebbly Sandstone

Sandstone

Admixture

Argillaceous

Glauconitic

Organic

Pyritic

Structure

Herringbone

Faintly Laminated

Low-angle Planar Laminated

Planar Cross-bedded

Planar Laminated

Trough Cross-bedded

Contacts

Gradational

Straight

Accessories

Calcite Nodules

Pyrite Nodules

Coal

Py Pyrite

Pebbles

Shale Clasts

Fossils Broken

Mottled Bedding

Parallel Wavy Bedding

Fossils

Planar Lamination

Slumped Bedding

Sedimentary Structures

Wispy Lamination

Herringbone Cross-bedding

Planar Cross Lamination

Trough Cross Lamination

mud drapes with sand

Trace Fossils

Ophiomorpha

Thalassinoides

Vertical Spreiten

Facies

Cross-bedded (bidirectional) fU glauc sandstone

Low-angle to planar bedded pebbly sandstone

Massive to faintly laminated glauco nitic fU-mL sandstone with occasional mud

None None

Depositional Environment

Subaqueous subtidal platform tidal sa

Suspension settling in trough of tidal sand

Zones

#1 Core #1

#2 Core #2

#3 Core #3

M missing

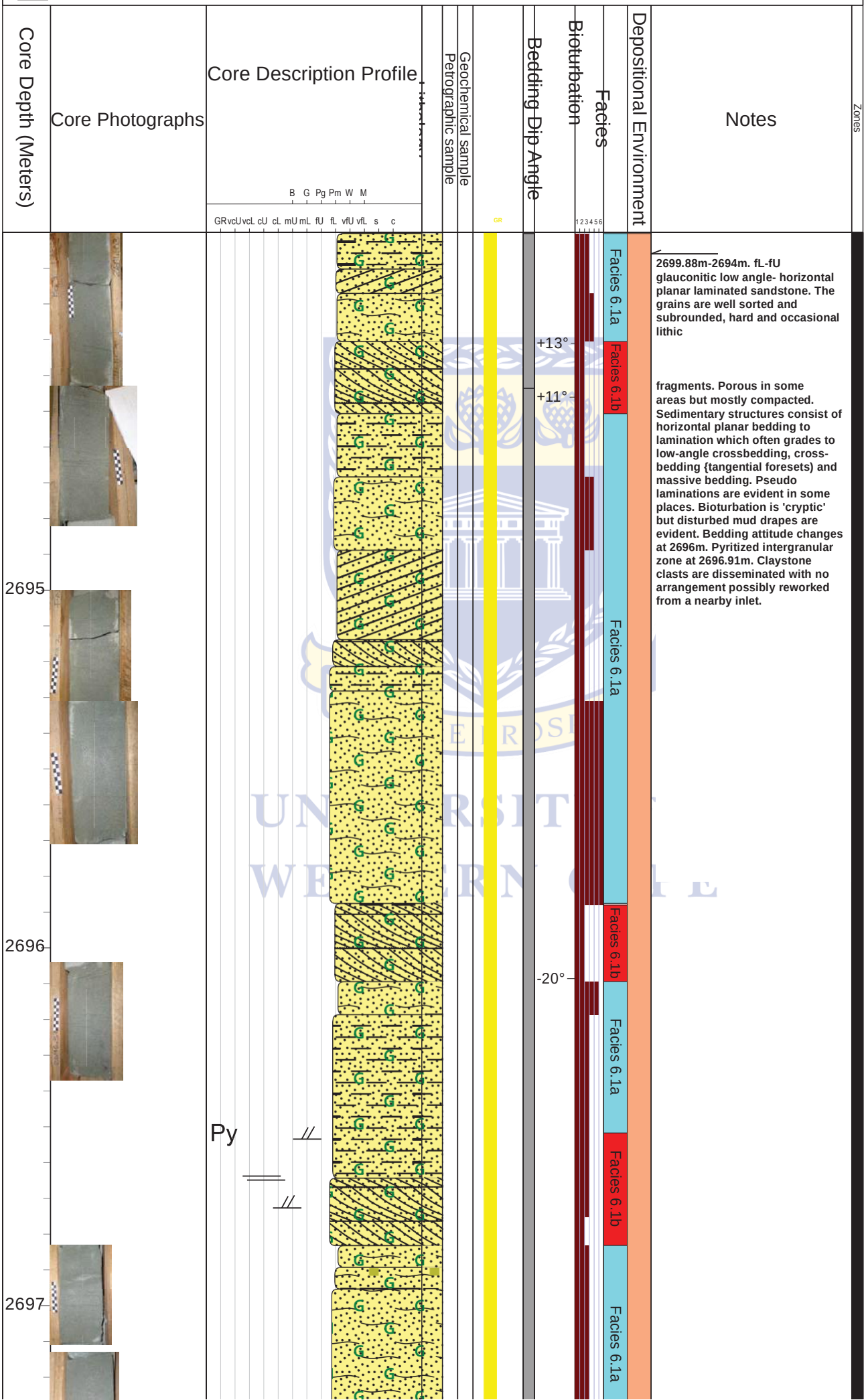

2698

2699

2700

2701

-18°

+8.5°

-12°

-28°

Facies 6.1b

Facies 6.1a

Facies 6.1b

2699,88m-2709.35m. fL bioturbated glauconitic sandstone. grains are

moderately well sorted and rounded to subrounded, highly compacted.
Sedimentary structures include faint horizontal to low angle bedding, cross bedding with changes in bedding angle and direction {2700.83m), herringbone cross bedding {2707.4m) and massive bedding in part, Mud drapes are also common, consisting of single and double mud layers that are partly straight to crinkled.
Disturbed drpaes are also common. Pyrite is common and pyritized zone occurs at 2701.59m. Bioturbation is common with trace fossils of *Ophiomorpha iregulaire* and *Thalassinoides*

{2702.46m, 2702.88m, 2705.49m). Occasional

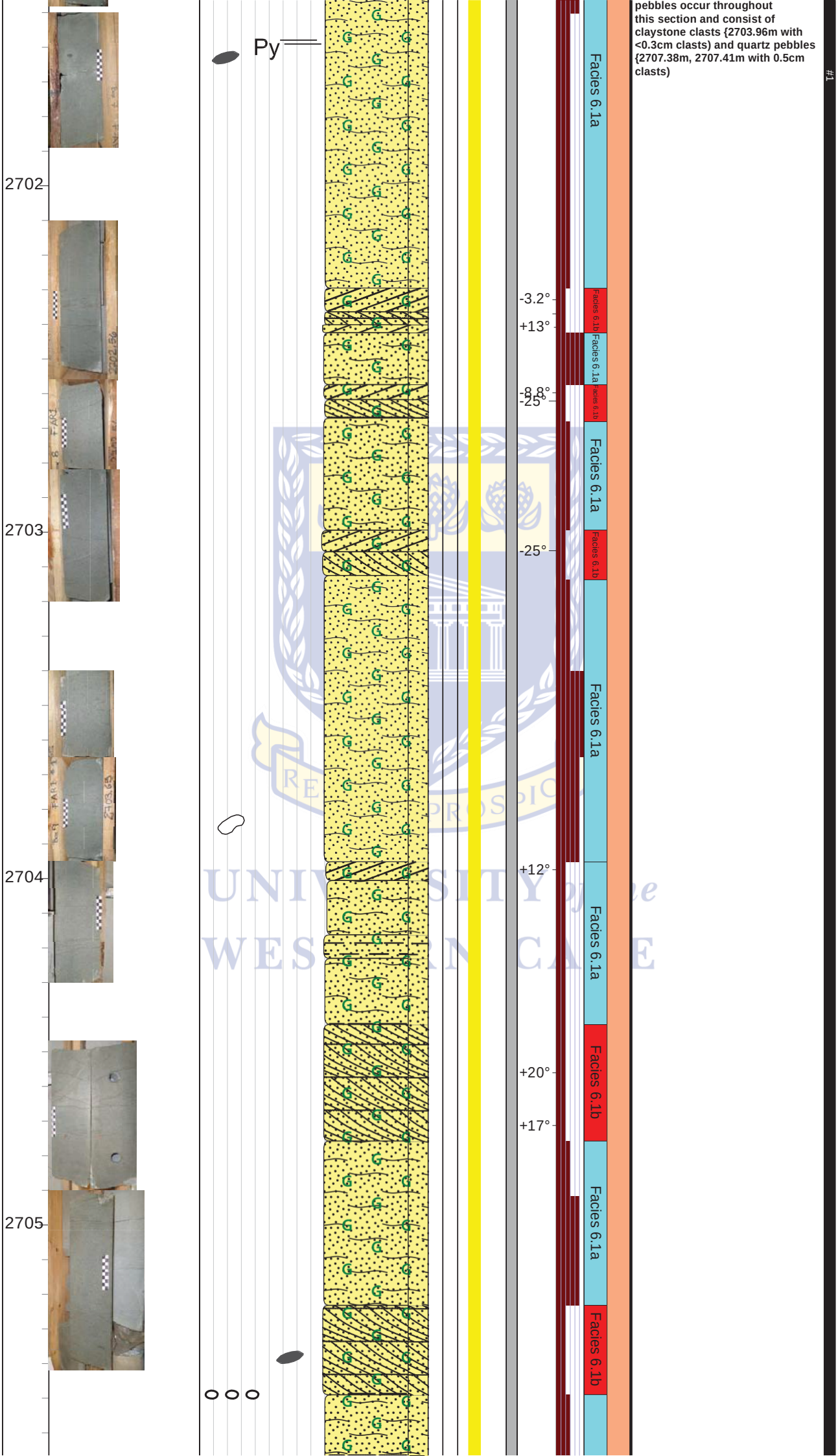

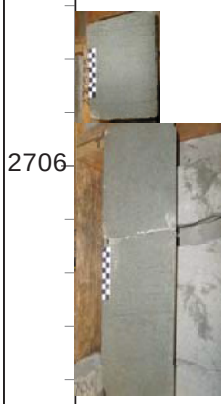

2706

2707

2708

2709

Facies 6.1a

-14°

Facies 6.1a

-20°

Facies 6.1b

+7.9°

+28°

None

Missing Core

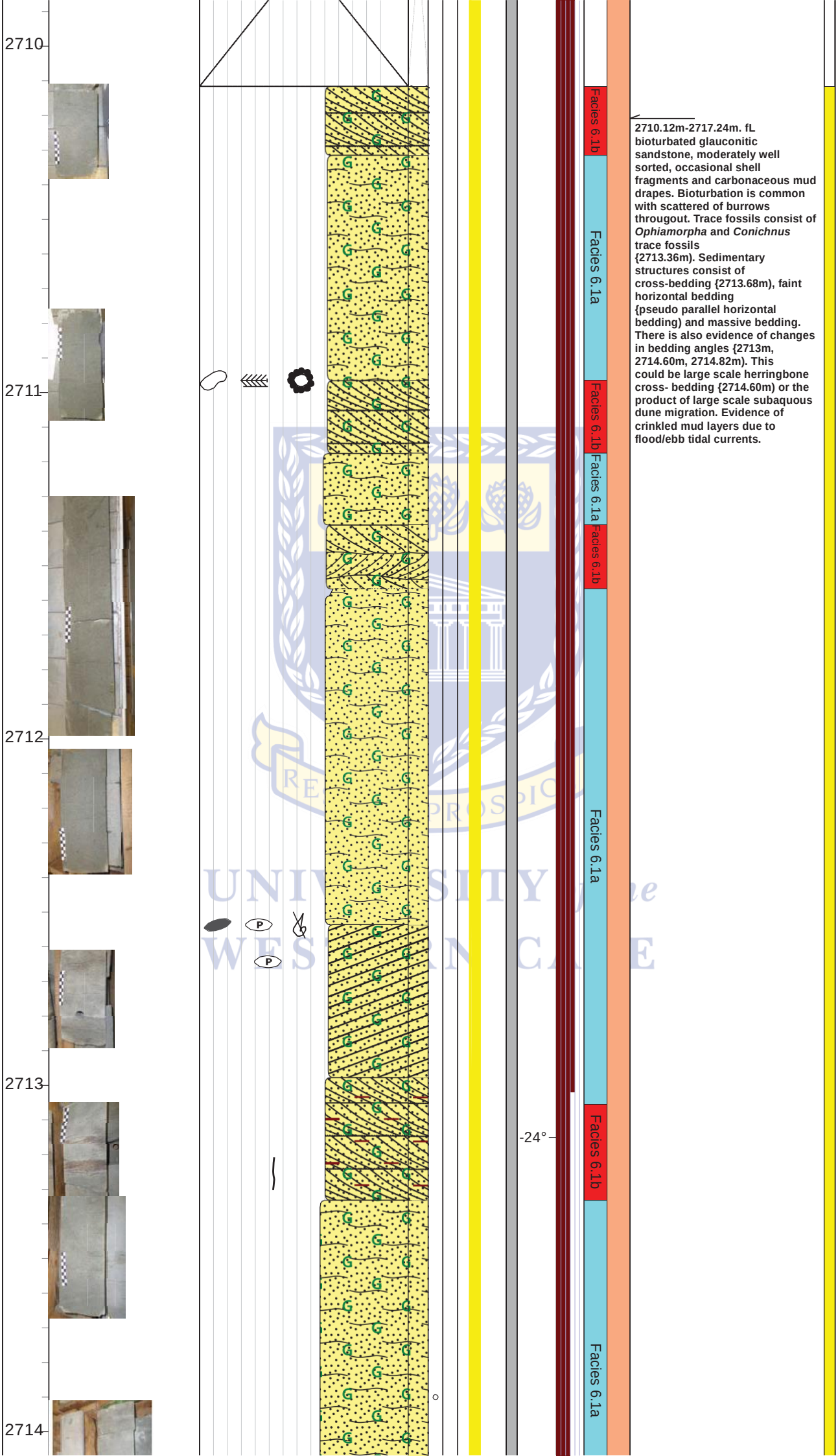

2710.12m-2717.24m. fL bioturbated glauconitic sandstone, moderately well sorted, occasional shell fragments and carbonaceous mud drapes. Bioturbation is common with scattered of burrows througout. Trace fossils consist of *Ophiamorpha* and *Conichnus* trace fossils {2713.36m). Sedimentary structures consist of cross-bedding {2713.68m), faint horizontal bedding {pseudo parallel horizontal bedding) and massive bedding. There is also evidence of changes in bedding angles {2713m, 2714.60m, 2714.82m). This could be large scale herringbone cross- bedding {2714.60m) or the product of large scale subaquous dune migration. Evidence of crinkled mud layers due to flood/ebb tidal currents.

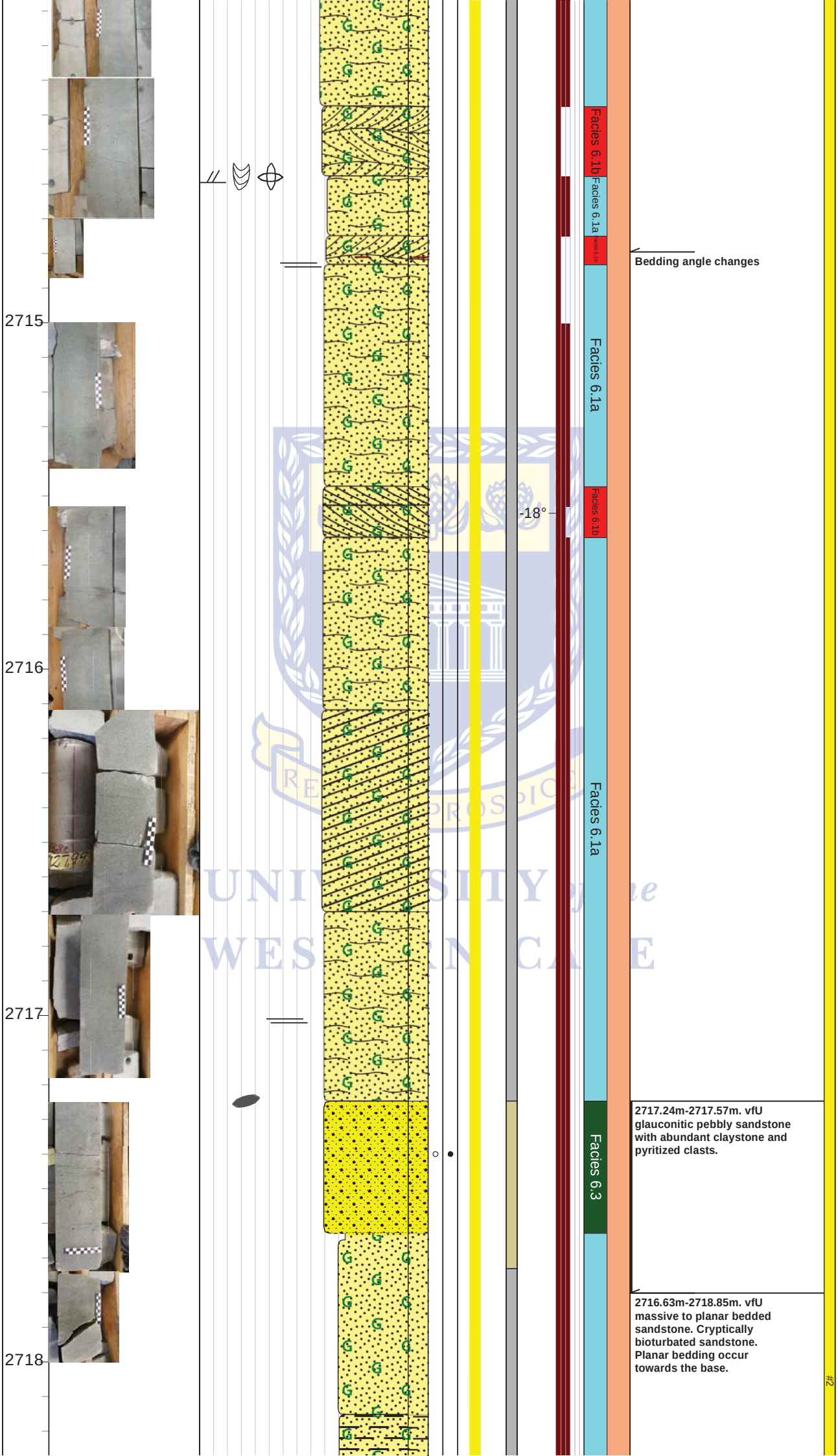

2719

2720

2721

2722

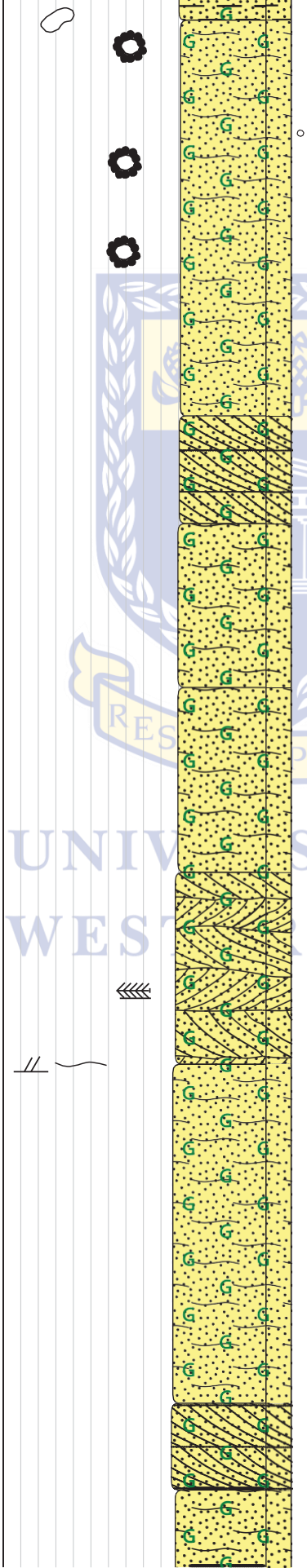

Facies 6.1a

Facies 6.1b

Facies 6.1a

Facies 6.1b

Facies 6.1a

Facies 6.1b

Tidal sand ridges

2719.77m-2718.91m.
Massive clean white sandstone. Trace fossils consist of *Ophiomorpha* type burrows. Very well

sorted sandstone evidence of beach/foreshore is approached

2719.83m-2726.02m. vfU glauconitic sandstone, medium to light grey, sedimentary structures include planar tabular cross-bedding, herringbone cross bedding and massive bedding. Disturbed or massive bedding throughout. Weakly defined and cryptic bioturbation textures at

2719.47m. Trace fossils are *Thalassinoides (2719.7m/ 2721.82m/2722.37m)* and

***Ophiomorpha* filled burrows. Ophiomorpha burrows towards 2720m consist of clean white sandstone composition, due to the layer above. Compacted sandstone porosity poor due to cementation of pores. disturbed bedding at 2725.01m more intense. Base of this cross bedded unit occurs at 2725.75. This bed is usually found interbedded with massive sandstone and cross bedding sandstone**

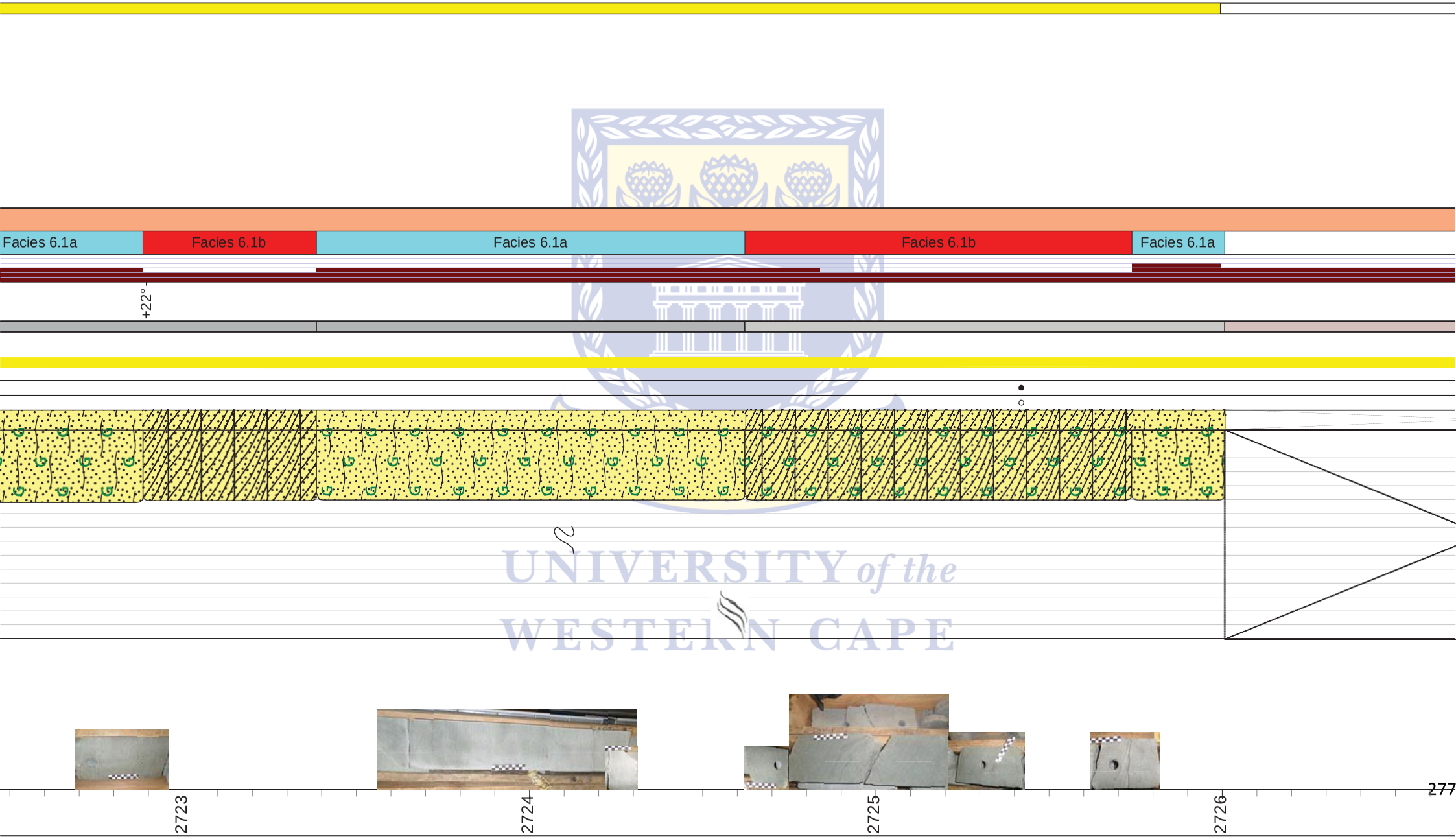

Missing Core

2727

2728

2729

2730

None

Facies 6.1a

Facies 6.1b

Fa

-19°

-19°

M

2727.52m-2740.75m. vfU-fL gluconitic sandstone, light grey to medium in color. Grains are well rounded and moderately well sorted. Sedimentary structures consist of faint laminations to massive bedding {2738.17m), sigmoidal-tangential {asymptotic) cross bedding, angular {planar tabular normal) cross bedding at 2733.33m, ripple scale and dune scale herringbone cross- bedding, Horizontal to low angle cross-bedding {2732.32m/2736.2m), Bioturbation intensity is moderate to high with the occurrence of 'cryptic' bioturbation at 2739.62m and throughout. Trace fossils {horizontal burrows abd) are *Thalassinoides (2736.98m).* Disturbed mud drapes are common with trace fossil accumulations. Erosive mud drapes {crickled) are also common, could be ebb- flood tide fluctuations {erosion on upper part of dune) or strong vortex within the dune migration phases {erosion on lower part of dune bedform). Evidence of single mud drape layers are common with dominant and subordinate current stages {ebb-flood) at 2739.62m.

2736
2737
2738
2739
+3.7°
Facies 6.1a
#3

2740

2741

2742

2743

-9.3°

-20°

+3.9°

Facies 6.1b

Facies 6.1a

Facies 6.1b

Facies 6.1

2740.75m-2743.85m. fL cross bedded glauconitic sandstone, light grey with well sorted and subrounded grains. Towards the top of this unit {2740.75m), mud drape intensity start to increase {becoming double and triple mud layers), possibly due to bioturbation decreasing with *Ophiamorpha* burrows becoming visible or change in 'colonization' window. There is also a change in bedding angle {2742.29m).Faint low angle cross bedding is common towards the bottom with faint horizontal laminations.

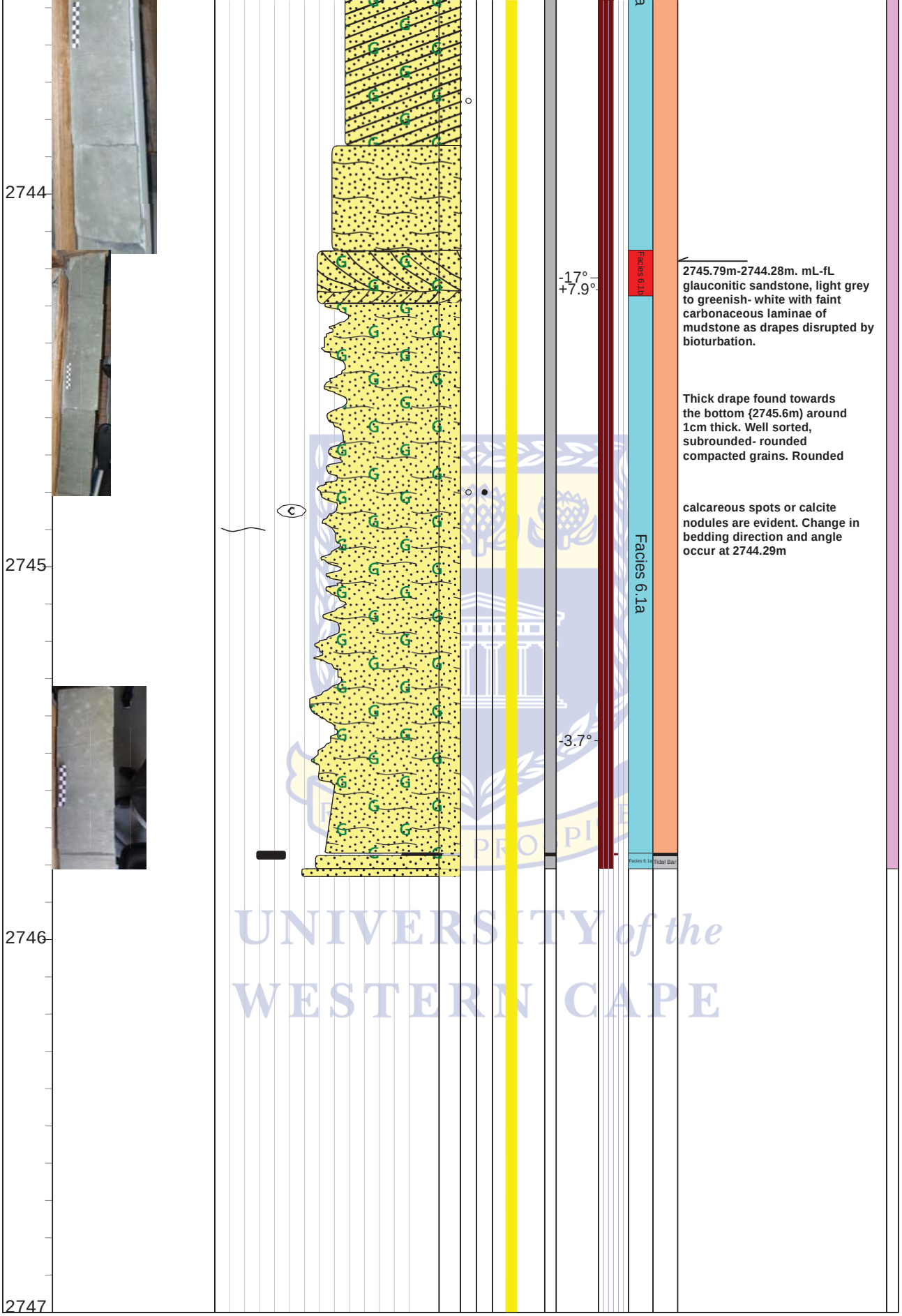

Appendix B: Petrographic data

Modal counts

Table B1: Detrital modal count data of mineral components of selected sandstone samples in the 1AT!-V horizon reservoir interval. Qm (monocrystalline quartz with undulose and non-undulose extinction); Qp (polycrystalline quartz); Q (Total quartz grains [Qm+Qp]);P (plagioclase); K (K-feldspar); F (total feldspar grains [P+K]); Ls (sedimentary lithic fragments); Lv (volcanic lithic fragments); Lp (plutonic lithic fragments); Lm (metamorphic lithic fragments); L (total lithic fragments); M (miscellaneous); Acce (accessory minerals) (modified after Dickinson, 1985)

Sample name	**Qm (undulose)**	**Qm (none-undulose)**	**Qm**	**Qp**	**K**		**P**	**Ls**	**Lv**	**Lp**	**Lm**	**M**	**Matrix**	**Acce**	**Q**	**F**	**L**
F-A12#1	36	187	223	12	3		18	15	0	8	5	16	7	16	235	21	28
F-A12#2	38	185	223	15	6		17	34	0	3	2	0	20	0	238	23	39
F-A12#3	22	203	225	33	1		22	17	1	1	0	0	12	0	258	23	19
F-A12#5	65	117	182	53	1		37	4	1	0	22	0	0	0	235	38	27
F-A12#7	40	186	226	15	0		47	6	2	3	1	0	58	11	241	47	12
F-A12#9	66	128	194	26	15		47	13	0	0	5	0	3	1	220	62	17
F-A12#11	58	112	170	11	13		97	9	0	0	0	0	4	0	181	110	9
F-A12#12a	108	78	186	11	17		65	20	1	0	0	0	11	2	197	80	21
F-A12#13	72	102	174	26	17		56	21	0	0	6	0	3	1	200	73	26
F-A5#1	84	108	192	12	29		60	4	0	3	0	0	3	1	204	89	6
F-A5#2	98	98	196	8	5.6		64	15	0	0	0	0	27	0	204	69.6	15
F-A5#3	68	87	155	21	29		80	15	0	0	0	0	2	0	176	109	15
F-A5#4	95	97	192	37	3		34	31	1	1	1	0	7	0	229	38	34
F-A5#5	86	96	182	36	11		30	36	0	4	0	0	0	1	218	41	40
F-A5#8	68	99	167	57	13		45	15	1	2	0	0	3	0	224	58	18
F-A5#10	55	90	145	41	30		68	14	0	2	0	0	0	0	186	98	16

F-AR1#1	63	80	143	22	53		51	23	0	7	0	0	2	1	165	104	30
F-AR1#4	70	122	192	14	12		10	9	5	0	5	0	0	46	206	22	19
F-AR1#5	81	106	187	24	30		47	2	0	1	0	0	12	0	211	77	3
F-AR1#7	125	86	211	24	20		36	9	0	0	0	0	3	0	235	56	9
F-AR1#11	83	101	184	32	15		50	16	0	3	0	0	31	1	216	65	19

Table B2: Detrital recalculated modal count data of mineral components of selected sandstone samples in the 1AT!-V horizon reservoir interval. Qm (monocrystalline quartz with undulose and non-undulose extinction); Qp (polycrystalline quartz); Q (Total quartz grains [Qm+Qp]); P (plagioclase); K (K-feldspar); F (total feldspar grains [P+K]); Ls (sedimentary lithic fragments); Lv (volcanic lithic fragments); Lp (plutonic lithic fragments); Lm (metamorphic lithic fragments); L (total lithic fragments); Lt (Qp+L); Lsm (metasedimentary lithic fragments [Ls+Lm]); Lvm (metavolcanic lithic fragments [Lv+Lm); M (miscellaneous); Acce (accessory minerals) (after Ingersoll et al. (1984))

Sample name	**Q**	**F**	**L**	**Lm**	**Lv**	**Ls**	**Qp**	**Lvm**	**Lsm**	**Lt**	**Qm**	**F**
F-A12#1	82.75	7.394	9.9	25	0	75	38	15.6	62.5	40	78.5	7.394
F-A12#2	79.33	7.667	13	5.6	0	94	29	3.92	70.6	54	74.3	7.667
F-A12#3	86	7.667	6.3	0	5.6	94	65	1.96	33.3	52	75	7.667
F-A12#5	78.33	12.67	9	81	3.7	15	66	28.8	32.5	80	60.7	12.67
F-A12#7	80.33	15.67	4	11	22	67	63	12.5	29.2	27	75.3	15.67
F-A12#9	73.58	20.74	5.7	24	0	76	60	9.3	39.5	43	64.9	20.74
F-A12#11	60.33	36.67	3	0	0	100	55	0	45	20	56.7	36.67
F-A12#12a	66.11	26.85	7	0	4.8	95	34	3.13	62.5	32	62.4	26.85
F-A12#13	66.89	24.41	8.7	19	0	81	50	9.62	50	52	58.2	24.41
F-A5#1	68.23	29.77	2	0	0	100	80	0	20	18	64.2	29.77
F-A5#2	70.69	24.12	5.2	0	0	100	35	0	65.2	23	67.9	24.12
F-A5#3	58.67	36.33	5	0	0	100	58	0	41.7	36	51.7	36.33
F-A5#4	76.08	12.62	11	3	3	94	53	2.86	45.7	71	63.8	12.62
F-A5#5	72.91	13.71	13	0	0	100	50	0	50	76	60.9	13.71
F-A5#8	74.67	19.33	6	0	6.3	94	78	1.37	20.5	75	55.7	19.33
F-A5#10	62	32.67	5.3	0	0	100	75	0	25.5	57	48.3	32.67
F-AR1#1	55.18	34.78	10	0	0	100	49	0	51.1	52	47.8	34.78
F-AR1#4	83.4	8.907	7.7	26	26	47	42	30.3	42.4	33	77.7	8.907

F-AR1#5	72.51	26.46	1	0	0	100	92	0	7.69	27	64.3	26.46
F-AR1#7	78.33	18.67	3	0	0	100	73	0	27.3	33	70.3	18.67
F-AR1#11	72	21.67	6.3	0	0	100	67	0	33.3	51	61.3	21.67

Detailed petrographic descriptions of selected samples

Table B3: Individual sample descriptions showing the overall mineral components and reservoir potential (conventional core analysis). Representitave images are shown only (on right or second column). Conventional core analysis contained porosity and permeability data. Categories for porosity consisted of poor porosity (<15%), good porosity (15 > x < 25) and excellent porosity (>25%). Categories for permeability consisted of poor permeability (<100mD), good permeability (100 > x < 250 and excellent permeability (> 250mD)

Sample number: F-A5#17 **Depth:** 2730.62m	**Modal count:** N/A **Facies:**Facies 5.1a **Microfacies name:** Claystone
General description: **Texture**: Claystone with minor silt-sized grains, poorly sorted with grains being subangular/subrounded bimodal grains and disseminated throughout. The matrix are largely defined as clay minerals. **Mineralogy**: ***Composition:*** 1) ***Framework minerals:*** • Monocrystalline Quartz (15%) with unit and undulose extinction, quartz are oblate • Plagioclase feldspar (<10%) (twinned and embayed by clay minerals) ***2) Ductile minerals:*** • Clays (60%) (illite/smectite) -Largely found throughout this section, interstitial clays b) Muscovite flakes (<5%) ***3) Authigenic minerals:***	

• Chalcedony (10%) ball-like structures at 0.5µm • Quartz been broken up by clay minerals evidence of silica dissolution • Clay-rich cement (Possibly chlorite/smectite) ***4) Matrix:*** Clay minerals ***5) Cement:*** Clay cement ***Reservoir potential*:** Non-reservoir unit. No Primary or secondary porosity structures, possible microcracks due to pore fluid traps (trapped water).	
Sample Number: F-A5#16 **Depth:** 2729.92m	**Modal count:** QFL N/A **Facies:**Facies 5.1a **Microfacies :**Silty claystone
General description: **Texture**: Quartz grains are angular-subangular and poorly sorted (bimodal distribution) **Mineralogy**: ***Composition:*** ***1) Framework minerals:*** • Monocrystalline quartz (30%), with unit extinction • Rare to minor plagioclase largely replaced by clay minerals ***2) Ductile Minerals:*** a) Clay minerals consist of kaolinite, smectite/illite but possibly more smectite/chlorite ***3) Authigenic Minerals:*** Smectite/illite ***4) Matrix:*** Clay minerals ***5) Cement:***Clay cement (illite) ***Reservoir potential*:** Primary porosity is poor, but secondary porosity still evident (Non-reservoir unit)	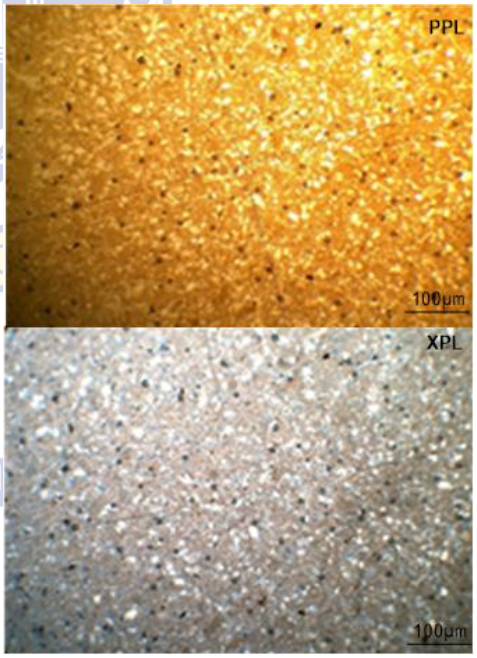

Sample Number: F-A5#15 **Depth:** 2718.46m	**Modal count:** QFL N/A **Facies:**Facies 5.1b **Microfacies:**Silty Claystone
General description: **Texture**: Silty claystone that contains subangular – angular quartz grains and are poorly sorted (bimodal) grains scattered quartz. Silt-sized grains disseminated. Whole sample is in optical continuity where whole matrix is one mineral. **Mineralogy**: ***Composition:*** ***1) Framework minerals:*** • Band of quartz (Qm) compacted. Polycrystalline quartz also evident ***2) Ductile minerals:*** Clay minerals (Same as authigenic) ***3) Authigenic minerals:*** Chlorite/Sericite and Siderite ***4) Matrix:*** Clay-rich (Sericite) ***5) Cement:*** Clay cement (spots of Fe-rich calcite) **Reservoir potential:** Poor (No evidence of primary or secondary porosity) (Non-reservoir unit)	
Sample Number: F-A5#14 **Depth:** 2715.56m	**Modal count:** QFL N/A **Facies:**Facies 5.1a **Microfacies :**Silty claystone
General description: **Texture**: Silty claystone with grains that are poorly sorted with abundant subangular quartz grains. Patches of grains are in optical continuity. Some laminations are seen. **Mineralogy:** ***Composition:*** ***1) Framework minerals:*** • Quartz grains (37.5µm) • Quartz are spotted (due to grinding)	

<table>
<tr>
<td>

- No visible feldspars or lithic fragments

2) ***Ductile Minerals:*** Micaceous minerals (muscovite)

3) ***Authigenic Minerals:***

- Illite and sericite, with kaolinite (with wavy extinction)
- Calcite spots
- Chalcedony also evident

4) ***Matrix:*** Clay-rich (clay minerals)

5) ***Cement:*** Calcite, siderite and clay minerals

Reservoir potential: No Primary porosity, but evidence of microcracks (secondary porosity) (Non-reservoir unit)

</td>
<td> 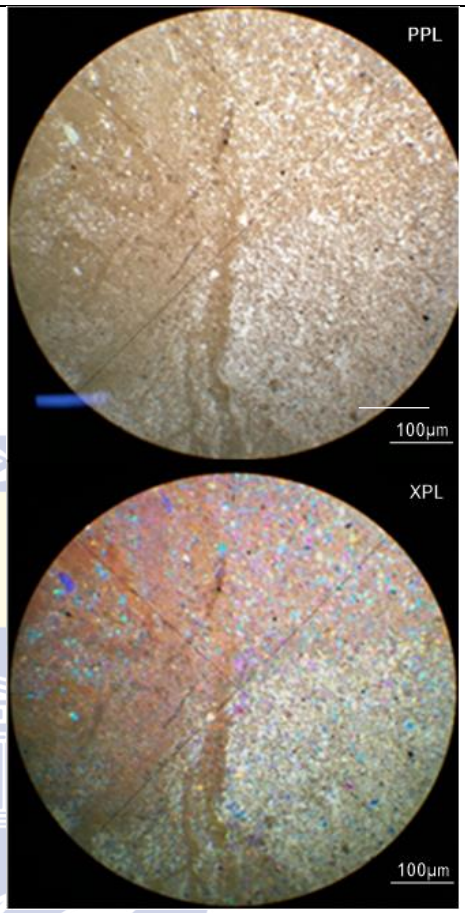
</td>
</tr>
<tr>
<td>Sample Number: F-A5#13

Depth: 2711.05m</td>
<td>Modal count: QFL N/A

Facies:Facies 5.1b

Microfacies :Silty Claystone</td>
</tr>
<tr>
<td>

General description:

Texture: Claystone with silt-sized grains, poorly sorted with grains being subangular/subrounded bimodal grains and disseminated throughout. The matrix are largely defined as clay minerals

Mineralogy:

Composition:

1) ***Framework minerals:***
   - Monocrystalline Quartz (15%) with unit and undulose extinction, quartz are oblate
   - Plagioclase feldspar (<10%) (twinned

</td>
<td> 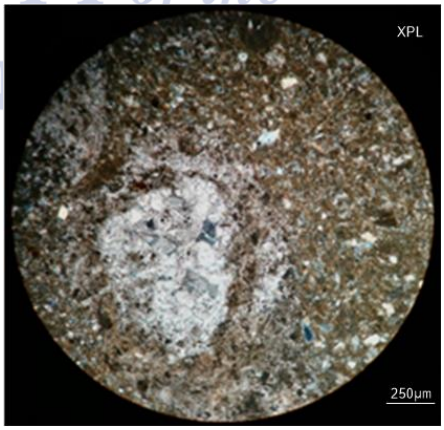
</td>
</tr>
</table>

and embayed by clay minerals) ***2) Ductile Minerals:*** • Clays (60%) (illite/smectite) -Largely found throughout this section, interstitial clays b) Muscovite flakes (<5%) ***3) Authigenic Minerals:*** • Chalcedony (10%) ball-like structures at 0.5µm • Quartz been broken up by clay minerals evidence of silica dissolution • Clay-rich cement (Possibly chlorite/smectite and kaolinite) ***1) Matrix:*** Clay-rich matrix ***2) Cement:*** Clay and silica rich cement ***Reservoir potential*:**Non-reservoir mudstone.No Primary or secondary porosity structures, possible microcracks due to pore fluid traps (trapped water)	
Sample Number: F-A5#12 **Depth:** 2710.09	**Modal count:** QFL N/A **Facies:** Facies 5.1b **Microfacies :**Siltstone
<u>General description</u>: **Texture**:A siltstone with textural variability consisting of grains are poorly to moderately sorted with majority of the quartz grains showing angular shapes. There is a bimodal distribution of grains with clay minerals and quartz grains. There are evidence of claystone clasts (elongated). There are evidence of alteration or leaching. **Mineralogy**: ***Composition:*** ***1) Framework minerals:*** • Monocrystalline quartz that are largely angular-subangular • Plagioclase feldspar (some showing extinction)	

2) ***Ductile minerals:*** Micaceous minerals present as muscovite 3) ***Authigenic minerals:*** Sulphides (pyrite) and authigenic clay minerals. 4) **Matrix**: Matrix are largely made up of clay minerals 5) **Cement:** Quartz overgrowths evidence of silica cementation with clay mineral cement ***Reservoir potential*:**Non-reservoir unit that is dominated by sulphides and clay minerals.Primary porosity destroyed by clay cement, Secondary porosity preserved as micro cracks but largely filled in by silica precipitation	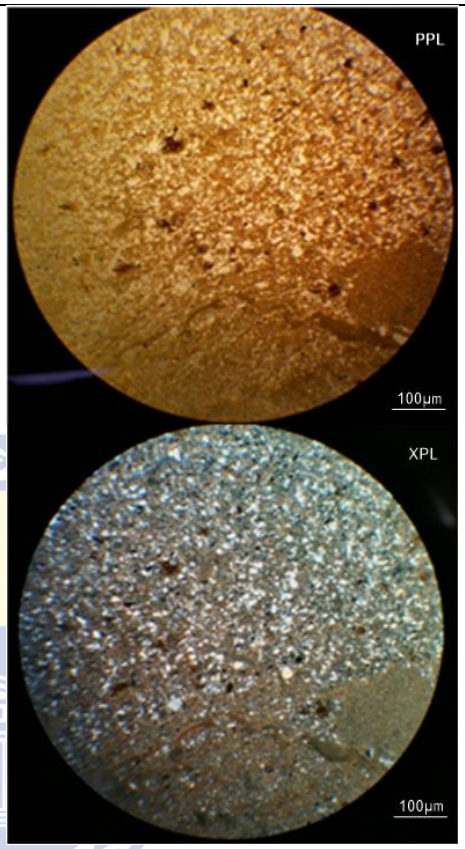
Sample Number: F-A5#11 **Depth:** 2708.34m	**Modal count:** QFL N/A **Facies:**Facies 5.1b **Microfacies :**Siltstone/vfL sandstone contact
<u>General description</u>: **Texture**: Claystone/siltstone with sandstone clasts. Grains are poorly sorted within the vfL sandstone, but moderately sorted within the siltstone. **Mineralogy:** ***Composition:*** 1) ***Framework minerals:*** • Monocrystalline quartz grains are subrounded-subangular showing undulose and unit extinction (70µm in places). • Plagioclase feldspar also occurs unaltered • Mudstone stringers with sandstone	

clasts as lithic fragments

2) Ductile Minerals: Largely just clay minerals

3) Authigenic Minerals: Chalcedony and Iron-rich calcite

4) Matrix: Clay minerals

5) Cement: Clay minerals

***Reservoir potential*:**represents a non-reservoir unit. The claystone laminations acts as a barrier, thus decreasing permeability (non-reservoir claystone). Microfractures might enhance secondary porosity but are largely filled by siderite. The partial dissolution of feldspar could enhance porosity. Localized chalcedony and calcite structures might degrade the pore system. The spacing between grains within the vfL sandstone are around 20-30 micrometers but this is largely filled by clay minerals.

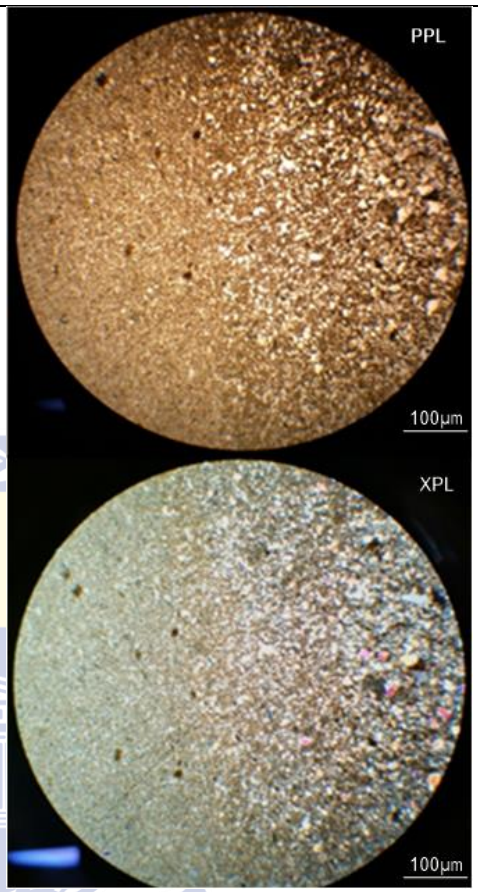

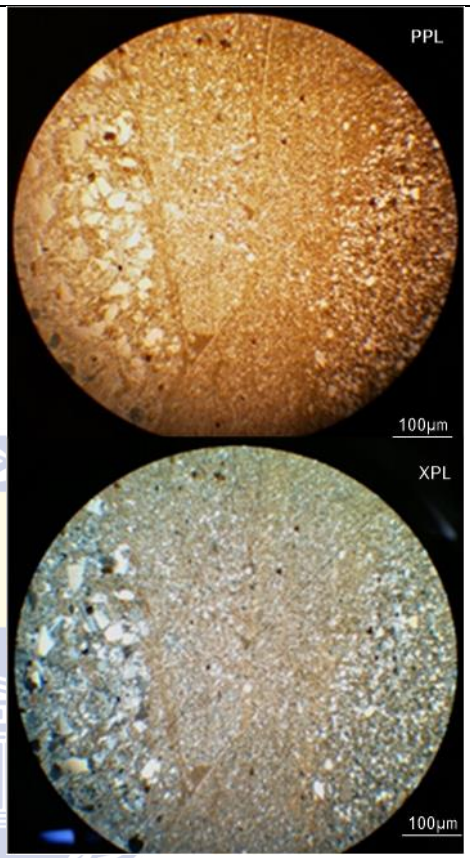

Sample Number: F-A5#10

Depth: 2706.12m

Modal count: $Q_{62}F_{33}L_6$

Facies: Facies 7.1

Microfacies: Quartzofeldspathic

General description:

Texture: A fU sandstone that is moderately well sorted and has subrounded-subangular grains. A very compacted sandstone, which reduce porosity without the effects of cementation. Mature sandstone unit. Grain boundaries consist of concavo-convex grain boundary contacts. Some grains are coated with ferruginous opaque material (possibly hematite). Heavy minerals consist mostly of zircon

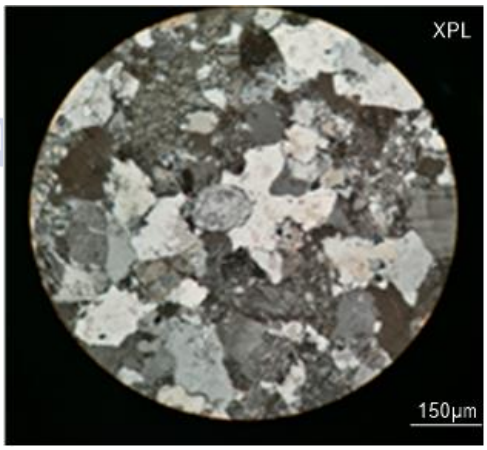

Mineralogy:

Composition:

1) ***Framework minerals:***

- Monocrystalline quartz consist of undulose and unit extinct quartz that are largely

equidimensional (with some subangular grains as well). Some quartz has inclusions of high interference mineral grains (Zircon). Polycrystalline quartz are abundant • Plagioclase feldspars (around 30µm wide) are abundant. Microcline is also evident but with lesser orthoclase of the K-feldspars. These feldspars are altered in some places as well (sericitized grains) • Lithic fragments consisted of meta-quartzitic grains and siltstone lithic fragments **2) Matrix:** Matrix are scarce, but were evident consist of silt-sized grains. ***3) Ductile Minerals:***Clay minerals ***4) Authigenic Minerals:*** Vermicular kaolinite, quartz overgrowths, feldspar overgrowths. ***5)Cement:*** Silica and Calcite cement (with calcite being the oldest (eogenetic) in a paragenetic sequence) ***Reservoir potential*:** A very tight sandstone unit with good porosity but low permeability due to compaction and dissolution. The cements obstructs fluid flow. Porosity is possibly enhanced by feldspar dissolution. Primary porosity is destroyed due to compaction but secondary porosity is still preserved due to microcracks.	
Sample Number: F-A5#9 **Depth:** 2705.20m	**Modal count:** QFL N/A **Facies:**Facies 7.2 **Microfacies:**Quartzolithic (?)
General description: Texture:Ripple laminated vfU sandstone that has angular-subangular grains and are poorly to moderately sorted. Grains are more elongated than equidimensional. The unit is compacted with sutured and long contact boundaries. This unit consist of multi-modal sandstone with claystone towards the bottom grading to coarser vfU sandstone and eventually to siltstone (Normal	

grading on ripple forests and mud draped)

Mineralogy:

Composition:

1)Framework minerals:

- Monocrystalline quartz are largely subangular with subrounded finer grains. Grains show normal and undulose extinction. Undulose extinction shows double-sided wavy extinction possibly due to long contacts. Polycrystalline quartz are evident.
- Plagioclase feldspars are abundant with typical lamellae and are fractured in some cases. Plagioclase are largely altered and unaltered. Microcline is more dominant than Orthoclase. Orthoclase are largely untwinned.
- Lithic fragments consist mostly of metasedimentary and sedimentary lithic fragments but are few

2) Ductile Minerals: Clay minerals are largely detrital but are abundant. Mica minerals consist largely of muscovite but are scarce.

3) Authigenic Minerals:Some clay minerals with calcite grains and sulphide nodules (opaque pyrite). Vermicular kaolinite also present.

***4) Matrix*:**Matrix consist largely of silt sized quartz grains and clay minerals

5) Cement: Silica and calcite cement dominate

***Reservoir potential*:**Reservoir potentialsame as F-A5#10

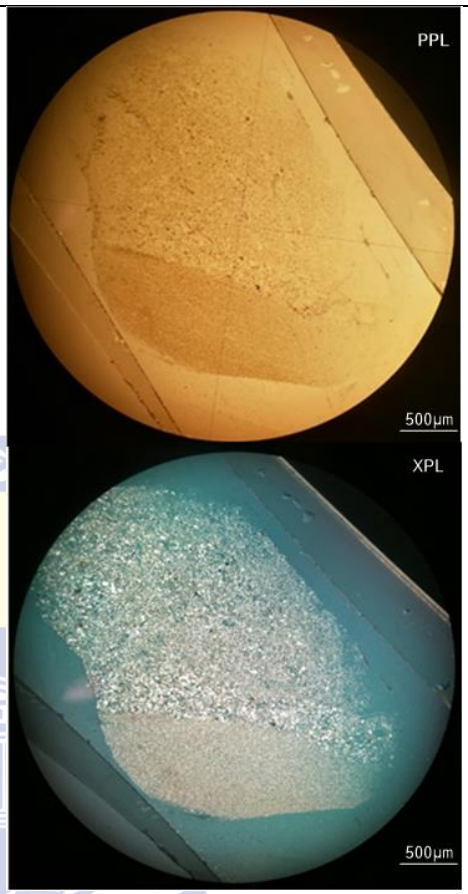

	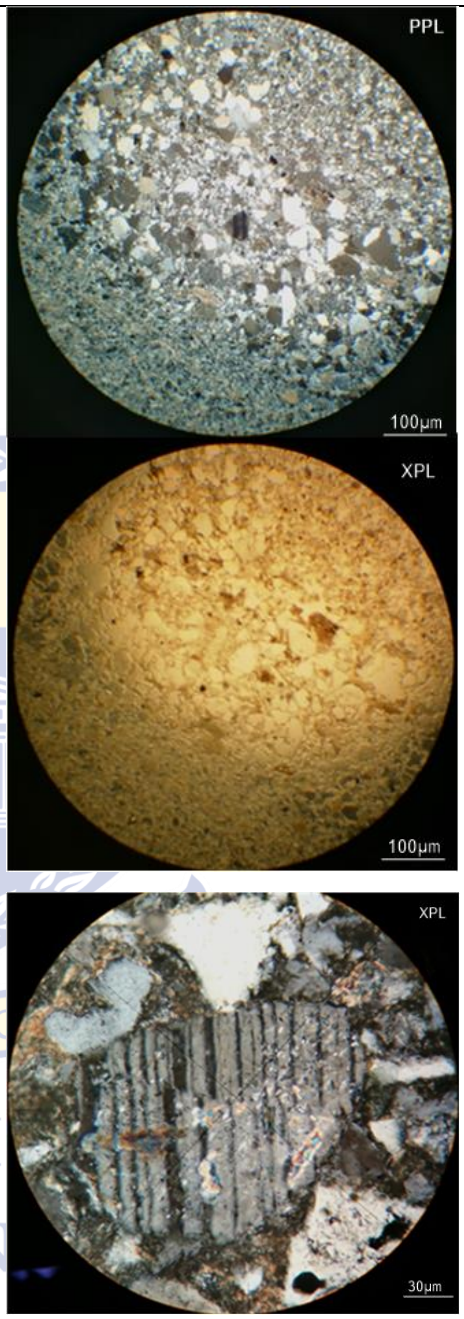
Sample Number: F-A5#8 **Depth:** 2702.84m	**Modal count:** $Q_{75}F_{19}L_{6}$ **Facies:**Facies 7.4 **Microfacies:**Quartzofeldspathic
General description: Texture: mL sandstone that consist of grains that are rounded to subrounded. The grains are largely moderately well sorted. Abraded zircon grains are	

common. Equidimensional grains are evident.

Mineralogy:

Composition:

1) ***Framework minerals:***
- Quartz with unit and undulose extinction. Quartz grains shows embayment (interpenetration textures) and sutured contacts as a result of extreme compaction. Polycrystalline quartz with undulose extinction
- Plagioclase feldspar is dominant, with microcline being more dominant than orthoclase as K-feldspars. Altered plagioclase is common
- Rock fragments consist of chert and metasedimentary fragments (rank 1)

2) ***Ductile Minerals:*** Mica minerals are more abundant than in previous (F-A5#9) sample. Clay minerals are also evident as coating.
3) ***Authigenic Minerals:*** Chalcedony
4) ***Matrix:*** silt-sized quartz grains
5) ***Cement:*** Silica cement as quartz overgrowths

***Reservoir potential*:** This sandstone contain a good porosity and poor to no permeability. Altered plagioclase possibly contributed to the high porosity but due to compaction and silica cement, created barriers to flow.

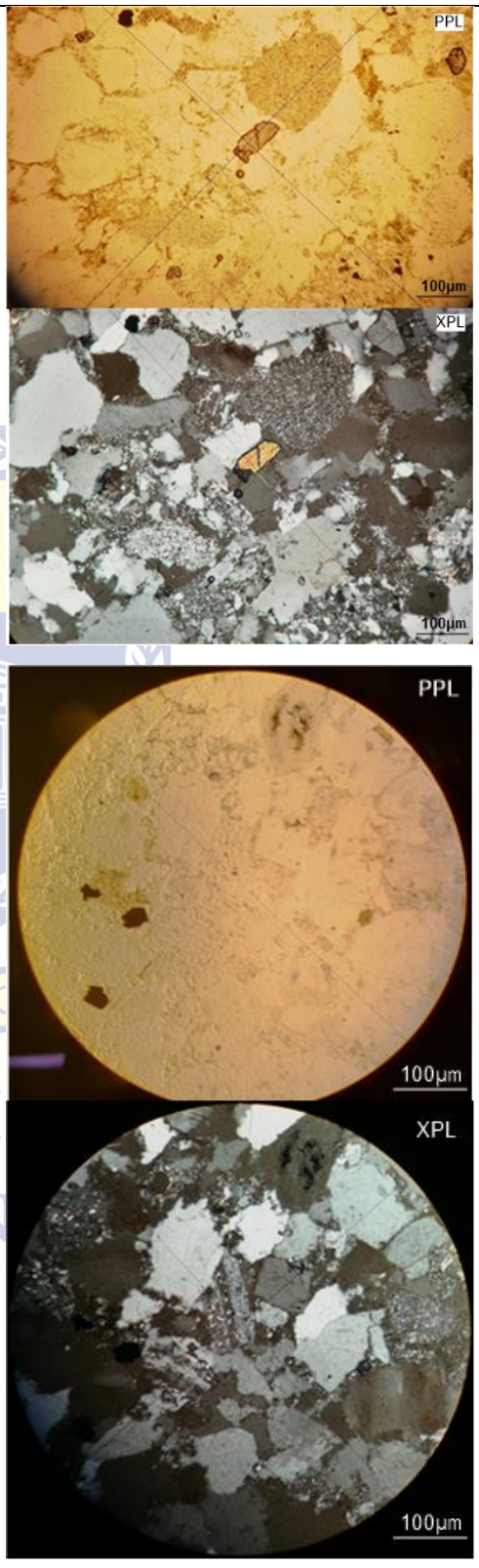

Sample Number: F-A5#7

Modal count: QFL N/A

Depth: 2701.54m	**Facies:**Facies 8.3 **Microfacies :**Quartzofeldspathic
General description: Texture: vfU sandstone with extraformational claystone clasts. Clasts are around 1mm in diameter (long axis). This unit is moderately sorted with rounded grains. The rip-up clasts are largely angular. Grains are equidimensional (slightly angular grains). Grain boundaries are sutured. Mineralogy: ***Composition:*** ***1) Framework minerals:*** • Monocrystalline quartz has undulose and unit extinction and are largely rounded-subrounded. Polycrystalline quartz are also evident and are possiblymetamorphic in origin with sheared quartzites • Plagioclase feldspar dominant and are quite large (elongated) • Rock fragments consist of sedimentary and metasedimentary fragments with extraformational claystone clasts (illite-smectite) with preserved laminations. 2) ***Ductile Minerals:*** Clay minerals 3) ***Authigenic Minerals:*** -Clay patched (clasts) made up of smectite-illite 4) ***Matrix:*** Clay rich matrix 5) ***Cement:***Largely silica cement ***Reservoir potential*:** This sandstone supports a good porosity but poor to no permeability. Dissolution of feldspars contributed to the enhanced porosity. Permeability was decreased due to compaction, clay matrix and silica dissolution.	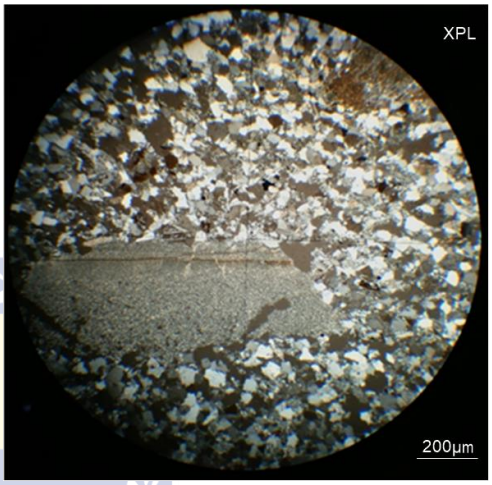 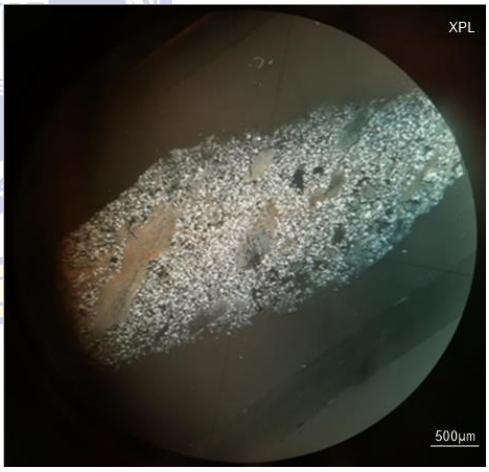
Sample Number: F-A5#6 **Depth:** 2700.19m	**Modal count:** QFL N/A **Facies:** Facies 8.5 **Microfacies:**Quartzofeldspathic
General description: Texture: vfL sandstone, moderately well sorted	

with angular to sub-rounded grains. Lamination in one side of the thin section is still present.

Mineralogy:

Composition:

1) ***Framework minerals:***
   - Clear monocrystalline quartz with undulose extinct quartz, polycrystalline quartz also evident with sutured intercrystalline sub-grain boundaries
   - Plagioclase feldspar dominant over K-feldspar (not much altered feldspars)
   - Rock fragments are made up of chert and metasedimentary grains
2) ***Ductile minerals:*** Mica (muscovite) but mostly clay minerals
3) ***Authigenic minerals:*** Sulphide (pyrite) nodules
4) ***Matrix:*** Clay-sized minerals
5) ***Cement:***Silica and clay cement

Reservoir potential:This sandstone supports a poor porosity and no permeability. Any porosity that is generated is therefore ineffective. The porosity possibly exists as secondary intergranular porosity.

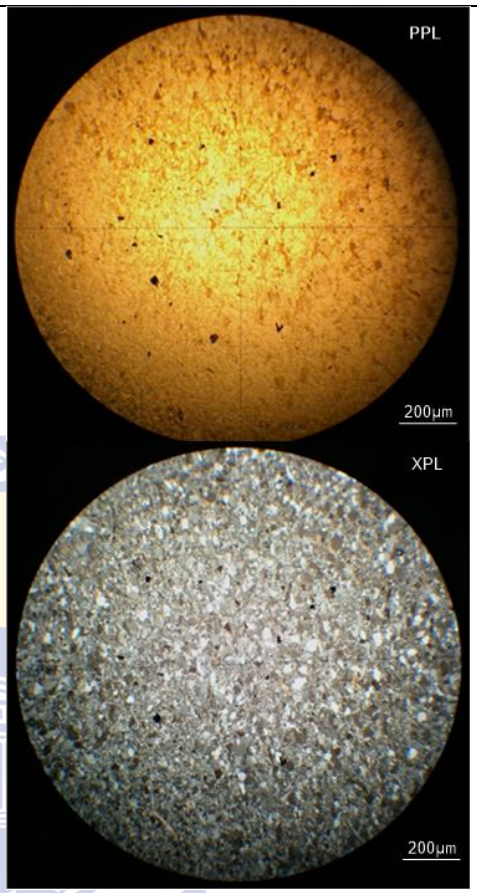

Sample Number: F-A5#5

Depth: 2698.49m

Modal count: $Q_{73}F_{14}L_{14}$

Facies: Facies 6.1b

Microfacies: Quartzofeldspatholithic

General description:

Texture: fU sandstone, well sorted with subrounded to largely rounded grains, First evidence of marine influence because of the appearance of glauconite.

Mineralogy:

Composition:

1) ***Framework minerals:***
   - Monocrystalline Quartz grains with undulose and unit extinction. Polycrystalline quartz are dominant and partially falls part of the matrix
   - Plagioclase feldspars are dominant

but are largely altered. Alteration of plagioclase feldspar is common. K-feldspars occurs largely as orthoclase that is untwinned. Microcline occurs but rarely.

- Lithic fragments are largely made up of sedimentary and metasedimentary grains. Abundant impure polycrystalline quartz (chert).

2) ***Ductile minerals:*** Glauconite (heavily compacted/deformed)
3) ***Authigenic minerals:*** Chalcedony and Clay minerals
4) ***Matrix:*** Silt-sized grains with organic matter in between.
5) ***Cement:*** Calcite cement is also common. Silica cement is also common with plagioclase overgrowths

***Reservoir potential*:** This sandstone supports a good porosity and poor permeability (first sign of permeability). The porosity is enhanced by plagioclase alteration and dissolution since compaction was evident. The permeability has increased but it is still poor. Permeability is enhanced possibly by the well-rounded grains but are largely heterogeneous since sutured boundaries and point contacts are common.

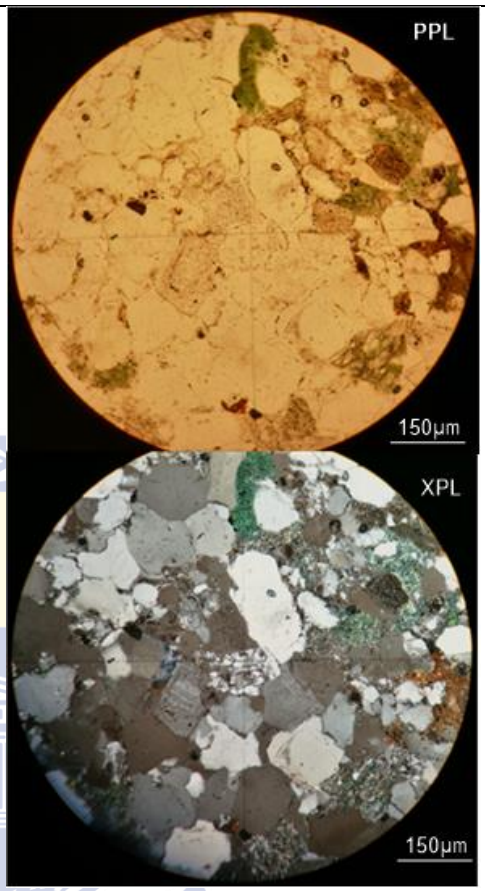

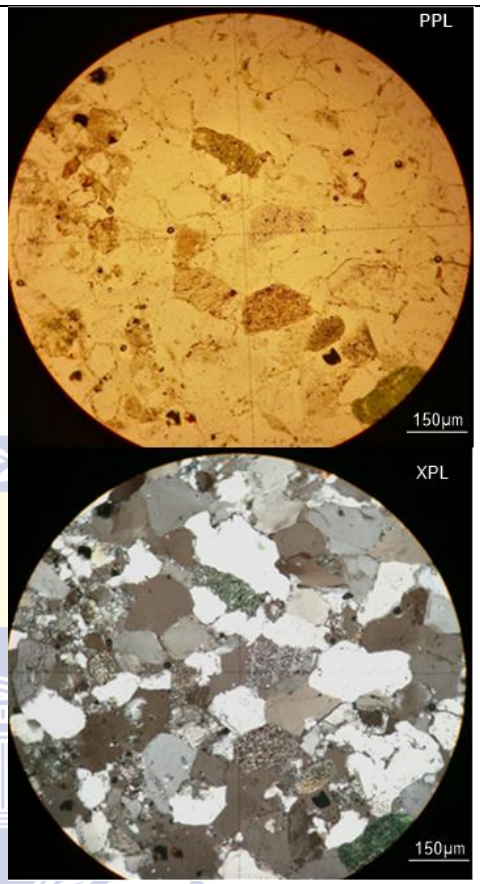

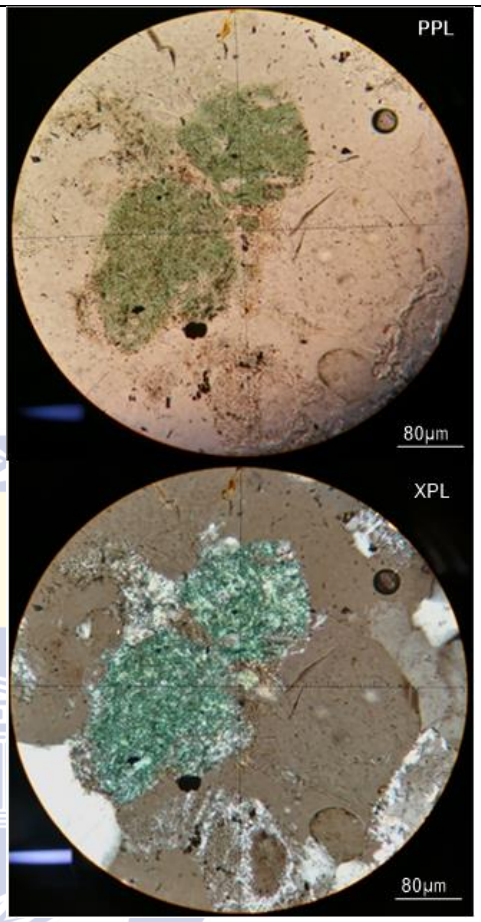

	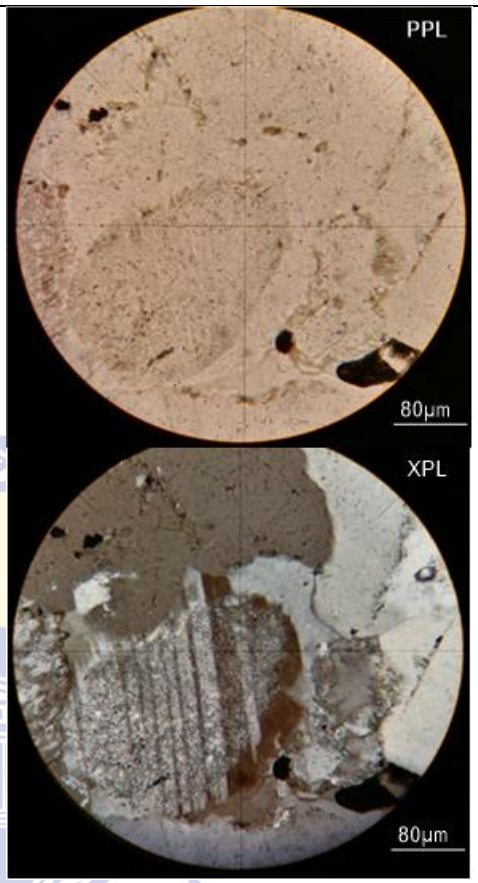
Sample Number: F-A5#4 **Depth:** 2697.18m	**Modal count:** $Q_{76}F_{12}L_{11}$ **Facies:**Facies 6.1a/6.3 **Microfacies:**Quartzofeldspathic
General description: Texture: mU sandstone, that consist of well-rounded grains and are moderately well sorted. Most grains shows fractures. Point contacts and long contacts are common. Mineralogy: ***Composition:*** ***1) Framework minerals:*** • Monocrystalline quartz shows both unit and undulose extinction. Polycrystalline quartz are also evident. • Plagioclase feldspar abundant and alteration is common. Orthoclase is evident but are largely untwinned.	

- Lithic fragments consist of sedimentary and metasedimentary grains, igneous fragments also occurs

2) ***Ductile Minerals:*** Glauconite still evident with clay minerals and carbonaceous material
3) ***Authigenic Minerals:*** Clay minerals from plagioclase alteration (sericite) and calcite.
4) ***Matrix:*** Silt-sized quartz grains with clay minerals
5) ***Cement:*** Largely silica with minor calcite cement

***Reservoir potential*:**This sandstone unit supports good porosity, with a fairly good permeability.Porosity is enhanced by the occurrence of plagioclase alteration which is common. Permeability is enhanced by the microfractured grains which allowed for fluid connectivity. This possibly contributed to the secondary porosity as well.

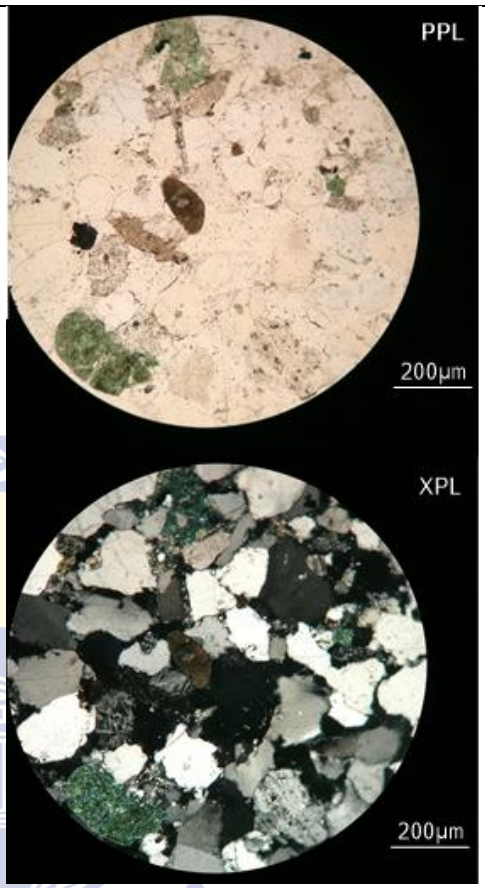

Sample Number: F-A5# 3

Depth: 2691.75m

Modal count: $Q_{58}F_{36}L_5$

Facies: Facies 9.2

Microfacies : Quartzofeldspathic

General description:

Texture: vfL-vfU sandstones, that consist of a bimodal sorting with parts showing moderately well sorted grains and other parts showing poorly sorted grains. The grain shapes are subangular to angular grains but heavily compacted.Sutured boundaries are common. Siltstone laminations are present.

Mineralogy:

Composition:

1) ***Framework minerals:***
- Mostly monocrystalline quartzthat are subangular to subrounded in shape. Polycrystalline quartz are also evident.

• Plagioclase feldspars still evident, with abundant alterations (sericite largely) • Lithic fragments consisted largely of metasedimentary and sedimentary impure polycrystalline quartz (chert) ***2) Ductile Minerals:*** Clay minerals, some glauconite (not much but present) and muscovite grains ***3) Authigenic Minerals:***Clay minerals with quartz overgrowths ***4) Matrix:*** Consisted of silt-sized grains (quartz and feldspars) and clay-sized material consisting of clay minerals. ***5) Cement:*** Largely consist of silica cement ***Reservoir potential*:** This sandstone supports a good-porosity but a poor to absent permeability. Feldspar alteration enhanced porosity but compacted nature, and silica cement possibly decreased permeability. Some of the silica cement occurred in patches (heterogeneous compaction due to mineral-specific resistance) which inhibited fluid flow.	
Sample Number: F-A5#2 **Depth:** 2686.31m	**Modal count:** $Q_{70}F_{24}L_{6}$ **Facies:**Facies 9.3 **Microfacies:**Quartzofeldspathic

General description:

Texture: vfL sandstone that is moderately well sorted, with some patches showing poorly sorted grains (bimodal). Subangular to angular grains. Carbonaceous/Clay laminae is evident (disrupted in places). This unit is also largely compacted.

Mineralogy:

Composition:

1) ***Framework minerals:***
- Monocrystalline quartz are largely angular to subangular in shape and exhibits undulose and unit extinct quartz. Polycrystalline is also present with sutured sub-crystals. Some of the quartz shows alteration as chalcedonic quartz and are not clear (diagenetic changes)
- Plagioclase are still dominant over the orthoclase minerals. Orthoclase are present but contains no twins. Alteration is common in the form of sericite, partially altered grains are also evident.

2) ***Ductile Minerals:***Clay minerals are evident and are associated with the carbonaceous streaks.
3) ***Authigenic Minerals:***
4) Matrix: Silt-sized quartzand clay matrix
5) ***Cement:*** Silica cement is largely evident as quartz overgrowths.

***Reservoir potential*:** This unit supports a good porosity but absent to rare permeability. The good porosity is due to the alteration of feldspars, the absent permeability is due to the compacted nature of the unit and the clay/carbonaceous laminae that caused barriers to flow.

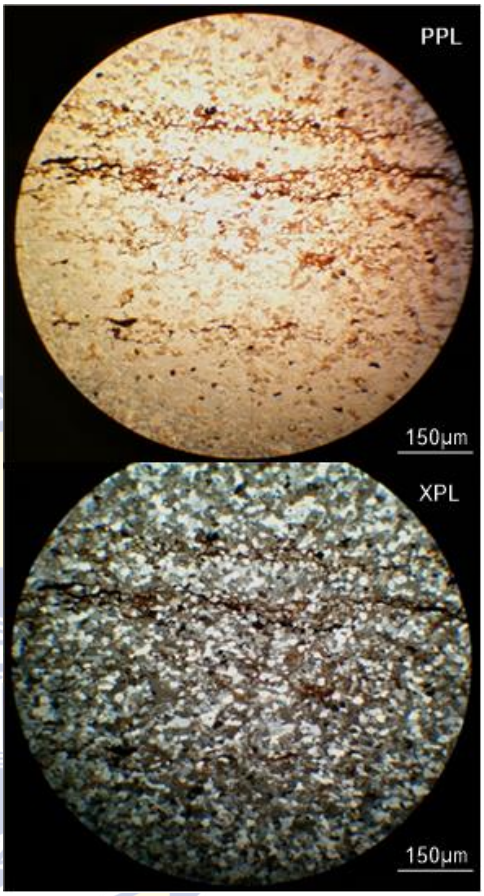

Sample Number: F-A5#1

Depth: 2684.25m

Modal count: $Q_{68}F_{30}L_3$

Facies: Facies 9.2

Microfacies: Quartzofeldspathic

General description:

Texture: fL sandstone unit that consist of sub-

rounded to rounded grains that is well sorted. Carbonaceous material still evident but less than samples F-A5 #2. Mineralogy: ***Composition:*** ***1) Framework minerals:*** • Monocrystalline quartz are evident with unit and undulose extinct quartz grains. Polycrystalline quartz grains exist as pure chert fragments. • Plagioclase evident and more than the K-feldspars grains • Lithic fragments are restricted to sedimentary/metapelitic grains ***2) Ductile Minerals:***Clay minerals and carbonaceous material. ***3) Authigenic Minerals:*** **Clay minerals** ***4) Matrix:*** Silt-sized quartz-dominated grains ***5) Cement:*** Largely silica cement ***Reservoir potential*****:** This sandstone supports a fairly good porosity and poor to no permeability. Porosity is enhanced in part by plagioclase alteration. Permeability is destroyed by compaction and silica cement	
Sample Number: F-A12#15 **Depth:** 2769.23m	**Modal count:** QFL N/A **Facies:**Facies 1.1 **Microfacies:**Heterolythic Quartzofeldspathic
General description: Texture: vfL sandstone and Siltstone/claystone heterolythic unit (double mud drapes). The grains in the vfL sandstone are poorly-moderately sorted with subangular-subrounded shapes.This unit also shows signs of compaction (silica dissolution). Claystone drapes has silt-sized quartz grains making it a clayey mudstone. Opaque minerals common as well as zircon grains. Opaque minerals largely found in the claystone drapes. The micro-contacts shows largely gradation from claystone to	

silty claystone and to vfL sandstone.

Mineralogy:

Composition:

1) ***Framework minerals:***
- Monocrystalline quartz that are largely angular and exhibits unit and undulose extinction. Polycrystalline quartz is present but very rare.
- Plagioclase feldspar are evident but less
- Some siltstone bands (angular frags if quartz feldspar)
- Lithic fragments consist of sedimentary lithic grains

2) ***Ductile Minerals:***Some occurrence of glauconite in the vfL sandstone. Quartz overgrowths are also present.
3) ***Authigenic minerals:***Clay minerals with quartz overgrowths
4) ***Matrix:***Silt-sized quartz grains and clay minerals in the sandstone unit. Clay matrix in the silty-mudstone.
5) ***Cement:*** Cement: Clay mineral cement

***Reservoir potential*:** This unit supports a poor porosity and permeability. The horizontal permeability is decreased due to the occurrence of clay cement and the vertical permeability is decreased due to the claystone barrier/drape. The porosity is low possibly because of the compaction and the absence of significant feldspars.

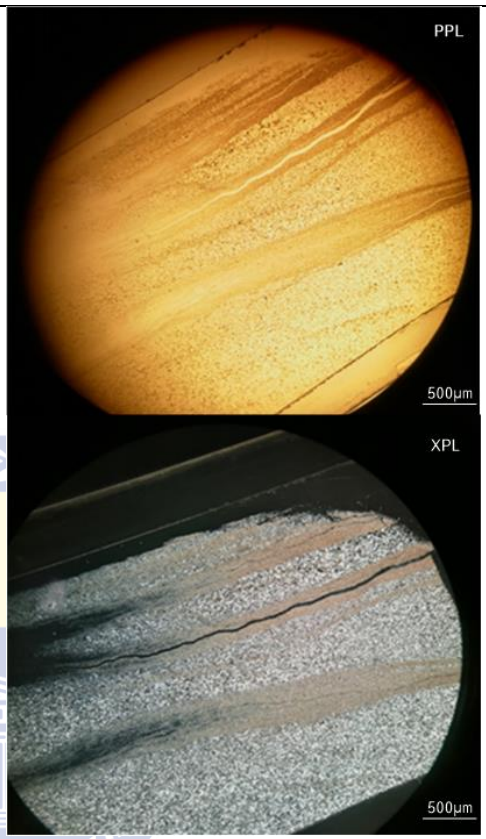

	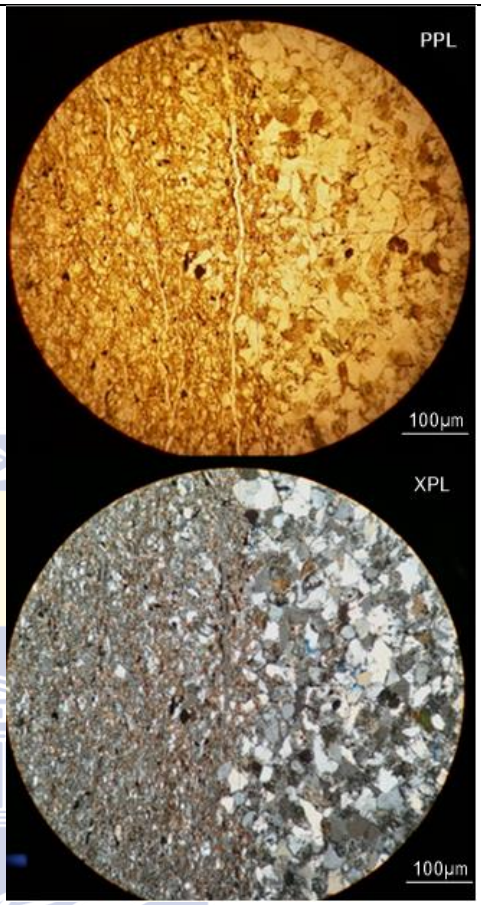
Sample Number: F-A12#14 **Depth:** 2750.93m	**Modal count:** QFL N/A **Facies:** Facies 3.2 **Microfacies:**vfL-siltstone (Quartzofeldspathic)
General description: Texture: vfL sandstone with siltstone bands (ripple laminated). The vfL unit is poorly sorted and consist of sub-rounded to rounded grains. Cross-laminated simple bedsets. Organic/Carbonaceous material is common. Mineralogy: ***Composition:*** ***1) Framework minerals:*** • Mostly monocrystalline quartzare subrounded and exhibits undulose and nit extinct quartz	

<table>
<tr>
<td>

- Plagioclase feldspars are common but mostly fully altered
- Lithic fragments are restricted to impure polycrystalline quartz of sedimentary origin

2) Ductile Minerals: Micaceous minerals are rare with muscovite being more dominant than biotite. Clay minerals occurs as well

3) Authigenic Minerals: Clay minerals and kaolinite are present

***Reservoir potential*:** This sandstone unit supports a poor porosity and permeability. The siltstone bands acts as barriers to flow. Porosity is possibly low due to a clay rich matrix.

</td>
<td>
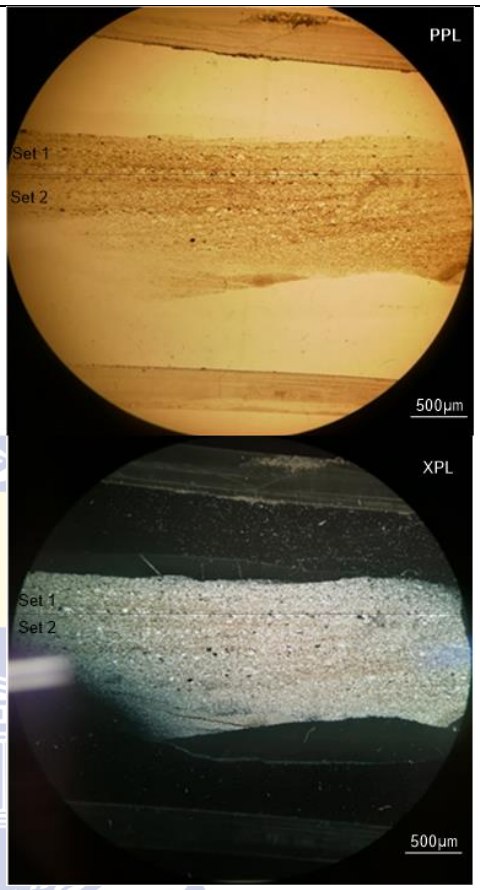

</td>
</tr>
<tr>
<td>

Sample Number: F-A12#13

Depth: 2747.79m

</td>
<td>

Modal count: $Q_{66}F_{24}L_{9}$

Facies: Facies 3.2

Microfacies: Quartzofeldspathic

</td>
</tr>
</table>

General description:

Texture: fU sandstone unit that is moderately sorted to poorly sorted in some parts (bimodal). The grains are sub-rounded in shape. Laminations partly seen in thin section (siltstone bands). Opaque minerals are abundant

Mineralogy:

Composition:

1) ***Framework minerals:***
- Monocrystalline quartz are sub-rounded and exhibits both undulose and unit extinction. Polycrystalline quartz are abundant. Sub-crystals within the polycrystalline quartz are sutured (largely indicative of metamorphic polycyclic grains.
- Plagioclase feldspars are abundant. K-feldspars are rare. Alteration of the feldspars are common as well (sericite and partially altered sericite)
- Lithic Fragments consist mostly of sedimentary and metasedimentary lithic grains (rank 1).

2) ***Ductile Minerals:*** Clay minerals with carbonaceous matter
3) ***Authigenic Minerals:*** Quartz overgrowths with abundant poikilotopic calcite cement. Pyrite nodules also occurs in places.
4) ***Matrix:*** Silt-sized quartz grains and clay minerals in part
5) ***Cement:*** Abundant poikilotopic calcite cement and silica cement still visible in parts.

***Reservoir potential*:** This unit supports a poor porosity and poor to absent permeability. The porosity is decreased by the occurrence of the poikilotopic calcite cement. Minor intragranular porosity exists possibly due to plagioclase alteration. The poikilotopic calcite cement also restricts flow and leads to an absent to low permeability.

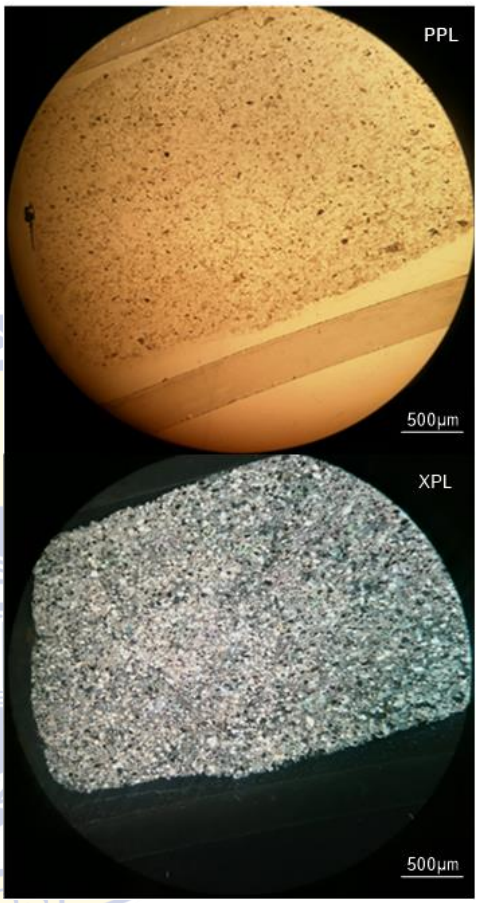

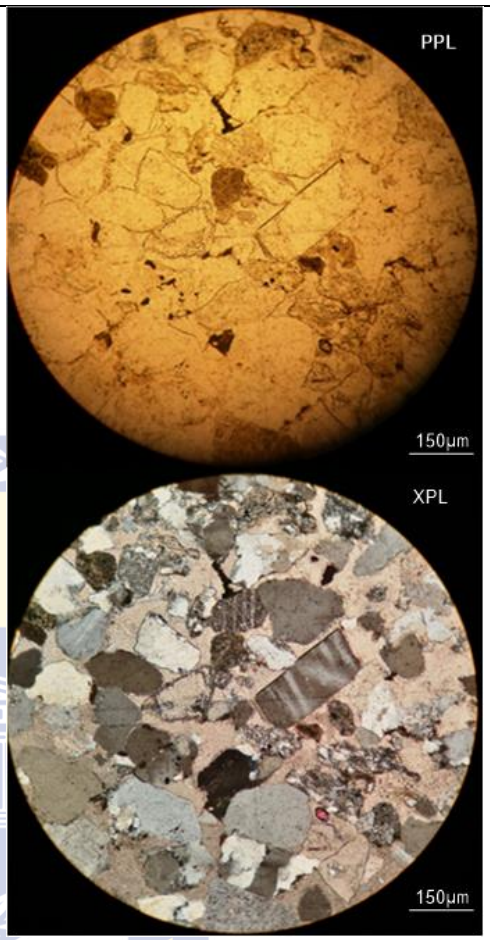

<table>
<tr><td></td><td> 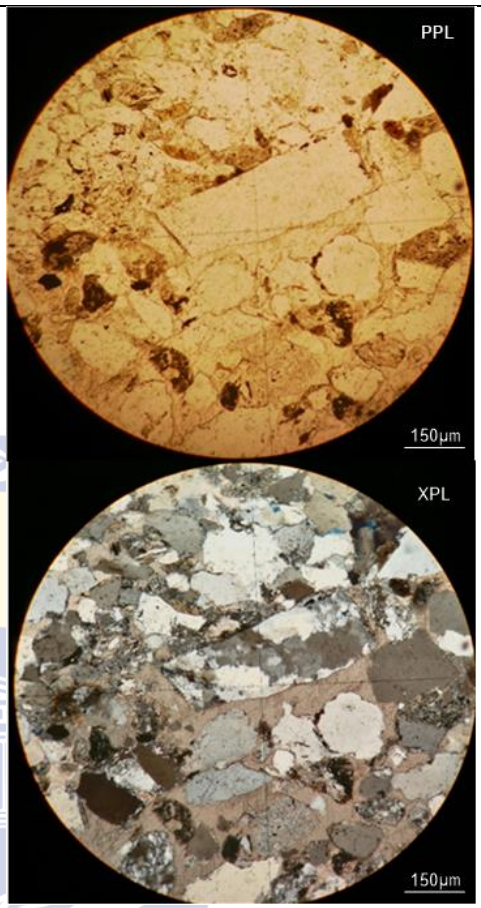
</td></tr>
<tr><td>Sample Number: F-A12#12B

Depth: 2745.80m</td><td>Modal count: QFL N/A

Facies:Facies 3.1

Microfacies:Silty claystone</td></tr>
<tr><td>General description:

Texture: A black claystone with siltstone bands. Carbonaceous material are abundant. Laminations can be seen from thin section.

Mineralogy:

Composition:

1) Framework minerals:
• Monocrystalline quartz are found with silt-sized grains. Polycrystalline quartz are absent.
• Plagioclase feldspars are absent
• No lithic fragments</td><td></td></tr>
</table>

2) ***Ductile Minerals:*** Clay minerals 3) ***Authigenic Minerals:*** Clay minerals are evident as kaolinite and illite. Sulphides arepresent as pyrite. 4) ***Matrix:*** Clay minerals 5) ***Cement:*** Clay cement (illite) ***Reservoir potential*:**This unit supports a poor porosity (9.3%**)**. This is largely as a result of secondary porosity enhancement (microcracks). Permeability is restricted because of the clay matrix. Overall this is a non-reservoir unit.	
Sample Number: F-A12#12A **Depth:** 2745.39m	**Modal count:** $Q_{65}F_{27}L_{7}$ **Facies:**Facies 3.2 **Microfacies:**Quartzofeldspathic
General description: Texture: vfL sandstone that contains grains that are subangular to subrounded (bimodal in part with silt-sized grains) and are largely poorly sorted. Some laminations are present with the occurrence of silt-sized grains and clay minerals. Heavy minerals are also present (rounded zircons). Mineralogy: ***Composition:*** 1) ***Framework minerals:*** • Monocrystalline quartz are common with unit extinction, but rare occurrence of undulose extinct quartz. Where undulose extinction occurs are heavily strained or deformed. Polycrystalline are present but rare. • Plagioclase are abundant.K-feldspars are also present in the form of orthoclase (no twinning). Plagioclase alteration is also common • Lithic fragments are mostly in the form of sedimentary lithic fragments (siltstone and claystone) 2) ***Ductile Minerals:*** Clay minerals and rare	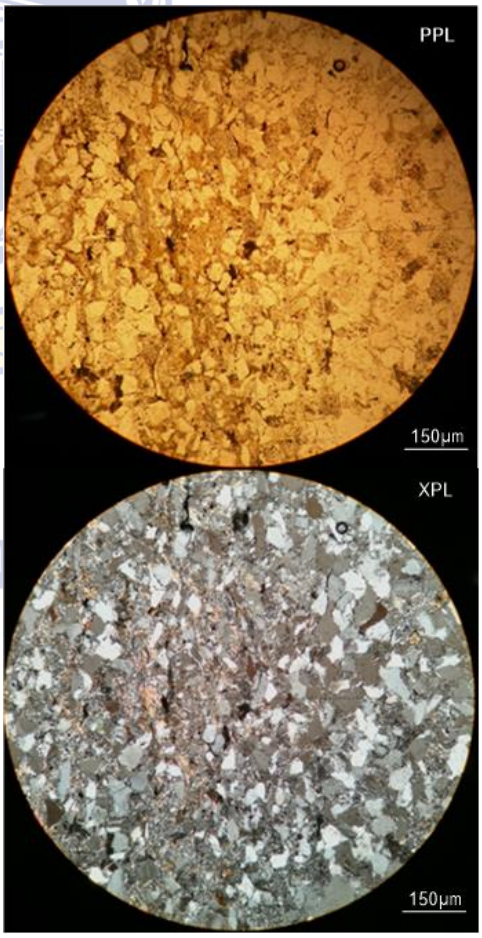

micas (biotite and muscovite seen)

3) ***Authigenic Minerals:***Calcite and clay minerals
4) ***Matrix:*** Mostly clay and silt-sized quartz grains
5) ***Cement:*** Clay cement, calcite and abundant quartz overgrowths (silica cement)

***Reservoir potential*:** This unit supports a poor porosity (8.8%) and poor permeability. Permeability has improved from the previous sample but is still restricted due to clay, calcite, silica cement and grain size sorting (bimodal). Porosity is now enhanced due to intra-particle alteration (mostly sericite from plagioclase).

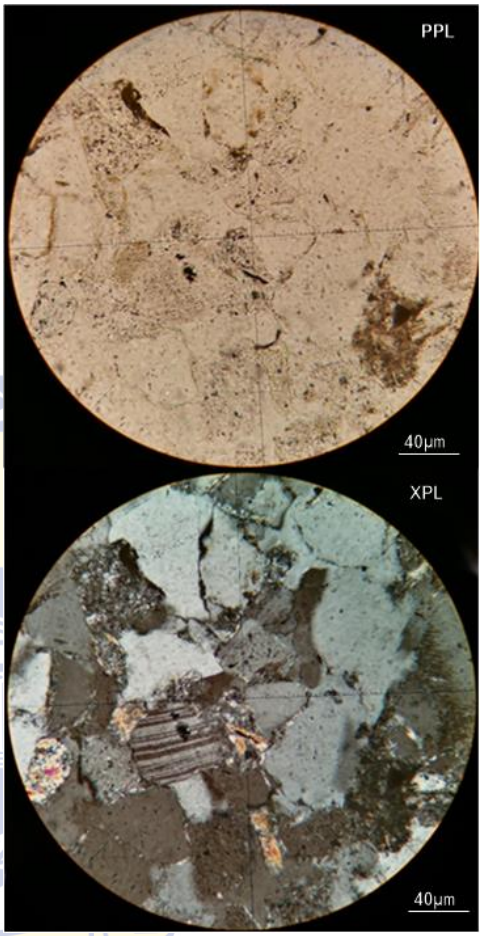

Sample Number: F-A12#11

Depth: 2743.70m

Modal count: $Q_{60}F_{36}L_3$

Facies: Facies 3.2

Microfacies : Quartzofeldspathic

General description:

Texture: vfU sandstone that has rounded to sub-rounded grains and are largely moderately sorted but has patches of poorly sorted grain distribution as well. Carbonaceous streaks are common.

Mineralogy:

Composition:

1) ***Framework minerals:***

- Monocrystalline quartz with undulose and unit extinct quartz
- Plagioclase feldspar dominant. Plagioclase

is usually altered to sericite. • Lithic fragments consist of sedimentary lithic fragments with minor metapelitic (rank 1) grains ***2) Ductile Minerals:*** Clay minerals and micas (mostly in the form of muscovite) ***3) Authigenic Minerals:*** Clay and cement ***4) Matrix:*** Clay mineral matrix ***5) Cement:*** Clay minerals with quartz overgrowths ***Reservoir potential*:**This unit supports a poor porosity and permeability. The clay mineral matrix reduced the porosity and permeability.	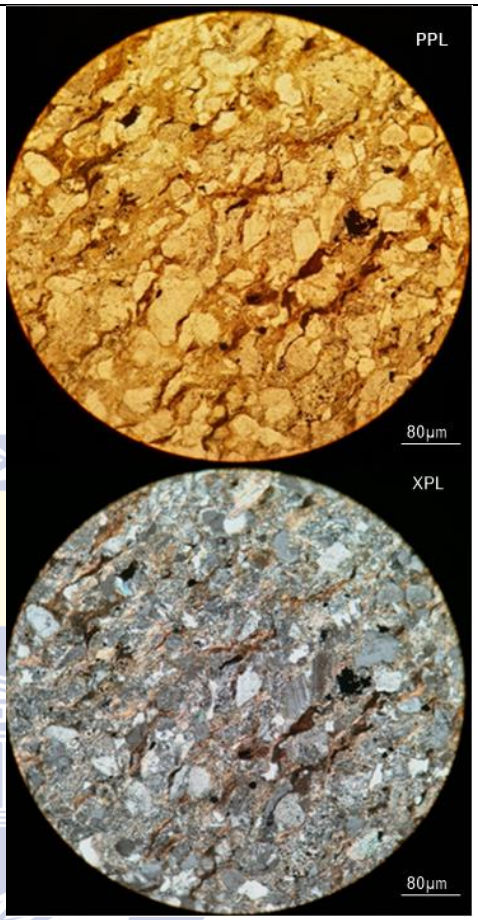
Sample Number: F-A12 #10 **Depth:** 2726.58m	**Modal count:** QFL N/A **Facies:**Facies 4.4 **Microfacies:**Caliche
General description: Texture: A brecciated deposit that is calcareous and consist of angular claystone clasts. The unit is largely poorly sorted due to burrowing. Clasts (granule)and burrows occur with burrows larger than 5mm in long axis diameter. High calcite content in the vfL host sandstone. Mineralogy: ***Composition:*** 1) ***Framework minerals:*** • Monocrystalline quartz grains shows undulose and unit extinction. Polycrystalline quartz is absent.	

- Plagioclase feldspars are common
- Lithic fragments are restricted to intraformational grains of claystone.

2) ***Ductile minerals:*** Clay minerals
3) ***Authigenic minerals:*** Clay cementwithin the clast. Calcite cement dominant in the host unit.
4) ***Matrix:*** Clay minerals in the clast are largely smectite and kaolinite. The host unit contains silt-sized quartz grains.
5) ***Cement:*** Clay mineral cement in the clast and the host unit consist mostly of calcite cement. Quartz cement also forms in microcracks

***Reservoir potential*:** This unit supports a poor porosity and permeability. Permeability is enhanced but largely due to microfractures. Porosity is also enhanced due to secondary porosity in quartz.

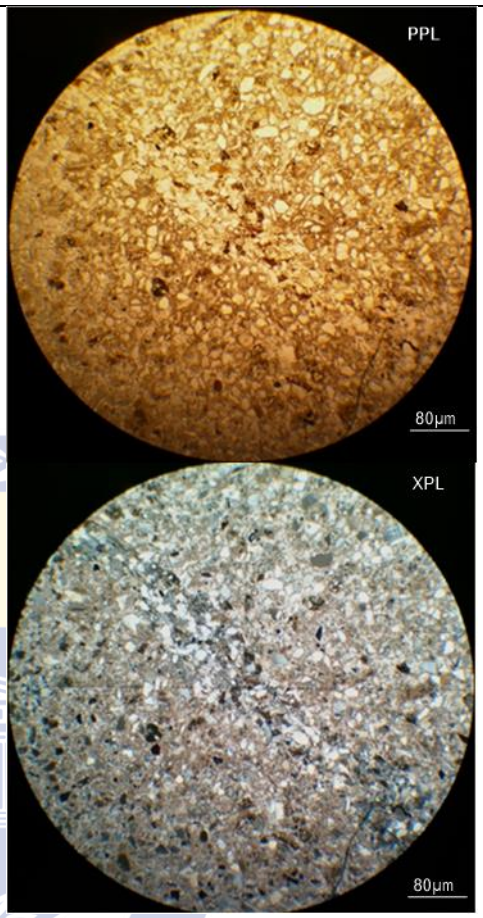

<table>
<tr><td></td><td> 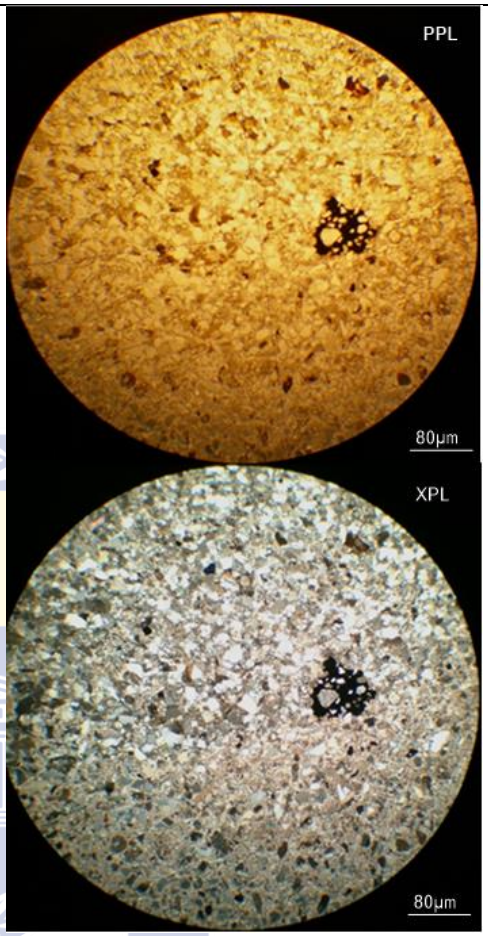
</td></tr>
<tr><td>Sample Number: F-A12#9

Depth: 2713.30m</td><td>Modal count: $Q_{73}F_{21}L_6$

Facies: Facies 4.3

Microfacies:Quartzofeldspathic</td></tr>
<tr><td>General description:

Texture: fU sandstone that contains subrounded to rounded grains and are moderately well sorted. Grain boundary contacts consist largely of concavo-convex, long contacts and sutured boundaries. Compacted sandstone unit.

Mineralogy:

Composition:

1) Framework minerals:
• Monocrystalline quartz (sub-rounded)are abundant and shows unit and undulose extinct quartz. These quartz grains also</td><td></td></tr>
</table>

shows inclusions of muscovite. Grains are largely deformed/strainedwith overgrowths. Polycrystalline is also common and contains sub-grains that are sutured

- Plagioclase feldspar is common. Orthoclase (untwinned) is also common with microcline as K-feldspars. Altered feldspars are more common than previous sample
- Lithic fragments consist of sedimentary (siltstone) and metasedimentary (rank 1) fragments

2) ***Ductile Minerals:*** Clay minerals with micas (mostly muscovite) being rare.
3) ***Authigenic Minerals:***Calcite grains are also evident.
4) ***Matrix***: Contains silt-sized quartz grains, largely compacted so matrix is not distinct.
5) ***Cement:***Quartz overgrowths or silica cementation is common.

***Reservoir potential*:** This unit supports amoderate porosity (12.5%) with poor permeability. This unit is highly compacted and porosity is only increased as secondary intra-granular porosity through plagioclase and orthoclase alteration. Permeability is restricted due to compaction, forming silica cement which inhibits flow.

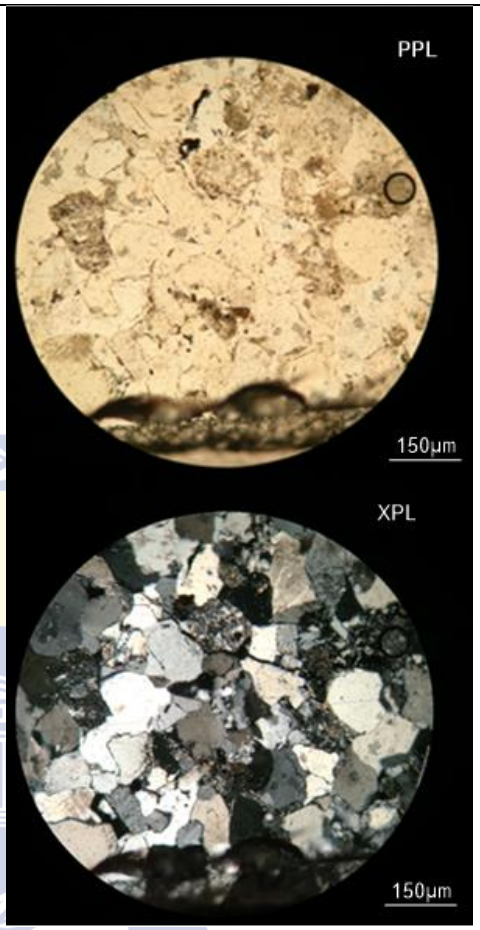

Sample Number: F-A12#8

Depth: 2706.68m

Modal count: QFL N/A

Facies: Facies 5.1

Microfacies: Mudstone

General description:

Texture: A siltstone unit with silty mudstone streaks. Grains are largely sub-angular to sub-rounded and are rather moderately sorted (immature). There are some carbonaceous material along the contacts.

Mineralogy:

Composition:

1) Framework minerals:

- Monocrystalline quartz grains with unit and undulose extinction, grains are largely

angular. Polycrystalline quartz are absent • Plagioclase feldspar are rare and consist mainly of plagioclase. • Lithic fragments are absent ***2) Ductile minerals:*** Largely made up of clay minerals, possibly montmorillonite smectite (confirmed by geochemistry) ***3) Authigenic minerals:*** Clay minerals and sulphide specks (pyrite) ***4) Matrix:*** Clay minerals ***5) Cement:*** Clay mineral cement ***Reservoir potential*:** A non-reservoir unit. Contains some porosity (still poor) due to silt-sized grains but no permeability in both vertical and horizontal distributions due to clay cement and matrix.	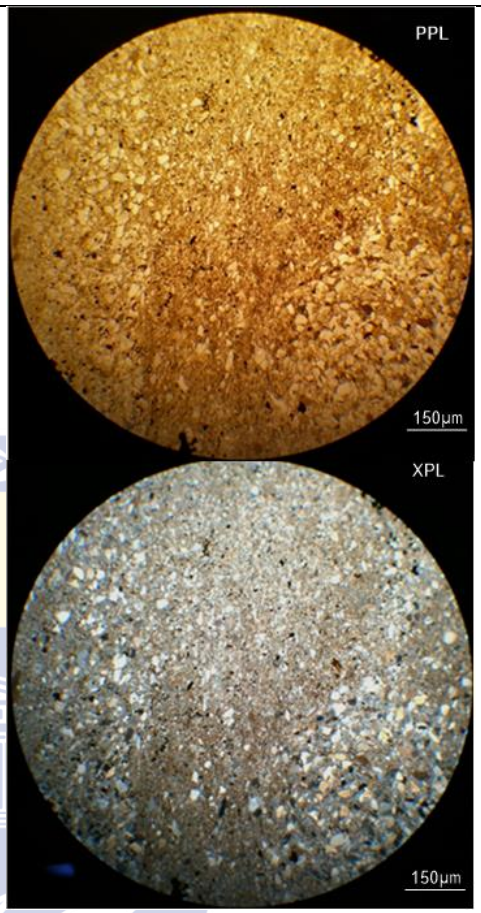
Sample Number: F-A12#7 **Depth:** 2700.23m	**Modal count:** $Q_{80}F_{16}L_4$ **Facies:**Facies 5.1 **Microfacies:**Quartzofeldspathic (Siltstone)
General description: Texture: Coarse Siltstone with sub-angular to angular grains and is moderately sorted throughout. Bioturbated and mottled unit. Mineralogy: ***Composition:*** 1) ***Framework minerals:*** • Monocrystalline quartz occurs with undulose and unit extinct quartz. Polycrystalline quartz are rare • Plagioclase is common with the K-feldspars being rare. Not much alteration occurs	

• Sedimentary lithic fragments occurs but not often. Plutonic, volcanic and metasedimentary lithic fragments occurs as well ***2) Ductile Minerals:***Clay minerals are also common with the occurrence of one or two micaceous grains (muscovite). ***3) Authigenic Minerals:***Calcite occurs frequently with siderite as well. Smectite also occurs ***4) Matrix:*** Fine silt-sized quartz grains with clay minerals (smectite-montmorillonite) ***5) Cement:***Siderite is a common cement (blobs) with minor calcite cement and in parts contain Fe-oxyhydroxide minerals. ***Reservoir potential*:** A non-reservoir unit. Poor porosity and permeability due to cement minerals.	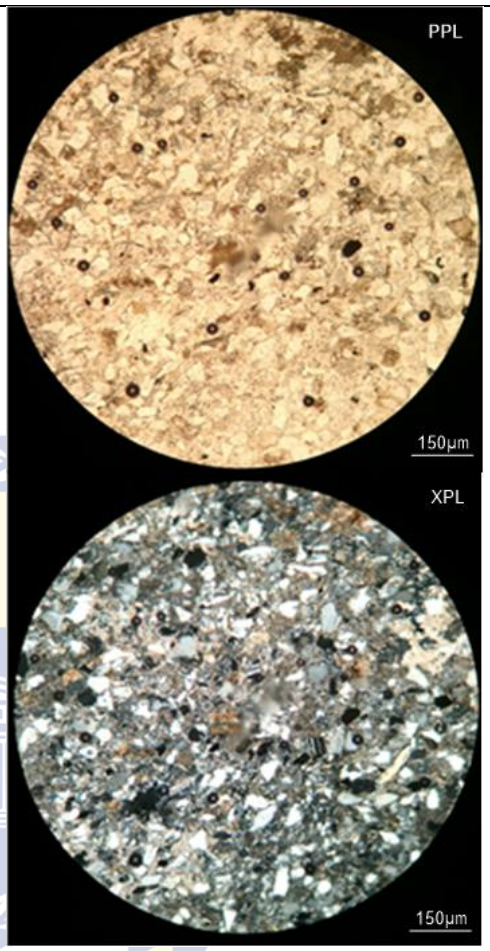
Sample Number: F-A12#6 **Depth:** 2697.00m	**Modal count:** QFL N/A **Facies:**Facies 5.1 **Microfacies:**Claystone
General description: Texture: Claystone, Largely altered minerals. Considered low energy environment Mineralogy: ***Composition:*** ***1) Framework minerals:*** • Monocrystalline quartz (subangular) are evident in parts. Polycrystalline quartz not evident. • Traces of plagioclase feldspars but largely altered to clay minerals. No visible evidence of K-feldspars.	

<table>
<tr>
<td>

- Rock fragment are absent

2) ***Ductile Minerals:***Largely consist of clay minerals. Kaolinite are largely evident as detrital grains with small speck resembling micro-quartz but shimmering nature reveals kaolinite. Illite and illite-smectite are also present.
3) ***Authigenic Minerals:***Clay minerals (illite)
4) ***Matrix:*** Clay minerals
5) ***Cement:*** Clay mineral cement (illite)

***Reservoir potential*:** Non reservoir unit. Poor porosity and permeability.

</td>
<td> 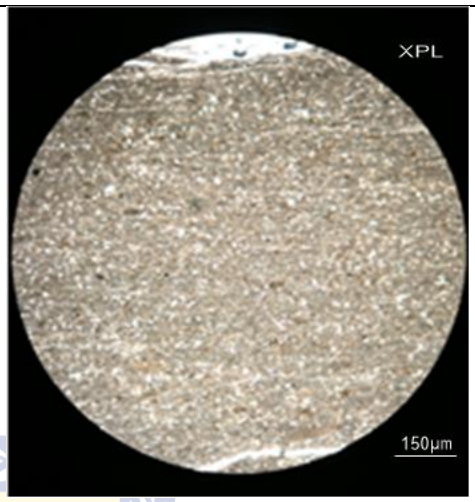
</td>
</tr>
<tr>
<td>Sample Number: F-A12 #5

Depth: 2691.44m</td>
<td>Modal count: $Q_{78}F_{13}L_{9}$

Facies:Facies 4.3

Microfacies :Quartzofeldspathic</td>
</tr>
<tr>
<td>

General description:

Texture: vfU sandstone that consist of sub-rounded to rounded grains that is moderately to poorly sorted (submature). Point contacts are common, with long contacts being rare.

Mineralogy:

Composition:

1) ***Framework minerals:***

- Monocrystalline quartz showing undulose and unit extinct grains. These quartz grains are largely angular to sub-angular. Polycrystalline tend to be abundant in this sample (sutured and long contact sub-crystal boundary)
- Plagioclase feldspar occurs more frequent as compared to its rarer counterpart, K-feldspar. Plagioclase alteration is common, fully altered and partially altered to sericite.
- Lithic fragments consist mostly of meta-sedimentary fragments (rank 1 metapelites) and minor sedimentary fragments (claystone and impure polycrystalline quartz)

</td>
<td></td>
</tr>
</table>

2) ***Ductile Minerals:***Clay minerals (smectite-montmorillonite) are common forming grain-rimming that are largely localized (pore-filling cement). Micaceous minerals are restricted to muscovite in some parts. 3) ***Authigenic Minerals:*** Consist mostly of calcite, sericite and sulphide mineral specks (pyrite). 4) ***Matrix:*** Silt-sized quartz fragments. 5) ***Cement:*** Poikilotopic calcite cement is common (some sparatic but largely poikilotopic), but where absent contains clay minerals (smectite/montmorillonite) ***Reservoir potential*:** This unit supports a poor porosity (4.1%) and poor to absent permeability. The porosity is enhanced by plagioclase alteration (secondary porosity). Permeability is mostly restricted by clay mineral cement and matrix, as well as the poikilotopic calcite cement.	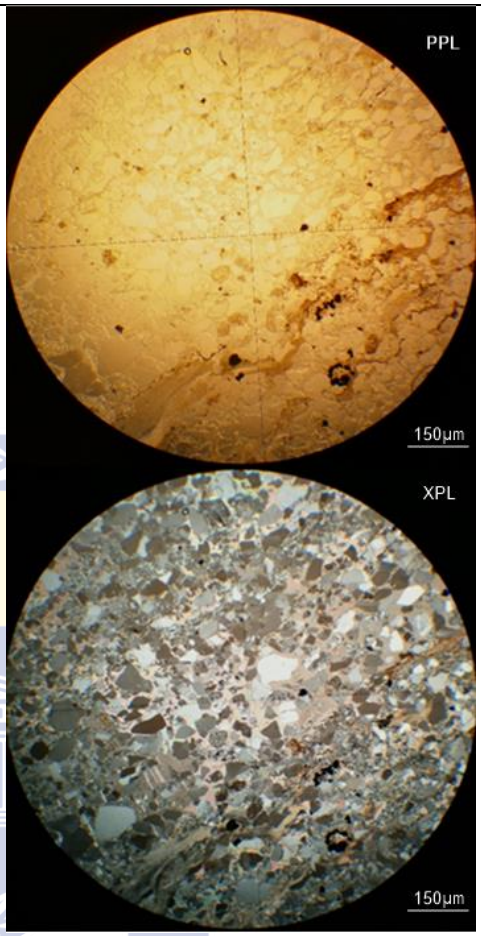
Sample Number: F-A12#4 **Depth:** 2682.57m	**Modal count:** QFL N/A **Facies:**Facies 5.1 **Microfacies :**Siltstone
General description: Texture: vfL sandstone that is moderately well sorted and contains sub-rounded to sub-angular grains. Carbonaceous material also occurs. Mineralogy: ***Composition:*** 1) ***Framework minerals:*** • Monocrystalline quartz shows undulose and unit extinction. Polycrystalline rarely occurs. • Plagioclase feldspars occurs with untwinned orthoclase (K-feldspar). There are minor	

alterations but rare. • Lithic fragments is restricted to impure polycrystalline quartz ***2) Ductile Minerals:***Clay minerals are abundant with minor micaceous minerals (muscovite) ***3) Authigenic Minerals:*** Clay minerals (illite, kaolinite and smectite). Calcite also present as grains (sparatic). Fe oxyhydroxide minerals also occur. ***4) Matrix:*** Consist largely of clay minerals ***5) Cement:*** Clay minerals (sericite, Kaolinite and illite) ***Reservoir potential*:** This unit supports a poor porosity (3.6%) and rare to absent permeability. This unit is dominated by a clay matrix and cement therefore permeability will be decreased. Porosity is restricted to the occurrence of intergranular pore spaces (primary porosity largely).	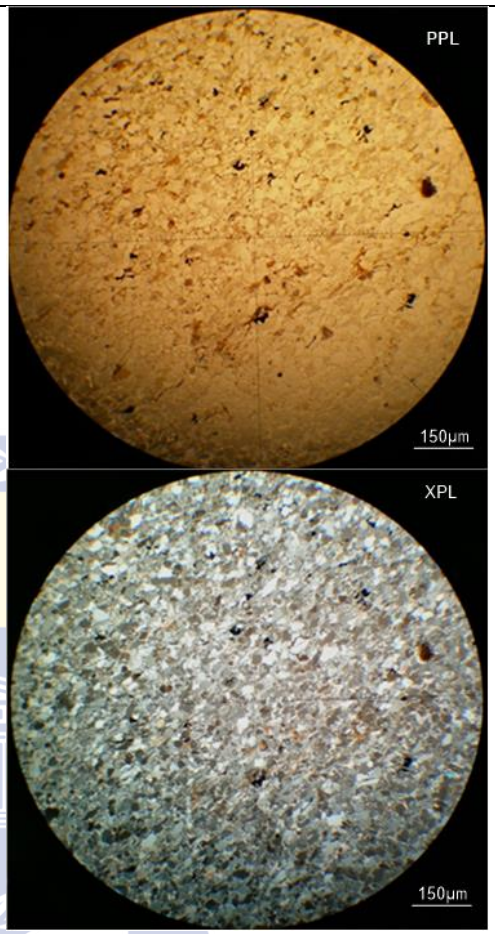
Sample Number: F-A12#3 **Depth:** 2677.82m	**Modal count:** $Q_{86}F_8L_6$ **Facies:**Facies 6.1 **Microfacies:**Quartzofeldspathic
General description: Texture: A fU sandstone that contains sub-rounded to rounded grains and are moderately well sorted (although poorly sorted in some cases). The roundness and sorting were based on quartz grains that showed quartz overgrowths because of the extreme compaction this unit was under. Microfossils in the form of echinoderms are common. These echinodermsare partially filled by glauconite as well. Mineralogy: ***Composition:*** 1) ***Framework minerals:***	

<table>
<tr>
<td>

- Monocrystalline quartz shows unit and undulose extinction. The quartz are largely rounded to subrounded. Polycrystalline quartz grains are found often.
- Plagioclase grains are common. Plagioclase is often partially to fully altered. Sub-equal amounts of fresh plagioclase feldspar and its altered counterpart (sericite). Untwinned orthoclase also occurs.
- Lithic fragments consist mostly of sedimentary siltstone and claystone clasts. The claystone clasts are also largely compacted forming a pseudo-matrix. Minor igneous (plutonic (metafelsitic) and volcanic (metabasitic)) fragments. Metamorphic fragments also occur and are restricted to metapelites (rank 1)

2) ***Ductile minerals:*** Clay minerals are common in the form of glauconite, illite and kaolinite. Kaolinite occurs mostly in the pseudomatrices created by claystone clasts.

3) Authigenic minerals: Clay minerals with silica cements in the form of quartz overgrowths. Calcite cement occurs as small herringbone features.

4) Matrix: Silt-sized quartz and lithic fragments grains.

5) Cement: Poikilotopic (minor sparitic) calcite cement and silica cement.

***Reservoir potential*:** This unit supports a moderate porosity (11%) with poor permeability. The porosity is enhanced by feldspar alterations (secondary intra-granular porosity). The occurrences of clay cements, silica cement (compacted) and calcite cements is the reason for the poor to absent permeability.

</td>
<td>
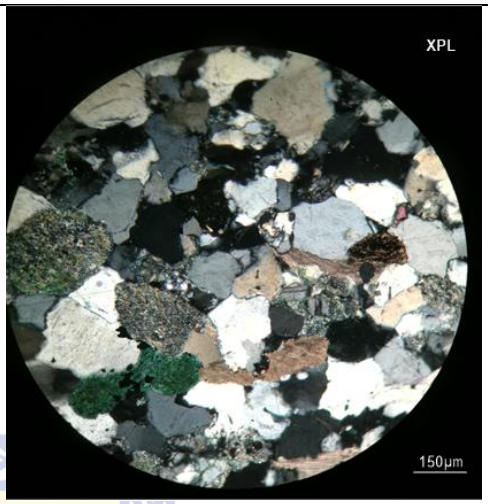

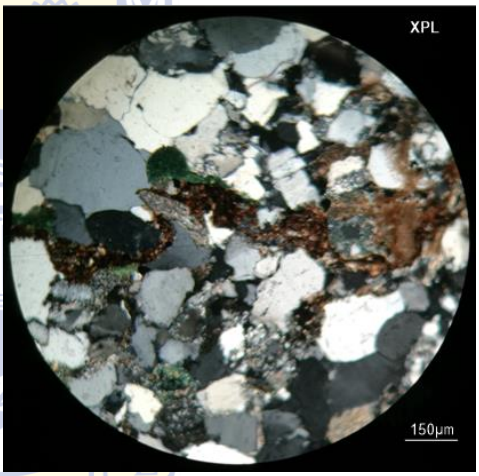

</td>
</tr>
<tr>
<td>Sample Number: F-A12#2

Depth: 2674.78m</td>
<td>Modal count: $Q_{79}F_8L_{13}$

Facies:Facies 6.1

Microfacies:Quartzolithic</td>
</tr>
<tr>
<td>General description:

Texture: fU-mL sandstone that contain sub-rounded to rounded grains that are well sorted. Calcite</td>
<td></td>
</tr>
</table>

shows herringbone twins. Compacted unit.

Mineralogy:

Composition:

1) ***Framework minerals:***
- Monocrystalline quartz shows undulose and unit extinction. The grains are mostly rounded to sub-rounded. Polycrystalline quartz is also evident.
- Plagioclase feldspar is more abundant than K-feldspars. Alteration is common among the plagioclase and untwinned orthoclase. Plagioclase shows overgrowths.
- Lithic fragments sedimentary lithic fragments (siltstone fragments). Plutonic igneous fragments also occur with metasedimentary (rank 1 metapelitic) lithic fragments.

2) ***Ductile Minerals:*** Clay minerals are common as illite/smectite. Glauconite also occurs frequently within the samples. Micaceous minerals are rare (muscovite)

3) ***Authigenic Minerals:***Calcite and clay minerals (glauconite)

4) ***Matrix:*** Matrix consist of silt-sized quartz grains and clay minerals.

5) ***Cement:***Silica cement is common due to highly compacted unit**.** Clay cement is restricted to the occurrence of claystone lithic clasts that has formed a pseudomatrix. Poikilotopic calcite cement occurs disseminated (patches).

***Reservoir potential*:** This unit supports a poor porosity and poor permeability. Permeability is decreased by the occurrence of cementation. Porosity is enhanced by the secondary intra-granular porosity. Bioturbation could also been a factor in primary porosity but completelydestroyed by compaction.

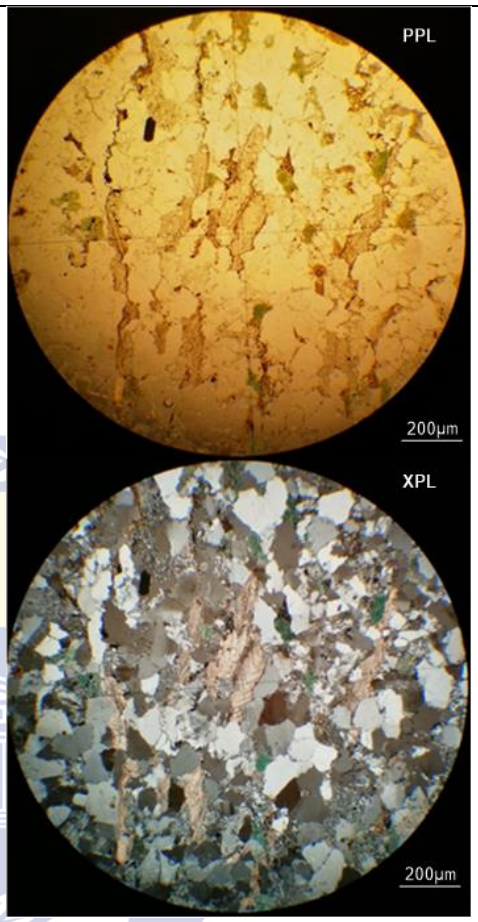

Sample Number: F-A12#1

Depth: 2662.27m

Modal count: $Q_{83}F_7L_{10}$

Facies: Facies 6.1

Microfacies: Quartzolithic

General description:

Texture: fU-mL sandstone that has sub-rounded grains and are well to moderately well-sorted. Carbonaceous patches also occurs.

Mineralogy:

Composition:

1) ***Framework minerals:***
- Monocrystalline quartz shows undulose and unit extinction. Quartz are strained and shows double extinction in parts. The quartz grains are largely rounded to sub-rounded. Polycrystalline quartz also occurs with sutured sub-grain contacts (chert).
- Plagioclase feldspar also occurs altered and unaltered grains. K-feldspars are rarely seen but untwinned orthoclase and microcline is evident in parts.
- Lithic fragments consist mostly of sedimentary and plutonic fragments. Sedimentary lithic fragments are mostly in the form of siltstone, claystone and impure polycrystalline quartz. Metamorphic rock fragments are restricted to metapelite (rank 1) lithic fragments only.

2) ***Ductile minerals:*** Clay minerals are partly visible as grain-rims and consist mostly of smectite. Glauconite is also common throughout, even occurring as an alteration directly from plagioclase feldspar.

3) ***Authigenic minerals:***Glauconite, Fe oxy-hydroxide minerals are also common as grain rimming and compacted pseudo matrix.

4) ***Matrix:*** Largely as silt-sized quartz grains with few clay minerals

5) ***Cement:*** Silica cementation is common with minor poikilotopic calcite cement. Clay mineral cement is largely restricted to the formation of oxy-hydroxide minerals.

***Reservoir potential*:** This unit supports a fairly moderate porosity (11.2) with poor to absent permeability. The porosity is enhanced by the

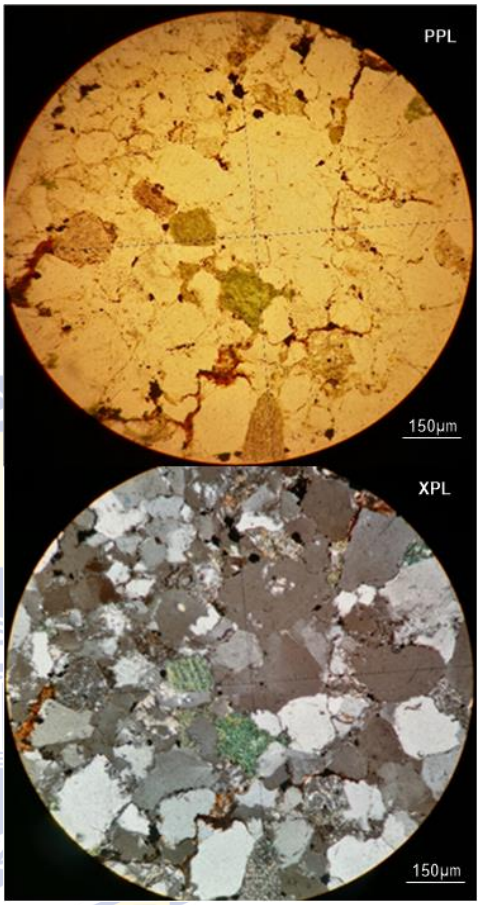

occurrence of altered feldspars (secondary intra-granular porosity). Permeability, however is restricted due to the occurrence of extensive cementation.	
Sample Number: F-AR1#11 **Depth:** 2744.80m	**Modal count:** $Q_{72}F_{22}L_7$ **Facies:**Facies 6.1a **Microfacies :**Quartzofeldspathic
General description: Texture: mL sandstone that contains sub-rounded to rounded grains and are well sorted. Mineralogy: ***Composition:*** ***1) Framework minerals:*** • Monocrystalline quartz shows both unit and undulose extinct quartz and they occur sub-equal in abundance. Polycrystalline quartz also occurs with sutured sub-grain boundaries. • Plagioclase feldspars are common. Partially altered (sericite spots). Untwinned orthoclase also occurs. • Lithic fragments consist largely of sedimentary lithic grains (impure polycrystalline quartz, claystone and siltstone fragments) 2) ***Ductile minerals:*** Glauconite occurs and are largely deformed by more hard minerals like quartz. Micaceous minerals consist largely of microcline and lesser amounts of biotite. 3) ***Authigenic minerals:***Pyrite is common. Clay minerals also occurs as diagenetic. ***4) Matrix:***Silt-sized quartz grains and some clay minerals (Kaolinite as confirmed by XRD as well) 5) ***Cement:*** Poikilotopic calcite cement patches (possibly relict disseminated shell debris). Silica cement is largely evident due to the compaction. Pyrite cement also occurs associated with organic matter.	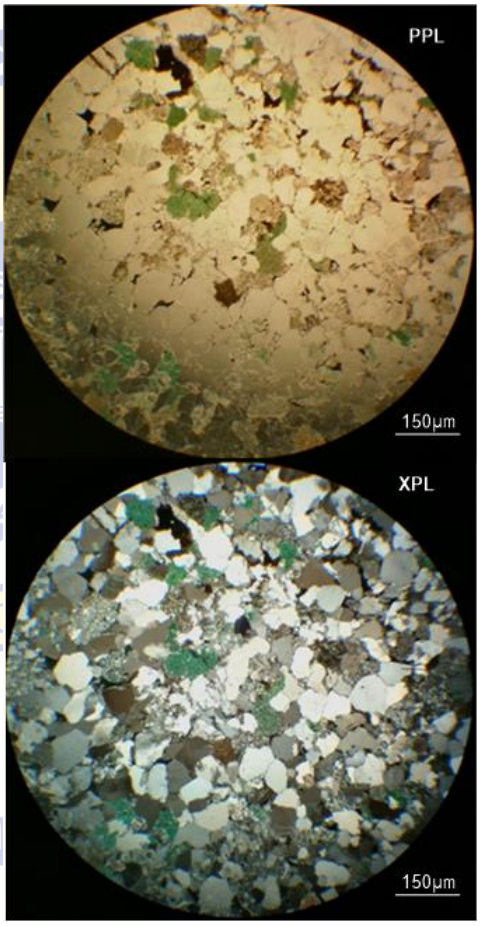

***Reservoir potential*:** This unit supports a moderate to good porosity (16%) with poor permeability. Porosity is enhanced by the secondary intra-granular porosity with feldspar alteration (spotted alteration is common). Permeability is decreased due to compaction, forming silica and calcite cement that inhibits fluid flow.	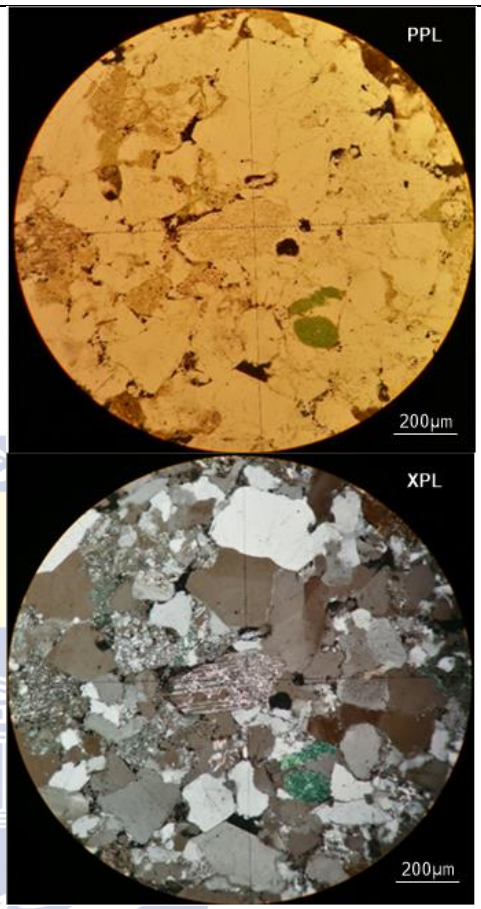

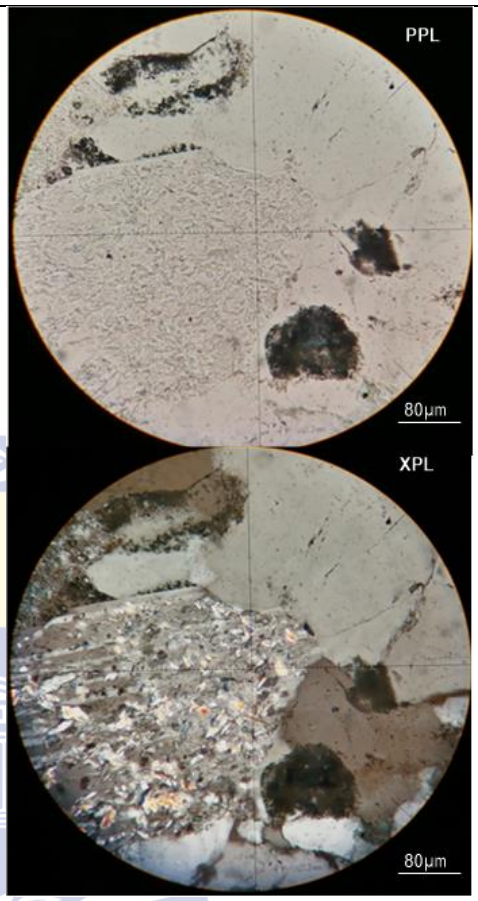

Sample Number: F-AR1#10

Depth: 2743.74m

Modal count: QFL N/A

Facies: Facies 6.1a

Microfacies: Quartzofeldspathic

General description:

Texture: vfU sandstone that contains grains that are sub-rounded to rounded and are moderately to moderately well-sorted. Compacted unit with interpenetration textures seen.

Mineralogy:

Composition:

1) ***Framework minerals:***

- Monocrystalline quartz shows unit and undulose extinction. The quartz grains are mostly rounded in shape. These quartz grains also have inclusions, mica and zircon grains. Polycrystalline quartz also occurs

with sutured sub-grain boundary contacts. • Plagioclase also occurs frequently • Lithic fragments consist largely of sedimentary lithic grains (impure polycrystalline quartz, claystone and siltstone fragments) 2) ***Ductile Minerals:*** Glauconite occurs and are largely deformed by more hard minerals like quartz. Micaceous minerals consist largely of microcline and lesser amounts of biotite. 3) ***Authigenic Minerals:***Pyrite is common. Clay minerals also occurs as diagenetic. ***4)*** ***Matrix:***Silt-sized quartz grains and some clay minerals (Kaolinite as confirmed by XRD as well) 5) ***Cement:*** Poikilotopic calcite cement patches (possibly relict disseminated shell debris). Silica cement is largely evident due to the compaction. Pyrite cement also occurs associated with organic matter. ***Reservoir potential*****:** (same as previous sample) This unit supports a moderate to good porosity (16%) with poor permeability. Porosity is enhanced by the secondary intra-granular porosity with feldspar alteration (spotted alteration is common). Permeability is decreased due to compaction, forming silica and calcite cement that inhibits fluid flow.	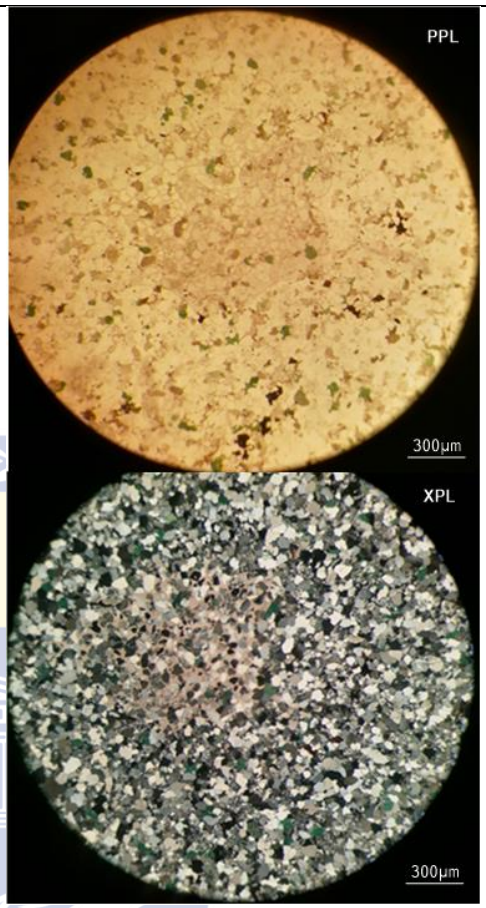
Sample Number: F-AR1#9 **Depth:** 2740.77m	**Modal count:** QFL N/A **Facies:**Facies 6.1b **Microfacies:**Quartzofeldspathic
General description: Texture: vfU sandstone that contains grains that are sub-rounded to rounded and are moderately to moderately well-sorted. Compacted unit with interpenetration textures seen. Mud drapes are common as well (silts-sized quartz grains in mud drapes). Mineralogy:	

Composition: ***1) Framework minerals:*** • Monocrystalline quartz shows unit and undulose extinction. The quartz grains are mostly rounded in shape. These quartz grains also have inclusions, micas and zircon grains. Polycrystalline quartz also occurs with sutured sub-grain boundary contacts. • Plagioclase also occurs frequently. Untwinned orthoclase also occurs. Microcline is evident but rare. • Lithic fragments consist largely of sedimentary lithic grains (impure polycrystalline quartz, claystone and siltstone fragments) 2) ***Ductile Minerals:*** Glauconite occurs and are largely deformed by more hard minerals like quartz. Micaceous minerals consist largely of microcline and lesser amounts of biotite. 3) ***Authigenic Minerals:*** Pyrite is common. Clay minerals also occurs as diagenetic. ***4) Matrix:***Silt-sized quartz grains and some clay minerals (Kaolinite as confirmed by XRD as well) 5) ***Cement:*** Poikilotopic calcite cement patches (possibly relict disseminated shell debris). Silica cement is largely evident due to the compaction. Pyrite cement also occurs associated with organic matter. ***Reservoir potential:*** Same as previous sample	
Sample Number: F-AR1#8 **Depth:** 2737.41m	**Modal count:** QFL N/A **Facies:**Facies 6.1a **Microfacies:**Quartzofeldspathic
General description: Texture: fL sandstone that contains grains that are sub-rounded to rounded and are moderately to moderately well-sorted. Compacted unit with interpenetration textures seen. Mud drapes are common as well (silts-sized quartz grains in mud	

drapes).

Mineralogy:

Composition:

1) ***Framework minerals:***

- Monocrystalline quartz shows unit and undulose extinction. The quartz grains are mostly rounded in shape. Some of the quartz grains are also spherical to elongated. These quartz grains also have inclusions, micas and zircon grains. Polycrystalline quartz also occurs with sutured sub-grain boundary contacts.
- Plagioclase also occurs frequently. Untwinned orthoclase also occurs. Microcline is evident but rare.
- Lithic fragments consist largely of sedimentary lithic grains (impure polycrystalline quartz, claystone and siltstone fragments)

2) ***Ductile Minerals:*** Glauconite occurs and are largely deformed by more hard minerals like quartz. Glauconite is also spherical (well rounded). Some glauconite is also partially to fully altered. Micaceous minerals consist largely of microcline and lesser amounts of biotite.
3) ***Authigenic Minerals:***Pyrite (sulphide) is common. Clay minerals also occurs as diagenetic.
4) ***Matrix:***Silt-sized quartz grains and some clay minerals (Kaolinite as confirmed by XRD as well)
5) ***Cement:*** Poikilotopic calcite cement patches (possibly relict disseminated shell debris). Silica cement is largely evident due to the compaction. Overprinting is common between grains, such as orthoclase replaced by calcite. Pyrite cement also occurs associated with organic matter.

Reservoir potential:*Same as previous sample but with porosity at 15.2%*

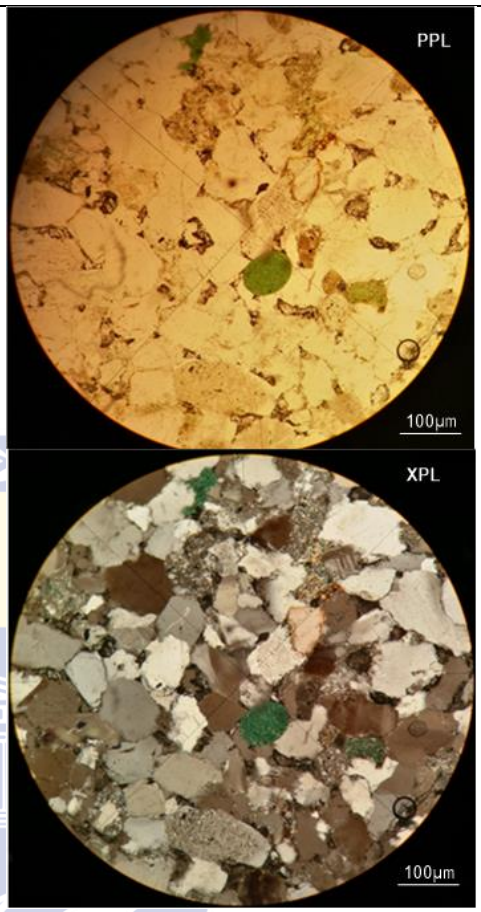

Sample Number: F-AR1#7 **Depth:** 2735.44m	**Modal count:** $Q_{78}F_{19}L_3$ **Facies:** Facies 6.1a **Microfacies:**Quartzofeldspathic
General description: Texture: vfU to fL sandstone that contains grains that are sub-rounded to rounded and are moderately to moderately well-sorted. Compacted unit with interpenetration textures seen. Mud drapes are common as well (silts-sized quartz grains in mud drapes). Mineralogy: ***Composition:*** ***1) Framework minerals:*** • Monocrystalline quartz shows unit and undulose extinction. The quartz grains are mostly rounded in shape. Some of the quartz grains are also spherical to elongated. These quartz grains also have inclusions, micas and zircon grains. Polycrystalline quartz also occurs with sutured sub-grain boundary contacts. • Plagioclase also occurs frequently. Untwinned orthoclase also occurs with its alteration product (sericite). Microcline is evident but rare. Plagioclase are largely partially altered with some showing full alteration to sericite. • Lithic fragments consist largely of sedimentary lithic grains (impure polycrystalline quartz, claystone and siltstone fragments) 2) ***Ductile Minerals:*** Glauconite occurs and are largely deformed by more hard minerals like quartz. Glauconite is also spherical (well rounded). Some glauconite is also partially to fully altered. Micaceous minerals consist largely of microcline and lesser amounts of biotite. 3) ***Authigenic Minerals:***Pyrite (sulphide) is common. Clay minerals also occurs as diagenetic.	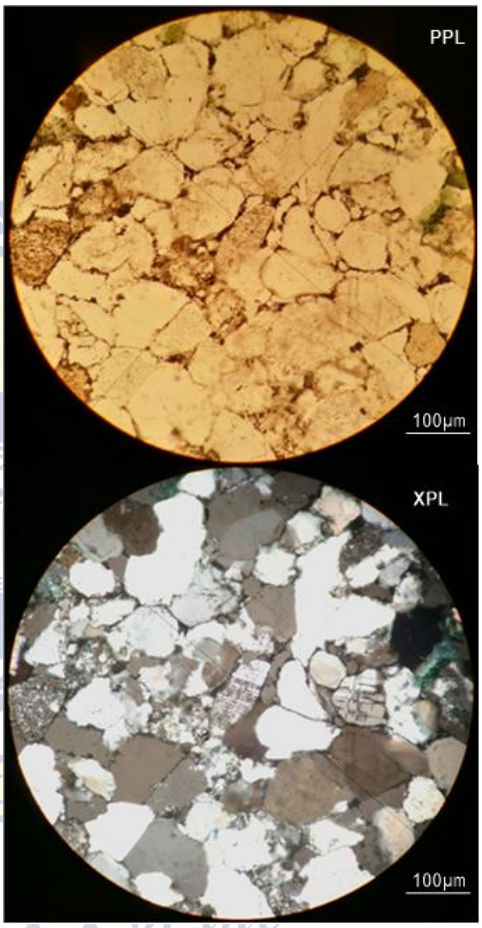

4) ***Matrix:***Silt-sized quartz grains and some clay minerals (Kaolinite as confirmed by XRD as well) 5) ***Cement:*** Poikilotopic calcite cement patches (possibly relict disseminated shell debris). Silica cement is largely evident due to the compaction. Overprinting is common between grains, such as orthoclase replaced by calcite. Pyrite cement also occurs associated with organic matter. ***Reservoir potential*:** Porosity decreased to 14% from previous sample and its formation is the same as previous sample.	
Sample Number: F-AR1#6 **Depth:** 2729.63m	**Modal count:** QFL N/A **Facies:**Facies 6.1b **Microfacies:**Quartzofeldspathic
General description: Texture: vfU sandstone that contains grains that are sub-rounded to sub-angular and are moderately to moderately well-sorted. Compacted unit with interpenetration textures seen. Mud drapes are common as well (silts-sized quartz grains in mud drapes). Mineralogy: ***Composition:*** ***1) Framework minerals:*** • Monocrystalline quartz shows unit and undulose extinction. The quartz grains are mostly rounded in shape. The quartz grains also shows fractures in some places. These quartz grains also have inclusions, micas and zircon grains. Polycrystalline quartz also occurs with sutured sub-grain boundary contacts. • Plagioclase also occurs frequently. Untwinned orthoclase also occurs with its alteration product (sericite). Microcline is evident but rare. Plagioclase are largely partially altered with some showing full	

alteration to sericite.

- Lithic fragments consist largely of sedimentary lithic grains (impure polycrystalline quartz, claystone and siltstone fragments)

2) ***Ductile minerals:*** Glauconite are abundant. Glauconite is also spherical (well rounded). Some glauconite is also partially to fully altered. Micaceous minerals consist largely of microcline and lesser amounts of biotite.
3) ***Authigenic minerals:***Pyrite (sulphide) is common. Clay minerals also occurs as diagenetic.
4) ***Matrix:***Silt-sized quartz grains and some clay minerals (Kaolinite as confirmed by XRD as well)
5) ***Cement:*** Poikilotopic calcite cement patches (possibly relict disseminated shell debris). Silica cement is largely evident due to the compaction. Pyrite cement also occurs associated with organic matter.

***Reservoir potential*:** Porosity increased to 17% from previous sample. Poor permeability is still evident. The increase in porosity is a result of the fractured quartz seen in some of the samples but are largely the results of alteration of feldspars (more orthoclase alteration). Permeability is decreased due to compaction.

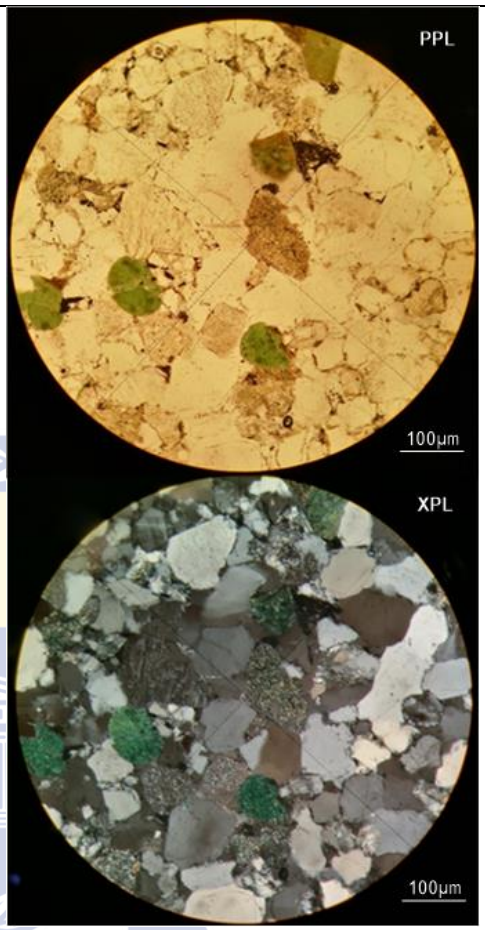

	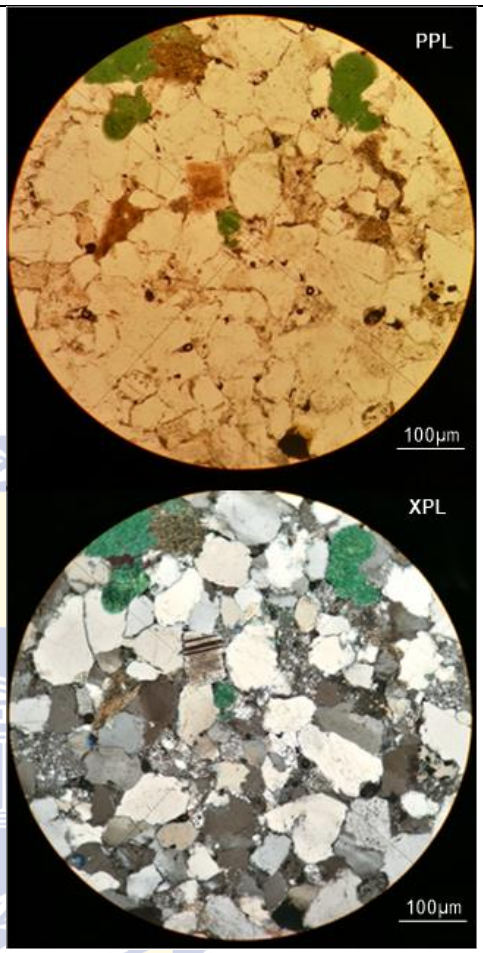
Sample Number: F-AR1#5 **Depth:** 2725.42m	**Modal count:** $Q_{72}F_{26}L_{1}$ **Facies:**Facies 6.1b **Microfacies:**Quartzofeldspathic
General description: Texture: vfU sandstone that contains grains that are sub-rounded to sub-angular and are moderately to moderately well-sorted. Compacted unit with interpenetration textures seen. Mud drapes are common as well (silts-sized quartz grains in mud drapes). Mineralogy: ***Composition:*** ***1) Framework minerals:*** • Monocrystalline quartz shows unit and undulose extinction. The quartz grains are	

mostly rounded in shape. The quartz grains also shows fractures in some places. These quartz grains also have inclusions, micas and zircon grains. Polycrystalline quartz also occurs with sutured sub-grain boundary contacts.

- Plagioclase (albite) also occurs frequently. Untwinned orthoclase also occurs with its alteration product (sericite). Microcline is evident but rare. Plagioclase are largely partially altered with some showing full alteration to sericite.
- Lithic fragments consist largely of sedimentary lithic grains (impure polycrystalline quartz, claystone and siltstone fragments)

2) ***Ductile Minerals:*** Glauconite are abundant. Glauconite is also spherical (well rounded). Some glauconite is also partially to fully altered. Micaceous minerals consist largely of microcline and lesser amounts of biotite.
3) ***Authigenic Minerals:***Pyrite (sulphide) is common. Clay minerals also occurs as diagenetic.
4) ***Matrix:***Silt-sized quartz grains and some clay minerals (Kaolinite as confirmed by XRD as well)
5) ***Cement:*** Poikilotopic calcite cement patches (possibly relict disseminated shell debris). Silica cement is largely evident due to the compaction. Pyrite cement also occurs associated with organic matter.

***Reservoir potential*:** Porosity decreased to 14% from previous sample. Poor permeability is still evident. Moderate to poor porosity is a result of silica and calcite cementation. Permeability is decreased due to compaction.

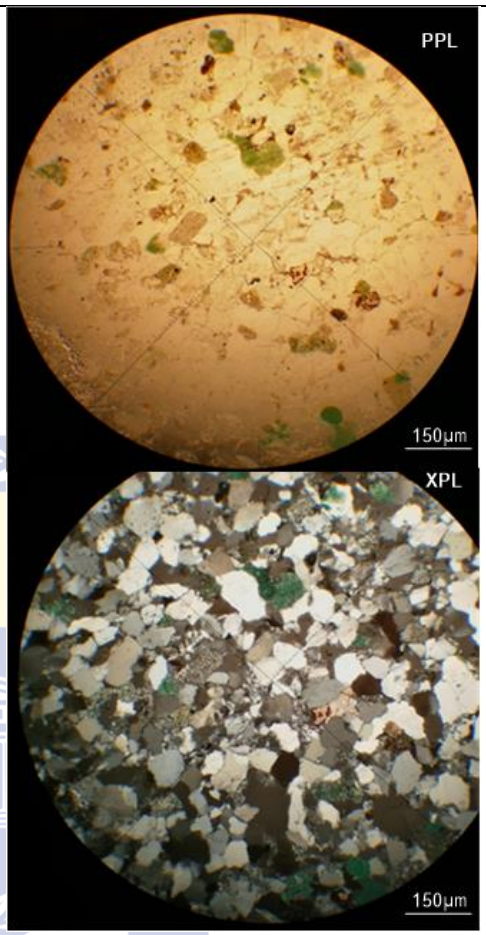

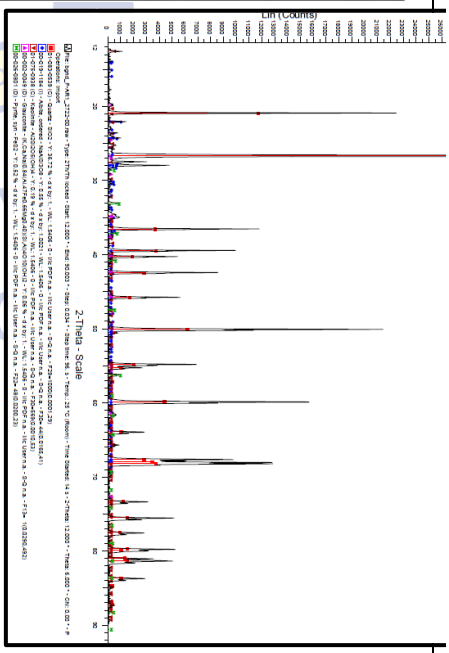

- XRD analysis confirms quartz, albite, kaolinite,

	glauconite and pyrite in decreasing abundance.
Sample Number: F-AR1#4 **Depth:** 2719.19m	**Modal count:** $Q_{83}F_9L_8$ **Facies:**Facies 6.1a **Microfacies:**Quartzofeldspathic
General description: Texture: vfU sandstone that contains grains that are sub-rounded to rounded and are moderately to well-sorted. Compacted unit with interpenetration textures seen. Mineralogy: ***Composition:*** ***1) Framework minerals:*** • Monocrystalline quartz shows unit and undulose extinction. The quartz grains are mostly rounded in shape. The quartz grains also shows fractures in some places. Polycrystalline quartz also occurs with sutured sub-grain boundary contacts. • Plagioclase also occurs frequently. Untwinned orthoclase also occurs with its alteration product (sericite). Microcline is evident but rare. Plagioclase are largely partially altered with some showing full alteration to sericite. • Lithic fragments consist largely of sedimentary lithic grains (impure polycrystalline quartz, claystone and siltstone fragments). Metafelsitic, metapelites and volcanic lithic fragments are also common. 2) ***Ductile Minerals:*** Glauconite are abundant. Glauconite is also spherical (well rounded). Some glauconite is also partially to fully altered. Micaceous minerals consist largely of microcline and lesser amounts of biotite. 3) ***Authigenic Minerals:***Pyrite (sulphide) is	

common. Clay minerals also occurs as diagenetic. ***4) Matrix:***Silt-sized quartz grains and some clay minerals (Kaolinite as confirmed by XRD as well) 5) ***Cement:*** Poikilotopic calcite cement patches (possibly relict disseminated shell debris). Silica cement is largely evident due to the compaction. Pyrite cement also occurs associated with organic matter. ***Reservoir potential*:** Very good porosity (20%) and poor permeability. Porosity is enhanced by feldspar alteration with the occurrence of micro-fractures as well. The alteration of volcanic fragments could also have enhanced porosity. Permeability is decreased due to silica cementation and compaction.	
Sample Number: F-AR1#3 **Depth:** 2717.41m	**Modal count:** QFL N/A **Facies:**Facies 6.3 **Microfacies:**Quartzofeldspathic
General description: Texture: fL sandstone that contains grains that are sub-rounded to sub-angular and are moderately to moderately well-sorted. Compacted unit with interpenetration textures seen. Siltstone intra-basinal elongated clasts (300-400µm) are common. Sulphide clasts occur (pyrite) difficult to identify authigenic or detrital. Mineralogy: ***Composition:*** ***1) Framework minerals:*** • Monocrystalline quartz shows unit and undulose extinction. The quartz grains are mostly rounded in shape. Polycrystalline quartz also occurs with sutured sub-grain boundary contacts. • Plagioclase also occurs frequently. Untwinned orthoclase also occurs with its alteration product (sericite). Microcline is evident but rare. Plagioclase are largely	

partially altered with some showing full alteration to sericite.

- Lithic fragments consist largely of sedimentary lithic grains (impure polycrystalline quartz, claystone and siltstone fragments). Metafelsitic, metapelites and volcanic lithic fragments are also common.

2) ***Ductile minerals:*** Glauconite are abundant. Glauconite is also spherical (well rounded). Some glauconite is also partially to fully altered. Micaceous minerals consist largely of microcline and lesser amounts of biotite.
3) ***Authigenic minerals:***Pyrite (sulphide) is common. Clay minerals also occurs as diagenetic.
4) ***Matrix:***Silt-sized quartz grains and some clay minerals (Kaolinite as confirmed by XRD as well)
5) ***Cement:*** Silica cement is largely evident due to the compaction. Pyrite cement also occurs associated with organic matter.

***Reservoir potential*:** Good porosity (17%) and poor permeability. Porosity is enhanced by feldspar alteration. The alteration of volcanic fragments could also have enhanced porosity. Permeability is decreased due to silica cementation and compaction.

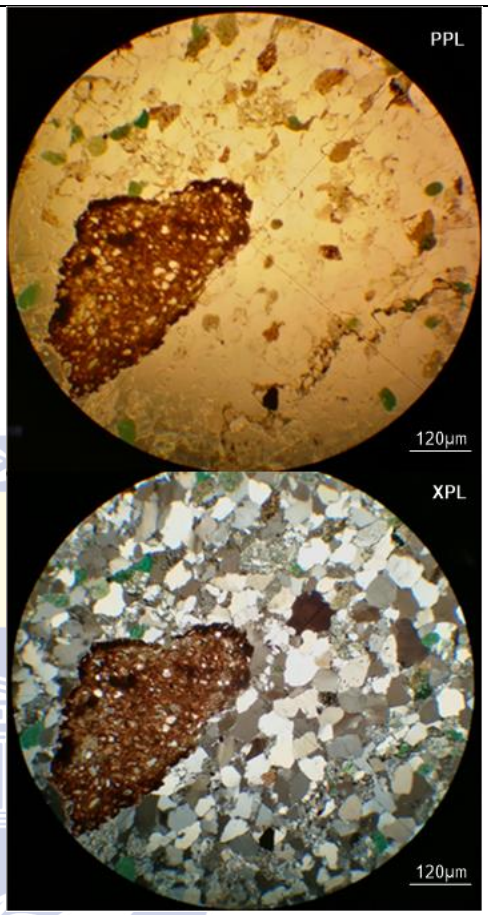

Sample Number: F-AR1#2

Depth: 2713.91m

Modal count: QFL N/A

Facies: Facies 6.1a

Microfacies: Quartzofeldspathic

General description:

Texture: fL sandstone that contains grains that are sub-rounded to sub-angular and are moderately to moderately well-sorted. Poorly sorted in some parts. Point contacts are common. Siltstone intra-basinal elongated clasts (300-400µm) are common. Sulphides are rather abundant and forms sulphide cement.

Mineralogy:

Composition:

1) ***Framework minerals:***

- Monocrystalline quartz shows unit and undulose extinction. The quartz grains are mostly rounded in shape. Polycrystalline quartz also occurs with sutured sub-grain boundary contacts.
- Plagioclase (albite) also occurs frequently. Untwinned orthoclase also occurs with its alteration product (sericite). Microcline is evident but rare. Plagioclase are largely partially altered with some showing full alteration to sericite.
- Lithic fragments consist largely of sedimentary lithic grains (impure polycrystalline quartz, claystone and siltstone fragments). Metafelsitic, metapelites and volcanic lithic fragments are also common.

2) ***Ductile minerals:*** Glauconite are abundant. Glauconite is also spherical (well rounded). Some glauconite is also partially to fully altered. Micaceous minerals consist largely of microcline and lesser amounts of biotite.

3) ***Authigenic minerals:***Pyrite (sulphide) is common. Clay minerals also occurs as diagenetic.

4) ***Matrix:***Silt-sized quartz grains and some clay minerals (Kaolinite as confirmed by XRD)

5) ***Cement:*** Silica cement is evident but occurs in patches due to the differential compaction. Pyrite cement also occurs associated with organic matter.

***Reservoir potential*:** This unit supports agood porosity (19.7%) and good permeability (220mD). Porosity is enhanced by feldspar alteration. The alteration of volcanic fragments could also have enhanced porosity (secondary macroporosity). Permeability increased possibly as a result of pore connectivity.

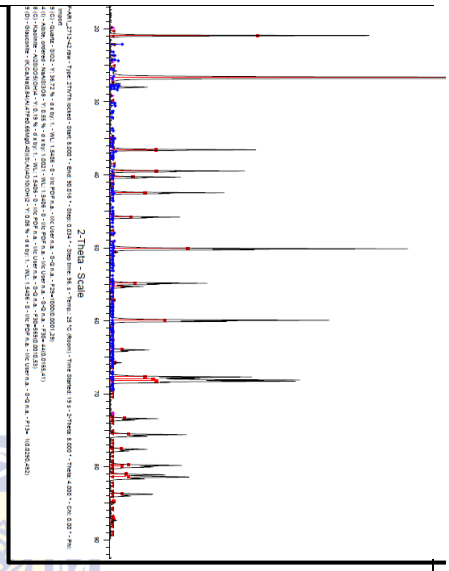

- XRD analysis confirms quartz, albite, kaolinite and glauconite in decreasing abundance.

Sample Number: F-AR1#1

Modal count: $Q_{55}F_{35}L_{10}$

Depth: 2698.67m	**Facies:**Facies 6.1a **Microfacies :**Quartzofeldspathic
General description: Texture: fL sandstone that contains grains that are sub-rounded to sub-angular and are moderately sorted. Some patches also contains fU- to mL-sized grains. Point contacts are common. Siltstone intra-basinal elongated clasts (300-400µm) are common. Sulphides are rather abundant and forms sulphide cement. Mineralogy: ***Composition:*** ***1) Framework minerals:*** • Monocrystalline quartz shows unit and undulose extinction. The quartz grains are mostly rounded in shape. Polycrystalline quartz also occurs with sutured sub-grain boundary contacts. • Plagioclase (albite) also occurs frequently. Untwinned orthoclase also occurs with its alteration product (sericite). Microcline is evident but rare. Plagioclase are largely partially altered with some showing full alteration to sericite. • Lithic fragments consist largely of sedimentary lithic grains (impure polycrystalline quartz, claystone and siltstone fragments). Metafelsitic, metapelites and volcanic lithic fragments are also common. 2) ***Ductile minerals:*** Glauconite are abundant. Glauconite is also spherical (well rounded). Some glauconite is also partially to fully altered. Micaceous minerals consist largely of microcline and lesser amounts of biotite. 3) ***Authigenic minerals:***Clay minerals also occurs as diagenetic. ***4) Matrix:***Silt-sized quartz grains and some clay minerals (Kaolinite as confirmed by XRD) 5) ***Cement:*** Silica cement is evident but occurs in patches due to the differential	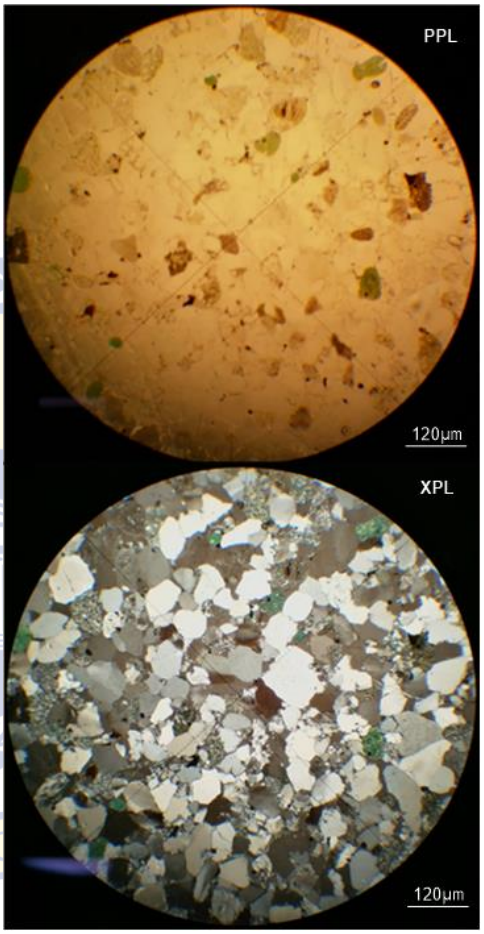

compaction. Pyrite cement also occurs associated with organic matter. ***Reservoir potential*:** This unit supports agood porosity (20.3%) and very good permeability (326mD). Porosity is enhanced by feldspar alteration and the poorly-sorted patches. The alteration of volcanic fragments could also have enhanced porosity (secondary macroporosity). Permeability is increased possibly as a result of pore connectivity. Also, in terms of the overall unit, the porosity and permeability increases as the depth decreases.	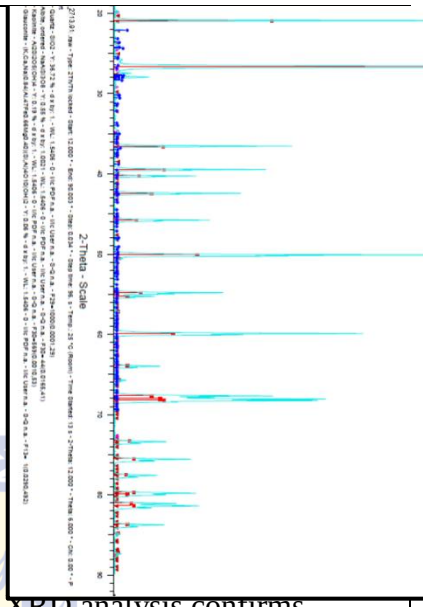 • XRD analysis confirms quartz, albite, kaolinite and glauconite in decreasing abundance.

Appendix C: Geochemical data

Raw geochemical data

Table C1: Major element chemistry showing all the major oxides (in %) of selected samples in the 1AT1-V horizon reservoir interval. Averages of the fine and coarse fractions and referenced sediment values has been added (PAAS- Post Archean Shale, NASC- North Amercican Sandstone Composite and UCC- Upper Continental Crust reference values).

Sample name	**Rock sample**	**Al_2O_3 (%)**	**CaO (%)**	**Cr_2O_3 (%)**	**Fe_2O_3 (%)**	**K_2O (%)**	**MgO (%)**	**MnO (%)**	**Na_2O (%)**	**P_2O_5 (%)**	**SiO_2 (%)**	**TiO_2 (%)**	**L.O.I. (%)**
F-A5*1	Sandstone (fL)	4.12	0.97	0	1.3	0.6	0.26	0.03	1.18	0.05	89.2	0.3	1.239
F-A5*3	Sandstone (vfL-vfU/siltstone bands)	7.24	0.16	0	1.9	1.3	0.44	0.01	1.81	0.07	83.6	0.4	2.722
F-A5*4	Sandstone (mU)	3.42	0.65	0	2.2	0.9	0.44	0.1	0.68	0.15	88.7	0.2	1.63
F-A5*5	Sandstone (glauconitic fU)	3.35	0.29	0	1.6	0.8	0.31	0.04	0.75	0.1	90.9	0.2	1.071
F-A5*7	Sandstone (vfU)/Clst clasts	11.13	0.21	0	2.1	2.7	0.78	0.01	2.13	0.1	76.5	0.5	2.882
F-A5*8	Sandstone (mL)	4.11	0.19	0.01	1.4	0.9	0.27	0.01	0.99	0.08	90.1	0.3	0.798
F-A5*9	Sandstone (vfU)/Siltstone drapes	12.14	0.22	0.01	2.5	2.7	0.87	0.01	2.49	0.1	74.9	0.6	3.01
F-A5*10	Sandstone (fU)	5.27	0.17	0.01	1.8	1.1	0.43	0.01	1.23	0.07	87.1	0.3	0.981
F-A5*11	Mudstone with sandstone clasts	13.62	0.69	0.01	3.8	3.3	1.41	0.04	1.95	0.11	69.8	0.7	4.053
F-A5*14	Silty Claystone	14.24	2.7	0.01	3.5	4.2	1.61	0.04	1.27	0.06	65.1	0.5	6.777
F-A5*17	Claystone	13.78	1.76	bdl	3.6	3.9	1.67	0.06	1.26	0.13	67	0.5	6.086
F-AR1*11	Sandstone (glauconitic fL)	4.36	0.66	0.01	2.5	1.2	0.48	0.18	0.76	0.1	87.1	0.2	1.535
F-AR1*7	Sandstone (glauconitic vfU-	3.91	0.29	0.01	2.1	1.1	0.41	0.05	0.64	0.09	89.4	0.2	1.164

	fL)												
F-AR1*5	Sandstone (glauconitic vfU)	3.98	0.2	0.01	2.3	1.1	0.41	0.02	0.64	0.1	89.1	0.3	1.173
F-AR1*3	Sandstone (glauconitic fL minor siltstone clasts)	4.52	0.33	0.01	3.1	1.3	0.61	0.36	0.68	0.12	86	0.3	2.202
F-AR1*1	Sandstone (fU-mL)	2.98	0.16	0.01	2	0.9	0.29	0.02	0.52	0.1	90.7	0.2	1.487
F-A12*1	Sandstone (glauconitic fU-mL) Carb/Calc	3.9	2.67	0.01	6.4	1	0.74	1.1	0.56	0.16	74.1	0.3	5.122
F-A12*2	Sandstone (glauconitic fU-mL)	4.15	1.49	0.01	1.9	1.1	0.41	0.14	0.71	0.12	86.6	0.3	2.182
F-A12*4	Siltstone	12.19	0.62	0.01	2.6	2.7	0.65	0.06	1.8	0.09	74.2	0.6	3.532
F-A12*5	Sandstone (vfU) Calc with clay matrix	6.54	13.25	0.01	2.1	1.5	0.46	0.13	1.22	0.07	62.5	0.3	11.4
F-A12*6	Siltstone	13.14	0.35	0.01	3.2	3.5	1.26	0.06	0.96	0.1	70.9	0.4	5.457
F-A12*7	Sandstone (vfL)	8.68	5.29	0.01	1.7	1.9	0.66	0.06	1.73	0.07	73.2	0.4	6.262
F-A12*8	Mudstone	14.74	0.26	0.01	4.1	3.5	1.03	0.02	1.96	0.13	66.8	0.8	5.284
F-A12*9	Sandstone (fU)	4.78	0.69	0.01	1.2	1.1	0.26	0.02	1.08	0.07	88.6	0.3	1.252
F-A12*10	Brecciated vfL sandstone (burrowed)	5.51	15.14	0.01	4.5	1.3	6.87	0.42	1	0.04	44.2	0.2	20.78
F-A12*11	Sandstone (vfU)	17.95	0.24	0.01	3.7	4.2	1.06	0.02	2.56	0.11	62.7	0.8	5.279
F-A12*12a	Sandstone (vfL)	6.95	0.4	0.01	2	1.4	0.46	0.02	1.44	0.1	84.5	0.4	1.604

F-A12*12	Silty Claystone	23.09	0.24	0.01	4.9	6.1	1.72	0.02	1.47	0.13	52.9	1.1	7.409
F-A12*13	Sandstone (fU)	3.9	12.09	0.01	1.5	0.9	0.32	0.1	0.87	0.06	70.2	0.2	9.584
F-A12*14	Sandstone (vfU-siltstone bands)	14.27	0.29	0.01	3.7	3.1	0.98	0.02	2.35	0.1	68.8	0.6	4.807
Average	Average	8.399	2.089	0.01	2.7	2	0.92	0.11	1.29	0.1	76.8	0.4	4.292
Coarse	Coarse	6.398	2.437	0.01	2.4	1.5	0.79	0.13	1.22	0.09	79.9	0.3	
Fine	Fine	14.97	0.946	0.01	3.7	3.9	1.34	0.04	1.52	0.11	66.7	0.6	
REFERENCED SEDIMENT VALUES	**PAAS (Taylor and McLennan, 1985; McLennan, 2001)**	18.9	1.3		6.5	3.7	2.2	0.11	1.2	0.16	62.8	1	
REFERENCED SEDIMENT VALUES	**NASC (Gromet et al., 1984)**	16.9	3.36		5.7	4	2.86	0.06	1.14	0.11	64.8	0.7	
REFERENCED SEDIMENT VALUES	**UCC (Rudnick and Gao, 2003)**	15.4	3.59		5	2.8	2.48	0.1	3.27	0.15	66.6	0.6	

Table C2: Trace element chemistry of samples in the 1AT1-V horizon reservoir interval. Averages of the fine and coarse fractions and referenced sediment values has been added (PAAS- Post Archean Shale, NASC- North Amercican Sandstone Composite and UCC-Upper Continental Crust reference values).

Sample name	Sc (ppm)	V (ppm)	Cr (ppm)	Co (ppm)	Ni (ppm)	Cu (ppm)	Zn (ppm)	Rb (ppm)	Sr (ppm)	Y (ppm)	Zr (ppm)	Nb (ppm)	Mo (ppm)
F-A5*1	7.45	55.1	375.6	3.9	15.3	14.1	32	26.5	69	13.7	416	6.93	22.4
F-A5*3	8.99	54.2	182	5.59	16.5	14	30	53.5	77	18.5	389	8.7	10.1
F-A5*4	6.46	55.9	382.5	4.87	17	12.4	19	35.6	60	15.5	112	4.17	23.6
F-A5*5	6.56	56.1	385	4.94	28.3	39.4	33	34.3	110	11.7	125	4.69	24
F-A5*7	11.5	92.5	217.2	4.58	16.4	12	50	114	107	26.9	392	12.5	11.7
F-A5*8	6.6	60.3	467.8	3.35	16	12.8	22	36.1	71	13.8	211	6.39	28.2
F-A5*9	11.1	76	232.1	5.83	20.7	16.7	34	114	110	26.4	322	12.9	12.2
F-A5*10	7.3	59.5	408	3.15	16.6	12.4	30	43.6	159	15.6	280	6.49	24.8
F-A5*11	13.1	75.2	72.25	5.01	17	17.8	53	142	120	37.7	527	14	2.71
F-A5*14	13.8	53.5	47.55	5.95	16	19	61	187	156	38.3	234	13	1.63
F-A5*17	13	56.7	52.35	5.93	24.8	34.9	62	177	171	36.2	208	12.9	1.54
F-AR1*11	6.72	62	375.4	5.18	19.7	13.7	176	48.9	69	16.9	115	4.96	22.1
F-AR1*7	6.98	58.1	363.5	4.5	16.2	13.7	28	43.7	50	14.7	95.1	4.33	21.6

F-AR1*5	6.81	61.7	414	6.26	18.2	13.2	24	44.3	46	15	231	5.98	24
F-AR1*3	7.48	53.6	208.2	6.71	17.1	10.4	34	52.5	57	21.7	177	6.66	12.7
F-AR1*1	6.21	42.2	211.5	4.76	23.6	26.2	17	34.5	38	15	98.1	3.86	12.8
F-A12*1	7.34	63.8	314.6	17	35.6	10.6	72	41	90	26.6	368	6.79	18.7
F-A12*2	6.65	46.6	212.7	5.22	14.1	8.07	35	42.3	71	16.8	190	5.25	12.2
F-A12*4	9.69	60.1	187.6	6.46	18.1	17.3	41	104	115	25.2	495	12.6	10.6
F-A12*5	7.5	47.8	222.2	4.14	15.1	14.1	29	62.3	521	22.2	274	6.66	12.4
F-A12*6	11.4	57.8	58.75	5.99	15.7	20.2	48	162	105	31.2	114	11.8	1.81
F-A12*7	8.01	43.7	68.15	2.66	10.8	9.87	48	83.2	235	20.8	182	8.25	3.36
F-A12*8	13.3	90.6	167.8	9.5	26.2	22.6	58	157	137	34.5	326	17.6	8.51
F-A12*9	6.46	48.9	319	2.54	11.8	11.5	32	42.3	77	14	167	5.66	18.7
F-A12*10	8.74	45.3	117	3.51	9.78	10.6	43	49.3	904	37.4	141	4.74	6.45
F-A12*11	12.3	91.9	146.5	9.45	29.7	46.3	35	166	159	37	411	17.9	7.14
F-A12*12a	7.84	55.4	291.5	6.46	19.2	13.5	31	54.8	71	22.7	577	8.67	17.9
F-A12*12	21.3	145	92.55	12.7	24.8	37	56	271	166	49.2	349	25.4	1.09
F-A12*13	5.79	45.6	327.3	2.97	13.5	14.1	18	36.6	457	20.3	179	4.46	19.2
F-A12*14	9.76	67	103.7	7.91	19.6	15.7	28	120	126	26.5	393	14	5.83

Average	9.2	62.7	234.1	5.9	18.8	17.8	43	86	157	24.1	270	9.27	13.3
Coarse	7.85	58.4	275.9	5.45	18.3	15.9	39	59.9	162	20.4	254	7.43	16.2
Fine	13.7	77	96.97	7.36	20.4	24.1	54	171	138	36	322	15.3	3.99
PAAS (Taylor and McLennan, 1985; McLennan, 2001)	16	150	110	20	55			160	200	27	210	19	
NASC (Gromet et al., 1984)	16	130	125	26	58			125	142	27	200	13	
UCC (Rudnick and Gao, 2003)	15	97	92	17.3	47	28	67	82	320	35	193	12	

Table C2: Continued

Sample name	Cs (ppm)	Ba (ppm)	La (ppm)	Ce (ppm)	Pr (ppm)	Nd (ppm)	Sm (ppm)	Eu (ppm)	Gd (ppm)	Tb (ppm)	Dy (ppm)	Ho (ppm)	Er (ppm)
F-A5*1	1.4	279	19.03	41	4.9	17.3	3.68	0.94	2.8	0.6	2.6	0.66	1.58
F-A5*3	3.2	205	25.1	54	6.1	22.7	4.69	0.77	4	0.6	3.4	0.67	2.18
F-A5*4	2.2	1031	17.99	39	4.5	16.9	3.52	0.75	3.3	0.5	2.8	0.55	1.59
F-A5*5	2.3	3136	16.85	36	4.5	15.8	3.63	0.95	3.2	0.6	2.4	0.73	1.45
F-A5*7	9.4	2081	36.3	72	8.6	32	6.13	1.2	5.3	0.8	4.7	0.96	2.88
F-A5*8	2.3	1247	17.76	35	4.6	17.2	3.85	0.81	3.4	0.5	2.6	0.52	1.43
F-A5*9	8.8	424	32.45	67	7.8	27.8	5.45	0.98	4.3	0.7	4.5	0.95	2.98
F-A5*10	2.6	3680	19.76	39	4.9	18.6	3.94	0.94	3.7	0.5	2.8	0.58	1.74
F-A5*11	33	477	40	81	9.7	36.6	7.71	1.32	6.9	1	6.8	1.37	4.2
F-A5*14	29	496	50.18	104	12	46.5	9.41	1.45	8.1	1.1	7.1	1.4	4.17
F-A5*17	25	475	38.65	79	9.3	35.6	7.51	1.17	6.8	1	6.6	1.26	3.87
F-AR1*11	2.1	268	21.52	47	5.1	19.6	3.94	0.82	3.6	0.5	3.2	0.58	1.7
F-AR1*7	2.2	306	18.18	39	4.5	17.2	3.68	0.69	3.2	0.5	2.9	0.55	1.57
F-AR1*5	2.3	190	24.48	56	6.4	24.6	4.94	1.1	3.9	0.5	2.8	0.56	1.58

F-AR1*3	2.2	217	29.03	62	6.7	25.1	4.63	0.94	4.3	0.6	3.9	0.72	2.3
F-AR1*1	1.5	342	20.69	44	5	19.2	4.05	0.76	3.4	0.5	2.7	0.59	1.54
F-A12*1	2	405	36.1	74	8.6	32.9	6.41	1.22	5.3	0.7	4.7	0.93	2.63
F-A12*2	2.3	341	18.92	41	4.7	19.1	4.08	0.82	3.9	0.5	3.1	0.64	1.75
F-A12*4	6.1	453	35.27	73	8.9	33.2	6.44	1.14	4.9	0.7	4.6	0.93	2.89
F-A12*5	3.5	383	24.04	45	5.5	21.5	4.12	0.8	3.9	0.5	3.9	0.75	2.23
F-A12*6	14	700	30.12	66	7.3	27.4	5.77	0.93	5.5	0.8	5.3	1.08	3.33
F-A12*7	5.1	418	21.63	44	5.4	21	4.83	0.94	4.6	0.7	3.7	0.83	2.1
F-A12*8	12	653	53.2	103	12	44.5	8.17	1.5	6.3	1	6.3	1.26	3.72
F-A12*9	2.3	536	18.43	35	4.6	17.3	3.74	0.79	3.2	0.6	2.6	0.58	1.47
F-A12*10	2.6	583	23.48	47	5.6	22.2	5.66	1.23	5.8	0.9	6.2	1.21	3.53
F-A12*11	10	832	60.05	115	14	48.9	8.01	1.29	6	0.9	6.5	1.36	4.27
F-A12*12a	2.9	348	26.45	60	7.2	28.2	6.35	1.22	6.2	0.8	4.6	0.82	2.38
F-A12*12	24	779	64.15	131	14	50.1	8.45	1.48	6.8	1.1	8.3	1.8	5.8
F-A12*13	1.9	582	15.01	32	4.1	17.1	3.92	0.87	4.2	0.6	3.6	0.67	1.85
F-A12*14	7.6	480	36.35	77	8.4	30.1	5.31	0.94	4.5	0.7	4.6	0.98	3.05
Average	7.5	745	29.7	61	7.2	26.9	5.4	1.02	4.7	0.7	4.3	0.88	2.59

Coarse	3.6	796	25.2	52	6.1	23.1	4.72	0.95	4.2	0.6	3.7	0.76	2.16
Fine	20	576	44.51	91	11	39.1	7.64	1.28	6.5	1	6.4	1.3	4
PAAS (Taylor and McLennan, 1985; McLennan, 2001)	15	650	38	80	8.8	33.9	5.55	1.08	4.7	0.8	4.5	0.99	2.85
NASC (Gromet et al., 1984)	5.2	636	31.1	67		27.4	5.59	1.18		0.9			
UCC (Rudnick and Gao, 2003)	4.9	628	31	63	7.1	27	4.7	1	4	0.7	3.9	0.83	2.3

Table C2: Continued

Sample name	**Tm (ppm)**	**Yb (ppm)**	**Lu (ppm)**	**Hf (ppm)**	**Ta (ppm)**	**Pb (ppm)**	**Th (ppm)**	**U (ppm)**

F-A5*1	0.35	1.75	0.4	11	0.7	10.5	6	1.85
F-A5*3	0.31	2.13	0.3	10.4	0.7	9.77	8.12	2.16
F-A5*4	0.2	1.29	0.2	3.09	0.3	11.6	4.26	1.84
F-A5*5	0.39	1.28	0.3	3.82	0.6	8	4.28	1.66
F-A5*7	0.45	2.8	0.4	10.9	0.9	11.5	11.8	2.31
F-A5*8	0.29	1.36	0.3	5.57	0.5	7.65	4.32	1.07
F-A5*9	0.43	3.02	0.5	8.99	1	17.2	12.2	3.36
F-A5*10	0.27	1.61	0.3	7.27	0.5	9.71	5.46	1.55
F-A5*11	0.62	4.25	0.6	14.8	1.1	16.4	16.1	3.09
F-A5*14	0.63	4.05	0.6	7.19	1	14.6	16.6	1.93
F-A5*17	0.56	3.55	0.5	6.14	1	15.1	15.8	2.75
F-AR1*11	0.23	1.5	0.2	3.11	0.4	8.7	5.23	1.18
F-AR1*7	0.32	1.45	0.2	2.74	0.3	8.07	4.62	1.1
F-AR1*5	0.22	1.45	0.2	5.89	0.4	7.88	4.78	1.53
F-AR1*3	0.32	2.24	0.3	4.9	0.5	10.8	6.47	1.74
F-AR1*1	0.24	1.3	0.2	2.98	0.3	7.59	4.05	0.98
F-A12*1	0.39	2.55	0.4	9.95	0.5	19.7	6.85	1.91

F-A12*2	0.23	1.58	0.2	4.77	0.4	9.15	5.12	1.36
F-A12*4	0.43	2.95	0.4	13.1	0.9	14.4	10.5	3.62
F-A12*5	0.33	2.38	0.3	7.36	0.5	16.2	7.01	2.4
F-A12*6	0.48	3.25	0.5	3.64	1	20.8	14.5	3.63
F-A12*7	0.32	1.8	0.3	5.16	0.6	14.2	8.13	1.72
F-A12*8	0.59	3.9	0.6	9.24	1.3	21.5	16.4	3.63
F-A12*9	0.28	1.42	0.3	4.65	0.5	12.1	4.83	1.69
F-A12*10	0.51	3.35	0.4	3.79	0.3	8.94	5.16	1.53
F-A12*11	0.65	4.5	0.7	11.7	1.5	40.5	18.7	6.86
F-A12*12a	0.36	2.44	0.4	15.3	0.6	10.3	9.53	2.84
F-A12*12	0.88	5.74	0.8	10.2	2	22.8	26.3	8.88
F-A12*13	0.25	1.54	0.2	4.93	0.4	9.87	3.98	1.2
F-A12*14	0.47	3.21	0.5	10.9	1.5	30.3	13.1	4.14
Average	0.4	2.52	0.4	7.44	0.7	14.2	9.34	2.52
Coarse	0.34	2.08	0.3	6.91	0.6	13.1	7.12	2.09
Fine	0.6	3.95	0.6	9.18	1.2	17.9	16.6	3.93
PAAS (Taylor and McLennan, 1985;	0.41	2.82	0.4	5	1.3	20	14.6	3.1

McLennan, 2001)								
NASC (Gromet et al., 1984)		3.06	0.5	6.3	1.1	20	12.3	2.7
UCC (Rudnick and Gao, 2003)	0.3	2	0.3	5.3	0.9	17	10.5	2.7

Table C3: Chemical Index of Weathering (CIW), Chemical Index of Alteration (CIA), Plagioclase Index of Alteration (PIA), Index of Compositional Variation (ICV) and CIA_{molar} (molar proportions of the CIA) values of the finer and coarser sediments in the 1AT1-V horizon reservoir interval

Sample name	CIW	CIA	PIA	ICV	CIA_{molar}
F-A5*1	52.6528	48.55573	58.67653	1.145631	2.361572
F-A5*3	68.89661	60.98231	77.61592	0.831492	24.92982
F-A5*4	60.865	52.21503	55.1839	1.488304	3.155068
F-A5*5	65.54381	55.84604	63.33337	1.2	6.374185
F-A5*7	74.12176	62.19629	71.05616	0.756514	29.21229
F-A5*8	67.55331	57.96329	69.40123	1	11.92309
F-A5*9	72.9732	62.20738	73.17171	0.762768	30.41809
F-A5*10	69.31896	59.78581	72.4138	0.952562	17.08156
F-A5*11	75.32162	63.05502	67.41185	0.866373	10.92237
F-A5*14	79.67151	63.67018	61.40038	0.962079	9.271412
F-A5*17	79.2711	63.68682	61.8697	0.927431	9.042212
F-AR1*11	64.02095	53.83846	55.09314	1.369266	3.65819
F-AR1*7	71.21875	58.52643	61.11449	1.219949	7.437441
F-AR1*5	73.75166	60.42108	64.0352	1.248744	10.96689
F-AR1*3	72.45148	59.36996	61.25176	1.473451	7.557706
F-AR1*1	72.21876	59.05232	62.82941	1.352349	10.26106

F-A12*1	68.6061	57.72493	59.25361	3.279487	4.360569
F-A12*2	64.38186	54.6539	56.74872	1.445783	3.666097
F-A12*4	74.88441	63.4868	69.14558	0.735029	10.8713
F-A12*5	62.32581	53.83034	57.33	2.899083	3.377366
F-A12*6	85.57115	68.63782	67.59243	0.745053	20.70099
F-A12*7	63.67145	55.24915	60.87715	1.352535	4.168124
F-A12*8	79.94758	66.28822	71.34778	0.790366	31.24932
F-A12*9	61.19386	53.42133	60.17826	0.947699	3.838676
F-A12*10	62.91035	54.49258	58.26034	5.333938	3.463934
F-A12*11	79.43264	66.1294	72.15471	0.700279	41.22087
F-A12*12a	69.18046	60.11321	70.46358	0.879137	9.594244
F-A12*12	88.99722	71.03776	69.79878	0.669554	53.00207
F-A12*13	58.00419	50.80675	55.55216	4.1	2.817602
F-A12*14	76.4606	64.93659	73.42426	0.774352	27.1339

Table C4: Major and trace element ratios of samples of the 1AT1-V horizon reservoir interval

Sample name	Si/Al	K/Al	Na/Al	Fe_2O_3/Al_2O_3	K_2O/Al_2O_3	MgO/Al_2O_3	CaO/Al_2O_3	Na_2O/Al_2O_3	K_2O/Na_2O	Al_2O_3/TiO_2	SiO_2/Al_2O_3
F-A5*1	19.12	0.23	0.40	0.32	0.15	0.06	0.24	0.29	0.52	12.12	21.65
F-A5*3	10.20	0.27	0.35	0.26	0.17	0.06	0.02	0.25	0.70	16.45	11.55
F-A5*4	22.91	0.39	0.28	0.63	0.25	0.13	0.19	0.20	1.26	17.10	25.94
F-A5*5	23.97	0.38	0.31	0.48	0.24	0.09	0.09	0.22	1.09	16.75	27.13
F-A5*7	6.07	0.37	0.27	0.19	0.24	0.07	0.02	0.19	1.25	21.00	6.87
F-A5*8	19.36	0.35	0.34	0.35	0.23	0.07	0.05	0.24	0.94	14.17	21.92
F-A5*9	5.45	0.34	0.29	0.20	0.22	0.07	0.02	0.21	1.07	21.68	6.17
F-A5*10	14.59	0.33	0.33	0.33	0.21	0.08	0.03	0.23	0.91	17.57	16.52
F-A5*11	4.53	0.37	0.20	0.28	0.24	0.10	0.05	0.14	1.67	20.33	5.13
F-A5*14	4.03	0.46	0.13	0.24	0.29	0.11	0.19	0.09	3.27	30.30	4.57
F-A5*17	4.29	0.45	0.13	0.26	0.29	0.12	0.13	0.09	3.12	28.12	4.86
F-AR1*11	17.64	0.43	0.24	0.56	0.27	0.11	0.15	0.17	1.57	18.17	19.97
F-AR1*7	20.19	0.44	0.23	0.53	0.28	0.10	0.07	0.16	1.72	19.55	22.86
F-AR1*5	19.77	0.43	0.23	0.59	0.28	0.10	0.05	0.16	1.72	14.74	22.38
F-AR1*3	16.80	0.44	0.21	0.69	0.28	0.13	0.07	0.15	1.87	14.58	19.02
F-AR1*1	26.88	0.45	0.24	0.68	0.29	0.10	0.05	0.17	1.63	17.53	30.43

F-A12*1	16.78	0.40	0.20	1.64	0.25	0.19	0.68	0.14	1.77	12.19	19.00
F-A12*2	18.42	0.40	0.24	0.47	0.26	0.10	0.36	0.17	1.49	16.60	20.86
F-A12*4	5.38	0.35	0.21	0.21	0.22	0.05	0.05	0.15	1.50	21.77	6.09
F-A12*5	8.44	0.37	0.26	0.31	0.23	0.07	2.03	0.19	1.25	20.44	9.55
F-A12*6	4.77	0.42	0.10	0.25	0.27	0.10	0.03	0.07	3.65	30.56	5.40
F-A12*7	7.45	0.35	0.28	0.20	0.22	0.08	0.61	0.20	1.11	24.11	8.44
F-A12*8	4.00	0.37	0.19	0.28	0.24	0.07	0.02	0.13	1.79	19.14	4.53
F-A12*9	16.37	0.34	0.32	0.24	0.22	0.05	0.14	0.23	0.97	17.70	18.53
F-A12*10	7.09	0.36	0.25	0.82	0.23	1.25	2.75	0.18	1.25	26.24	8.03
F-A12*11	3.09	0.37	0.20	0.21	0.23	0.06	0.01	0.14	1.64	22.16	3.49
F-A12*12a	10.74	0.32	0.29	0.28	0.20	0.07	0.06	0.21	0.97	16.16	12.16
F-A12*12	2.02	0.41	0.09	0.21	0.26	0.07	0.01	0.06	4.12	20.99	2.29
F-A12*13	15.90	0.35	0.31	0.39	0.23	0.08	3.10	0.22	1.01	17.73	18.00
F-A12*14	4.26	0.34	0.23	0.26	0.21	0.07	0.02	0.16	1.30	22.65	4.82

Table C4: Continued

Sample name	La/Sc	Sc/Th	Co/Th	Zr/Th	V/Cr	Th/Sc	Zr/Sc	Y/Ni	Ba/La	Th/U	K/Rb	K_2O/Rb	Rb/Al_2O_3

F-A5*1	2.55	1.24	0.65	69.30	0.15	0.81	55.81	0.89	14.69	3.24	190.84	0.02	6.44
F-A5*3	2.79	1.11	0.69	47.84	0.30	0.90	43.21	1.12	8.19	3.76	195.70	0.02	7.38
F-A5*4	2.79	1.52	1.14	26.37	0.15	0.66	17.41	0.91	57.33	2.32	200.54	0.02	10.41
F-A5*5	2.57	1.53	1.15	29.19	0.15	0.65	19.04	0.41	186.14	2.58	198.72	0.02	10.23
F-A5*7	3.17	0.97	0.39	33.33	0.43	1.03	34.22	1.64	57.31	5.10	194.04	0.02	10.22
F-A5*8	2.69	1.53	0.77	48.83	0.13	0.65	31.96	0.86	70.21	4.02	213.95	0.03	8.78
F-A5*9	2.92	0.91	0.48	26.47	0.33	1.10	29.00	1.27	13.07	3.63	193.79	0.02	9.39
F-A5*10	2.71	1.34	0.58	51.37	0.15	0.75	38.39	0.94	186.28	3.53	213.25	0.03	8.27
F-A5*11	3.05	0.82	0.31	32.74	1.04	1.23	40.15	2.22	11.93	5.22	190.67	0.02	10.39
F-A5*14	3.63	0.83	0.36	14.11	1.12	1.20	16.92	2.39	9.88	8.61	184.73	0.02	13.10
F-A5*17	2.97	0.82	0.37	13.14	1.08	1.21	15.93	1.46	12.28	5.74	184.12	0.02	12.86
F-AR1*11	3.20	1.29	0.99	22.03	0.17	0.78	17.13	0.86	12.47	4.43	202.02	0.02	11.22
F-AR1*7	2.61	1.51	0.97	20.57	0.16	0.66	13.63	0.91	16.83	4.20	209.20	0.03	11.16
F-AR1*5	3.59	1.43	1.31	48.30	0.15	0.70	33.87	0.82	7.77	3.13	206.37	0.02	11.12
F-AR1*3	3.88	1.16	1.04	27.36	0.26	0.87	23.68	1.27	7.47	3.73	200.82	0.02	11.62
F-AR1*1	3.33	1.53	1.17	24.22	0.20	0.65	15.80	0.63	16.53	4.12	204.83	0.02	11.56
F-A12*1	4.92	1.07	2.48	53.79	0.20	0.93	50.23	0.75	11.22	3.59	200.23	0.02	10.52
F-A12*2	2.85	1.30	1.02	37.14	0.22	0.77	28.62	1.19	18.02	3.76	208.28	0.03	10.18
F-A12*4	3.64	0.92	0.61	46.89	0.32	1.09	51.03	1.39	12.83	2.91	214.59	0.03	8.57
F-A12*5	3.21	1.07	0.59	39.02	0.22	0.94	36.49	1.48	15.91	2.92	203.88	0.02	9.53
F-A12*6	2.65	0.78	0.41	7.87	0.98	1.28	10.08	1.99	23.22	4.01	178.86	0.02	12.36

F-A12*7	2.70	0.99	0.33	22.43	0.64	1.01	22.75	1.92	19.33	4.72	191.69	0.02	9.58
F-A12*8	4.01	0.81	0.58	19.86	0.54	1.24	24.56	1.32	12.27	4.52	185.48	0.02	10.66
F-A12*9	2.85	1.34	0.53	34.67	0.15	0.75	25.90	1.18	29.06	2.86	206.09	0.02	8.85
F-A12*10	2.69	1.69	0.68	27.39	0.39	0.59	16.16	3.82	24.81	3.36	210.70	0.03	8.94
F-A12*11	4.87	0.66	0.51	21.96	0.63	1.52	33.32	1.25	13.85	2.73	210.04	0.03	9.25
F-A12*12a	3.37	0.82	0.68	60.52	0.19	1.21	73.53	1.18	13.16	3.36	212.08	0.03	7.88
F-A12*12	3.01	0.81	0.48	13.26	1.57	1.23	16.36	1.98	12.14	2.96	185.47	0.02	11.75
F-A12*13	2.59	1.46	0.75	44.94	0.14	0.69	30.85	1.51	38.74	3.32	199.52	0.02	9.39
F-A12*14	3.72	0.75	0.61	30.10	0.65	1.34	40.27	1.35	13.19	3.15	211.51	0.03	8.42

Table C5: Correlation matrix of major element oxides for the coarser grained fraction of samples of the 1AT1-V horizon reservoir interval

	Al_2O_3	CaO	Fe_2O_3	K_2O	MgO	Na_2O	P_2O_5	SiO_2	TiO_2	L.O.I.
Al2O3	1.00	-0.13	0.67	0.98	0.93	0.94	0.10	-0.85	0.97	0.43
CaO	-0.13	1.00	-0.27	-0.14	-0.15	-0.10	-0.38	-0.40	-0.20	0.82
Fe_2O_3	0.67	-0.27	1.00	0.73	0.82	0.45	0.54	-0.55	0.64	0.21
K_2O	0.98	-0.14	0.73	1.00	0.95	0.87	0.21	-0.84	0.93	0.41
MgO	0.93	-0.15	0.82	0.95	1.00	0.82	0.32	-0.81	0.87	0.41
Na_2O	0.94	-0.10	0.45	0.87	0.82	1.00	-0.10	-0.78	0.94	0.39
P_2O_5	0.10	-0.38	0.54	0.21	0.32	-0.10	1.00	0.05	0.05	-0.22
SiO_2	-0.85	-0.40	-0.55	-0.84	-0.81	-0.78	0.05	1.00	-0.78	-0.84
TiO_2	0.97	-0.20	0.64	0.93	0.87	0.94	0.05	-0.78	1.00	0.34
L.O.I.	0.43	0.82	0.21	0.41	0.41	0.39	-0.22	-0.84	0.34	1.00

Table C6: Correlation matrix of the major element oxides for the finer grained fraction of samples of the 1AT1-V horizon reservoir interval

	Al_2O_3	CaO	Fe_2O_3	K_2O	MgO	Na_2O	P_2O_5	SiO_2	TiO_2	CaO*	L.O.I.
Al_2O_3	1	-0.2665	0.8551	0.9468	0.5291	-0.0409	0.4224	-0.9618	0.8839	-0.5232	0.6988
CaO	-0.2665	1	-0.2393	0.0002	0.4314	-0.3607	-0.5893	0.0318	-0.5244	0.8348	0.3273
Fe_2O_3	0.8551	-0.2393	1	0.817	0.6257	0.1138	0.6028	-0.8838	0.8243	-0.4835	0.6502
K_2O	0.9468	0.0002	0.817	1	0.7317	-0.2967	0.3013	-0.9832	0.699	-0.3375	0.8783
MgO	0.5291	0.4314	0.6257	0.7317	1	-0.471	0.1468	-0.6899	0.2063	0.2002	0.7965
Na_2O	-0.0409	-0.3607	0.1138	-0.2967	-0.471	1	0.2483	0.1372	0.4091	-0.1108	-0.5589
P_2O_5	0.4224	-0.5893	0.6028	0.3013	0.1468	0.2483	1	-0.3536	0.5676	-0.4922	0.0994
SiO_2	-0.9618	0.0318	-0.8838	-0.9832	-0.6899	0.1372	-0.3536	1	-0.7808	0.369	-0.842
TiO_2	0.8839	-0.5244	0.8243	0.699	0.2063	0.4091	0.5676	-0.7808	1	-0.6284	0.3404
CaO*	-0.5232	0.8348	-0.4835	-0.3375	0.2002	-0.1108	-0.4922	0.369	-0.6284	1	-0.1448
L.O.I.	0.6988	0.3273	0.6502	0.8783	0.7965	-0.5589	0.0994	-0.842	0.3404	-0.1448	1

Table C7: Correlation matrix of the major element oxides for the finer grained fraction of samples of the 1AT1-V horizon reservoir interval

	Sc	V	Co	Ni	Cu	Zn	Rb	Sr	Y	Zr	Nb	Mo	Cs	Ba	La	Ce	Pr	Nd	Sm	Eu	Gd	Tb	Dy	Ho	Er	Tm	Yb	Lu	Hf	Ta	Pb	Th	U
Sc	1.00	0.85	0.58	0.36	0.32	0.01	0.93	0.00	0.87	0.64	0.95	-0.62	0.95	0.03	0.89	0.87	0.88	0.86	0.84	0.64	0.66	0.81	0.85	0.88	0.92	0.87	0.92	0.86	0.68	0.87	0.73	0.95	0.82
V	0.85	1.00	0.53	0.46	0.37	0.14	0.78	-0.09	0.70	0.47	0.79	-0.18	0.83	0.23	0.80	0.77	0.80	0.77	0.71	0.65	0.51	0.62	0.68	0.70	0.75	0.76	0.75	0.69	0.50	0.71	0.59	0.76	0.69
Co	0.58	0.53	1.00	0.67	0.48	0.02	0.62	-0.26	0.66	0.43	0.63	-0.41	0.50	-0.24	0.79	0.85	0.79	0.78	0.70	0.52	0.54	0.58	0.68	0.66	0.72	0.61	0.74	0.60	0.46	0.63	0.67	0.69	0.76
Ni	0.36	0.46	0.67	1.00	0.90	0.05	0.38	-0.19	0.34	0.12	0.37	-0.05	0.33	0.25	0.53	0.54	0.54	0.50	0.43	0.39	0.23	0.34	0.36	0.49	0.43	0.55	0.44	0.44	0.16	0.42	0.45	0.42	0.55
Cu	0.32	0.37	0.48	0.90	1.00	-0.08	0.39	0.05	0.33	0.06	0.36	-0.11	0.33	0.28	0.51	0.47	0.51	0.47	0.40	0.36	0.20	0.40	0.35	0.54	0.41	0.61	0.42	0.49	0.10	0.44	0.52	0.41	0.57
Zn	0.01	0.14	0.02	0.05	-0.08	1.00	0.05	-0.10	0.02	-0.15	-0.04	0.04	0.01	-0.09	0.02	0.02	0.00	0.00	-0.03	-0.03	-0.01	-0.06	0.03	-0.03	-0.01	-0.08	-0.03	-0.10	-0.15	-0.07	-0.06	0.00	-0.09
Rb	0.93	0.78	0.62	0.38	0.39	0.05	1.00	0.15	0.93	0.49	0.95	-0.69	0.97	-0.03	0.92	0.90	0.91	0.90	0.86	0.63	0.71	0.84	0.91	0.94	0.95	0.86	0.93	0.83	0.53	0.90	0.87	0.96	0.88
Sr	0.00	-0.09	-0.26	-0.19	0.05	-0.10	0.15	1.00	0.26	-0.01	0.08	-0.18	0.14	0.12	-0.02	-0.06	0.00	0.02	0.06	0.11	0.24	0.29	0.23	0.22	0.17	0.09	0.10	0.07	0.01	0.11	0.18	0.08	0.08
Y	0.87	0.70	0.66	0.34	0.33	0.02	0.93	0.26	1.00	0.56	0.91	-0.69	0.88	-0.14	0.92	0.91	0.92	0.93	0.91	0.68	0.84	0.89	0.99	0.93	0.98	0.81	0.96	0.80	0.61	0.81	0.82	0.94	0.87
Zr	0.64	0.47	0.43	0.12	0.06	-0.15	0.49	-0.01	0.56	1.00	0.69	-0.31	0.49	-0.04	0.55	0.58	0.60	0.61	0.69	0.69	0.67	0.70	0.61	0.58	0.61	0.59	0.67	0.72	1.00	0.64	0.42	0.68	0.60
Nb	0.95	0.79	0.63	0.37	0.36	-0.	0.95	0.08	0.91	0.69	1.00	-0.	0.93	-0.	0.92	0.90	0.92	0.90	0.87	0.69	0.71	0.87	0.89	0.93	0.95	0.90	0.97	0.92	0.73	0.95	0.85	0.98	0.91

						04						63		02																		
Mo	-0.62	-0.18	-0.41	-0.05	-0.11	0.04	-0.69	-0.18	-0.69	-0.31	-0.63	1.00	-0.63	0.34	-0.59	-0.59	-0.56	-0.58	-0.58	-0.27	-0.56	-0.63	-0.67	-0.68	-0.68	-0.51	-0.64	-0.53	-0.34	-0.58	-0.58	-0.67	-0.53
Cs	0.95	0.83	0.50	0.33	0.33	0.01	0.97	0.14	0.88	0.49	0.93	-0.63	1.00	0.08	0.85	0.82	0.84	0.83	0.80	0.62	0.66	0.80	0.84	0.89	0.90	0.84	0.88	0.80	0.54	0.86	0.76	0.92	0.79
Ba	0.03	0.23	-0.24	0.25	0.28	-0.09	-0.03	0.12	-0.14	-0.04	-0.02	0.34	0.08	1.00	-0.07	-0.13	-0.07	-0.10	-0.10	0.16	-0.07	-0.03	-0.15	0.00	-0.08	0.11	-0.09	0.03	-0.03	0.04	-0.09	-0.06	-0.05
La	0.89	0.80	0.79	0.53	0.51	0.02	0.92	-0.02	0.92	0.55	0.92	-0.59	0.85	-0.07	1.00	0.99	0.99	0.99	0.92	0.71	0.72	0.82	0.91	0.91	0.95	0.86	0.96	0.84	0.59	0.85	0.87	0.94	0.92
Ce	0.87	0.77	0.85	0.54	0.47	0.02	0.90	-0.06	0.91	0.58	0.90	-0.59	0.82	-0.13	0.99	1.00	0.99	0.99	0.92	0.73	0.74	0.82	0.91	0.90	0.95	0.84	0.95	0.83	0.62	0.84	0.84	0.93	0.91
Pr	0.88	0.80	0.79	0.54	0.51	0.00	0.91	0.00	0.92	0.60	0.92	-0.56	0.84	-0.07	0.99	0.99	1.00	0.99	0.94	0.76	0.76	0.85	0.92	0.92	0.95	0.87	0.96	0.85	0.64	0.85	0.85	0.95	0.93
Nd	0.86	0.77	0.78	0.50	0.47	0.00	0.90	0.02	0.93	0.61	0.90	-0.58	0.83	-0.10	0.99	0.99	0.99	1.00	0.97	0.78	0.81	0.86	0.93	0.91	0.95	0.83	0.95	0.82	0.64	0.81	0.83	0.94	0.91
Sm	0.84	0.71	0.70	0.43	0.40	-0.03	0.86	0.06	0.91	0.69	0.87	-0.58	0.80	-0.10	0.92	0.92	0.94	0.97	1.00	0.85	0.91	0.91	0.93	0.89	0.91	0.79	0.91	0.78	0.73	0.75	0.72	0.91	0.85
Eu	0.64	0.65	0.52	0.39	0.36	-0.03	0.63	0.11	0.68	0.69	0.69	-0.27	0.62	0.16	0.71	0.73	0.76	0.78	0.85	1.00	0.81	0.82	0.72	0.73	0.68	0.66	0.69	0.69	0.71	0.59	0.49	0.70	0.65
Gd	0.66	0.51	0.54	0.23	0.20	-0.01	0.71	0.24	0.84	0.67	0.71	-0.56	0.66	-0.07	0.72	0.74	0.76	0.81	0.91	0.81	1.00	0.89	0.89	0.77	0.80	0.61	0.76	0.61	0.69	0.58	0.54	0.77	0.67
Tb	0.81	0.62	0.58	0.34	0.40	-0.06	0.84	0.29	0.89	0.70	0.87	-0.63	0.80	-0.03	0.82	0.82	0.85	0.86	0.91	0.82	0.89	1.00	0.92	0.94	0.90	0.85	0.89	0.87	0.74	0.81	0.75	0.90	0.85
Dy	0.85	0.68	0.68	0.36	0.35	0.03	0.91	0.23	0.99	0.61	0.89	-0.67	0.84	-0.15	0.91	0.91	0.92	0.93	0.93	0.72	0.89	0.92	1.00	0.93	0.97	0.82	0.95	0.80	0.65	0.79	0.80	0.94	0.87

Ho	0.88	0.70	0.66	0.49	0.54	-0.03	0.94	0.22	0.93	0.58	0.93	-0.68	0.89	0.00	0.91	0.90	0.92	0.91	0.89	0.73	0.77	0.94	0.93	1.00	0.96	0.93	0.95	0.92	0.63	0.89	0.87	0.96	0.92
Er	0.92	0.75	0.72	0.43	0.41	-0.01	0.95	0.17	0.98	0.61	0.95	-0.68	0.90	-0.08	0.95	0.95	0.95	0.95	0.91	0.68	0.80	0.90	0.97	0.96	1.00	0.88	0.99	0.87	0.65	0.88	0.87	0.98	0.92
Tm	0.87	0.76	0.61	0.55	0.61	-0.08	0.86	0.09	0.81	0.59	0.90	-0.51	0.84	0.11	0.86	0.84	0.87	0.83	0.79	0.66	0.61	0.85	0.82	0.93	0.88	1.00	0.90	0.95	0.64	0.91	0.82	0.91	0.89
Yb	0.92	0.75	0.74	0.44	0.42	-0.03	0.93	0.10	0.96	0.67	0.97	-0.64	0.88	-0.09	0.96	0.95	0.96	0.95	0.91	0.69	0.76	0.89	0.95	0.95	0.99	0.90	1.00	0.91	0.71	0.91	0.87	0.98	0.94
Lu	0.86	0.69	0.60	0.44	0.49	-0.10	0.83	0.07	0.80	0.72	0.92	-0.53	0.80	0.03	0.84	0.83	0.85	0.82	0.78	0.69	0.61	0.87	0.80	0.92	0.87	0.95	0.91	1.00	0.76	0.93	0.83	0.91	0.90
Hf	0.68	0.50	0.46	0.16	0.10	-0.15	0.53	0.01	0.61	1.00	0.73	-0.34	0.54	-0.03	0.59	0.62	0.64	0.64	0.73	0.71	0.69	0.74	0.65	0.63	0.65	0.64	0.71	0.76	1.00	0.69	0.47	0.72	0.65
Ta	0.87	0.71	0.63	0.42	0.44	-0.07	0.90	0.11	0.81	0.64	0.95	-0.58	0.86	0.04	0.85	0.84	0.85	0.81	0.75	0.59	0.58	0.81	0.79	0.89	0.88	0.91	0.91	0.93	0.69	1.00	0.89	0.93	0.90
Pb	0.73	0.59	0.67	0.45	0.52	-0.06	0.87	0.18	0.82	0.42	0.85	-0.58	0.76	-0.09	0.87	0.84	0.85	0.83	0.72	0.49	0.54	0.75	0.80	0.87	0.87	0.82	0.87	0.83	0.47	0.89	1.00	0.87	0.95
Th	0.95	0.76	0.69	0.42	0.41	0.00	0.96	0.08	0.94	0.68	0.98	-0.67	0.92	-0.06	0.94	0.93	0.95	0.94	0.91	0.70	0.77	0.90	0.94	0.96	0.98	0.91	0.98	0.91	0.72	0.93	0.87	1.00	0.94
U	0.82	0.69	0.76	0.55	0.57	-0.09	0.88	0.08	0.87	0.60	0.91	-0.53	0.79	-0.05	0.92	0.91	0.93	0.91	0.85	0.65	0.67	0.85	0.87	0.92	0.92	0.89	0.94	0.90	0.65	0.90	0.95	0.94	1.00

Major, weathering indices trace element (HFSE and LILE) within stratigraphic variation for F-A12, F-A5 and F-AR1

Major elements and weathering indices variation

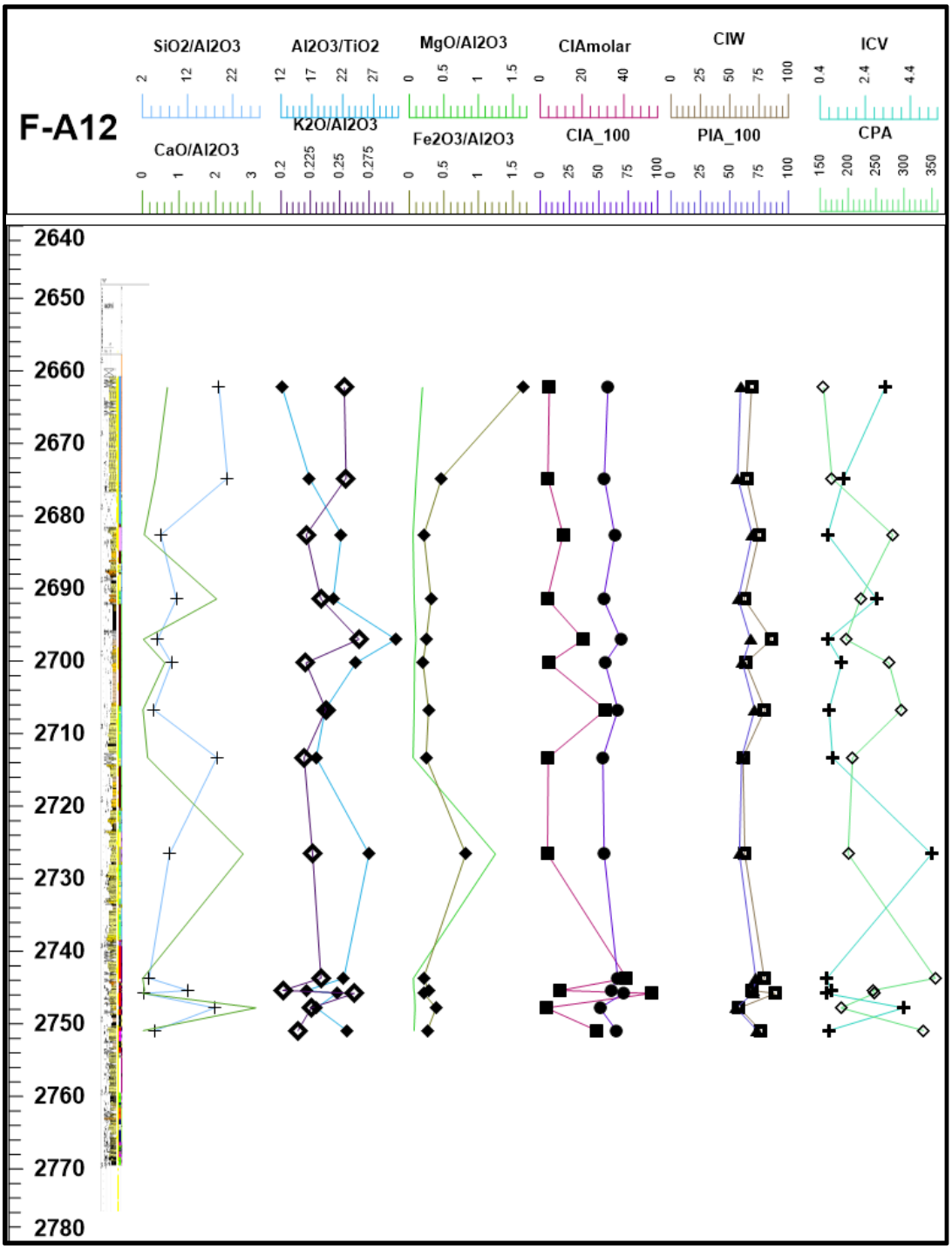

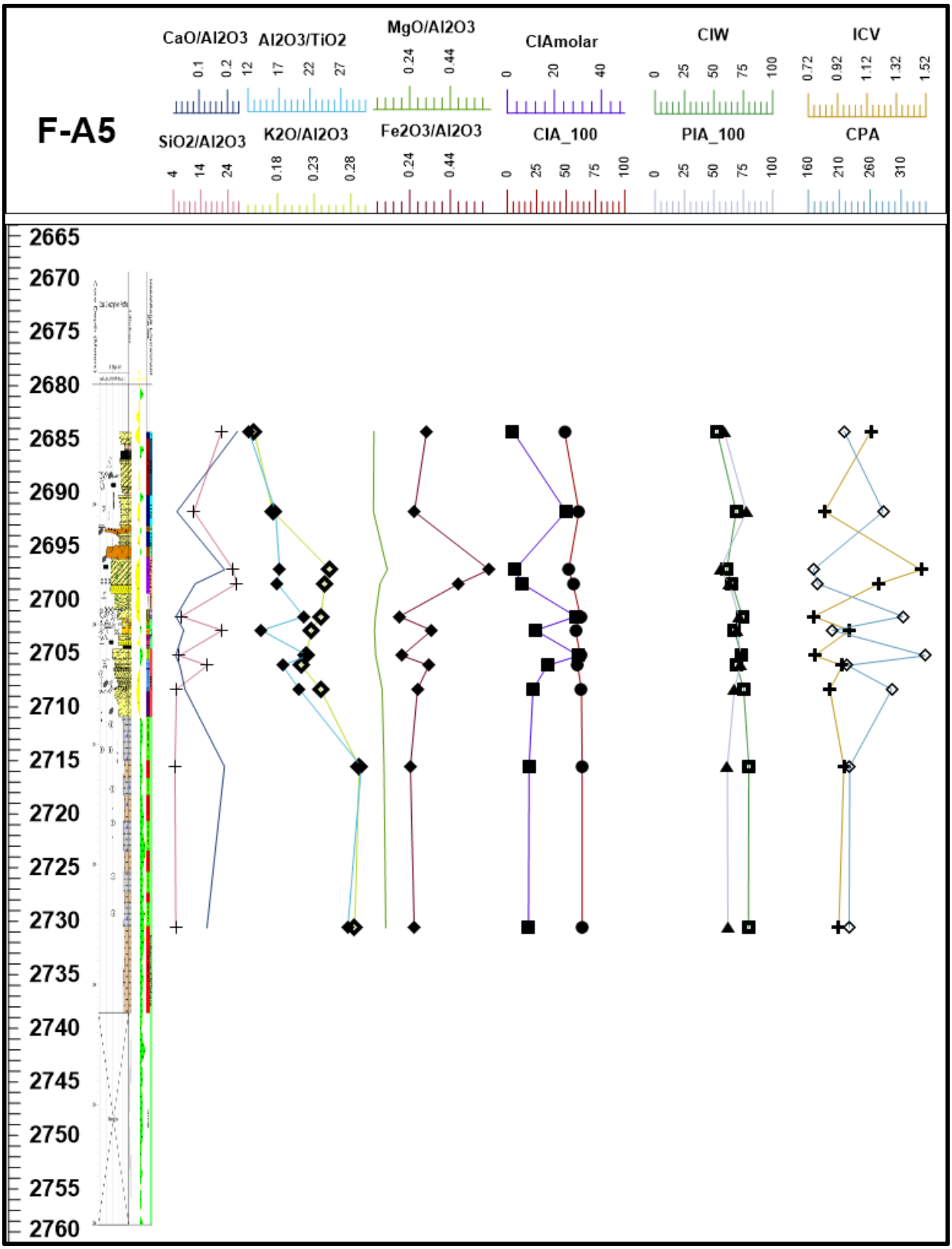
F-A5
CaO/Al2O3
0.1
0.2
Al2O3/TiO2
12
17
22
27
MgO/Al2O3
0.24
0.44
CIAmolar
0
20
40
CIW
0
25
50
75
100
ICV
0.72
0.92
1.12
1.32
1.52
SiO2/Al2O3
4
14
24
K2O/Al2O3
0.18
0.23
0.28
Fe2O3/Al2O3
0.24
0.44
CIA_100
0
25
50
75
100
PIA_100
0
25
50
75
100
CPA
160
210
260
310
2665
2670
2675
2680
2685
2690
2695
2700
2705
2710
2715
2720
2725
2730
2735
2740
2745
2750
2755
2760

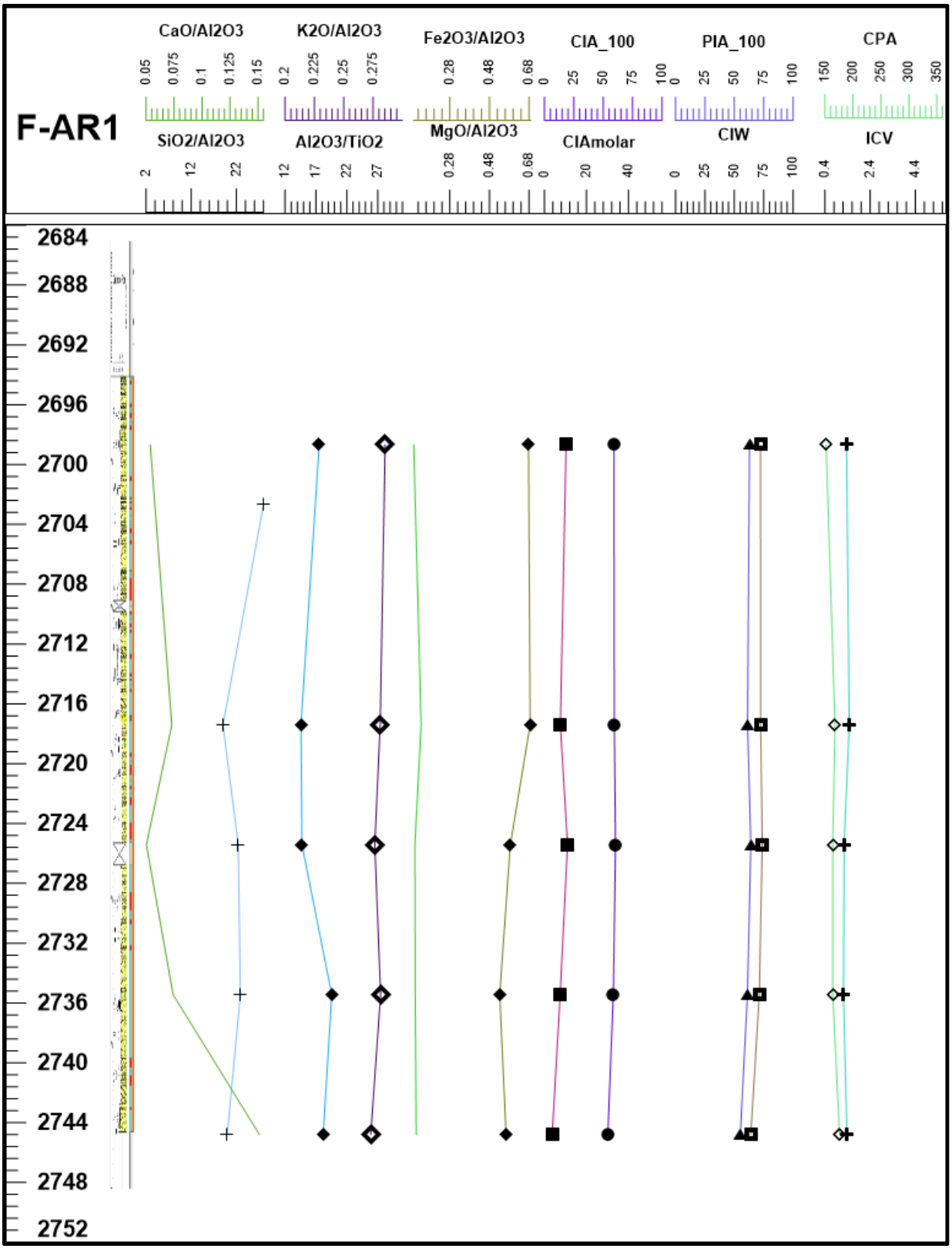
F-AR1
CaO/Al2O3
0.05
0.075
0.1
0.125
0.15
K2O/Al2O3
0.2
0.225
0.25
0.275
Fe2O3/Al2O3
0.28
0.48
0.68
CIA_100
0
25
50
75
100
PIA_100
0
25
50
75
100
CPA
150
200
250
300
350
SiO2/Al2O3
2
12
22
Al2O3/TiO2
12
17
22
27
MgO/Al2O3
0.28
0.48
0.68
CIAmolar
0
20
40
CIW
0
25
50
75
100
ICV
0.4
2.4
4.4
2684
2688
2692
2696
2700
2704
2708
2712
2716
2720
2724
2728
2732
2736
2740
2744
2748
2752

Trace element within stratigraphic variation

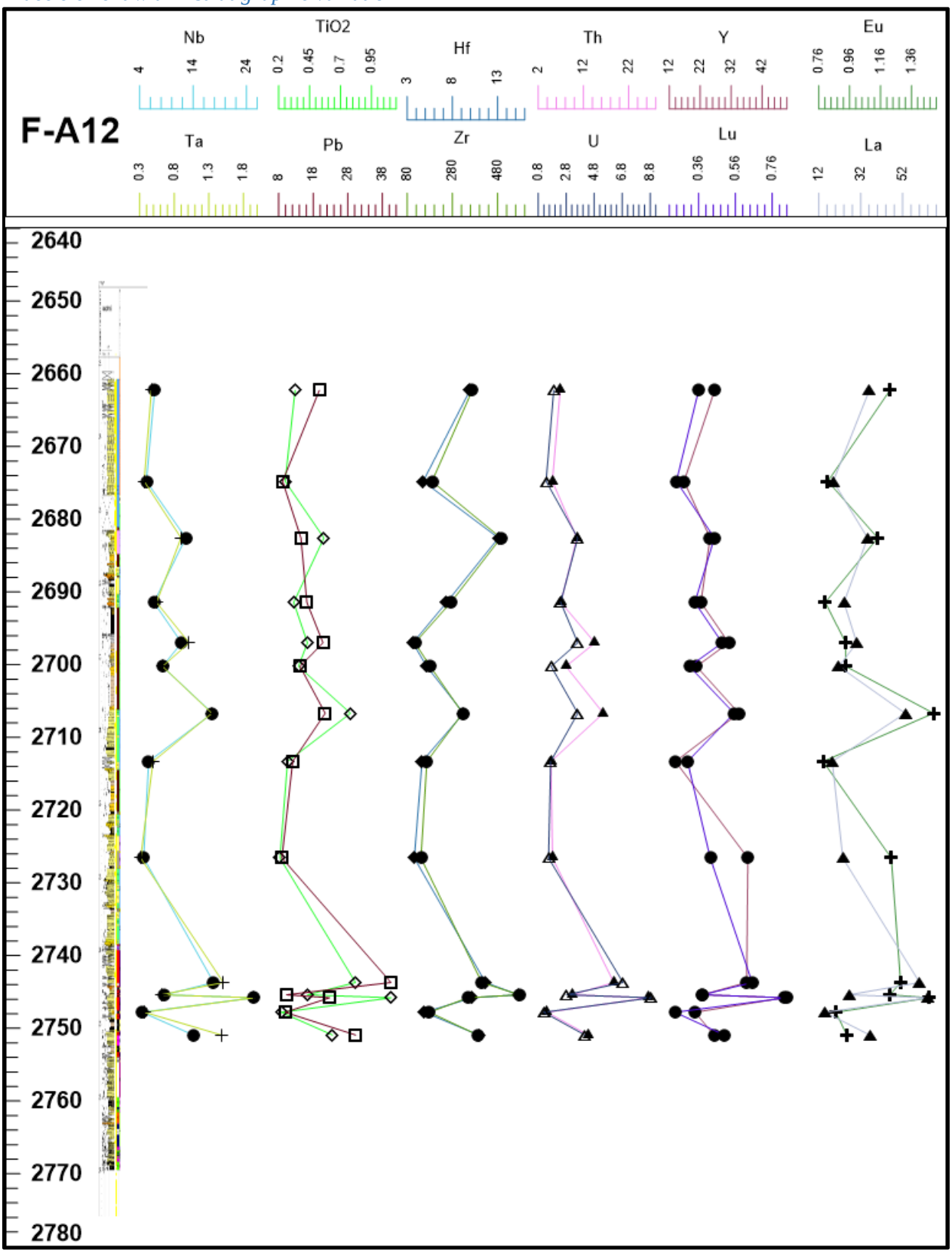

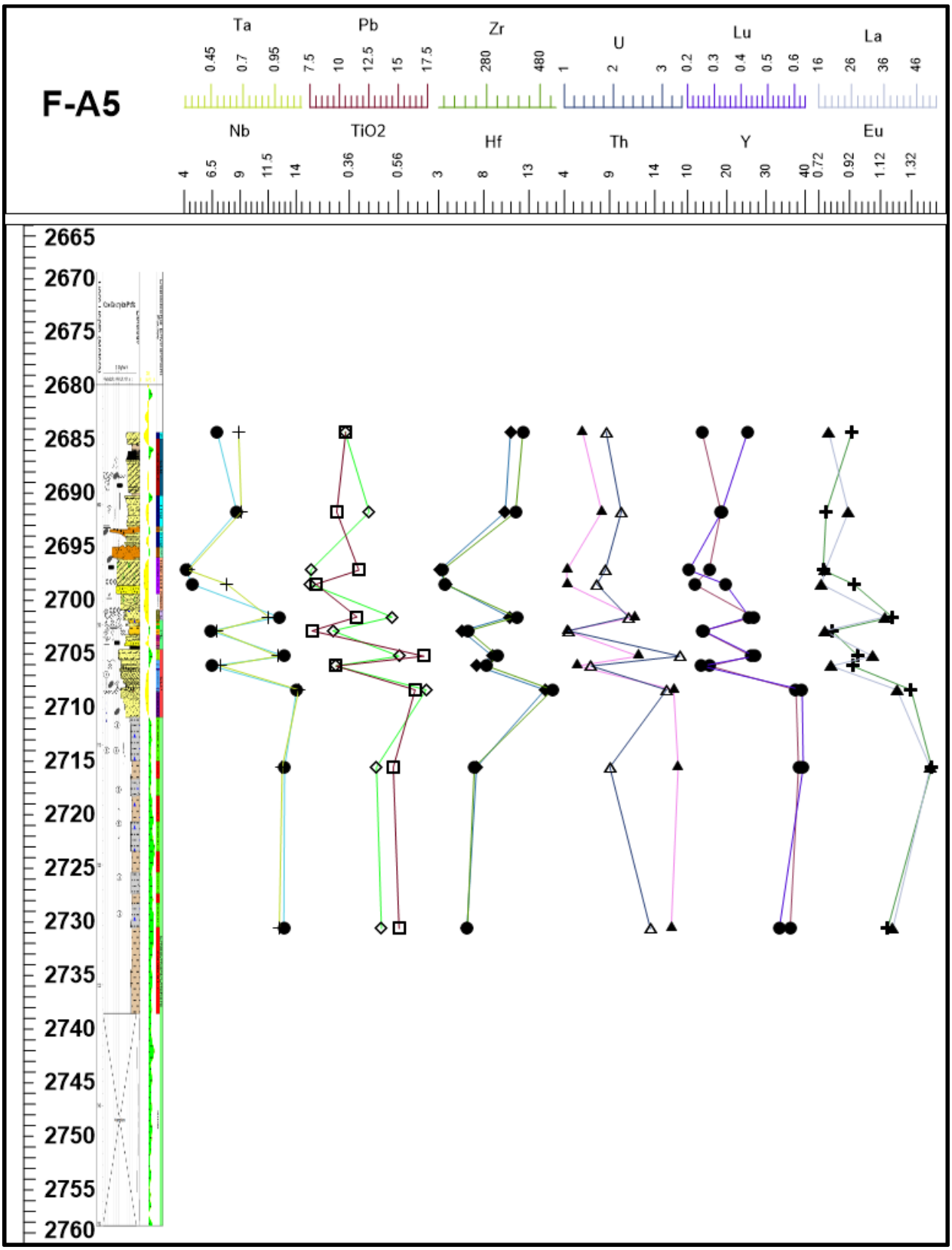
F-A5
Ta
0.45
0.7
0.95
Pb
7.5
10
12.5
15
17.5
Zr
280
480
U
1
2
3
Lu
0.2
0.3
0.4
0.5
0.6
La
16
26
36
46
Nb
4
6.5
9
11.5
14
TiO2
0.36
0.56
Hf
3
8
13
Th
4
9
14
Y
10
20
30
40
Eu
0.72
0.92
1.12
1.32
2665
2670
2675
2680
2685
2690
2695
2700
2705
2710
2715
2720
2725
2730
2735
2740
2745
2750
2755
2760

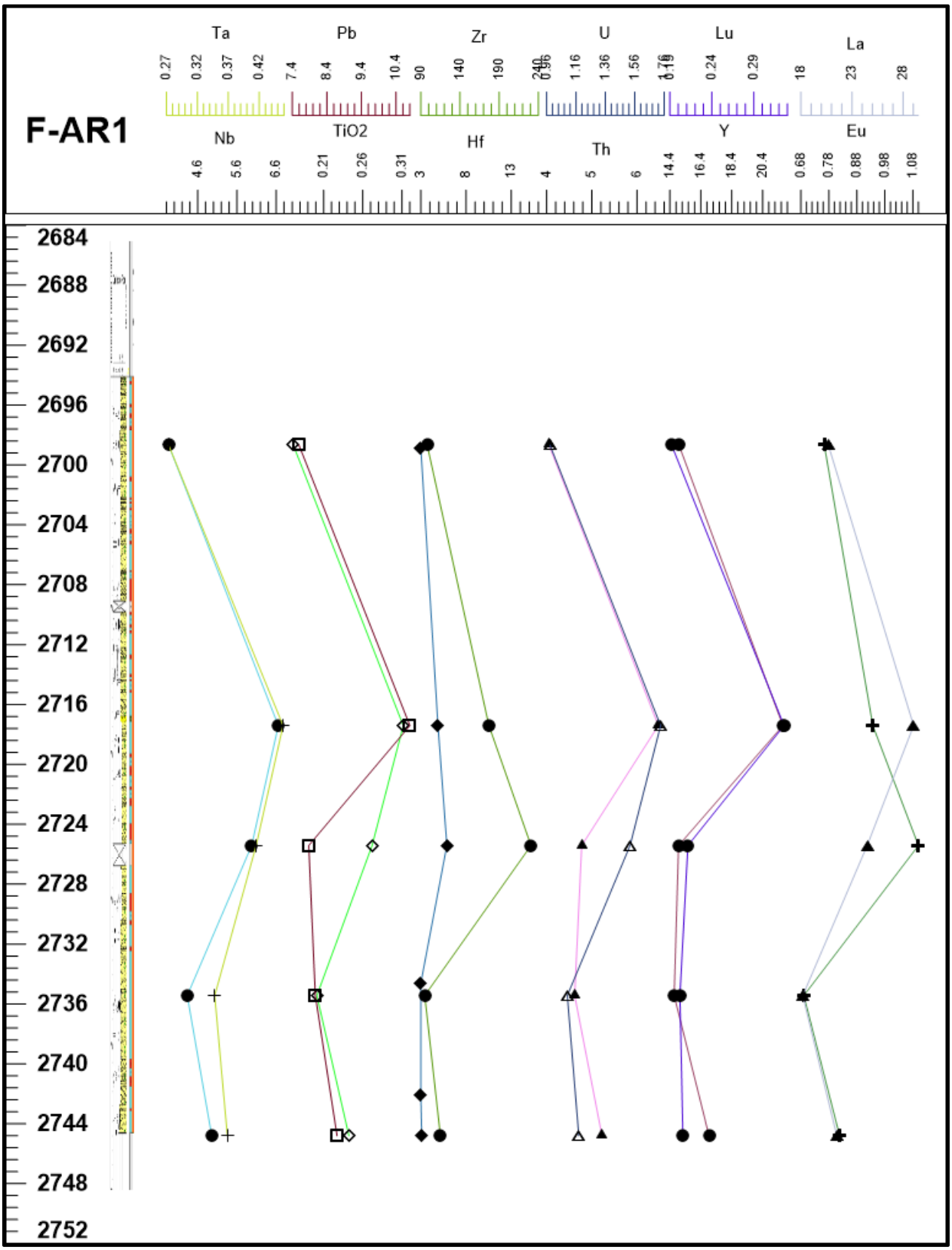
F-AR1
Ta
0.27
0.32
0.37
0.42
Pb
7.4
8.4
9.4
10.4
Zr
90
140
190
240
U
0.96
1.16
1.36
1.56
1.76
Lu
0.19
0.24
0.29
La
18
23
28
Nb
4.6
5.6
6.6
TiO2
0.21
0.26
0.31
Hf
3
8
13
Th
4
5
6
Y
14.4
16.4
18.4
20.4
Eu
0.68
0.78
0.88
0.98
1.08
2684
2688
2692
2696
2700
2704
2708
2712
2716
2720
2724
2728
2732
2736
2740
2744
2748
2752

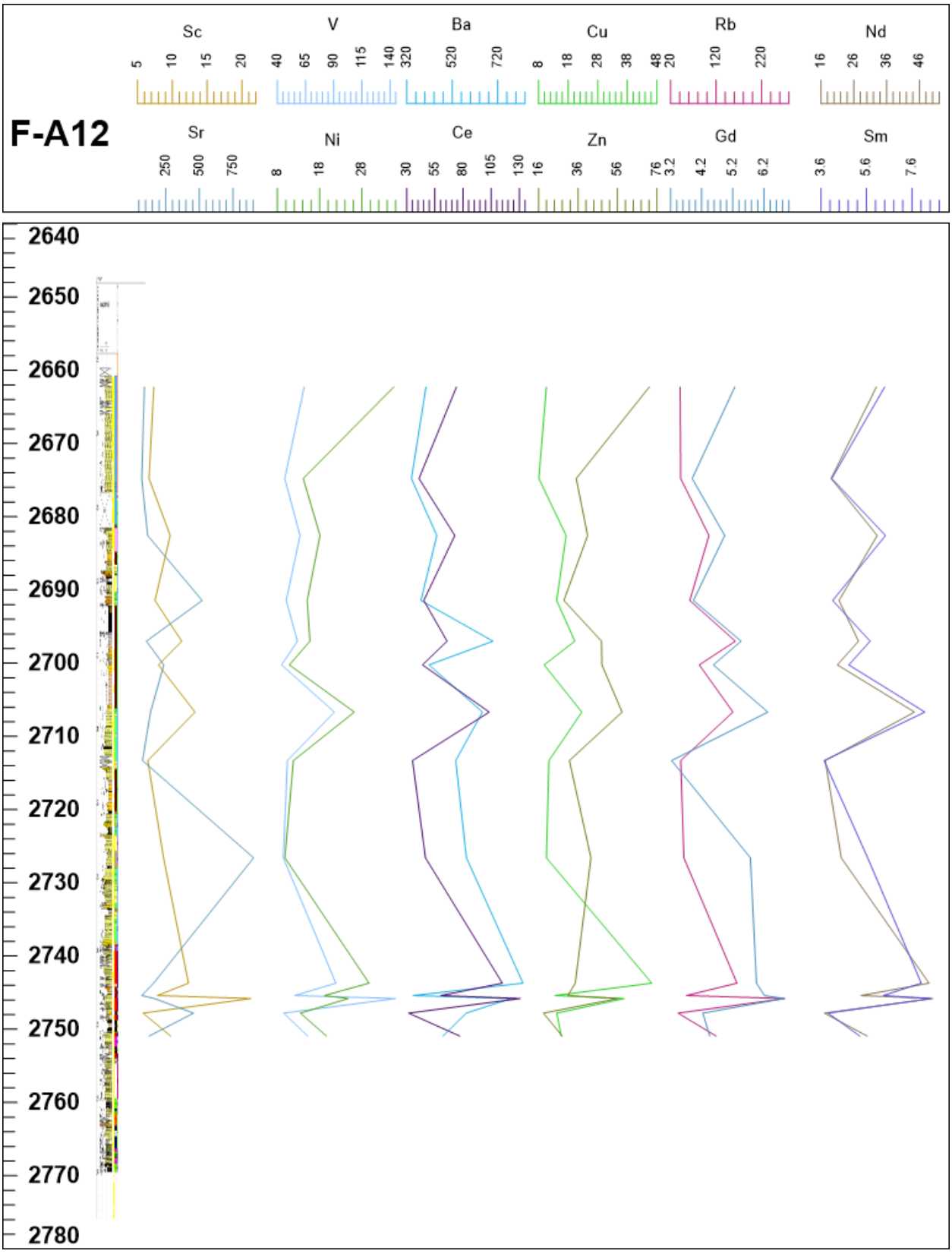
F-A12
Sc
5
10
15
20
V
40
65
90
115
140
320
Ba
520
720
Cu
8
18
28
38
48
20
Rb
120
220
Nd
16
26
36
46
Sr
250
500
750
Ni
8
18
28
Ce
30
55
80
105
130
Zn
16
36
56
76
Gd
3.2
4.2
5.2
6.2
Sm
3.6
5.6
7.6
2640
2650
2660
2670
2680
2690
2700
2710
2720
2730
2740
2750
2760
2770
2780

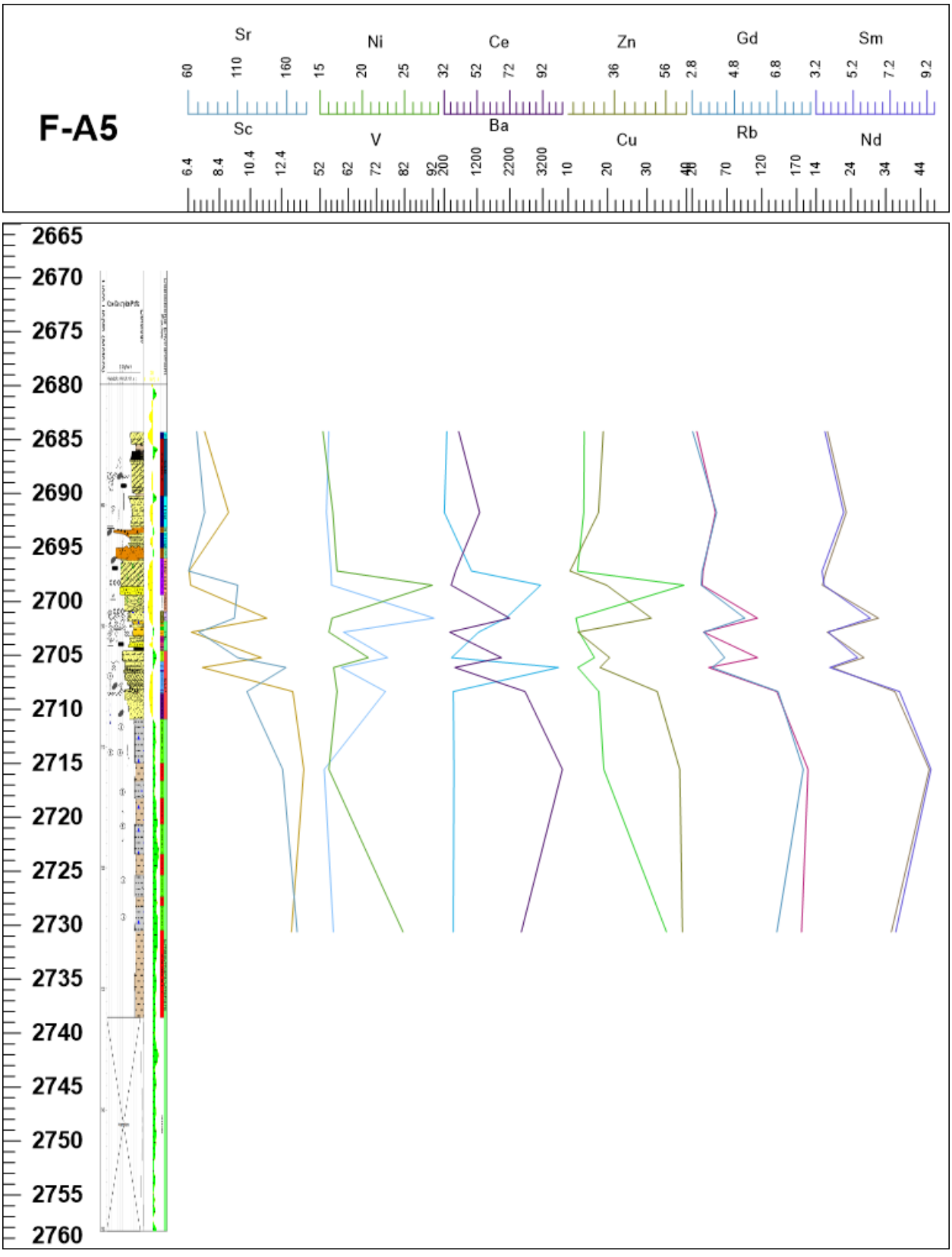
F-A5
Sr
Ni
Ce
Zn
Gd
Sm
Sc
V
Ba
Cu
Rb
Nd
2665
2670
2675
2680
2685
2690
2695
2700
2705
2710
2715
2720
2725
2730
2735
2740
2745
2750
2755
2760

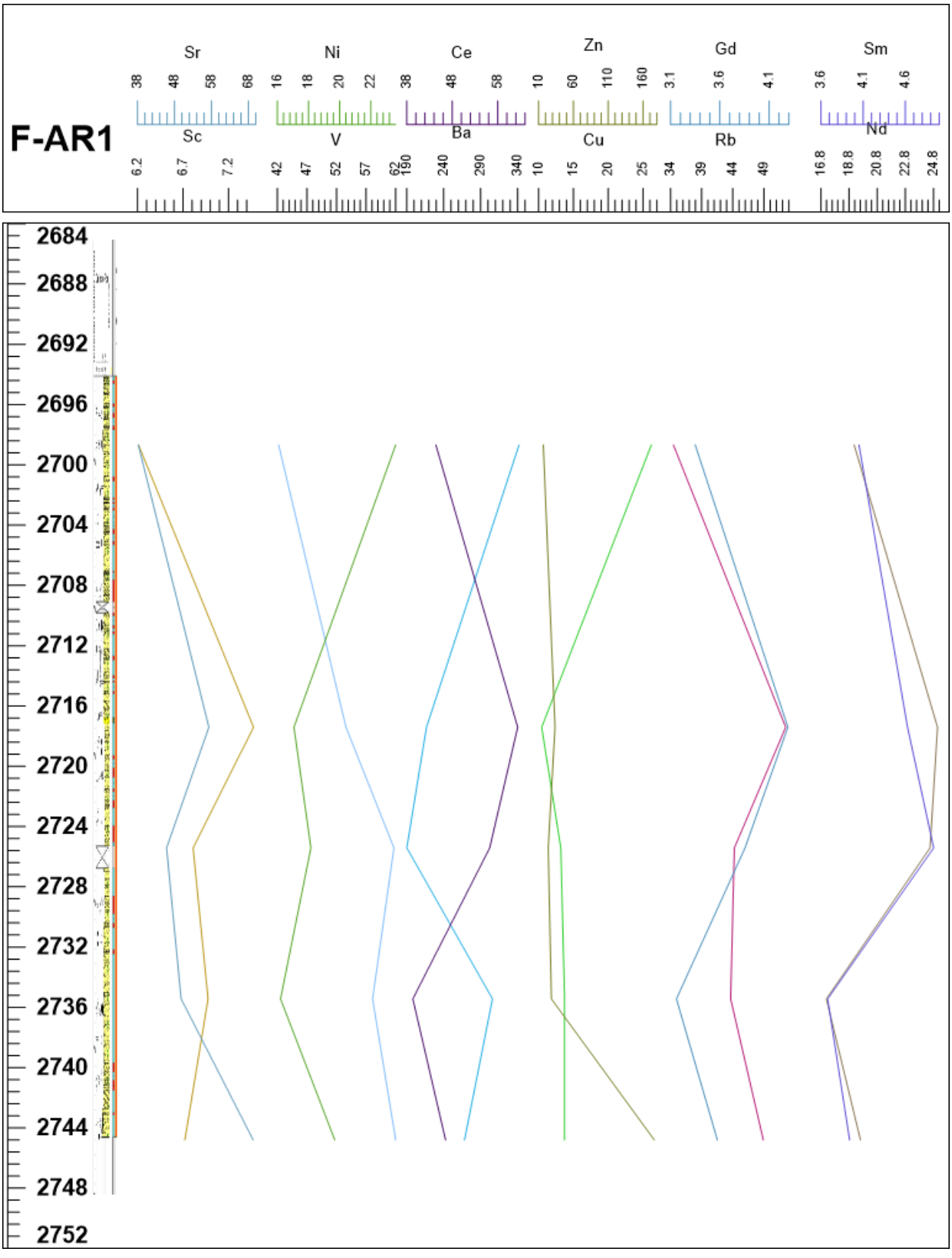
F-AR1
Sr
38
48
58
68
Ni
16
18
20
22
Ce
38
48
58
Zn
10
60
110
160
Gd
3.1
3.6
4.1
Sm
3.6
4.1
4.6
Sc
6.2
6.7
7.2
V
42
47
52
57
62
Ba
190
240
290
340
Cu
10
15
20
25
Rb
34
39
44
49
Nd
16.8
18.8
20.8
22.8
24.8
2684
2688
2692
2696
2700
2704
2708
2712
2716
2720
2724
2728
2732
2736
2740
2744
2748
2752

Principle component and Discrimnant function analysis

Principle component data

Table C8: Variation array of major element data

Xi\Xj	Al2O3	CaO	Fe2O3	K2O	MgO	Na2O	SiO2	TiO2	Clr Variances
Al2O3		1.11	0.1967	0.0274	0.0704	0.0336	0.3841	0.0302	0.0689
CaO	-2.7051		1.0072	1.1215	0.9937	1.0806	0.7975	1.052	0.7327
Fe2O3	-1.0303	1.6748		0.1357	0.0653	0.2773	0.14	0.1484	0.0837
K2O	-1.4627	1.2424	-0.4324		0.034	0.107	0.3548	0.0694	0.0686
MgO	-2.5058	0.1994	-1.4754	-1.0431		0.15	0.2738	0.0851	0.0464
Na2O	-1.6358	1.0693	-0.6055	-0.1731	0.87		0.3627	0.0375	0.0935
SiO2	2.6695	5.3746	3.6998	4.1322	5.1753	4.3053		0.2631	0.1593
TiO2	-2.8718	-0.1667	-1.8415	-1.4091	-0.3661	-1.236	-5.5413		0.0481

Table C9: Variation array of trace element data

Xi\Xj	Sc	V	Co	Ni	Rb	Sr	Y	Zr	Nb	La	Gd	Yb	Hf	Ta	Th	U	clr variances
Sc		0.0192	0.0911	0.0762	0.1037	0.145	0.0206	0.1834	0.0588	0.0276	0.0252	0.0309	0.1613	0.0979	0.0647	0.1043	0.0185
V	2.0216		0.0902	0.0575	0.151	0.1904	0.0521	0.2306	0.1023	0.0489	0.0452	0.0681	0.2104	0.141	0.1183	0.1449	0.0473
Co	-0.4674	-2.489		0.0588	0.2076	0.3605	0.0842	0.2942	0.1733	0.0675	0.0859	0.093	0.2723	0.22	0.156	0.1502	0.0932
Ni	0.8228	-1.1988	1.2902		0.2549	0.2779	0.1111	0.3455	0.2059	0.0963	0.0836	0.1329	0.3137	0.2285	0.2058	0.2004	0.1084
Rb	1.9474	-0.0742	2.4148	1.1246		0.1778	0.0604	0.2757	0.0544	0.0657	0.1256	0.0596	0.2478	0.0967	0.0384	0.0988	0.069
Sr	2.3692	0.3476	2.8366	1.5464	0.4218		0.1668	0.3073	0.149	0.201	0.1664	0.1758	0.2831	0.1407	0.1671	0.2009	0.1372
Y	0.853	-1.1686	1.3204	0.0302	-1.0944	-1.5162		0.1947	0.0493	0.012	0.0224	0.0143	0.1729	0.1082	0.0376	0.0833	0.0173
Zr	3.3545	1.3329	3.8219	2.5317	1.4071	0.9853	2.5015		0.1003	0.1891	0.1969	0.1383	0.0026	0.127	0.1325	0.1561	0.1225
Nb	-0.0948	-2.1164	0.3726	-0.9176	-2.0422	-2.464	-0.9478	-3.4493		0.0457	0.0918	0.0217	0.0829	0.0243	0.0134	0.0515	0.0194

La	1.1215	-0.9001	1.5889	0.2986	-0.826	-1.2478	0.2684	-2.2331	1.2162		0.0392	0.0139	0.1659	0.0931	0.0404	0.0709	0.0165
Gd	-0.6809	-2.7025	-0.2135	-1.5037	-2.6283	-3.0501	-1.5339	-4.0354	-0.5861	-1.8023		0.0505	0.1776	0.152	0.0886	0.131	0.0355
Yb	-1.4249	-3.4465	-0.9575	-2.2477	-3.3723	-3.7941	-2.278	-4.7794	-1.3301	-2.5464	-0.7441		0.1172	0.0586	0.0144	0.0473	0.0077
Hf	-0.2407	-2.2623	0.2267	-1.0635	-2.1881	-2.6099	-1.0937	-3.5952	-0.1459	-1.3621	0.4402	1.1842		0.1034	0.1106	0.1328	0.1025
Ta	-2.6296	-4.6512	-2.1622	-3.4524	-4.577	-4.9988	-3.4826	-5.9841	-2.5348	-3.751	-1.9487	-1.2047	-2.3889		0.0449	0.0602	0.0489
Th	-0.1571	-2.1787	0.3103	-0.9799	-2.1045	-2.5263	-1.0101	-3.5116	-0.0623	-1.2786	0.5238	1.2678	0.0836	2.4725		0.041	0.0225
U	-1.4174	-3.4389	-0.95	-2.2402	-3.3648	-3.7866	-2.2704	-4.7719	-1.3226	-2.5388	-0.7365	0.0076	-1.1767	1.2122	-1.2603		0.0475

Discrimnant function plots

Facies trends through geochemical major eleemnts showing

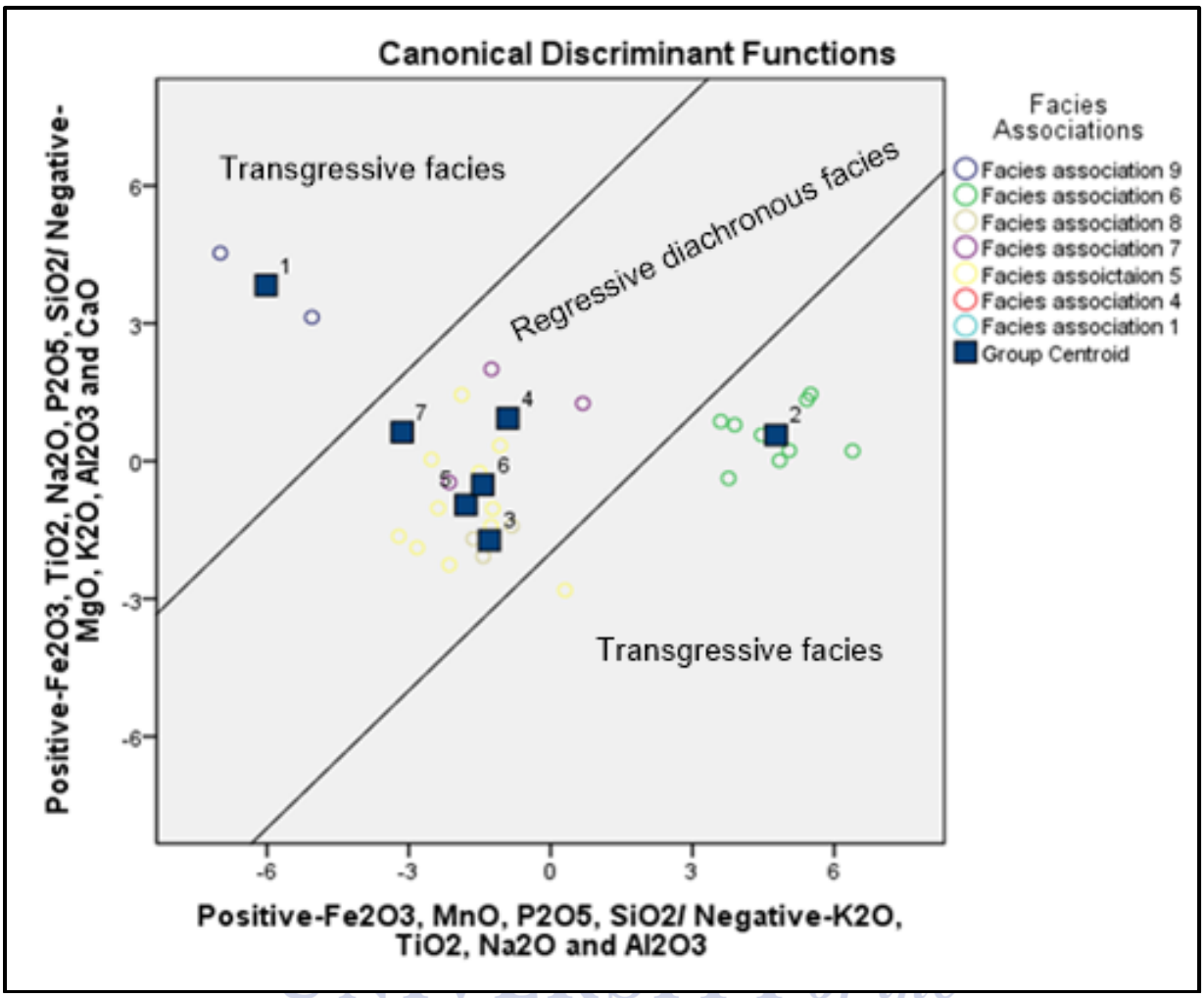

96.7% of the original cases correctly classified

Facies correlation trends through geochemical trace elements from discriminant functions

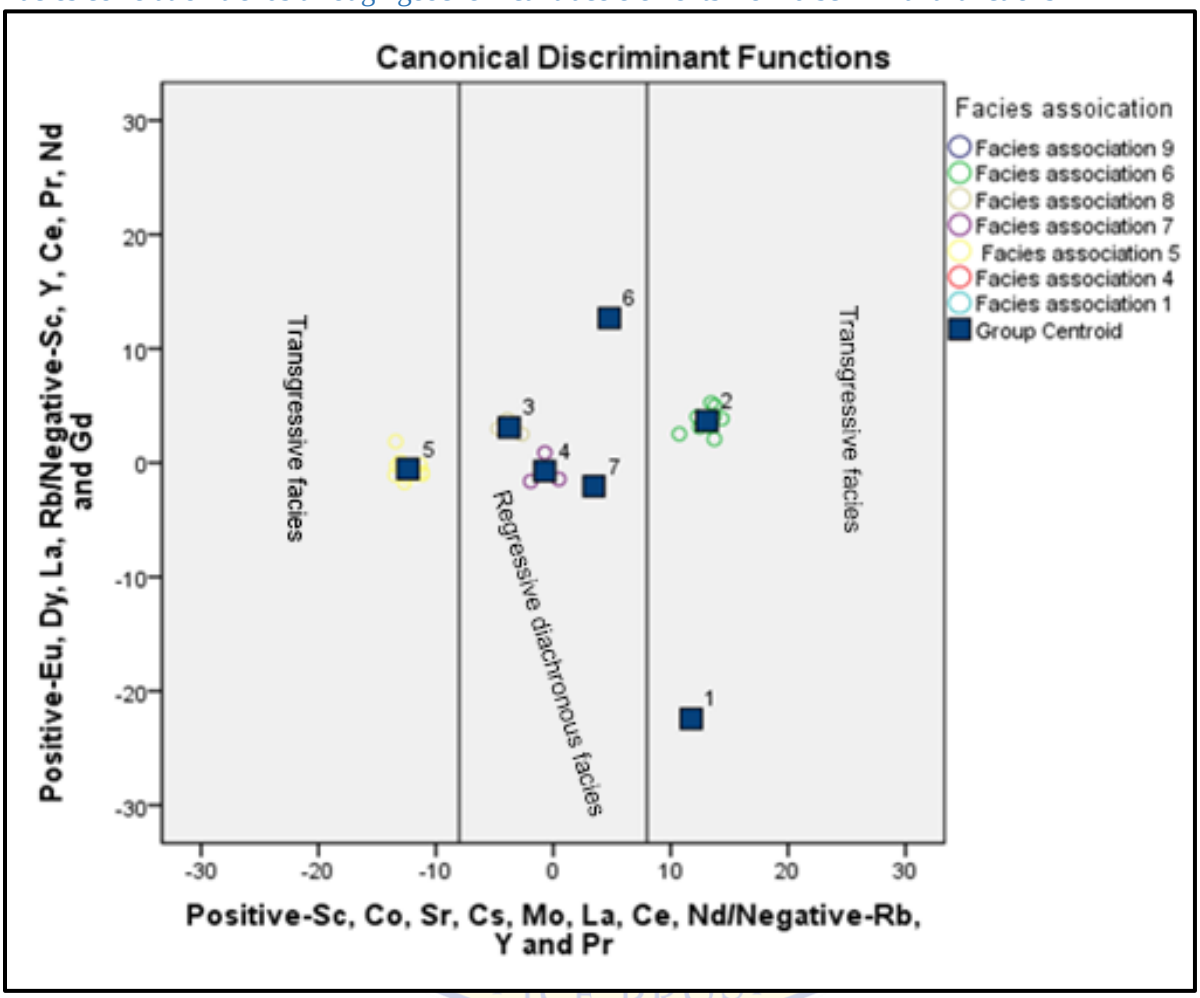

100% of original groups correctly classified

Provenance-related trace elements subjected to discriminant function analysis

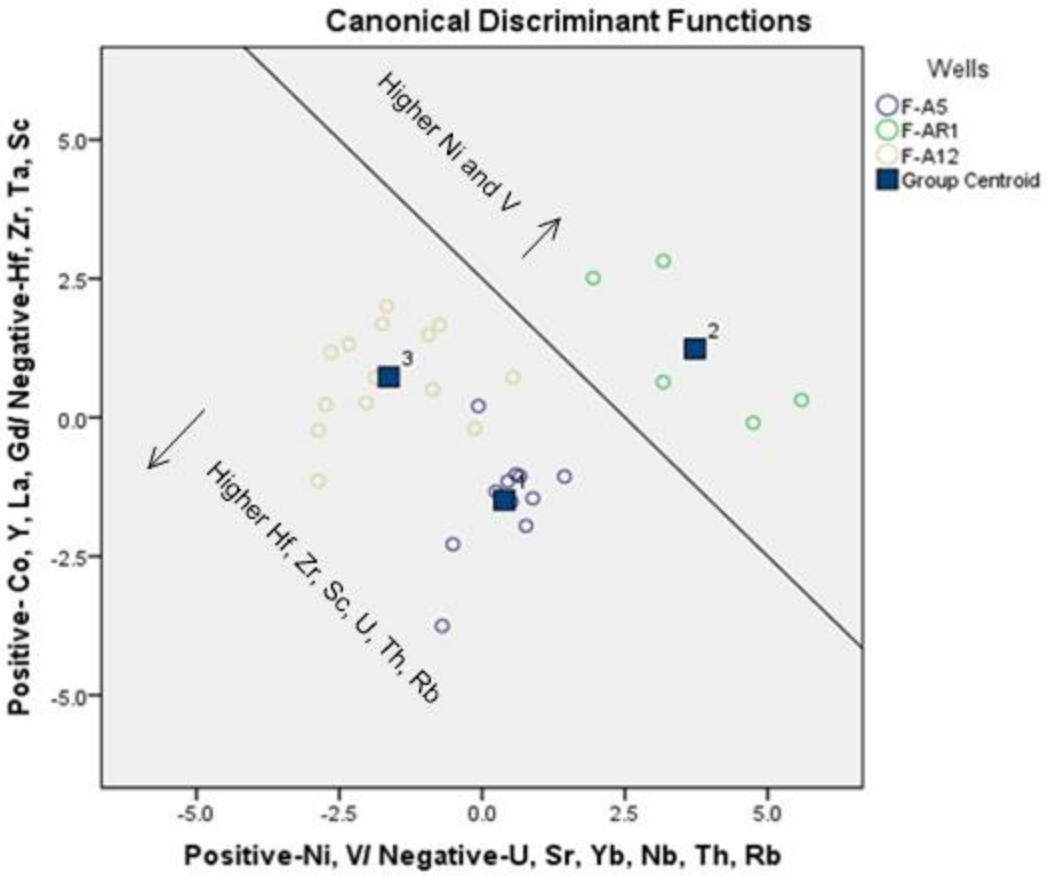

93.3% of original grouped cases correctly classified